ULTIMATE STRENGTH OF UNSTIFFENED AND RING STIFFENED CIRCULAR CYLINDERS

A Thesis submitted for
the Degree of Doctor of Philosophy
in the Faculty of Engineering
of The University of Glasgow

by

ANASTASIOS SACHINIS
B.Sc.

Department of Naval Architecture
and Ocean Engineering

March, 1982

To my parents, my sister
and my wife, with
gratitude

NOMENCLATURE

CHAPTER 1

E	Young's modulus
I	Moment of Inertia of column cross-section
L	Cylindrical shell length
m	Number of longitudinal half waves
n	Number of circumferential waves
P_{cl}	Classical buckling load
P_E	Euler's elastic buckling load
r	Radius of gyration
R	Radius of circular cylinder
R/T	Radius-to-thickness ratio
t	Thickness of cylinder wall
w_o	Initial out-of-plane deformation
w_o^*	Maximum initial out-of-plane deformation
ν	Poisson's ratio
σ_{cl}	Classical buckling stress

CHAPTER 2

c	Viscous coefficient
k	Damping factor
k_{cr}	Critical damping factor
k_{ij}	Elements of stiffness matrix
t	Time
$\ddot{x}$	Acceleration component
$\dot{x}_p$	Velocity at time $t - \frac{\Delta t}{2}$

$\dot{x}_c$	Velocity at time $t + \frac{\Delta t}{2}$
x_p	Displacement at time $t - \Delta t$
x_c	Displacement at time t
α	Minimum eigenvalue of the stiffness matrix
β	Maximum eigenvalue of the stiffness matrix
Δt	Time increment
Δt_{cr}	Critical time increment
ρ	Fictitious density

CHAPTER 3

A	Area of triangular element after straining
A_i	Area of triangular element before straining
b_w, b_u, b_v	Numerical sum of the absolute coefficients of each row of the stiffness matrix
f	Yield function
(i,j)	Position of a node
k_x, k_y, k_{xy}	Generalised flexural total strains
M_x, M_θ, $M_{x\theta}$, $M_{\theta x}$	Bending moments per unit width
M_o	Uniaxial yield moment/unit width
N_x, N_θ, $N_{x\theta}$, $N_{\theta x}$	In-plane stress resultants per unit width
N_o	Uniaxial yield force/unit width
p	External pressure
Q_x, Q_θ	Transverse shearing force intensities
u	In-plane displacement in x-direction
v	In-plane displacement in y-direction
w	Out-of-plane deflection in z-direction
x, y, z	Co-ordinates
$[C]$, $[D]$, $[R]$	Tangential elasto-plastic modular matrices relating to generalised stress resultants
$[E]$	Modular matrix (3 x 3)
$[I]$	Identity matrix

δx, δy, δs	Side lengths of triangular element after straining
δx_i, δy_i, δs_i	Side lengths of triangular element before straining
Δx, δx	Node spacing in x-direction
$R\Delta\theta$	Node spacing in θ-direction
ϵ_x, ϵ_y, ϵ_{xy}	Generalised in-plane total strains
λ	Plastic strain-multiplier
ρ_w, ρ_u, ρ_v	Fictitious densities
σ_o, σ_y	Yield stress
σ_x, σ_θ, $\sigma_{x\theta}$, $\sigma_{\theta x}$	Stress components
ϕ_x, ϕ_θ	Angles of rotation of element sides

CHAPTER 4

d_f^s, d_f^ϕ	Fictitious density reduction factors
H	Horizontal force
k_ϕ	Damping factor
k_s	Beam-column curvature
k_x^G	Generalised flexural total strain
M	Bending moment
M_b	Bending moment on column ends
m_s	Number of longitudinal half waves
n	Normal force
P	Axial load
Q	Shear force
Q(x)	Uniform lateral load
R_s	Radius of curvature
s	Column deflection on plane of bending
s_o	Initial column deformation
s_o^*	Maximum column deformation
s^t	$s + s_o$

V	Vertical force
ε_x^s	Beam-column in-plane strain
ε_x^G	Generalised total in-plane strain
ρ_s, ρ_ϕ	Fictitious densities
ϕ	Column end rotation
$\dot{\phi}$	Column angular end velocity

CHAPTER 5

i_b	Node at mid-section end
i_m	Node at mid-height of column
k_s	Damping factor
L_c	Length of mid-section
L_s	Column length
S_m	s-displacement at i_m node
ρ_m	Fictitious density
ω	Rotation of mid-section

CHAPTER 6

b	Combination between axial-compression and bending
M	Bending moment
M_p	Fully-plastic moment = $4R^2t\sigma_y$
P_{cr}	Euler buckling load
s_t	Total column deflection = $s + s_o$
w/T	Deflection-to-thickness ratio
ε	Maximum in-plane displacement at one edge divided by the half length of the shell
ε_y	Yield strain
λ	$= \frac{L}{\pi r}\sqrt{\frac{\sigma_y}{E}}$
σ_{av}	Average compressive stress
σ_m	Maximum compressive strength

p^*	Superscript referring to the corresponding value in the end of the previous load increment
f, b, in	When are used as superscripts or subscripts refer to values corresponding to fictitious , boundary and internal nodes respectively
p	When is used as a subscript refers to values in the plastic region
Δ, δ	Indicate increment

CONTENTS

		Page
NOMENCLATURE		iii
REFERENCES		4
ACKNOWLEDGEMENTS		11
SUMMARY		12
CHAPTER 1	INTRODUCTION AND LITERATURE REVIEW	14
1.1	Introduction	14
1.2	Theory of Circular Cylindrical Shells	17
1.3	Experiments on Circular Cylindrical Shells	20
1.4	Theory of Long Circular Columns	21
1.5	Experiments on Long Circular Columns	25
1.6	Interactive Buckling of Circular Cylindrical Shells	26
1.7	Aim of Thesis	27
1.8	Scope of Thesis	27
1.9	Layout of Computing Programs	28
CHAPTER 2	OUTLINE OF NUMERICAL TECHNIQUE	30
2.1	Introduction	30
2.2	Historical Development	31
2.3	Basic D.R. Formulation	32
CHAPTER 3	CYLINDRICAL SHELL ANALYSIS	35
3.1	Introduction	35
3.2	Strain-Displacement Relationships	35
3.2.1	Definition of Engineering Strains	35
3.2.2	Alternative Definition of Strains	37
3.2.3	Derivation to account for Initial Out-of-plane Distortions	39
3.3	Derivation of Curvature Expressions	45
3.4	Derivation of Governing Equations	47
3.5	Study for an Optimum Yield Criterion	51
3.5.1	Ilyushin's Yield Criterion	51
3.5.2	Modified Ivanov's Yield Criterion	54
3.5.3	Multi-layer Approach	57
3.5.4	Comparison	59
3.5.5	Correction back to the Yield Surface	61

		Page
3.6	Discretisation of Cylindrical Shell	62
3.7	Imperfections	64
3.8	Boundary Conditions	65
3.9	Loading	66
3.10	Adaptation of the Numerical Technique	67
	3.10.1 Derivation of Fictitious Nodes	67
	3.10.2 Derivation of Fictitious Densities	69
	3.10.3 Automatic Calculation Technique for Damping Factor	74
3.11	Flow Charts	76
3.12	Convergence Studies	80
3.13	Comparison with Other Solutions	81
3.14	Comparison with Experimental Data	81
CHAPTER 4	BEAM-COLUMN OVERALL AND LOCAL INTERACTIVE BUCKLING ANALYSIS	83
4.1	Introduction	83
4.2	Kinematic Relationships	83
4.3	Derivation of Governing Equations	86
4.4	Discretisation of Beam-Column	89
4.5	Yield Criterion	90
4.6	Imperfections	90
4.7	Boundary Conditions	91
4.8	Loading	91
4.9	Adaptation of the Numerical Technique	92
	4.9.1 Derivation of Fictitious Nodes	92
	4.9.2 Derivation of Fictitious Densities	94
4.10	Flow Chart	96
4.11	Convergence Studies	99
4.12	Comparison with Other Solutions	99
4.13	Comparison with Experimental Data	100
CHAPTER 5	SIMPLIFIED APPROACH TO BEAM-COLUMN INTERACTIVE BUCKLING	101
5.1	Introduction	101
5.2	Theoretical Approach	101
	5.2.1 Seeking a Suitable Method	101
	5.2.2 Theoretical Formulation	102
	5.2.3 Limitation of the Technique	104
	5.2.4 Imperfections	104

		Page
5.3	Flow Chart	104
5.4	Comparison with Other Solutions	107
5.5	Comparison with Experimental Data	107
CHAPTER 6	PARAMETRIC STUDIES	108
6.1	Introduction	108
6.2	Circular Cylindrical Shells	108
6.2.1	Axial-Compression	108
6.2.2	Axial-Compression plus Bending	110
6.2.3	External Pressure plus Axial Loading and Bending	111
6.2.4	Residual Axial-Compressive Strength of Damaged Cylinders	113
6.3	Beam-Column Elasto-Plastic Results	114
6.4	Comparison with Existing Rules	115
CHAPTER 7	CONCLUSIONS AND FUTURE WORK	117
7.1	Conclusions Concerning Numerical Technique	117
7.2	Conclusions on the Cylindrical Shell Analysis	118
7.3	Conclusion on the Beam-Column Overall and Local Interactive Buckling Analysis	119
7.4	Conclusions on the Simplified Approach to Beam-Column Interactive Buckling	120
7.5	Conclusions on Parametric Studies of Cylindrical Shells	120
7.5.1	Axial Compression	121
7.5.2	Axial Compression plus Bending	122
7.5.3	Axial Compression plus Bending plus External Pressure	122
7.6	Conclusions on Beam-Columns	123
7.7	Recommendations for Future Work	124
APPENDIX I	General Strain-Displacement Relationships	125
APPENDIX II	Development of Graphical Subroutines	131
APPENDIX III	Preliminary Design of a Pressure Chamber	133
FIGURES		144

REFERENCES

1. Ship Design and Construction, Ed. A.M. D'ARCHANGELO, Publ. The Society of Naval Architects and Marine Engineers, p.584, 1969.

2. FAULKNER, D.: Some thoughts on the nature of Hazards affecting structures in deeper waters, Jnl. SUT, vol. 3, no. 1, April 1977, pp. 16-21.

3. LORENZ, R.: Die nichtachsensymmetrische knickung dünnwanger Hohlzylinder, Phys. Z., vol. 13, pp. 241-260, 1911.

4. TIMOSHENKO, S.: Theory of Elastic Stability, 1st Edition, McGraw-Hill Book Company Inc., New York and London, 1936.

5. TIMOSHENKO, S.P. and GERE, J.M.: Theory of Elastic Stability, 2nd ed., McGraw Hill, New York, 1961.

6. SOUTHWELL, R.V.: On the Collapse of Tubes by External Pressure, Phil. Mag., vol. 25, pp. 687-698, 1913.

7. VON MISES, R.: Der kritische Ausendruck zylindrischer Rohre, Z. Ver. Deutsch. Ing., vol. 58, pp. 750-755, 1914.

8. FLÜGGE, W.: Die Stabilitat der kreiszylinderschall, Ing. -Arch, vol. 3, pp. 436-506, 1932.

9. DONNELL, L.H.: Stability of Thin-Walled Tubes under Torsion, NACA Rep. 479, 1933.

10. VON KARMAN, T. and TSIEN, H.S.: The Buckling of Thin Cylindrical Shells under Axial Compression, J. Aeronaut. Sci., vol. 8, pp. 303-312, August 1941.

11. DONNELL, L.H. and WAN, C.C.: Effects of Imperfections on Buckling of Thin Cylinders and Columns under Axial Compression, J. Appl. Mech., vol. 17, pp. 73-83, 1950.

12. KOITER, W.T.: On the stability of Elastic Equilibrium (in Dutch with English summary), thesis, Delft, H.J. Paris, Amsterdam, 1945. English translation, Air Force Flight Dyn. Lab. Tech. Rep. AFFDL-TR-70-25, February 1970.

13. KOITER, W.T.: Elastic Stability and Postbuckling Behaviour, Proc. Symp. Non-linear probl., University of Wiscons. in Press, Madison, 1963, pp. 257-275.

14. BRAZIER, L.G. (1927): On the flexure of thin cylindrical shells and other "thin" sections, Proc. Roy. Soc. (London), A116, 104-114.

15. HARDING, J.E.: The Elasto-Plastic Analysis of Imperfect Cylinders, Proc. Instn. Civ. Engrs., Part II, vol. 65, London, December 1978.

16. LUNDQUIST, E.E.: Strength Tests on Thin-Walled Duraluminium Cylinders in Compression, NACA Rep. 473, 1933.

17. DONNELL, L.H.: A New Theory for the Buckling of Thin Cylinders under Axial Compression and Bending, Trans. ASME, vol. 56, p. 795, 1934.

18. BRUSH, D.O. and ALMROTH, B.O.: Buckling of Bars, Plates and Shells, McGraw Hill, 1975.

19. SUER, H.S., Harris, L.A., SKENE, W.T. and BENJAMIN, R.J.: The bending stability of thin-walled unstiffened circular cylinders including effects of internal pressure, J. Aeronaut. Sci., 25, 281-287, 1958.

20. LEUMONT, W.J. Jr.: Collapse tests of pressurised membrane-like circular cylinders for combined compression and bending, Tech. Notes, natu. aeronaut. Space Admin., No. D-2814, 1-16, 1965.

21. HARDING, J.E. and DOWLING, P.J.: Correlation between experimental and analytical results for the buckling of ring stiffened shells, Conference, Integrity of Offshore Structures, Ed. D. Faulkner, M.J. Cowling and P.A. Frieze, Univ. of Glasgow, Applied Science Publishers, 1981.

22. FLETCHER, SIR BANISTER: A History of Architecture, 15th Edition. B.T. Batsford, London, 1950, p.28.

23. HOFF, N.J.: Buckling and Stability, Jour. Roy. Aeor. Soc., vol. 58, no. 517, Jan. 1954.

24. The Architecture of Vitruvious Pollio (1791), translated from the original Latin by W. Newton, Architect, London, 1791; Book the fourth, Chapter I: of the Three Kinds of Columns and their Invention.

25. TIMOSHENKO, S.P.: History of the Strength of Materials, McGraw-Hill, New York, pp. 30-40, 1953.

26. SHANLEY, F.R.: Inelastic Column Theory, Jour. Aeronaut Sci., p. 261, 1947.

27. CHWALLA, W.: Die Stabilität zentrisch und exzentrisch gedrückter Stäbe aus Baustahl, Sitzungsberichte der Akädemie de Wissenschaften in Wien, Abt. IIα, p. 469, (1928).

28. BLEICH, F.: Buckling Strength of Metal Structures, Eng. Society, Monograph, McGraw-Hill, New York, 1959.

29. MESLOH, R., JOHNS, T.G. and SORENSON, J.E.: The Propagating Buckle, BOSS '76, Behaviour of Offshore Structures, The Norwegian Institute of Technology, 1976

30. KYRIAKIDES, S. and BABCOCK, C.D.: On the Dynamics and the Arrest of the Propagating Buckle in Offshore Pipelines, Offshore Technology Conference, 1979, OTC 3479.

31. BOUWKAMP, J.G. and STEPHEN, R.M.: Structural behaviour of a large diameter pipeline under combined loading, J. Trans. Div., Am. Soc. Civ. Engrs., 99, TE3, pp. 521-536, 1973.

32. BOUWKAMP, J.G.: Buckling and Post-Buckling Strength of Circular Tubular Sections, Seventh Annual Offshore Technology Conference, May 1975.

33. CHEN, W.F. and ROSS, D.A.: Tests of Fabricated Tubular Columns, Journal of the structural division, A.S.C.E., March 1977.

34. SMITH, C.S., KIRKWOOD, W.J. and SWAN, J.W.: Buckling strength and post-collapse behaviour of tubular bracing members including damage effect., Dept. of Energy Report No. OT-R 7837, AMTE Report No. AMTE(S) TM 79343,1979.

35. OTTER, J.R.H.: Computations for Prestressed Concrete Reactor Pressure Vessels using Dynamic Relaxation, Nucl. Struct. Engng, 1, pp. 61-75, 1965.

36. OTTER, J.R.H.: Dynamic Relaxation, Proc. Inst. Civ. Engrs., 35, pp. 633-656, 1966.

37. OTTER, J.R.H., CASSEL, E. and HOBBS, R.E.: Dynamic Relaxation, Proc. Inst. Civ. Engrs. 35, pp. 723-750, (1967).

38. DAY, A.X.: An Introduction to Dynamic Relaxation, The Engineer, 219, pp. 218-221, (1965).

39. RUSHTON, K.R.: Dynamic Relaxation Solutions of Elastic Plate Problems, J. Strn. Anal., vol. 3, pp. 23-32, 1968.

40. RUSHTON, K.R.: Large Deflexion of Variable Thickness Plates, Int. J. Mech. Sci., vol. 10, pp. 723-735, 1968.

41. RUSHTON, K.R.: Dynamic Relaxation Solution for the Large Deflection of Plates with Specified Boundary Stresses, J. Strn. Anal., vol. 4, pp. 75-80, 1969.

42. WILLIAMS, D.G.: Some Examples of the Elastic Behaviour of Initially Deformed Bridge Panels, Civil Eng. & Pub. Wks. Rev., pp. 1107-1112, 1971.

43. LOWE, P.A. and FLINT, A.R.: Prediction of Collapse Loadings for Composite Highway Bridges, Proc. Instn. Civ. Engrs., vol. 48, pp. 645-659, 1971.

44. CASSELL, A.C.: Shells of Revolution under Arbitrary Loading and the use of Fictitious Densities in Dynamic Relaxation, Proc. Instn. Civ. Engrs., vol. 45, pp. 65-78, 1970.

45. FRIEZE, P.A., HOBBS, R.E. and DOWLING, P.J.: Application of Dynamic Relaxation to the Large Deflection Elasto-Plastic Analysis of Plates, Computers & Structures, vol. 8, pp. 331-310, 1978.

46. HARDING, J.E., HOBBS, R.E. and NEAL, B.G.: The Elasto-Plastic Analysis of Imperfect Square Plates under In-Plane Loading, Proc. Instn. Civ. Engrs., vol. 63, Part 2, pp. 137-158, 1977.

47. PAPADRAKAKIS, M.: A method for the Automatic Evaluation of the Dynamic Relaxation Parameters, Computer Methods in Applied Mechanics and Engineering 25 (1981), pp. 35-48, North-Holland publishing company.

48. WOOD, W.L.: Comparison of dynamic relaxation with three other iterative methods, Engineer, Lond., 1967, 221 (Nov. 24), pp. 683-687.

49. CASSELL, A.C. and HOBBS, R.E.: Numerical Stability of Dynamic Relaxation Analysis of Non-Linear Structures, Int. J. Num. Methods in Eng., vol. 1, 1976.

50. SACHINIS, A. and FRIEZE, P.A.: Kinematic Relationships for Initially Distorted Cylinders, Report no. NAOE-HL-81-08, Dept. of Naval Architecture & Ocean Engineering, University of Glasgow, 1981.

51. DONNELL, L.H.: Beams, Plates and Shells, McGraw-Hill Book Company, 1976 edition.

52. TIMOSHENKO, S.: Theory of Plates and Shells, McGraw-Hill Book Company, 1st edition, 1940.

53. ILYUSHIN, A.A.: Plasticité, Editions Eyrolles, Paris, 1956.

54. CRISFIELD, M.A.: Large-deflection elasto-plastic buckling analysis of plates using finite elements, TRRL Report LR 593, 1973.

55. MASSONET, C.: General theory of elasto-plastic membrane-plates, Engineering Plasticity, edited by J. Heyman and F.A. Leakie, Cambridge University press, 1968, pp. 443-473.

56. CRISFIELD, M.A.: Ivanov's yield criterion for thin plates and shells using finite elements, TRRL Laboratory Report 919, 1979.

57. BURGOYNE, C.J.: Discussion on Paper 8154, 'Elasto-plastic buckling in short thin-walled beams and columns', Proc. Instn. Civ. Engrs., Part 2, 65, December 1978, pp. 857-874; discussion Proc. Instn. Civ. Engrs., Part 2, 67, June 1979, pp. 559-560.

58. IVANOV, G.V.: Inzhenernyi Zhurnal Mekhanika Trerdogo Tela, No. 6, 1967, pp. 74-75.

59. ZIENKIEWICZ, O.C., VALLIAPAN, S. and KING, I.P.: Elasto-plastic solutions of engineering problems, Initial stress, finite element approach, Int. Journal of Numerical Meth. in Eng., 1, 1969, pp. 75-100.

60. YAMADA, Y., YOSHIMURA, N. and SAKURAI, T.: Plastic stress-strain matrix and its application for the solution of elasto-plastic problems by the finite element method. Int. Journal of Mech. Sci., 10, pp. 343-354, 1968.

61. FRIEZE, P.A. and SACHINIS, A.: Buckling Analysis of Singly- and Doubly-Curved Shells using Dynamic Relaxation, Numerical Methods for Non-Linear Problems, Proc. of the Intern. Conf. held at University College, Swansea, 2-5 Sept. 1980.

62. LYNCH, R.D., KELSEY, S. and SAXE, H.C.: The application of Dynamic Relaxation to the Finite Element Method of Structural Analysis, Project THEMIS University of NOTRE DAME, 19.

63. BASU, A.K. and DAWSON, J.M.: Orthotropic sandwich plates, Part 1: Dynamic relaxation treatment, Part 2: Analysis and application to multicell and voided bridge decks, Proc. Instn. Civ. Engrs., 1970, 45(Feb), pp. 87-114.

64. HARDING, J.E.: Ring-stiffened cylinders under axial and external pressure loading, Proc. Instn. Civ. Engrs., Part 2, 1981, 71, Sept., pp. 863-878.

65. WALKER, A.C., ANDRONICOU, A., SRIDHARAN, S.: Theoretical Analysis of Stringer and Ring Stiffened Shells, Buckling of Shells in Offshore Structures, Ed. J.E. Harding, P.J. Dowling & N. Agelidis, Granada Publ.

66. DOWLING, P.J. and HARDING, J.E.: Experimental Behaviour of Ring and Stringer Stiffened Shells, Buckling of shells in offshore structures, Ed. J.E. Harding, P.J. Dowling & N. Agelidis, Granada Publ.

67. CHEN, W.F. and ATSUTA, T.: Theory of Beam Columns, vol. 1, McGraw-Hill Book Company, 1976 ed.

68. A.P.I. Recommended Practice for Planning, Designing, and Constructing Fixed Offshore Platforms, Issued by American Petroleum Institute, API RP2A, 12th Ed., January 1981.

69. Rules for the Design Construction and Inspection of Offshore Structures, 1977, Appendix C, Steel Structures, Reprint with corrections (1979), Det norske Veritas.

70. VANDEPITTE, D. and RATHÈ, J.: Buckling of Circular Cylindrical Shells under Axial Load in the Elasto-Plastic Region, State University at Gent, Belgium, June 1980.

71. Specification for Unfired Fusion Welded Pressure Vessels, BS5500: 1976, British Standards Institution.

72. Det norske Veritas, "Rules for the Construction and Classification of Diving Systems", 1975.

73. SANDERS, J.L.: Non-Linear Theories for Thin Shells, Q. Appl. Maths., 1963, 21, pp. 26-36.

ACKNOWLEDGEMENTS

The work presented in this thesis is part of the NA3 project sponsored by the Science and Engineering Research Council (S.E.R.C.), Marine Technology Directorate. The author wishes to express his gratitude to Dr. P.A. Frieze, Lecturer in the Department of Naval Architecture and Ocean Engineering for his continuous supervision, expert advice and guidance throughout the accomplishment of the present thesis. He is also grateful to Professor D. Faulkner, Professor of Naval Architecture and Ocean Engineering, for his approval in offering financial support in the form of a Research Assistantship.

The author also wishes to express his thanks to the consultants of the Glasgow University Computing Service for their assistance during the development of the programs, and also to the operators who showed great co-operation, patience and understanding during the generation of results.

In appreciation of the great help offered by Mrs. T. Anderson, computing assistant in the Department of Naval Architecture and Ocean Engineering, in carrying out parametric studies, the author expresses his gratitude.

The author would like to acknowledge the high standard of draughting and excellent response of Mrs. H. Guile who prepared most of the figures.

The help of Mrs. R. Young, tracer of the Faculty of Engineering, and Mr. J. MacCallum, tracer of the Department of Naval Architecture and Ocean Engineering, for their part in preparing some figures is acknowledged.

Finally, the author expresses his gratitude to Mrs. L. Robinson for the excellent typing of this thesis, under difficult circumstances.

SUMMARY

The work presented in this thesis aims to investigate the pre- and post-buckling elasto-plastic behaviour of general circular cylindrical shells subjected to load combinations of axial-compression, bending and external pressure.

Theoretical formulations are described which cater for both local and overall instability behaviour of cylindrical shells. Dynamic Relaxation in conjunction with finite differences is used to solve the shell equilibrium equations together with kinematic and constitutive relationships.

Plasticity is introduced using a multi-layer approach based upon the von Mises yield criterion in conjunction with the Prandtl-Reuss flow rule. This was selected after a comparative study on Ilyushin's and Ivanov's modified single-layer approaches.

Results derived from the present formulations are compared with existing theoretical and experimental results.

Parametric studies were undertaken and the derived results are discussed.

Conclusions regarding the numerical technique and the parametric studies are included. Recommendations concerning further developments are made.

The derivation of general strain-displacement relationships, including initial imperfections and small rigid body rotations, is presented in

Appendix I.

Appendix II describes the development of graphical subroutines which enable a rapid presentation of results to be performed.

Appendix III presents a preliminary design for a pressure chamber to enable combined loading tests on tubes to be conducted.

CHAPTER 1

INTRODUCTION AND LITERATURE REVIEW

1.1 Introduction

In engineering design cylindrical shells play an important role when it comes to weight critical applications since these thin-walled structures exhibit very favourable strength over weight ratios. Unfortunately, they are also very susceptible to buckling instabilities. The thin-walled cylindrical shell is often said to be one of the most important structural elements. For a long time it has been used extensively in aerospace structures, some transportation vehicles, bridges, submarines, tower shafts and silos.

Buckling of thin-walled shell structures has now become a subject of interest to Naval Architects. Here, reference can be made to a variety of different designs for large diameter tubular members of semi-submersible offshore drilling rigs and floating buoy oil storage tanks.

Long unstiffened circular tubes of low radius-to-thickness ratio ($R/T<30$) are also used extensively in offshore structures. Circular tubes are the predominant elements in the primary structural framework of fixed platforms and mobile drilling rigs. These cylindrical bracing members, particularly those in the splash zone, are often subjected to impact loading arising from supply and support vessel collision or accidental drop of weights from the platforms deck and, to a lesser extent, to wave slamming. These are the main hazards that can reduce the strength and stiffness of these members.

Another booming engineering field where long tubes are of great importance is the technology of pipelaying in deep water. It is sometimes hard to remember that only five to six years ago it was thought

ambitious and somewhat risky to lay a pipe in 100m of water.

In the North Sea, the laying of very long pipes in water up to 150m deep is now commonplace. This has shown that pipes can be laid successfully in 300m, and several studies are now looking at the problems of placing pipes in much deeper waters, to 1000m and beyond.

Thus, it is not surprising that in the last few decades, literally hundreds of technical papers dealing with shell stability have been published.

Actual submersible structures are far from perfect or even true to specified imperfections that can be satisfactorily approximated on a theoretical basis. Among the degrading factors that will occur in practical cases are the following:

1. Lack of uniformity of the physical properties of the base material.
2. Lack of uniformity in the physical dimensions of the base material.
3. Imperfect workmanship.
4. Welding residual stresses.
5. Initial stresses due to rolling or forming of structural material.
6. Stress concentrations from items such as access fittings and local attachments.
7. Even residual stresses that result from the steel making process; i.e., from rolling billets into flat plating and later heat treatment.

When these degrading factors are combined with a factor of safety, e.g. as low as 1.5, it is almost essential that model tests of any intended

structure involving cylindrical elements be undertaken to confirm the design before actual full-scale production begins[1].

The lack of validation for theoretical analysis concerning structures with moderate to large levels of geometric imperfections is of particular concern in the marine structures field. Marine structures, in their hostile marine environments, are subjected to various levels of damage over their life. These together with their fabrication shortcomings amplify any geometric imperfections to such an extent that comparison with even the most imperfect aerospace structures is invalid [2]. In addition, full-scale proof testing of components, as is customary in aerospace design, is impracticable and so there is some concern in the marine industry about the lack of theories capable of predicting the reductions of elastic buckling loads in cylinders having moderate to large imperfections. The fact that marine structures are usually constructed of relatively stocky geometries and from material with yield stresses such that over these geometric ranges plasticity could provide additional and possibly significant loss of stiffness, can only add to this unease.

With the advance of Offshore Technology, a need for yet more thorough and careful study of circular cylindrical elements is required. The consequences of failure and delay are extremely expensive and, although analyses using sophisticated numerical techniques are not necessarily inexpensive, their effectiveness can have a very high economic return. Consider for example, a laybarge costing £100,000 a day which is laying a 200km pipeline at a rate of one double joint every 15 minutes. If an engineering research project costs £50,000 and, as a result, it is possible to cut the time per double joint by just 10 seconds or to avoid one 10-hour delay, the study has saved more than its own cost. A second example would be the ability to analyse the residual strength of a dam-

aged member and indicate if it is adequate in its present condition. The alternative of shutting down the platform to replace the member because of inadequate knowledge has severe economic consequences.

In general the stability of thin-walled cylindrical shells is one of those problems which continues to pose a serious challenge to the problem solving skills of today's engineers.

1.2 Theory of Circular Cylindrical Shells

For almost eight decades the buckling of the thin-walled, circular, cylindrical shell under axial compression has proved to be an enigma. Stability equations for cylindrical shells have been available in the literature since the late 1800s. The buckling of axially compressed cylindrical shells was first solved independently by Lorenz[3], Timoshenko[4,5] and Southwell[6] at the beginning of this century. Their theory led to a bifurcation load $P_{cl} = (2\pi Rt)\sigma_{cl}$ for the perfect cylinder with radius R and wall thickness t,

$$\sigma_{cl} = \frac{1}{\sqrt{3(1 - \nu^2)}} \frac{Et}{R} \simeq 0.6 \frac{Et}{R} \tag{1.1}$$

for $\nu = 0.3$, which gives

$$P_{cl} = 1.2\pi Et^2 \tag{1.2}$$

which is called the classical buckling load. Here E is Young's modulus and ν Poisson's ratio.

Solutions for buckling under uniform external pressure were given by Southwell in 1913[6], and by von Mises in 1914[7]. In 1932 Flügge[8] presented a comprehensive treatement of cylindrical shell stability including combined loading and cylinders subjected to bending. Donnell[9] in 1934 presented an approximate large deflection theory which included initial imperfections. He defined failure as the load at which the maximum stress reached the yield point of the material. However, in

order to reduce the computational difficulties he had to introduce so many simplifying assumptions that he later considered the solution obtained unsatisfactory. It has been long felt that the buckling phenomenon of shells can be explained by means of a non-linear large deflection theory. This belief was confirmed in 1941 when von Karman and Tsien[10] published a paper in which their landmark analysis of the postbuckling equilibrium of axially compressed cylindrical shells showed that the secondary equilibrium path drops sharply downward from the bifurcation point (Fig. 1.1). Although the authors did not analyse initially imperfect shells, their results suggest that the corresponding equilibrium path for such a shell might have the form illustrated in Figure (1.2), where buckling occurs at the markedly lower value of the load corresponding to the limit point B rather than at the bifurcation point A.

A well-known analysis of initially imperfect cylindrical shells presented by Donnell and Wan in 1950[11] yielded equilibrium paths of the form shown in Figure (1.2). The Donnell-Wan analysis was based on the non-linear large deflection equilibrium equations and analysed a thin-walled shell with an initial shape which deviated only slightly from cylindrical. The analysis had the limitation, however, that the function representing the initial deviation from a perfectly cylindrical shape was assumed for simplicity to be of the form of the constantly changing displacement mode. Consequently, it does not represent a particular initial shape. Rigorous confirmation of the influence of initial imperfections was given by Koiter in 1945[12]. His work in this paper received little attention until a summary[13] appeared in 1963. The Koiter analysis focuses attention on initial-post-buckling behaviour and provides a theory that is exact in the asymptotic sense, i.e. exact at the bifurcation point itself and a close approximation for the post-buckling configurations near the bifurcation point. When the initial portion of the secondary path has a positive

slope, considerable post-buckling strength can be developed by the structure, and loss of stability on the primary path does not result in structural collapse. On the other hand, when the initial portion of the secondary path has a negative slope, the buckling is precipitous and the magnitude of the critical load is subject to the influence of initial imperfections. The analysis in Reference (12) showed that a limited amount of information about the secondary path can be obtained by examination of the state of equilibrium at the bifurcation point. Along the primary path, equilibrium is always stable below the bifurcation point and unstable beyond. At the bifurcation point itself, however, equilibrium is stable in some cases and unstable in others. In any case Koiter's general theory of elastic stability marked the beginning of the imperfection sensitivity design philosophy.

Little attention has been given in the literature to the problem of the buckling of circular cylinders under pure bending, and under combined bending and external pressure loading. Brazier in 1927[14] studied the stability of an infinitely long cylinder under bending where loss of stability occurred as a result of excessive ovalisation of the cylinder cross-section. This ovalisation, commonly referred to as the Brazier effect, is caused by the fact that the longitudinal tensile and compressive stresses have components directed toward the midplane of the cylinder. The effect of these components is to flatten the cylinder, resulting in a steadily decreasing resistance to bending moment. As shown in Figure (1.3), a limit-point maximum is eventually reached, and collapse of the shell results. The Brazier effect is dominant in very long cylinders under bending where end conditions have a negligible restraining effect on sections furthest from the ends.

In the case of buckling analyses of structures composed of elastic-plastic materials, there is the added complexity of a stress-strain relationship which is not only non-linear, but also has different paths for

loading into and unloading from the plastic range.

The advent of computers and the development of numerical techniques, in the early 1970s, have provided an easy way to study the elasto-plastic behaviour of cylinders with great accuracy. Many elastic or elasto-plastic solutions have been obtained during the last decade using finite element or finite difference techniques. In 1978 Harding[15] presented a comprehensive study on unstiffened imperfect cylindrical shells under axial compression and external pressure. These were elasto-plastic results which gave some insight into the large scatter of experimental results for cylindrical shells under axial compression. He used a program which incorporated a multilayer representation of plasticity combined with the von Mises' yield criterion.

1.3 Experiments on Circular Cylindrical Shells

For a great number of the cylinders of different materials and sizes tested in axial compression during the period from 1927 to 1970, there is severe disagreement with the theoretical results for perfect cylinders. For large R/T's the actual buckling loads are only 20 to 50 per cent of the classical buckling load. The main reason for this disagreement has been found to be the large imperfection sensitivity of cylinders under axial compression.

Early attempts by Flügge[8], Lundquist in 1933[16] and Donnell in 1934[17] failed to establish a correlation between theoretical and experimental buckling loads for axially compressed cylindrical shells. Experimental results were scattered well below the analytical results. Also the analyses indicated that the buckles were either axisymmetric or of the so-called checkerboard type.

$$w_o = w_o^* \sin\left(\frac{mx\pi}{L}\right)\sin(n\theta) \qquad (1.3)$$

In contrast, buckles observed in tests are diamond shaped with primarily inward displacements. This descrepancy was noticed by the early investigators, but only later was it possible by use of high-speed photography[18] to establish what actually happened in the transition to the buckled state.

The analysis of the postbuckling behaviour of axially loaded cylinders has contributed to a better understanding of the reasons for the scatter in tests results and of the discrepancy between experimental and theoretical results.

In 1958 Suer et al[19] carried out an extensive series of tests on cylinders in bending both with and without internal pressure present. The length of the cylinders was long enough to avoid any affect of the boundaries. Also, the shells were thin enough so that elastic buckling occurred. Their results agreed with those produced by Donnell in 1934 and Lundquist in 1933.

In 1956 Leaumont[20] presented experimental collapse loads for combined compression and bending of internally pressurised membrane-like cylinders. The shells were made of polyester film with R/T ratios of 3,000, 6,000 and 12,000 and were tested at different pressures. The experimental results showed a linear interaction between axial compression and bending moment at buckling, for all pressures at which the tests were carried out.

In recent years a series of experiments on large- and small-scale ring-stiffened cylinders under concentric and eccentric axial compression has been carried out at Imperial College[21] with the aim of using the results to calibrate a computer based analysis and to provide data to check design curves deduced from the analytical studies. The models were at a scale of approximately 1:4 and 1:20, respectively.

1.4 Theory of Long Circular Columns

Columns have been used for centuries as compression members in

buildings. At the beginning of recorded history, between 2500 and 2200 B.C., the Egyptians hewed columns out of rock in the tombs of Beni Hasan[22]. However, in the minds of men in the Western World the word column is associated rather with the collonades of ancient Greek and Roman public buildings[23]. Apparently the columns of the classic period were designed entirely empirically, and their ultimate strength was determined entirely by the crushing strength of the material similar to that of the fracture strength in tension members. However, it was vaguely understood that column strength is somehow related to the column length. In order to illustrate the Design Philosophy of Columns in ancient times, the following quotation from a translation of the book "De Architectura" by Vitruvius [24] will be given. This quotation is mentioned also by Hoff[23] but it is always worthwhile to recall. Vitruvius speaks of the Greek Colonists in Asia Minor.

> "There began to erect fanes, and constitute temples to the immortal gods. First they erected the temple of Apollo Panionios, in manner they had seen it in Achaia; which manner they call Doric, because they had seen it first in the Dorian cities. In this temple they were desirous of using columns; but being ignorant of their symmetry, and of the proportions necessary to enable them to sustain the weight, and give them a handsome appearance, they measured the human foot of a man to be the sixth part of the height, they gave that proportion to their columns, making the thickness of the shaft at the base equal to the sixth part of the height, including the capital. Thus the Doric Column, having the proportions, firmness, and beauty of the human body, first began to be used in buildings.
>
> "Afterwards, to construct the temple of Diana, they sought a new order from the same traces, copying the gracefulness of women, and making the thickness of the columns an eighth part of the height,

in order to give them a taller appearance. Thus arose the invention of these two different orders: one of the masculine appearance, naked and unadorned; the other imitating the slenderness and fine proportions of women. But posterity, improving in ingenuity and judgement, and delighting in more graceful proportions, fixed the height of Doric Columns at seven times their diameter; and of the Ionic, at eight and a half. This latter order was called Ionic because it was first used by Ion.

"The third which is called Corinthian, is in imitation of the delicacy of virgins; for in that tender age, the limbs are formed more slender and are more graceful in attire."

No progress can be recorded in column design until 1759. Leonhard Euler was the first to derive the Euler column formula and proved theoretically that there is another criterion for column strength which is independent of crushing or yielding of material. This is called the stability limit load of a column. The corresponding mode of failure is known as buckling phenomenon. For a simply supported column subjected to an axial compression P at the ends as shown in Figure (1.4), the stability limit load or Euler's elastic buckling load is given by

$$P_E = \frac{\pi^2 EI}{L^2} \qquad (1.4)$$

in which L is the column length and I is the moment of inertia of the column cross-section. The Euler formula is applicable to all elastic columns provided that the right hand side of equation (1.4) is multiplied by an appropriate coefficient, corresponding to different boundary conditions.

In this early development, column behaviour was analysed by using linear theory based on linear elastic material properties and a small deflection approximation of the column. In 1770, Euler and Lagrange presented

the non-linear large deflection theory which solved the elastica problem, i.e., the post-buckling deformation of elastic columns[25]. At the time, the Euler formula was mistakenly assumed to be applicable to short as well as slender columns. For a short column, however, the behaviour and strength are determined almost entirely by the strength properties of the material, plastification or yielding in the case of steel. This is in contrast to a long column where the behaviour is determined almost entirely by the elastic flexural stiffness, EI.

When the column is of intermediate length, yielding of the material will precede but interact with the elastic stability limit. Thus plastic stability analysis governs this situation. On plastic stability theory, Engesser first presented his original tangent-modulus theory in 1889, which replaced the elastic modulus E in the Euler formula by the tangent modulus E_t of the material. Later he proposed a theoretically more reasonable theory, the reduced-modulus theory, for the plastic stability of columns in which an "effective" modulus which lies between E and E_t was adopted. The latter theory had been accepted until Shanley[26], in 1947, showed that the tangent-modulus theory is the more realistic one.

In the plastic range, the behaviour of columns in this intermediate length range is affected significantly by factors which hasten the onset of yielding such as residual stresses and accidental crookedness in the column. Elastic beam-columns were solved by Timoshenko[4] in 1936 and many others for various end conditions. Plastic studies were started by von Karman (1908, 1910) and Chwalla (1928)[27]. Since then, many methods have been reported most of which have been numerical approaches. Early developments of columns and beam-columns have been reviewed by Bleich (1952)[28] and Timoshenko (1953)[25].

In 1969, Battelle's Columbus Laboratories initiated a large research program to investigate the buckling behaviour of offshore pipelines[29].

This research showed that a new phenomenon of buckling existed and the name given to this was "propagating buckle". When a local transverse buckle occurs in a long cylinder, for example a pipeline, subjected to external pressure and bending, the action of the external pressure alone can be sufficient to transform the transverse buckle into a longitudinal one. This buckle, once formed, then "propagates" along the pipeline with some finite velocity. The propagating buckle is one of the new problems that has appeared as a result of the increased interest in offshore natural resources. Studies of this phenomenon have led to design criteria for buckle arrestors for offshore pipelines[30].

1.5 Experiments on Long Circular Columns

A lot of experimental work has been carried out on buckling of long columns in both the elastic and plastic ranges. A review of early experimental work has already been given in the Section on short cylinders.

In 1973 Bouwkamp and Stephen[31] carried out full-scale tests on a number of 48 in. diameter welded steel pipes in order to examine their buckling characteristics. The pipes were subjected to a loading system consisting of a constant axial force and internal pressure, together with a momotonically increasing bending moment. After this work Bouwkamp[32], in order to assess the buckling and post-buckling strength of circular tubular columns, as used in typical offshore structures, studied a number of model pipes. The R/T and L/r values of the pipe columns were similar to those of tubular brace members of an actual tower structure. The pipes were 12 3/4 in. O.D. and 8 5/8 in. O.D., with wall thicknesses of 0.250 in. and 0.219 in. respectively. Results of axial load tests agreed reasonably well with predicted load values.

In the first half of the last decade, Mesloh, Johns and Sorenson[29], pioneers of the "propagating buckle", conducted experiments on long circular pipes. Their aim was to determine the effect of interaction of bending

moment or strain and external pressure on the buckling locus for, a number of circular pipes having a range of R/T's between 10 and 50. Their work also resulted in an empirical expression for the propagation pressure as a function of the pipe material and dimensions.

In 1977 Chen[33] presented a paper on the experimental investigation of fabricated tubular columns under concentric axial load. The research programme was carried out at Lehigh University and Purdue University. Included in the investigation was the measurement of residual stresses in a typical fabricated cylindrical column, the testing of three stub-columns, and the testing of 10 full-scale pin-ended columns under axial load with slenderness ratios ranging from 39 to 83 and diameter to wall thickness ratios of 48 and 70.

The most recent experimental work on columns is that by Smith et al[34]. They tested a series of 16 circular tubes representing offshore steel bracing members at about 1:4 scale under axial compression. The aim of this work was to check the accuracy of a large-deflection elasto-plastic beam-column analysis in representing the collapse and post-collapse behaviour of tubular members, including the performance of damaged members. The work aimed to provide empirical information about the influence of local instability and damage, in the form of dents, on collapse and post-collapse behaviour. The diameter to thickenss ratios varied from 61.5 to 100.0 and thicknesses from 1.05mm to 2.11mm. The length was kept constant to 2150mm.

1.6 Interactive Buckling of Circular Cylindrical Shells

The buckling strength of circular cylindrical shells has been the subject of several studies. However, these investigations have generally been focussed on either the local instability of cylinders with large R/T ratios or on the ultimate strength of cylinders with small R/T ratios.

The development of local buckling depends on the type of loading and the dimensions of the cylindrical shell. Usually, circular cylinders

are classified as short, moderately long and long cylinders. While long cylinders will exhibit the typical column-type buckling, short and moderately long columns will buckle with more of a local mode depending on the radius to thickness ratio, R/T, and the length-to-thickness ratio L/T. It seems that for tubular members with R/T ratios of 10 to 30, as commonly used in offshore structures, the local buckling strength is considerably larger than the column buckling strength. Only in case of considerably larger R/T ratios may local instability become a dominant factor. This is the area where interaction between overall and local buckling occurs.

No theoretical approach has apparently been developed to analyse this problem, and any experience on this topic is based on experimental results.

Some recent experiments on tubular members tested by Smith et al[34] showed a tendency to fail in a rather local mode. The R/T ratios of those tubes were 30.1 and 43.65 with corresponding L/r's of 60.9 and 68.4 respectively.

1.7 Aim of Thesis

The object of the work in this thesis is to establish theoretical means to enable the elasto-plastic behaviour of general cylindrical shells under combined load in the pre- and post-buckling regime to be studied. In particular, the interaction between overall and local instability is pursued.

1.8 Scope of Thesis

In Chapter 2, a review of the development of Dynamic Relaxation as a useful numerical technique is discussed. A description and basic formu-

lation of the numerical method are outlined.

In Chapter 3, the detailed development of a formulation regarding local instability of circular cylindrical shells is outlined. Adaptation of the numerical technique is included and correlations with available theoretical and experimental results are reported.

In Chapter 4, a rigorous interactive formulation between overall and local instability of circular beam-columns is developed. Detailed adaptation of the numerical technique is described, and comparisons with well established theoretical and experimental results are presented.

In Chapter 5, a simplified interactive formulation between overall and local instability of circular beam-columns is outlined. Limitations and applicability of the method are discussed.

In Chapter 6, parametric studies conducted using the analysis developed in the previous chapters are reported. In these studies results on local and overall buckling behaviour of general circular cylindrical shells are presented and comparisons are made with existing Design Rules.

In Chapter 7, conclusions concerning the usefulness and suitability of the numerical technique are recorded. Further, observations derived from the parametric studies and recommendations for future work are presented.

1.9 Layout of Computing Programs

A suite of computing programs was written to perform the analyses based on the theoretical approaches developed in this thesis. The layout of this suite can be seen in Figure (1.5) . ANSA1 refers to local buckling, while ANSA2 and ANSA3 refer to interaction between overall and local buckling. ANSA1IL, ANSA1IV and ANSA1ML differ on the plasticity formulation as follows: ANSA1IL used Ilyushin's yield criterion, ANSA1IV Ivanov's modified

yield criterion and ANSAlML used the multi-layer approach.

These main programs are related according to the Venn diagram shown in Figure (1.6).

The above programs were developed on the ICL 2976 main frame computer of the University of Glasgow.

CHAPTER 2

OUTLINE OF NUMERICAL TECHNIQUE

2.1 Introduction

Dynamic relaxation (DR) when used in conjunction with centre finite differences is a numerical technique that has proved to be a very useful tool in the ultimate load analysis of plated structures. It is a step-by-step integration procedure with respect to time and is based on the fact that when a structure is subjected to a loading, it finally reaches the static equilibrium position under the action of the applied load.

Out-of-balance forces are derived locally by discretising the structure's equilibrium equations at each node. Each out-of-balance force is equated with an equation of motion governing structural dynamic response by introducing point masses and viscous damping forces at the nodes. The equation of motion is discretised by using central finite differences with respect to time and by rearranging the terms of the equation of motion an expression for current velocities can be obtained. Then, by integrating the velocitites with respect to time the current displacements are calculated. Kinematic and constitutive relationships supply the remainder of the equations necessary to undertake an analysis. By retaining these in a form separate from the equilibrium equations, both displacement and stress boundary conditons can be handled readily.

Each time-step involves the following cycle of calculations:

a) calculate stresses using current strain vectors;

b) apply stress boundary conditions;

c) derive new velocities from current lack of equilibrium;

d) calculate new displacements by integrating current velocities;

e) apply displacement boundary conditions;

f) calculate strain vectors from new displacements;

A DR solution can start from a condition of zero displacements or stresses everywhere when the loads are suddenly applied or, as is clearly more efficient, from the previous static result. A static solution represents convergence and is optimally achieved by suitable choices of the mass density-time increment and viscous damping coefficients.

The damping coefficient which causes the structure to approach the static position most rapidly is known as the critical damping factor. In practice for almost any damping factor the static position will be reached, so that although equilibrium will be the most rapidly reached with the critical damping factor, any factor may in fact be used. For example, for curve *b* (Fig. 2.1) a damping factor less than the critical damping factor was used in the calculation, and in curve *c* a greater damping factor. It is seen that both these curves converge to the static position. Curve *a* shows an undamped solution which was obtained with a damping factor equal to zero.

2.2 Historical development

The name "Dynamic Relaxation" appears to have been introduced by Otter[35-37] or Day[38] in the mid-1960's. These papers[35-38] reflect the beginning of the engineers interest in DR and introduce the idea of obtaining a static solution from a dynamic transient analysis method.

Numerical stability was controlled by restricting the time increment on an ad hoc basis while no guidance was given on the choice of damping factor. Rushton[39] also studied plates in the small deflection range and discussed damping in some detail. Automatic empirical procedures for

determining the critical damping factor were also outlined.

Rushton later extended his formulation to include large deflection behaviour[40,41] based on the von Karman equations. Initial out-of-plane distortions were first considered by Williams[42] in a similar large deflection analysis. Material non-linearity was introduced by Lowe in a small deflection solution for reinforced concrete slabs[43]. He was also the first to apply to the analysis of plates the idea of fictitious densitites, a concept formulated only a short time previously by Cassell[44] for the automatic calculation of the mass density-time increment coefficient governing convergence. This particular development marked a significant step forward in the evolution of DR.

Large deflections and plasticity were first combined by Frieze in a single-layer formulation for the buckling analysis of plates[45]. In a similar procedure, Harding adopted a multi-layer approach using the Mises-Hencky criterion to monitor yield on each of the layers[46].

The most recent contribution to the development of DR is the work by Papadrakakis[47] who advocates that the use of kinetic damping instead of viscous damping simplifies the method, since only a bound for the maximum eigenvalue is required.

2.3 Basic DR formulation

Non-graded interlacing meshes have been adopted for the discretisation of elements in most of the recent DR with finite difference formulations.

At each node generated by this discretisation, the equations of motion are equated with the out-of-balance forces (or lack of equilibrium) in the following form:

$$\rho\ddot{x} + c\dot{x} = [\text{lack of equilibrium}] \qquad (2.1)$$

where ρ is the mass-density, c the viscous coefficient and ($\dot{}$) indicates differentiation with respect to time. Considering an increment of time Δt, $\ddot{x}$ and $\dot{x}$ can be replaced by finite difference expressions involving the velocities at times $t + \Delta t/2$ and $t - \Delta t/2$, $\dot{x}_c$ and $\dot{x}_p$ repectively. If c is replaced in non-dimensional form by $k\rho/\Delta t$, (2.1) can be rearranged as

$$\dot{x}_c = \frac{1 - \frac{k}{2}}{1 + \frac{k}{2}} \dot{x}_p + \frac{\Delta t}{\rho(1 + \frac{k}{2})} \quad [\text{ lack of equilibrium }] \tag{2.2}$$

The displacement at time $t + \Delta t$ is then found from

$$x_c = x_p + \dot{x}_c \Delta t \tag{2.3}$$

where x_p is the displacement at time t. As in all iterative procedures, the convergence of (2.2) is determined by the choices of k, Δt and ρ. In order to achieve a static solution the damping factor k must evidently be non-zero and the time increment Δt must not exceed the critical value beyond which numerical instability occurs. To damp out the oscillations in the shortest possible time the system should be critically damped with respect to the fundamental mode although other mode shapes are usually represented in the oscillations. However, since the critical value of the damping factor is not usually known exactly, and since underdamping retards convergence much more than similar degree of over-damping[48], it is preferable to choose for k a value somewhat less than the estimated k_{cr}.

Rushton initially used stability criteria based on established iterative techniques to determine Δt in his large deflection analyses while k was found from the system's dynamic behaviour[49]. It was found, however, that Δt had to be reduced on an ad hoc basis to prevent divergence of the solution. He also found that Δt could be reduced even to unity since the dynamic behaviour of the plate as such was of no particular interest.

Otter et al[36] showed that DR is analogous to the second order Richardson process (also known as Frankel's method). Pursuing this analogy further Cassell[44] has obtained the following expressions for optimum convergence.

$$k_{cr} = 4\sqrt{\frac{\alpha\beta}{\alpha+\beta}} \qquad (2.4) \qquad \text{and} \quad \frac{\Delta t_{cr}^2}{\rho} = \frac{4}{\alpha+\beta} \qquad (2.5)$$

where α and β are respectively the magnitudes of the minimum and maximum eigenvalues of the stiffness matrix of the structure. Frequently $\alpha << \beta$ and the mass density time increment coefficient, (2.5), becomes

$$\frac{\Delta t^2}{\rho} = \frac{4}{\beta} \qquad (2.6)$$

Gershgorin's theorem is used to provide an upper bound estimate for β. It was then found that this analogy could be extended to each row of the stiffness matrix to provide near-optimum control of convergence on a node-by-node basis[49]. Nevertheless, since the dynamic response per se was of no particular interest, Δt was assumed equal to unity, thereby reducing (2.6) to a simpler form.

$$\rho = \frac{1}{4}\beta$$

or

$$\rho = \frac{1}{4}\Sigma|k_{ij}| \qquad (2.7)$$

where k_{ij} are the elements of the stiffness matrix of the structure.

CHAPTER 3

CYLINDRICAL SHELL ANALYSIS

3.1 Introduction

This chapter develops the essential components of the cylindrical shell analysis, reports on mesh convergence studies and presents comparisons between solutions generated by the analysis as programmed and other numerical and experimental results.

The necessary components of the analysis are the following:

a) kinematic relationships,

b) equilibrium equations,

c) boundary conditions,

d) yield function and flow rule, and

e) constitutive relationships.

The kinematic relationships are developed in three stages. The first relates to out-of-plane distortions and is presented in detail in this chapter. The second and third consider in-plane and rigid-body rotations and are described in Appendix (I). The stage one derivation forms the basis of the programmed analysis.

3.2 Strain-Displacement Relationships

3.2.1 *Definition of Engineering Strains*

The strain in a plane can easily be described by using three independent non-dimensional quantities which can be defined in various ways. Assuming the strains are finite, they can be mathematically defined as the strains referred to the sides of a triangle with lengths $\delta x, \delta y, \delta s$ and $(\delta\hat{x}\delta y)=\theta$. Before deformation the sides of a triangle are of lengths δx_i, δy_i, δs_i and $(\delta\hat{x}_i\delta y_i) = \theta_i$.

Let ε_x be the strain referred to the side δx and ε_y be the strain referred to the side δy, and ε_{xy} be the change of the angle θ_i after deformation. The commonly used 'engineering' strains are defined as

$$(\varepsilon_x)_{eng} = \frac{\delta x - \delta x_i}{\delta x_i} \tag{3.1}$$

$$(\varepsilon_y)_{eng} = \frac{\delta y - \delta y_i}{\delta y_i} \tag{3.2}$$

and the shear strain as

$$(\varepsilon_{xy})_{eng} = \sin^{-1}\left(\frac{\delta x^2 + \delta y^2 - \delta s^2}{2\delta x \delta y}\right)$$

This definition considers $(\delta\hat{x}_i \delta y_i) = 90^o$, but due to initial imperfections this angle will be different from 90^o and thus a general formula for 'engineering' shear strain has to be developed.

This can be done as follows:

$$\varepsilon_{xy} = \theta_i - \theta$$

Therefore

$$\sin\varepsilon_{xy} = \sin(\theta_i - \theta)$$

$$= \sin\theta_i \cos\theta - \sin\theta\cos\theta_i$$

$$\sin\theta_i \approx \sin\theta \approx 1$$

$$\cos\theta_i = \frac{\delta x_i^2 + \delta y_i^2 - \delta s_i^2}{2\delta x_i \delta y_i} \qquad \text{(cosine-rule)}$$

$$\cos\theta = \frac{\delta x^2 + \delta y^2 - \delta s^2}{2\delta x \delta y}$$

Therefore

$$\sin\varepsilon_{xy} = \cos\theta - \cos\theta_i$$

or $\varepsilon_{xy} = \sin^{-1} (\cos\theta - \cos\theta_i)$

Therefore

$$\varepsilon_{xy} = \sin^{-1} \left(\frac{\delta x^2 + \delta y^2 - \delta s^2}{2\delta x \delta y} - \frac{\delta x_i^2 + \delta y_i^2 - \delta s_i^2}{2\delta x_i \delta y_i} \right) \qquad (3.3)$$

3.2.2 *Alternative Definition of Strains*

It must be clearly understood that $\varepsilon_j (j = x,y)$ is not strain in the j-direction but strain along δj which lies close to, but not necessarily along the j-axis.

Because δx, δy are determined by Pythagoras' theorem, their calculation includes square roots which makes manipulations of these expressions difficult. Consequently definitions of strain were proposed[50] which obviated the need to find these square roots. Such a derivation is presented below.

From equation (3.1)

$$\varepsilon_x = \frac{\delta x}{\delta x_i} - 1 \quad \text{or} \quad 1 + \varepsilon_x = \frac{\delta x}{\delta x_i}$$

or $$(1+\varepsilon_x)^2 = \frac{\delta x^2}{\delta x_i^2} \quad \text{or} \quad 1 + 2\varepsilon_x + \varepsilon_x^2 = \frac{\delta x^2}{\delta x_i^2} \qquad (3.4)$$

Assuming $\varepsilon_x^2 \ll 1$, equation (3.4) becomes

$$1 + 2\varepsilon_x = \frac{\delta x^2}{\delta x_i^2} \quad \text{or} \quad \varepsilon_x = \frac{\delta x^2 - \delta x_i^2}{2\delta x_i^2} \qquad (3.5)$$

Similarly,

$$\varepsilon_y = \frac{\delta y^2 - \delta y_i^2}{2\delta y_i^2} \qquad (3.6)$$

ε_x and ε_y are called 'normal' strains.

To derive the shear strain expression, consider the area of the triangle to be the same before (A_i) and after (A) straining.

Then $A = A_i$,

or $\frac{1}{2}\,\delta x_i \delta y_i \sin\theta_i = \frac{1}{2}\,\delta x \delta y \sin\theta$

but $\sin\theta_i \simeq \sin\theta \simeq 1$

Therefore

$$\delta x_i \delta y_i = \delta x \delta y \tag{3.7}$$

Recalling equation (3.3), ε_{xy} becomes

$$\varepsilon_{xy} = \sin^{-1}\left(\frac{\delta x^2 + \delta y^2 - \delta s^2}{2\delta x_i \delta y_i} - \frac{\delta x_i^2 + \delta y_i^2 - \delta s_i^2}{2\delta x_i \delta y_i}\right) \tag{3.8}$$

Assuming that $-\frac{\pi}{2} < \varepsilon_{xy} < \frac{\pi}{2}$ and ε_{xy} very small

$$\varepsilon_{xy} = \frac{\delta x^2 + \delta y^2 - \delta s^2}{2\delta x_i \delta y_i} - \frac{\delta x_i^2 + \delta y_i^2 - \delta s_i^2}{2\delta x_i \delta y_i} \tag{3.9}$$

This can be used as the general expression for shear strain. However, it can be simplified in the case of no initial shear distortion since

$$\theta_i = 90^\circ \quad \text{so that} \quad \delta s_i^2 = \delta x_i^2 + \delta y_i^2$$

and $$\varepsilon_{xy} = \frac{\delta x^2 + \delta y^2 - \delta s^2}{2\delta x_i \delta y_i} \tag{3.10}$$

Thus, both the 'engineering' and the 'normal' shear strains reduce to the same expression if appropriate simplifications are made.

3.2.3 *Derivation to Account for Initial Out-of-Plane Distortions*

In the analysis which follows, terms up to the second degree are included and small angle theory is appplied throughout. Also, Pythagoras' theorem and binomial series are used extensively throughout the derivation.

The points O, P, and Q are the vertices of a small triangular element before deformation lying at the middle surface of a cylindrical shell with angle POQ = 90°, as it is shown in the figure below. The displacement components of the point O are u, v, and w where u is measured along the length of the cylinder, v, tangentially to the Y-axis, and w normal to the original middle surface.

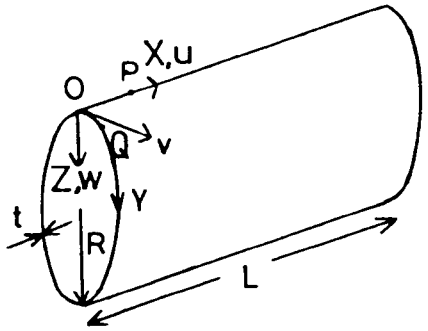

The figures below show the positions of O, P, and Q before straining with out-of-plane displacements and O', P', and Q' represent the displaced positions of O, P, and Q after straining.

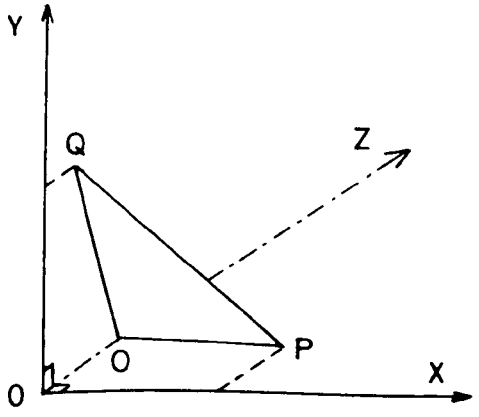

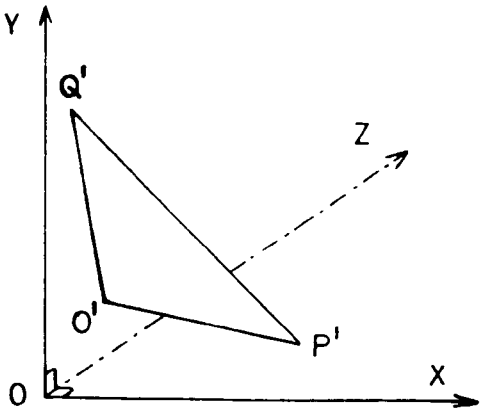

Co-ordinates of points O, P, and Q and O', P', and Q' are as follows:

	x	y	z
O	O.	O	w_O
P	δx	O	$w_O + \frac{\partial w_O}{\partial x}\ \delta x$
Q	O	$\delta y - \frac{w_O}{R}\ \delta y$ *	$w_O + \frac{\partial w_O}{\partial y}\ \delta y$
O'	u	v	$w + w_O$
P'	$u + \delta x + \frac{\partial u}{\partial x}\ \delta x$	$v + \frac{\partial v}{\partial x}\ \delta x$	$w + w_O + \left(\frac{\partial w}{\partial x} + \frac{\partial w_O}{\partial x}\right)\ \delta x$
Q'	$u + \frac{\partial u}{\partial y}\ \delta y$	$v + \delta y + \left(\frac{\partial v}{\partial y} - \frac{w+w_O}{R}\right)\delta y$	$w + w_O + \left(\frac{\partial w}{\partial y} + \frac{\partial w_O}{\partial y} + \frac{v}{R}\right)\ \delta y$

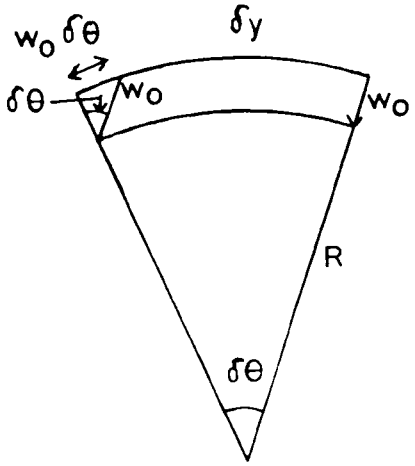

* $\delta y - w_O\delta\theta = \delta y - w_O \frac{\delta y}{R}$

The component $\frac{v}{R}\ \delta y$ in the z co-ordinate of Q' is due to the fact that the v displacement is tangential to the Y-curved axis. Thus there would be a component on the Z-axis of $v\delta\theta = \frac{v}{R}\ \delta y$.

For convenience let

$$u_x = \frac{\partial u}{\partial x}\ ,\quad v_x = \frac{\partial v}{\partial x}\ ,\quad w_x = \frac{\partial w}{\partial x}\ ,\quad w_{O_x} = \frac{\partial w_O}{\partial x}$$

$$u_y = \frac{\partial u}{\partial y}\ ,\quad v_y = \frac{\partial v}{\partial y}\ ,\quad w_y = \frac{\partial w}{\partial y}\ ,\quad w_{o_y} = \frac{\partial w_o}{\partial y}$$

Now, from equation (3.5)

$$\varepsilon_x = \frac{(O'P')^2 - (OP)^2}{2(OP)^2}$$

where

$$(OP)^2 = \delta x^2 + \left(\frac{\partial w_o}{\partial x}\right)^2 \delta x^2 = \left[1 + \left(\frac{\partial w_o}{\partial x}\right)^2\right] \delta x^2 = (1 + w_{o_x}^2)\,\delta x^2$$

and

$$(O'P')^2 = \left(\delta x + \frac{\partial u}{\partial x}\,\delta x\right)^2 + \left(\frac{\partial v}{\partial x}\right)^2 \delta x^2 + \left(\frac{\partial w}{\partial x} + \frac{\partial w_o}{\partial x}\right)^2 \delta x^2$$

$$= (1 + u_x)^2\,\delta x^2 + v_x^2\ \delta x^2 + (w_x + w_{o_x})^2\,\delta x^2$$

Therefore

$$\varepsilon_x = \frac{(1 + u_x)^2 + v_x^2 + (w_x + w_{o_x})^2 - (1 + w_{o_x}^2)}{2(1 + w_{o_x}^2)}$$

$$= \tfrac{1}{2}\left[\,1 + u_x^2 + 2u_x + v_x^2 + w_x^2 + w_{o_x}^2 + 2w_x w_{o_x} - 1 - w_{o_x}^2\,\right]\left[\,1 + w_{o_x}^2\,\right]^{-1}$$

$$= \tfrac{1}{2}\,(2u_x + u_x^2 + v_x^2 + w_x^2 + 2w_x w_{o_x})\,(1 - w_{o_x}^2)$$

$$= u_x + \tfrac{1}{2}(u_x^2 + v_x^2 + w_x^2 + 2w_x w_{o_x}) \qquad (3.11)$$

Rearranging equation (3.4) without neglecting ε_x^2 term

$$\varepsilon_x = \frac{\delta x^2 - \delta x_i^2}{2\delta x_i^2} - \frac{\varepsilon_x^2}{2}$$

The first term of the R.H.S. of equation (3.11) when substituted into the $-\tfrac{1}{2}\,\varepsilon_x^2$ term leads to $-\tfrac{1}{2}\,u_x^2$, so that

$$\varepsilon_x = u_x + \tfrac{1}{2}\,(v_x^2 + w_x^2 + 2w_x w_{o_x}) \qquad (3.12)$$

From equation (3.6)

$$\varepsilon_y = \frac{(O'Q')^2 - (OQ)^2}{2(OQ)^2}$$

where

$$(OQ)^2 = \left(\delta y - \frac{w_o}{R}\,\delta y\right)^2 + \left(\frac{\partial w_o}{\partial y}\right)^2 \delta y^2 = \left(1 - \frac{w_o}{R}\right)^2 \delta y^2 + w_{o_y}^2\, \delta y^2$$

$$(O'Q')^2 = \left(\frac{\partial u}{\partial y}\right)^2 \delta y^2 + \left[\delta y + \left(\frac{\partial v}{\partial y} - \frac{w+w_o}{R}\right)\delta y\right]^2 + \left(\frac{\partial w}{\partial y} + \frac{\partial w_o}{\partial y} + \frac{v}{R}\right)^2 \delta y^2$$

$$= u_y^2\, \delta y^2 + \left(1 + v_y - \frac{w+w_o}{R}\right)^2 \delta y^2 + \left(w_y + w_{o_y} + \frac{v}{R}\right)^2 \delta y^2$$

Therefore

$$\varepsilon_y = \frac{u_y^2 + \left(1 + v_y - \frac{w+w_o}{R}\right)^2 + \left(w_y + w_{o_y} + \frac{v}{R}\right)^2 - \left(1 - \frac{w_o}{R}\right)^2 - w_{o_y}^2}{2\left[\left(1 - \frac{w_o}{R}\right)^2 + w_{o_y}^2\right]}$$

$$= \tfrac{1}{2}\left[u_y^2 + \left(1 - \frac{w_o}{R}\right)^2 + \left(v_y - \frac{w}{R}\right)^2 + 2\left(1 - \frac{w_o}{R}\right)\left(v_y - \frac{w}{R}\right)\right.$$

$$\left. + \left(w_y + \frac{v}{R}\right)^2 + w_{o_y}^2 + 2\left(w_y + \frac{v}{R}\right) w_{o_y} - \left(1 - \frac{w_o}{R}\right)^2 - w_{o_y}^2\right]$$

$$\left[1 - 2\,\frac{w_o}{R} + \left(\frac{w_o}{R}\right)^2 + w_{o_y}^2\right]^{-1}$$

$$= \tfrac{1}{2}\left[u_y^2 + v_y^2 + \left(\frac{w}{R}\right)^2 - 2\,\frac{w}{R}\,v_y + 2v_y - 2\,\frac{w}{R} - 2\,\frac{w_o}{R}\,v_y\right.$$

$$\left. + 2\,\frac{w}{R}\,\frac{w_o}{R} + w_y^2 + \left(\frac{v}{R}\right)^2 + 2\,\frac{v}{R}\,w_y + 2w_y w_{o_y} + 2\,\frac{v}{R}\,w_{o_y}\right]\left[1 + 2\,\frac{w_o}{R}\right]$$

$$= v_y - \frac{w}{R} + \tfrac{1}{2}\left[u_y^2 + v_y^2 + w_y^2 + \left(\frac{w}{R}\right)^2 + \left(\frac{v}{R}\right)^2 - 2\,\frac{w}{R}\,v_y\right.$$

$$\left. + 2\,\frac{v}{R}\,w_y + 2\,\frac{v}{R}\,w_{o_y} + 2w_y w_{o_y} + 2\,\frac{w_o}{R}\,v_y - 2\,\frac{w}{R}\,\frac{w_o}{R}\right]$$

Now, by repeating the exercise undertaken with respect to ε_x, the terms v_y^2, $\left(\frac{w}{R}\right)^2$ and $-2\,\frac{w}{R}\,v_y$ drop out to give,

$$\varepsilon_y = v_y - \frac{w}{R} + \tfrac{1}{2}\left[u_y^2 + w_y^2 + \left(\frac{v}{R}\right)^2 + 2\,\frac{v}{R}\,w_y + 2\,\frac{v}{R}\,w_{o_y}\right.$$

$$\left. + 2w_y w_{o_y} + 2\,\frac{w_o}{R}\,v_y - 2\,\frac{w}{R}\,\frac{w_o}{R}\right] \qquad (3.13)$$

From equation (3.9)

$$\varepsilon_{xy} = \frac{(O'P')^2 + (O'Q')^2 - (P'Q')^2}{2(OP)(OQ)} - \frac{(OP)^2 + (OQ)^2 - (PQ)^2}{2(OP)(OQ)}$$

where

$$(PQ)^2 = \delta x^2 + \left(1 - \frac{w_o}{R}\right)^2 \delta y^2 + \left(\frac{\partial w_o}{\partial x} - \frac{\partial w_o}{\partial y}\right)^2 \delta y^2$$

$$= (OP)^2 + (OQ)^2 - 2\,\frac{\partial w_o}{\partial x}\,\frac{\partial w_o}{\partial y}\,\delta y^2$$

Therefore

$$(OP)^2 + (OQ)^2 - (PQ)^2 = 2w_{o_x} w_{o_y}\,\delta y^2$$

$$(P'Q')^2 = \left(\delta x + \frac{\partial u}{\partial x}\,\delta x - \frac{\partial u}{\partial y}\,\delta y\right)^2 + \left[\delta y + \left(\frac{\partial v}{\partial y} - \frac{w+w_o}{R}\right)\delta y - \frac{\partial v}{\partial x}\,\delta x\right]^2$$

$$+ \left[\left(\frac{\partial w}{\partial y} + \frac{\partial w_o}{\partial y} + \frac{v}{R}\right)\delta y - \left(\frac{\partial w}{\partial x} + \frac{\partial w_o}{\partial x}\right)\delta x\right]^2$$

$$= (\delta x + u_x \delta x - u_y \delta y)^2 + \left[\delta y + \left(v_y - \frac{w+w_o}{R}\right)\delta y - v_x \delta x\right]^2$$

$$+ \left[\left(w_y + w_{o_y} + \frac{v}{R}\right)\delta y - (w_x + w_{o_x})\,\delta x\right]^2$$

$$= (1 + u_x)^2\,\delta x^2 + u_y^2\,\delta y^2 - 2(1 + u_x)\,u_y\,\delta x\delta y$$

$$+ \left(1 + v_y - \frac{w+w_o}{R}\right)^2 \delta y^2 + v_x^2\,\delta x^2 - 2\left(1 + v_y - \frac{w+w_o}{R}\right) v_x\,\delta x\delta y$$

$$+ \left(w_y + w_{o_y} + \frac{v}{R}\right)^2 \delta y^2 + (w_x + w_{o_x})^2\,\delta x^2 - 2\left(w_y + w_{o_y} + \frac{v}{R}\right)(w_x + w_{o_x})\,\delta x\delta y$$

$$= (O'P')^2 + (O'Q')^2 - 2(1 + u_x)\, u_y \delta x \delta y$$

$$- 2\left(1 + v_y - \frac{w+w_o}{R}\right) v_x \delta x \delta y \quad - 2\left(w_y + w_{o_y} + \frac{v}{R}\right)(w_x + w_{o_x})\ \delta x \delta y$$

$$(OP)^2 (OQ)^2 = (1 + w_{o_x}^2) \left[\left(1 - \frac{w_o}{R}\right)^2 + w_{o_y}^2\right] \delta x^2 \delta y^2$$

$$= (1 + w_{o_x}^2) \left[1 + \left(\frac{w_o}{R}\right)^2 - 2\,\frac{w_o}{R} + w_{o_y}^2\right] \delta x^2 \delta y^2$$

$$= \left[1 - \frac{2w_o}{R} + \left(\frac{w_o}{R}\right)^2 + w_{o_y}^2 + w_{o_x}^2\right] \delta x^2 \delta y^2$$

Therefore

$$(OP)(OQ) = \left[1 - 2\,\frac{w_o}{R} + \left(\frac{w_o}{R}\right)^2 + w_{o_y}^2 + w_{o_x}^2\right]^{\frac{1}{2}} \delta x \delta y$$

Therefore

$$\varepsilon_{xy} = \left(u_y + u_x u_y + v_x + v_y v_x - v_x \frac{w}{R} - v_x \frac{w_o}{R} + w_x w_y\right.$$

$$\left. + w_y w_{o_x} + w_{o_y} w_x + w_{o_y} w_{o_x} + \frac{v}{R} w_x + \frac{v}{R} w_{o_x} - w_{o_x} w_{o_y}\right) \left(1 + \frac{w_o}{R}\right)$$

or

$$\varepsilon_{xy} = v_x + u_y + u_x u_y + v_x v_y - v_x \frac{w}{R} + w_x w_y + w_y w_{o_x}$$

$$+ w_{o_y} w_x + \frac{v}{R} w_x + \frac{v}{R} w_{o_x} + \frac{w_o}{R} u_y \qquad (3.14)$$

Comparing relationships (3.12), (3.13) ignoring w_o, with the respective relationships of Reference (51) page 335, it is apparent that the author did not undertake the routine check of assessing the value of ε_x^2 which was initially discarded in arriving at equations (3.5) and (3.6).

Also, it is easily shown that

$$\left[(O'P')(O'Q')\right]^{-\frac{1}{2}} = 1 - u_x\, v_y + \frac{w}{R} + \frac{w_o}{R}$$

Using equation (3.8), therefore

$$(\varepsilon_{xy})_{eng} = \varepsilon_{xy} + \left(u_y + u_x u_y + v_x + v_y v_x - v_x \frac{w}{R} - v_x \frac{w}{R} - v_x \frac{w_o}{R}\right.$$

$$\left. + w_x w_y + w_y w_{o_x} + w_{o_y} w_x + w_{o_y} w_{o_x} + \frac{v}{R} w_x + \frac{v}{R} w_{o_x}\right)\left(1 - u_x - v_y + \frac{w}{R}\right)$$

$$= v_x + u_y + u_x u_y + v_x v_y - v_x \frac{w}{R} + w_x w_y + w_y w_{o_x} + w_{o_y} w_x$$

$$+ w_{o_y} w_{o_x} + \frac{v}{R} w_x + \frac{v}{R} w_{o_x} + \frac{w_o}{R} u_y - u_x u_y - u_x v_x$$

$$- v_y u_y - v_y v_x + u_y \frac{w}{R} + v_x \frac{w}{R}$$

or

$$(\varepsilon_{xy})_{eng} = v_x + u_y + w_x w_y + w_y w_{o_x} + w_{o_y} w_x + \frac{v}{R} w_x + \frac{v}{R} w_{o_x}$$

$$+ \frac{w_o}{R} u_y - u_x v_x - v_y u_y + u_y \frac{w}{R}$$

Even though the denominator of $(\varepsilon_{xy})_{eng}$ is more complicated than the denominator of the previous expression, in the end the number of terms remains the same.

3.3 Derivation of Curvature Expressions

The next figure shows an element OABC, after deformation, of a continuous curved surface such as the middle surface of a cylindrical shell having axes X, Y, Z with origin O. In order to establish formulae for the three curvature changes k_x, k_y and k_{xy} very small displacements u, v, and w are considered and the rotations produced by each of these displacements are calculated.

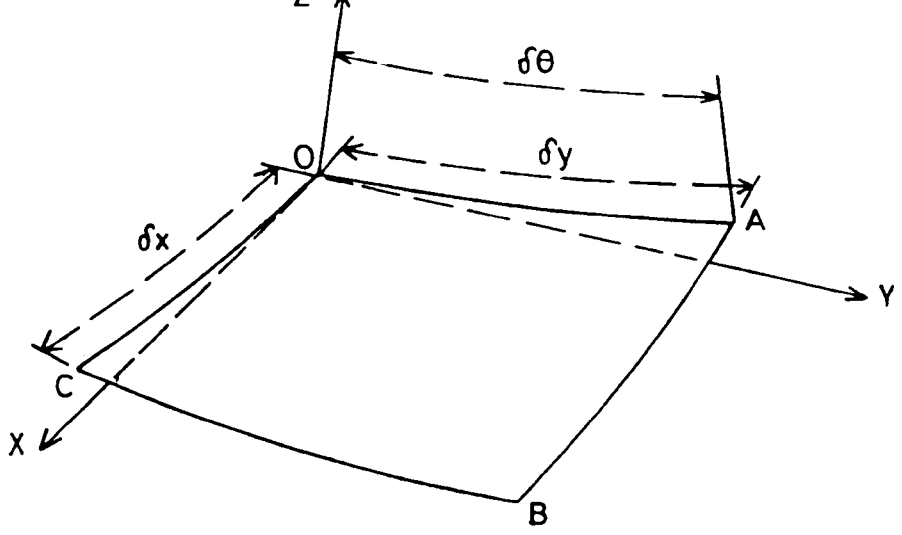

Because of displacement w, the rate of change in the X-direction, $-\frac{\partial}{\partial x}$, of the slope of the surface in the X-direction, $\frac{\partial w}{\partial x}$, is defined as the curvature of the surface in the X-direction.

$$k_x = -\frac{\partial^2 w}{\partial x^2} \tag{3.15a}$$

Due to the curvature of the cylindrical shell, the initial angle between these lateral sides of the element OABC is $\delta\theta$. However, because of the displacements v and w, this angle will change and rotation of the lateral side OC with respect to the X-axis becomes

$$-\frac{v}{R} + \frac{1}{R}\frac{\partial w}{\partial \theta}$$

The corresponding rotation for the lateral side AB is

$$-\frac{v}{R} + \frac{1}{R}\frac{\partial w}{\partial \theta} + \frac{\partial}{\partial \theta}\left(-\frac{v}{R} + \frac{1}{R}\frac{\partial w}{\partial \theta}\right) d\theta$$

Hence, the curvature of the surface in the Y-direction is defined as the rate of change, $-\frac{1}{R}\frac{\partial}{\partial \theta}$, of the slope of the surface in the Y-direction.

$$k_y = -\frac{1}{R}\frac{\partial}{\partial \theta}\left(\frac{1}{R}\frac{\partial w}{\partial \theta} - \frac{v}{R}\right)$$

or

$$k_y = -\frac{1}{R^2}\frac{\partial^2 w}{\partial \theta^2} + \frac{1}{R^2}\frac{\partial v}{\partial \theta} \tag{3.15b}$$

In calculating the twist of the element, it is noted that the generator, during deformation, rotates with respect to the Y-axis through an angle equal to $-\frac{\partial w}{\partial x}$. Considering now a similar element of a generator at a

circumferential distance $R\delta\theta$ from the first one, it is seen that its rotation about the Y-axis, corresponding to displacement w, is

$$-\frac{\partial w}{\partial x} + \frac{\partial}{\partial \theta}\left(\frac{\partial w}{\partial x}\right) d\theta$$

or $$-\frac{\partial w}{\partial x} + \frac{\partial^2 w}{\partial \theta \partial x} d\theta$$

Due to the angle $\delta\theta$ between the two elements, the latter rotation has a component with respect to the Y-axis equal to

$$-\frac{\partial v}{\partial x} d\theta$$

From the above results it is concluded that the twist of the surface is

$$k_{xy} = -\frac{1}{R}\left(\frac{\partial^2 w}{\partial \theta \partial x} - \frac{\partial v}{\partial x}\right) \tag{3.16}$$

3.4 Derivation of Governing Equations

Consider a thin-walled circular shell of length L, wall thickness t, and underformed middle surface radius R, with $t \ll R$, as it is shown in the Figure on page 39. The middle surface of the cylinder is referred to in cylindrical coordinates (x, θ) and distances from the middle surface are measured by a coordinate z, positive inward. Displacement components in the X, Y and Z directions are denoted by u, v, and w, respectively. The cylinder is considered to be subjected to a lateral pressure p, positive inward.

The Love-Kirchoff assumptions, which are essential to the derivation of the shell equations, are mentioned briefly:

(i) Normals to the undeformed middle plane remain straight, normal and inextensional during deformation, so that transverse normal and shearing strains may be neglected in the derivation of the kinematic relations.

(ii) Transverse normal stresses are assumed to be small compared with the other stress components, and may thus be neglected in the stress-strain relations.

Internal forces and moments are expressed in terms of forces and moments per unit length of the shell element as shown in the Figure 3.1.

The force and moment intensities are related to the internal stresses by the equations[52]:

$$
\begin{aligned}
N_x &= \int_{-t/2}^{t/2} \sigma_x \left(1 - \frac{z}{R}\right) dz & N_\theta &= \int_{-t/2}^{t/2} \sigma_\theta \, dz \\
N_{x\theta} &= \int_{-t/2}^{t/2} \sigma_{x\theta} \left(1 - \frac{z}{R}\right) dz & N_{\theta x} &= \int_{-t/2}^{t/2} \sigma_{\theta x} dz \\
Q_x &= \int_{-t/2}^{t/2} \sigma_{xz} \left(1 - \frac{z}{R}\right) dz & Q_\theta &= \int_{-t/2}^{t/2} \sigma_{\theta z} dz \qquad (3.17) \\
M_x &= \int_{-t/2}^{t/2} \sigma_x \left(1 - \frac{z}{R}\right) z dz & M_\theta &= \int_{-t/2}^{t/2} \sigma_\theta z dz \\
M_{x\theta} &= \int_{-t/2}^{t/2} \sigma_{x\theta} \left(1 - \frac{z}{R}\right) z dz & M_{\theta x} &= \int_{-t/2}^{t/2} \sigma_{\theta x} z dz
\end{aligned}
$$

where N_x, N_θ, $N_{x\theta}$ and $N_{\theta x}$ are the in-plane normal and shearing force intensities,

Q_x and Q_θ are the transverse shearing force intensities, and

M_x, M_θ, $M_{x\theta}$ and $M_{\theta x}$ are the bending and twisting moment intensities.

The stresses σ_x, σ_θ etc., denote stress components at any point through the shell wall thickness. The forces and moments defined by equations (3.17) are in equilbirium with the external forces acting on the entire shell

element. The non-linear equilibrium equations may thus be derived by summation of forces and moments for a cylindrical shell element in a slightly deformed configuration, as shown in Figure 3.2. The angles of rotation ϕ_x and ϕ_θ are regarded as small and sines and cosines of the angles are replaced by the angles themselves in radians and unity, respectively. Furthermore, quadratic terms representing non-linear interaction between the small transverse shearing forces and the rotations are assumed to be negligibly small.

The following equilibrium equations are derived by summing up the forces in the X, Y and Z directions:

$$\frac{\partial N_x}{\partial x} + \frac{1}{R}\frac{\partial N_{\theta x}}{\partial \theta} = 0 \tag{3.18a}$$

$$\frac{\partial N_{x\theta}}{\partial x} + \frac{1}{R}\frac{\partial N_\theta}{\partial \theta} + Q_\theta = 0 \tag{3.18b}$$

$$\frac{1}{R}\frac{\partial Q_\theta}{\partial \theta} + \frac{\partial Q_x}{\partial x} + \frac{N_\theta}{R} + N_x\frac{\partial \phi_x}{\partial x} + N_{x\theta}\frac{\partial \phi_\theta}{\partial x} + \frac{1}{R}N_{\theta x}\frac{\partial \phi_x}{\partial \theta} + \frac{1}{R}N_\theta\frac{\partial \phi_\theta}{\partial \theta} = -p \tag{3.18c}$$

Summation of moments relative to the X and Y directions gives:

$$Q_\theta = \frac{1}{R}\frac{\partial M_\theta}{\partial \theta} + \frac{\partial M_{x\theta}}{\partial x} \tag{3.19a}$$

$$Q_x = \frac{\partial M_x}{\partial x} + \frac{1}{R}\frac{\partial M_{\theta x}}{\partial \theta} \tag{3.19b}$$

Summation of moments about the Z-axis leads to an identity.

For sufficiently shallow shells the Q_θ term in equation (3.18b) makes a negligible contribution to the equilibrium of forces in the circumferential direction [5, 18] and consequently, is omitted from equation (3.18b). The use of equations (3.19) to eliminate the transverse shear terms in equation (3.18c) leads to the following three equilibrium equations:

$$\frac{\partial N_x}{\partial x} + \frac{1}{R}\frac{\partial N_{\theta x}}{\partial \theta} = 0 \qquad (3.20a)$$

$$\frac{\partial N_{x\theta}}{\partial x} + \frac{1}{R}\frac{\partial N_{\theta}}{\partial \theta} = 0 \qquad (3.20b)$$

$$\frac{\partial^2 M_x}{\partial x^2} + \frac{1}{R}\frac{\partial^2 M_x}{\partial x \partial \theta} + \frac{1}{R}\frac{\partial^2 M_{\theta x}}{\partial x \partial \theta} + \frac{1}{R^2}\frac{\partial^2 M_{\theta}}{\partial \theta^2} + \frac{N_{\theta}}{R} + N_x \frac{\partial \phi_x}{\partial x}$$

$$+ N_{x\theta}\frac{\partial \phi_{\theta}}{\partial x} + \frac{1}{R} N_{\theta x}\frac{\partial \phi_x}{\partial \theta} + \frac{1}{R} N_{\theta}\frac{\partial \phi_{\theta}}{\partial \theta} + p = 0 \qquad (3.20c)$$

It is possible to rewrite equations (3.20) in a simpler form by noting that for sufficiently thin shells, z/R may be neglected relative to unity in equations (3.17), thus $N_{x\theta} = N_{\theta x}$ and $M_{x\theta} = M_{\theta x}$. Substituting

$$\phi_x = \frac{\partial w_t}{\partial x} \qquad \text{and} \qquad \phi_{\theta} = \frac{1}{R}\frac{\partial w_t}{\partial \theta} - \frac{v}{R}$$

where $w_t = w + w_o$, and w_o is the initial distortion, equations (3.20) take their final form,

$$\frac{\partial N_x}{\partial x} + \frac{1}{R}\frac{\partial N_{x\theta}}{\partial \theta} = 0 \qquad (3.21a)$$

$$\frac{\partial N_{x\theta}}{\partial x} + \frac{1}{R}\frac{\partial N_{\theta}}{\partial \theta} = 0 \qquad (3.21b)$$

$$\frac{\partial^2 M_x}{\partial x^2} + \frac{2}{R}\frac{\partial^2 M_x}{\partial x \partial \theta} + \frac{1}{R^2}\frac{\partial^2 M_{\theta}}{\partial \theta^2} + \frac{N_{\theta}}{R} + N_x\left(\frac{\partial^2 w}{\partial x^2} + \frac{\partial^2 w_o}{\partial x^2}\right)$$

$$+ \frac{2}{R} N_{x\theta}\left(\frac{\partial^2 w}{\partial x \partial \theta} + \frac{\partial^2 w_o}{\partial x \partial \theta} - \frac{\partial v}{\partial x}\right) + \frac{N_{\theta}}{R^2}\left(\frac{\partial^2 w}{\partial \theta^2} + \frac{\partial^2 w_o}{\partial \theta^2} - \frac{\partial v}{\partial \theta}\right) + p = 0 \qquad (3.21c)$$

The above set of equilibrium equations (3.21) are those on which the Donnell (1933) equations are based[9].

3.5 Study for an Optimum Yield Criterion

3.5.1 *Ilyushin's Yield Criterion*

In 1948, Ilyushin[53] used the von Mises' yield function to derive a complex yield surface for thin shells. The main assumption used in the derivation of Ilyushin's surface is that the equivalent stress is at yield (as defined by von Mises' yield criterion) throughout the full depth of the section. In cases where bending dominates, this condition is achieved only at an infinite equivalent plastic curvature. For many problems this is not a serious drawback. Ilyushin[53,54] derived the following approximate yield criterion for a thin shell:

$$f = \frac{\bar{N}}{N_o^2} + \frac{s\overline{MN}}{\sqrt{3}M_o N_o} + \frac{\bar{M}}{M_o^2} \leq 1 \qquad (3.22)$$

where $\bar{N}$, $\overline{MN}$ and $\bar{M}$ are given by:

$$\bar{N} = N_x^2 + N_\theta^2 - N_x N_\theta + 3N_{x\theta}^2 \qquad (3.23a)$$

$$\bar{M} = M_x^2 + M_\theta^2 - M_x M_\theta + 3M_{x\theta}^2 \qquad (3.23b)$$

$$\overline{MN} = M_x N_x + M_\theta N_\theta - \tfrac{1}{2}(M_x N_\theta + M_\theta N_x) + 3M_{x\theta} N_{x\theta} \qquad (3.23c)$$

and $$s = \frac{\overline{MN}}{|\overline{MN}|} \qquad (3.24)$$

N_o is the uniaxial yield force, and M_o is the uniaxial yield moment and are defined as:

$$N_o = \sigma_o t \qquad (3.25)$$

and $$M_o = \tfrac{1}{4}\sigma_o t^2 \qquad (3.26)$$

where σ_o is the uniaxial yield stress.

In order for plastic flow to take place, the generalised stress resultants must remain on the yield surface, therefore

$$\delta f = 0 \tag{3.27}$$

or by differentiating (3.22) and using the expression (3.23), (3.27) becomes

$$\{f_n\}^T \{\Delta N\} + \{f_m\}^T \{\Delta M\} = 0 \tag{3.28}$$

where

$$\{f_n\} = \frac{1}{N_o^2} \left\{\frac{\partial \overline{N}}{\partial N}\right\} + \frac{s}{\sqrt{3} M_o N_o} \left\{\frac{\partial \overline{MN}}{\partial M}\right\} \tag{3.29a}$$

$$\{f_m\} = \frac{s}{\sqrt{3} M_o N_o} \left\{\frac{\partial \overline{MN}}{\partial N}\right\} + \frac{1}{M_o^2} \left\{\frac{\partial \overline{M}}{\partial M}\right\} \tag{3.29b}$$

In order to avoid discontinuity in calculating s as $\overline{MN}$ tends to zero, e.g. $|\overline{MN}| < 10^{-4}$, s is taken as zero. By using the Prandtl-Reuss flow rule, the plastic strain component is normal to the yield surface. Thus,

$$\{\Delta \epsilon_p\} = \lambda \{f_n\} \tag{3.30a}$$

$$\{\Delta k_p\} = \lambda \{f_m\} \tag{3.30b}$$

where λ is a positive scalar.

The elastic incremental generalised stress-strain laws are[54] assumed to be Hookean in nature[55]

$$\{\Delta N\} = t[E] \left[\{\Delta \epsilon_t\} - \{\Delta \epsilon_p\}\right] \tag{3.31a}$$

$$\{\Delta M\} = \frac{t^3}{12}[E] \left[\{\Delta k_t\} - \{\Delta k_p\}\right] \tag{3.31b}$$

Combining equations (3.30), (3.31) in conjunction with the equation (3.28) provides the following expressions for the plastic strain rate multiplier λ.

$$\lambda = \frac{1}{m+n} \left(t\{f_n\}^T [E] \{\Delta \epsilon_t\} + \frac{t}{12} \{f_m\}^T [E] \{\Delta k_t\}\right) \tag{3.32a}$$

where

$$n = t\{f_n\}^T[E]\{f_n\} \tag{3.32b}$$

$$m = \frac{t^3}{12}\{f_m\}^T[E]\{f_m\} \tag{3.32c}$$

In order to find a relation between the plastic strain increments and the total strain increments, λ is substituted with its equivalent expression (3.32a) into equations (3.30). By rearranging the terms the following expressions are derived.

$$\{\Delta\epsilon_p\} = \frac{1}{m+n}\left\{t[N][E]\{\Delta\epsilon_t\} + \frac{t^3}{12}[NM][E]\{\Delta k_t\}\right\} \tag{3.33a}$$

$$\{\Delta k_p\} = \frac{1}{m+n}\left\{t[NM]^T[E]\{\Delta\epsilon_t\} + \frac{t^3}{12}[M][E]\{\Delta k_t\}\right\} \tag{3.33b}$$

where

$$\begin{aligned}[N] &= \{f_n\}\{f_n\}^T \\ [M] &= \{f_m\}\{f_m\}^T \\ [NM] &= \{f_n\}\{f_m\}^T\end{aligned} \tag{3.34}$$

Substituting the equivalent expressions (3.33) for $\{\Delta\epsilon_p\}$ and $\{\Delta K_p\}$ into equations (3.31), the following relationships between the generalised stress resultant increments and the total generalised strain increments are obtained:

$$\begin{aligned}\{\Delta N\} &= [C]\{\Delta\epsilon_t\} + [R]\{\Delta k_t\} \\ \{\Delta M\} &= [R]^T\{\Delta\epsilon_t\} + [D]\{\Delta k_t\}\end{aligned} \tag{3.35}$$

where $[C]$, $[D]$ and $[R]$ are the tangential elasto-plastic modular matrices and are given by:

$$\begin{aligned}[C] &= t[E]\left\{[I] - \frac{t}{m+n}[N][E]\right\} \\ [D] &= \frac{t^3}{12}[E]\left\{[I] - \frac{t^3}{12(m+n)}[M][E]\right\} \\ [R] &= -\frac{t^4}{12(m+n)}[E][NM][E]\end{aligned} \tag{3.36}$$

During loading of a shell and before any part of the shell has entered plasticity, or in the case of unloading from the yield surface, the elastic rigidities come into action by substitution for the elasto-plastic ones.

3.5.2 *Modified Ivanov's Yield Criterion*

Crisfield[56], following the work of Burgoyne[57] who has claimed that the use of one of Ivanov's approximations[58] leads to a more exact representation of the true surface to Ilyushin's exact yield functions, has made an allowance for first "fibre yield". This modification is achieved by replacing the uniaxial yield moment (M_o) by αM_o in the Ivanov's approximate yield function[56]. This replacement provides a good approximation to the uniaxial moment/plastic curvature relationship with increasing equivalent plastic curvature.

The Ivanov's yield criterion, after modification, can be written as:

$$f = \frac{\bar{N}}{N_o^2} + \frac{1}{2}\frac{\bar{M}}{M_e^2} - \frac{1}{4}\frac{s}{q} + \frac{rH}{2M_e^2 N_o} \tag{3.37}$$

where,

$$\begin{aligned} \bar{N} &= N_x^2 + N_\theta^2 - N_x N_\theta + 3N_{x\theta}^2 \\ \bar{M} &= M_x^2 + M_\theta^2 - M_x M_\theta + 3M_{x\theta}^2 \\ \overline{MN} &= M_x N_x + M_\theta N_\theta - \frac{1}{2}(M_x N_\theta + M_\theta N_x) + 3M_{x\theta}\, N_{x\theta} \end{aligned} \tag{3.38}$$

and also,

$$q = \bar{N}M_e^2 + 0.48\,\bar{M}\,N_o^2$$

$$r = \sqrt{N_o^2\bar{M}^2 + 4M_e^2\overline{MN}^2}$$

$$s = \bar{N}\,\bar{M} - \overline{MN}^2$$

and finally,

$$N_o = \sigma_o t \qquad \text{(uniaxial yield force/unit width)}$$

$$M_o = \frac{1}{4}\sigma_o t^2 \qquad \text{(uniaxial yield moment/unit width)}$$

$$M_e = \alpha M_o$$

with $\alpha = 1.0 - 0.4\text{EXP}(-2.6\sqrt{\bar{k}_{ps}})$ (3.40)

$\bar{k}_{ps}$ is the non-dimensional equivalent plastic curvature obtained by summing all the incremental equivalent plastic curvatures.

$$\Delta\bar{k}_{ps}^2 = \left(\frac{Et}{3\sigma_o}\right)^2 \Delta k_{ps}^2 = \left(\frac{Et}{3\sigma_o}\right)^2 \frac{4}{3}\left(\Delta k_{px}^2 + \Delta k_{p\theta} + \Delta k_{px}\Delta k_{p\theta} + \frac{1}{4}\Delta k_{px\theta}^2\right) \tag{3.41}$$

Differentiation of equation (3.37) gives

$$\Delta f = \{f_n\}^T\{\Delta N\} + \{f_m\}^T\{\Delta M\} + \frac{\partial f}{\partial \alpha}\frac{\partial \alpha}{\partial k_{ps}}\Delta k_{ps} \tag{3.42}$$

where

$$\{f_n\} = b_1\left\{\frac{\partial \bar{N}}{\partial N}\right\} + b_2\left\{\frac{\partial \bar{M}}{\partial M}\right\}$$

$$\{f_m\} = b_2\left\{\frac{\partial \bar{N}}{\partial N}\right\} + b_3\left\{\frac{\partial \bar{M}}{\partial M}\right\} \tag{3.43}$$

after substituting

$$\frac{\partial \overline{MN}}{\partial N} = \frac{1}{2}\frac{\partial \bar{M}}{\partial M} \qquad \text{and} \qquad \frac{\partial \overline{MN}}{\partial M} = \frac{1}{2}\frac{\partial \bar{N}}{\partial N}$$

The coefficients b_1, b_2 and b_3 are given by the following expressions:

$$b_1 = \frac{1}{N_o^2} - \frac{\bar{M}}{4q} + \frac{sM_e^2}{4q^2} \tag{3.44a}$$

$$b_2 = \overline{MN}\left(\frac{1}{4q} + \frac{H}{rN_o}\right) \tag{3.44b}$$

$$b_3 = \frac{1}{2M_e^2} - \frac{\bar{N}}{4q} + \frac{0.12sN_o^2}{q^2} + \frac{H\bar{M}N_o}{2rM_e^2} \tag{3.44c}$$

Differentiation of (3.37) with respect to α gives:

$$\frac{\partial f}{\partial \alpha} = -\frac{1}{\alpha}\frac{\bar{M}}{M_e^2} + \frac{s\bar{N}M_e^2}{2\alpha q^2} - \frac{rH}{\alpha N_o M_e^2} + \frac{2H\bar{M}\bar{N}^2}{\alpha r N_o} \tag{3.45}$$

Also from equation (3.40), after differentiation

$$\frac{\partial \alpha}{\partial k_{ps}} = \frac{0.52}{\sqrt{k_{ps}}}\left(\frac{Et}{3\sigma_o}\right)^{\frac{1}{2}} \text{EXP}(-2.6\sqrt{k_{ps}}) \tag{3.46}$$

In order to avoid the discontinuity in equations (3.44b,c) and (3.45), as $r \to 0$, H is set to zero instead of its usual value of unity when $r < 10^{-4}$. Assuming that the yield function (3.37) can be treated as a plastic potential, and since the plastic strain rate vector is normal to the yield surface,

$$\begin{aligned} \{\Delta\varepsilon_p\} &= \lambda\{f_n\} \\ \{\Delta k_p\} &= \lambda\{f_m\} \end{aligned} \tag{3.47}$$

where λ is a positive scalar. Therefore, from equation (3.41)

$$\Delta k_{ps} = B\lambda \tag{3.48}$$

where

$$B = 2\sqrt{b_2^2\bar{N} + b_3^2\bar{M} + 2b_2b_3\bar{MN}} \tag{3.49}$$

The incremental generalised elastic stress-strain laws are defined as follows:

$$\begin{aligned} \{\Delta N\} &= t[E]\left[\{\Delta\varepsilon_t\} - \{\Delta\varepsilon_p\}\right] \\ \{\Delta M\} &= \frac{t^3}{12}[E]\left[\{\Delta k_t\} - \{\Delta k_p\}\right] \end{aligned} \tag{3.50}$$

For tangential behaviour, $\delta f = 0$. Therefore, combining equations (3.42), (3.47), (3.50) and after rearrangement of the terms, an expression for the scalar λ, is obtained.

$$\lambda = \frac{1}{j + g - B \frac{\partial f}{\partial \alpha} \frac{\partial \alpha}{\partial k_{ps}}} \left[\{f_n\}^T [E] \{\Delta \varepsilon_t\} + \frac{t^3}{12} \{f_m\}^T [E] \{\Delta k_t\} \right] \tag{3.51}$$

where

$$j = t\{f_n\}^T [E] \{f_n\}$$

$$g = \frac{t^3}{12} \{f_m\}^T [E] \{f_m\} \tag{3.52}$$

Introduction of equations (3.47) and (3.51) into equations (3.50) gives the following relationships:

$$\{\Delta N\} = [C] \{\Delta \varepsilon_t\} + [R] \{\Delta k_t\}$$

$$\{\Delta M\} = [R]^T \{\Delta \varepsilon_t\} + [D] \{\Delta k_t\} \tag{3.53}$$

The rigidities $[C]$, $[D]$ and $[R]$ are given by

$$[C] = t[E] \left[[I] - \frac{t}{p} [N] [E] \right]$$

$$[D] = \frac{t^3}{12} [E] \left[[I] - \frac{t}{12p} [M] [E] \right] \tag{3.54}$$

$$[R] = \frac{-t^4}{12p} [E] [NM] [E]$$

where

$$p = j + g - B \frac{\partial f}{\partial \alpha} \frac{\partial \alpha}{\partial k_{ps}}$$

$$[N] = \{f_n\}\{f_n\}^T$$

$$[M] = \{f_m\}\{f_m\}^T$$

$$[NM] = \{f_n\}\{f_m\}^T$$

3.5.3 *Multi-layer Approach*

This method is also referred to as the "volume approach" because it involves a volume integral. It is based on von Mises' yield criterion.

At any level z, plasticity is governed by the von Mises' yield

criterion:

$$(f)_z = \frac{1}{\sigma_o^2}\left(\sigma_x^2 + \sigma_\theta^2 - \sigma_x\sigma_\theta + 3\sigma_{x\theta}^2\right) \leq 1 \tag{3.55}$$

where σ_x and σ_θ are the direct components of stress, and $\sigma_{x\theta}$ is the shear stress.

For plastic flow to take place, the direction of the change in stress must be tangential to the yield function, i.e.

$$\left\{\frac{\partial f}{\partial \sigma}\right\}^T \{\Delta\sigma\} = 0 \tag{3.56}$$

Using the Prandtl-Reuss flow rule, the plastic strain component is normal to the yield surface. Thus,

$$\{\Delta\varepsilon_p\}_z = \lambda\left\{\frac{\partial f}{\partial \sigma}\right\}_z \tag{3.57}$$

where λ is a positive scalar. The incremental stress-strain laws are given by:

$$\{\Delta\sigma\}_z = [E]\left\{\{\Delta\varepsilon_t\} - \{\Delta\varepsilon_p\}\right\}_z \tag{3.58}$$

Combining equations (3.55) and (3.58), (following the work by Zienkiewicz et al[59] and Yamada et al,[60] as Crisfield mentions in Ref. (54), the relationship between the stress increments and the total strain increments may be written as:

$$\{\Delta\sigma\}_z = \left[E^*(\sigma)\right]_z \{\Delta\varepsilon_t\}_z \tag{3.59}$$

where $\left[E^*(\sigma)\right]_z$ is the tangential elasto-plastic modular matrix which is a function of the current stress level and is given by:

$$\left[E^*(\sigma)\right]_z = [E]\left\{[I] - \frac{1}{r}[\sigma][E]\right\} \tag{3.60}$$

where $[I]$ is the identity matrix, and

$$r = \left\{\frac{\partial f}{\partial \sigma}\right\}^T [E]\left\{\frac{\partial f}{\partial \sigma}\right\} \qquad \text{and} \qquad [\sigma] = \left\{\frac{\partial f}{\partial \sigma}\right\}\left\{\frac{\partial f}{\partial \sigma}\right\}^T \tag{3.61}$$

Let the incremental stress resultants $\{\Delta N\}$, $\{\Delta M\}$ be defined by

$$\{\Delta N\} = \int_{-t/2}^{t/2} \{\Delta\sigma\} dz$$
$$\{\Delta M\} = \int_{-t/2}^{t/2} z\{\Delta\sigma\} dz \tag{3.62}$$

and let the total strain vary linearly through the depth of the plate so that

$$\{\Delta\varepsilon_t\}_z = \{\Delta\varepsilon_t\} + z\{\Delta k_t\} \tag{3.63}$$

where $\{\Delta\varepsilon_t\}$ defines the strains at $z = 0$, and $\{\Delta k_t\}$ defines the (negative) curvatures. The combination of equations (3.59), (3.62) and (3.63) gives

$$\{\Delta N\} = [C]_v \{\Delta\varepsilon_t\} + [R]_v \{\Delta k_t\}$$
$$\{\Delta M\} = [R]_v \{\Delta\varepsilon_t\} + [D]_v \{\Delta k_t\} \tag{3.64}$$

where $[C]_v$, $[R]_v$ and $[D]_v$ are the tangential elasto-plastic modular matrices that relate to the generalised stress resultants and are given by

$$[C]_v = \int [E^*(\sigma)]_z dz$$
$$[D]_v = \int [E^*(\sigma)]_z z^2 dz \tag{3.65}$$
$$[R]_v = \int [E^*(\sigma)]_z z dz$$

3.5.4 *Comparison*

A few examples of a cylindrical shell under axial loading and bending combined with axial loading are shown in Figures (3.3, 3.4). These illustrate the response of the structure in the elasto-plastic region found by treating the plasticity by each of the yield formulations outlined

in Section 3.5.

It is observed that Ilyushin's yield criterion overestimates the peak and also the post-buckling path of the stress-strain curve. This happens because yielding is recorded suddenly throughout the thickness of the shell plating, in contrast with the multilayer or Ivanov's approach where plasticity takes place gradually, starting from the extreme fibres of the section. Due to this gradual penetration of plasticity, the change of curvature of the stress-strain curve around the peak is smoother. This comparison also shows that although both the multilayer and Ivanov's approaches give the same peak on the stress-strain curve, the latter causes a more rapid drop of the slope of the curve in the post-buckling region[61].

Comparisons of the computing storage capacity and of the actual running time per load increment for the three different approaches are shown in the following table. It was found that Ilyushin's and Ivanov's approaches needed 15.8% and 13.1% less storage respectively than the multilayer one. On the time basis, Ilyushin's and Ivanov's approaches were faster by 5.8% and 5.2% respectively, than the multilayer approach.

Approaches treating plasticity	Storage capacity of program	Time/load increment
Multilayer	100%	100%
Ilyushin's	84.2%	94.2%
Ivanov's	86.9%	94.8%

If the same comparison had taken place, but using the finite element instead of the finite difference technique, the differences would have been much greater especially those related to time. This would have happened because calculation of the rigidities occurs only once in each increment when the finite difference technique is used, while, in the case of the finite element technique, the calculation is repeated every iteration.

In situations where complicated structures are analysed so that the time factor is important, single-layer formulations are to be preferred.

Throughout the present analyses the multilayer approach was used in order to produce an 'exact' solution.

The multilayer approach has been formulated in the program with four options concerning the choice of numbers of layers. 3, 5, 7 or 9 layers can be chosen in order for integrations to be performed through the thickenss of the shell.

Figure (3.5) shows the effect on a stress-strain curve of using different numbers of layers. The 5, 7 and 9 layers have produced the same result, but the 3 layers choice was found to have overestimated the post-buckling behaviour of the curve.

The 5-layer formulation has thus been employed throughout the analyses. Numerical integration through the thickness of the shell is performed using Simpson's formula.

3.5.5 *Correction back to the Yield Surface*

For loading of the shell in the plastic region flow occurs tangentially to the yield surface. For other than very small increments, expansion of the yield surface will occur. For elastic-perfectly plastic materials this cannot be tolerated, and a correction has to be applied. This is performed by introducing a factor F_y as follows:

$$F_y = \frac{1}{\sqrt{f}}$$

where f is the yield function. This empirical formula is based on the fact that the yield function is proportional to the square of the stress resultants and moments.

At the end of each increment all the stress resultants and moments

are multiplied by F_y, thus returning the point to the original yield surface.

3.6 Discretisation of Cylindrical Shell

The cylindrical shell was divided into small rectangular elements as shown in Figure (3.17) and central finite differences were used to approximate the partial derivatives. An interlacing mesh was used to define displacements and stresses since first order derivatives are more accurately represented in this way. The adopted mesh can be seen in Figure (3.18). The following strains, curvatures, force and moment intensities were calculated at the indicated positions (see Fig. 3.18):

$\varepsilon_x, \varepsilon_\theta, k_x, k_\theta, N_x, N_\theta, M_x, M_\theta$: •

$\varepsilon_{x\theta}, k_{x\theta}, k_{\theta x}, N_{x\theta}, M_{x\theta}$: o

First and second derivatives of the displacements were calculated using central finite differences. In the x-direction and at the (•) position:

$$\left(\frac{\partial u}{\partial x}\right)_{i,j} = \frac{u(i,j) - u(i-1,j)}{\Delta x}$$

$$\left(\frac{\partial v}{\partial x}\right)_{i,j} = \frac{\dfrac{v(i+1,j) - v(i-1,j)}{2\Delta x} + \dfrac{v(i+1,j-1) - v(i-1,j-1)}{2\Delta x}}{2}$$

$$= \frac{v(i+1,j) - v(i-1,j) + v(i+1,j-1) - v(i-1,j-1)}{4\Delta x}$$

$$\left(\frac{\partial x}{\partial x}\right)_{i,j} = \frac{w(i+1,j) - w(i-1,j)}{2\Delta x}$$

$$\left(\frac{\partial^2 w}{\partial x^2}\right)_{i,j} = \frac{\dfrac{w(i+1,j) - w(i,j)}{\Delta x} - \dfrac{w(i,j) - w(i-1,j)}{\Delta x}}{\Delta x}$$

$$= \frac{w(i+1,j) - 2w(i,j) + w(i-1,j)}{\Delta x^2}$$

Also, in the θ direction with respect to the x direction at the (•) position,

$$\left(\frac{\partial^2 w}{\partial x \partial \theta}\right)_{i,j} = \frac{\frac{w(i+1,j+1) - w(i-1,j+1)}{2\Delta x} - \frac{w(i+1,j-1) - w(i-1,j-1)}{2\Delta x}}{2\Delta\theta}$$

$$= \left[w(i+1,j-1) - w(i-1,j+1) - w(i+1,j-1) + w(i-1,j-1)\right]/(4\Delta x \Delta\theta)$$

and similarly for the other variables which were defined at the (•) position.

In the θ direction and at the (.) position

$$\left(\frac{\partial v}{\partial \theta}\right)_{i,j} = \frac{v(i,j) - v(i,j-1)}{\Delta\theta}$$

$$\left(\frac{\partial w}{\partial \theta}\right)_{i,j} = \frac{w(i,j+1) - w(i,j-1)}{2\Delta\theta}$$

$$\left(\frac{\partial^2 w}{\partial \theta^2}\right)_{i,j} = \frac{\frac{w(i,j+1) - w(i,j)}{\Delta\theta} - \frac{w(i,j) - w(i,j-1)}{\Delta\theta}}{\Delta\theta}$$

$$= \frac{w(i,j+1) - 2w(i,j) + w(i,j-1)}{\Delta\theta^2}$$

and similarly for the other variables which were defined at the (•) position.

For the calculation of derviatives at a (o) position

$$\left(\frac{\partial v}{\partial x}\right)_{i,j} = \frac{v(i,j) - v(i-1,j)}{\Delta x}$$

$$\left(\frac{\partial w}{\partial x}\right)_{i,j} = \frac{\frac{w(i,j+1) - w(i-1,j+1)}{\Delta x} + \frac{w(i,j) - w(i-1,j)}{\Delta x}}{2}$$

$$= \frac{w(i,j+1) - w(i-1,j+1) + w(i,j) - w(i-1,j)}{2\Delta x}$$

$$\left(\frac{\partial u}{\partial \theta}\right)_{i,j} = \frac{u(i,j+1) - u(i,j)}{\Delta\theta}$$

$$\left(\frac{\partial w}{\partial \theta}\right)_{i,j} = \frac{\frac{w(i+1,j+1) - w(i+1,j)}{\Delta\theta} - \frac{w(i,j+1) - w(i,j)}{\Delta\theta}}{2\Delta\theta}$$

$$\left(\frac{\partial^2 w}{\partial x \partial \theta}\right)_{i,j} = \frac{\frac{w(i+1,j+1) - w(i,j+1)}{\Delta x} - \frac{w(i+1,j) - w(i,j)}{\Delta x}}{\Delta\theta}$$

$$= \frac{w(i+1,j+1) - w(i,j+1) - w(i+1,j) + w(i,j)}{\Delta x \Delta\theta}$$

and similarly for the remaining variables at the (o) position. Now, having all the derivatives in finite difference form, the equilibrium equations(3.21), the strain-displacement and the stress-strain relationships can be expressed in a finite difference form.

3.7 Imperfections

A sinusoidal type of initial imperfection was considered both in the longitudinal and circumferential directions.

$$w_o = w_o^* \cos(n\theta) \sin(\frac{m\pi x}{L})$$

where w_o^* is the amplitude of the wave, n is the number of circumferential waves and m is the number of longitudinal half waves.

The combinations of circumferential and longitudinal waves that were used in the present study are as follows:

(m,n) : (1,1), (5,1), (1,2), (1,4), i.e. mode 1, mode 6, mode 2 and mode 3 respectively of Reference(15) (Fig.3.19). This selection of modes ca be justified on the basis of elastic theory. For short cylindrical shells ($\frac{L}{R} < \frac{1.73}{\sqrt{R/T}}$) subjected to axial compression only one half wave will form in the axial direction during buckling[52]. The buckling of the shell will be symmetrical with respect to the axis of the cylinder, i.e. n = O. When L/R is somewhat bigger than $\frac{1.73}{\sqrt{R/T}}$, one half wave again will form in the axial direction during buckling but the number of circumferential waves will no longer be zero. Several lobes will appear around the circumference and their number will increase with cylinder length up to the limit when two half waves will be formed in the axial direction. The form of buckling will again be symmetrical with respect to the axis.

Preliminary runs have shown that there is little effect on the ultimate collapse load of varying the number of initial circumferential

waves. In contrast, the effect on strength of variation of the longitudinal wave length is significant.

The simplicity of mode selection has enabled the present analyses to be performed with relatively coarse finite difference meshes as discussed in Section 3.12.

Three different levels of w_o^* were chosen: (i) R/2000, (ii) R/1000 and R/400. These enabled comparisons to be made with existing results and also to assess the effect of level of imperfections on the strength of the structure.

3.8 Boundary Conditions

Boundary conditions are divided into two categories, circumferential boundary conditions and end ones. The first ones were applied along the generator AA' (Fig. 3.20) where the circumferential numbering of nodes begins and ends. These boundary conditions are illustrated in the Figure (3.20).

During the analyses, half of the cylindrical shell was analysed since symmetric imperfections about the plane (P) were assumed and since the same boundary conditions were considered at each end, symmetry of buckling could be expected. This consideration almost halved the actual running time of the computer program.

The end boundary conditions considered in the analyses were those approximating to heavy ring stiffereners in typical offshore platforms. Hence, zero tangential and normal displacements were assumed around the circumference of the cylinder ends (v,w=0). Simply supported ends were assumed to provide a lower bound on shell buckling behaviour. The fourth boundary condition necessary to define the shell ends completely was used for the application of load (see Section 3.9.1).

Boundary conditions similar to those used in classical buckling theory for axial compression were also included in the program, i.e., the circumferential stress intensity was assumed equal to zero. In this way the cylinder was allowed to expand uniformly around the circumference. Thus, taking $\dot{N}_\theta = 0$ at the boundaries, the w displacement at the end of the cylinder can be calculated:

$$N_\theta = \Delta N_\theta + N_\theta^p$$

$$= C_\theta \Delta\varepsilon_x + C_x \Delta\varepsilon_\theta + N_\theta^p = 0$$

where N_θ^p is the circumferential stress intensity in the previous load increment.

Solving for $\Delta\varepsilon_\theta$

$$\Delta\varepsilon_\theta = -\frac{(C_\theta \Delta\varepsilon_x + N_\theta^p)}{C_x}$$

$$\text{or } \varepsilon_\theta = \varepsilon_\theta^p - \frac{(C_\theta \Delta\varepsilon_x + N_\theta^p)}{C_x}$$

$$\text{or } \frac{1}{R}\frac{\partial v}{\partial \theta} - \frac{w_b}{R} + \{\text{other terms}\} = \varepsilon_\theta^p - \frac{(C_\theta \Delta\varepsilon_x + N_\theta^p)}{C_x}$$

$$\text{and } w_b = -R\varepsilon_\theta^p + \frac{\partial v}{\partial \theta} + \frac{R(C_\theta \Delta\varepsilon_x + N_\theta^p)}{C_x} + \{\text{other terms}\}$$

3.9 Loading

In the present analyses the axial compressive loading was applied as a sequence of increments of end axial displacement. This type of loading helped significantly in the tracing of the post-buckling behaviour of the structure, as long as no "snap-back" was expected of the loading path.

The size of these increments was varied according to the expected behaviour of the cylinder. Usually, when the structure was still elastic, three to four increments were adequate to describe the loading path since it was generally linear. As soon as the structure entered plasticity the increments were made relatively small in order to satisfactorily trace the change in curvature of the loading path. Later, when the post-buckling path had been established, larger increments of axial displacement were

considered. An average of 60 increments was used for each analysis.

Wherever external pressure was included, pressure loading was applied first keeping the cylinder ends in a constrained condition with zero net axial load. After an equilibrium state has been established, subsequent increments of compressive axial displacements were applied.

In the case of damaged cylinders subjected to axial compressive loading the following procedure was followed. A short cylindrical shell was considered with zero out-of-plane distortions and a point load was applied at a node at the middle of the shell. The load was increased gradually until the solution diverged indicating a failure of the numerical method. The cylinder was unloaded three times during the loading procedure. Following this, axial in-plane compressive displacements were applied in order to assess the residual strength of the cylinder.

3.10 Adaptation of the Numerical Technique

3.10.1 *Derivation of Fictitious Nodes*

Due to discretisation of the cylindrical shell some partial derivatives need to be calculated at the end boundaries. For this purpose fictitious nodes were considered (Fig.3.20a) and the respective displacements, u, v and w calculated.

The local bending moment at each node of the end boundaries is zero. Therefore,

$$M_x = 0$$

$$\text{or } \Delta M_x + M_x^p = 0 \qquad (3.66)$$

Using equation (3.64), equation (3.66) becomes:

$$R_x\Delta\varepsilon_x + R_\theta\Delta\varepsilon_\theta + R_{x\theta}\Delta\varepsilon_{x\theta} + D_x\Delta k_x + D_\theta\Delta k_\theta + D_{x\theta}\Delta k_{x\theta} + M_x^p = 0 \qquad (3.67a)$$

where R_x, R_θ, $R_{x\theta}$, D_x, D_θ, $D_{x\theta}$ are the rigidities at a particular node and M_x^p is the value of M_x at the end of the previous load increment. Substituting,

$$\Delta k_x = k_x - k_x^p$$

and rearranging the terms of equation (3.67a)

$$k_x = k_x^p - (R_x\Delta\varepsilon_x + R_\theta\Delta\varepsilon_\theta + R_{x\theta}\Delta\varepsilon_{x\theta} + D_\theta\Delta k_\theta + D_{x\theta}\Delta k_{x\theta} + M_x^p)/D_x$$

$$\text{or} - \frac{w_{in} - 2w_b + w_f}{\Delta x^2} = k_x^p - (R_x\Delta\varepsilon_x + \ldots + M_x^p)/D_x$$

and hence,

$$w_f = 2w_b - w_{in} - \Delta x^2 k_x^p + \Delta x^2 (R_x\Delta\varepsilon_x + \ldots + M_x^p)/D_x \qquad (3.67b)$$

where w_b, w_{in} and w_f are the out-of-plane displacements at a boundary, internal and fictitious node respectively.

The fictitious in-plane displacement, u_f, was found assuming a linear variation of the u displacement.

$$\frac{u_{in} + u_f}{2} = u_b \quad \text{or} \quad u_f = 2u_b - u_{in}$$

where u_b, u_{in} are the in-plane displacements at a boundary and internal node respectively.

By considering the equilibrium equation (3.21b) at the boundary, the fictitious v displacement can be calculated. Thus,

$$\frac{N_{x\theta}^{in} - N_{x\theta}^{f}}{\Delta x} + \frac{1}{R}\frac{\partial N\theta}{\partial\theta} = 0$$

$$\text{or } N_{x\theta}^{f} = N_{x\theta}^{in} + \frac{1}{R}\frac{\partial N\theta}{\partial\theta}\Delta x$$

$$\text{or } C'_x\Delta\varepsilon_x + C'_\theta\Delta\varepsilon_\theta + C'_{x\theta}\Delta\varepsilon_{x\theta} + R'_x\Delta k_x + R'_\theta\Delta k_\theta + R'_{x\theta}\Delta k_{x\theta} + (N_{x\theta}^{f})^p$$

$$= N_{x\theta}^{in} + \frac{1}{R}\frac{\partial N_\theta}{\partial\theta}\Delta x \qquad (3.68)$$

Substituting,

$$\Delta\varepsilon_{x\theta} = \varepsilon_{x\theta} - \varepsilon^{p}_{x\theta}$$

and rearranging the terms of equation (3.68)

$$\varepsilon_{x\theta} = \left[N^{in}_{x\theta} + \frac{1}{R}\frac{\partial N_{\theta}}{\partial\theta}\Delta x - (C'_{x}\Delta\varepsilon_{x} + C'_{\theta}\Delta\varepsilon_{\theta} + R'\Delta k_{x} + R'_{\theta}\Delta k_{\theta} + \right.$$

$$\left. + R'_{x\theta}\Delta k_{x\theta} + (N^{f}_{x\theta})^{p})\right]/C'_{x\theta} + \varepsilon^{p}_{x\theta} \qquad (3.69)$$

or $$\frac{v_b - v_f}{\Delta x} + \{\text{other terms of } \varepsilon_{x\theta}\} = \{\text{R.H.S. of (3.69)}\}$$

Hence,

$$v_f = v_b + \Delta x \{\text{other terms of } \varepsilon_{x\theta}\} - \Delta x \{\text{R.H.S. of (3.69)}\}$$

3.10.2 *Derivation of Fictitious Densities*

Fictitious densitites were derived separately for the w, u and v displacements at every node, using the following expressions which were derived in Section 2.3.

$$\rho_w = 0.25\ b_w \qquad (3.70a)$$

$$\rho_u = 0.25\ b_u \qquad (3.70b)$$

$$\rho_v = 0.25\ b_v \qquad (3.70c)$$

Each of b_w, b_u and b_v were calculated by considering the numerical sum of the absolute coefficients of each row of the stiffness matrix for each node.

The stiffness matrix is written explicitly, by expressing the equilibrium equations (3.21) in an analytical form including only u, v and w displacement terms, by using finite difference formulation.

Due to the complexity of these expressions, the development has been carried out in the elastic range initially. Namely, only terms including elastic rigidities were considered.

In the first stage of calculation of b_w, b_u and b_v, the stress intensities and the moments were written explicitly in terms of displacements.

$$N_x = C_x\left[\frac{\partial u}{\partial x} + \frac{1}{2}\left(\frac{\partial v}{\partial x}\right)^2 + \frac{1}{2}\left(\frac{\partial w}{\partial x}\right)^2 + \frac{\partial w}{\partial x}\frac{\partial w_o}{\partial x} \right]$$
$$+ C_\theta\left[\frac{1}{R}\frac{\partial v}{\partial \theta} - \frac{w}{R} + \frac{1}{2R^2}\left(\frac{\partial u}{\partial \theta}\right)^2 + \frac{1}{2R^2}\left(\frac{\partial w}{\partial \theta}\right)^2 + \frac{1}{2}\left(\frac{v}{R}\right)^2 \right.$$
$$\left. + \frac{v}{R^2}\frac{\partial w}{\partial \theta} + \frac{v}{R^2}\frac{\partial w_o}{\partial \theta} + \frac{1}{R^2}\frac{\partial w}{\partial \theta}\frac{\partial w_o}{\partial \theta} + \frac{w_o}{R^2}\frac{\partial v}{\partial \theta} - \frac{w}{R}\frac{w_o}{R} \right] \qquad (3.71a)$$

$$N_\theta = C_x\left[\frac{1}{R}\frac{\partial v}{\partial \theta} - \frac{w}{R} + \frac{1}{2R^2}\left(\frac{\partial u}{\partial \theta}\right)^2 + \frac{1}{2R^2}\left(\frac{\partial w}{\partial \theta}\right)^2 + \frac{1}{2}\left(\frac{v}{R}\right)^2 \right.$$
$$\left. + \frac{v}{R^2}\frac{\partial w}{\partial \theta} + \frac{v}{R^2}\frac{\partial w_o}{\partial \theta} + \frac{1}{R^2}\frac{\partial w}{\partial \theta}\frac{\partial w_o}{\partial \theta} + \frac{w_o}{R^2}\frac{\partial v}{\partial \theta} - \frac{w}{R}\frac{w_o}{R} \right]$$
$$+ C_\theta\left[\frac{\partial u}{\partial x} + \frac{1}{2}\left(\frac{\partial v}{\partial x}\right)^2 + \frac{1}{2}\left(\frac{\partial w}{\partial x}\right)^2 + \frac{\partial w}{\partial x}\frac{\partial w_o}{\partial x} \right] \qquad (3.71b)$$

$$N_{x\theta} = C_{x\theta}\left[\frac{\partial v}{\partial x} + \frac{1}{R}\frac{\partial u}{\partial \theta} + \frac{1}{R}\frac{\partial w}{\partial \theta}\frac{\partial w}{\partial x} + \frac{1}{R}\frac{\partial w}{\partial \theta}\frac{\partial w_o}{\partial x} + \frac{1}{R}\frac{\partial w_o}{\partial \theta}\frac{\partial w}{\partial x} \right.$$
$$\left. + \frac{v}{R}\frac{\partial w}{\partial x} + \frac{v}{R}\frac{\partial w_o}{\partial x} + \frac{w_o}{R^2}\frac{\partial u}{\partial \theta} - \frac{\partial u}{\partial x}\frac{\partial v}{\partial x} - \frac{1}{R^2}\frac{\partial v}{\partial \theta}\frac{\partial u}{\partial \theta} + \frac{w}{R^2}\frac{\partial u}{\partial \theta} \right] \qquad (3.71c)$$

$$M_x = -D_x\frac{\partial^2 w}{\partial x^2} \qquad (3.71d)$$

$$M_\theta = -D_\theta\left(\frac{1}{R^2}\frac{\partial^2 w}{\partial^2 \theta} - \frac{1}{R^2}\frac{\partial v}{\partial \theta}\right) \qquad (3.71e)$$

$$M_{x\theta} = -D_{x\theta}\left(\frac{2}{R}\frac{\partial^2 w}{\partial x \partial \theta} - \frac{2}{R}\frac{\partial v}{\partial x}\right) \qquad (3.71f)$$

In the second stage the first and second derivatives of the displacements were expressed in finite difference form and the coefficients of these terms were calculated as follows:

a) At the (.) nodes,

$$\overline{\frac{\partial u}{\partial x}} = \frac{2}{\Delta x}, \qquad \overline{\frac{\partial v}{\partial x}} = \frac{4}{4\Delta x} = \frac{1}{\Delta x}, \qquad \left(\overline{\frac{\partial v}{\partial x}}\right)^2 = 2\,\frac{1}{\Delta x}\left|\frac{\partial v}{\partial x}\right|$$

$$\overline{\frac{\partial w}{\partial x}} = \frac{2}{2\Delta x} = \frac{1}{\Delta x}, \qquad \left(\overline{\frac{\partial w}{\partial x}}\right)^2 = 2\,\frac{1}{\Delta x}\left|\frac{\partial w}{\partial x}\right|,$$

$$\left(\overline{\frac{\partial w}{\partial x}\frac{\partial w_o}{\partial x}}\right) = \frac{1}{\Delta x}\left|\frac{\partial w_o}{\partial x}\right|, \qquad \overline{\frac{\partial v}{\partial \theta}} = \frac{2}{\Delta \theta}, \qquad \overline{w} = 1,$$

$$\overline{\frac{\partial u}{\partial \theta}} = \frac{4}{2\Delta\theta} = \frac{2}{\Delta\theta}\,, \qquad \left(\overline{\frac{\partial u}{\partial \theta}}\right)' = 2\,\frac{2}{\Delta\theta}\,\left|\frac{\partial u}{\partial \theta}\right|\,, \qquad \overline{\frac{\partial w}{\partial \theta}} = \frac{2}{2\Delta\theta} = \frac{1}{\Delta\theta}\,,$$

$$\left(\overline{\frac{\partial w}{\partial \theta}}\right)^2 = 2\,\frac{1}{\Delta\theta}\,\left|\frac{\partial w}{\partial \theta}\right|\,, \qquad \overline{v} = 1, \qquad (\overline{v})^2 = 2|v|\,,$$

$$\left(\overline{v\,\frac{\partial w}{\partial \theta}}\right)' = \left|\frac{\partial w}{\partial \theta}\right| + \frac{1}{\Delta\theta}\,|v|\,, \qquad \left(\overline{v\,\frac{\partial w_o}{\partial \theta}}\right) = \left|\frac{\partial w_o}{\partial \theta}\right|\,,$$

$$\left(\overline{\frac{\partial w}{\partial \theta}\,\frac{\partial w_o}{\partial \theta}}\right) = \frac{1}{\Delta\theta}\,\left|\frac{\partial w_o}{\partial \theta}\right|\,, \qquad \left(\overline{w_o\,\frac{\partial v}{\partial \theta}}\right) = \frac{2}{\Delta\theta}\,|w_o|\,,$$

$$(\overline{w\,w_o}) = |w_o|\,, \qquad \left(\overline{\frac{\partial^2 u}{\partial x^2}}\right) = \frac{4}{\Delta x^2}\,, \qquad \left(\overline{\frac{\partial^2 w}{\partial \theta^2}}\right) = \frac{4}{\Delta\theta^2}$$

b) At the (o) nodes,

$$\overline{\frac{\partial v}{\partial x}} = \frac{2}{\Delta x}\,, \qquad \overline{\frac{\partial u}{\partial \theta}} = \frac{2}{\Delta\theta}\,, \qquad \overline{\frac{\partial u}{\partial x}} = \frac{4}{4\Delta x} = \frac{1}{\Delta x}\,,$$

$$\overline{\frac{\partial w}{\partial x}} = \frac{4}{2\Delta x} = \frac{2}{\Delta x}\,, \qquad \overline{\frac{\partial w}{\partial \theta}} = \frac{4}{2\Delta\theta} = \frac{2}{\Delta\theta}\,,$$

$$\left(\overline{\frac{\partial w}{\partial x}\,\frac{\partial w}{\partial \theta}}\right) = \frac{2}{\Delta x}\,\left|\frac{\partial w}{\partial \theta}\right| + \frac{2}{\Delta\theta}\,\left|\frac{\partial w}{\partial x}\right|\,, \qquad \left(\overline{\frac{\partial w}{\partial \theta}\,\frac{\partial w_o}{\partial x}}\right) = \frac{2}{\Delta\theta}\,\left|\frac{\partial w_o}{\partial x}\right|$$

$$\left(\overline{\frac{\partial w_o}{\partial \theta}\,\frac{\partial w}{\partial x}}\right) = \frac{2}{\Delta x}\,\left|\frac{\partial w_o}{\partial \theta}\right|, \qquad \overline{v} = 1\,, \qquad \left(\overline{v\,\frac{\partial w}{\partial x}}\right) = \left|\frac{\partial w}{\partial x}\right| + \frac{2}{\Delta x}\,|v|,$$

$$\left(\overline{v\,\frac{\partial w_o}{\partial x}}\right) = \left|\frac{\partial w_o}{\partial x}\right|, \qquad \left(\overline{w_o\,\frac{\partial u}{\partial \theta}}\right) = \frac{2}{\Delta\theta}\,|w_o|\,,$$

$$\left(\overline{\frac{\partial u}{\partial x}\,\frac{\partial v}{\partial x}}\right) = \frac{1}{\Delta x}\,\left|\frac{\partial v}{\partial x}\right| + \frac{2}{\Delta x}\,\left|\frac{\partial u}{\partial x}\right|\,, \qquad \overline{\frac{\partial v}{\partial \theta}} = \frac{4}{4\Delta\theta} = \frac{1}{\Delta\theta}\,,$$

$$\left(\overline{\frac{\partial v}{\partial \theta}\,\frac{\partial u}{\partial \theta}}\right) = \frac{1}{\Delta\theta}\,\left|\frac{\partial u}{\partial \theta}\right| + \frac{2}{\Delta\theta}\,\left|\frac{\partial v}{\partial \theta}\right|\,, \qquad \left(\overline{w\,\frac{\partial u}{\partial \theta}}\right) = \left|\frac{\partial u}{\partial \theta}\right| + \frac{2}{\Delta\theta}\,|w|\,,$$

$$\overline{\frac{\partial^2 w}{\partial x\,\partial \theta}} = \frac{4}{\Delta x\,\Delta\theta}$$

For the third stage the coefficients of the stress intensities and moments were found by substituting the displacement coefficients, into expressions

3.71 leading to absolute coefficients for an (i,j) node of

$$\left[\overline{N_x}\right]_{i,j} = C_x \left[\frac{2}{\Delta x} + \frac{1}{\Delta x}\left|\frac{\partial v}{\partial x}\right| + \frac{1}{\Delta x}\left|\frac{\partial w}{\partial x}\right| + \frac{1}{\Delta x}\left|\frac{\partial w_o}{\partial x}\right|\right]_{i,j}$$
$$+ C_\theta \left[\frac{1}{R}\frac{2}{\Delta\theta} + \frac{1}{R} + \frac{1}{R^2}\frac{2}{\Delta\theta}\left|\frac{\partial u}{\partial\theta}\right| + \frac{1}{R^2}\frac{1}{\Delta\theta}\left|\frac{\partial w}{\partial\theta}\right|\right.$$
$$+ \frac{1}{R^2}|v| + \frac{1}{R^2}\left|\frac{\partial w}{\partial\theta}\right| + \frac{1}{R^2}\frac{1}{\Delta\theta}|v| + \frac{1}{R^2}\left|\frac{\partial w_o}{\partial\theta}\right|$$
$$\left. + \frac{1}{R^2}\frac{1}{\Delta\theta}\left|\frac{\partial w_o}{\partial\theta}\right| + \frac{1}{R^2}\frac{2}{\Delta\theta}|w_o| + \frac{1}{R^2}|w_o|\right]_{i,j} \qquad (3.72a)$$

$$\left[\overline{N_\theta}\right]_{i,j} = C_x \left[\frac{1}{R}\frac{2}{\Delta\theta} + \frac{1}{R} + \frac{1}{R^2}\frac{2}{\Delta\theta}\left|\frac{\partial u}{\partial\theta}\right| + \frac{1}{R^2}\frac{1}{\Delta\theta}\left|\frac{\partial w}{\partial\theta}\right|\right.$$
$$+ \frac{1}{R^2}|v| + \frac{1}{R^2}\left|\frac{\partial w}{\partial\theta}\right| + \frac{1}{R^2}\frac{1}{\Delta\theta}|v| + \frac{1}{R^2}\left|\frac{\partial w_o}{\partial\theta}\right|$$
$$\left. + \frac{1}{R^2}\frac{1}{\Delta\theta}\left|\frac{\partial w_o}{\partial\theta}\right| + \frac{1}{R^2}\frac{2}{\Delta\theta}|w_o| + \frac{1}{R^2}|w_o|\right]_{i,j}$$
$$+ C_\theta \left[\frac{2}{\Delta x} + \frac{1}{\Delta x}\left|\frac{\partial v}{\partial x}\right| + \frac{1}{\Delta x}\left|\frac{\partial w}{\partial x}\right| + \frac{1}{\Delta x}\left|\frac{\partial w_o}{\partial x}\right|\right]_{i,j} \qquad (3.72b)$$

$$\left[\overline{N_x}\right]_{i,j} = C_{x\theta}\left[\frac{2}{\Delta x} + \frac{1}{R}\frac{2}{\Delta\theta} + \frac{1}{R}\frac{2}{\Delta x}\left|\frac{\partial w}{\partial\theta}\right| + \frac{1}{R}\frac{2}{\Delta\theta}\left|\frac{\partial w}{\partial x}\right|\right.$$
$$+ \frac{1}{R}\frac{2}{\Delta\theta}\left|\frac{\partial w_o}{\partial x}\right| + \frac{1}{R}\frac{2}{\Delta x}\left|\frac{\partial w_o}{\partial\theta}\right| + \frac{1}{R}\left|\frac{\partial w}{\partial x}\right|$$
$$+ \frac{1}{R}\frac{2}{\Delta x}|v| + \frac{1}{R}\left|\frac{\partial w_o}{\partial x}\right| + \frac{1}{R^2}\frac{2}{\Delta\theta}|w_o|$$
$$+ \frac{1}{\Delta x}\left|\frac{\partial v}{\partial x}\right| + \frac{2}{\Delta x}\left|\frac{\partial u}{\partial x}\right| + \frac{1}{R^2}\frac{1}{\Delta\theta}\left|\frac{\partial u}{\partial\theta}\right| + \frac{1}{R^2}\frac{2}{\Delta\theta}\left|\frac{\partial v}{\partial\theta}\right|$$
$$\left. + \frac{1}{R^2}\left|\frac{\partial u}{\partial\theta}\right| + \frac{1}{R^2}\frac{2}{\Delta\theta}|w|\right]_{i,j} \qquad (3.72c)$$

$$\left[\overline{M_x}\right]_{i,j} = D_x \frac{4}{\Delta x^2} \qquad (3.72d)$$

$$\left[\overline{M_\theta}\right]_{i,j} = D_\theta\left(\frac{1}{R^2}\frac{4}{\Delta\theta^2} + \frac{1}{R^2}\frac{2}{\Delta\theta}\right) \qquad (3.72e)$$

$$\left[\overline{M_{x\theta}}\right]_{i,j} = D_{x\theta}\left(\frac{2}{R}\frac{4}{\Delta x\Delta\theta} + \frac{2}{R}\frac{2}{\Delta x}\right) \qquad (3.72f)$$

For the fourth stage, the equilibrium equations (3.21) were expressed in finite difference form, thus,

$$\frac{N_x(i+1,j) - N_x(i,j)}{\Delta x} + \frac{1}{R}\frac{N_{x\theta}(i,j) - N_{x\theta}(i,j-1)}{\Delta\theta} = 0 \qquad (3.73a)$$

$$\frac{N_{x\theta}(i,j) - N_{x\theta}(i-1,j)}{\Delta x} + \frac{1}{R}\frac{N_{\theta}(i,j+1) - N_{\theta}(i,j)}{\Delta\theta} = 0 \qquad (3.73b)$$

$$\frac{M_x(i+1,j) - 2M_x(i,j) + M_x(i-1,j)}{\Delta x^2} +$$

$$2\,\frac{M_{x\theta}(i,j) - M_{x\theta}(i,j-1) + M_{x\theta}(i-1,j-1) - M_{x\theta}(i-1,j)}{R\Delta x\Delta\theta} +$$

$$\frac{1}{R^2}\,\frac{M_{\theta}(i,j+1) - 2M_{\theta}(i,j) + M_{\theta}(i,j-1)}{\Delta\theta^2} + \frac{N_{\theta}(i,j)}{R} +$$

$$N_x(i,j)\left(\frac{\partial^2 w}{\partial x^2} + \frac{\partial^2 w_o}{\partial x^2}\right)_{i,j} + \frac{1}{R^2}N_{\theta}(i,j)\left(\frac{\partial^2 w}{\partial\theta^2} + \frac{\partial^2 w_o}{\partial\theta^2} - \frac{\partial v}{\partial\theta}\right)_{i,j} +$$

$$\frac{2}{R}N_{x\theta}(i,j)\left(\frac{\partial^2 w}{\partial x\partial\theta} + \frac{\partial^2 w_o}{\partial x\partial\theta} - \frac{\partial v}{\partial x}\right) + p(i,j) = 0 \qquad (3.73c)$$

For the fifth and final stage the b_u, b_v and b_w were calculated by substituting in the above equations the coefficients calculated at the third stage (3.72). Thus,

$$b_u = \frac{1}{\Delta x}\left(\overline{[N_x]}_{i+1,j} + \overline{[N_x]}_{i,j}\right) + \frac{1}{R\Delta\theta}\left(\overline{[N_{x\theta}]}_{i,j} + \overline{[N_{x\theta}]}_{i,j-1}\right) \qquad (3.74a)$$

$$b_v = \frac{1}{\Delta x}\left(\overline{[N_{x\theta}]}_{i,j} + \overline{[N_{x\theta}]}_{i-1,j}\right) + \frac{1}{R\Delta\theta}\left(\overline{[N_{\theta}]}_{i,j+1} + \overline{[N_{\theta}]}_{i,j}\right) \qquad (3.74b)$$

$$b_w = \frac{1}{\Delta x^2}\left(\overline{[M_x]}_{i+1,j} + 2\overline{[M_x]}_{i,j} + \overline{[M_x]}_{i-1,j}\right)$$

$$+ \frac{2}{R\Delta\theta\Delta x}\left(\overline{[M_{x\theta}]}_{i,j} + \overline{[M_{x\theta}]}_{i,j-1} + \overline{[M_{x\theta}]}_{i-1,j-1} + \overline{[M_{x\theta}]}_{i-1,j}\right)$$

$$+ \frac{1}{R^2\Delta\theta^2}\left(\overline{[M_{\theta}]}_{i,j+1} + 2\overline{[M_{\theta}]}_{i,j} + \overline{[M_{\theta}]}_{i,j-1}\right) + \frac{1}{R}\overline{[N_{\theta}]}_{i,j}$$

$$+ \overline{[N_x]}_{i,j}\left(\left|\frac{\partial^2 w}{\partial x^2}\right| + \left|\frac{\partial^2 w_o}{\partial x^2}\right|\right)_{i,j} + \frac{4}{\Delta x^2}N_x(i,j)$$

$$+ \frac{1}{R^2}\overline{[N_{\theta}]}_{i,j}\left(\left|\frac{\partial^2 w}{\partial\theta^2}\right| + \left|\frac{\partial^2 w_o}{\partial\theta^2}\right| + \left|\frac{\partial v}{\partial\theta}\right|\right)_{i,j} + \left(\frac{1}{R^2\Delta\theta^2} + \frac{2}{\Delta\theta}\right)N_{\theta}(i,j)$$

$$+ \frac{2}{R}\left(\frac{4}{\Delta x\Delta\theta} + \frac{2}{\Delta x}\right)N_{x\theta}(i,j) + \frac{2}{R}\overline{[N_{x\theta}]}_{i,j}\left(\left|\frac{\partial^2 w}{\partial x\partial\theta}\right| + \left|\frac{\partial^2 w_o}{\partial x\partial\theta}\right| + \left|\frac{\partial v}{\partial x}\right|\right)_{i,j} \qquad (3.74c)$$

During early stages of program development the expressions for b_u, b_v and b_w were evaluated at every iteration. It was noticed that after ascertaining the number of iterations the numerical values of b_u, b_v and b_w converged to steady values. Thus, the number of iterations for calculating the fictitious densities was reduced down to one twentieth of the total number of iterations. A more thorough study showed that even if the calculation took place at only the first iteration of each iterative cycle, the results were still satisfactory. Derivation of the fictitious densities was made by including all the elasto-plastic elements of the stiffness matrix in an attempt to see if convergence would be improved. Comparison between the stress-strain curves produced by using elastic and elasto-plastic fictitious densities showed no practical differences.

In some cases it was noticed that convergence was underestimated, resulting in failure of the iterative procedure. This problem was tackled by introducing density factors. In this way the fictitious densities were usually doubled and satisfactory convergence achieved.

This problem was encountered in cases where combined pressure, bending and axial loading was applied to cylindrical shells of small R/T.

3.10.3 *Automatic Calculation Technique for Damping Factor*

Some investigators have developed methods which lead to the calculation of damping factors. These methods illustrate how to calculate the minimum and maximum eigenvalues of the stiffness matrix[62, 47] and consequently the damping factor by applying the formula

$$k = \frac{4\sqrt{\alpha\beta}}{\alpha+\beta} \qquad (3.75)$$

where α and β are the minimum and maximum eigen values of the stiffness matrix respectively.

Rushton[39] has suggested a rather simple method, based on the

damped vibration of a simply supported uniformly loaded beam. Combination of the critical damping (3.76) for the fundamental mode and the angular frequency (3.77) of the undamped vibration of this beam gives equation (3.78).

$$k = 2\sqrt{m}\pi^2 \tag{3.76}$$

$$\omega = \frac{\pi^2}{\sqrt{m}} \tag{3.77}$$

$$k = 2m\omega \tag{3.78}$$

Therefore, the critical damping factor can be determined from the frequency of the undamped vibration and for unit mass

$$k = 2\omega \tag{3.79}$$

The angular frequency can be estimated by allowing the structure to oscillate without damping and calculating the total kinetic energy at each iteration. If the kinetic energy has a maximum after N iterations then the angular frequency ω is given by

$$\omega = \frac{2\pi}{4N\Delta t} \quad \text{rad/sec} \tag{3.80}$$

and the critical damping factor k is given by

$$k = \frac{\pi}{N\Delta t} \tag{3.81}$$

or for unit time increment

$$k = \frac{\pi}{N} \tag{3.82}$$

This procedure has been used successfully for a large number of problems concerning beams and plates[39, 40, 41].

Rushton's method has been modified and used by Basu et al[63] in the analysis of bridge decks.

In the case of cylindrical shells, it was found that the damping factors obtained using formula (3.82) were insufficient and a factor J_k was introduced as follows:

$$k = J_k \frac{\pi}{N} \tag{3.83}$$

where J_k is an integer taking values in the domain (1,4). This domain has been chosen only for the present analyses and it is not absolute. This method has been programmed and it is easy to use. J_k is determined by a trial and error method.

3.11 Flow Charts

The following flow charts refer to the formulation developed in this chapter. The first chart describes the main stages of the ANSAlML computing program based on the multi-layer approach. The program is governed mainly by two loops, the DR iterative loop and the load increment loop. Given that, at the end of the DR iterative loop, convergence is achieved, all the nodes (i,j) are checked for yielding. If yielding occurs, the elasto-plastic rigidites are calculated according to the flow chart on page 78, and are used in the next load increment.

At the end of each load increment all the values necessary to initialise the next increment are recorded in special files. These data recordings proved to be very useful, particularly when the computer happened to break down. Following these occasions, the files were recalled at the beginning of the program and analysis continued normally from the load increment at which the break-down occurred.

The chart also shows how the pressure can be applied either incrementally or all at once.

The second chart shows the main stages of the ANSAlIL and ANSAlIV programs. These differ from the ANSAlML program only in the calculation of plastic rigidities. They both use a single-layer approach as discussed in Sections 3.5.1 and 3.5.2.

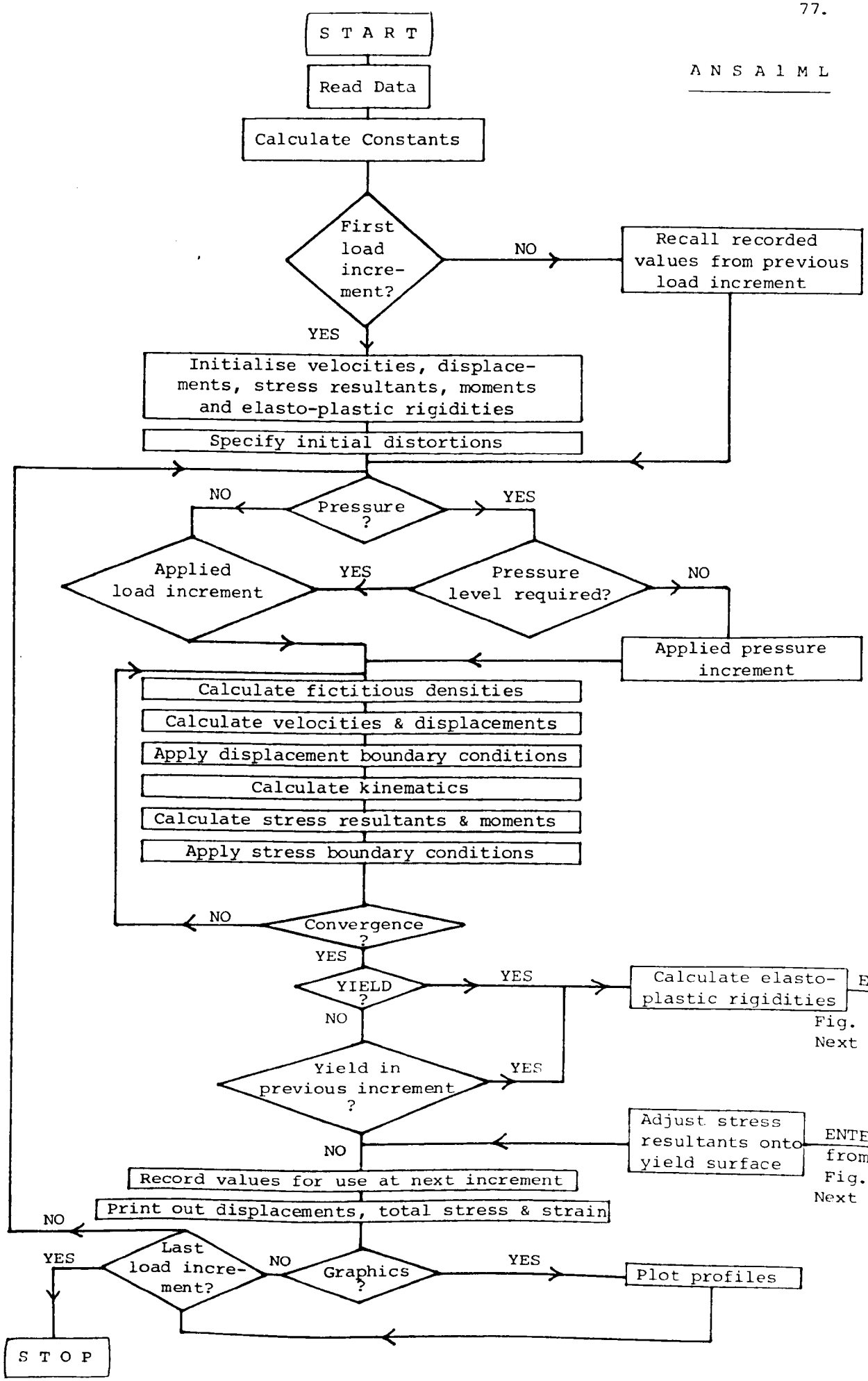
S T A R T
Read Data
Calculate Constants
First load increment?
NO
Recall recorded values from previous load increment
YES
Initialise velocities, displacements, stress resultants, moments and elasto-plastic rigidities
Specify initial distortions
NO
Pressure ?
YES
Applied load increment
YES
Pressure level required?
NO
Applied pressure increment
Calculate fictitious densities
Calculate velocities & displacements
Apply displacement boundary conditions
Calculate kinematics
Calculate stress resultants & moments
Apply stress boundary conditions
NO
Convergence ?
YES
YIELD ?
YES
Calculate elasto-plastic rigidities
EXI
Fig.
Next pa
NO
Yield in previous increment ?
YES
Adjust stress resultants onto yield surface
ENTER from Fig.
Next pa
NO
Record values for use at next increment
Print out displacements, total stress & strain
NO
YES
Last load increment?
NO
Graphics ?
YES
Plot profiles
S T O P

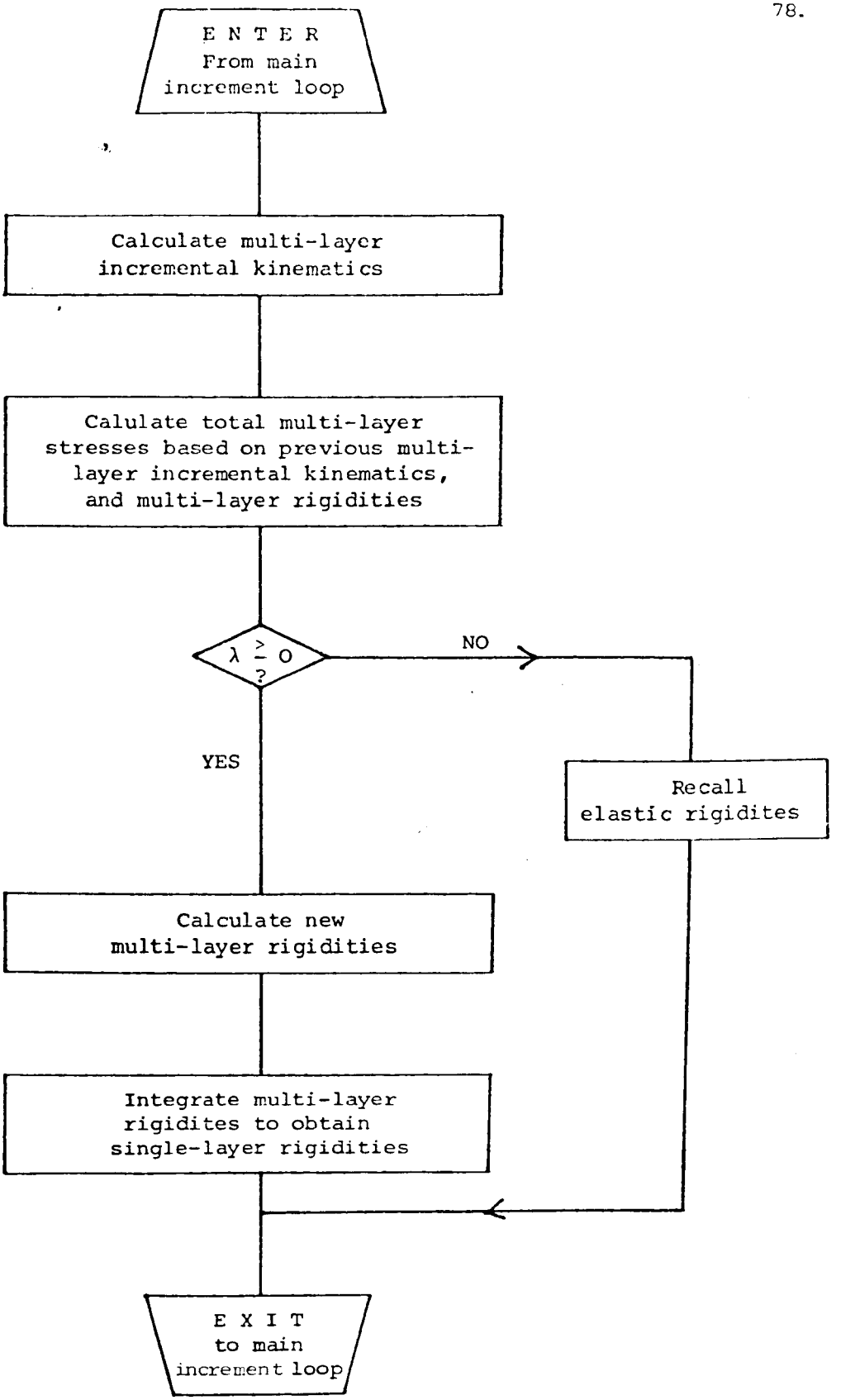

FLOW CHART FOR THE CALCULATION OF SINGLE-LAYER RIGIDITIES USING THE MULTI-LAYER APPROACH

A N S A l I L
&
A N S A l I V

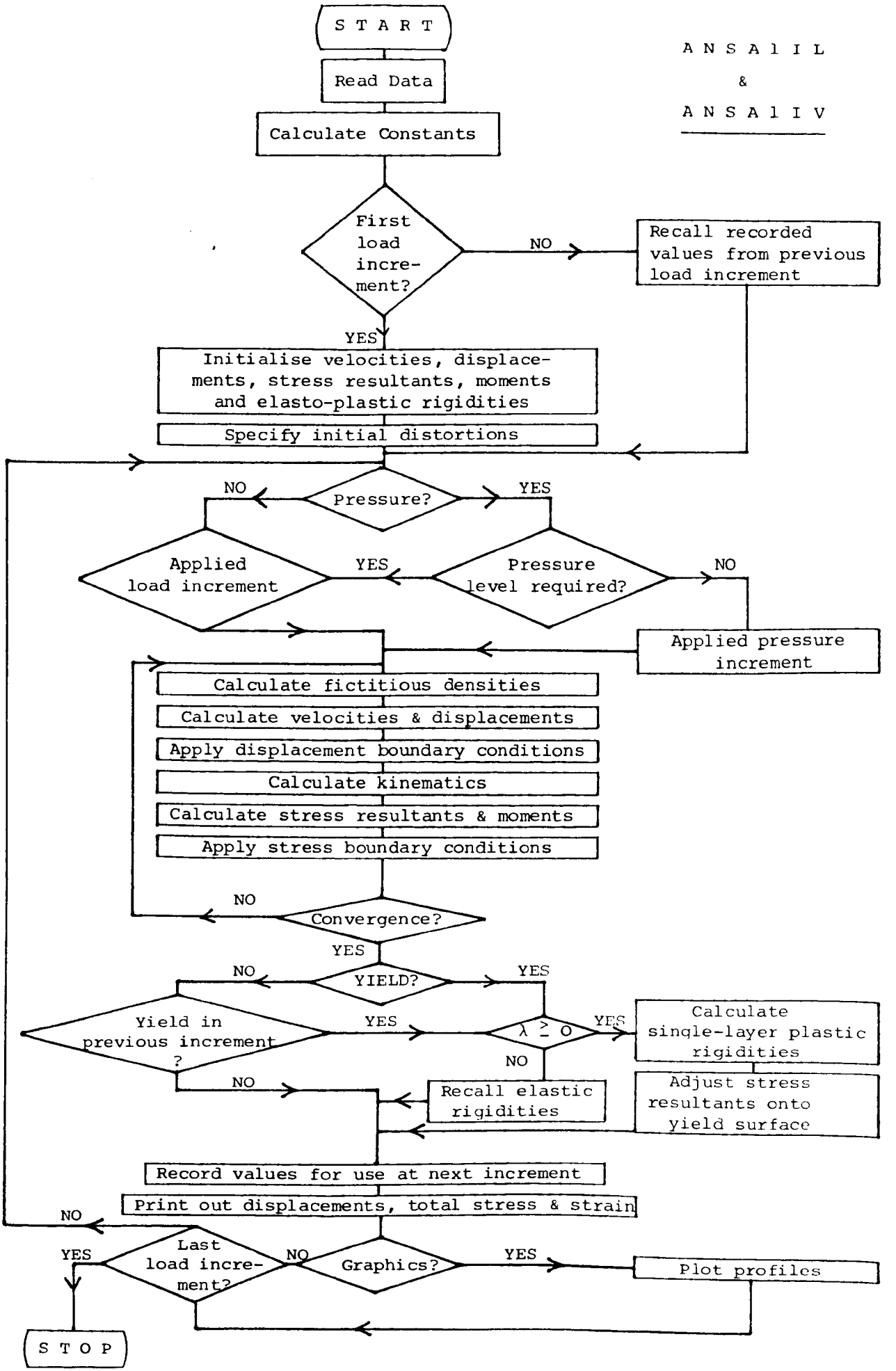

3.12 Convergence Studies

An investigation to establish optimum mesh sizes was undertaken before any parametric studies were performed. Several mesh sizes were examined and the results for some of them are illustrated in Figures (3.6-3.9) . This study was conducted in two stages. Firstly, the number of circumferential nodes was kept constant while the number of nodes along the length of the cylindrical shell was varied. In these particular examples the angle between two successive nodes was 22.5^{o}, namely 16 nodes around the circumference. The consideration of three different mesh sizes was found to be adequate to satisfactorily accomplish the covergence studies. The three selected mesh sizes were as follows: 3 x 16, 5 x 16 and 11 x 16. The number of nodes 3, 5 and 11 refers to half of the cylinder length. Three nodes were found to be inadequate. On the contrary, 5 and 11 were found to give very similar results. However, the 5 x 16 mesh size failed to complete the analysis in cases where large values of R/T's were involved, usually R/T>200, or in cases where complex load was involved.

This weakness arose because a change in mode occurred along the cylinder length and the number of nodes was inadequate to describe this new mode. This situation was observed to happen just at the peak of the stress-strain curve and further loading of the cylinder was impossible. Therefore, the 11 x 16 mesh was used to undertake any analysis.

For the second stage, the number of nodes along the cylinder length was kept constant, namely 11, while the number of nodes around the circumference was varied (Fig. 3.9).

Three different meshes were examined; 11 x 4, 11 x 8 and 11 x 16. In other words, the angle θ between two successive nodes was 90^{o}, 45^{o} and 22.5^{o} respectively. The 11 x 4 mesh produced too high results and failed to describe the circumferential wave pattern accurately.

Both the 11 x 8 and 11 x 16 meshes generated almost identical results, but again, in order to develop accurate patterns of the initial and final circumferential waves, the 11 x 16 mesh was selected to undertake most of the analyses.

3.13 Comparison with Other Solutions

The only existing elasto-plastic solutions available in the literature are those due by Harding[15, 64]. A comparison between his results and those of the present solution are presented in Figures (3.13-3.16)

The comparison shows that there is a good agreement between the two solutions for cylinders loaded in axial compression (Fig.3.13-3.15).Fig.3.16 shows a comparison between the two solutions for cylinders under conbined axial compression and bending moment. Both solutions relate to the mode 6 initial imperfection and a satisfactory comparison was achieved.

The fact that Harding has used different equations and also solved his equilibrium equations in an incremental form could lead to the small discrepancies noted between the solutions.

3.14 Comparison with Experimental Data

A lot of experimental work has been carried out in the last few decades on the behaviour of unstiffened circular cylinders subjected to axial compression, but unfortunately very little information is available to enable comparisons with the present formulations to be performed. However, a few recent experiments on ring-stiffened cylinders subjected to axial compression have been performed and sufficient information is available on them so that correlation with the present formulations can be undertaken.

Walker et al[65] have carried out a series of tests on stringer-

and ring-stiffened shells and the results compared against theoretical ones generated by a finite element formulation. The experimental and theoretical stress-strain curves of one bay ring-stiffened cylinder are plotted against the corresponding curve produced by the present formulation (Fig. 3.10). The comparison shows a 12% overestimation of the average stress-strain curve peak. This sort of discrepancy was expected since no residual stresses were taken into account in the present analysis. Another recent series of experiments on ring-stiffened cylinders subjected to axial loading has been carried out by Harding and Dowling[21,66]. These cylinders were 3-bay ring-stiffened cylinders. Figure (3.11) and (3.12) show theoretical stress-strain curves produced by a theoretical formulation[15] using as input, data from the experiments. The experimental collapse load is also noted. The same experimental data have been used to carry out the analysis with the present formulation. The analysis was based on zero residual stresses and on axisymmetric imperfections having wave amplitude of 0.20 mm. The predictions for the collapse loads seem to be within reasonable range considering the uncertainty of the factors involved during the experiments.

CHAPTER 4

BEAM-COLUMN OVERALL AND LOCAL INTERACTIVE BUCKLING ANALYSIS

4.1 Introduction

In this chapter the development of a formulation capable of performing a beam-column analysis in which local shell buckling is also possible is presented. Local shell buckling is treated using the cylindrical shell analysis developed in the previous chapter.

Mesh convergence studies are reported and comparisons between solutions produced by the analysis as programmed and other numerical and experimental results are presented.

4.2 Kinematic Relationships

For the following derivations, several assumptions were made: These are,

i) Bending of the beam-column is in one plane;

ii) Plane sections remain plane after deformation;

iii) Fibres remain normal to the deflected axes after deformation, i.e. shear deformation is neglected.

The figures below show a one-dimensional element before and after straining.

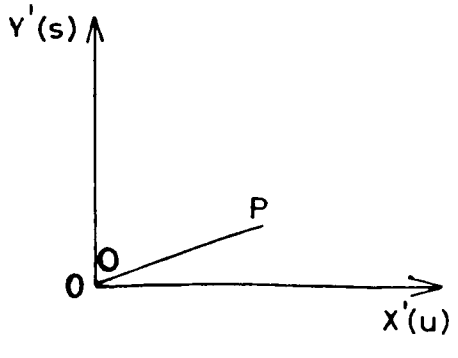

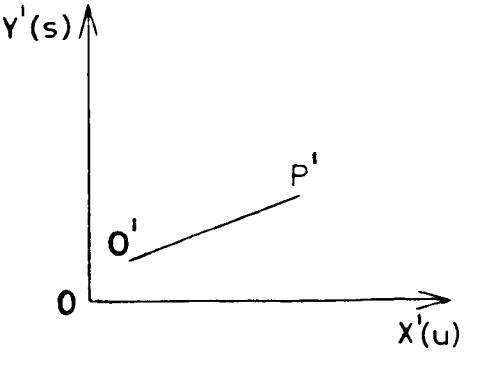

The co-ordinates of O, P and O', P' are given in the following table.

	x	y
O	O	s_o
P	δx	$s_o + \frac{ds_o}{dx}\delta x$
O'	u	$s + s_o$
P'	$u + \delta x + \frac{du}{dx}\delta x$	$s + s_o + \left(\frac{ds}{dx} + \frac{ds_o}{dx}\right)\delta x$

Following the procedure descibed in Section 3.2.3 the in-plane strain (ε_x^s) can be derived. For convenience,

$$s_{o_x} = \frac{ds_o}{dx}, \quad s_x = \frac{ds}{dx}, \quad u_x = \frac{du}{dx}, \quad s_{xx} = \frac{d^2s}{dx^2}$$

In this case,

$$(OP)^2 = (1 + s_{o_x}^2)\delta x^2$$

and

$$(O'P')^2 = (1 + u_x)^2\delta x^2 + (s_x + s_{o_x})^2\delta x^2$$

From equation (3.5)

$$\varepsilon_x^s = \frac{(O'P')^2 - (OP)^2}{2(OP)^2}$$

or

$$\varepsilon_x^s = \frac{(1 + u_x)^2\delta x^2 + (s_x + s_{o_x})^2\delta x^2 - (1 + s_{o_x}^2)\delta x^2}{2(1 + s_{o_x}^2)\delta x^2}$$

$$= \frac{1}{2}(1 + u_x^2 + 2u_x + s_x^2 + s_{o_x}^2 + 2s_x s_{o_x} - 1 - s_{o_x}^2)(1 + s_{o_x}^2)^{-1}$$

$$= \frac{1}{2}(u_x^2 + 2u_x + s_x^2 + 2s_x s_{o_x})(1 - s_{o_x}^2)$$

$$= u_x + \frac{1}{2}(u_x^2 + s_x^2 + 2s_x s_{o_x}) \qquad (4.1)$$

Finally, after the deletion of the $\frac{1}{2}u_x^2$ term from equation (4.1), for

the reason advanced in Section (3.2.3), the in-plane strain takes its final form.

$$\varepsilon_x^s = u_x + \frac{1}{2}(s_x^2 + 2s_{o_x}s_x) \tag{4.2}$$

As shown in the figure below, the curvature k_s and the radius of curvature R_s are related to the column deflection s by

$$k_s = \frac{1}{R_s} = -\frac{s_{xx}}{(1 + s_x^2)^{3/2}} \tag{4.3}$$

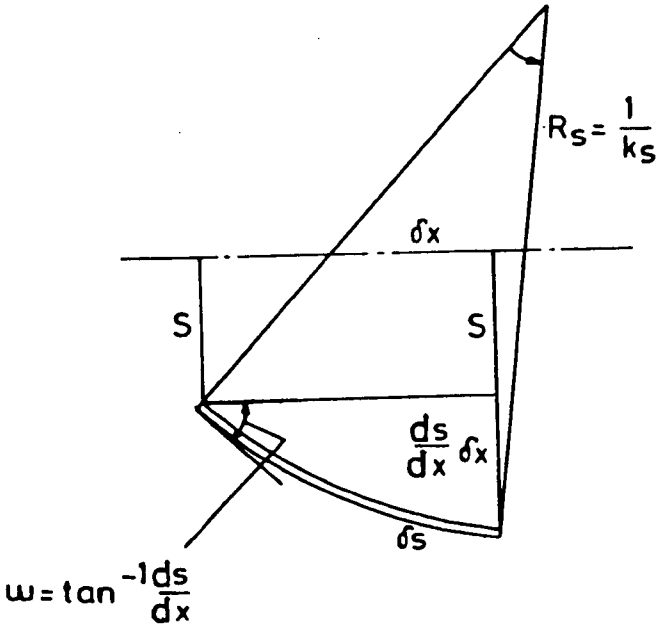

At this stage, a further assumption is made to help simplification. This is that the deflection is small so that the angle ω in radians is very small compared with unity; thus

$$s_x << 1 , \quad \sin\omega \simeq \omega , \quad \cos\omega \simeq 1 , \quad \tan\omega \simeq \omega ,$$

$$\omega = s_x , \quad \delta x \simeq \delta\alpha$$

Using this assumption the curvature (4.3) simplifies to

$$k_s = -s_{xx} \tag{4.4}$$

These kinematic relationships are valid only when the column is treated as a one-dimensional element.

In order to extend the formulation for circular cylindrical shells derived in Sections (3.2-3.4) to take into account column instability as well, the following formulation for the generalised kinematics has been employed and is illustrated in Figure (4.1).

$$\varepsilon_x^G = \varepsilon_x + (\varepsilon_x^s + k_s R\cos\theta) - u_x \qquad (4.5)$$

and

$$k_x^G = k_x - k_s\cos\theta \qquad (4.6)$$

where ε_x and k_x refer to the local behaviour of the shell wall: they are given by equations (3.12) and (3.15) respectively.

The term in brackets in equation (4.5), represents the effect of the axial strain (ε_x^s) at the shell wall. Similarly the effect of the overall curvature (k_s) has been resolved around the shell wall by $k_s\cos\theta$.

The u_x term is subtracted from equation (4.5) since it is included in both expressions for ε_x and ε_x^s.

4.3 Derivation of Governing Equations

The figure below shows a simply supported initially straight beam-column of length L which is subjected to an axial force P, and a uniform lateral load Q(x).

In order to examine the stability of the column it is necessary to consider the equilibrium of the column in its deflected form as shown by the solid line in the figure[67].

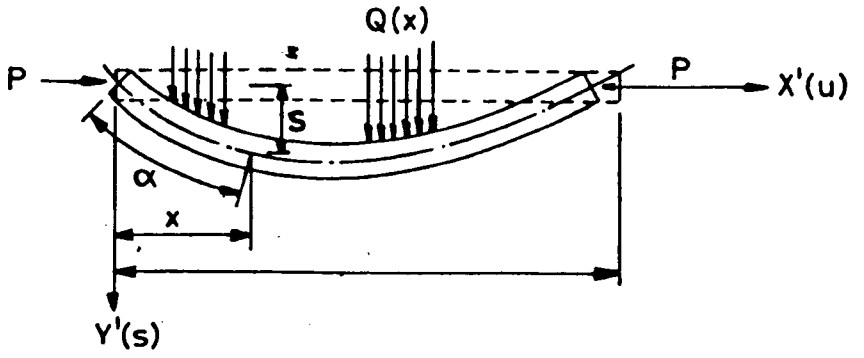

The stress resultants N and Q, namely the normal and shear forces, are normal and tengential to the cross-section of the column, and both can be resolved into horizontal and vertical forces, as shown in the following pair of figures.

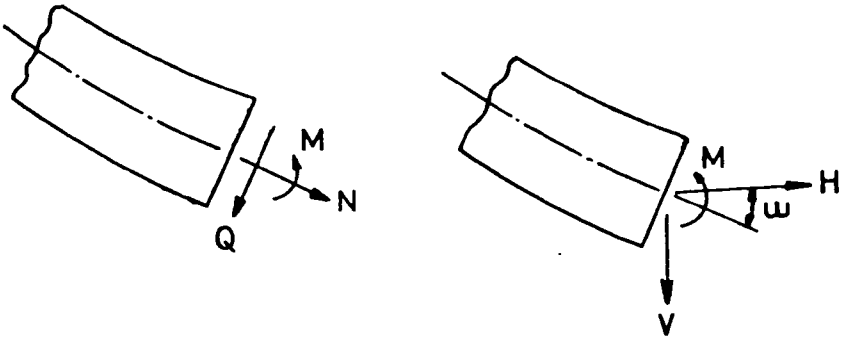

Horizontal Force : $H = N\cos\omega - Q\sin\omega$

Vertical Force : $V = H\sin\omega + Q\cos\omega$

Bending Moment : $M = M$

Now, considering a column element in the equilbirium state, as shown in the figure below, three equilbirium equations can be derived.

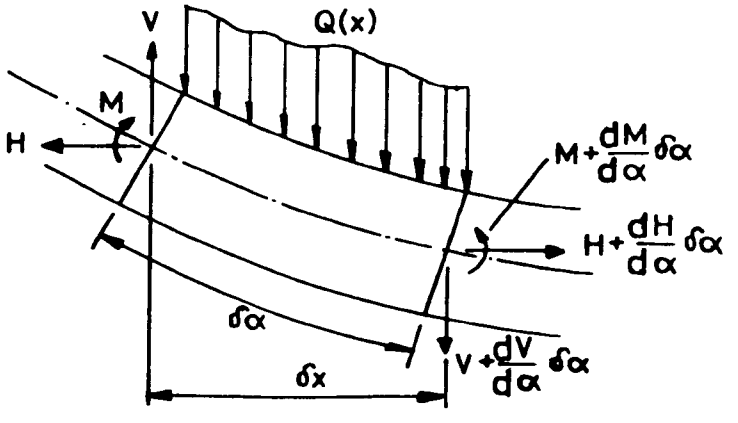

$$\text{Horizontal Force : } H + \frac{dH}{d\alpha}\delta\alpha - H = 0$$

$$\text{Vertical Force : } V + \frac{dV}{d\alpha}\delta\alpha - V + Q(x)\delta\alpha = 0$$

$$\text{Bending Moment : } M + \frac{dM}{d\alpha}\delta\alpha - M - \frac{\delta\alpha}{2}\left(V + \frac{dV}{d\alpha}\delta\alpha + V\right)\cos\omega + \frac{\delta\alpha}{2}\left(H + \frac{dH}{d\alpha}\delta\alpha + H\right)\sin\omega = 0$$

Since $\left(\frac{dV}{d\alpha}\right)\delta\alpha$ and $\left(\frac{dH}{d\alpha}\right)\delta\alpha$ are negligibly small compared with V and H, these equations reduce to

$$\frac{dH}{d\alpha} = 0$$

$$\frac{dV}{d\alpha} + Q(x) = 0$$

$$\frac{dM}{d\alpha} - V\cos\omega + H\sin\omega = 0$$

Applying small deflection theory, $dx \simeq d\alpha$ and

$$\frac{dH}{dx} = 0 \tag{4.7a}$$

$$\frac{dV}{dx} + Q(x) = 0 \tag{4.7b}$$

$$\frac{dM}{dx} - V + Hs_x^t = 0 \tag{4.7c}$$

where

$$s_x^t = s_x + s_{o_x} \tag{4.8}$$

Differentiating equation (4.7c) with respect to x,

$$M_{xx} - V_x + H_x s_x^t + Hs_{xx}^t = 0 \tag{4.9}$$

Substituting for V_x and H_x from equations (4.7a) and (4.7b) respectively and noting H = -P, the final form of the moment equilibrium equation is

$$M_{xx} + Q(x) - Ps_{xx}^t = 0$$

or

$$M_{xx} - P(s_{xx} + s_{o_{xx}}) + Q(x) = 0 \tag{4.10}$$

At any cross section, distance x from the origin, the stress resultant N (=H) and the bending moment M, are obtained by summing the local stress resultants (N_x) and their moments about a diameter of the cross section,

$$N = \sum_{j=1}^{j_m} (N_x)_j \tag{4.11}$$

$$M = \sum_{j=1}^{j_m} (N_x R\cos\theta)_j \tag{4.12}$$

where j_m is the number of circumferential nodes.

In order to introduce the column failure mode into the formulation for circular cylindrical shells derived in Section (3.4), equation (4.10) has been added to the system of equation (3.21). Equation (3.21c) has also been modified to account for the column deflection. This was achieved by including the term

$$-N_x\left(\frac{d^2s}{dx^2} + \frac{d^2s_o}{dx^2}\right)\cos\theta \tag{4.13}$$

The adapted system of equations is clearly stated below.

$$\frac{dM^2}{dx^2} - P\left(\frac{d^2s}{dx^2} + \frac{d^2s_o}{dx^2}\right) + Q(x) = 0 \tag{4.14a}$$

$$\frac{\partial N_x}{\partial x} + \frac{1}{R}\frac{\partial N_x}{\partial \theta} = 0 \tag{4.14b}$$

$$\frac{\partial N_{x\theta}}{\partial x} + \frac{1}{R}\frac{\partial N_\theta}{\partial \theta} = 0 \tag{4.14c}$$

$$\frac{\partial^2 M_x}{\partial x^2} + \frac{2}{R}\frac{\partial^2 M_x}{\partial x \partial \theta} + \frac{1}{R^2}\frac{\partial^2 M_\theta}{\partial \theta^2} + \frac{N_\theta}{R} + N_x\left(\frac{\partial^2 w}{\partial x^2} + \frac{\partial^2 w_o}{\partial x^2}\right)$$
$$- N_x\left(\frac{d^2s}{dx^2} + \frac{d^2s_o}{dx^2}\right)\cos\theta + \frac{2}{R}N_{x\theta}\left(\frac{\partial^2 w}{\partial x \partial \theta} + \frac{\partial^2 w_o}{\partial x \partial \theta} - \frac{\partial v}{\partial x}\right)$$
$$+ \frac{N_\theta}{R^2}\left(\frac{\partial^2 w}{\partial \theta^2} + \frac{\partial^2 w_o}{\partial \theta^2} - \frac{\partial v}{\partial \theta}\right) + p = 0 \tag{4.14d}$$

4.4 Discretisation of Beam-Column

The method of discretisation of the beam-column is similar to that described in Section (3.6), but with the addition of several extra

quantities. These are s, ε_x^s, k_s and M which are defined at the (•) positions as shown in Figure (3.18).

First and second derivatives of the deflection s were determined in a manner similar to that used for the w displacement in Section (3.6), namely,

$$\left(\frac{ds}{dx}\right)_i = \frac{s(i+1) - s(i-1)}{2\Delta x} \tag{4.15}$$

$$\left(\frac{d^2s}{dx^2}\right)_i = \frac{s(i+1) - 2s(i) + s(i-1)}{\Delta x^2} \tag{4.16}$$

The second derivative of moment (M) was defined similarly.

4.5 Yield Criterion

The Multilayer approach has been used throughout the column analysis as described in Section (3.5.3). The 5-layer formulation was again employed to cater for integration through the thickness of the column wall.

4.6 Imperfections

A sinusoidal deflection shape was assumed for the column in the form

$$s_o = s_o^* \sin\left(\frac{m_s x \pi}{L}\right) \tag{4.17}$$

where s_o^* is the amplitude of the wave and m_s the number of longitudinal half waves. Three different levels of s_o^* were chosen: i) L/2000, ii) L/1000, iii) L/500. These levels cover the practical range of column imperfections ($s_o^* \simeq$ L/1500), and the DNV ($s_o^* \leq$ L/667) and the API ($s_o^* \leq$ L/1000) tolerance requirements[68,69].

One half wave (m_s = 1) was assumed since this approximates the most common imperfection mode that is encountered in practice. It also represents the critical buckling mode for a simply-supported column.

4.7 Boundary Conditions

In the column formulation, both simply supported and clamped end boundary conditions were included. Since rigid boundaries were considered with respect to the Y'-direction, the s-displacement was taken equal to zero.

Boundary conditions in relation to local behaviour were the same as those used previously (Section 3.8).

The boundary conditions are discussed in more detail in Section (4.9.1).

4.8 Loading

Axial loading was applied by means of increments of in-plane displacement (u_b).

In the simply supported column case, rotation of the ends had to be permitted. This was accomplished by allowing the column ends to rotate at an angle ϕ until the bending moment at the ends became zero. The angle ϕ in radians was calculated by using a dynamic relaxation formulation, namely,

$$\dot{\phi} = \frac{1 - \frac{k_\phi}{2}}{1 + \frac{k_\phi}{2}} \dot{\phi}_p + \frac{M_b}{I} \frac{\Delta t}{\rho_\phi \left(1 + \frac{k_\phi}{2}\right)} \tag{4.18}$$

followed by integrating $\dot{\phi}$ with respect to time

$$\phi = \phi_p + \dot{\phi}\Delta t \tag{4.19}$$

where $\dot{\phi}$, $\dot{\phi}_p$ are current and previous values of angular velocities and ϕ, ϕ_p are current and previous values of angles. k_ϕ and ρ_ϕ are the damping factor and the fictitious density respectively. I is the moment of inertia of column cross-section.

Due to high values of the moment compared with those of the angle ϕ, the moment was scaled using the section moment of inertia. This accelerated the convergence of the value of the angle ϕ.

Because of the rotation ϕ, the in-plane displacements (u_b) are no longer uniform over the cross-section. They vary linearly along the diameter of the cross-section as shown in the figure below.

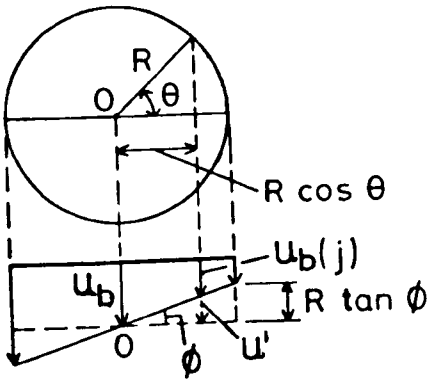

From the above figure,

$$u_b(j) = u_b - u' \tag{4.20}$$

Using similarity of triangles,

$$\frac{u'}{R\tan\phi} = \frac{R\cos\theta}{R}$$

or

$$u' = R\cos\theta\tan\phi$$

Equation 4.20 becomes

$$u_b(j) = u_b - R\cos\theta\tan\phi \tag{4.21}$$

4.9 Adaptation of the Numerical Technique

4.9.1 *Derivation of Fictitious Nodes*

Arising from discretisation of the beam-column, the first and second derivatives of the s-displacement need to be calculated at the boundaries. For this purpose, a value of s is required at a fictitious node.

In the case of a column with simply supported ends, the bending

moment at the boundaries is zero. Assuming that boundaries will remain elastic in this case, the expression for the bending moment can be written as

$$M_b = \frac{EI}{R_s},$$

or

$$M_b = -EIs^b_{xx} \tag{4.22}$$

Therefore,

$$s^b_{xx} = 0$$

or

$$\frac{s_{in} - 2s_b + s_f}{\Delta x^2} = 0$$

or

$$s_f = 2s_b - s_{in} \tag{4.23}$$

where s_b, s_{in} and s_f are the column deflections at the boundary, internal and fictitious node respectively.

In the case of a column with clamped boundaries the slope $\frac{ds}{dx}$ at the ends is taken equal to zero, namely

$$\frac{s_{in} - s_f}{2\Delta x} = 0$$

or

$$s_f = s_{in} \tag{4.24}$$

The expression (3.67b) for calculating the w-displacement at fictitious nodes had to be adjusted accordingly for simply supported ends. Following a similar procedure to that in Section (3.9.1), expression (3.67b) becomes

$$w_f = 2w_b - w_{in} - \Delta x^2 k^p_x + \Delta x^2 (R_x \Delta\varepsilon_x + \ldots + D_{x\theta} \Delta k_{x\theta} + M^p_x)/Dx$$

$$+ \Delta x^2 s_{xx} \cos\theta \tag{4.25}$$

When clamped boundaries are considered the slope $\frac{\partial w}{\partial x}$ at the ends was assumed equal to zero, namely

$$\left(\frac{w_{in} - w_f}{2\Delta x}\right)_j = 0$$

or

$$(w_f)_j = (w_{in})_j \tag{4.25}$$

The fictitious in-plane displacement (u_f) was found by assuming a linear variation of the u-displacement,

$$\left(\frac{u_{in} + u_f}{2}\right)_j = u_b(j)$$

or

$$u_f(j) = 2u_b(j) - u_{in}(j) \tag{4.27}$$

4.9.2 *Derivation of Fictitious Densities*

In this section, only the fictitious densities related to the s-displacements will be derived since fictitious densities for u, v and w displacements have been derived already in Section (3.92).

An adjustment in the density for w-displacement was necessary to account for the extra term in expression (4.13). Thus, relation (3.7a) becomes

$$\rho_w(i,j) = 0.25\left[b_w(i,j) + (\overline{N_x})_{i,j}\left(\left|\frac{d^2s}{dx^2}\right| + \left|\frac{d^2s_o}{dx^2}\right|\right)_i + \frac{4}{\Delta x^2}\,|N_x|_{i,j}\right] \tag{4.28}$$

Adapting equation (2.8)

$$\rho_s(i) = 0.25 b_s(i) \tag{4.29}$$

Using equation 4.14a, an expression for $b_s(i)$ can be developed,

$$b_s(i) = \left(\overline{\frac{d^2M}{dx^2}}\right)_i + |P|_i\left(\overline{\frac{ds^2}{dx^2}} + \overline{\frac{d^2s_o}{dx^2}}\right)_i + \overline{P}(i)\left(\left|\frac{ds^2}{dx^2}\right| + \left|\frac{d^2s_o}{dx^2}\right|\right)_i \tag{4.30}$$

where

$$\left(\overline{\frac{d^2M}{dx^2}}\right)_i = \frac{\overline{M}(i+1) + 2\overline{M}(i) + \overline{M}(i-1)}{\Delta x^2} \tag{4.31}$$

From equation (4.11)

$$\overline{P}(i) = \sum_{j=1}^{j_m} \overline{N}_x(i,j) \tag{4.32}$$

and from equation (4.12)

$$\overline{M}(i) = \sum_{j=1}^{j_m} \{\overline{N_x(i,j)R\cos\theta}\}$$

$$\simeq R \sum_{j=1}^{j_m} \overline{N}_x(i,j) \tag{4.33}$$

Substituting equation (4.32) into (4.33), equation (4.33) becomes

$$\overline{M}(i) = \overline{P}(i)R \tag{4.34}$$

Now, by introducing equation (4.34) into equation (4.31),

$$\left(\overline{\frac{d^2M}{dx^2}}\right)_i = \frac{R}{\Delta x^2}\{\overline{P}(i+1) + 2\overline{P}(i) + \overline{P}(i-1)\} \tag{4.35}$$

Recalling equation (4.16)

$$\left(\overline{\frac{ds^2}{dx^2}}\right)_i = \frac{4}{\Delta x^2} \tag{4.36}$$

Using equations (4.29), (4.30), (4.35) and (4.36) the fictitious densities $\rho_s(i)$ can be explicitly calculated.

$$\rho_s(i) = 0.25\left[\frac{R}{\Delta x^2}(\overline{P}(i+1) + 2\overline{P}(i) + \overline{P}(i-1)) + \frac{4}{\Delta x^2}|P(i)| + \overline{P}(i)\left(\left|\frac{d^2s}{dx^2}\right| + \left|\frac{d^2s_o}{dx^2}\right|\right)_i\right] \tag{4.37}$$

The fictitious density (ρ_ϕ) related to angle ϕ (Section 4.8) was set so

$$\rho_\phi = 0.25(\overline{P_b}) \tag{4.38}$$

This is an empirical relation which gives satisfactory convergence.

Both fictitious densities, $\rho_s(i)$ and ρ_ϕ, were found to vary with (L/r). This problem was resolved by introducing density factors, d_f^s and d_f^ϕ, to scale down the densities given by expressions (4.37) and (4.38) respectively. For easy reference, d_f^s and d_f^ϕ as used in the present analyses have been plotted against L/r. The graphs are presented in Figures (4.2, 4.3).

4.10 Flow Chart

The following flow chart shows the main stages of the ANSA2 program based on the formulation developed in this chapter. The program consists mainly of two loops, the DR iterative loop and the load increment one. At the end of the DR iterative loop, presuming convergence has been achieved, all the nodes are examined for yielding. If yielding has occurred, the elasto-plastic rigidities are calculated according to the flow chart on page 98. These values are saved for use in the next load increment.

In the case of a column with simply supported ends, end rotations are applied inside the DR iterative loop.

At the end of each load increment, required values for the next load increment are stored as discussed in Section 3.11.

Graphics can also be produced at a specified frequency of load increments in the manner described in Appendix II.

ANSA 2

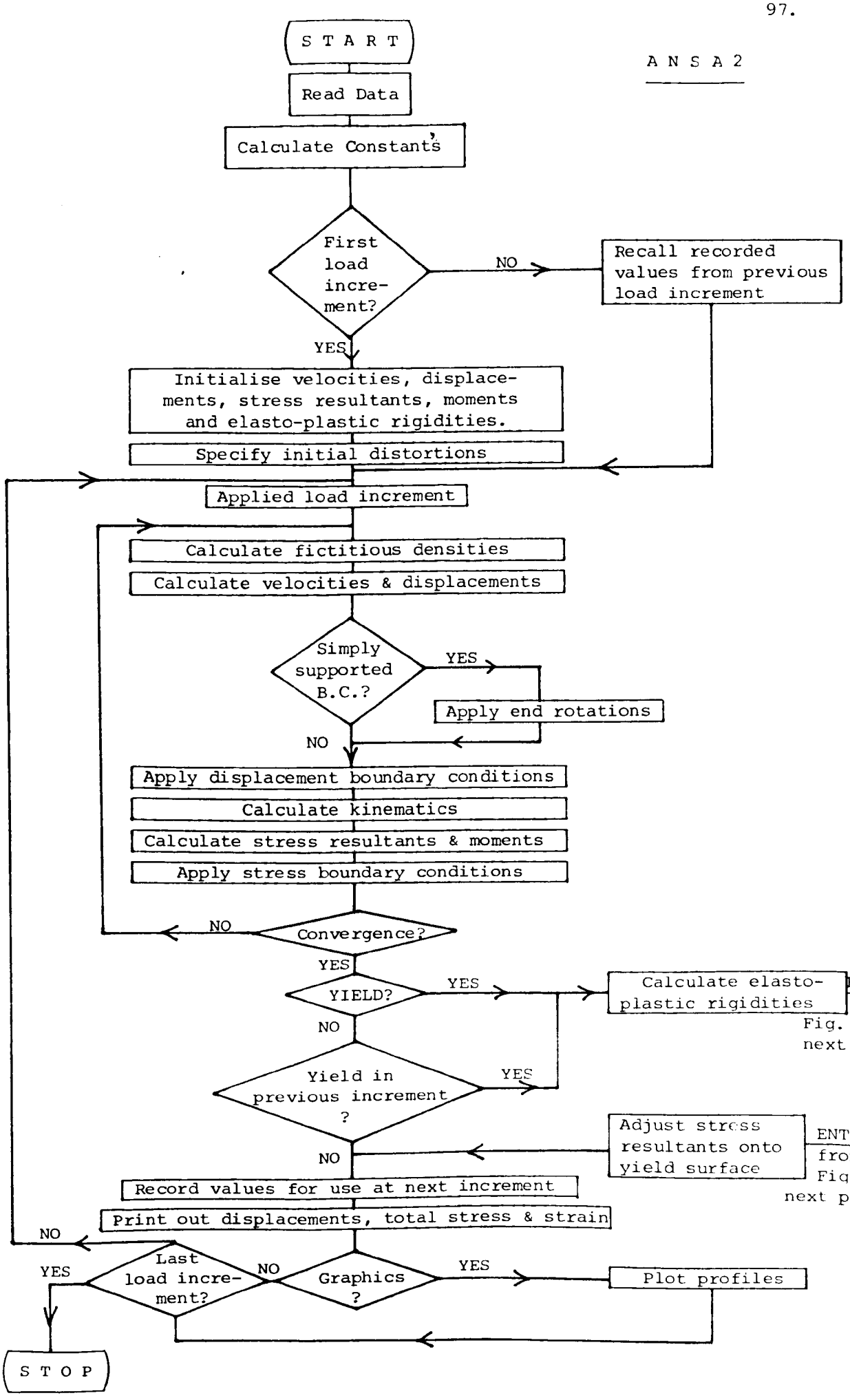
START
Read Data
Calculate Constants
First load increment?
NO
Recall recorded values from previous load increment
YES
Initialise velocities, displacements, stress resultants, moments and elasto-plastic rigidities.
Specify initial distortions
Applied load increment
Calculate fictitious densities
Calculate velocities & displacements
Simply supported B.C.?
YES
Apply end rotations
NO
Apply displacement boundary conditions
Calculate kinematics
Calculate stress resultants & moments
Apply stress boundary conditions
NO
Convergence?
YES
YIELD?
YES
Calculate elasto-plastic rigidities
EXI
Fig.
next pa
NO
Yield in previous increment ?
YES
Adjust stress resultants onto yield surface
ENTER
from
Fig.
next page
NO
Record values for use at next increment
Print out displacements, total stress & strain
NO
YES
Last load increment?
NO
Graphics ?
YES
Plot profiles
STOP

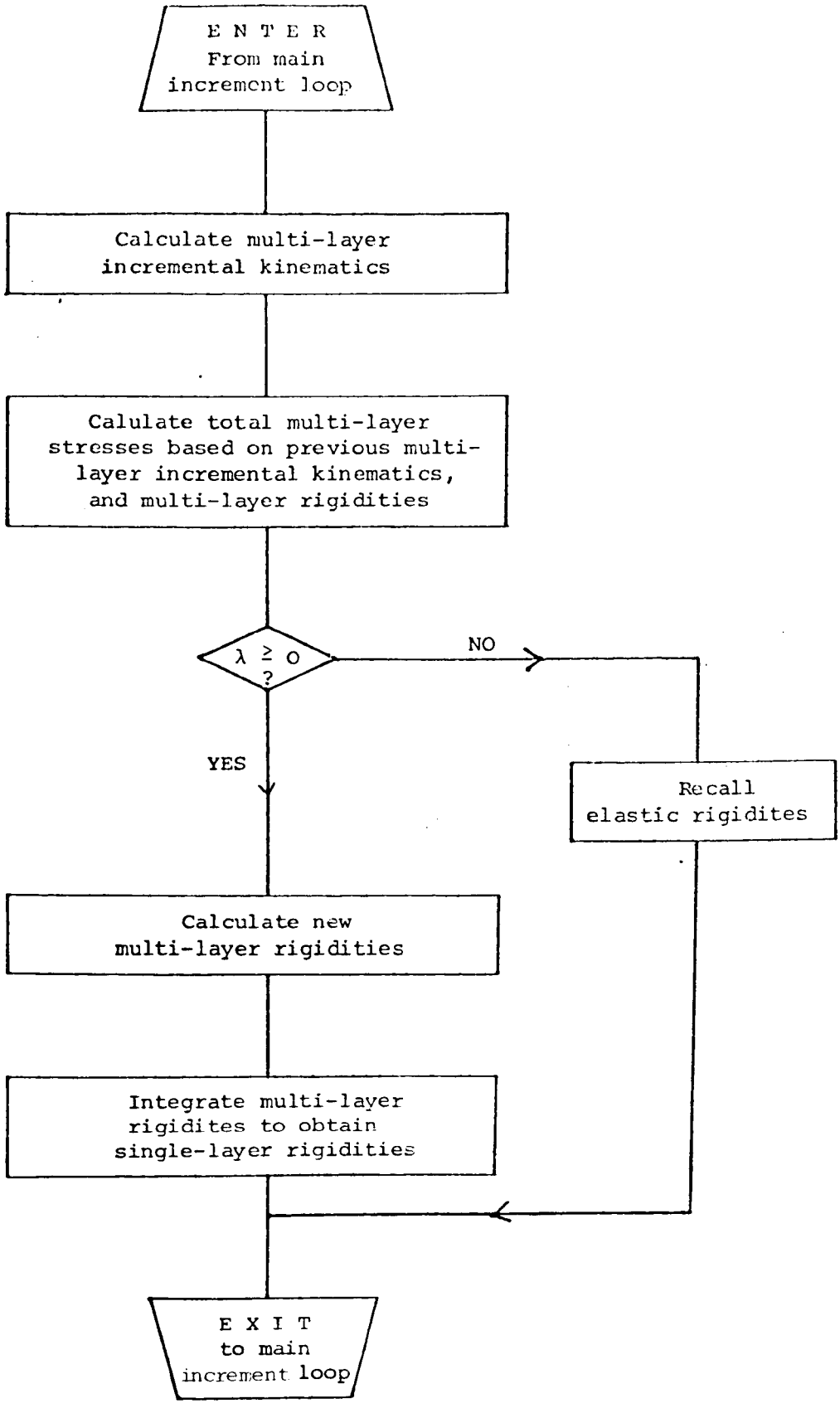

FLOW CHART FOR THE CALCULATION OF SINGLE-LAYER RIGIDITIES USING THE MULTI-LAYER APPROACH

4.11 Convergence Studies

Convergence studies were undertaken once the analysis was found to be performing satisfactorily. Three different mesh sizes were adequate to carry out the studies: the meshes used were 4 x 16, 6 x 16, 8 x 16. The procedure described in Section (3.12) was again used here. The number of nodes around the circumference was kept constant, in this case 16, and the number of nodes along the half length of the column was varied. The 4 x 16 mesh size gave rather higher results than the other two as can be seen in Figures (4.4, 4.5). Eight nodes were selected to undertake all the analyses. No influence of L/r was noticed on the required mesh size.

Variation of the number of nodes around the circumference did not affect the results significantly as can be seen in Figures (4.6, 4.7). The mesh-size finally selected to carry out the analyses was 8 x 16.

4.12 Comparison with Other Solutions

Smith et al recently developed a theoretical beam-column formulation which was used to back up their experimental work[34].

This formulation was based on a plane-frame analysis. The formulation accounts for initial deformation, residual stresses, load eccentricity, but no local buckling. Typical average stress-strain curves have been extracted from Reference (34) and plotted against respective ones generated by the present formulation (Fig.4.8,4.9): both solutions seem to give very similar results. Figure (4.10) shows a complete comparison between the two solutions regarding variation of collapse loads with slenderness for three different levels of column initial bow.

4.13 Comparison with Experimental Data

The most recent experimental work is that due to Smith et al [34] as previously indicated. Two examples were selected from their work and correlation between those and the respective solutions produced by the present formulation was attempted.

The first example is illustrated in Figure(4.11a) and shows a comparison between the theoretical and experimental average stress-strain curves from Reference (34) and the corresponding theoretically based curves produced by the present formulation. Figure (4.11b) compares the corresponding displacements.

There is a good correlation between the theoretical and experimental results as can be seen in Figure (4.11) regarding prediction of maximum load capacity. After reaching the peak a sudden drop in load occurs in the present solution. This is due to the fact that snap-back has taken place which cannot be traced with the current technique.

Figure(4.12a) shows the comparison for the second example between the theoretically and experimentally derived average stress-strain curves. Figure(4.12b) shows the corresponding total displacements. These tubular members failed by local instability as is illustrated in Figure (6.224) where profiles of the deformed column can be seen.

CHAPTER 5

SIMPLIFIED APPROACH TO BEAM-COLUMN INTERACTIVE BUCKLING

5.1 Introduction

This chapter presents a detailed formulation for analysing interaction between local shell and overall buckling behaviour in cylindrical columns, comments on its capabilities and shows comparisons between solutions generated by the proposed analysis and other theoretical and experimental solutions.

5.2 Theoretical Approach

5.2.1 *Seeking a Suitable Method*

The beam-column formulation developed in the previous chapter presented a limited capability for undertaking interactive buckling analyses. This restriction was caused by the fact that the number of nodes produced by length-wise discretisation of the column was insufficient. A large increase in the number of nodes could have produced solutions, but at a tremendous increase in the requirement for computing time. This approach seemed to be a rather optimistic aspiration with the presently available computing facilities and so a search for an alternative approach seemed necessary.

Several theoretical approaches were surveyed and attempted in practice, but most of them were rejected mainly for their complexity and the difficulty in adapting the numerical technique to the problem in hand. The approach finally employed seemed to be reasonably adaptable and less complex.

5.2.2 *Theoretical Formulation*

Two basic assumptions were necessary for this approach. The first was that the deflected shape of the column was always sinusoidal. The second implied that local failure of the column wall would occur at the middle section of the column. The analysis would thus consist of a beam-column solution for overall buckling combined with a shell buckling analysis of a limited length of cylinder at mid-length of the column.

A suitable mesh was adapted for the middle part of the column of length L_s (see Fig. 5.1) and an analysis undertaken in the same manner as described in Chapter 3 . The set-up of the approach is illustrated in Figure (5.1).

The system of equations used is the same as 4.14 with the exception of the first equation (4.14a) which was used only to calculate the s-displacement (s_m) at the middle of the column. The dynamic relaxation formulation for this particular displacement is as follows:

$$\dot{s}_m = \frac{1 - \frac{k_s}{2}}{1 + \frac{k_s}{2}} (\dot{s}_m)^p + \frac{\Delta t}{\rho_m \left(1 + \frac{k_s}{2}\right)} \left[\text{lack of equilibirum}\right]_{i_m} \qquad (5.1)$$

where $(\dot{s}_m)^p$ and $\dot{s}_m$ are previous and current velocities of the displacement s_m. k_s and ρ_m are the damping factor and fictitious density respectively. The lack of equilibrium at node i_m is given by

$$\left[\text{lack of equiblibrium}\right]_{i_m} = \left(\frac{d^2M}{dx^2}\right)_{i_m} - P_{i_m}\left(\frac{d^2s}{dx^2} + \frac{d^2s_o}{dx^2}\right)_{i_m} \qquad (5.2)$$

Integrating the velocity $\dot{s}_m$ with respect to time, the displacement (s_m) can be calculated.

$$s_m = (s_m)^p + \dot{s}_m \Delta t \qquad (5.3)$$

where $(s_m)^p$ is the displacement at the previous increment.

Using the first assumption

$$s(i) = s^* \sin\left(\frac{\pi\left[(i-i_b)\Delta x + \frac{L_c - L_s}{2}\right]}{L_c}\right) \tag{5.4}$$

Evaluating expression (5.4) at the i_m node, the value of s* can be obtained.

$$s^* = \frac{s_m}{\sin\left(\frac{\pi\left[(i_m - i_b)\Delta x + \frac{L_c - L_s}{2}\right]}{L_c}\right)} \tag{5.5}$$

Differentiating s with respect to x

$$\left(\frac{ds}{dx}\right)_i = \frac{s^*\pi}{L_c} \cos\left(\frac{\pi\left[(i-i_b)\Delta x + \frac{L_c - L_s}{2}\right]}{L_c}\right) \tag{5.6}$$

Further differentiation gives

$$\left(\frac{d^2s}{dx^2}\right)_i = -\left(\frac{\pi}{L_c}\right)^2 s(i) \tag{5.7}$$

Assuming small deflection theory, the rotation ω of the ends of the central cylinder (see Fig. 5.1) is given by

$$\omega = \left(\frac{ds}{dx}\right)_{i_b}$$

$$= \frac{s^*\pi}{L_c} \cos\left(\frac{\pi(L_c - L_s)}{2L_c}\right)$$

$$= \frac{s_m \pi}{L_c} \operatorname{cotan}\left(\frac{\pi}{2} - \frac{\pi L_s}{2L_c}\right)$$

$$= \frac{s_m \pi}{L_c} \tan\left(\frac{\pi L_s}{2L_c}\right) \tag{5.8}$$

This rotation ω was used to calculate the fictitious u-displacements (u_f) in the same manner as described in Section (4.9.1).

$$u_f(j) = 2(u_b - R\cos\theta\tan\omega) - u_{in}(j) \tag{5.9}$$

Also at the boundaries of the middle section, the hoop stress (N_θ) was taken to be zero, so as to allow free expansion of the cylinder. In this way,

the w-displacement at the boundaries was obtained by using the expression for w_b in Section 3.8.

5.2.3 *Limitation of the Technique*

When conducting analyses it was found that significant increases in the R/T ratio led to major problems with the convergence of displacements. Attempts to achieve satisfactory convergence such as varying the damping factors, or introducing density factors, proved to be very time-consuming and required great experience. An effort to trace a regular pattern in the behaviour of the densities, following the success described in Section 4.9 ended unsuccessfully. The highest value of R/T that could be analysed reasonably confidently was around 40.

5.2.4 *Imperfections*

For column behaviour, sinusoidal type imperfections were used with one half wave along the length.

$$s_o(i) = s_o^* \sin\left(\frac{\pi\left[(i-i_b)\Delta x + \frac{L_c - L_s}{2}\right]}{L_c}\right)$$

5.3 Flow Chart

The flow chart shown on the next page outlines the main stages of the ANSA3 program based on the formulation developed in the present chapter. The major features of the chart have been discussed already in Section 3.11 and 4.10. The DR iterative loop has been extended to account for calculation of the s-displacement at mid-length as well as the rotations of the mid-length section. The chart on page 106 again shows the calculation of the elasto-plastic rigidities.

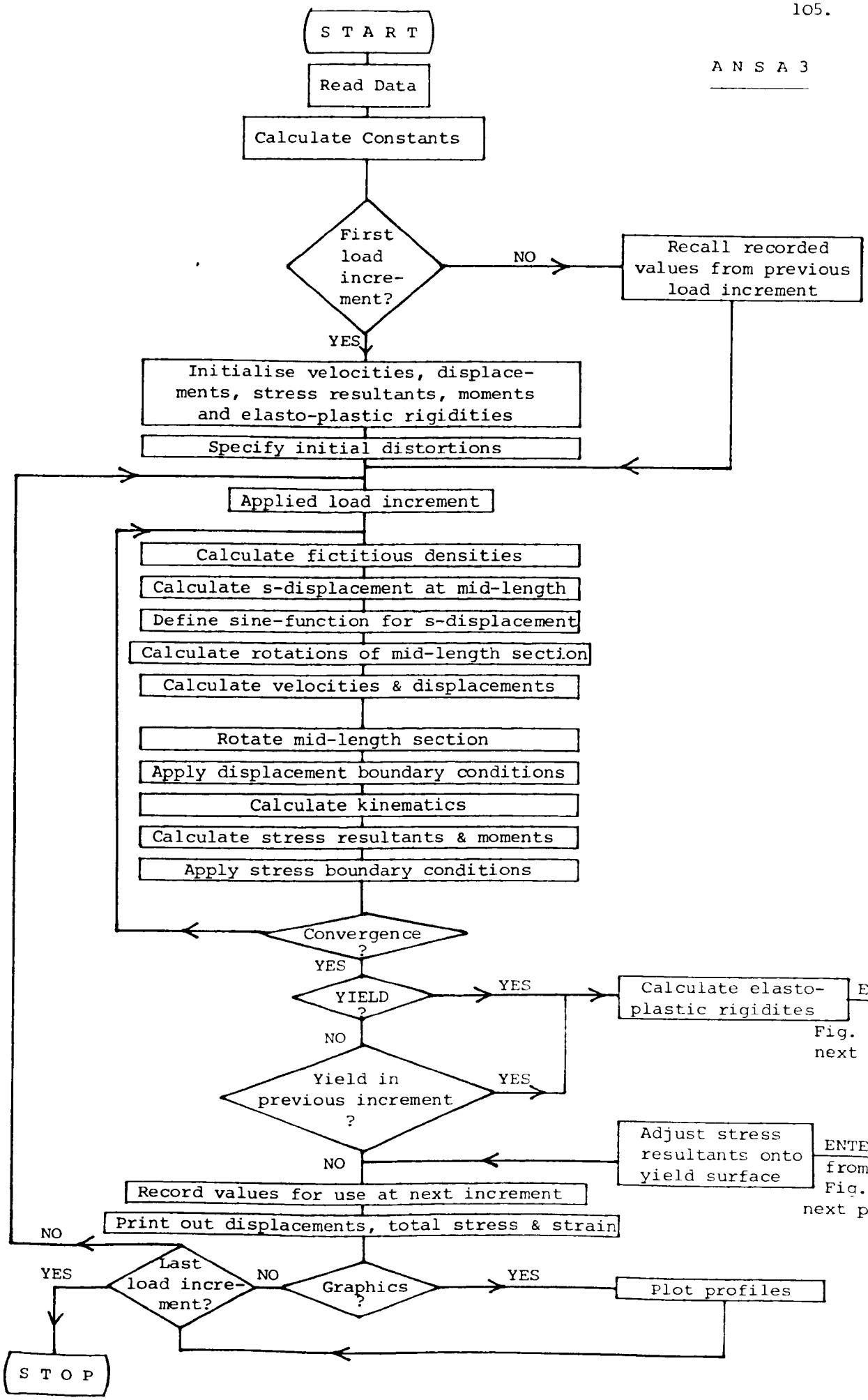
S T A R T
Read Data
Calculate Constants
First load increment?
NO
Recall recorded values from previous load increment
YES
Initialise velocities, displacements, stress resultants, moments and elasto-plastic rigidities
Specify initial distortions
Applied load increment
Calculate fictitious densities
Calculate s-displacement at mid-length
Define sine-function for s-displacement
Calculate rotations of mid-length section
Calculate velocities & displacements
Rotate mid-length section
Apply displacement boundary conditions
Calculate kinematics
Calculate stress resultants & moments
Apply stress boundary conditions
Convergence ?
YES
YIELD ?
YES
Calculate elasto-plastic rigidites
EXIT
Fig. next page
NO
Yield in previous increment ?
YES
Adjust stress resultants onto yield surface
ENTER from Fig. next page
NO
Record values for use at next increment
Print out displacements, total stress & strain
NO
YES
Last load increment?
NO
Graphics ?
YES
Plot profiles
S T O P

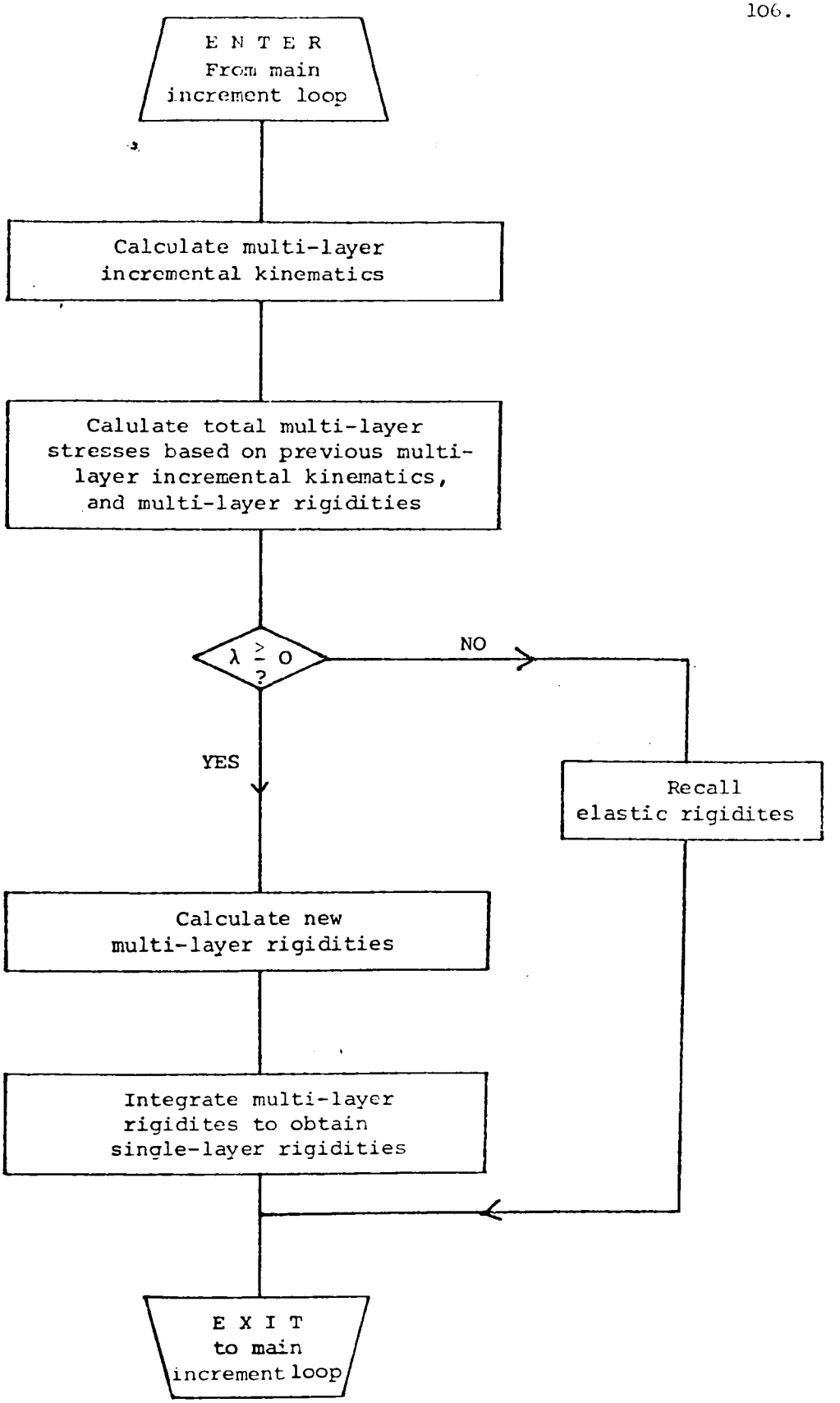

FLOW CHART FOR THE CALCULATION OF SINGLE-LAYER RIGIDITIES USING THE MULTI-LAYER APPROACH

5.4 Comparison with other Solutions

Figure (5.2a) illustrates a typical example of a column failing from overall instability as analysed by the present formulation. For comparison, a solution produced by the formulation in the previous chapter is also shown. The correlation between the two solutions is seen to be very satisfactory regarding the peaks of the average stress-strain curves, while a difference in the post-buckling paths can be observed. Figure (5.2b) shows the corresponding total displacements for the two solutions. Profiles of the deformed column wall from both solutions are shown in Figure (6.225).

5.5 Comparison with Experimental Data

The example from Reference 34 analysed by the formulation developed in Chapter 4 has also been analysed using the present technique. The comparison is shown in Figures (4.12a) and (4.12b). The present solution can be seen to produce slightly lower results compared with the previous solution. This particular tube failed by local buckling.

CHAPTER 6

PARAMETRIC STUDIES

6.1 Introduction

This chapter presents the results of parametric studies conducted firstly, on circular cylindrical shells subjected to axial compression and later to combinations of axial compression, bending and pressure and, secondly, on long columns subjected to axial compression.

6.2 Circular Cylindrical Shells

In the following studies the yield stress, Young's modulus and Poisson's ratio have remained unchanged throughout: The values used were 0.245 kN/mm^2, 207 kN/mm^2 and 0.3 respectively.

Loading of the cylinders in every example was continued until the strain (i.e. the maximum in-plane displacement at one edge divided by the half length of the shell) reached twice the yield strain.

6.2.1 Axial Compression

The radius to thickness ratios considered in this study were: 30, 100, 200, 500, 1000. This wide range covered the practical range (R/T<200) as well as that which might be proposed for weight-sensitive structures such as TLP's and semi-submersibles. These R/T ratios in conjunction with three different L/R ratios, namely, 0.10, 0.25 and 0.50 were the main parameters to be varied during the analyses. Circular cylinders having L/R ratios of this order are usually found as part of multi-bay ring stiffened cylinders in floating offshore structures. The analysis was also accompanied by a variation of mode and level of imperfection as

already discussed in Section 3.7. Average stress-strain curves have been produced for every case and plotted in groups. These groups are illustrated in Figures (6.2 - 6.25).

In mode one cases where big L/R's were involved, a steep drop of the post-peak path was observed. This steepness became more pronounced as R/T increased (Figs. 6.14 - 6.16).

This rather sudden drop was usually accompanied by a change in mode which is observed in all the cases where R/T>200. In the cases where R/T<200 the initial specified mode remained unchanged throughout the loading. On the contrary, in all mode six cases there is a smooth, almost constant load post-peak behaviour. This is due to the fact that no change of the initial mode occurred after post-peak (Figs. 6.5-7,11-13 etc.). In Figures (6.226,227) the loading history for particular examples can be seen. These particular examples were accompanied by a change of the initial mode.

Significant reduction of the elastic slopes occurs as the magnitude of imperfections increases. This can readily be seen by comparing the curves in Figures (6.2, 6.3 and 6.4).

The maximum average stresses from the above curves have been grouped and plotted, firstly, against radius-to-thickness (R/T) ratio and, secondly, against length-to-radius (L/R) ratio.

The resulting curves can be seen in Figures (6.26-41). Significant drops in strength are observed as R/T increases irrespective of the initial mode. Mode six has produced curves of lower strength than the rest of the modes while mode three is shown to produce a slight increase in strength compared with mode two. Mode one seemed to be most susceptible to L/R variation expecially when high levels of imperfections were present. For L/R greater than 0.25, this variable has little effect on strength. For values of L/R less than this, strength generally drops rapidly. However, this does not apply when R/T≤100 with the exception of modes two and

three when R/T=100. In these cases the effect is quite reversed.

The effect on strength of changing the level of imperfections was rather pronounced in all of the mode six cases (Figs. 6.29-31) and for mode one only when L/R=0.10 (Fig. 6.26). Strength in the presence of the remaining modes did not seem to be influenced significantly by increasing the level of imperfections (Figs. 6.27,6.28). Figures (6.32 and 6.33) show curves of mode two and three results respectively. The effect on strength of varying the ring spacing can be clearly seen. The strength seems to vary directly proportionally with L/R except when R/T=30 when the reverse occurs.

6.2.2 *Axial-Compression plus Bending*

For this parametric study the same R/T and L/R ratios were used as in the previous Section. Mode types and initial distortions were incorporated according to Section 3.7. Five different combinations of axial compression and bending were employed in the conduct of the study (Fig. 6.1). The results generated were grouped and plotted in the form of average stress-strain curves and moment-strain curves. The moment was non-dimensionalised by dividing by the fully-plastic moment $M_p = 4R^2t\sigma_y$. The curves are presented in Figures (6.42-102).

A significant drop in maximum axial strength was observed as R/T increased. A change of initial mode was noticed in most of the studied examples and profiles of these modes are illustrated in Figures (6.228-230). Only in some cases of low R/T ($\leq$100) ratio did the mode remain unchanged. It was also noticed that the peak of an average stress-strain curve did not necessarily correspond to the peak of the corresponding moment-strain curve. All the average stress-strain curves seem to be quite smooth and no sudden drop in the post-buckling régime was noticed. The reduction in strength tends to become smaller as R/T increases, especially for R/T$\geq$500. This was noticed in the corresponding moments as well.

A numerical increase in b (Fig. 6.1), provides the structure with

higher compressive strength while corresponding moments are dropping.

Variation of ring spacing has been shown to have a great influence on the elastic slopes of average stress-strain curves, although no significant change in the maximum compressive strength was noticed. These slopes tend to get smaller as ring spacing reduces and also to become more pronounced when R/T is large (R/T≥500).

Variation of level of imperfections has also been found to affect both the strength and the elastic slopes of average stress-strain curves.

The maximum stress from each average stress-strain curve and the corresponding moment on the moment-strain curve have been grouped and plotted (Figs. 6.103-120). In this way, non-dimensionalised interaction curves between maximum axial stress and moment have been produced. The interaction curves relating to mode one and the maximum initial deformation $w_o^* = R/400$ seem to be of the parabolic-type, while interaction curves relating to the smaller initial deformations and the rest of the modes seem to be of the linear-type.

From these figures, somewhat unusual behaviour of the interaction curve corresponding to R/T=500 can be observed, in that it tends to cross-over one of the neighbouring curves, either that of R/T=200 or R/T=1000. This seemed to happen at L/R=0.10 and L/R=0.50 and is due to the influence of mode change.

Mode two has produced slightly higher interaction curves than the mode one results, while the mode three ones are even higher (Figs. 6.117-120).

6.2.3 External Pressure plus Axial Loading and Bending

Four R/T ratios were examined in this analysis. These were 30, 100, 200 and 300. The L/R ratios were the same as in the previous Section. Again maximum deformations and mode types were incorporated according to Section 3.7. Three different pressure levels were employed: 50 m, 75 m and

100 m of water. The values of R/T and pressure level considered had to be restricted to the above ranges. This was because for further increases in pressure of R/T the strengths were so low as to have little meaning. The pressure was applied first, according to the procedure described in Section 3.9. The pressure was applied either all at once or incrementally depending on whether the cylinder entered plasticity while the pressure loading was still being applied. It was noticed that plasticity occurred at pressure levels of 70 m of water and above for the specific cases considered.

Immediately after pressure had been applied, incremental in-plane displacements were applied in a combined manner to account for axial compression and bending (Fig. 6.1). Average stress-strain and moment-strain curves have been produced and are shown in Figures (6.121-181).

It can be observed from these figures that the larger the R/T ratio, the more pronounced the pressure effect becomes. Pressure actually produced a stiffening effect at low levels of loading (pre-peak régime), while after peak the effect was reversed. This stiffening effect seemed to be rather suppressed in the case of L/R=0.10. The cylindrical shells studied under this rather complex loading showed great susceptibility in changing their initial mode. These occurred more than once during the loading cycle resulting in rather complicated and unpredictable modes. Pressure, as can be seen from the figures, did not affect the peaks in the average stress-strain curves as much as it did response in the post-peak régime.

Variation of level of imperfections affected the elastic slopes significantly especially when $w_o^* = R/400$, but not the maximum compressive strength to the same extent. This applies primarily to L/R=0.10, while for the other L/R ratios the effect was different. For these there was no influence on elastic slopes, but greater drops in strength in the post-peak régime were produced.

The average stress-strain curves within each group tend to cross-over one another either in the early or the later stages of loading, with some exceptions of, for example, the curves presented in Figures (6.121a) and (6.130a). The behaviour of the moment-strain curves seems also to be rather complex following a non-uniform pattern. In many examples (e.g. Fig. 6.121b) the curves also tend to intersect one another more than once. Again as in the previous examples, there is no correspondence between maximum compressive strength and maximum moment.

The maximum average stress and corresponding moment from each example have been grouped and plotted. These interaction curves between maximum stress and moment for each pressure level are shown in Figures (6.182-200).

Reducing the L/R ratio is seen to produce a drop in strength, especially in cases with large R/T's ($R/T \geq 200$). The effect on strength of varying the level of maximum deformation was insignificant. A comparison between mode one and mode six results showed no significant differences (Fig. 6.182-200). This supported the generation of the limited number of points presented in Figures (6.196-200). Deformations are shown in Figures (6.231-233).

The pattern of the interaction curves is seen not to be consistent. Part of this arises from the fact that the peaks in the stress-strain curves occur at significantly different levels of strain, for example see Figure (6.131a).

6.2.4 *Residual Axial-Compressive Strength of Damaged Cylinders*

In the following study an attempt was made to demonstrate the capability of the developed formulation (ANSA1) to undertake an analysis to assess the residual strength of damaged cylinders. Simulation of damage was achieved by applying a point load at mid-length of the cylinder. The cylinder was assumed to be perfect and loading was continued until no further satisfactory numerical convergence could be achieved. From three points along the loading path, unloading paths were produced to provide

three levels of damage. The applied point load in kN has been plotted against the corresponding deformation-to-thickness ratio (Figs. 6.201a-203a).

The early stage of the curves can be seen to rise steeply but this rapidly gives way to a long section of the response which is parabolic in nature. The broken line indicates the variation of permanent set with load.

Immediately after unloading, the cylinder was subjected to axial compression. The resulting average stress-strain curves are shown in Figures (6.201b-203b). As can be observed, the extent of damage does not effect the initial response of the cylinder, but mainly influences the onset and spread of plasticity with a consequential loss in maximum strength. Figure (6.204) shows maximum stress plotted against maximum deformation-to-thickness ratio: the loss of strength is not seen to be very significant for the range of damage investigated. For example, a three-fold increase in damage in a cylinder of R/T=100 and L/R=0.25 produced a drop in compressive strength of some 10%. Configurations from damaged profiles can be seen in Figure (6.234).

6.3 Beam-Column Elasto-Plastic Results

In the following study eight different length-to-radius of gyration ratios (L/r) were selected to cover the range of non-dimensional slenderness up to three, i.e. $\lambda=3$. These L/r ratios were 30, 50, 70, 90, 120, 160, 200 and 240. The yield stress, Young's modulus and Poisson's ratio had values 0.324 kN/mm^2, 207 kN/mm^2 and 0.3 respectively, which were kept constant throughout the study. It dealt mainly with simply-supported boundaries, with the exception of a few examples having clamped ends. The R/T ratios were selected from the region R/T≤30 where local buckling would have no affect. In the simply-supported cases the R/T ratio selected was 10 and in the cases where clamped ends were assumed, 17.5. Actually, no significant variation in collapse stress was noticed by using different R/T ratios from this range. Initial distortions were incorporated according to Section 4.6. The loading procedure has already been discussed in Section 4.8.

Average stress-strain and applied load-total displacement curves have been generated using the formulation developed in Chapter 4 (Figs.6.205-212) (ANSA2). The applied load and total displacement have been non-dimensionalised by dividing by the Euler critical load and thickness of the column wall respectively. From the figures showing average stress-strain curves, it is observed that in cases where L/r=30 and L/r>120, the load maintains a nearly constant value in the post-peak régime while in the range $30<L/r\leq120$, quite rapid unloading can follow the peak. This drop in load becomes less significant as the magnitude of the initial bow increases. The strength of the columns with L/r>120 coincides with their Euler buckling load. The curves relating to load-displacement generally show little growth in deflections during the basically elastic phase of loading. Post-peak, the curves tend to merge, a result which would be a likely outcome from a mechanism solution to this problem[34]. Collapse loads have been plotted against slenderness and are presented in Figure (6.213). Changes in the magnitude of initial bow, as can be seen from the Figure, affected the strength of the column only up to $\lambda\approx1.5$. Profiles illustrating deformations caused by overall collapse are shown in Figures (6.235-237).

A few examples of columns with clamped ends are presented in Figures (6.214-216), showing the effect of initial bow on column strength. Comparisons between these curves and the corresponding ones with simply-supported ends confirm the significant loss in strength of the latter. This limited number of examples was produced during the development phase of the program in order that substantiation of the analysis could be made against existing data[34]: good agreement was achieved.

6.4 Comparison with Existing Rules

Existing Design Rules are based mainly on experience, experiments and empirical formulas. In this Section a comparison is made between results generated by the present formulations and those predicted by existing Design Rules[68,69,70].

In the case of ring-stiffened cylinders subjected to axial compression, the results produced in Section 6.2 for mode one and mode six, and the design curves recommended by DNV, API and ECCS are plotted together in Figure (6.217). From this figure it can be seen that the DNV and ECCS design curves cross the mode six curve for R/T≈600, while the API curve only intersects this curve at R/T>100. If mode six can be assumed to give a lower bound, some of the Design Rules have doubtful safety margins, particularly at low R/T values. However, mode six is not necessarily felt to be a truly practical imperfection type. Analyses based on a reasonable interpretation of the DNV tolerance limits have produced results higher than those specified by the DNV Design Curve[69], (Fig. 6.218). The discrepancy between the results is more pronounced as R/T increases, while at low R/T's it tends to be negligible. In the absence of residual stresses, these results tend to indicate that the DNV strength curve has adequate margins, particularly at higher R/T values.

In the case of combined axial-compression and bending on cylindrical shells the results derived in Section 6.2.2 for mode one and mode six have been plotted together with the DNV[69], ECCS[64] and API[64] design curves and are presented in Figures (6.219-222). For R/T<200 DNV and ECCS design curves lie between the mode one and mode six curves, while API gives lower results. For R/T>200 the rules tend to recommend much lower values.

In the case of column design, the derived results in Section 6.3 have been plotted together with DNV/ECCS[69] and API/CRC[68] design curves and are shown in Figure (6.223).

The DNV/ECCS curve coincides with the L/500 imperfections curve over practically the entire slenderness range. The API/CRC curve is seen not to be consistent with any particular level of initial imperfection. At worst ($\lambda=\sqrt{2}$) the API/CRC curve over-estimates the strength of a practical structure ($s_o^* = L/1000$) by 5%.

CHAPTER 7

CONCLUSIONS AND FUTURE WORK

7.1 Conclusions Concerning Numerical Technique

Dynamic Relaxation has proved itself once again to be a powerful tool in the collapse load analysis of thin steel structures. Complete understanding of the method has been achieved and contributions towards improvement have been made.

a) A thorough study of the Dynamic Relaxation main parameters has led to the development of an empirical formula for automatic calculation of the damping factors. Re-estimation of damping factors can be made at any stage along the loading path.

b) Difficulties in achieving convergence have been generally overcome by introducing density factors. In the case of local buckling (ANSA1) density factors were used to magnify the densities, while in the column analysis (ANSA2) densities had to be reduced. For the latter, the factors were found to be a function of L/r. Simple diagrams were produced to facilitate selection of these density factors.

c) Studies showed that it is not essential to calculate fictitious densities at every iteration, and usually the values calculated during the first load increment seemed to be adequate to accomplish the complete analysis with no convergence problems.

d) Comparisons between the average stress-strain curves produced by using elastic and elasto-plastic fictitious densities showed no practical differences.

e) Adjustment of the velocities back to zero at the beginning of each new

loading increment improved convergence especially in those cases where the previous increment was governed by poor convergence.

f) Increments of strains and curvatures were calculated as the difference between current and previous value and not explicitly in terms of displacements.

7.2 Conclusions on the Cylindrical Shell Analysis

a) A thorough study into the derivation of strain-displacement relationships has led to the development of an easy approach based on elementary mathematics.

b) Comparison between the present and Sanders[73] strain-displacement relationships show them to be very similar despite the fact that the latter were derived using Tensors.

c) Comparisons of the computer storage capacity and of the actual running time per load increment show that single-layer representations of plasticity are 15% and 6% more efficient in these requirements than a similar multi-layer analysis. The multi-layer analysis solutions however are more accurate and this approach is recommended unless computer facilities are limited.

d) The application of axial compressive load in the form of incremental end displacements has enabled detailed studies of the post-buckling régime to be made except in those cases where snap-back occurs just after peak load.

e) Averaging the in-plane and flexural strains with respect to (o) fictitious nodes (Fig. 3.18) has permitted successful calculation of the plastic rigidities for these positions.

f) Convergence studies suggest that optimum mesh-sizes are dictated by the radius-to-thickness ratio. This is explained by the fact that

for large R/T ratios a greater number of nodes was required to accurately describe mode changes.

g) The use of an angle of 22.5^{o} between successive circumferential nodes proved successful in achieving a good level of accuracy in the results without requiring excessive computing time.

h) Comparisons between existing results and those generated by the present formulation (ANSA1) showed good agreement.

i) Despite the scarcity of detailed experimental data, comparisons with recent experimental results have shown agreement within 10% - 20% in predicting maximum compressive loads. This difference is partly due to the non-treatment of residual stresses.

7.3 Conclusions on the Beam-Column Overall and Local Interactive Buckling Analysis

a) A formulation (ANSA2) to account for interaction between overall and local collapse modes has been successfully developed. It combines the local shell buckling analysis with a beam-column solution to account for overall buckling.

b) Simply supported column ends can be successfully simulated by using a Dynamic Relaxation formulation to derive the end rotations necessary for the zero moment condition.

c) Convergnece studies suggest that seven intervals along the half column length are adequate to describe the column behaviour irrespective of the L/r ratio. Again, the ideal angle between successive circumferential nodes is 22.5^{o}.

d) Comparisons between average stress-strain curves for cylinders suffering overall buckling only derived with the present formulation (ANSA2) and other theoretical ones showed good agreement up to the collapse load while in the post-collapse régime the degree of correlation

depended on whether snap-back occurred or not. Where this pattern of behaviour occurred, the present analysis generated a curve similar to that expected of a very stiff test rig. For non-snap-back situations the present solution produced higher results. This difference is explained by the use of different plasticity theories.

e) A comparison between an existing experimental result and the respective one generated by the present formulation for an overall column failure showed excellent agreement in predicting the experimental collapse load.

7.4 Conclusions on the Simplified Approach to Beam-Column Interactive Buckling

a) Although seemingly working satisfactorily for $R/T<40$, further studies with this simplified interactive beam-column approach was hampered by convergence difficulties. The problem seemed particularly dependent on the fictitious densities.

b) For the range of problems investigated, this analysis was found to give good predictions of other numerical and experimental results. In particular, it predicted lower strengths in beam-columns where local buckling was expected to influence behaviour than the non-interactive beam-column analysis, viz. when $R/T>28$.

7.5 Conclusions on Parametric Studies of Cylindrical Shells

The problem of elasto-plastic buckling of circular cylindrical shells subjected to axial compression and more complex loading has been investigated numerically. The complex loading included combinations of axial compression and bending, and axial compression, bending and external pressure.

With reference to the results derived from these theoretical parametric studies the following observations can be made:

7.5.1 Axial Compression

a) Initial distortions of the m=1 and n=1 mode (mode 1) produce post-buckling curves which unload rapidly particularly for large L/R's. This is due to a mode change occuring as plasticity is initiated for the larger R/T's.

b) Mode one distortions tend to persist throughout the loading range when R/T<200. For R/T>200 a different mode develops post-peak.

c) For m=5, n=1 type initial shapes (mode 6) the longitudinal wave form is maintained throughout the complete loading cycle, irrespective of R/T.

d) Increases in the magnitude of imperfections causes reductions of the elastic slopes with a consequent reduction in the cylinders maximum strength.

e) Variation of ring-stiffener spacing has a significant effect on cylinder strength, and not always as expected. More closely spaced rings can apparently lead to reductions in strength.

f) Change of longitudinal wave length is more crucial than change in the circumferential one.

g) Behaviour in the post-peak régime is dictated mainly by the ring-stiffener spacing while that of the pre-buckling path is influenced by the imperfections magnitude.

h) Comparisons with existing Design Rules showed that the DNV and ECCS design curves predict buckling loads similar to those derived by assuming initial deformation of m=5, n=1 type (mode 6) and magnitude $w_o^* = R/400$, while the API strength curve predicts 10% lower values. Analysis based on the DNV tolerance limits generated buckling loads higher than those specified by the DNV Design Curve. These results indicate that the DNV strength curve has adequate margins, particularly at higher R/T values.

i) Results pertaining to damage indicated the effect on residual compressive strength was not necessarily significant. This was probably due to the fact that the damage examined was limited.

7.5.2 Axial Compression plus Bending

a) In general cylinders subjected to bending tend to change their initial mode during loading. In particular, the mode one longitudinal wave length reduces by $\frac{1}{3}$ after buckling.

b) Maximum compressive strengths do not necessarily correspond to maximum bending moments. With increasing ratios of bending to compressive strain, maximum bending moments occur at higher strain values than those corresponding to maximum compressive strengths.

c) Variation of ring spacing has a great influence on the elastic slopes of the average stress-strain curves without significantly affecting the maximum compressive strength.

d) Interaction between maximum compressive strength and corresponding moment is described either parabolically or by a linear relationship. Parabolic interaction applies for high levels of imperfections, linear to lower levels.

e) Comparisons with existing Design Rules showed that for $R/T<200$ the DNV and ECCS design curves lie between the mode 1 (m=1,n=1) and mode 6 (m=5,n=1) derived interaction curves, while the API give lower results. For $R/T>200$ the rules recommend much lower values. The analyses was based on a maximum deformation of $w_o^* = R/400$.

7.5.3 Axial Compression plus Bending plus External Pressure

a) External pressure was found to stiffen cylinders for loading in the pre-buckling régime but reduce their stiffness post-peak. This phenomenon was most pronounced in thin cylinders. The stiffening

effect in the pre-buckling phase arises from the opposing effects of hoop expansion under axial compressive loading.

b) Cylindrical shells subjected to these complex load patterns readily change their initial mode and in apparently unpredictable ways.

c) Pressure heads up to 100 m of water do not affect the maximum compressive strength of cylinders.

d) Variation of imperfection magnitude affects the elastic slopes significantly especially when a high imperfection level is used. Maximum compressive strength however is not affected to the same extent.

e) Again, reduction in ring-stiffener spacing leads to drops in strength particularly when $R/T \geq 200$.

7.6 Conclusions on Beam-Columns

Overall elasto-plastic buckling of circular beam-columns subjected to axial compression has been investigated numerically. Only the effect of initial out-of-straightness distortion was considered. The following observations can be made as a result of these studies:

a) Column strength was found to be dominated by slenderness (L/r), as expected, strength decreasing with increasing slenderness.

b) The influence of initial bow was found to be less important but still of significance for λ less than 1.5. For more slender columns, initial bow was of little importance.

c) For $0.6 \leq \lambda \leq 1.5$, rapid unloading occurred in the post-peak régime. For other slendernesses, unloading was far less rapid and for $\lambda \geq 2$, no obvious peak was detectable in the average stress-strain curve.

d) Columns with R/T's greater than 28 are susceptible to local buckling, the onset of local buckling occurring at progressively lower stress levels as R/T increases.

e) Comparisons with existing Design Rules for beam-columns showed that the DNV/ECCS Rules' strength for circular section was closely predicted by assuming an initial column bow of L/500. The API curve was found not to be consistent with any particular level of initial out-of-straightness, and appears to overestimate strength in the range of $\lambda>1.2$. For $\lambda>\sqrt{2}$, the API curve is just the Euler buckling curve.

7.7 Recommendations for Future Work

The following recommendations are suggested for future work:

a) Extension of the formulations to account for longitudinal and circumferential residual stresses.

b) Introduction of a displacement control mechanism so as to allow snap-back in the post-buckling régime to be traced.

c) Development of an improved procedure for calculating fictitious densities so that interactive buckling can be handled (ANSA3).

d) The provision of information on actual imperfections which are developed during fabrication in order that the numerical results can have direct relevance to practical structures.

e) The conduct of supportive experimental work, particularly under complex loading conditions.

f) Further numerical and experimental work on cylindrical shells damaged by point and line loads and then subjected to axial compression and complex loading.

g) Development of three-dimensional graphical subroutines are necessary to give further insight into sudden mode changes.

APPENDIX I

GENERAL STRAIN-DISPLACEMENT RELATIONSHIPS

1. Including u_o, v_o and w_o Initial Imperfections

The co-ordinates for the vertices of the triangular elements shown in the figures below are given in the following Table.

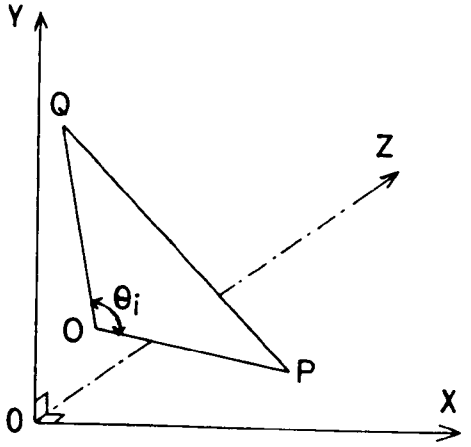

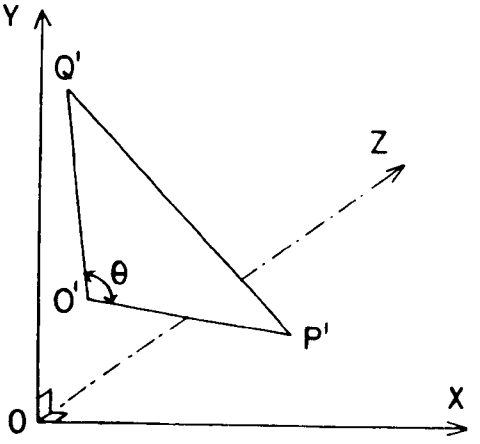

Co-ordinates of points O, P, and Q and O', P', and Q'

	x	y	z
O	u_o	v_o	w_o
P	$u_o + \delta x + \frac{\partial u_o}{\partial x}\delta x$	$v_o + \frac{\partial v_o}{\partial x}\delta x$	$w_o + \frac{\partial w_o}{\partial x}\delta x$
Q	$u_o + \frac{\partial u_o}{\partial y}\delta y$	$v_o + \frac{\partial v_o}{\partial y}\delta y + \delta y - \frac{w_o}{R}\delta y$	$w_o + \frac{\partial w_o}{\partial y}\delta y$
O'	$u + u_o$	$v + v_o$	$w + w_o$
P'	$u + u_o + \delta x + \frac{\partial u}{\partial x}\delta x + \frac{\partial u_o}{\partial x}\delta x$	$v + v_o + \frac{\partial v}{\partial x}\delta x + \frac{\partial v_o}{\partial x}\delta x$	$w + w_o + \left(\frac{\partial w}{\partial x} + \frac{\partial w_o}{\partial x}\right)\delta x$
Q'	$u + u_o + \frac{\partial u}{\partial y}\delta y + \frac{\partial u_o}{\partial y}\delta y$	$v + v_o + \delta y + \frac{\partial v}{\partial y}\delta y + \frac{\partial v_o}{\partial y}\delta y - \frac{w+w_o}{R}\delta y$	$w + w_o + \left(\frac{\partial w}{\partial y} + \frac{\partial w_o}{\partial y} + \frac{v}{R}\right)\delta y$

Following the same procedures as in Section (3.2.3) the expressions for ε_x, ε_y and ε_{xy} become

$$\varepsilon_x = u_x + v_x v_{o_x} - u_x u_{o_x} + \frac{1}{2}\left(v_x^2 + w_x^2 + 2w_x w_{o_x}\right)$$

$$\varepsilon_y = v_y - \frac{w}{R} + \frac{\partial v_o}{\partial y}\frac{w}{R} - \frac{\partial v}{\partial y}\frac{\partial v_o}{\partial y} + \frac{1}{2}\left[u_y^2 + w_y^2 + \left(\frac{v}{R}\right)^2 + 2\frac{v}{R}w_y + 2\frac{v}{R}w_{o_y} + 2w_y w_{o_y} + 2v_y\frac{w_o}{R} - 2\frac{w}{R}\frac{w_o}{R}\right] + \frac{\partial u}{\partial y}\frac{\partial u_o}{\partial y}$$

$$(\varepsilon_{xy})_{eng} = u_y + v_x + w_x w_y + w_y w_{o_x} + w_{o_y} w_x + w_x\frac{v}{R} + w_{o_x}\frac{v}{R} + u_y\frac{w_o}{R} - u_x v_x - u_y v_y + u_y\frac{w}{R} - u_y v_{o_y} - u_{o_y} v_y + u_{o_y}\frac{w}{R} - v_{o_x} u_x - v_x u_{o_x}$$

2. Including u_o, v_o, and w_o Initial Rotations and Rotations after Deformation

The co-ordinates of O, P, Q and O', P' and Q' are tabulated in the following page based on mathematical analysis given below.

Let OP_iQ_i describe the initial shape of the element and OPQ the shape after initial rotations have elapsed.

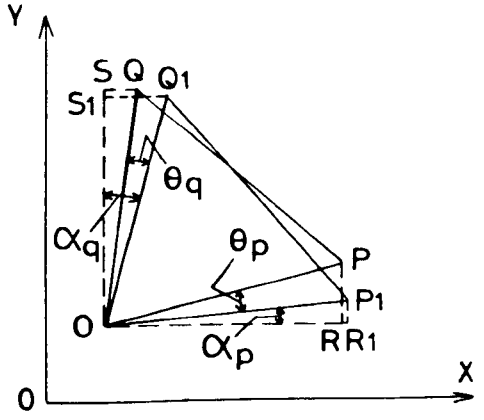

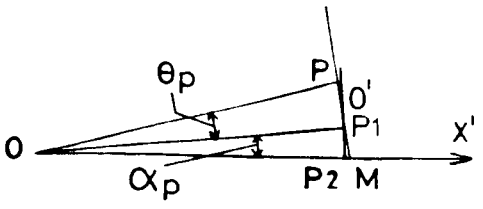

Co-ordinates of O, P, Q and O', P', Q'

	x	y	z
O	u_o	v_o	w_o
P	$u_o + \delta x + \frac{\partial u_o}{\partial x}\delta x + \frac{\partial v_o}{\partial x}\frac{\partial u_o}{\partial y}\delta x$	$v_o + \frac{\partial v_o}{\partial x}\delta x - \frac{\partial u_o}{\partial y}\delta x - \frac{\partial u_o}{\partial x}\frac{\partial u_o}{\partial y}\delta x$	$w_o + \frac{\partial w_o}{\partial x}\delta x$
Q	$u_o + \frac{\partial u_o}{\partial y}\delta y + \frac{\partial v_o}{\partial y}\frac{\partial v_o}{\partial x}\delta y + \frac{\partial v_o}{\partial x}\delta y - \frac{w_o}{R}\frac{\partial v_o}{\partial x}\delta y$	$v_o + \frac{\partial v_o}{\partial y}\delta y + \delta y - \frac{w_o}{R}\delta y - \frac{\partial u_o}{\partial y}\frac{\partial v_o}{\partial x}\delta y$	$w_o + \frac{\partial w_o}{\partial y}\delta y$
O'	$u + u_o$	$v + v_o$	$w + w_o$
P'	$u + u_o + \delta x + \frac{\partial u}{\partial x}\delta x + \frac{\partial u_o}{\partial x}\delta x + \frac{\partial v_o}{\partial x}\frac{\partial u_o}{\partial y}\delta x + \frac{\partial v}{\partial x}\frac{\partial u}{\partial y}\delta x + \frac{\partial u_o}{\partial y}\frac{\partial u}{\partial y}\delta x + \frac{\partial v_o}{\partial x}\frac{\partial u}{\partial y}\delta x$	$v + v_o + \frac{\partial v}{\partial x}\delta x + \frac{\partial v_o}{\partial x}\delta x - \frac{\partial u_o}{\partial y}\delta x - \frac{\partial u_o}{\partial x}\frac{\partial u_o}{\partial y}\delta x - \frac{\partial u}{\partial x}\frac{\partial u}{\partial y}\delta x - \frac{\partial u}{\partial y}\delta x - \frac{\partial u_o}{\partial x}\frac{\partial u}{\partial y}\delta x$	$w + w_o + \frac{\partial w}{\partial x}\delta x + \frac{\partial w_o}{\partial x}\delta x$
Q'	$u + u_o + \frac{\partial u}{\partial y}\delta y + \frac{\partial u_o}{\partial y}\delta y + \frac{\partial v_o}{\partial y}\frac{\partial v_o}{\partial x}\delta y + \frac{\partial v_o}{\partial x}\delta y - \frac{w_o}{R}\frac{\partial v_o}{\partial x}\delta y + \frac{\partial v}{\partial y}\frac{\partial v}{\partial x}\delta y - \frac{w}{R}\frac{\partial v}{\partial x}\delta y + \frac{\partial v_o}{\partial y}\frac{\partial v}{\partial x}\delta y + \frac{\partial v}{\partial x}\delta y - \frac{w_o}{R}\frac{\partial v}{\partial x}\delta y$	$v + v_o + \frac{\partial v}{\partial y}\delta y - \frac{w}{R}\delta y + \frac{\partial v_o}{\partial y}\delta y + \delta y - \frac{w_o}{R}\delta y - \frac{\partial u_o}{\partial y}\frac{\partial v_o}{\partial x}\delta y - \frac{\partial u}{\partial y}\frac{\partial v}{\partial x}\delta y - \frac{\partial u_o}{\partial y}\frac{\partial v}{\partial x}\delta y - \frac{\partial v_o}{\partial x}\frac{\partial v}{\partial x}\delta y$	$w + w_o + \frac{\partial w}{\partial y}\delta y + \frac{\partial w_o}{\partial y}\delta y + \frac{v}{R}\delta y$

$$OP_1 = OP \qquad OQ_1 = OQ$$

$$OR_1 = OP_1 \cos\alpha_p \qquad OS_1 = OQ_1 \cos\alpha_q$$

$$R_1P_1 = OP_1 \sin\alpha_p \qquad Q_1S_1 = OQ_1 \sin\alpha_q$$

$$\cos\theta_p \simeq 1 \qquad \cos\theta_q \simeq 1$$

From the figure, PM is tangent to a circle of radius $OP_1 = OP$ at point P which intersects OX' (OX'//OX) at M. $O'P_2$ is also tangent at point P_1. From geometry $OPO'P_1$ is an inscribed quadrilateral, because $O\hat{P}O' = O\hat{P}_1O' = 90^o$. Therefore, $P_1\hat{O}P = P_2\hat{O}'M = \theta_p$ and because angle α_p is very small,

$$\sin\theta_p \simeq \tan\theta_p = -\frac{\partial u_o}{\partial y}. \quad \text{Similarly, } \sin\theta_q \simeq -\frac{\partial v_o}{\partial x}.$$

For pure rotations

$$\theta_p = \theta_q$$

$$OR = OP_1 \cos(\alpha_p+\theta_p) = OP_1 \cos\alpha_p \cos\theta_p - OP_1 \sin\alpha_p \sin\theta_p$$
$$= OR_1 \cos\theta_p - P_1R_1 \sin\theta_p$$

$$PR = OP_1 \sin(\alpha_p+\theta_p) = OP_1 \sin\alpha_p \cos\theta_p + OP_1 \cos\alpha_p \sin\theta_p$$
$$= P_1R_1 \cos\theta_p + OR_1 \sin\theta_p$$

$$OS = OQ_1 \cos(\alpha_q-\theta_p) = OQ_1 \cos\alpha_q \cos\theta_q + OQ_1 \sin\alpha_q \sin\theta_q$$
$$= OS_1 \cos\theta_q + Q_1S_1 \sin\theta_q$$

$$QS = OQ_1 \sin(\alpha_q-\theta_q) = OQ_1 \sin\alpha_q \cos\theta_q - OQ_1 \sin\theta_q \cos\theta_q$$
$$= Q_1S_1 \cos\theta_q - OS_1 \sin\theta_q$$

Let $O'P_1'Q_1'$ represent the element after initial distortion, initial rotations and deformations have been included. OP'Q' describes the element after small rotations have occurred.

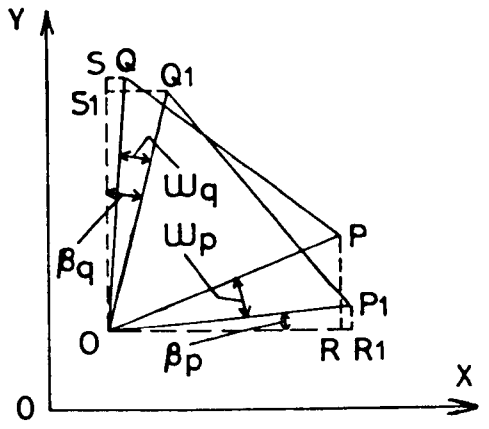

$$O'P_1' = O'P' \qquad O'Q_1' = O'Q'$$

$$O'R_1' = O'P_1' \cos\beta_p \qquad O'S_1' = O'Q_1' \cos\beta_q$$

$$R_1'P_1' = O'P_1' \sin\beta_p \qquad Q_1'S_1' = O'Q_1' \sin\beta_q$$

$$\cos\omega_p \simeq 1 \qquad \cos\omega_q \simeq 1$$

$$\sin\omega_p \simeq -\frac{\partial u}{\partial y} \quad \text{(Similarly as above)} \qquad \sin\omega_q \simeq -\frac{\partial v}{\partial x}$$

$$O'R' = O'P_1' \cos(\beta_p+\omega_p) = O'P_1' \cos\beta_p \cos\omega_p - O'P_1' \sin\beta_p \sin\omega_p$$
$$= O'R_1' \cos\omega_p - P_1'R_1' \sin\omega_p$$

$$P'R' = O'P_1' \sin(\beta_p+\omega_p) = O'P_1' \sin\beta_p \cos\omega_p + O'P_1' \cos\beta_p \sin\omega_p$$
$$= P_1'R_1' \cos\omega_p + O'R_1' \sin\omega_p$$

$$O'S' = O'Q_1' \cos(\beta_q-\omega_q) = O'Q_1' \cos\beta_q \cos\omega_q + O'Q_1' \sin\beta_q \sin\omega_q$$
$$= O'S_1' \cos\omega_q + Q'S_1' \sin\omega_q$$

$$Q'S' = O'Q_1' \sin(\beta_q-\omega_q) = O'Q_1' \sin\beta_q \cos\omega_q - O'Q_1' \sin\omega_q \cos\beta_q$$
$$= Q_1'S_1' \cos\omega_q - O'S_1' \sin\omega_q$$

Following the same procedures as in Section (3.2.3) the expressions for ε_x, ε_y and ε_{xy} become

$$\varepsilon_x = u_x + v_x v_{o_x} - u_x u_{o_x} + \frac{1}{2}\left(v_x^2 + u_y^2 + w_x^2 + 2w_x w_{o_x} - v_x u_{o_y}\right)$$

$$\varepsilon_y = v_y - \frac{w}{R} + v_{o_y}\frac{w}{R} - v_y v_{o_y} + \frac{1}{2}\left[u_{o_y}^2 + v_x^2 + w_y^2 + \left(\frac{v}{R}\right)^2 + 2\frac{v}{R}w_y\right.$$

$$\left. + 2\frac{v}{R}w_{o_y} + 2w_y w_{o_y} + 2v_y\frac{w_o}{R} - 2\frac{w}{R}\frac{w_o}{R}\right] + u_y u_{o_y} + u_y v_{o_x}$$

$$(\varepsilon_{xy})'_{eng} = u_y + v_x + w_x w_y + w_y w_{o_x} + w_{o_y} w_x + w_x\frac{v}{R} + w_{o_x}\frac{v}{R}$$

$$+ u_y\frac{w_o}{R} - u_x v_x - u_y v_y + u_y\frac{w}{R} - u_y v_{o_y} - u_{o_y} v_y$$

$$+ u_{o_y}\frac{w}{R} - v_{o_x} u_x - u_{o_x} v_x$$

The shear strain remains the same as before, i.e. in the case without rotation, because the angle between the element's sides are unaltered by more rotation.

Sanders[73] derived a similar set of expressions using a tensor-based approach, but ignoring both thin-plane and the out-of-plane initial imperfections. The following table indicates the tensor-based expression for the x-direction strain and the corresponding one found from the present analysis by deleting the term containing u_o, v_o and w_o. The only differences can be seen to be the constant associated with the square of the in-plane slope terms, which arises from the difference in definition between the tensor and 'engineering' approaches, and the cross-term of in-plane slopes which is not identified in the present derivation.

	ε_x
Sanders[73]	$\frac{\partial u}{\partial x} + \frac{1}{2}\left(\frac{\partial w}{\partial x}\right)^2 + \frac{1}{8}\left(\frac{\partial u}{\partial x}\right)^2 + \frac{1}{8R^2}\left(\frac{\partial u}{\partial \theta}\right)^2 - \frac{1}{4R}\frac{\partial v}{\partial x}\frac{\partial u}{\partial \theta}$
Present analysis	$\frac{\partial u}{\partial x} + \frac{1}{2}\left(\frac{\partial w}{\partial x}\right)^2 + \frac{1}{2}\left(\frac{\partial v}{\partial x}\right)^2 + \frac{1}{2R^2}\left(\frac{\partial u}{\partial \theta}\right)^2$

APPENDIX II

DEVELOPMENT OF GRAPHICAL SUBROUTINES

Two graphical subroutines have been written to illustrate mode shapes longitudinally and circumferentially. These subroutines are part of the main program and can be called at any time during the analysis. The technique adopted in these subroutines can be illustrated using the following figures.

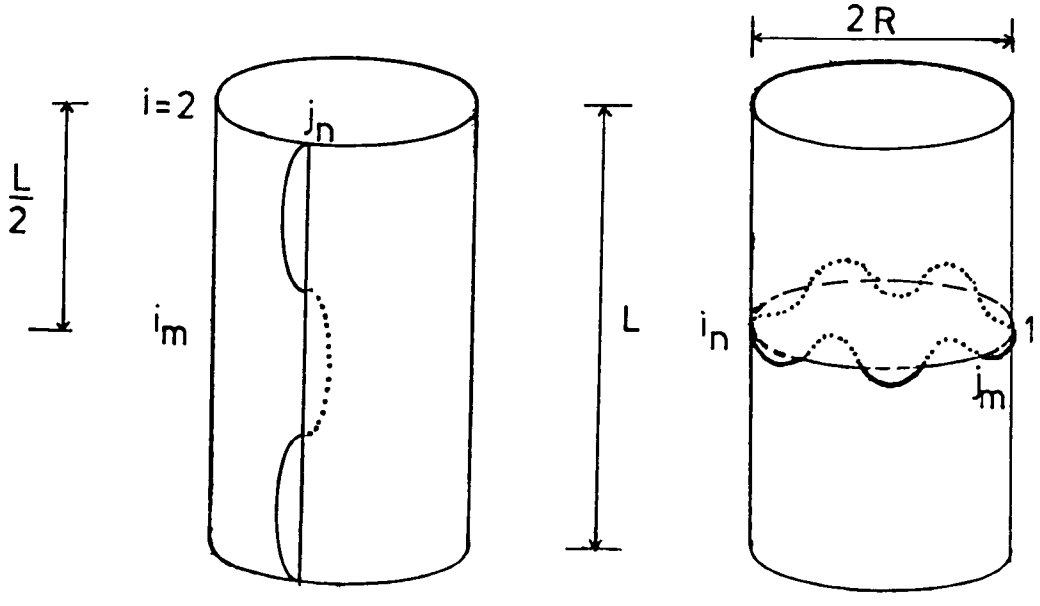

The program can output only one longitudinal and one circumferential profile at a specified frequency of load increments. The particular profiles required are specified by coordinates (i_n, j_n), usually $i_n = i_m$, where i_m is the mid-height axial node. The total deformations are calculated and non-dimensionalised with respect to the shell thickness at each node in question.

Axes are drawn and annotated automatically by estimating the maximum and minimum values of current deformations.

Following these calculations, standard subroutines are called to assist plotting. These subroutines are part of a package named GHOST mounted on the University's ICL 2976 main frame computer.

The output is plotted in the manner shown in the figures below.

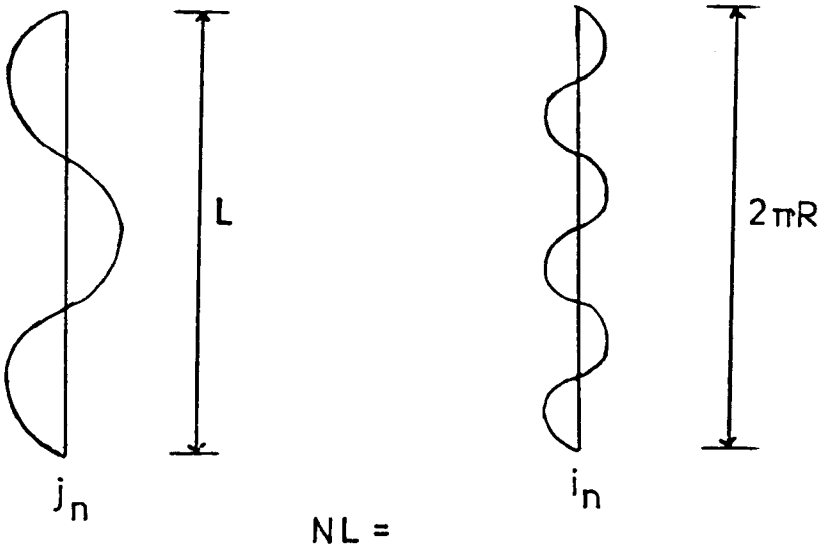

The longitudinal profile is plotted with respect to an initially straight generator at node j_n while the circumferential profile is plotted with respect to a developed initially circular circumference of length $2\pi R$. Every pair of profiles is identified by the number of loading increment, (e.g. NL = 1).

The development of these subroutines has significantly contributed to the rapid presentation of data in graphical form.

APPENDIX III

PRELIMINARY DESIGN OF A PRESSURE CHAMBER

1. Introduction

An investigation into the design of a pressure chamber has been carried out. Such a facility is required for experimental work on tubular members, subjected to axial load, bending and external pressure. The design of the chamber was dictated by the dimensions of an existing 2000 kN tension-compression machine in which the chamber had to be fitted (see Figure at the end of Appendix).

Another design limitation was that the main geometry of the dome ends should be selected from one of the standard designs available on the market. The pressure chamber was also to be designed to withstand a pressure head of 1500 m of water ($P = 0.0147\ kN/mm^2$). The British Standard[71] with some input from the DNV[72] code was used to carry out the design analysis.

The design procedure accompanied by calculations is illustrated in the following stages.

2. Selection of Material

The selected material was a Carbon Steel, to comply with B.S. 5500 grade M1 (see Table on the next page).

The minimum tensile strength for this material is $0.494\ kN/mm^2$ and the nominal design stress (σ) $0.196\ kN/mm^2$.

Table 2.3 Design strength values (N/mm²)

(b) Carbon and carbon manganese steels (BS 5500 grade M1) *(continued)*

Product form	Materials standards, BS references	Min. tensile strength	Thickness	Temperature, °C 20	50	100	150	200	250	300	350	Design lifetime (all thicknesses)	Temperature, °C 380	390	400	420	440	450	460	480
		N/mm²	mm									h								
Plate	1501 224 28A	432	Up to 16	184	184	165	145	132							92					
			>16 to 32	180	180	163	145	131	116	104	97									
			>32 to 64	170	170	158	142	129												
			>64 to 150	See note 1																
	28B	432	Up to 16	184	184	165						100 000			98	88	69	60	52	36
			>16 to 32	180	180	163	145	138	124	111	104	150 000				83	64	56	48	31
			>32 to 64	170	170	158						200 000				80	61	53	45	28
			>64 to 150	See note 1								250 000				77	59	51	42	26
	30A	464	Up to 16	197	197	177	157	142							98					
			>16 to 32	196	196	176	157	142	125	111	104									
			>32 to 64	185	185	170	154	139												
			>64 to 150	See note 1																
	30B	464	Up to 16	197	197	177						100 000			105	102	77	65	56	42
			>16 to 32	196	196	176	157	147	133	119	111	150 000				95	68	58	50	37
			>32 to 64	185	185	171						200 000				88	63	54	46	34
			>64 to 150	See note 1								250 000				83	59	51	43	31
	32A	494	Up to 16	210	210	189	167	151							105					
			>16 to 32	206	206	187	167	150	133	119	111									
			>32 to 64	196	196	180	164	147												
			>64 to 150	See note 1																
	32B	494	Up to 16	210	210	189						100 000			112	104	77	65	56	42
			>16 to 32	206	206	187	167	158	142	127	118	150 000				95	68	58	50	37
			>32 to 64	196	196	182						200 000				88	63	54	46	34
			>64 to 150	See note 1								250 000				83	59	51	43	31
			(Thickness) (Diameter)																	
Sections and bars	1502 211,221	432	Up to 16 Up to 25	170	170	156	142	133						Values up to 450 °C: as for 1501 211,221 26B depending on design lifetime						
			>16 to 32 >25 to 51	165	165	152	140	133	126	107	98									
			>32 to 64 >51 to 102	160	160	148	137	126												
			>64 to 100 >102 to 150	See note 1																
	1502 224	432	Up to 25	184	184	165	145	132						Values up to 450 °C: as for 1501 224 26B depending on design lifetime						
			>25 to 51	180	180	163	145	131	116	104	97									
			>51 to 102	170	170	156	142	129												
			>102 to 230	See note 1																

NOTE 1. For each 6.3 mm above 64 mm thickness (or 100 mm diameter in the case of sections and bars) reduce values up to 250 °C by 1 %.

NOTE 2. The values for forgings may be increased up to (but not greater than) the values permitted for plate in the equivalent material grade and equivalent ruling section on provision by the forgemaster of appropriate supporting data showing that the minimum acceptance criteria for equivalent plate are satisfied.

Table 2.3 Design strength values (N/mm²)

(b) Carbon and carbon manganese steels (BS 5500 grade M1) *(concluded)*

Product form	Materials standards, BS references		Min. tensile strength	Thickness	Temperature, °C								Design lifetime (all thicknesses)	Temperature, °C						
					20	50	100	150	200	250	300	350		380	390	400	420	440	450	460	480
			N/mm²	mm									h								
Forgings (see note 2)	1503 221	32A	494		164	164	153	147	140	132	120	115				107					
		32B			164	164	153	147	140	134	128	123				As 1501 221 32B depending on design lifetime					
		34A	525		175	175	163	157	148	140	130	125				108					
		34B			175	175	163	157	150	145	139	133				As 1501 223 30B depending on design lifetime					
	1503 223	28A	432		165	165	152	140	127	115	105	97				92					
		28B			165	165	152	140	130	121	112	103				98	As 1501 221 26B depending on design lifetime				
		32A	494		185	185	172	158	145	132	124	115				108					
		32B			185	185	172	160	151	142	132	123				115	As 1501 223 28B depending on design lifetime				
	1503 224	28A	432		154	154	141	128	119	115	104	97				92					
		28B			154	154	141	128	119	115	108	103				98	As 1501 224 28B depending on design lifetime				
		32A	494		175	175	164	152	142	132	120	115				108					
		32B			175	175	164	152	144	135	128	123				115	As 1501 224 32B depending on design lifetime				
Pipes and tubes	3601	410	410		157	157	144	132	120	109	98	90				82					
	3602*	27	417		165	165	148	132	127	119	105	96	100 000			92	91	69	60	52	36
													150 000				83	64	56	48	31
													200 000				80	61	53	45	28
													250 000				77	59	51	42	26
	3059 : Part 2	45	440		165	165	160	152	144	134	119	106	100 000			101	100	77	65	56	42
													150 000				95	68	58	50	37
													200 000				88	63	54	46	34
													250 000				83	59	51	43	31
	3603	27LT30	417		165	165															

* Time dependent values for 27H may be increased by 10% but ≯ 91.

NOTE 1. For each 6.3 mm above 64 mm thickness (or 100 mm diameter in the case of sections and bars) reduce values up to 250 °C by 1 %.

NOTE 2. The values for forgings may be increased up to (but not greater than) the values permitted for plate in the equivalent material grade and equivalent ruling section on provision by the forgemaster of appropriate supporting data showing that the minimum acceptance criteria for equivalent plate are satisfied.

3. Geometry of the Mid-Length Cylindrical Section

The overall diameter was chosen as D_o = 1103 mm and by using the following equation (of BS5500) the thickness (e) can be calculated.

$$e = \frac{PD_o}{2\sigma+P}$$

The thickness was thus estimated to be 40 mm and the length of this section was chosen as l = 1040 mm.

4. Geometry of the Dome End

The following geometry was employed to undertake calculation for the thickness of the dome end (see Figure on the next page).

Internal diameter	D_i = 1060 mm
Crown radius	R = 800 mm
Local radius	r = 212 mm
Height from knuckle to top	h = 308 mm

The calculation of thickness was based on B.S. 3.5.2 Section

$$\frac{P}{\sigma} = 0.075$$

$$\frac{h_e}{D_o} = \frac{h + e_d}{D_i + 2e_d} = \frac{308 + e_d}{1060 + 2e_d}$$

The value of e_d was found by trial and error. For

e_d = 30.5 mm

$$\frac{h_e}{D_o} = 0.31$$

Using Figure 3.5.2.3 of B.S. shown on the next page,

$$\frac{e_d}{D} = \frac{e_d}{D_i + 2e_d} = 0.028 \quad \text{or} \quad e_d = 30.5 \text{ mm}$$

Since the dome end is to have an elliptical opening (manhole), compensation for this loss of material has to be made in the form of

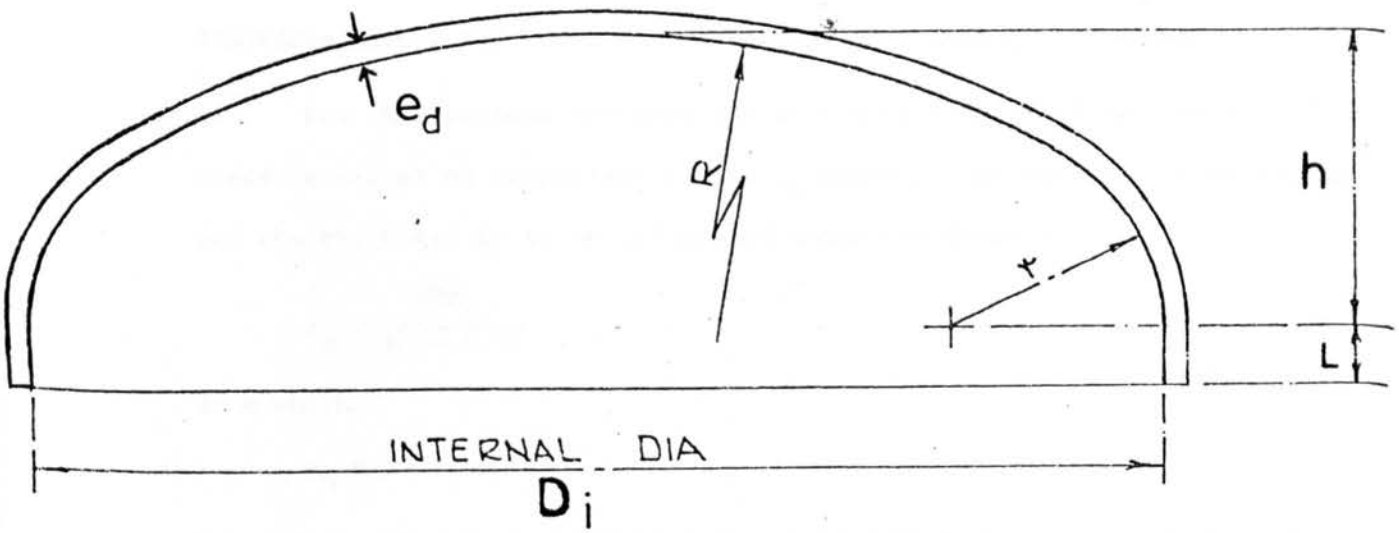

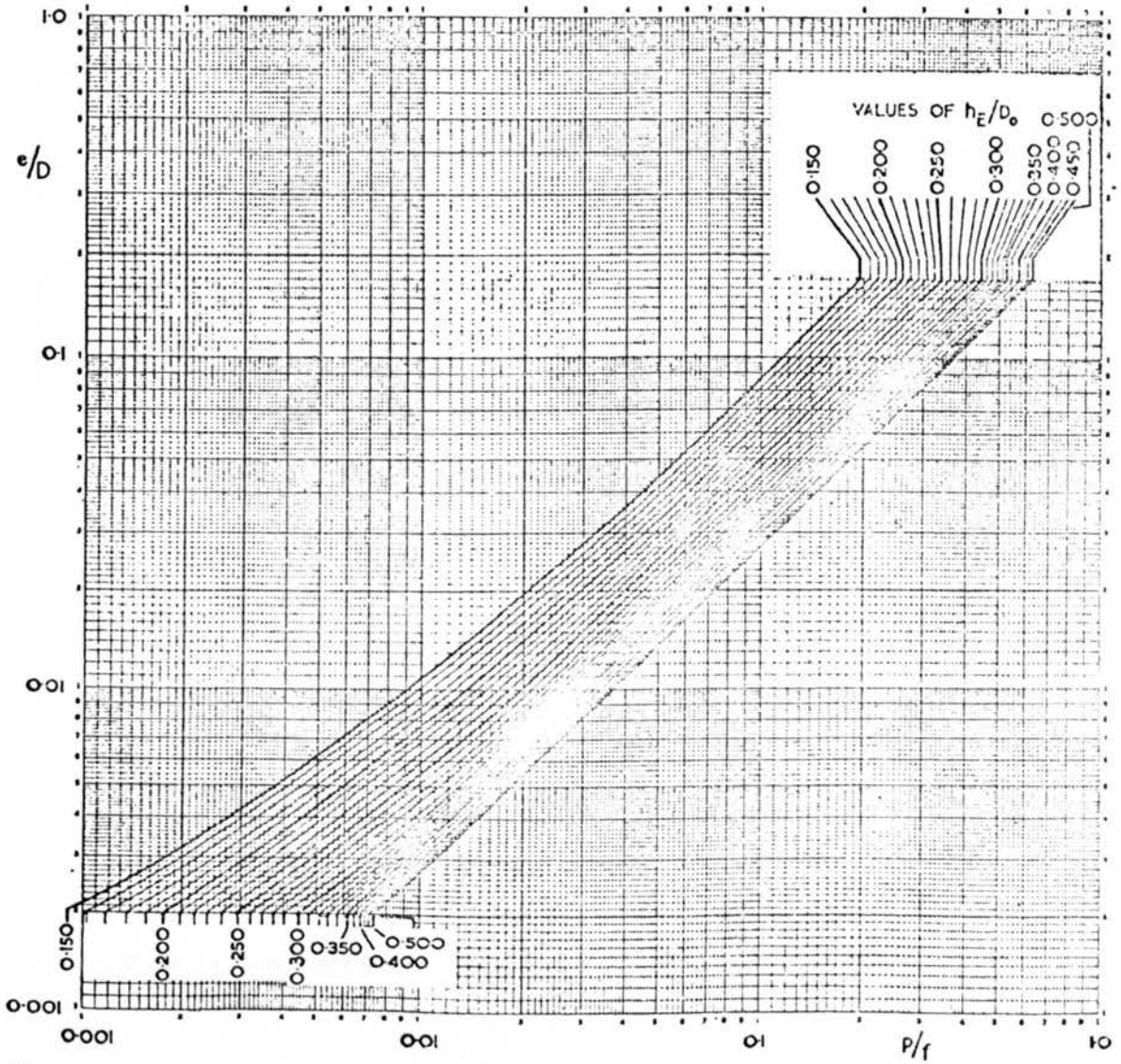

Figure 3.5.2.3 Design curves for unpierced domed ends

increased dome thickness. This calculation was carried out twice, firstly according to the B.S. code and, secondly, according to DNV codes.

a) For this purpose the dome end should be considered as a spherical pressure vessel of equivalent radius R_o equal to the external crown radius and the thickness is to be calculated using the formula

$$e_d = \frac{2PR_i}{4\sigma - 1.2P}$$

from which

$$e_d = 30.7 \text{ mm}$$

Now, if the thickness which will be calculated considering compensation is less than that just calculated, then no compensation needs to be made.

This calculation is performed according to Figure (3.5.4 (2)) of the B.S. shown on the next page.

$$\rho = \frac{d_m}{D_i + 2T_r} \sqrt{\frac{D_i + 2T_r}{2T_r}}$$

where d_m is the major axis of the opening and T_r the total thickness of shell as required by 3.5.4 Section of the B.S. for single openings

Assume $d_m = 290$ mm

$D_i = 1060$ mm

$T_r = 59.1$ mm (Guess)

Therefore,

$\rho = 0.778$ and

$C \frac{T_r}{T} = 2.1$

Taking C = 1.1 according to B.S., and T = 30.7 mm, the value of T_r is found as

$$T_r = 58.6 \text{ mm}$$

This is the thickness of the dome end including compensation.

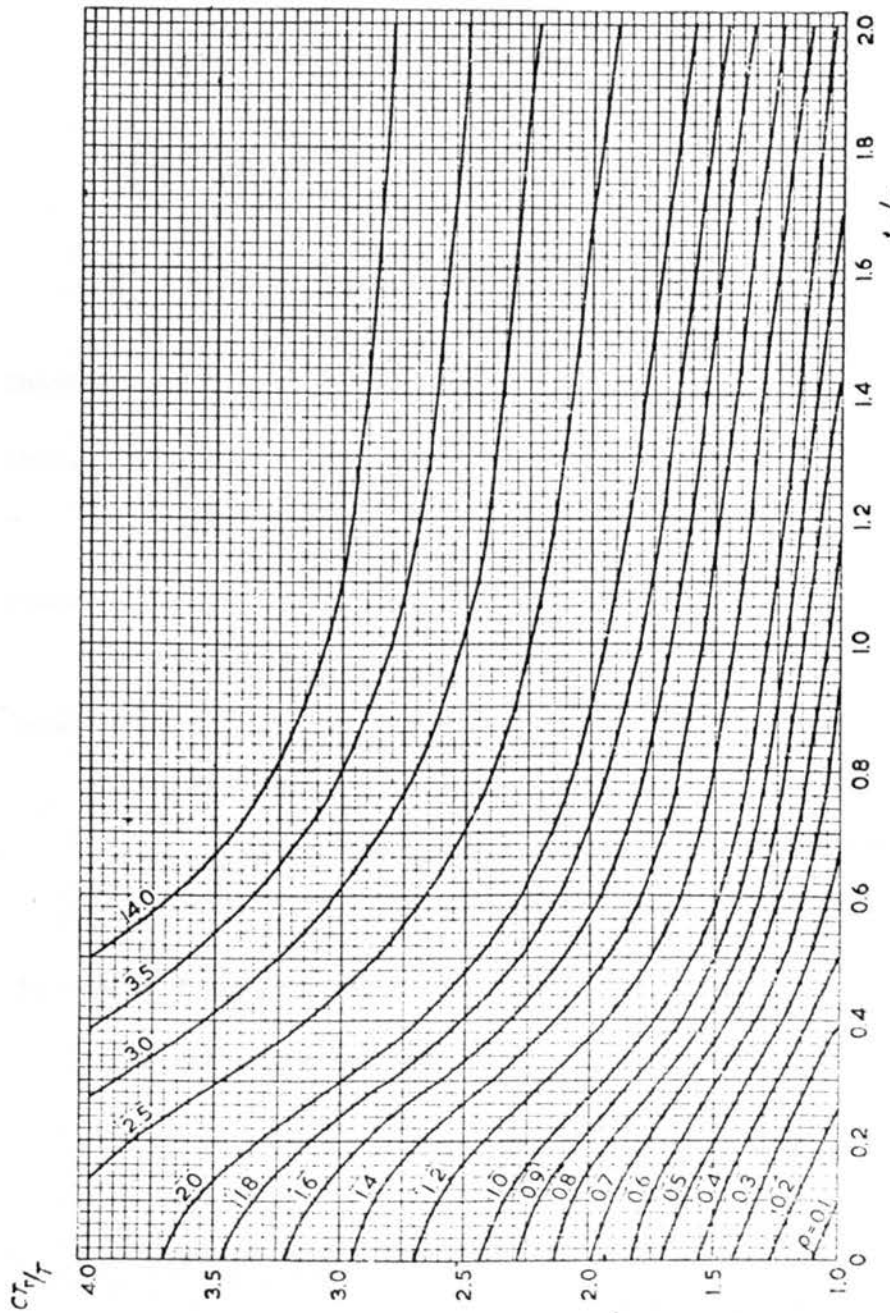

Figure 3.5.4(2) Design curves for flush nozzles in spherical shells ($d/D < 0.5$) and for flush nozzles in conical shells ($d/D < 0.3$)

b) The calculation for compensation will be made according to Figure (4.3) of the DNV codes shown on the next page.

For this calculation the following ratios have to be estimated.

Assuming a value of t = 50 mm,

$$\frac{d_m}{\sqrt{D_o t}} = \frac{d_m}{\sqrt{(D_i+2t)\,t}} = 1.2$$

$$\frac{H}{D_o} = \frac{h + t}{D_i + 2t} = \frac{308 + t}{1060 + 2t} = 0.309$$

Therefore, k = 1.14 (shape factor)

Thus,

$$t = \frac{PD_o}{20\sigma} k = \frac{P(D_i+2t)}{20\sigma} k$$

where

P = 147 Bars

leading to

t = 49.6 mm

Comparing the DNV and B.S. results, the DNV value is 15% smaller.

5. Total Height of Pressure Chamber

Height of bottom dome end	$= h + e_d + L$	$L \geq 2e_d$
	$= h + e_d + 3e_d$	take
	$= 430$ mm	$L = 3e_d$
Height of top dome end	$= h + T_r + L$	
	$= h + T_r + 3e_d$	
	$= 544$ mm	

Therefore,

total height of pressure chamber = 430 + 544 + 1040 = 2014 mm

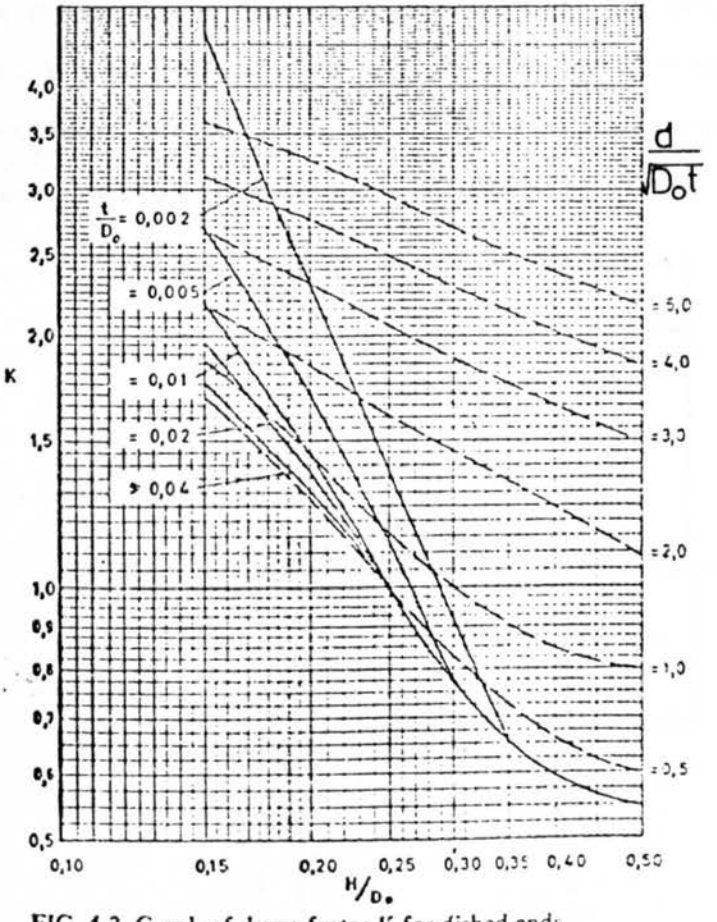

FIG. 4.3 Graph of shape factor K for dished ends

Note 1. In the case of ends containing only compensated openings, read K from full curves of t/D_o = 0.002 to t/D_o = 0.04 interpolating as necessary.

Note 2. In the case of ends containing uncompensated openings, read K from the broken line curves of $d/\sqrt{D_o t}$ = 5.0 to $d/\sqrt{D_o t}$ = 0.5 interpolating as necessary. In this case, K is to be taken as smaller than the value for a similar unpierced end.

Note 3. Linear interpolation is not recommended.

6. Flange Design

The reason for having a flange near the top of the chamber was to provide access to the interior so that models with cross-sections bigger than that of the manhole could be mounted.

Because of the high design pressure, an extensive study for an optimum flange design had to be carried out. In order to achieve this the B.S. flange design rules were programmed. The best results were obtained through the use of a full faced flange with a soft ring-type gasket. The particulars of this flange are presented in the following figure.

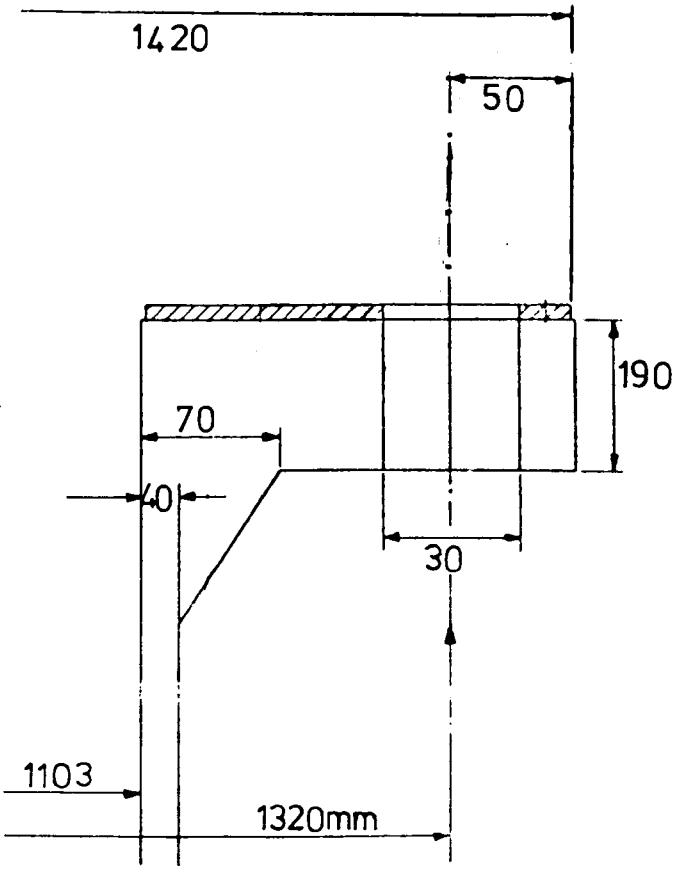

The particulars for the bolts are given below.

Nominal bolt stress	0.940 kN/mm²
Number of bolts	40
Bolt diameter	28.5 mm

Bolt hole diameter	31 mm

The gasket particulars were

Material	Soft Aluminium
Gasket factor	4
Minimum design seating stress	0.0606 kN/mm^2

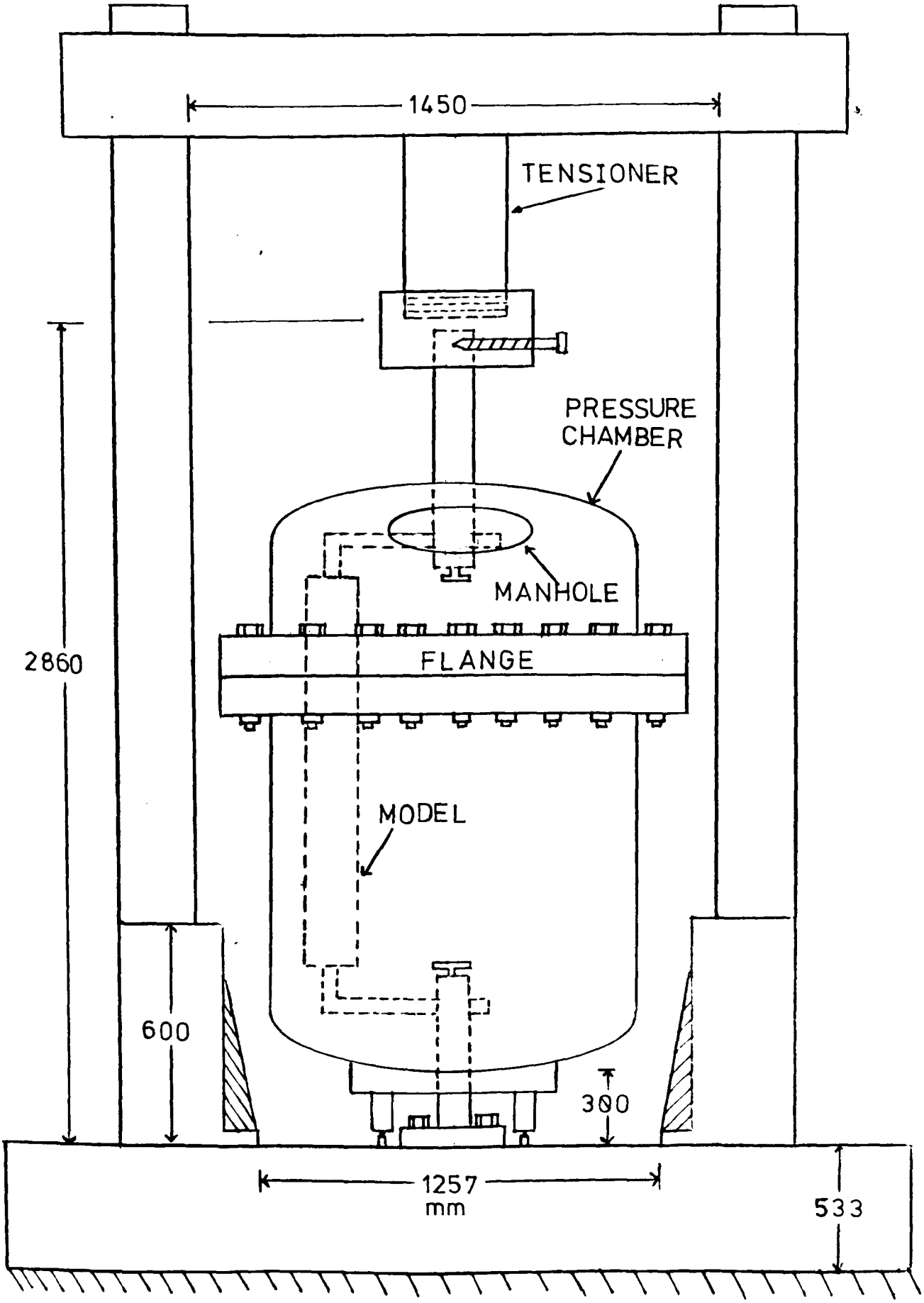

EXPERIMENTAL SET-UP

FIGURES

Figure No.		page
	CHAPTER 1	
1.1,1.2	Typical elastic load-strain curves	147
1.3	The Brazier effect	148
1.4	Typical beam-column	149
1.5	Layout of computing programs	149
1.6	Venn diagram showing relation of main programs	150
	CHAPTER 2	
2.1	Typical damped and undamped curves	150
	CHAPTER 3	
3.1	Internal forces and moments on an element	151
3.2	Equilibrium of an element under internal forces and moments	151
3.3,3.4	Average stress-strain curves showing comparison between single-layer and multi-layer approaches	152
3.5	Average stress-strain curves obtained with different number of layers through the shell wall thickness	153
3.6-3.9	Average stress-strain curves related to convergence studies	153-155
3.10-3.16	Comparions with other experimental and theoretical results	155-158
3.17	Cylindrical shell divided into small rectangular elements	159
3.18	Adopted centre finite difference mesh	159
3.19	Mode patterns	160
3.20	Illustration of boundary conditions	161

Figure No.	CHAPTER 4	page
4.1	Beam-column model to cater for interaction between local and overall instability	162
4.2,4.3	Density factors plotted against L/r	163
4.4-4.7	Average stress-strain curves related to convergence studies	164-165
4.8-4.12	Comparisons with other theoretical and experimental solutions	166-169
	CHAPTER 5	
5.1	Set-up of the simplified approach to beam-column interactive buckling	170
5.2	Comparison between ANSA2 and ANSA3 formulations	171
	CHAPTER 6	
6.1	Combinations of bending and axial compression	172
6.2-6.25	Average stress-strain curves related to axial compression	173-184
6.26-6.33	Maximum compressive strengths plotted against R/T ratios	185-188
6.34-6.41	Maximum compressive strengths plotted against L/R ratios	189-190
6.42a-6.102a	Average stress-strain curves related to combinations of bending and axial compression	191-250
6.42b-6.102b	Moment-strain curves related to combinations of bending and axial compression	191-250
6.103-6.120	Maximum compressive strength-corresponding moment interaction curves	251-259
6.121a-6.181a	Average stress-strain curves related to combinations of bending, axial compression and external pressure	260-320
6.121b-6.181b	Moment-strain curves related to combinations of bending, axial compression and external pressure	260-320
6.182-6.200	Maximum compressive strength-corresponding moment interaction curves	321-330
6.201-6.204	Results on damaged cylinders	331-334

Figure No.		page
6.205a-6.212a	Average stress-strain curves for circular columns under axial compression	335-342
6.205b-6.212b	Load-total deflection curves for circular columns under axial compression	335-342
6.213	Maximum compressive strength plotted against slenderness (λ)	343
6.214-6.216	Results on clamped circular columns	344-346
6.217-6.223	Comparisons with existing Design Rules	347-350
6.224-6.237	Longitudinal and circumferential deformations	351-392

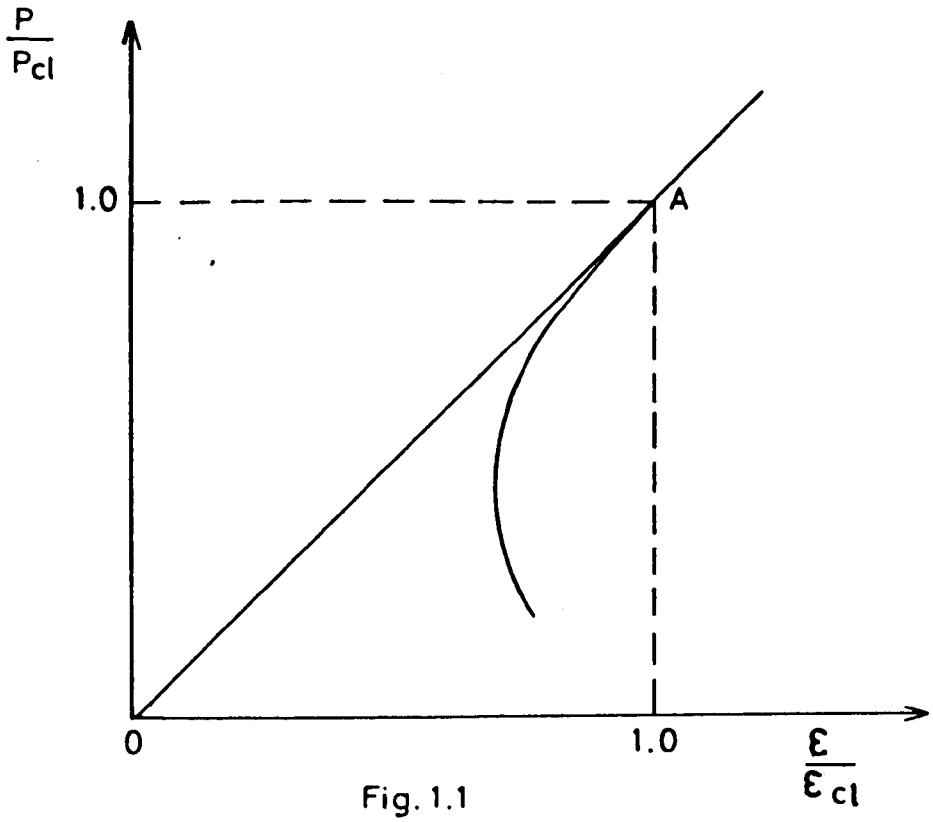

Fig. 1.1

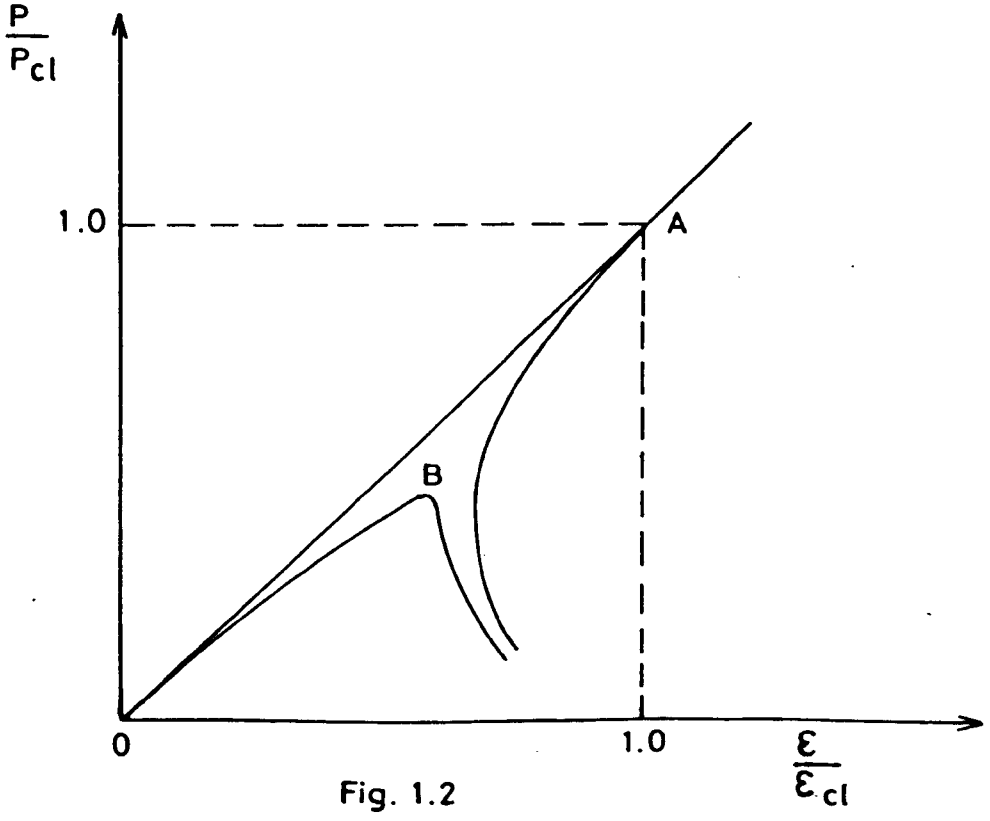

Fig. 1.2

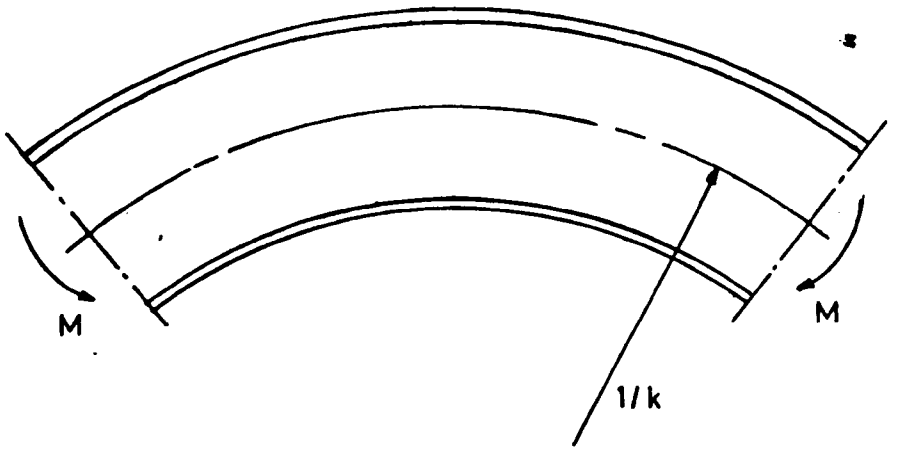

Fig. 1.3a

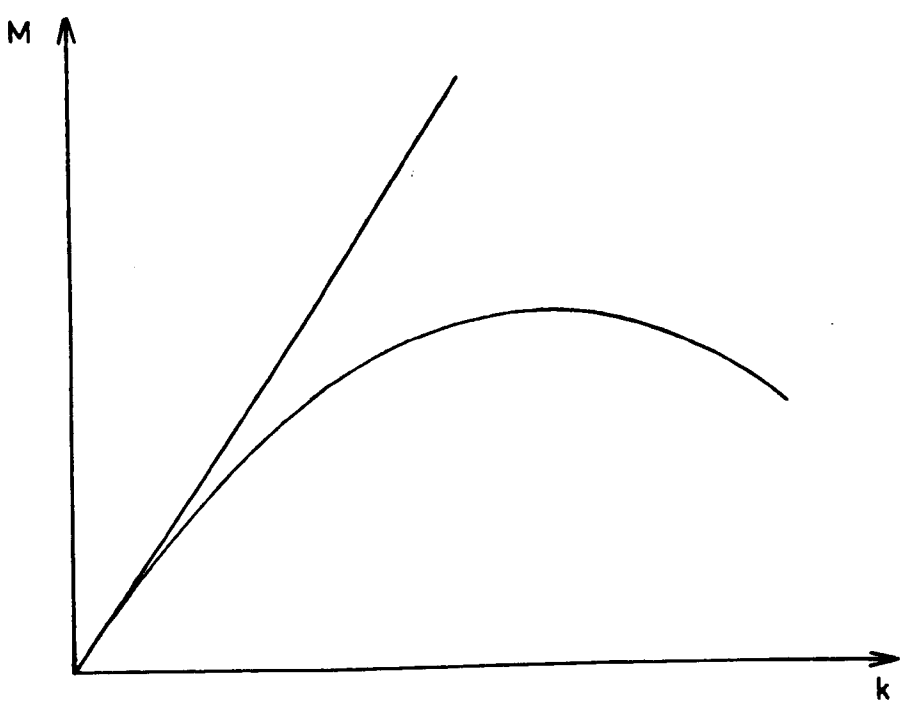

Fig. 1.3b

The Brazier effect

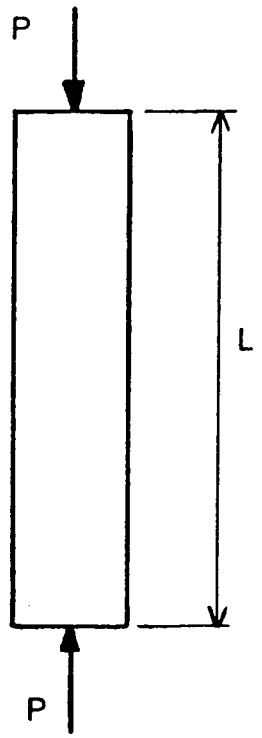
P
L
P

Fig. 1.4

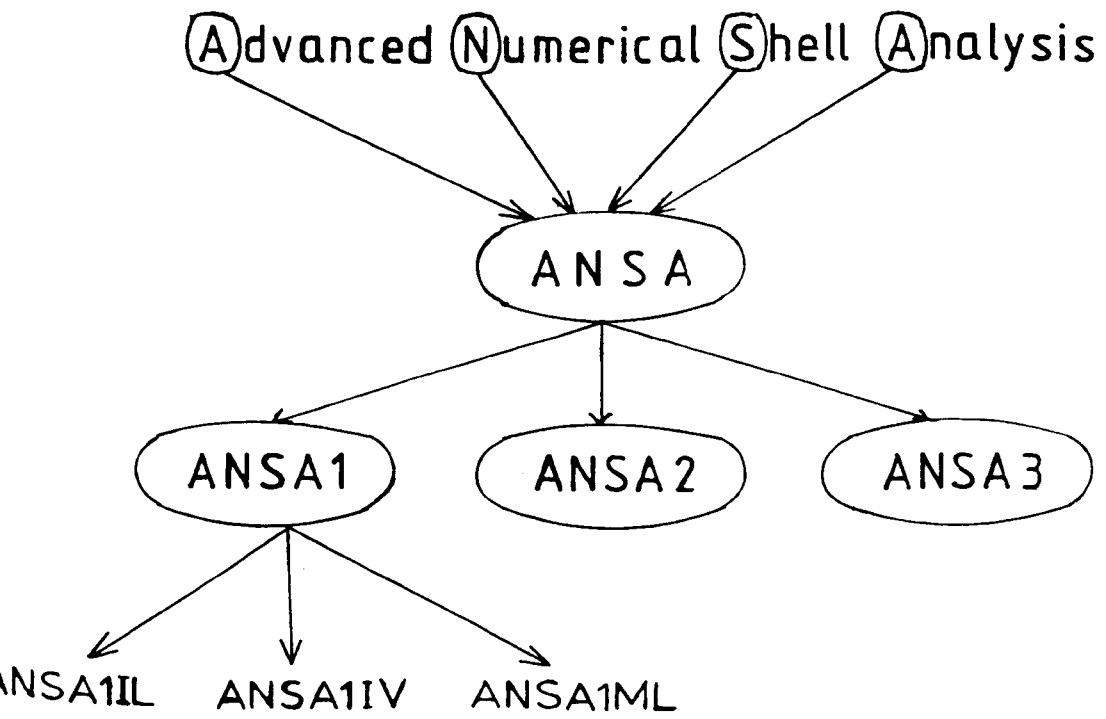
Advanced Numerical Shell Analysis
ANSA
ANSA1
ANSA2
ANSA3
ANSA1IL
ANSA1IV
ANSA1ML

Fig.1.5

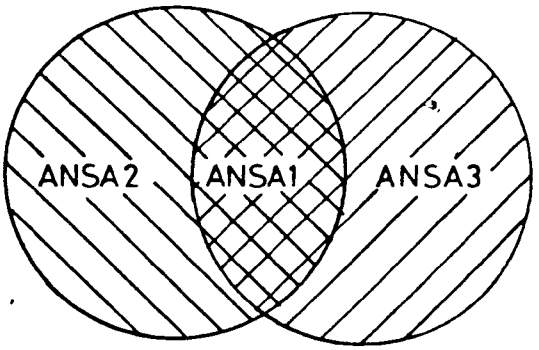

Fig. 1.6

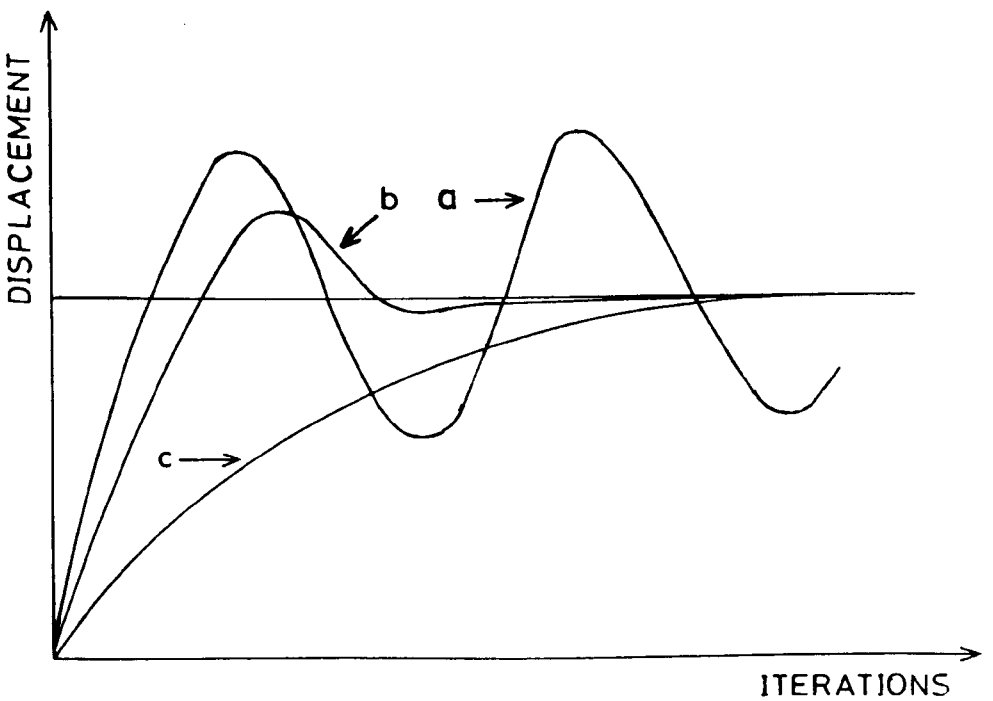

Fig. 2.1

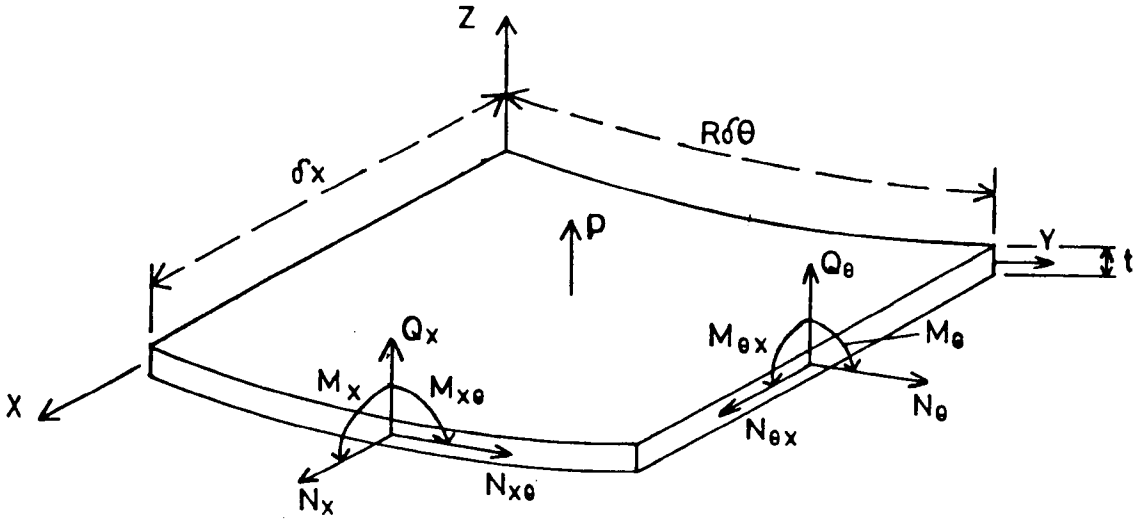

Fig. 3.1

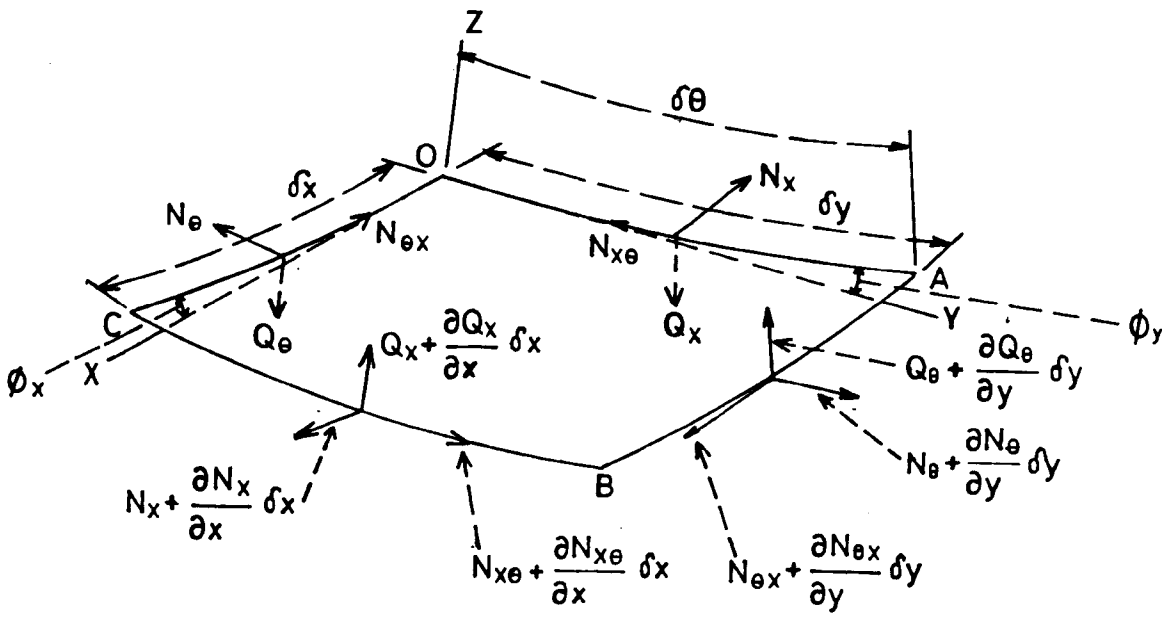

Fig. 3.2a

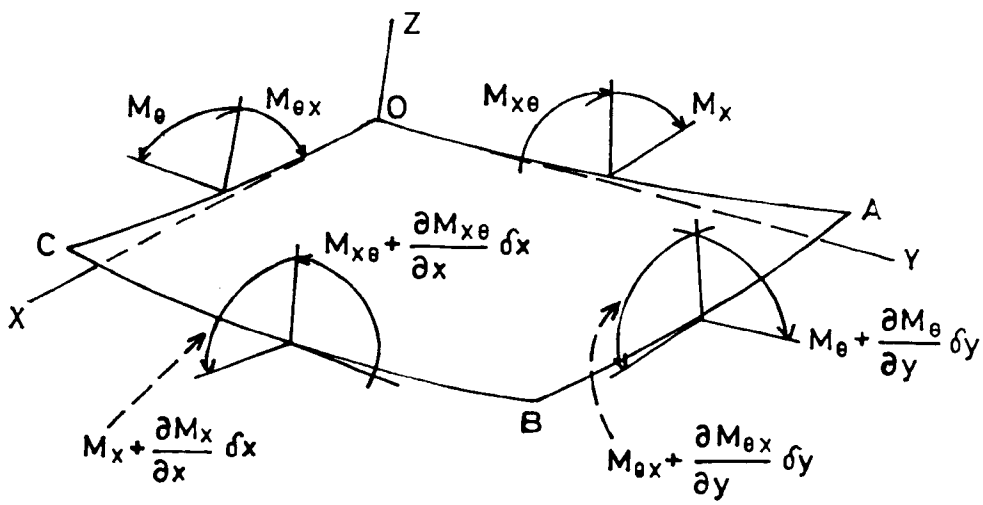

Fig. 3.2b

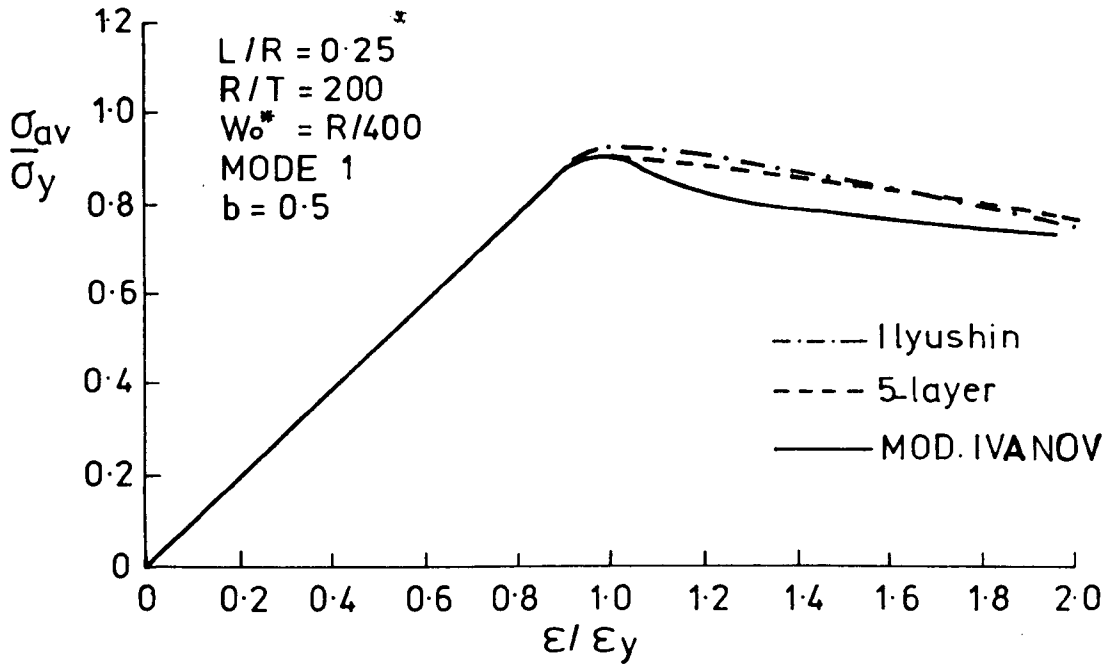
L/R = 0·25
R/T = 200
Wo* = R/400
MODE 1
b = 0·5
σav/σy
1·2
1·0
0·8
0·6
0·4
0·2
0
0 0·2 0·4 0·6 0·8 1·0 1·2 1·4 1·6 1·8 2·0
ε/εy
Ilyushin
5-layer
MOD. IVANOV

Fig. 3.3

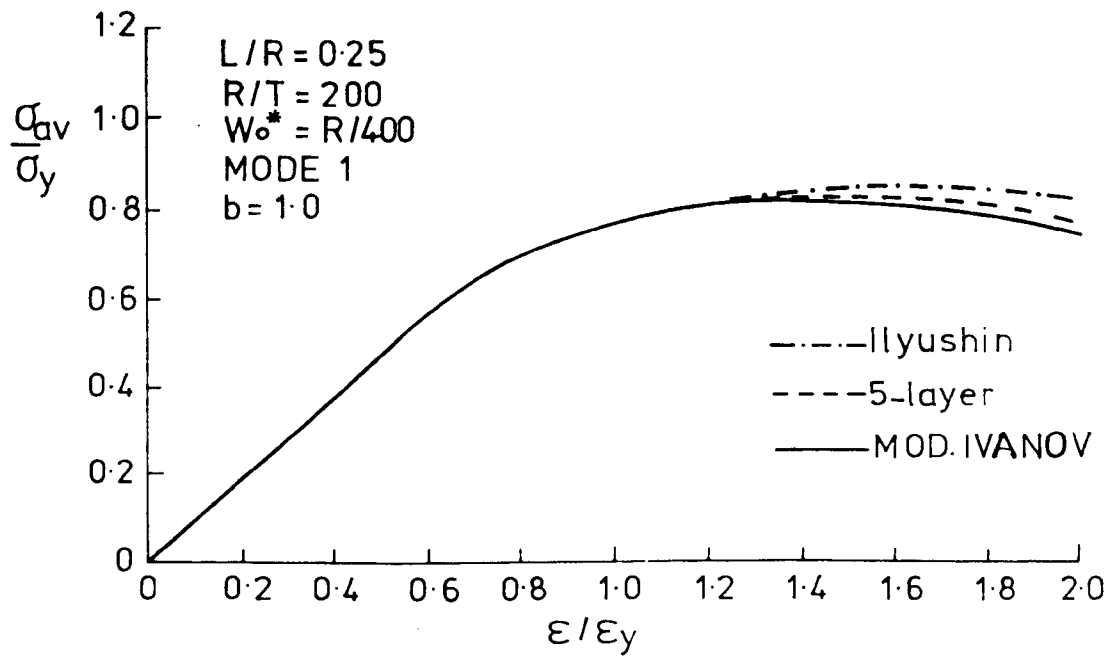
L/R = 0·25
R/T = 200
Wo* = R/400
MODE 1
b = 1·0
σav/σy
1·2
1·0
0·8
0·6
0·4
0·2
0
0 0·2 0·4 0·6 0·8 1·0 1·2 1·4 1·6 1·8 2·0
ε/εy
Ilyushin
5-layer
MOD. IVANOV

Fig. 3.4

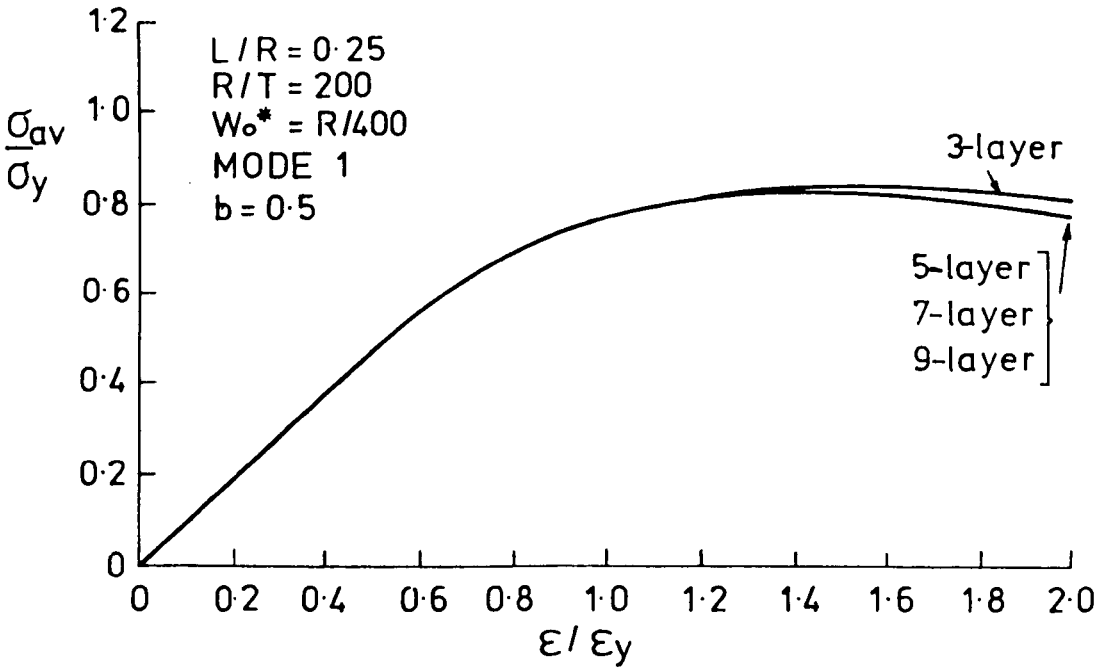
L / R = 0·25
R / T = 200
Wo* = R/400
MODE 1
b = 0·5
3-layer
5-layer
7-layer
9-layer
σav / σy
ε / εy
1·2
1·0
0·8
0·6
0·4
0·2
0
0·2
0·4
0·6
0·8
1·0
1·2
1·4
1·6
1·8
2·0

Fig. 3.5

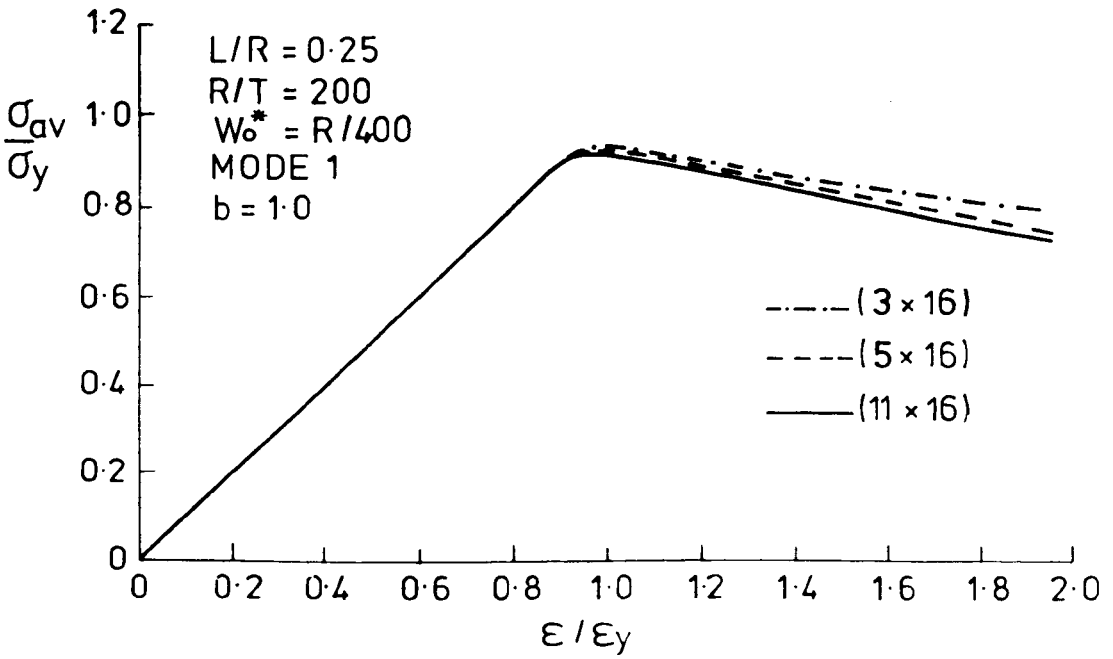
L/R = 0·25
R/T = 200
Wo* = R/400
MODE 1
b = 1·0
(3 × 16)
(5 × 16)
(11 × 16)
σav / σy
ε / εy
1·2
1·0
0·8
0·6
0·4
0·2
0
0·2
0·4
0·6
0·8
1·0
1·2
1·4
1·6
1·8
2·0

Fig. 3.6

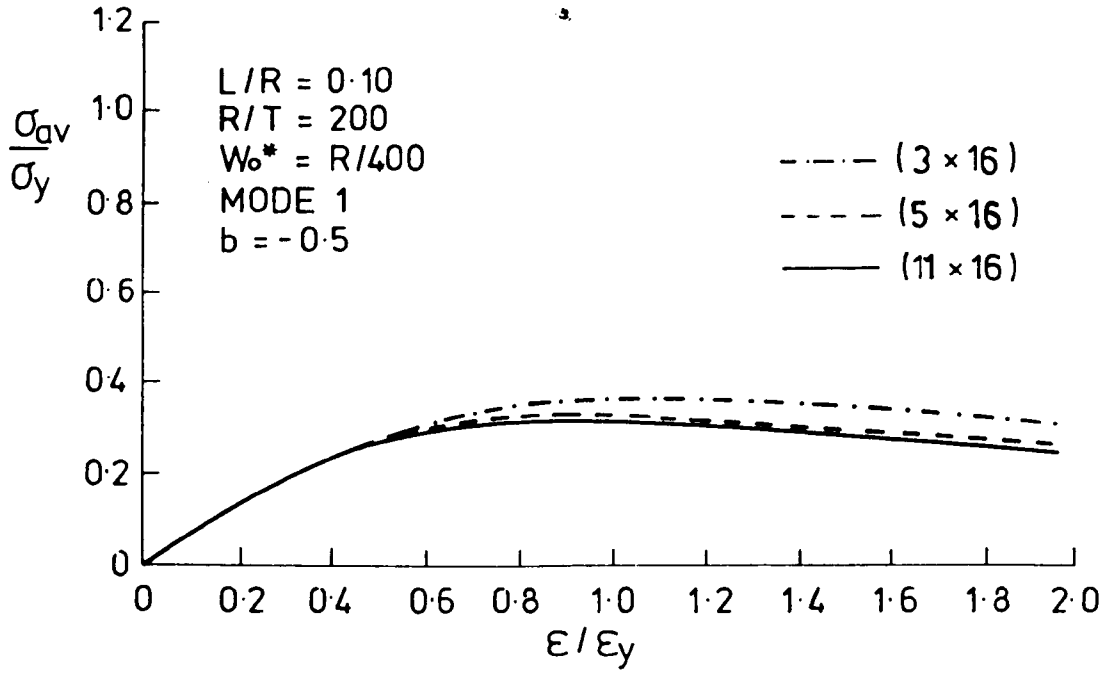
1·2
1·0
0·8
0·6
0·4
0·2
0
σav/σy
L/R = 0·10
R/T = 200
Wo* = R/400
MODE 1
b = -0·5
(3 × 16)
(5 × 16)
(11 × 16)
0
0·2
0·4
0·6
0·8
1·0
1·2
1·4
1·6
1·8
2·0
ε/εy

Fig. 3.7

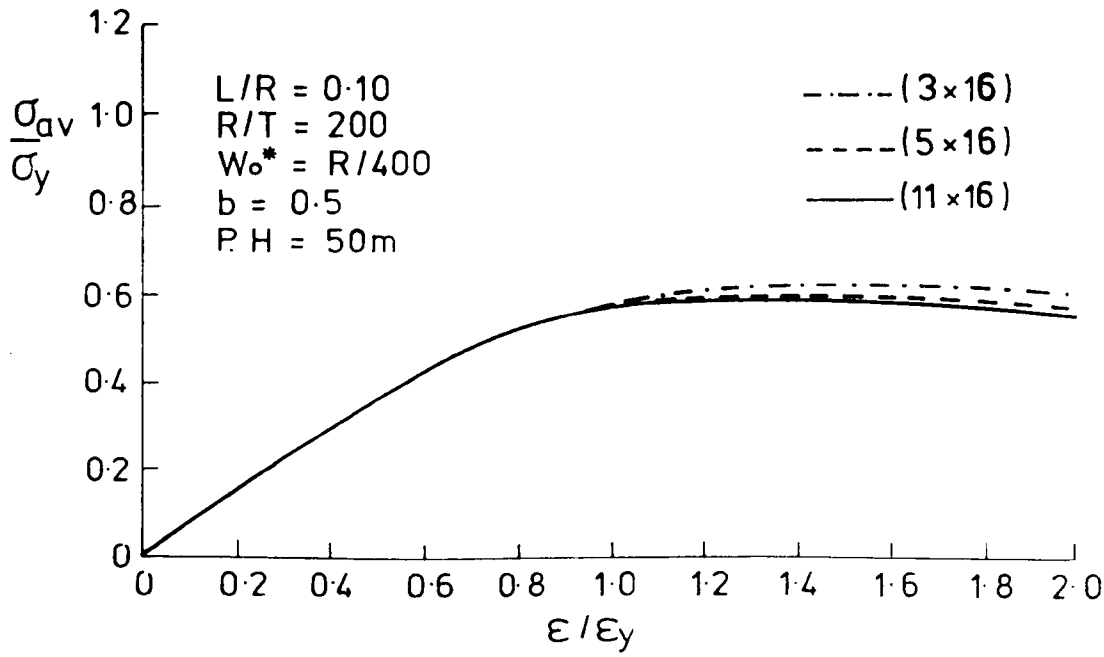
1·2
1·0
0·8
0·6
0·4
0·2
0
σav/σy
L/R = 0·10
R/T = 200
Wo* = R/400
b = 0·5
P.H = 50m
(3×16)
(5×16)
(11×16)
0
0·2
0·4
0·6
0·8
1·0
1·2
1·4
1·6
1·8
2·0
ε/εy

Fig. 3.8

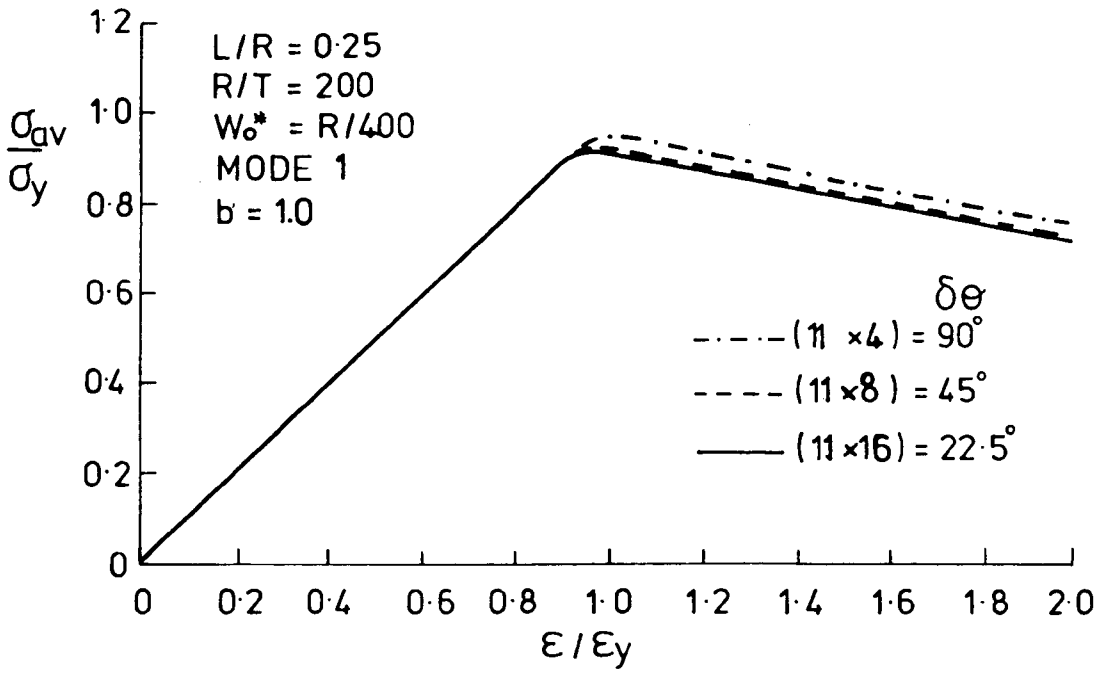

Fig. 3.9

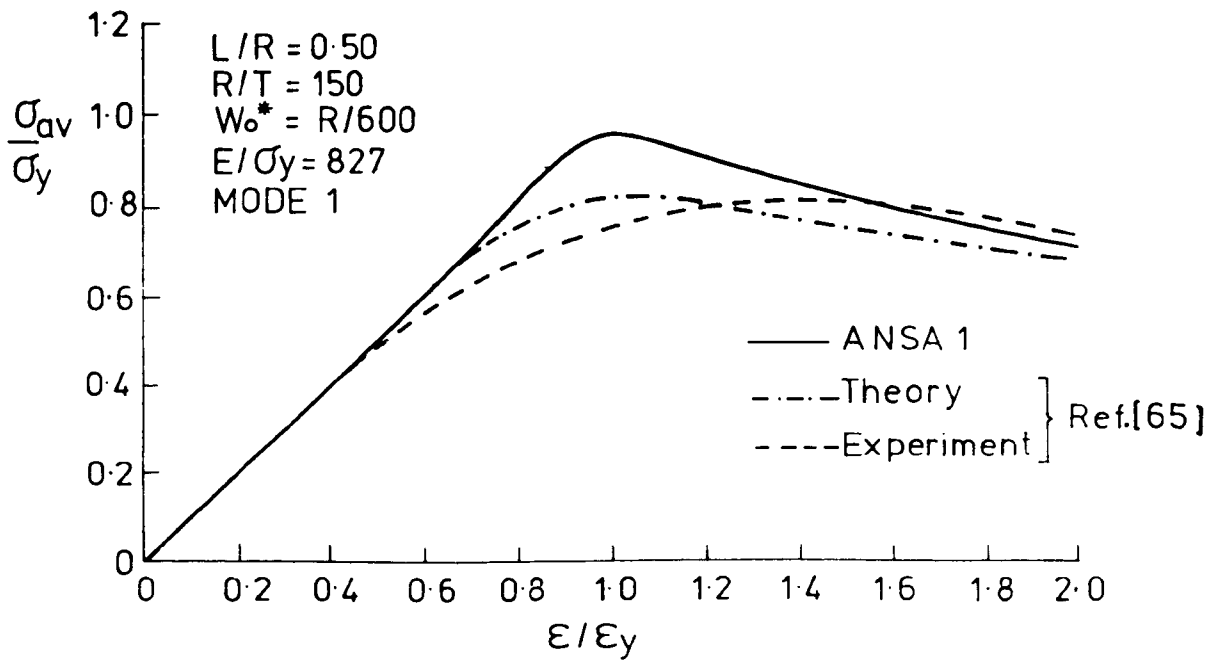

Fig. 3.10

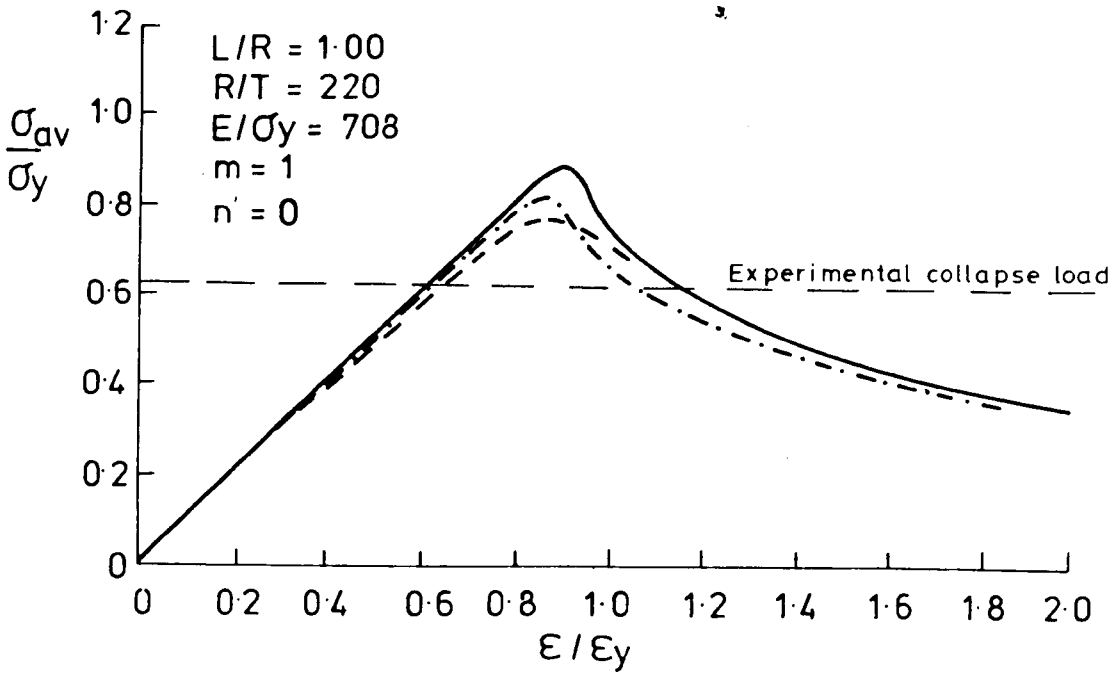

Fig. 3.11

ANSA 1
FULL CYLINDER $W_o^* > 1mm$
REF. [21,66] VERY LOW LEVEL OF RESIDUAL STRESSES.
PART CYLINDER $W_o^* > 0 \cdot 1mm$

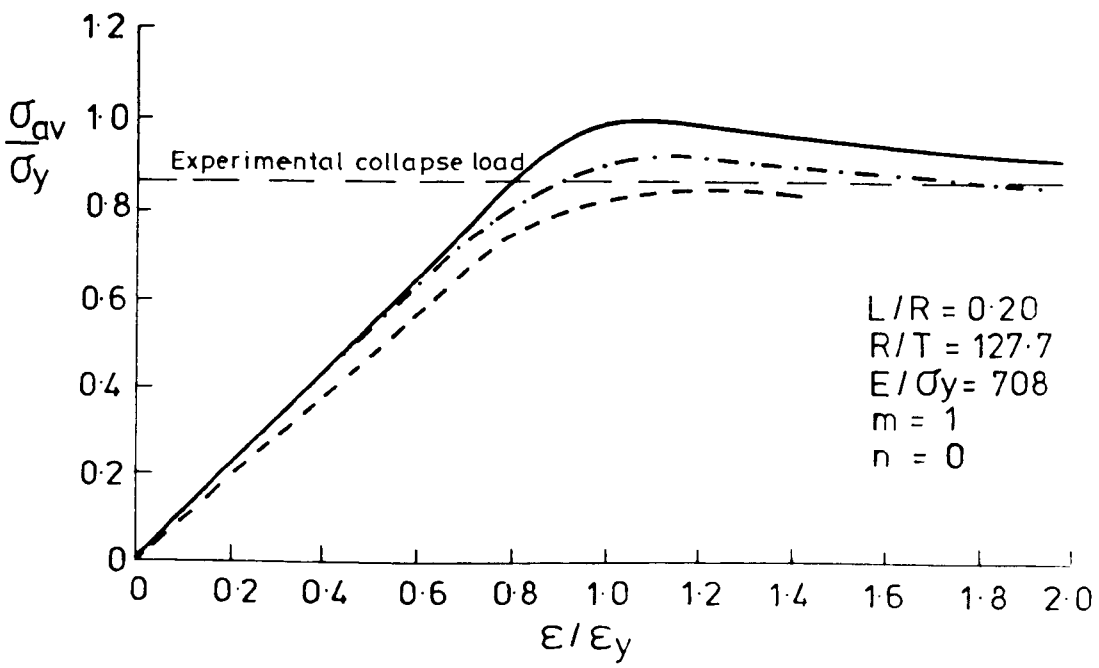

Fig. 3.12

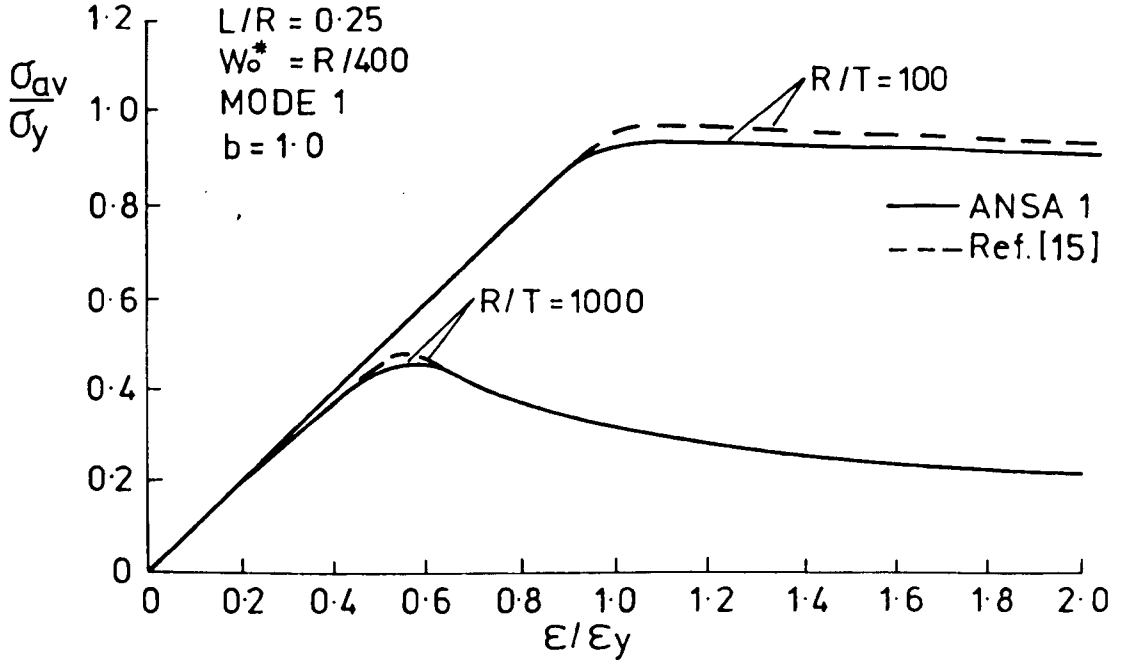

Fig. 3.13

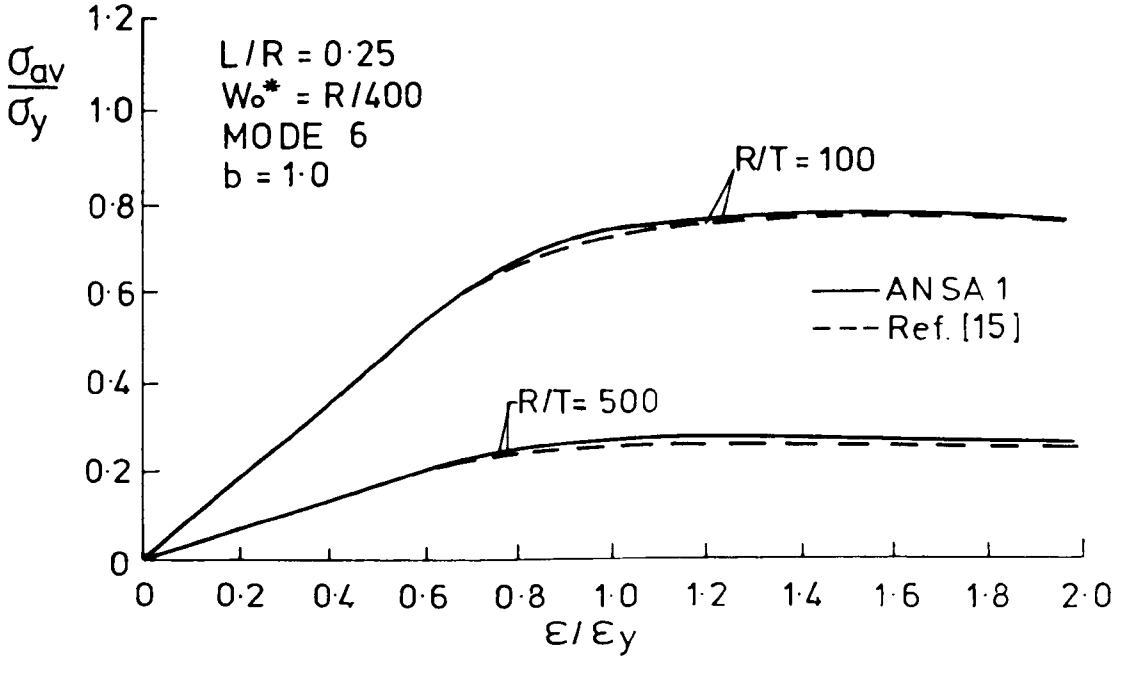

Fig. 3.14

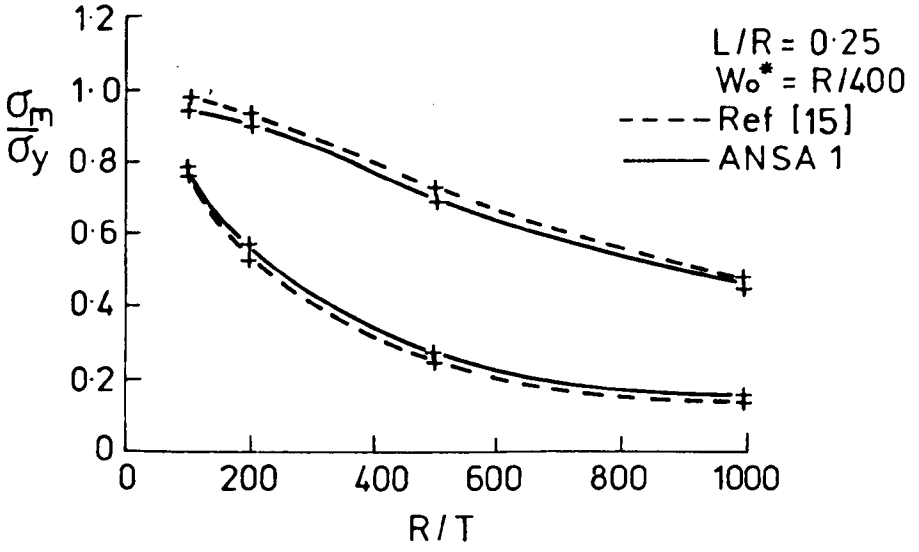

Fig. 3.15

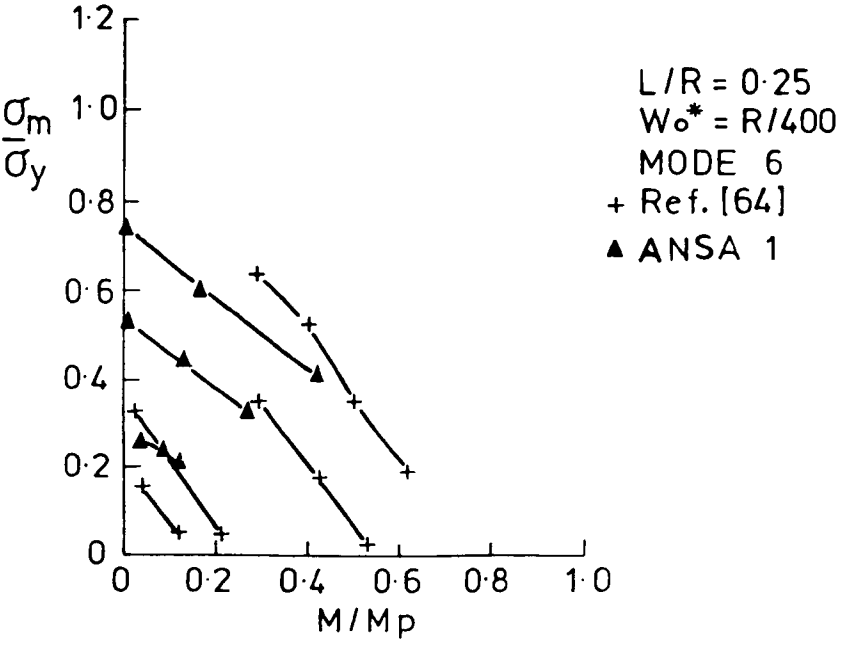

Fig. 3.16

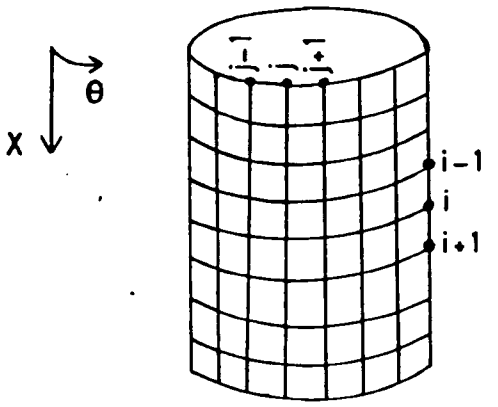

Fig. 3.17

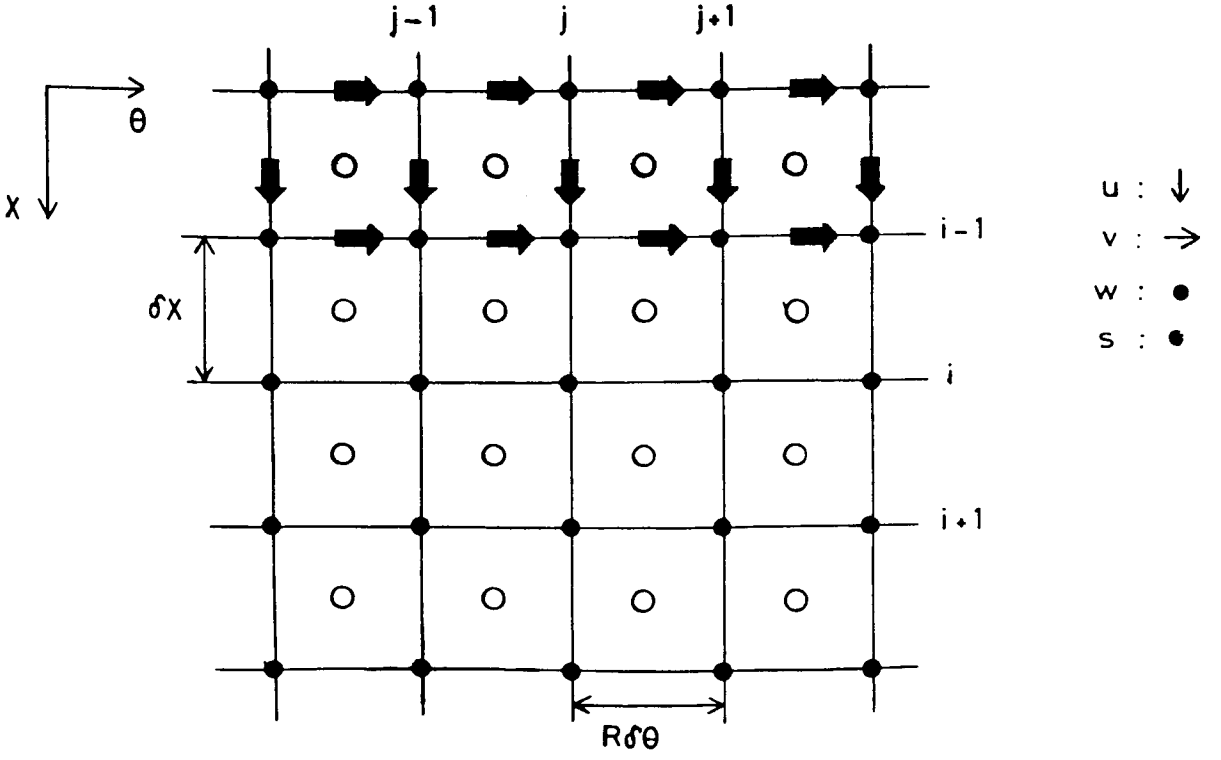

Fig. 3.18

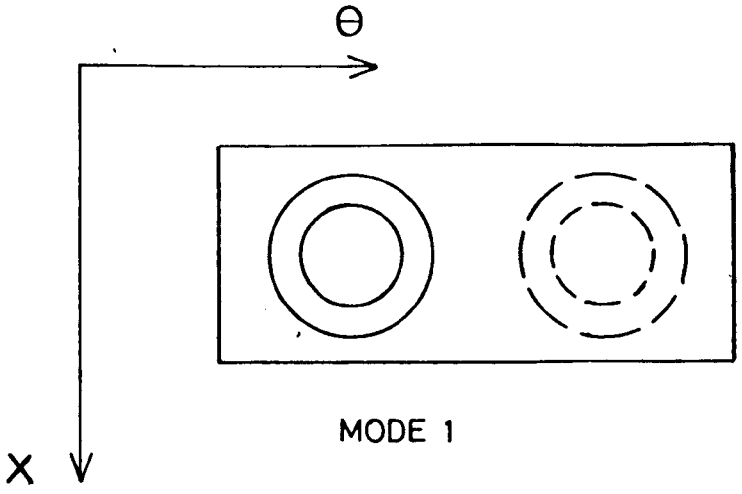

Fig. 3.19

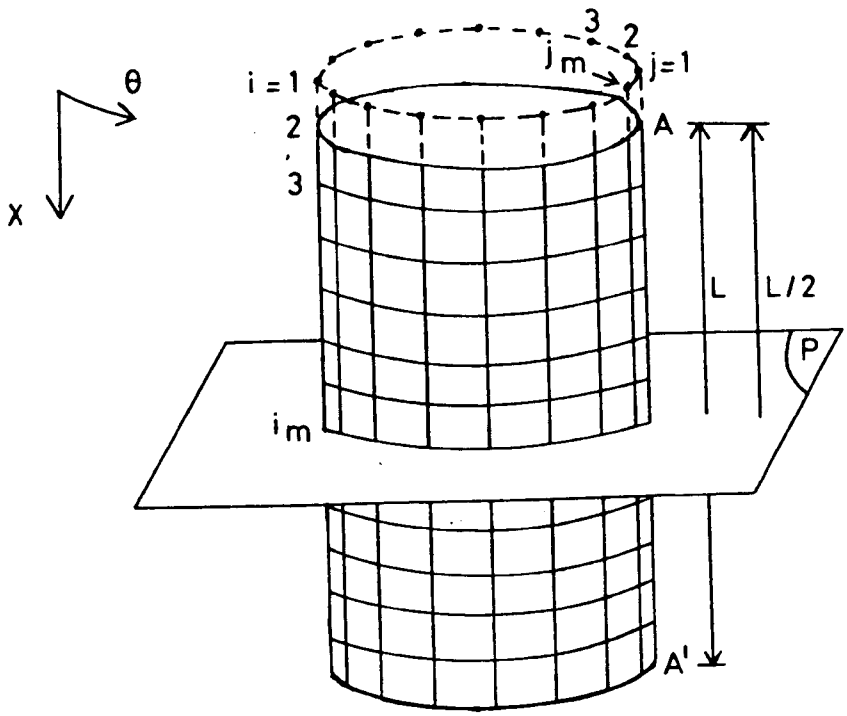

$j_{m+1} = 1$

$j_{m+2} = 2$

$i_{m+1} = i_{m-1}$

Fig. 3.20a

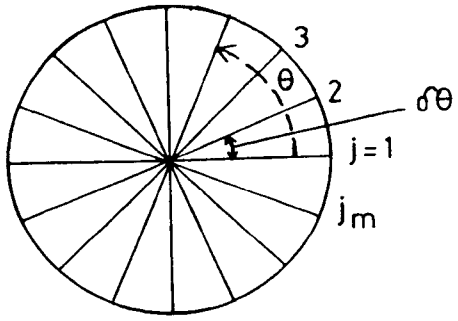

$$\delta\theta = \frac{2\pi}{j_m}$$

$$\theta = (j-1)\delta\theta$$

Fig. 3.20b

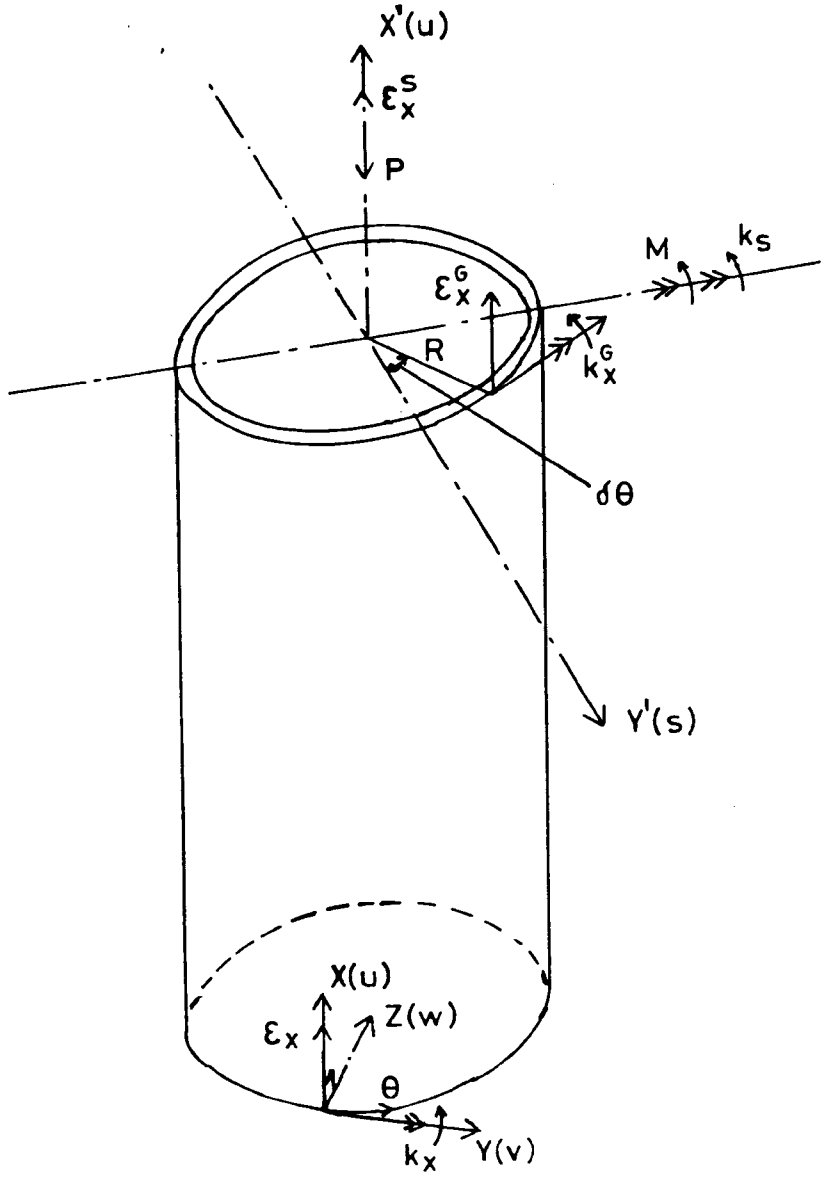
X'(u)
ε_x^s
P
M
k_s
ε_x^G
R
k_x^G
$\delta\theta$
Y'(s)
X(u)
ε_x
Z(w)
θ
k_x
Y(v)

Fig. 4.1

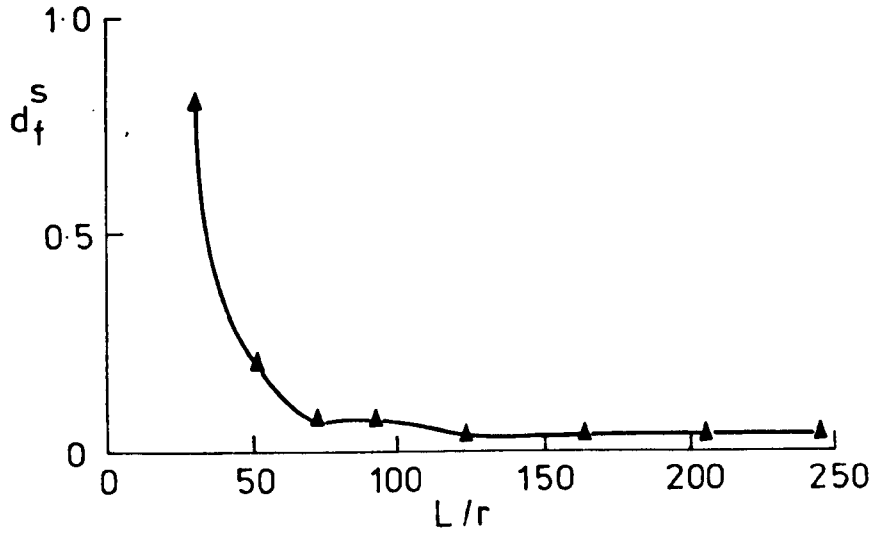
1·0
0·5
0
d_f^s
0
50
100
150
200
250
L/r

Fig. 4.2

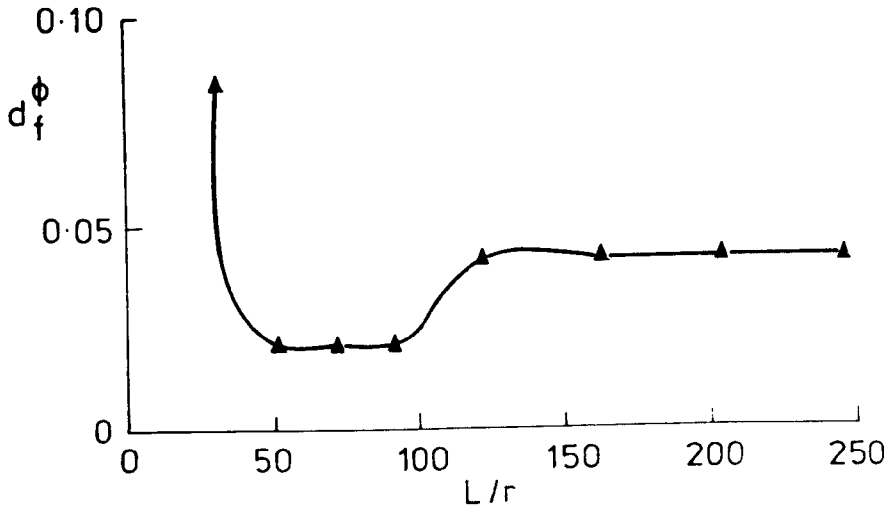
0·10
0·05
0
d_f^ϕ
0
50
100
150
200
250
L/r

Fig. 4.3

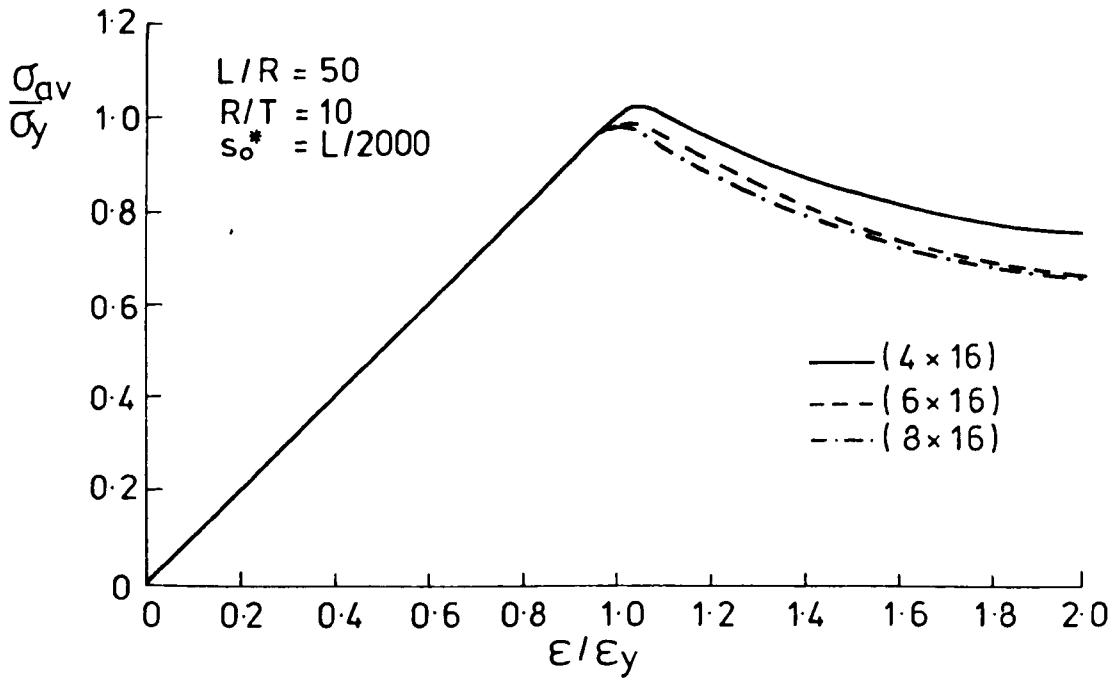
σav/σy
L/R = 50
R/T = 10
so* = L/2000
(4 × 16)
(6 × 16)
(8 × 16)
1·2
1·0
0·8
0·6
0·4
0·2
0
0 0·2 0·4 0·6 0·8 1·0 1·2 1·4 1·6 1·8 2·0
ε/εy

Fig. 4.4

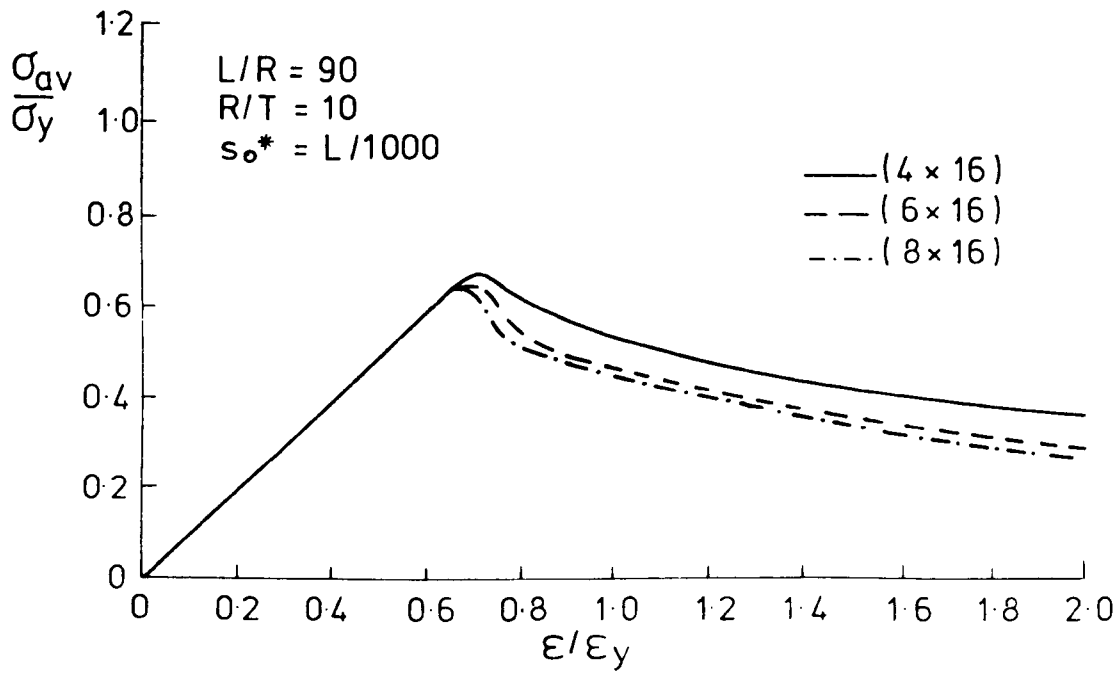
σav/σy
L/R = 90
R/T = 10
so* = L/1000
(4 × 16)
(6 × 16)
(8 × 16)
1·2
1·0
0·8
0·6
0·4
0·2
0
0 0·2 0·4 0·6 0·8 1·0 1·2 1·4 1·6 1·8 2·0
ε/εy

Fig. 4.5

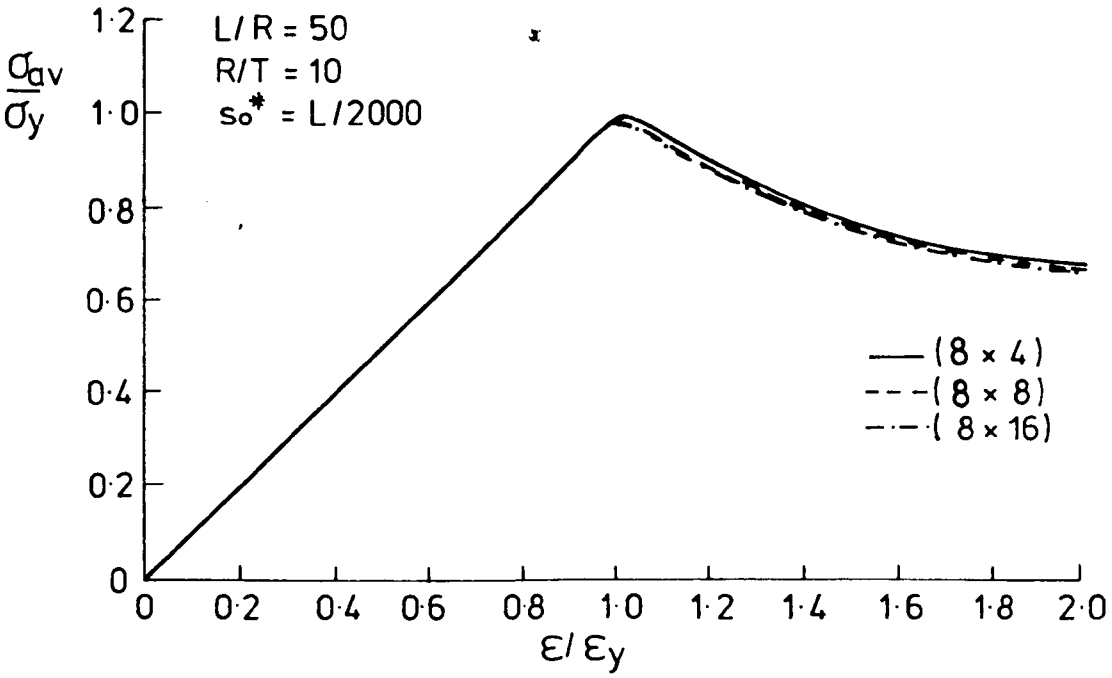
L/R = 50
R/T = 10
so* = L/2000
(8 × 4)
(8 × 8)
(8 × 16)
σav/σy
ε/εy
1·2
1·0
0·8
0·6
0·4
0·2
0
0·2
0·4
0·6
0·8
1·0
1·2
1·4
1·6
1·8
2·0

Fig. 4.6

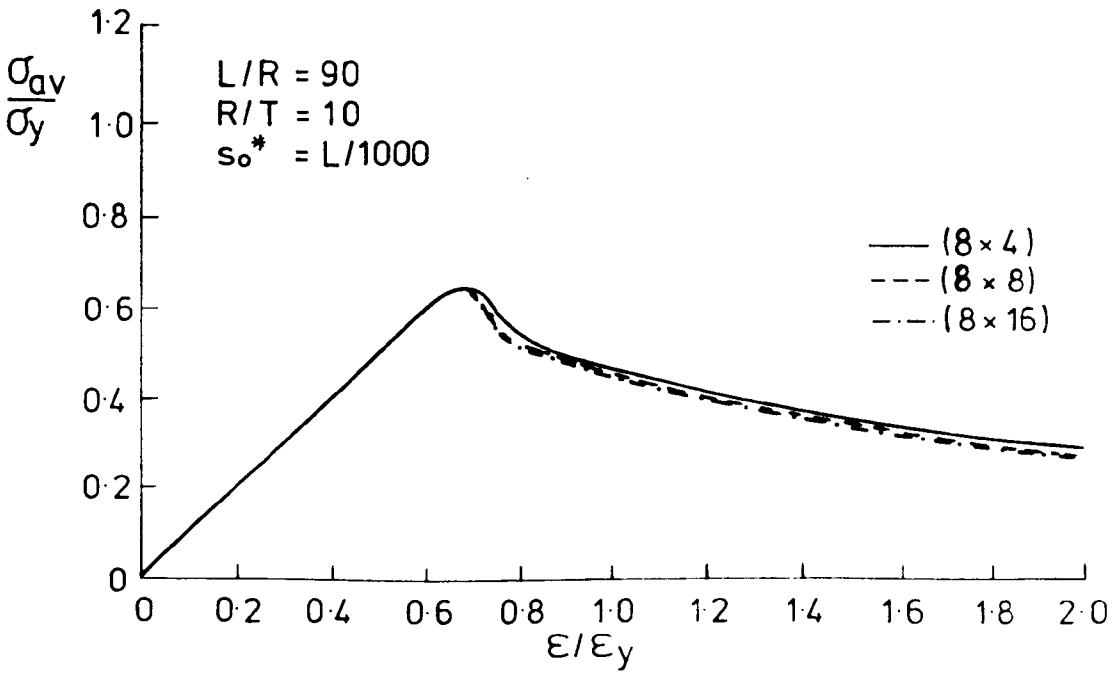
L/R = 90
R/T = 10
so* = L/1000
(8 × 4)
(8 × 8)
(8 × 16)
σav/σy
ε/εy
1·2
1·0
0·8
0·6
0·4
0·2
0
0·2
0·4
0·6
0·8
1·0
1·2
1·4
1·6
1·8
2·0

Fig. 4.7

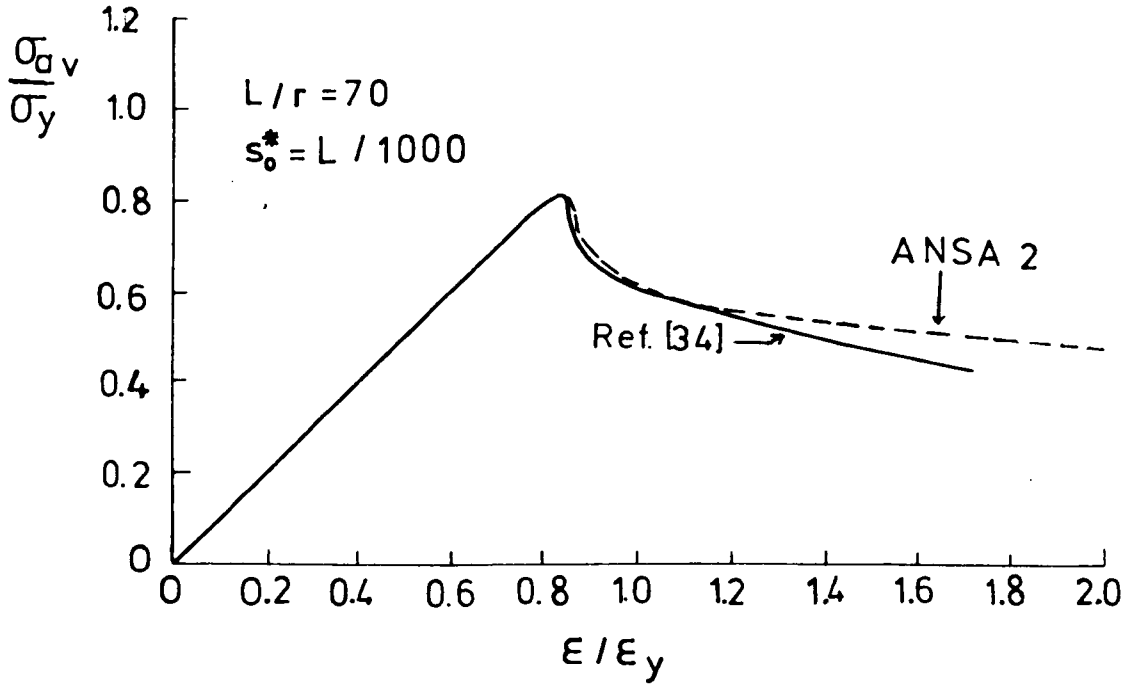
σav / σy
1.2
1.0
0.8
0.6
0.4
0.2
0
L / r = 70
s*o = L / 1000
ANSA 2
Ref. [34]
0 0.2 0.4 0.6 0.8 1.0 1.2 1.4 1.6 1.8 2.0
ε / εy

Fig. 4.8

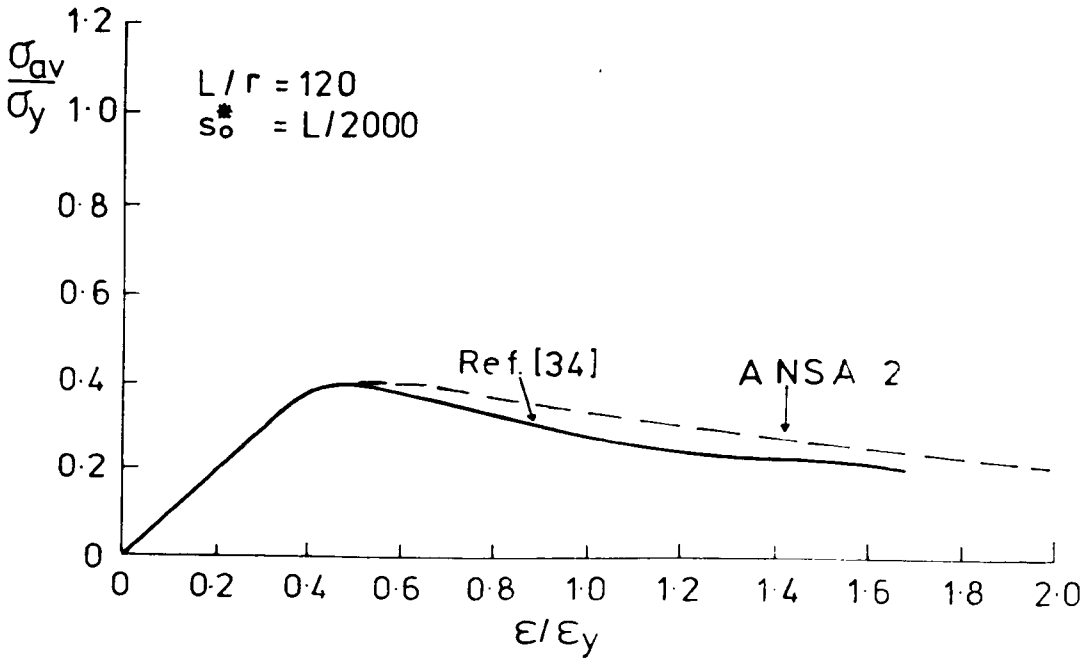
σav / σy
1·2
1·0
0·8
0·6
0·4
0·2
0
L / r = 120
s*o = L/2000
Ref. [34]
ANSA 2
0 0·2 0·4 0·6 0·8 1·0 1·2 1·4 1·6 1·8 2·0
ε / εy

Fig. 4.9

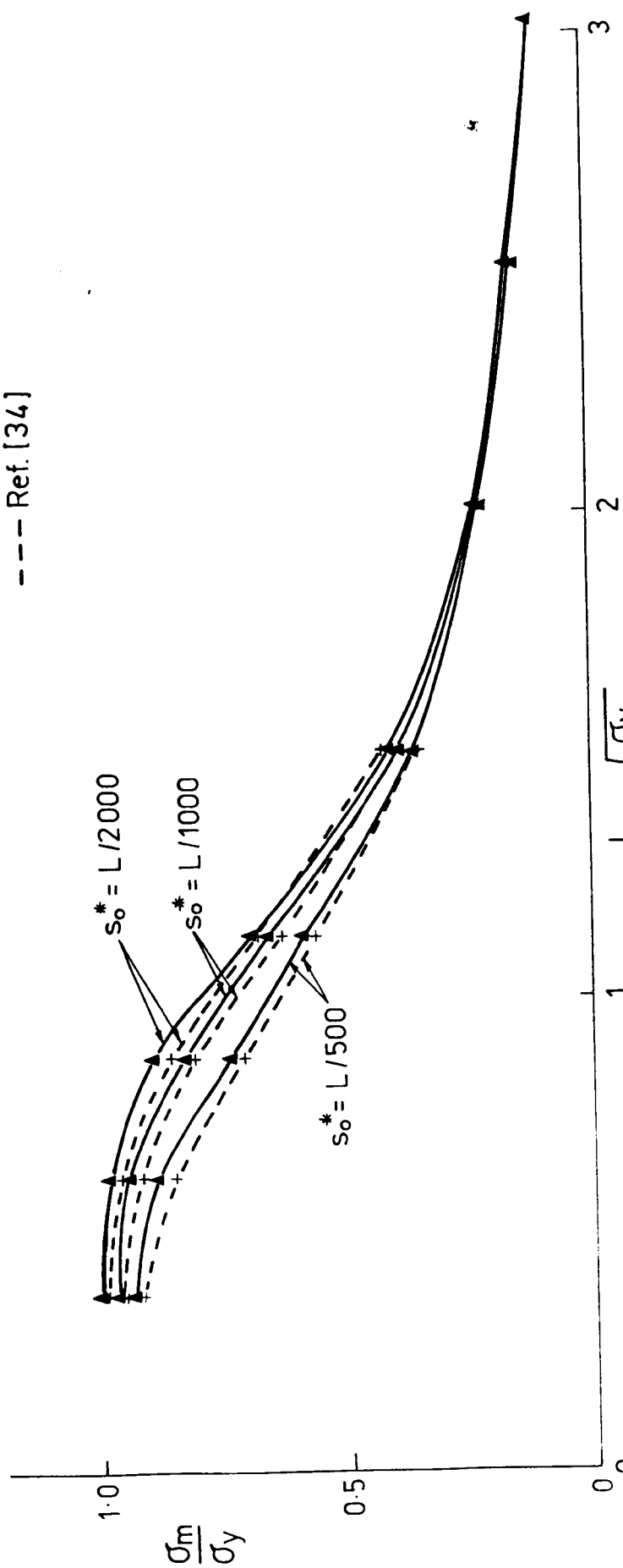
ANSA 2
Ref. [34]
$s_o^* = L/2000$
$s_o^* = L/1000$
$s_o^* = L/500$
$\frac{\sigma_m}{\sigma_y}$
1·0
0·5
0
0
1
2
3
$\lambda = \frac{L}{\pi r}\sqrt{\frac{\sigma_y}{E}}$

Fig. 4.10

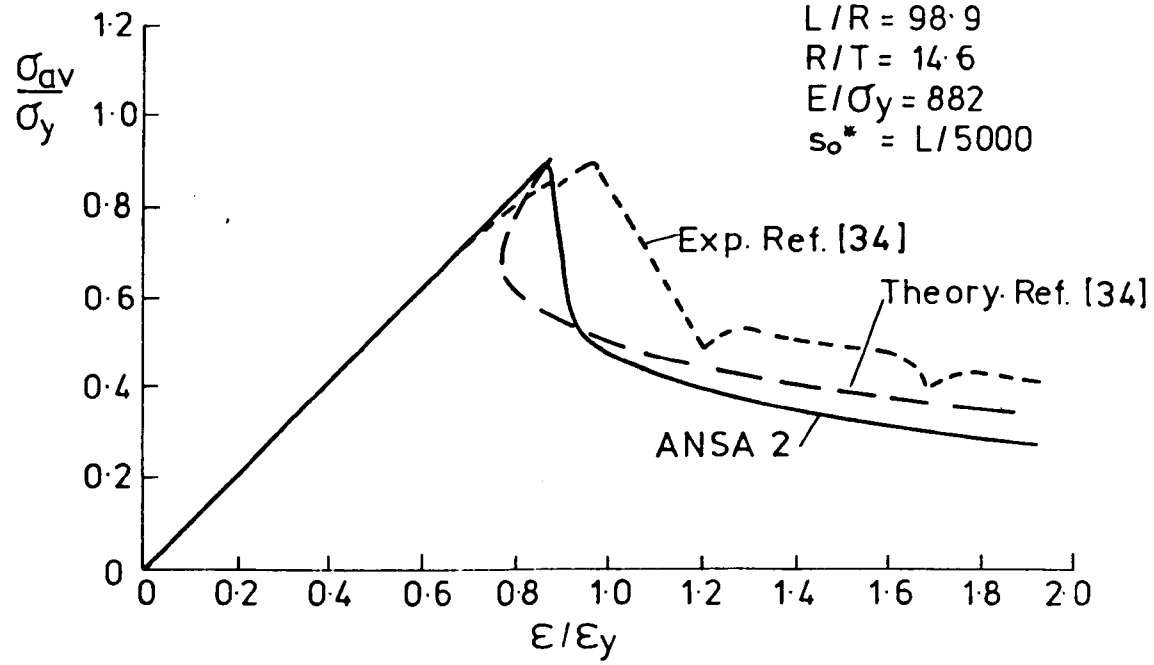

Fig. 4.11a

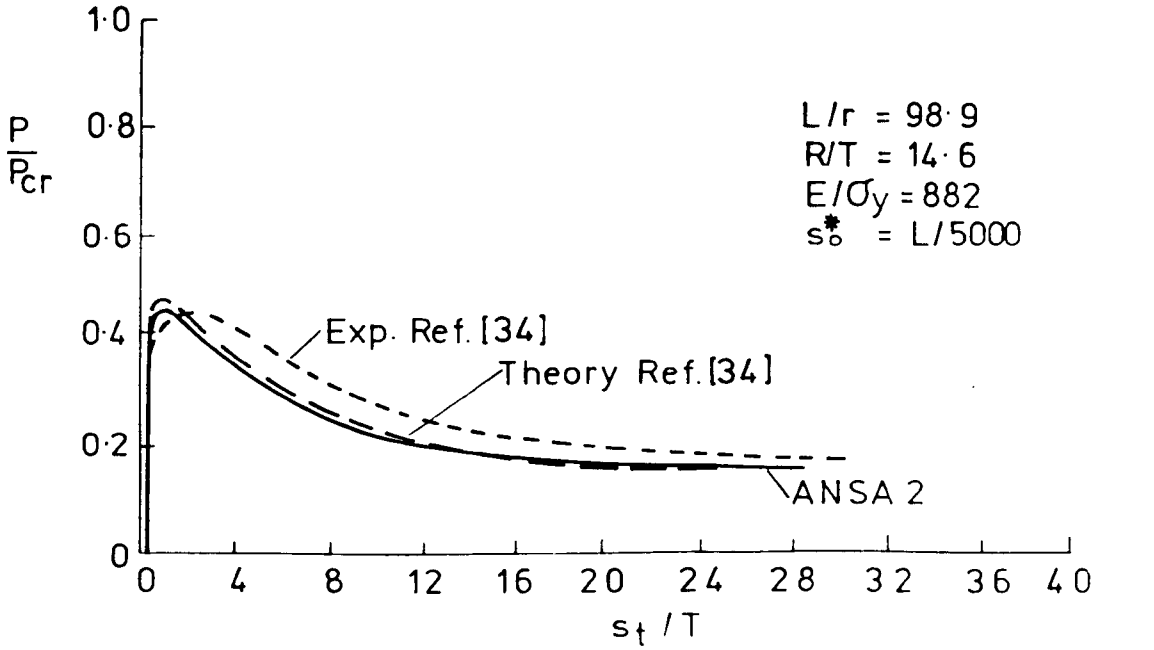

Fig. 4.11b

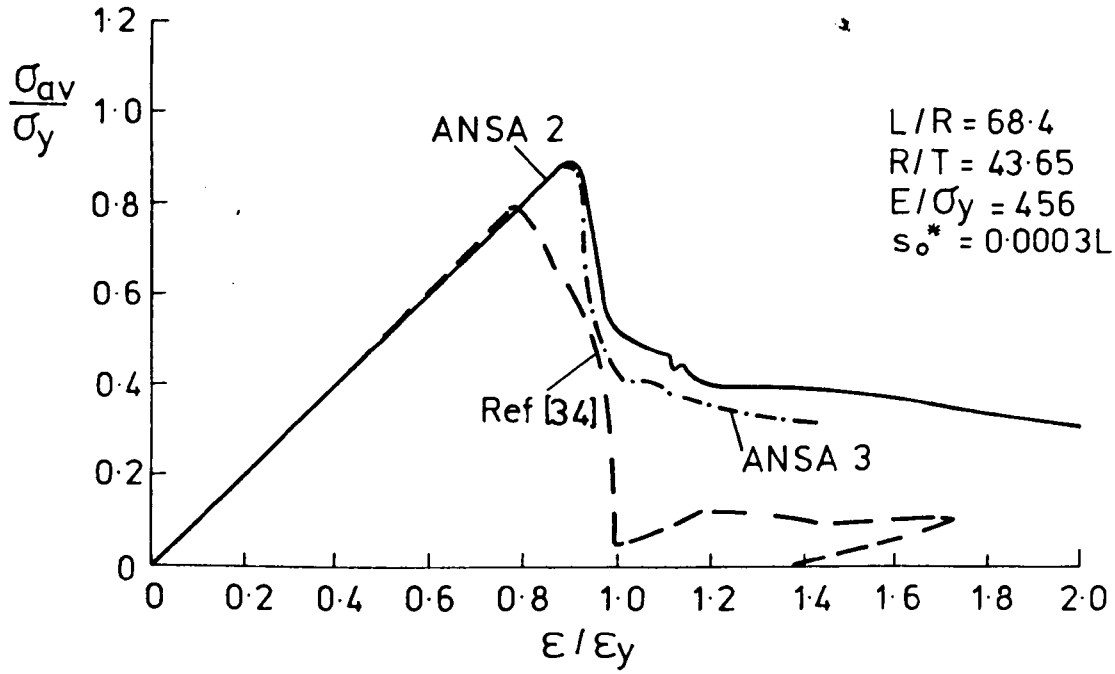

Fig. 4.12a

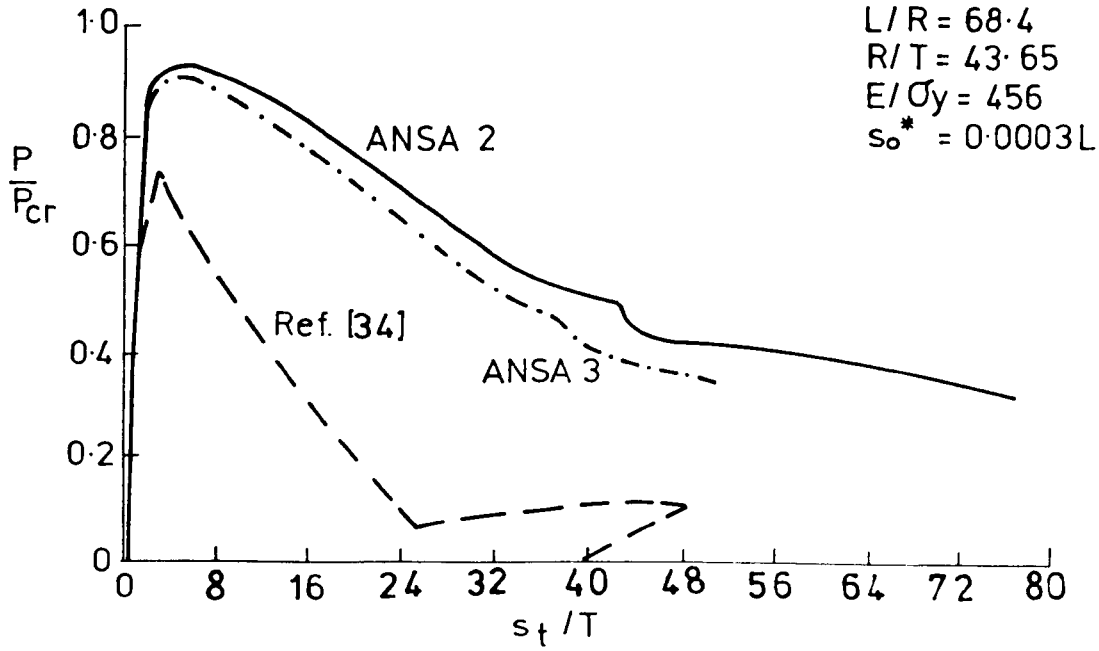

Fig. 4.12b

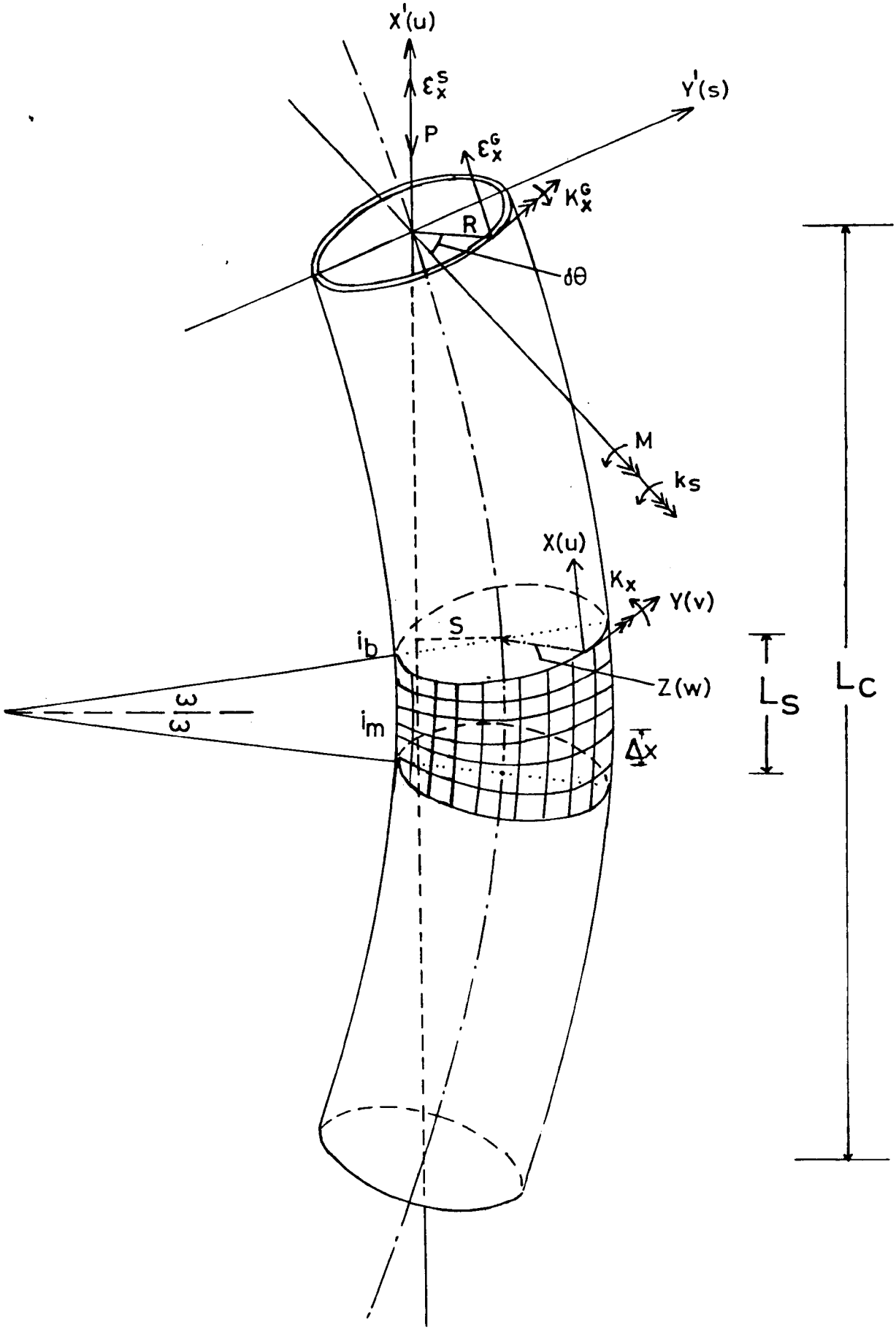
X'(u)
ε_x^s
P
Y'(s)
ε_x^G
K_x^G
R
dθ
M
k_s
X(u)
K_x
Y(v)
S
i_b
Z(w)
$\frac{\omega}{\omega}$
i_m
Δx
L_s
L_c

Fig. 5.1

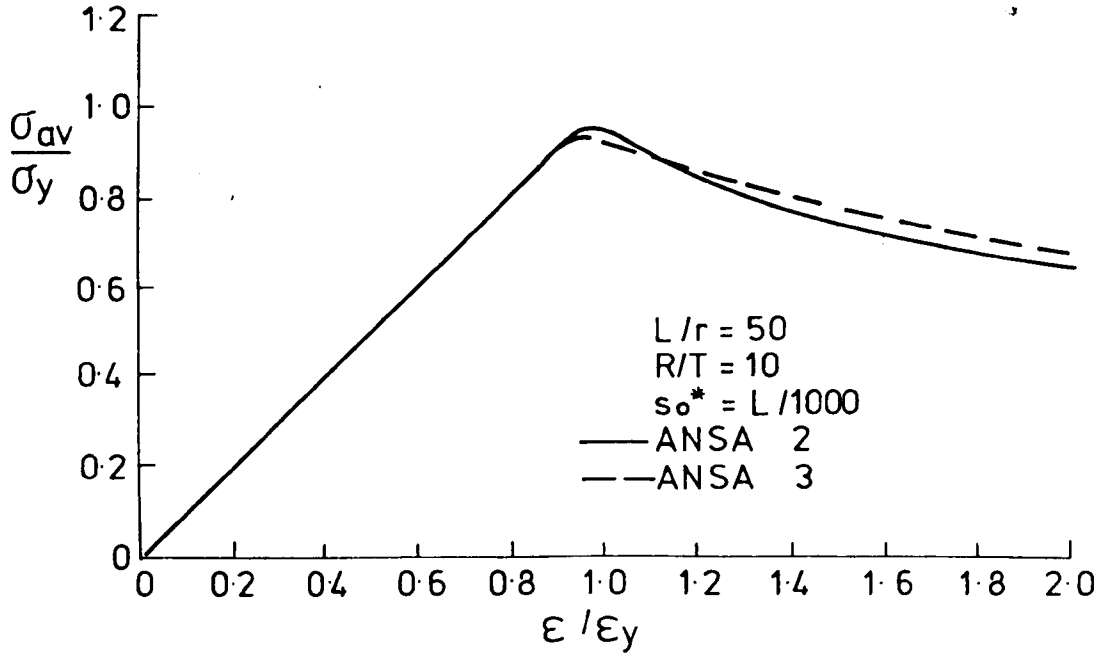

Fig. 5.2a

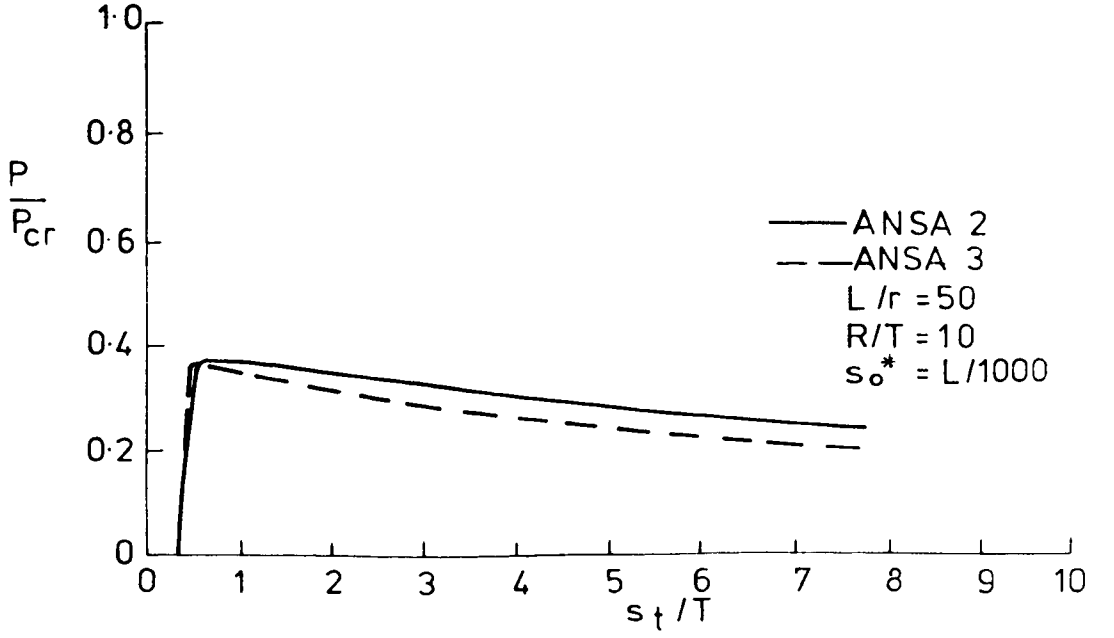

Fig. 5.2b

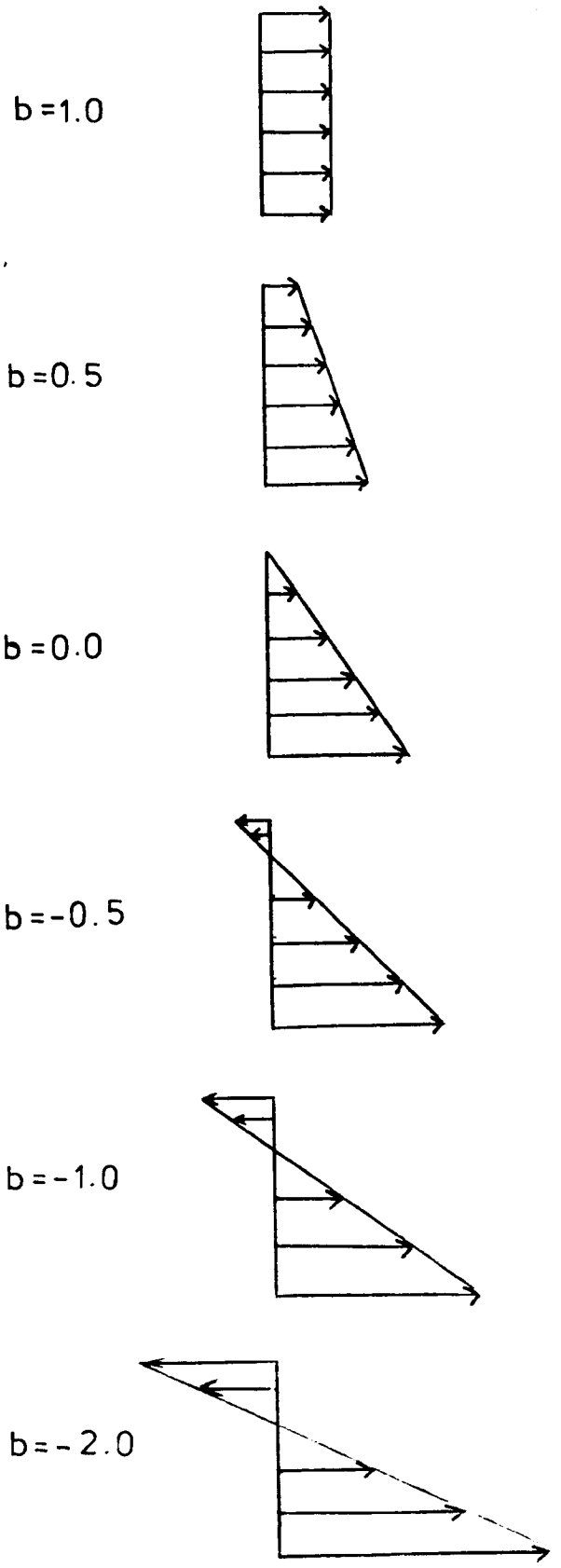

Fig. 6.1

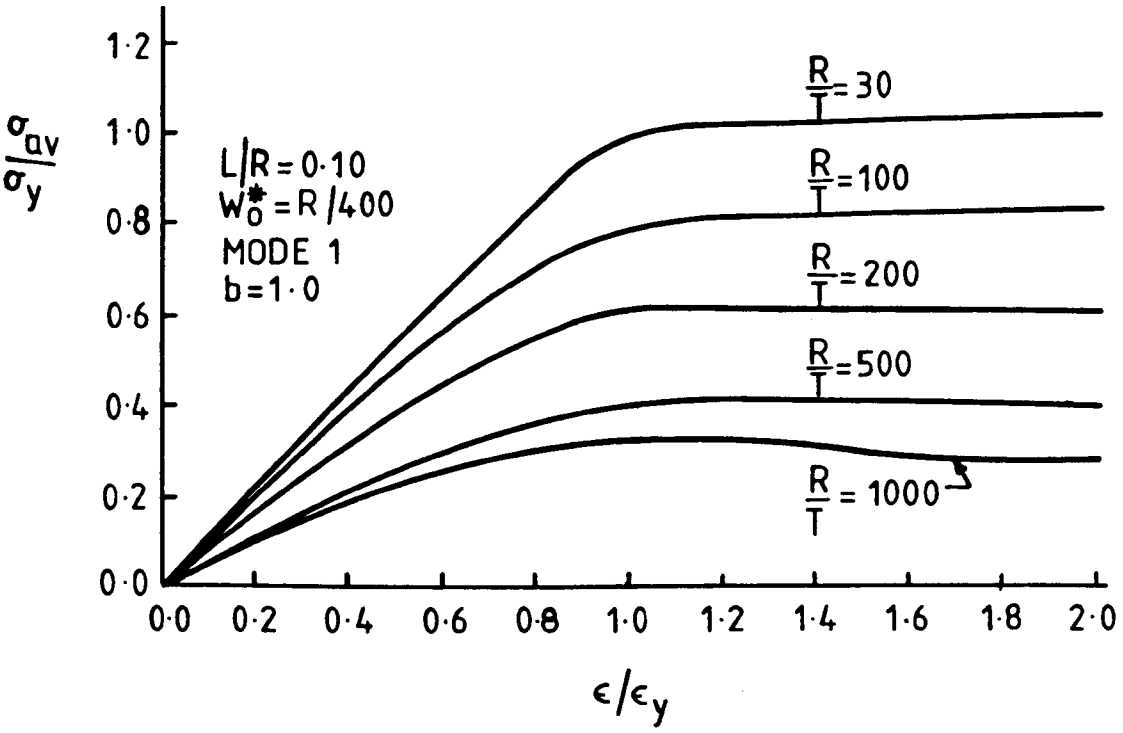
σav/σy
1·2
1·0
0·8
0·6
0·4
0·2
0·0
L/R = 0·10
W*o = R/400
MODE 1
b = 1·0
R/T = 30
R/T = 100
R/T = 200
R/T = 500
R/T = 1000
0·0 0·2 0·4 0·6 0·8 1·0 1·2 1·4 1·6 1·8 2·0
ϵ/ϵy

Fig. 6.2

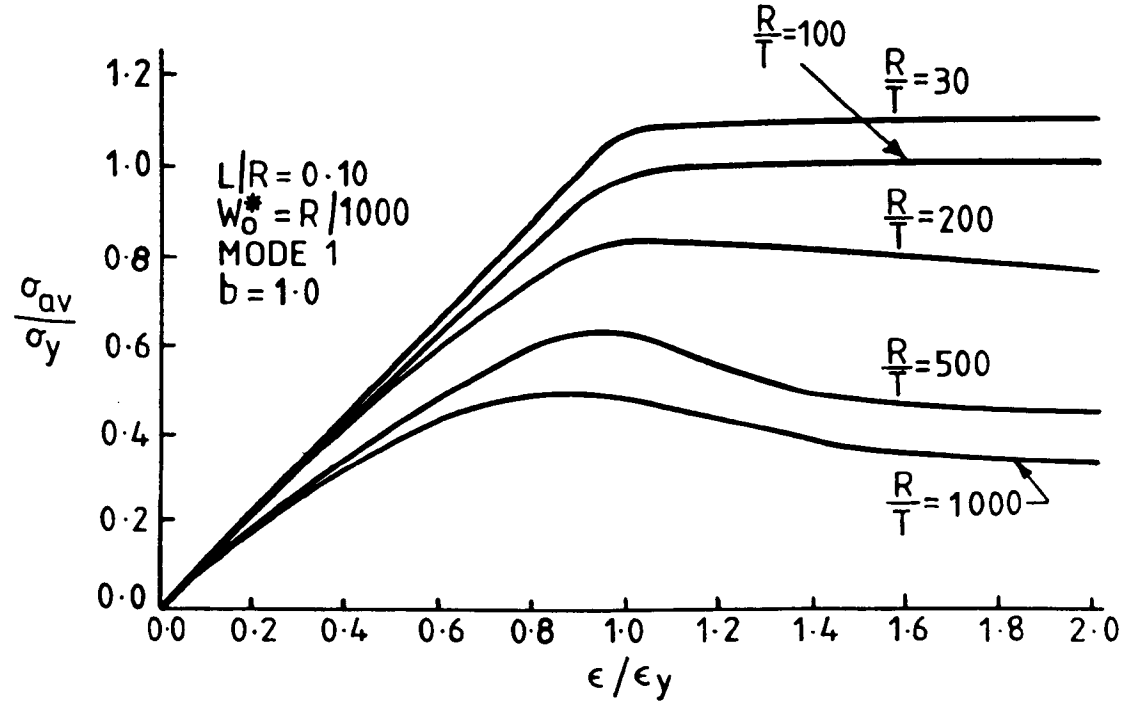
σav/σy
1·2
1·0
0·8
0·6
0·4
0·2
0·0
L/R = 0·10
W*o = R/1000
MODE 1
b = 1·0
R/T = 100
R/T = 30
R/T = 200
R/T = 500
R/T = 1000
0·0 0·2 0·4 0·6 0·8 1·0 1·2 1·4 1·6 1·8 2·0
ϵ/ϵy

Fig. 6.3

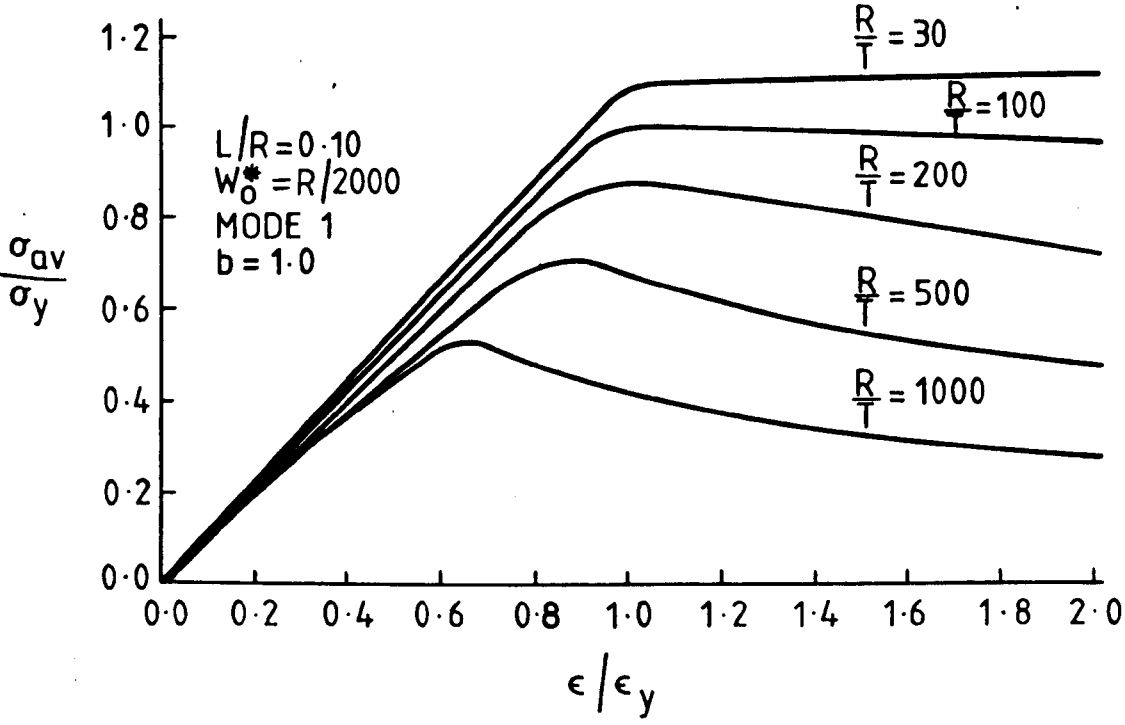
1·2
1·0
0·8
0·6
0·4
0·2
0·0
σav/σy
L/R=0·10
W*o=R/2000
MODE 1
b=1·0
R/T=30
R/T=100
R/T=200
R/T=500
R/T=1000
0·0 0·2 0·4 0·6 0·8 1·0 1·2 1·4 1·6 1·8 2·0
ε/εy

Fig. 6.4

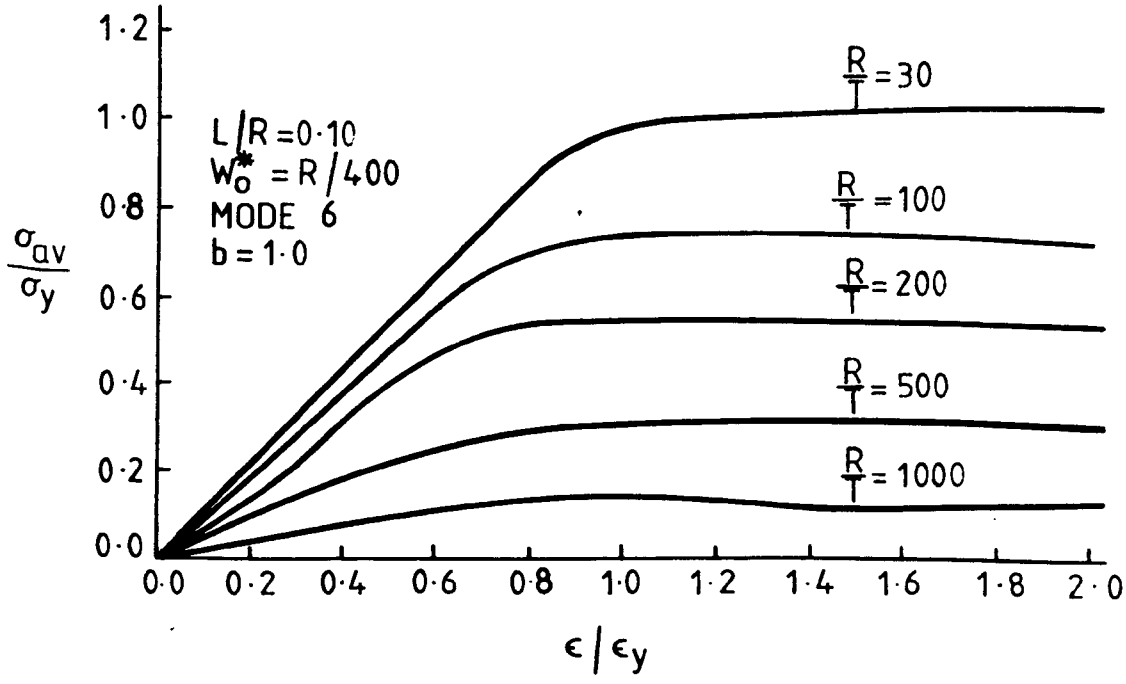
1·2
1·0
0·8
0·6
0·4
0·2
0·0
σav/σy
L/R=0·10
W*o=R/400
MODE 6
b=1·0
R/T=30
R/T=100
R/T=200
R/T=500
R/T=1000
0·0 0·2 0·4 0·6 0·8 1·0 1·2 1·4 1·6 1·8 2·0
ε/εy

Fig. 6.5

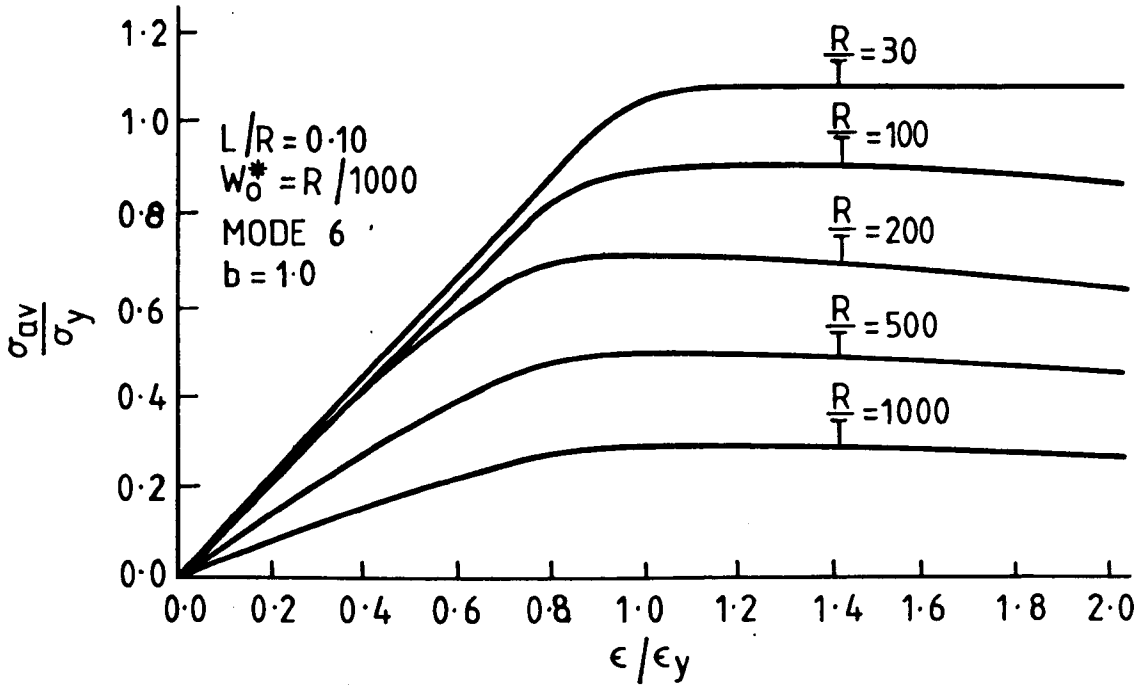
1·2
1·0
0·8
0·6
0·4
0·2
0·0
L/R = 0·10
W₀* = R/1000
MODE 6
b = 1·0
R/T = 30
R/T = 100
R/T = 200
R/T = 500
R/T = 1000
σav/σy
0·0 0·2 0·4 0·6 0·8 1·0 1·2 1·4 1·6 1·8 2·0
ϵ/ϵy

Fig. 6.6

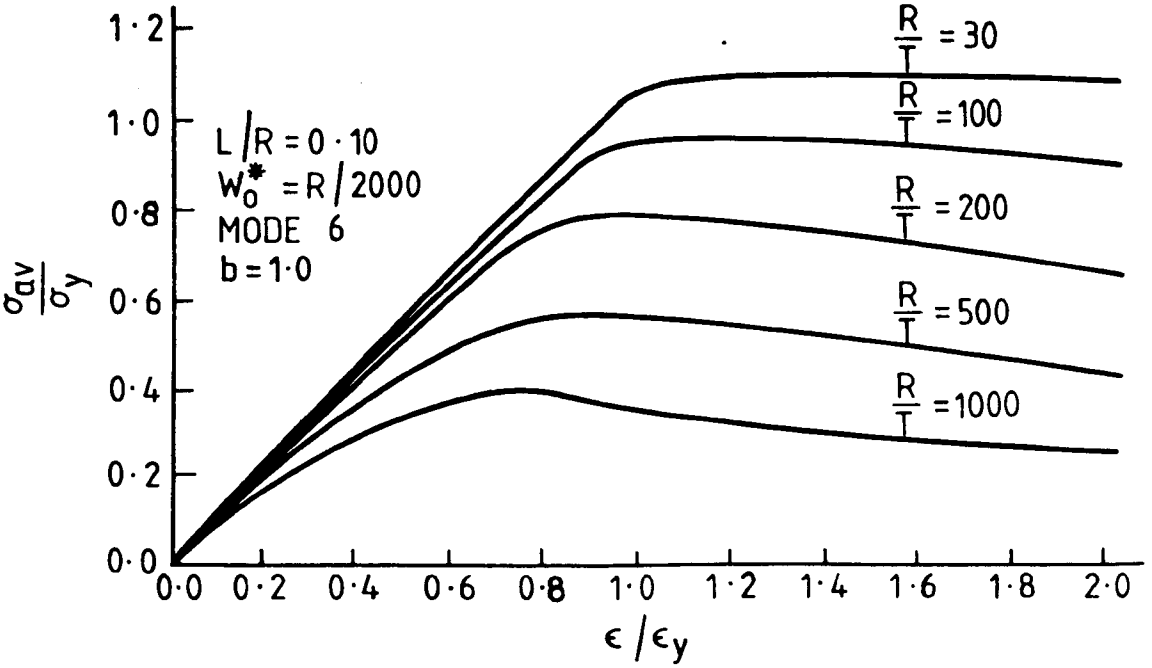
1·2
1·0
0·8
0·6
0·4
0·2
0·0
L/R = 0·10
W₀* = R/2000
MODE 6
b = 1·0
R/T = 30
R/T = 100
R/T = 200
R/T = 500
R/T = 1000
σav/σy
0·0 0·2 0·4 0·6 0·8 1·0 1·2 1·4 1·6 1·8 2·0
ϵ/ϵy

Fig. 6.7

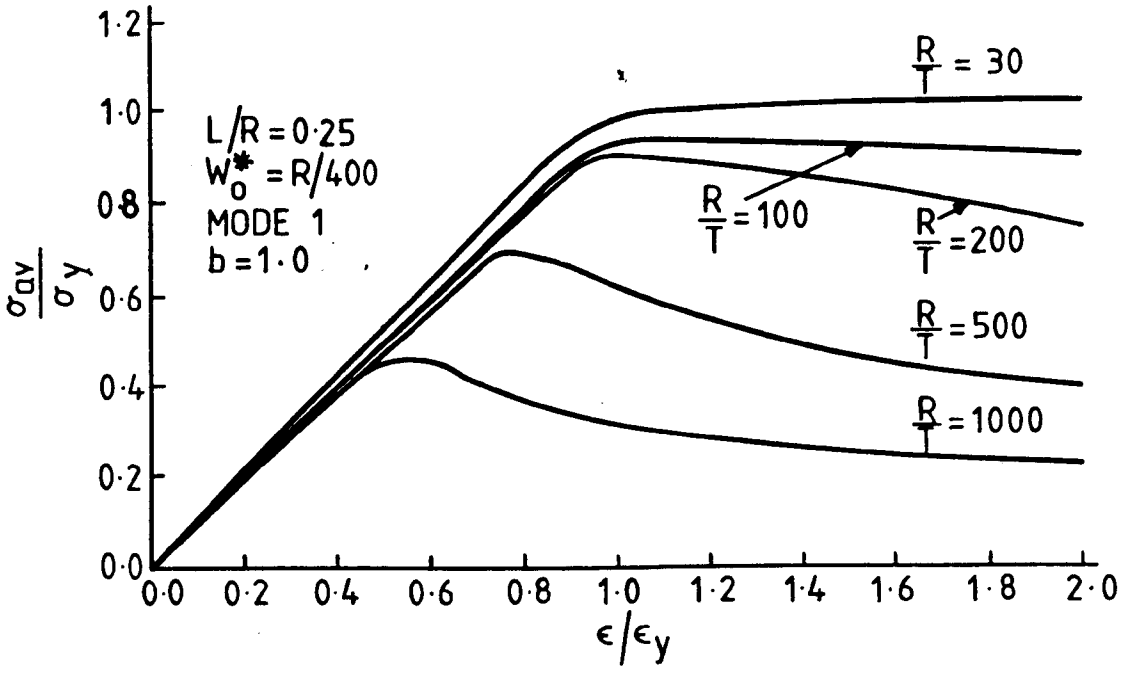
1·2
1·0
0·8
0·6
0·4
0·2
0·0
L/R = 0·25
W*o = R/400
MODE 1
b = 1·0
R/T = 30
R/T = 100
R/T = 200
R/T = 500
R/T = 1000
σav/σy
0·0 0·2 0·4 0·6 0·8 1·0 1·2 1·4 1·6 1·8 2·0
ε/εy

Fig. 6.8

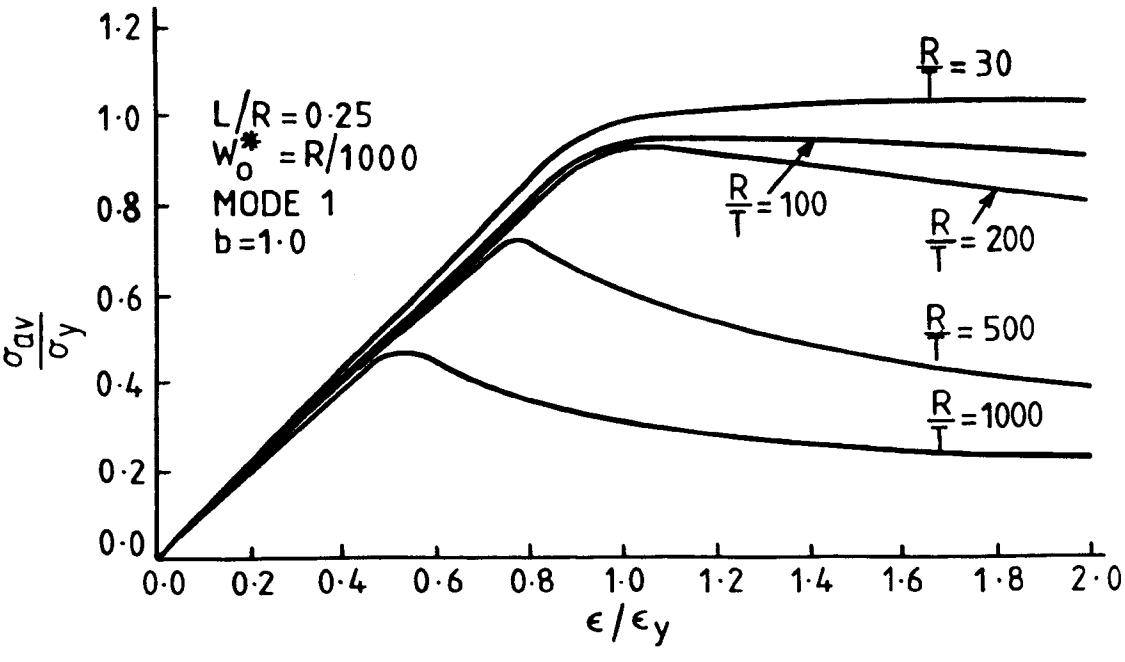
1·2
1·0
0·8
0·6
0·4
0·2
0·0
L/R = 0·25
W*o = R/1000
MODE 1
b = 1·0
R/T = 30
R/T = 100
R/T = 200
R/T = 500
R/T = 1000
σav/σy
0·0 0·2 0·4 0·6 0·8 1·0 1·2 1·4 1·6 1·8 2·0
ε/εy

Fig. 6.9

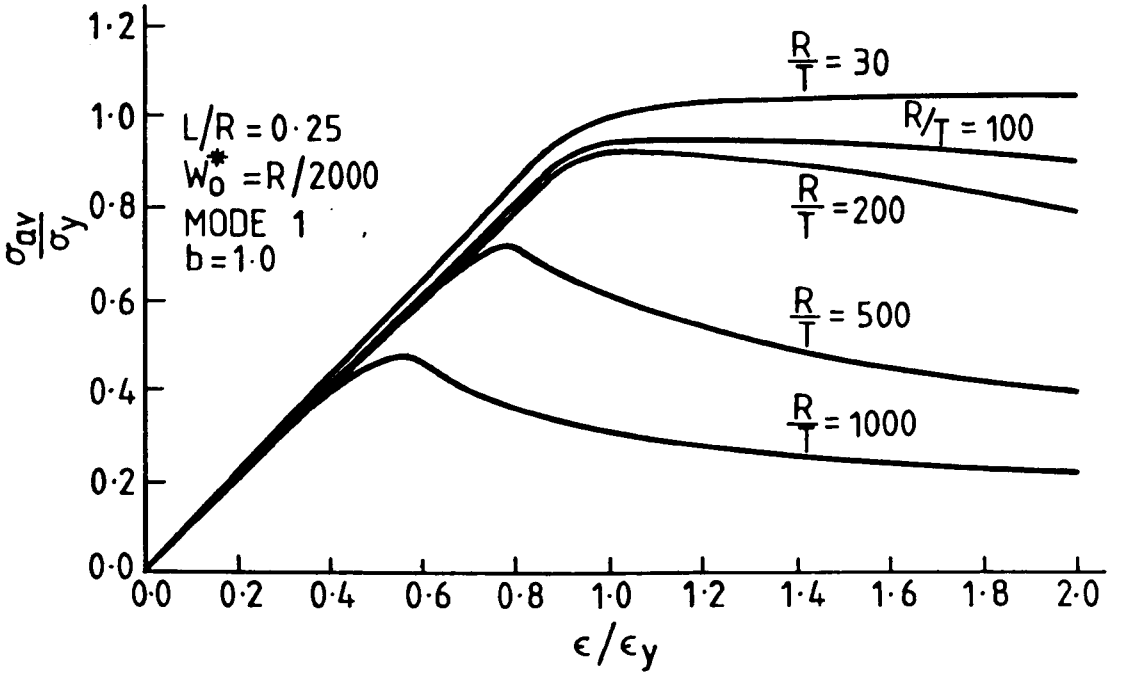

Fig. 6.10

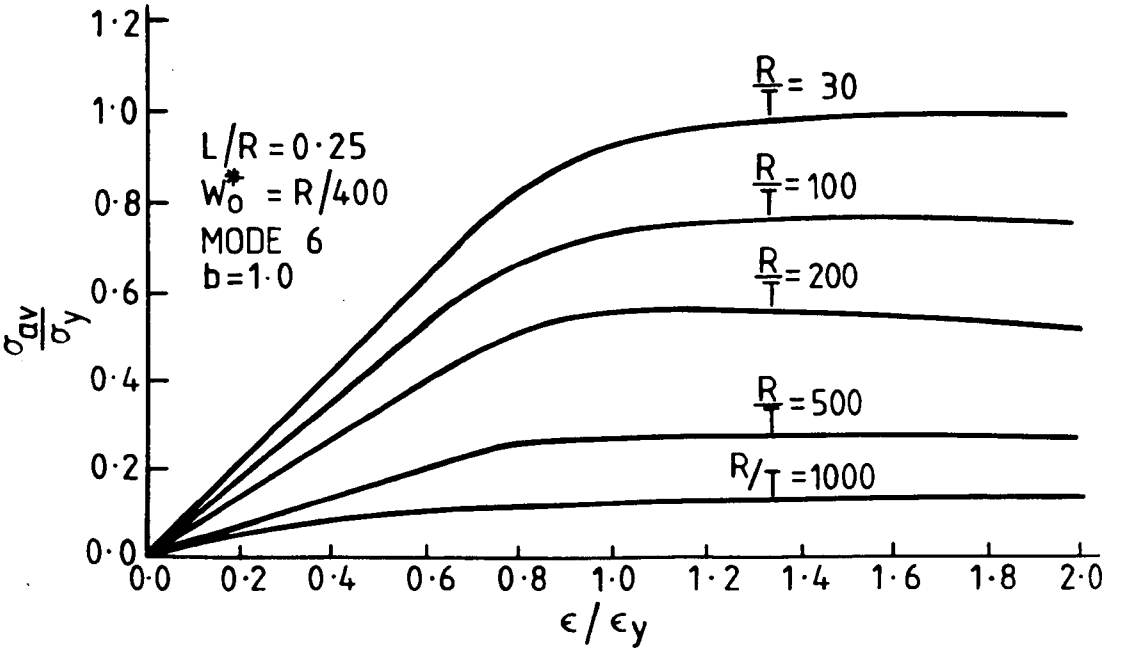

Fig. 6.11

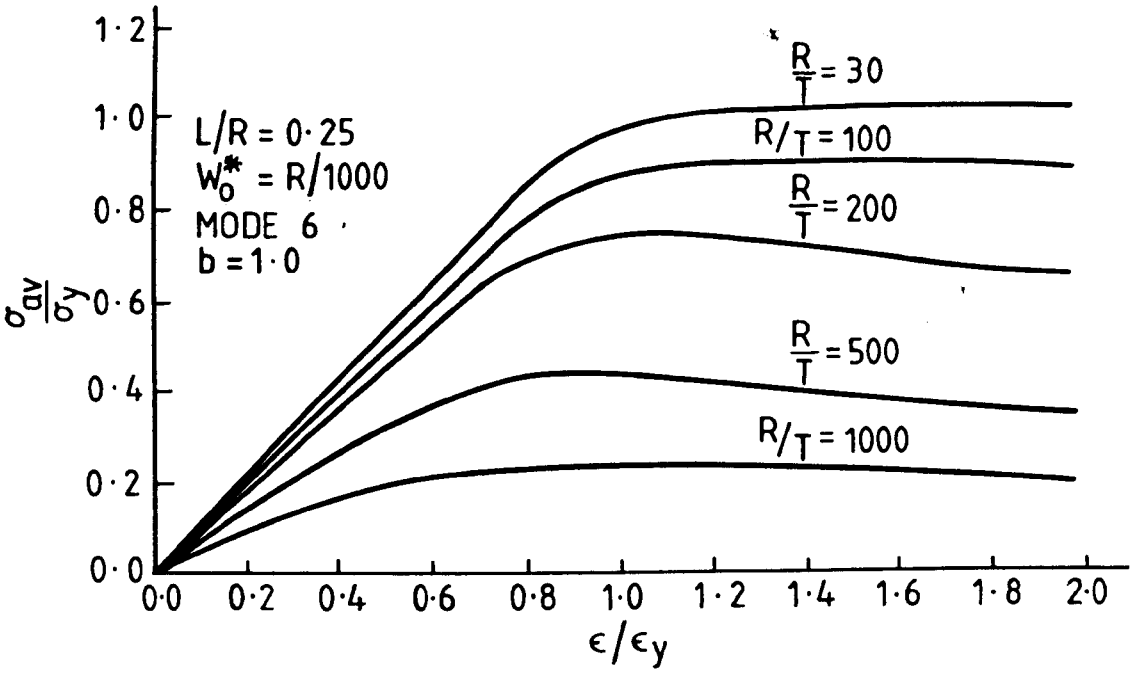

Fig. 6.12

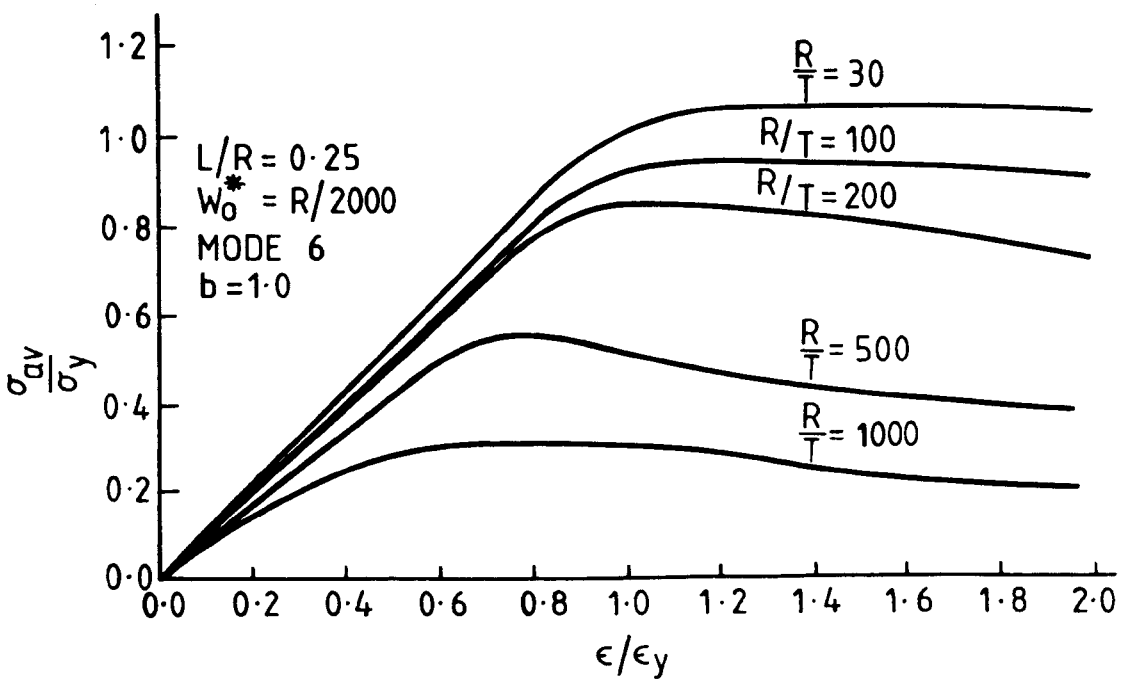

Fig. 6.13

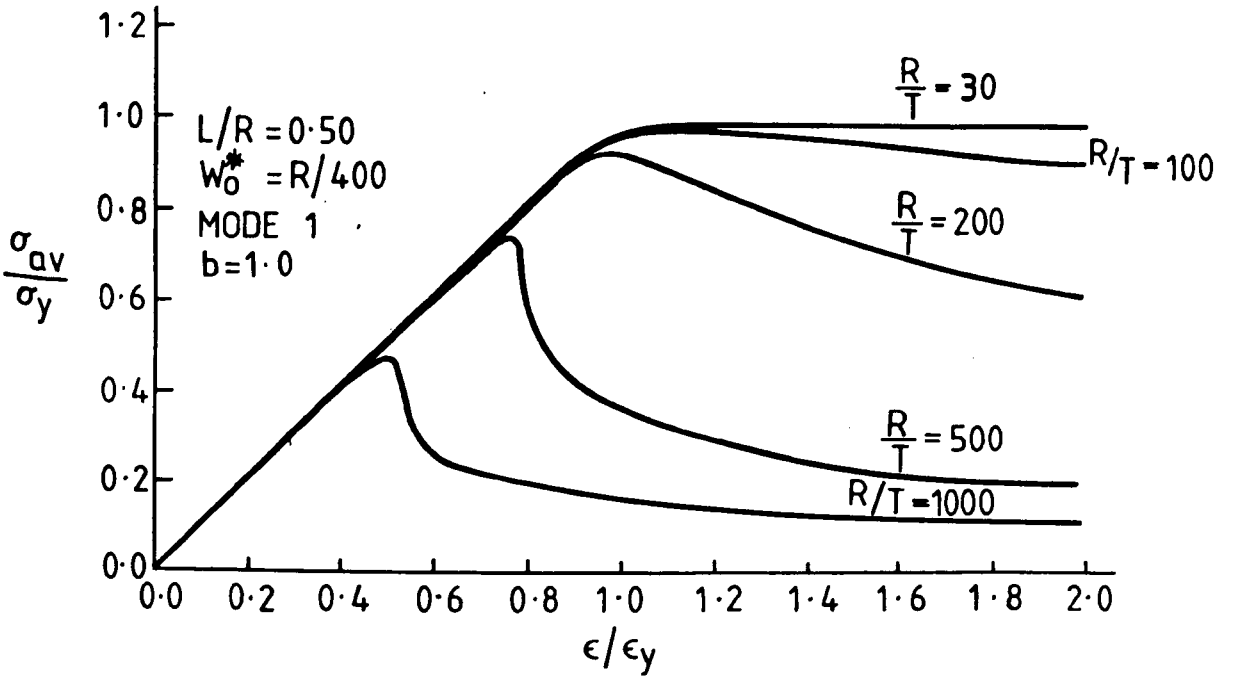

Fig. 6.14

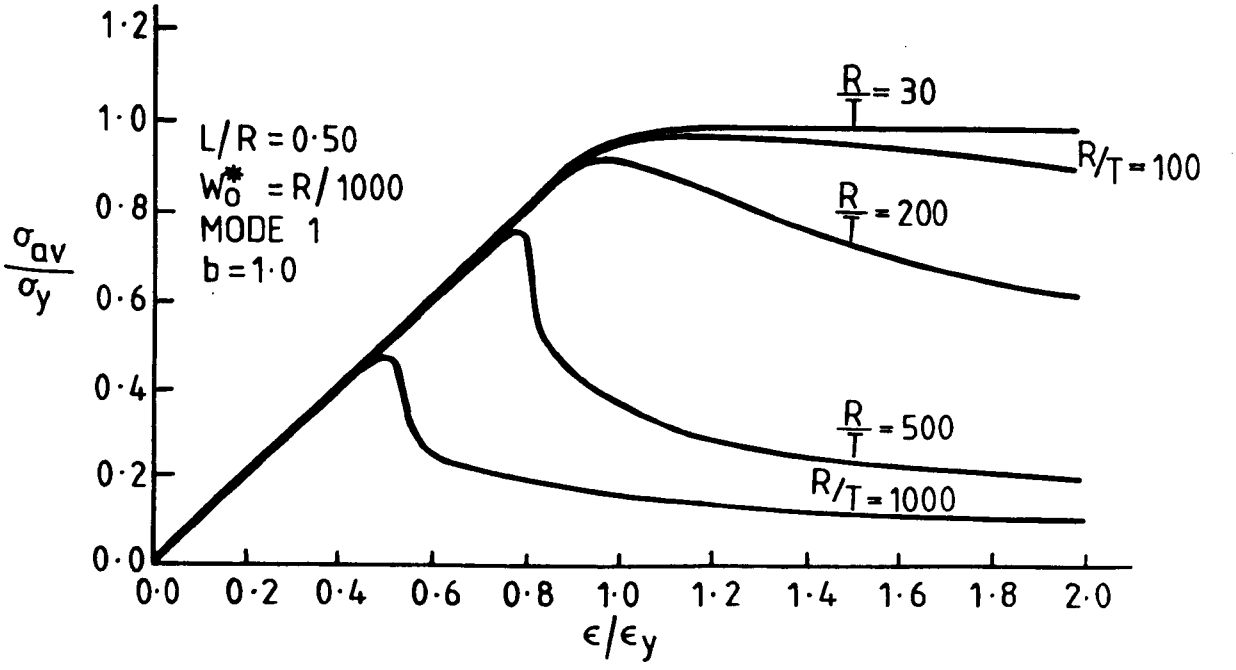

Fig. 6.15

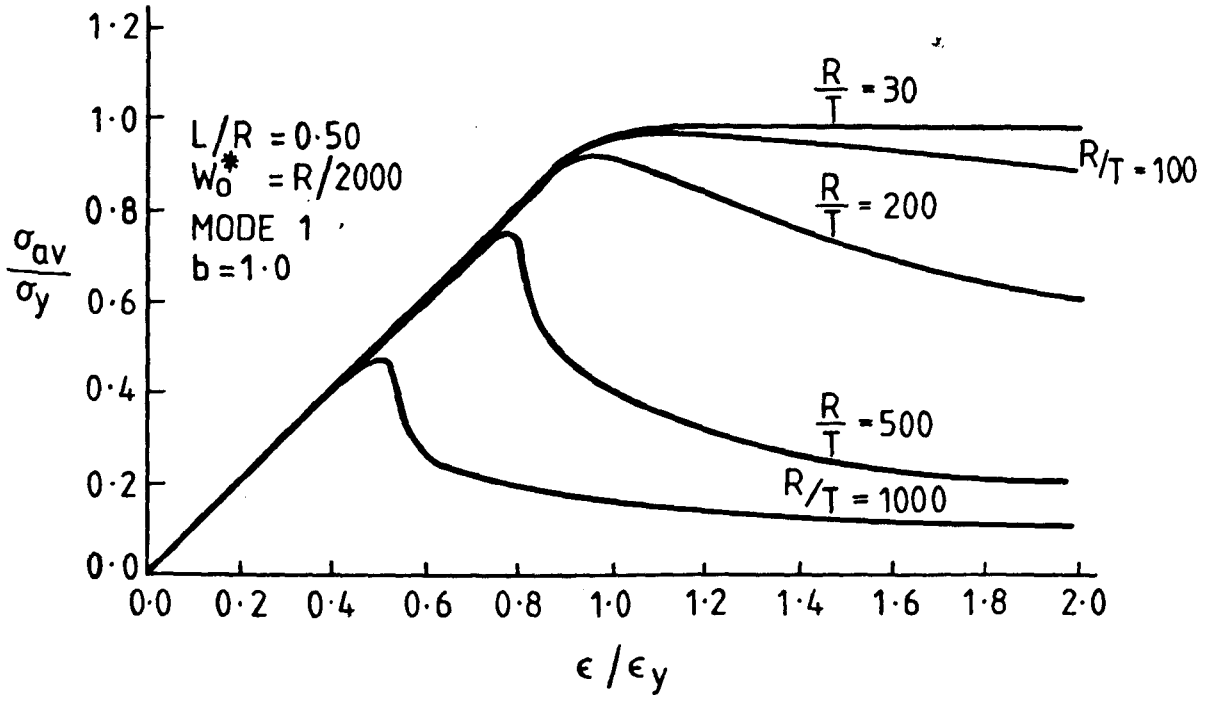

Fig. 6.16

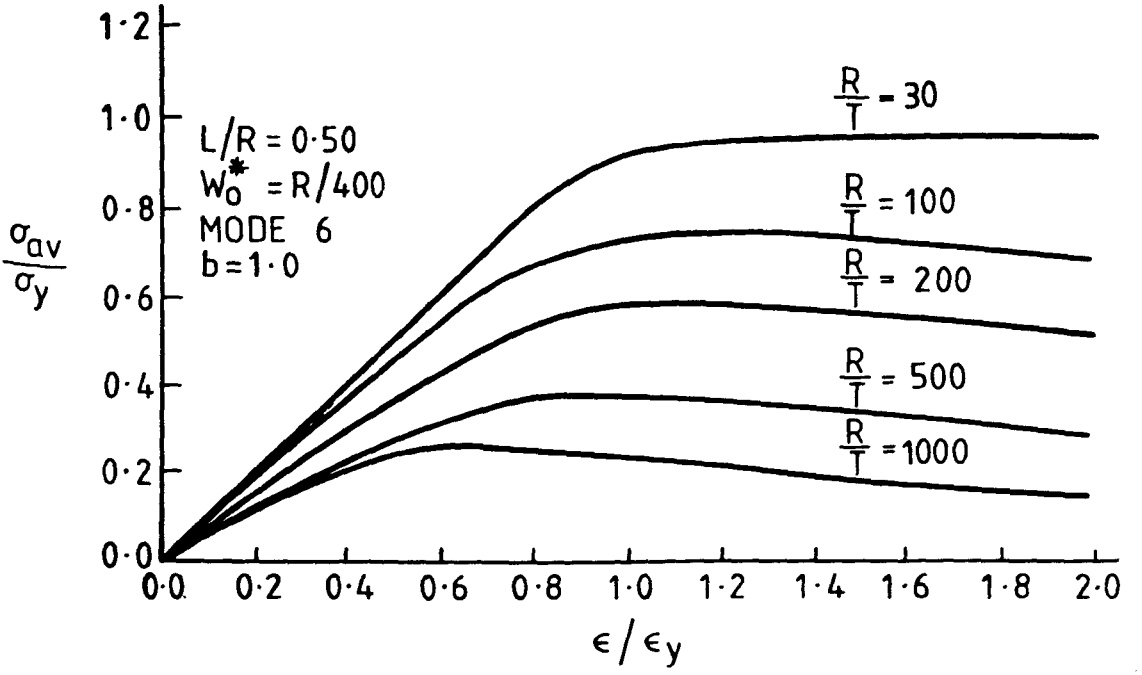

Fig. 6.17

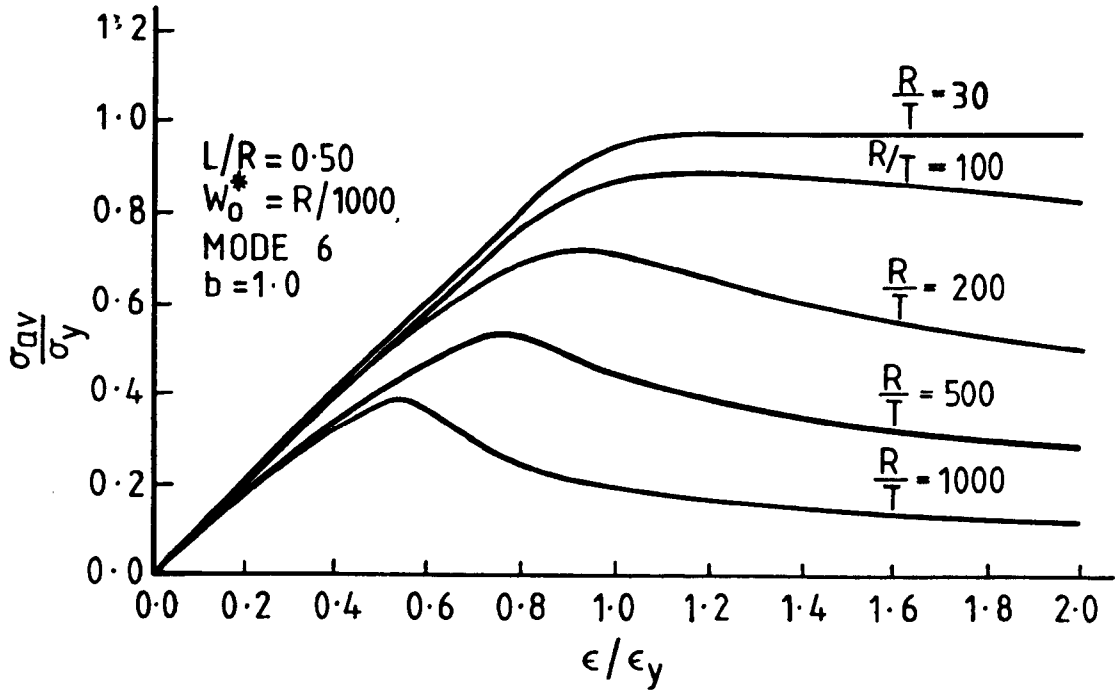

Fig. 6.18

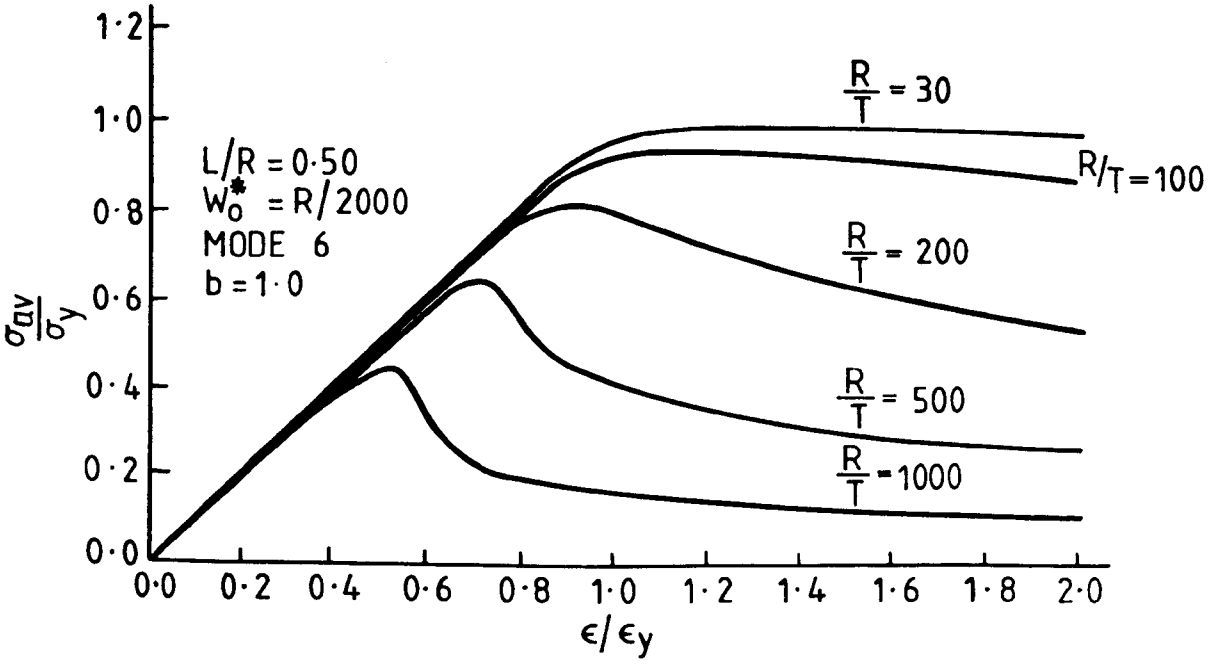

Fig. 6.19

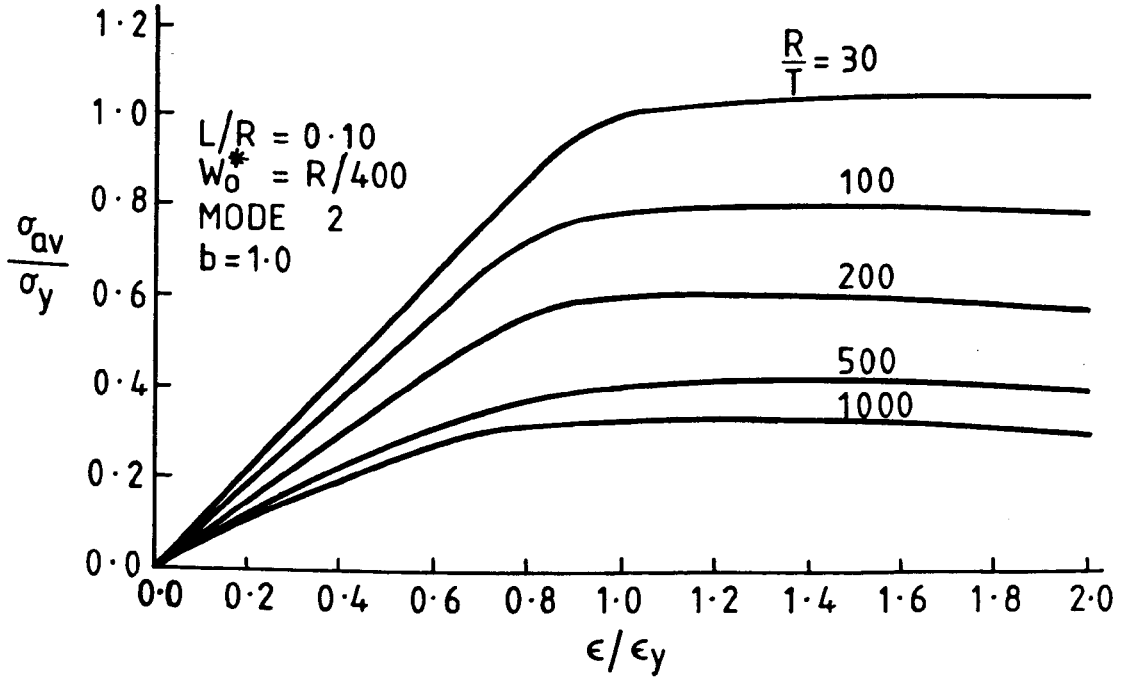

Fig. 6.20

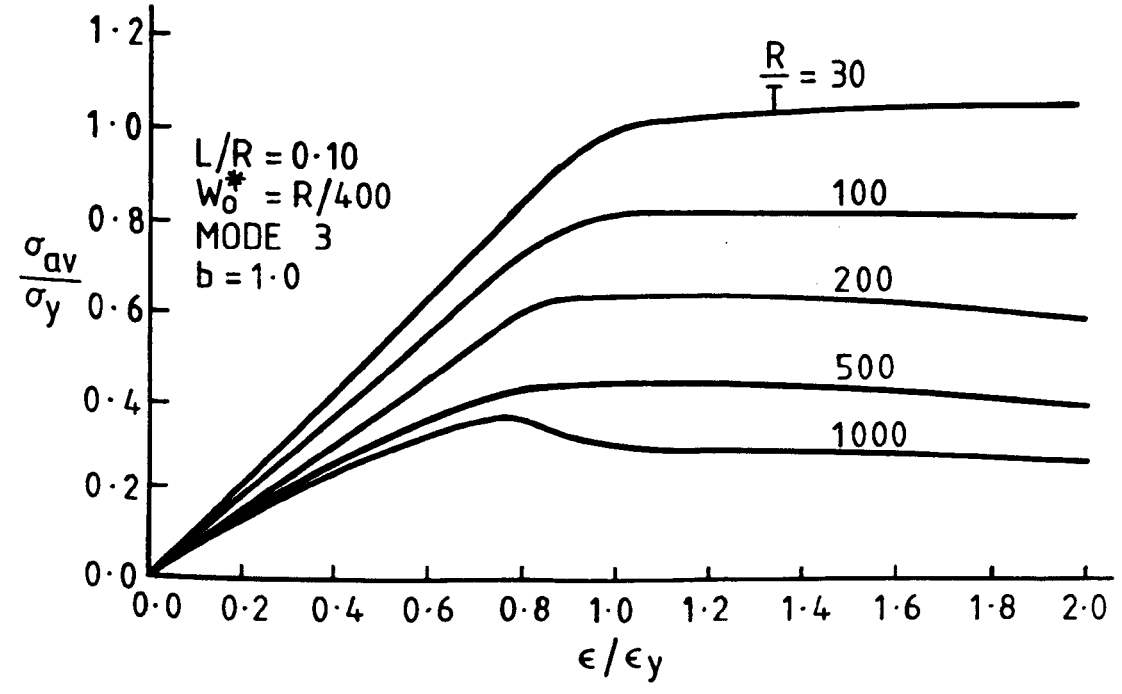

Fig. 6.21

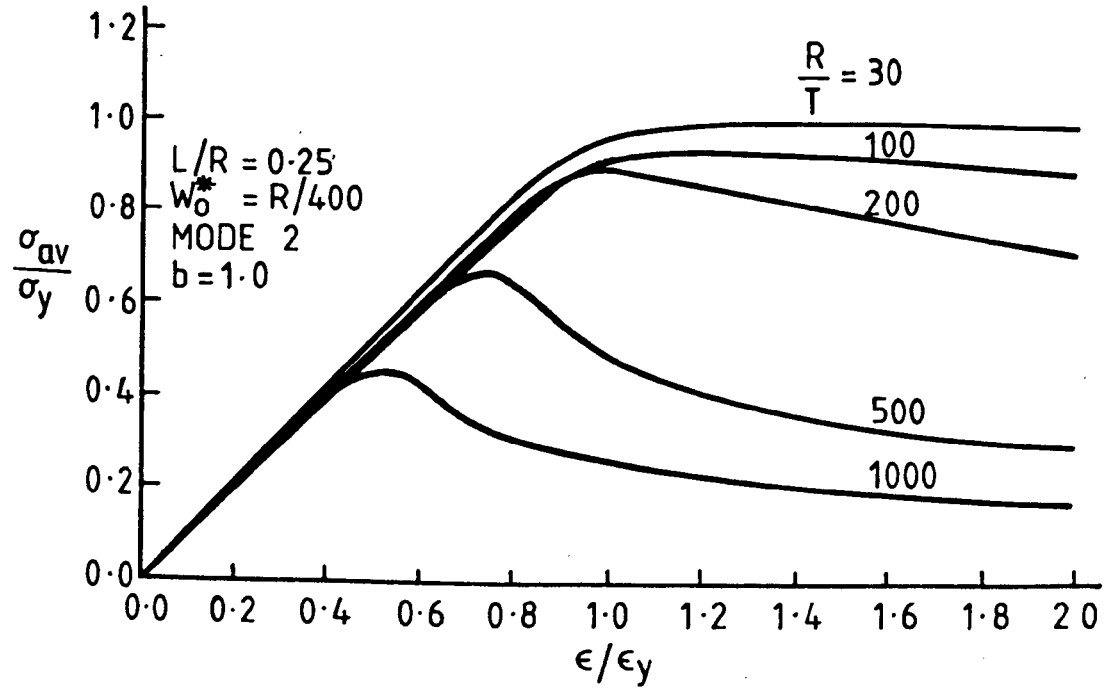

Fig. 6.22

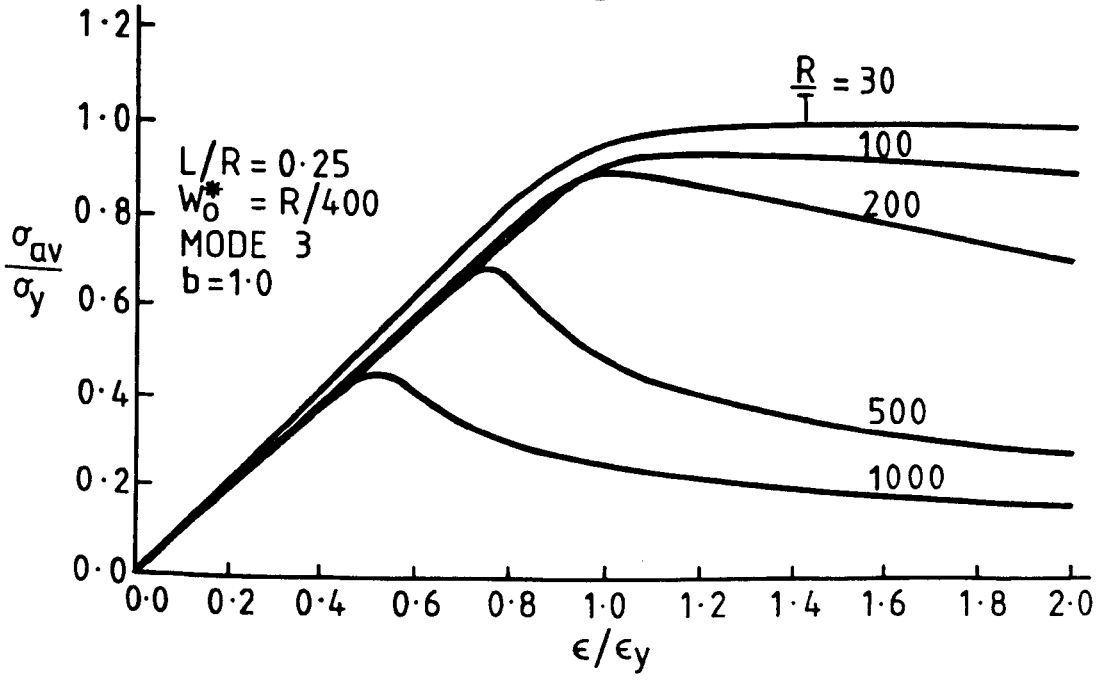

Fig. 6.23

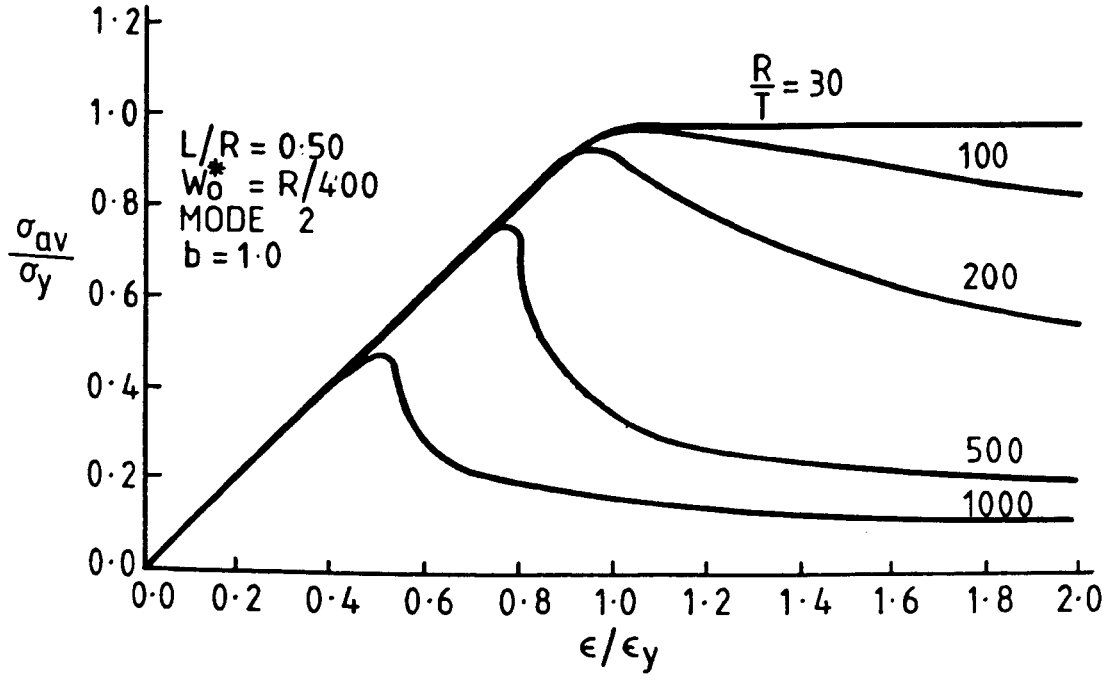

Fig. 6.24

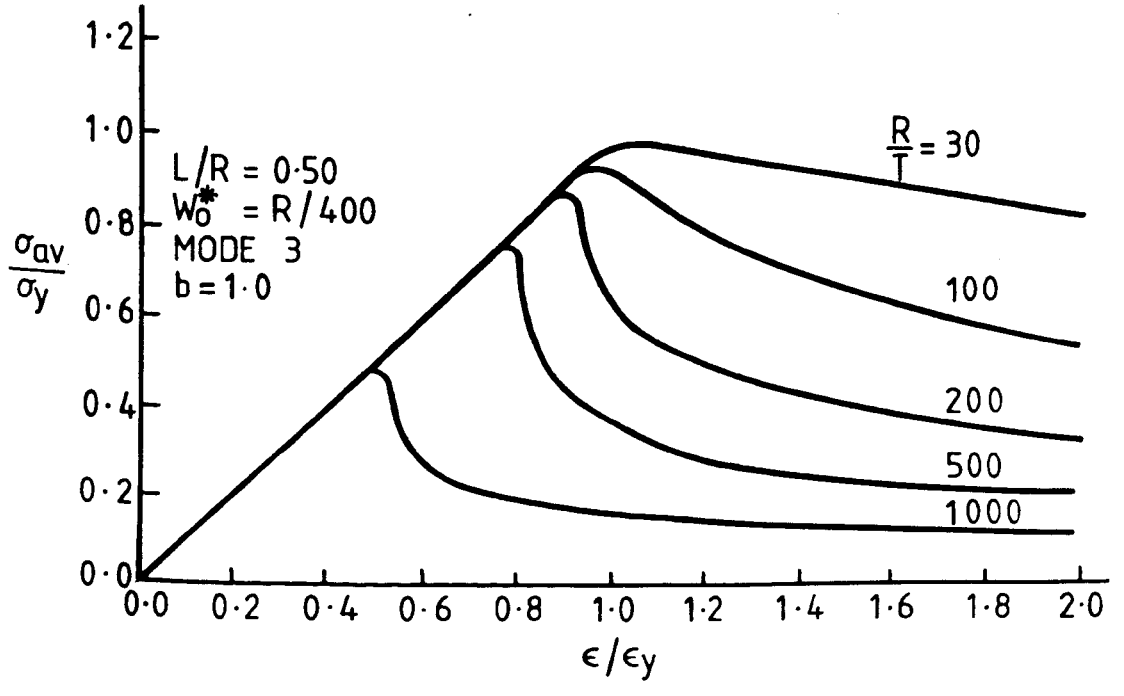

Fig. 6.25

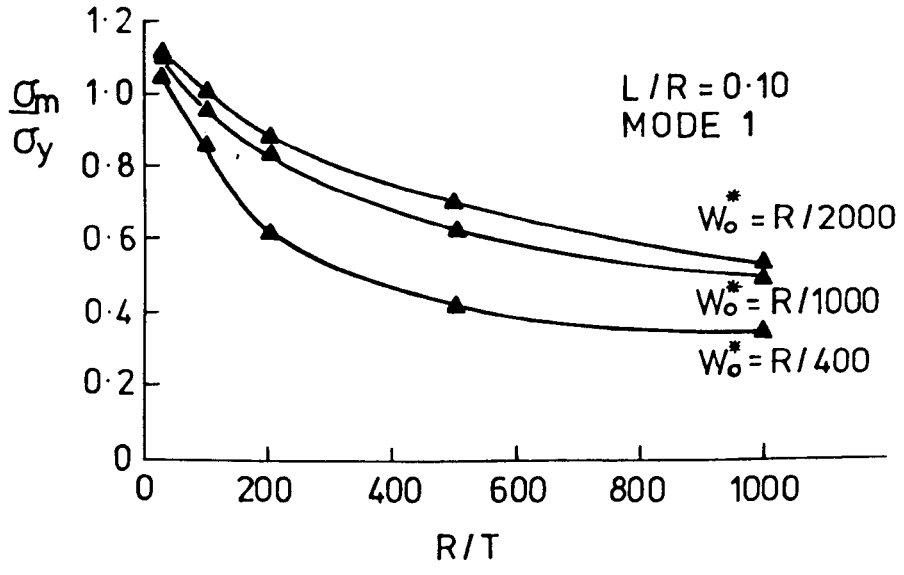

Fig. 6.26

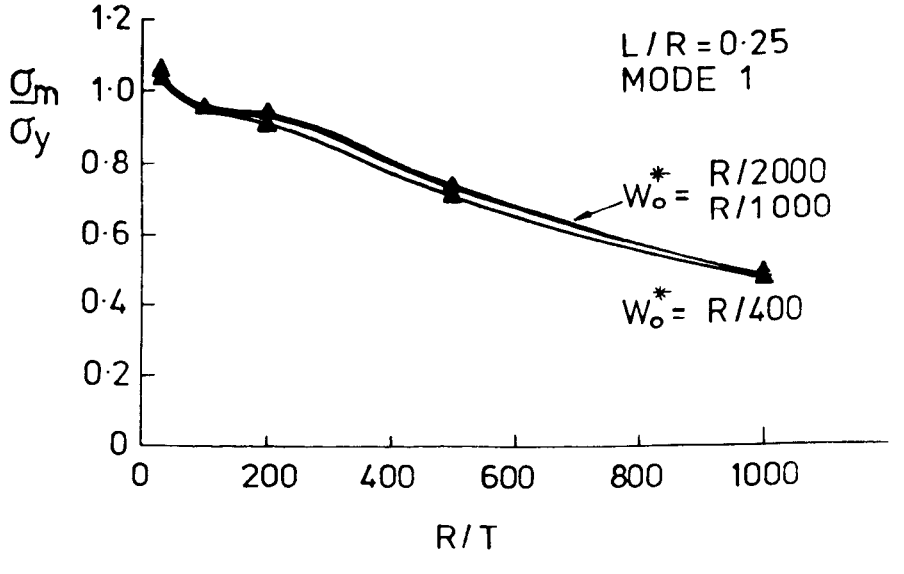

Fig. 6.27

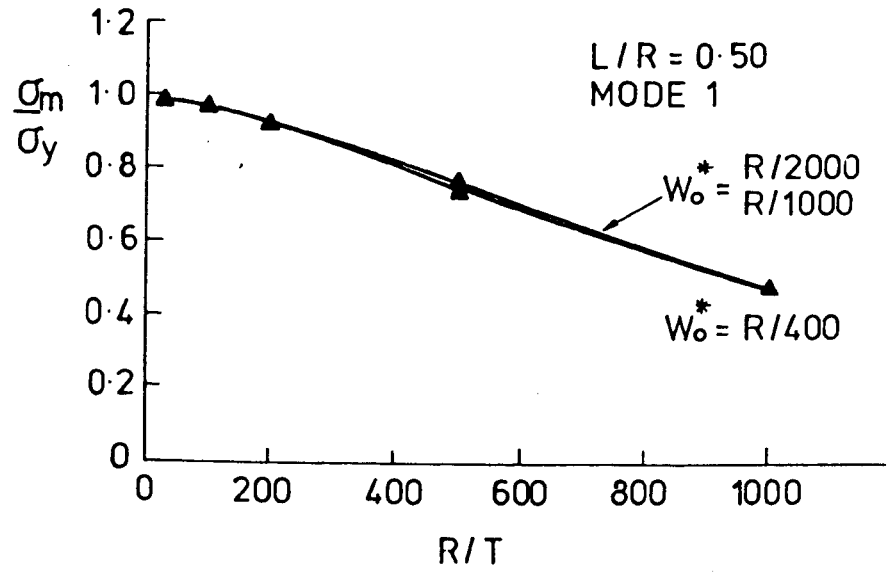

Fig. 6.28

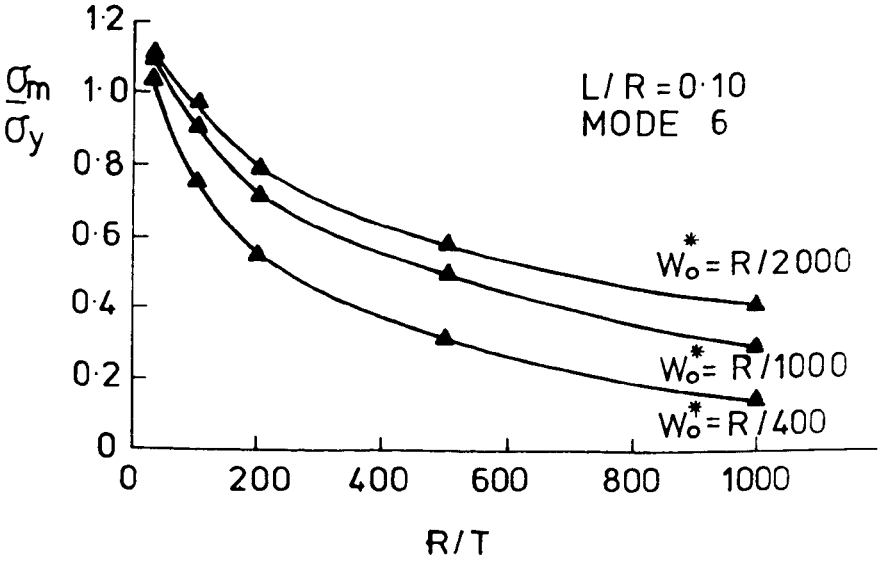

Fig. 6.29

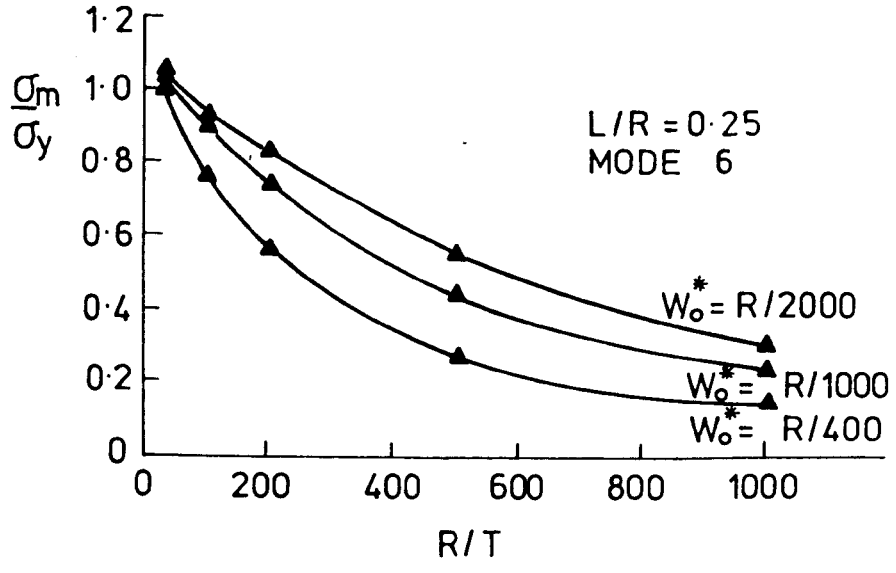

Fig. 6.30

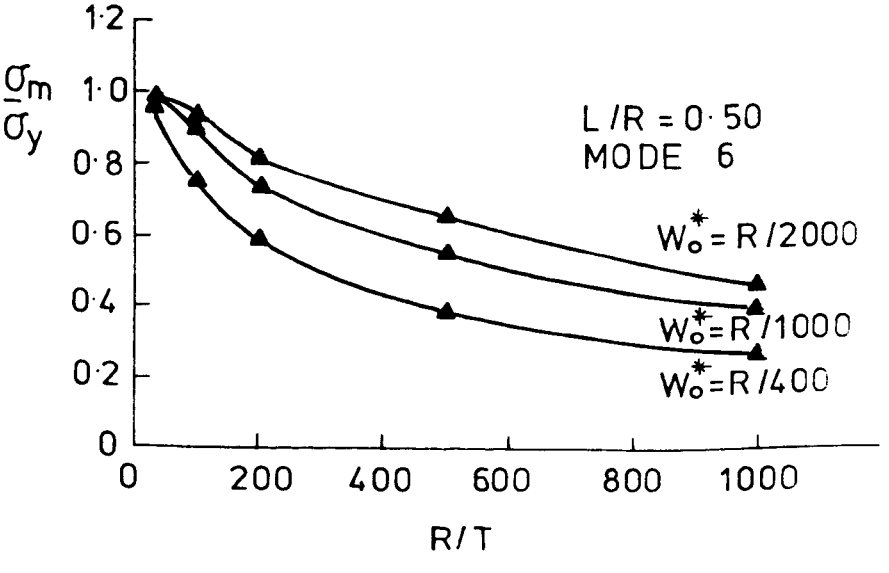

Fig. 6.31

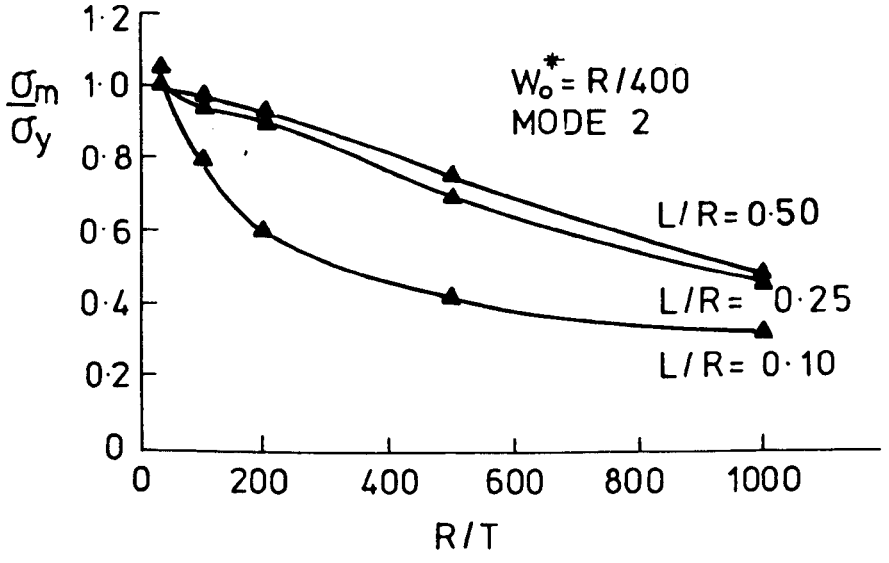

Fig. 6.32

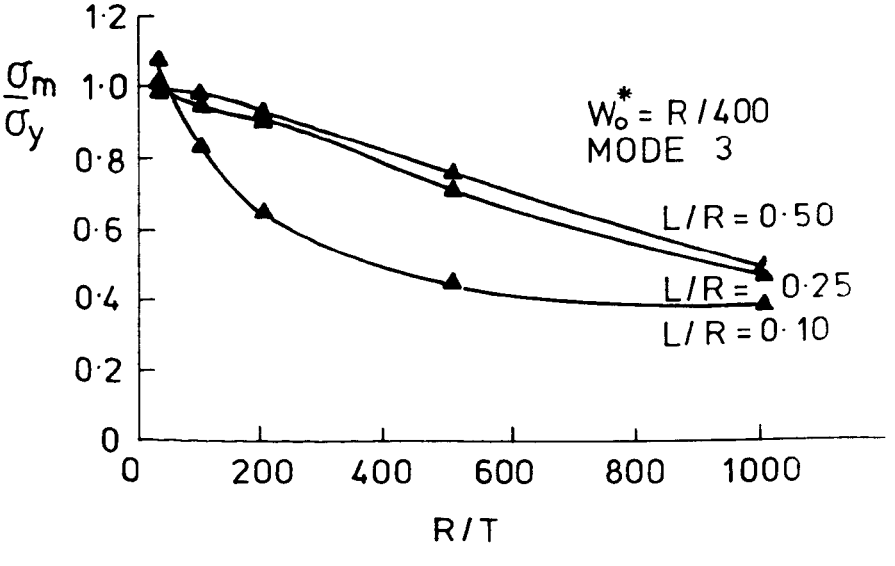

Fig. 6.33

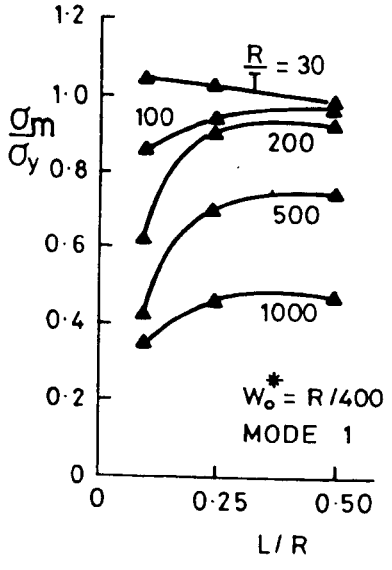

Fig. 6.34

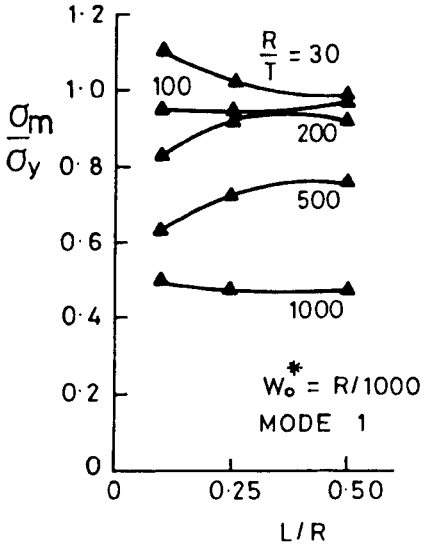

Fig. 6.35

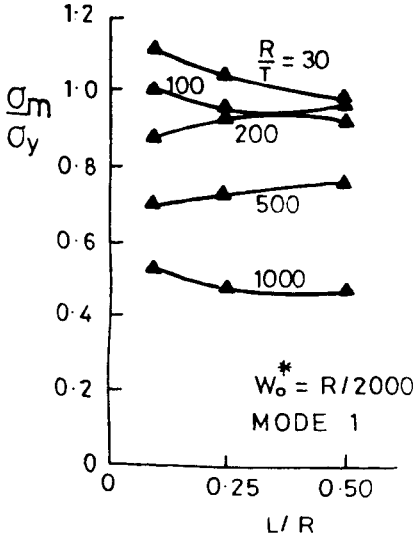

Fig. 6.36

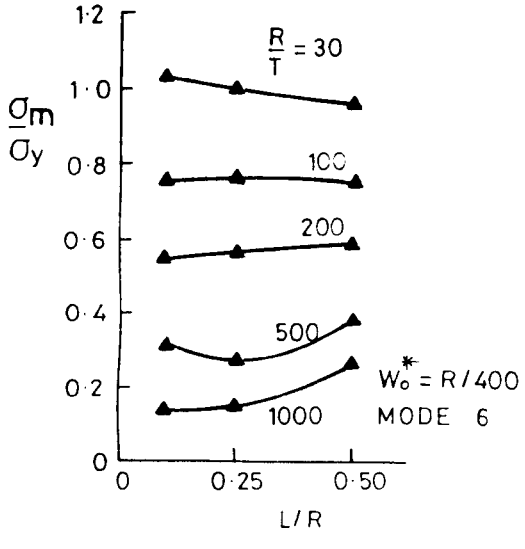

Fig. 6.37

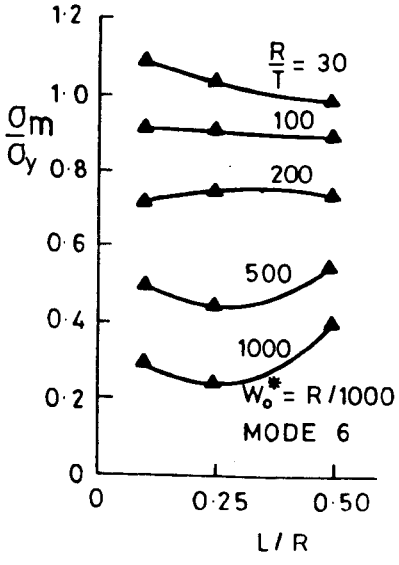

Fig. 6.38

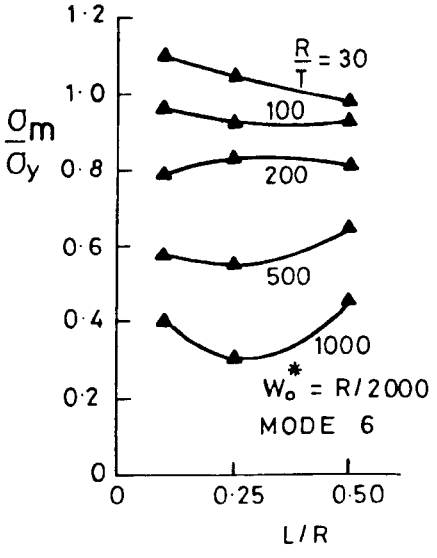

Fig. 6.39

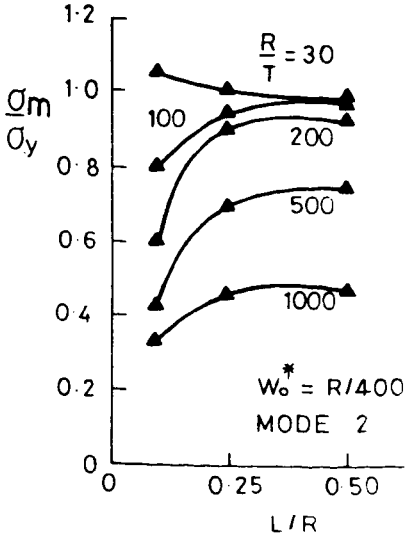

Fig. 6.40

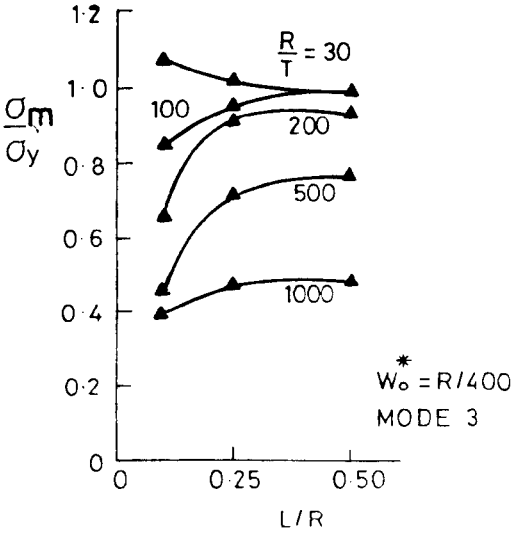

Fig. 6.41

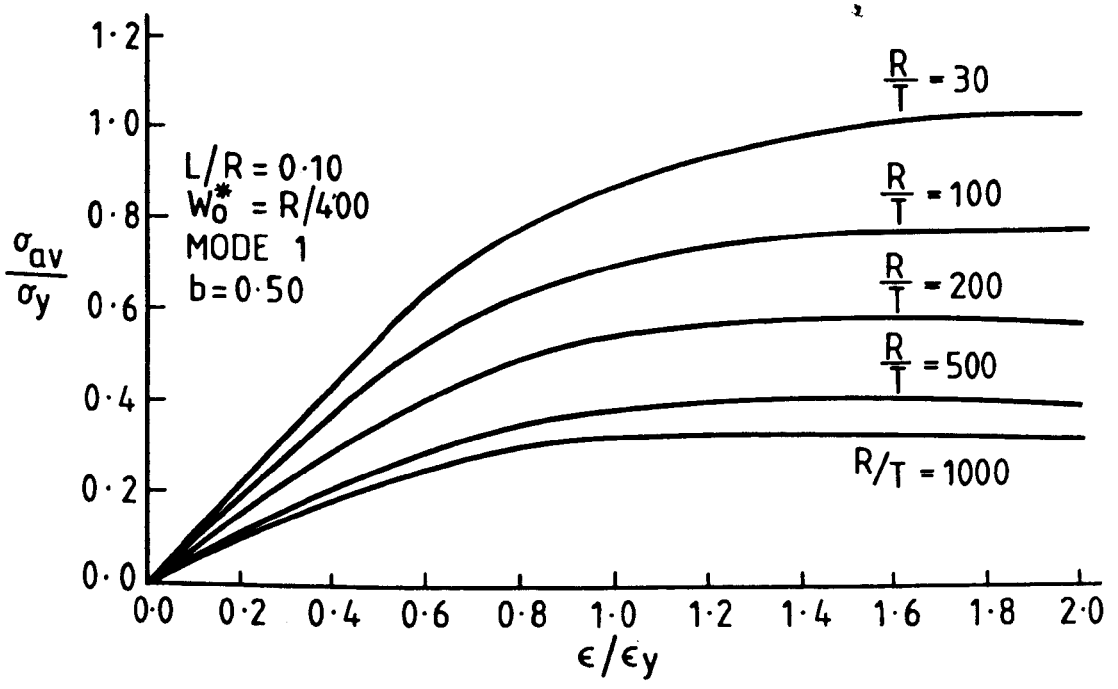

Fig. 6.42a

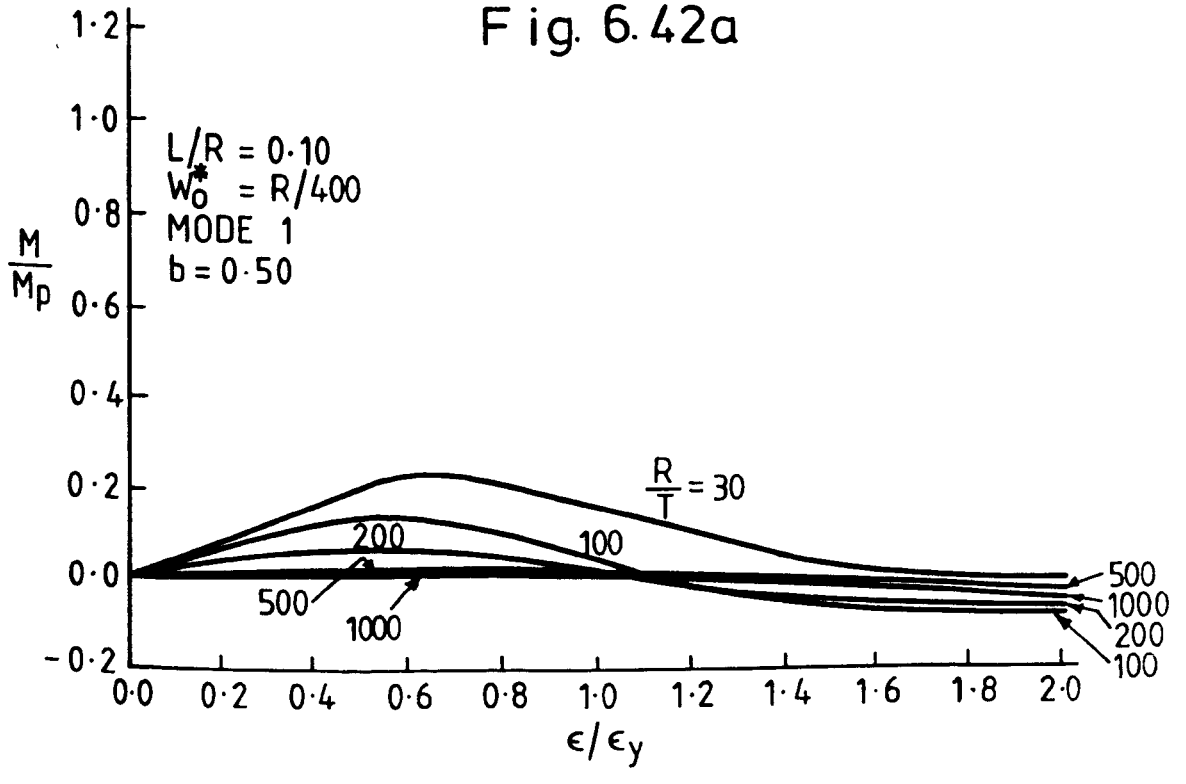

Fig. 6.42b

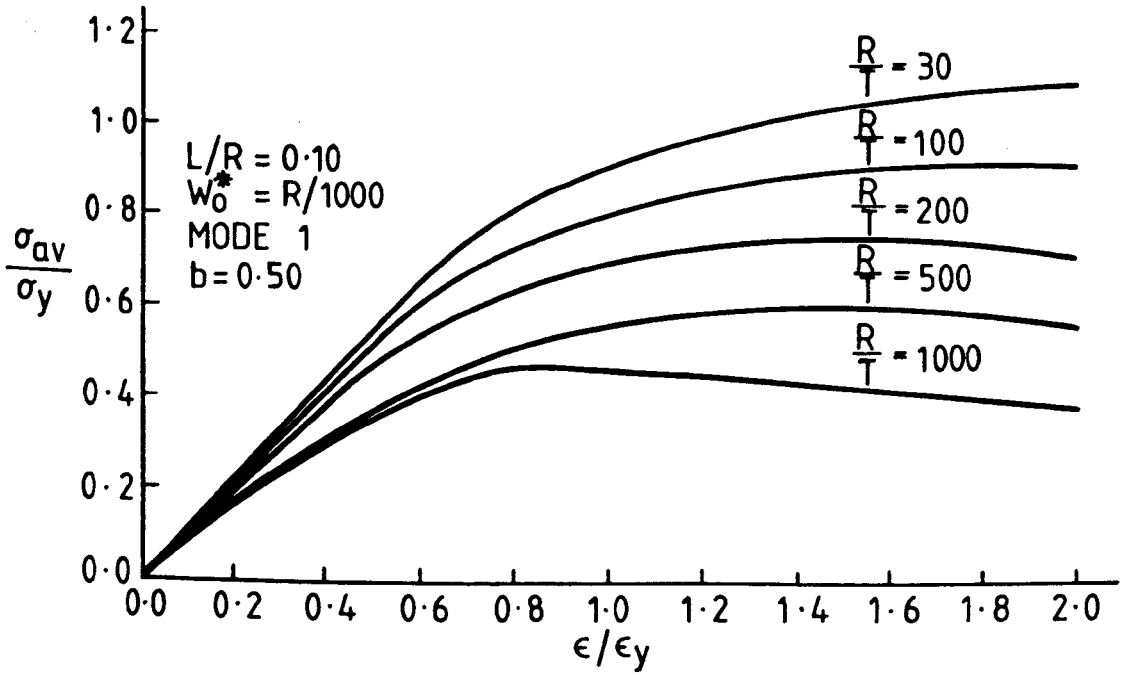

Fig. 6.43a

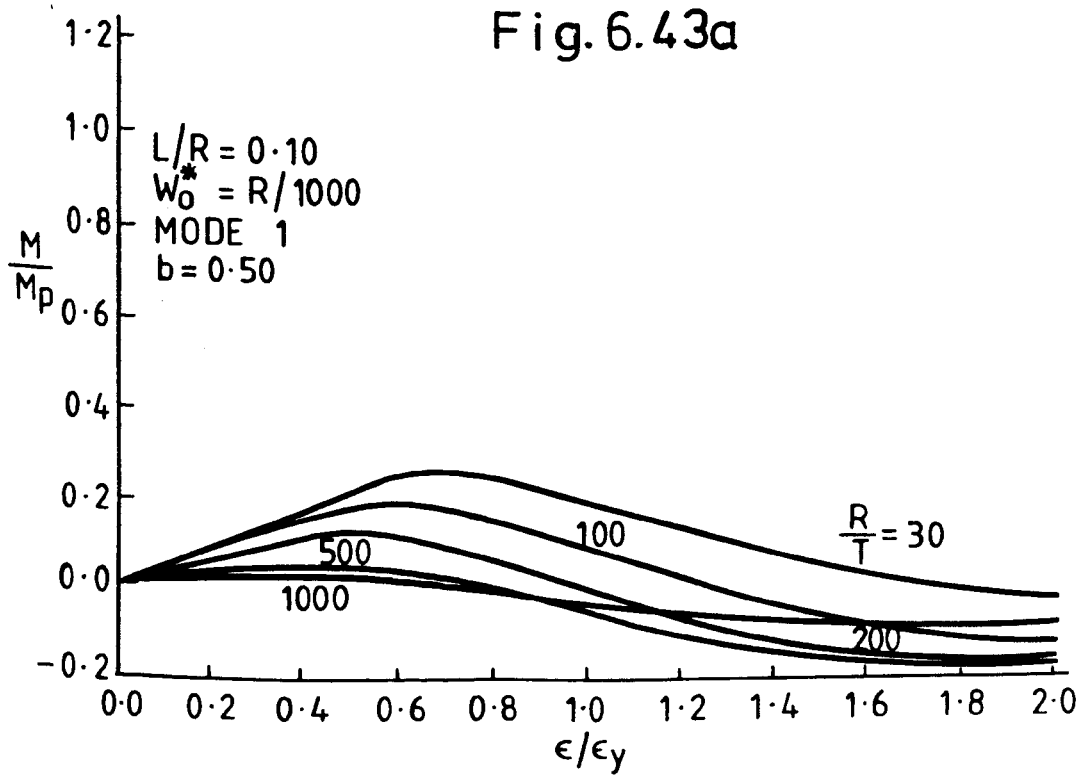

Fig. 6.43b

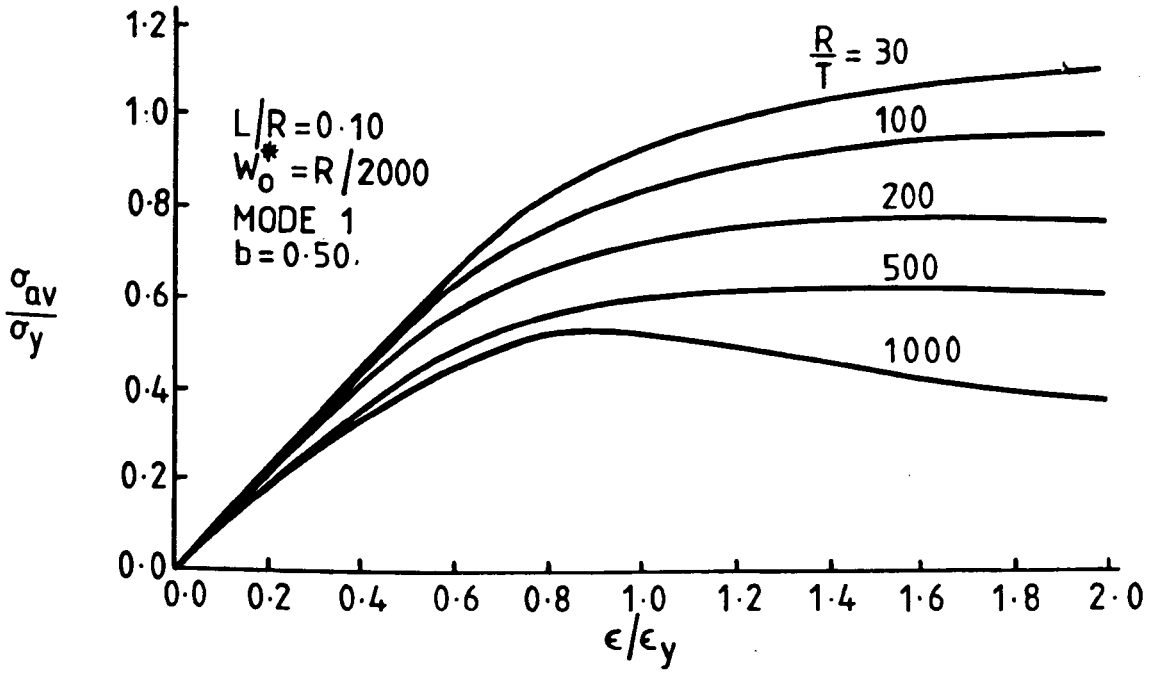

Fig. 6.44a

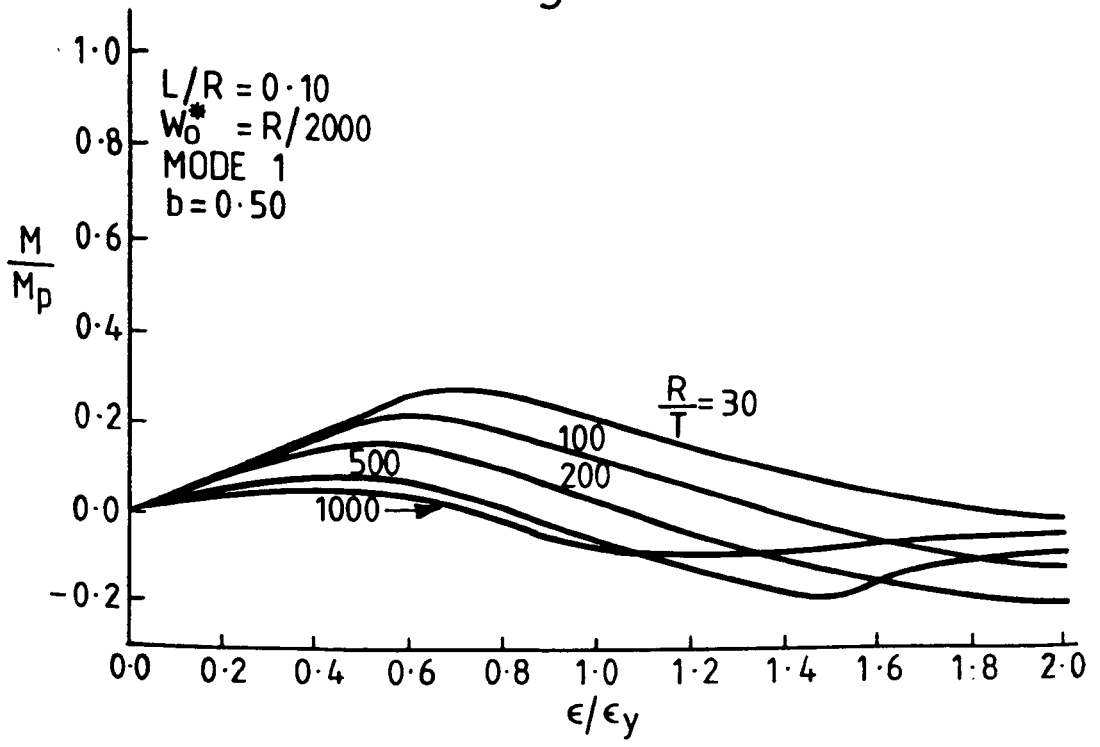

Fig. 6.44b

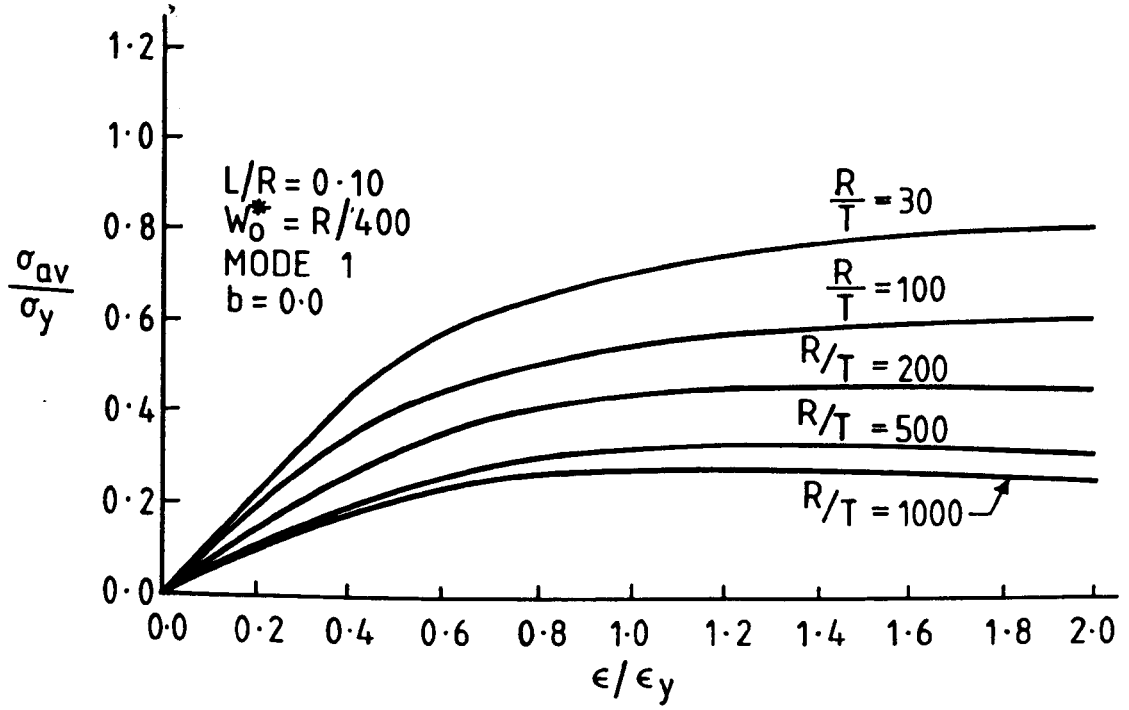

Fig. 6.45a

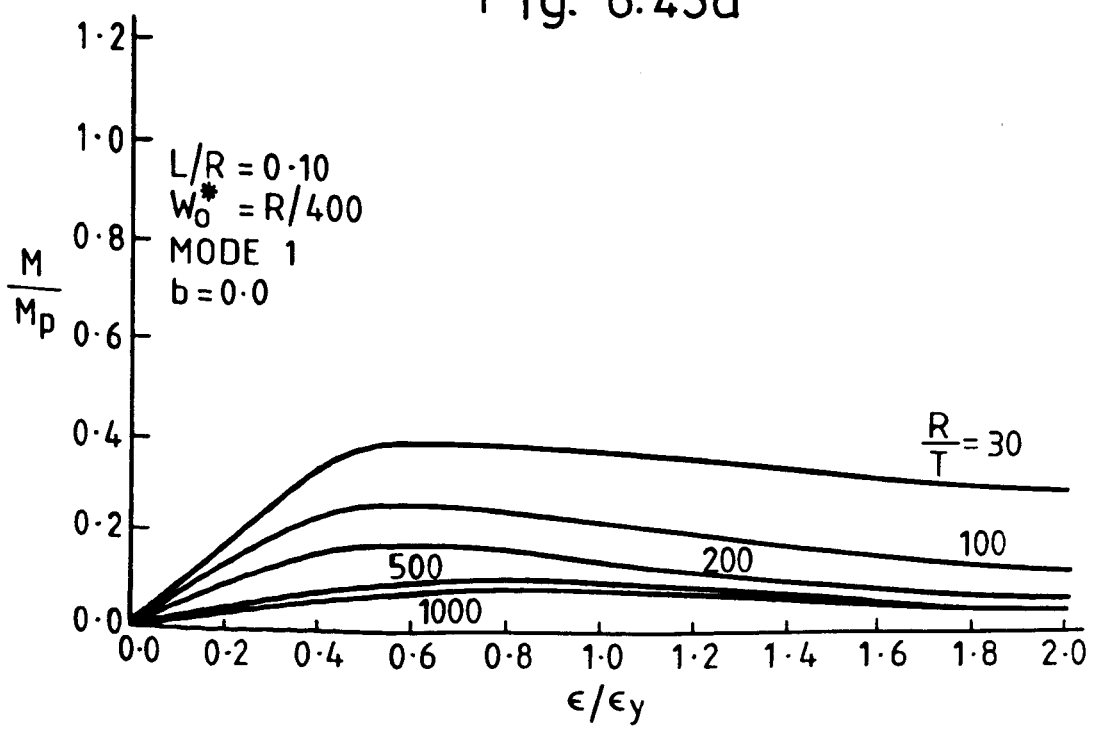

Fig. 6.45b

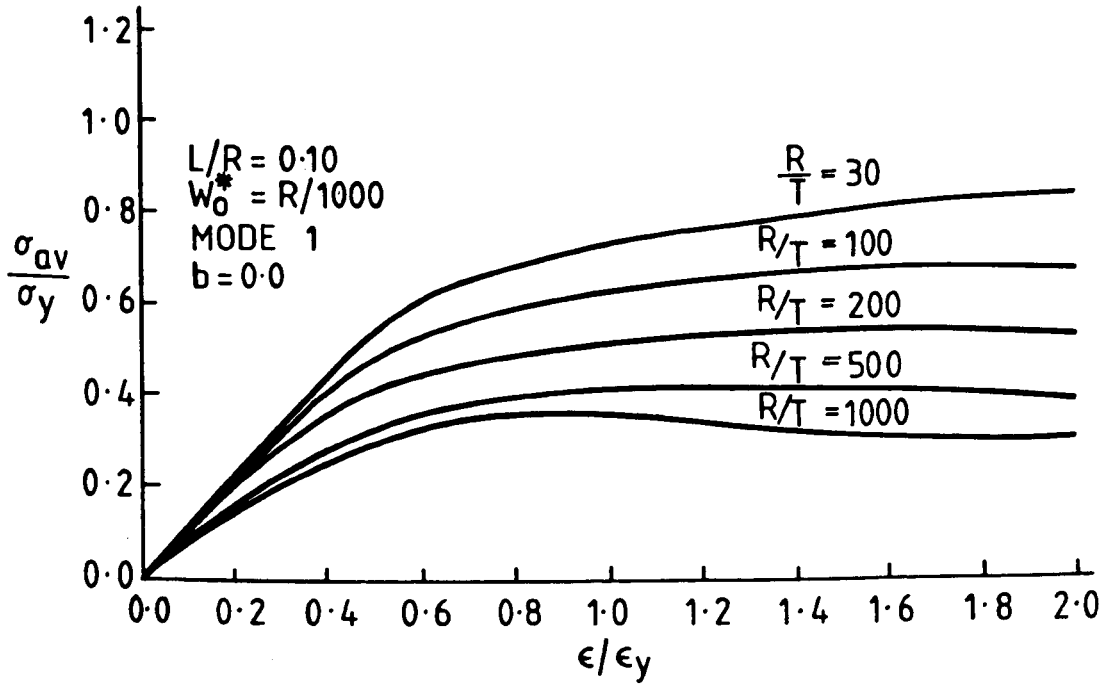

Fig. 6.46a

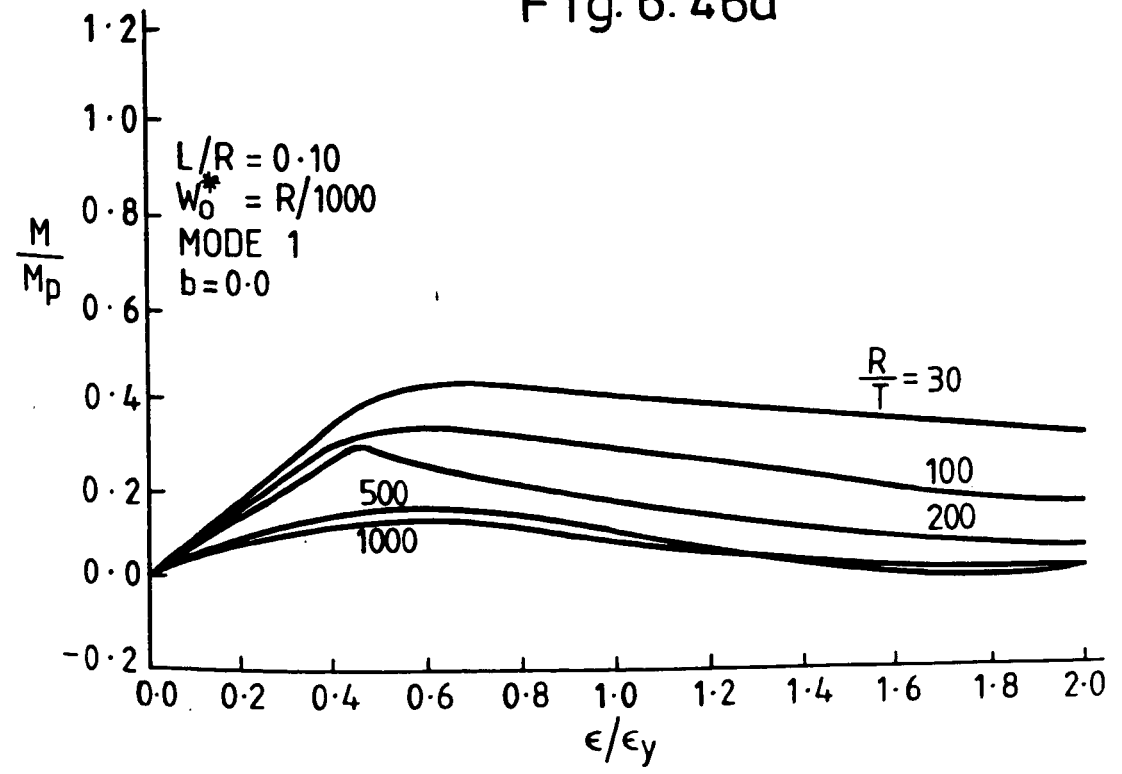

Fig. 6.46b

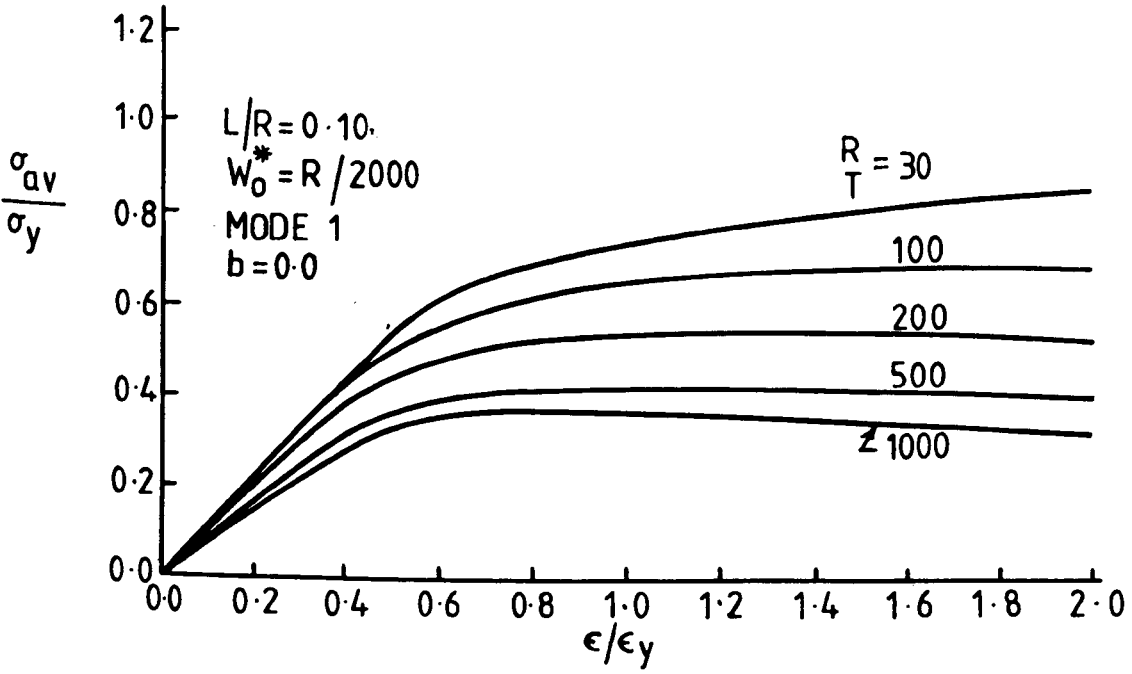

Fig. 6.47a

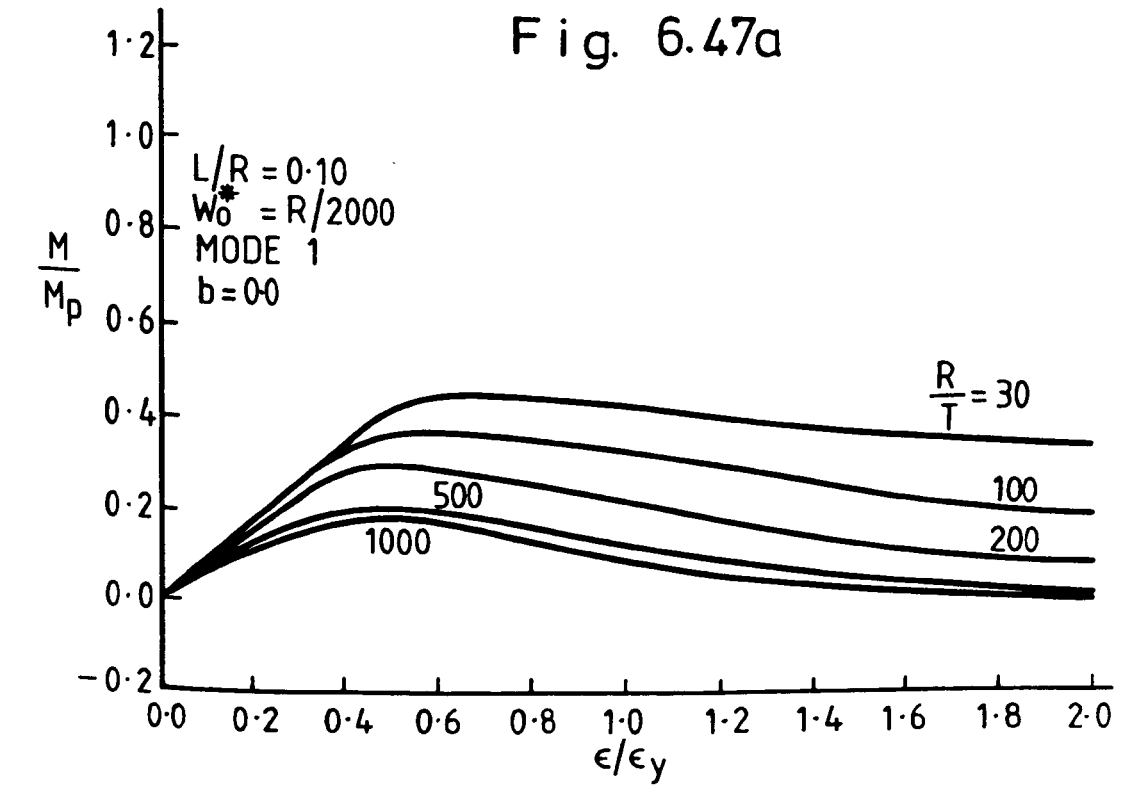

Fig. 6.47b

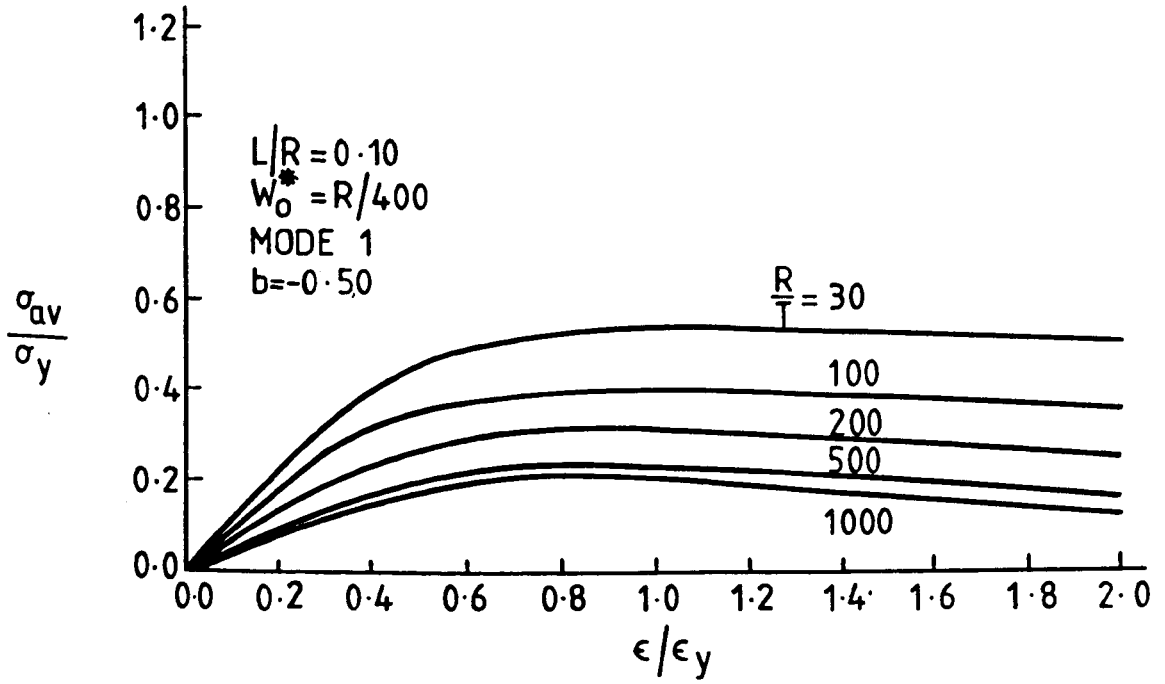

Fig. 6.48a

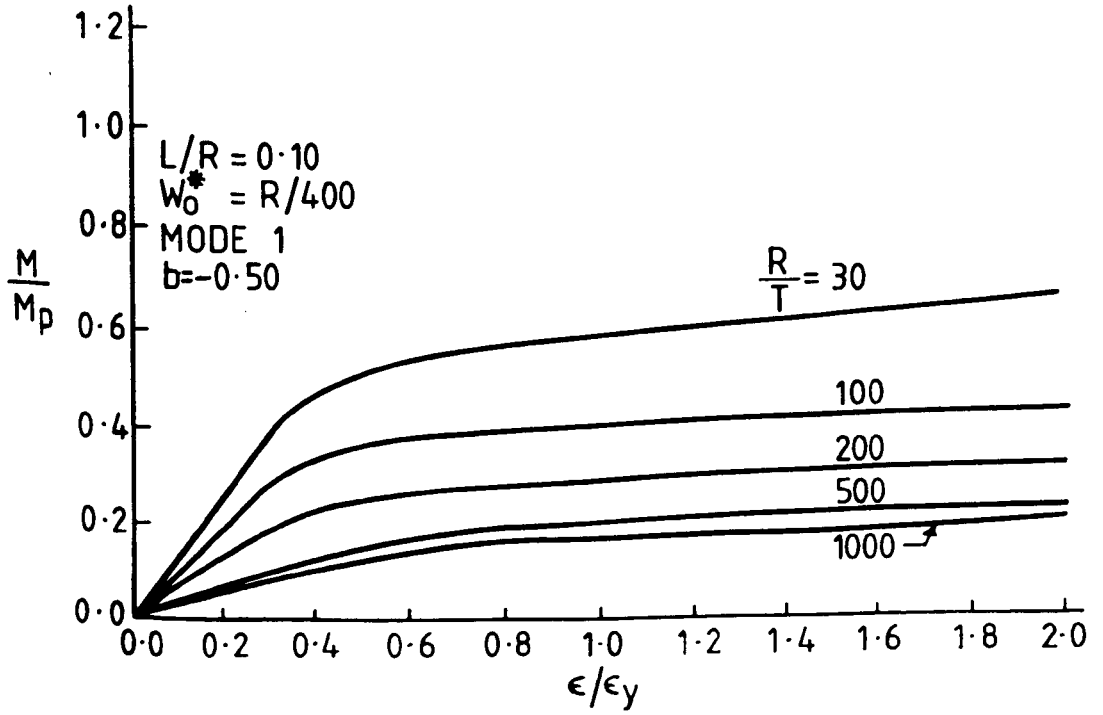

Fig. 6.48b

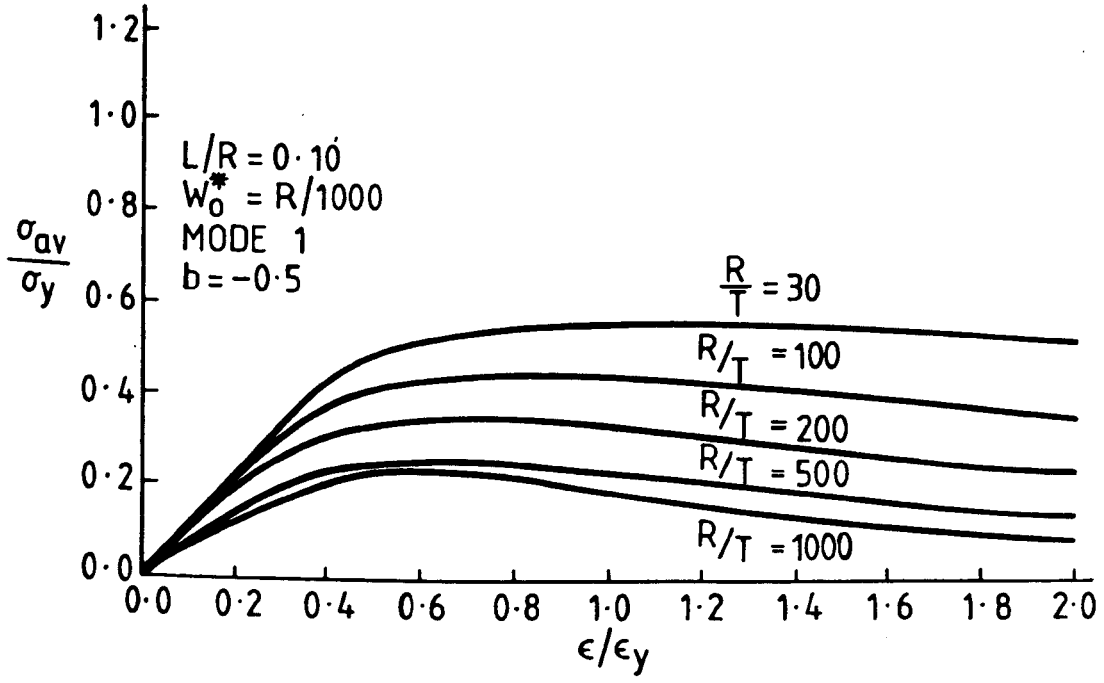

Fig. 6.49a

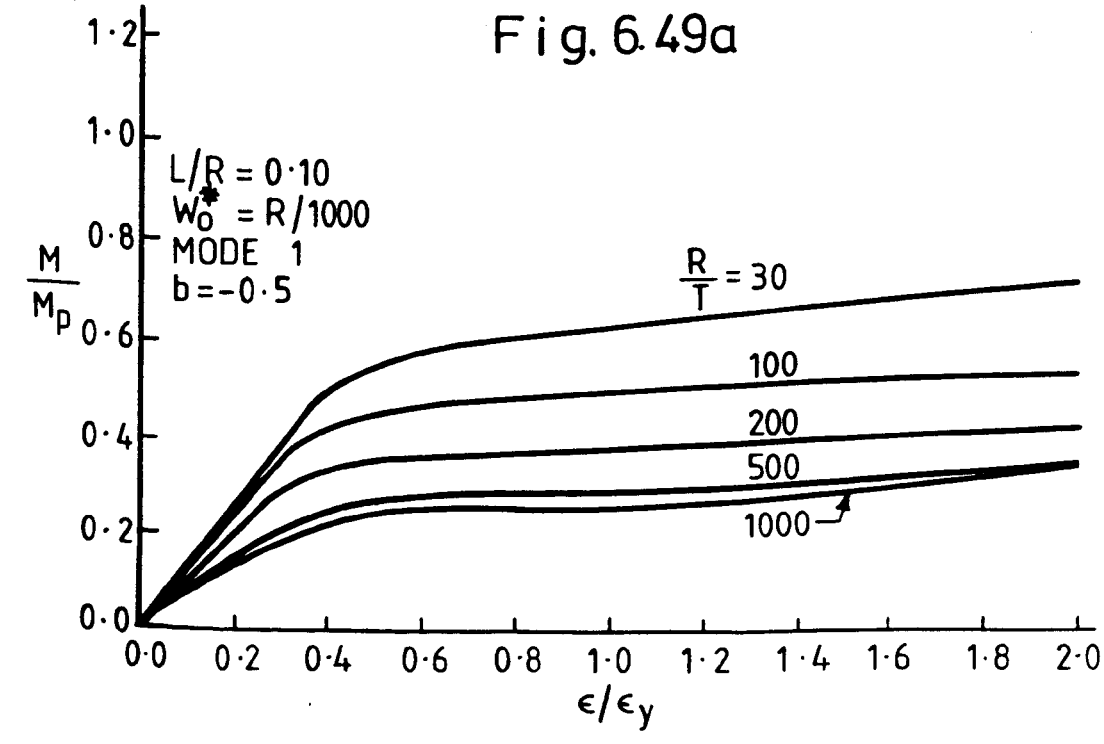

Fig. 6.49b

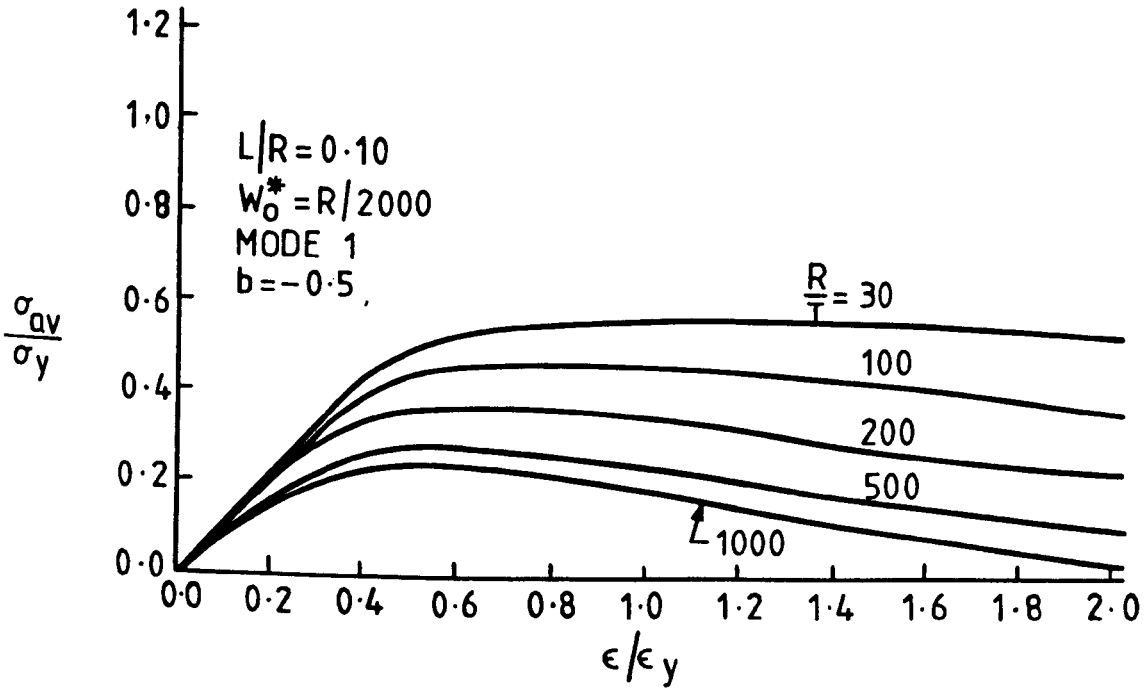

Fig. 6.50a

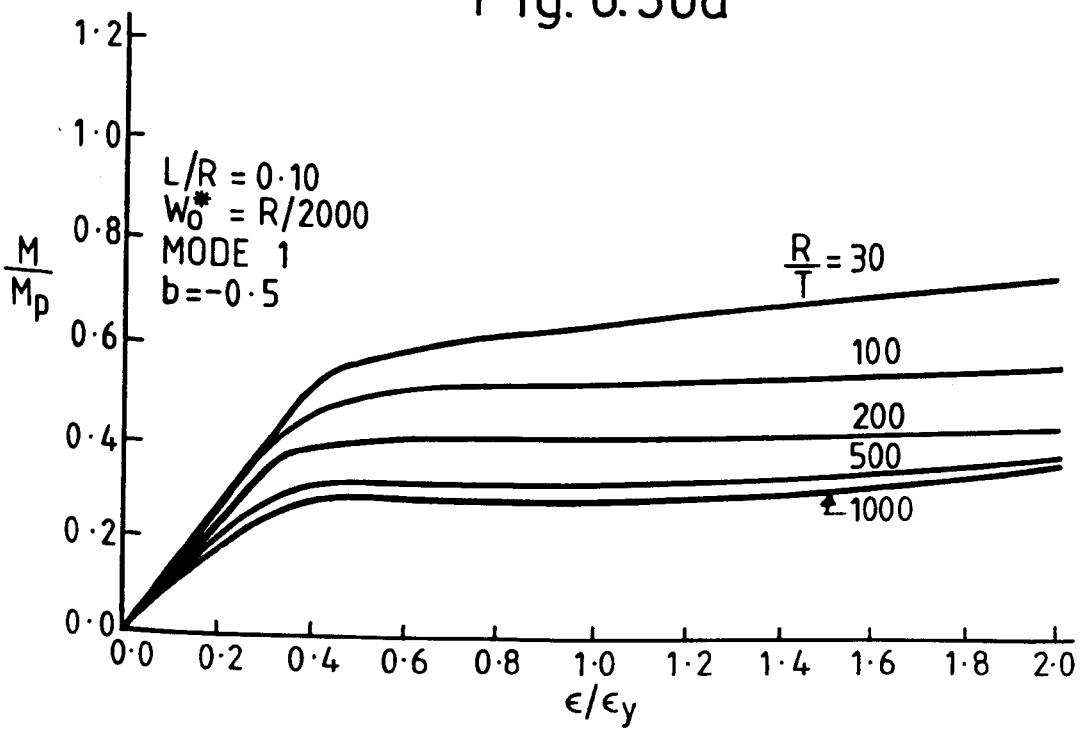

Fig. 6.50b

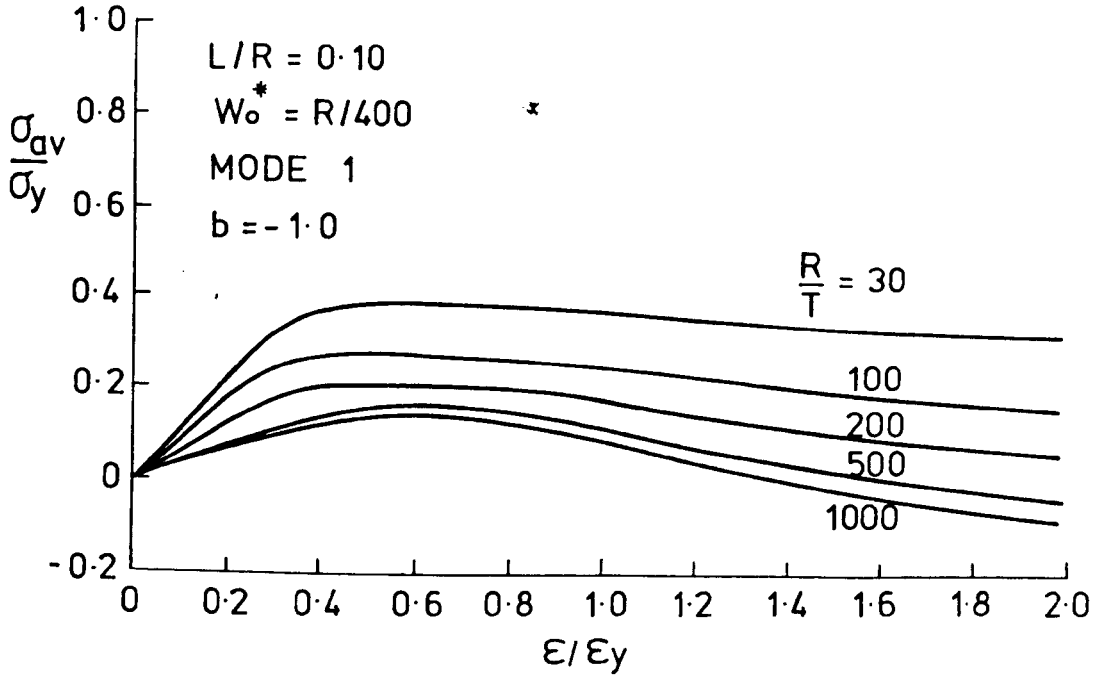

Fig. 6.51a

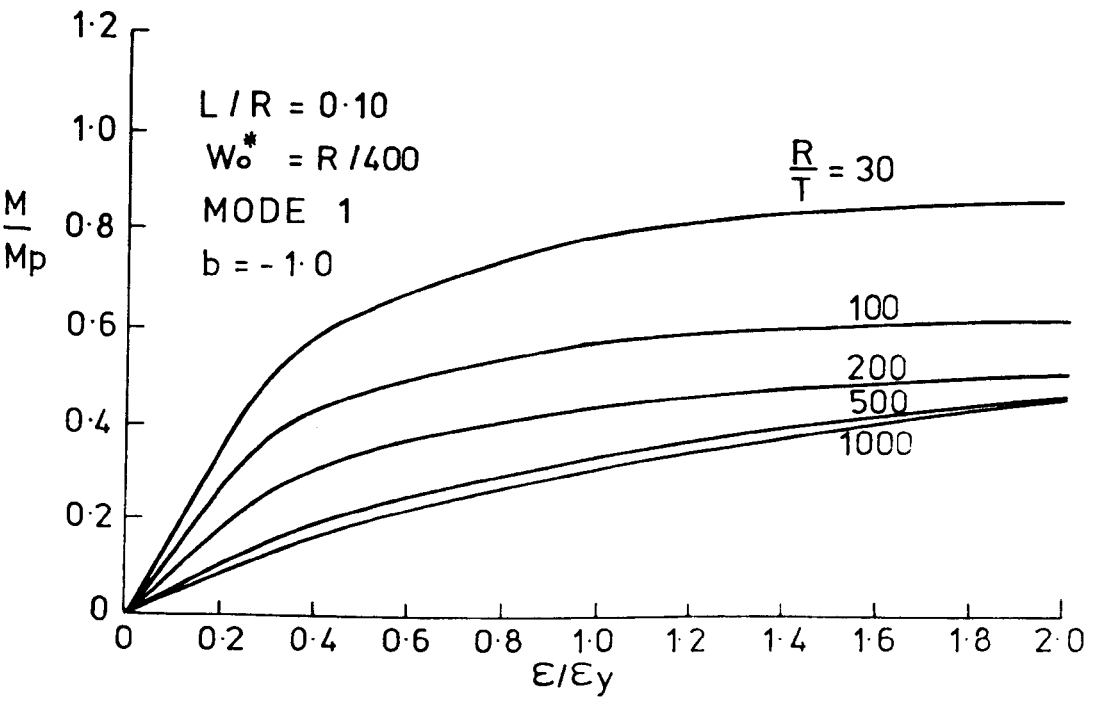

Fig. 6.51b

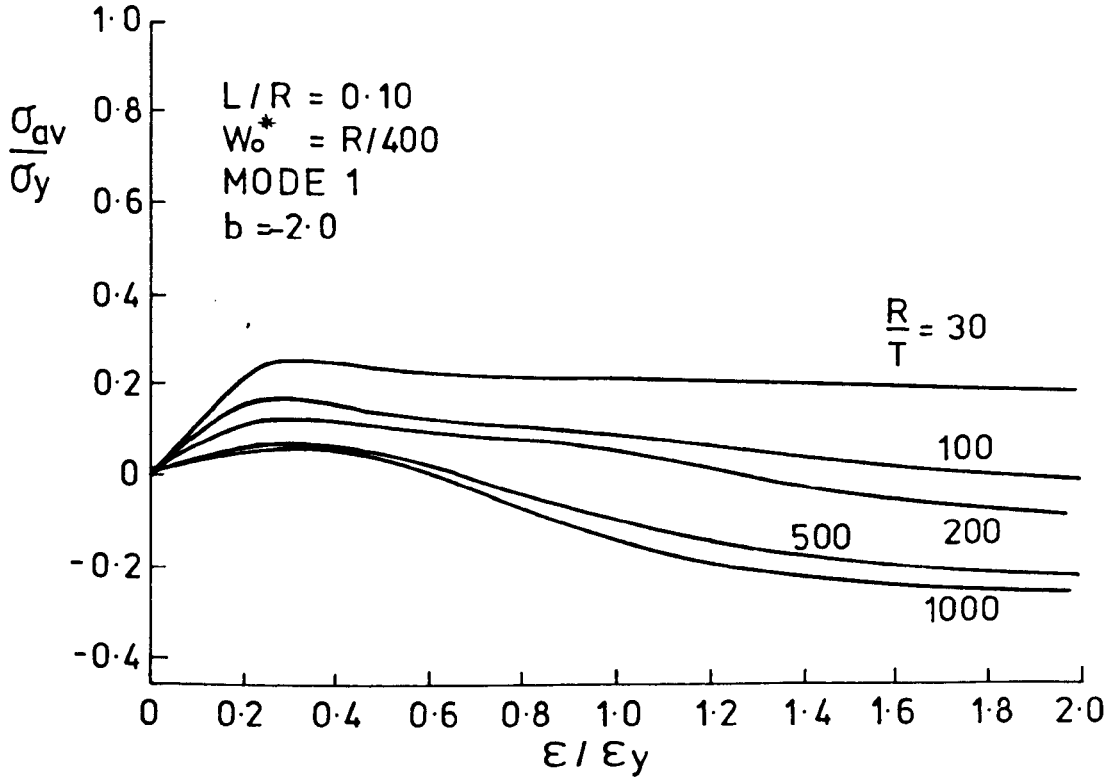

Fig. 6.52a

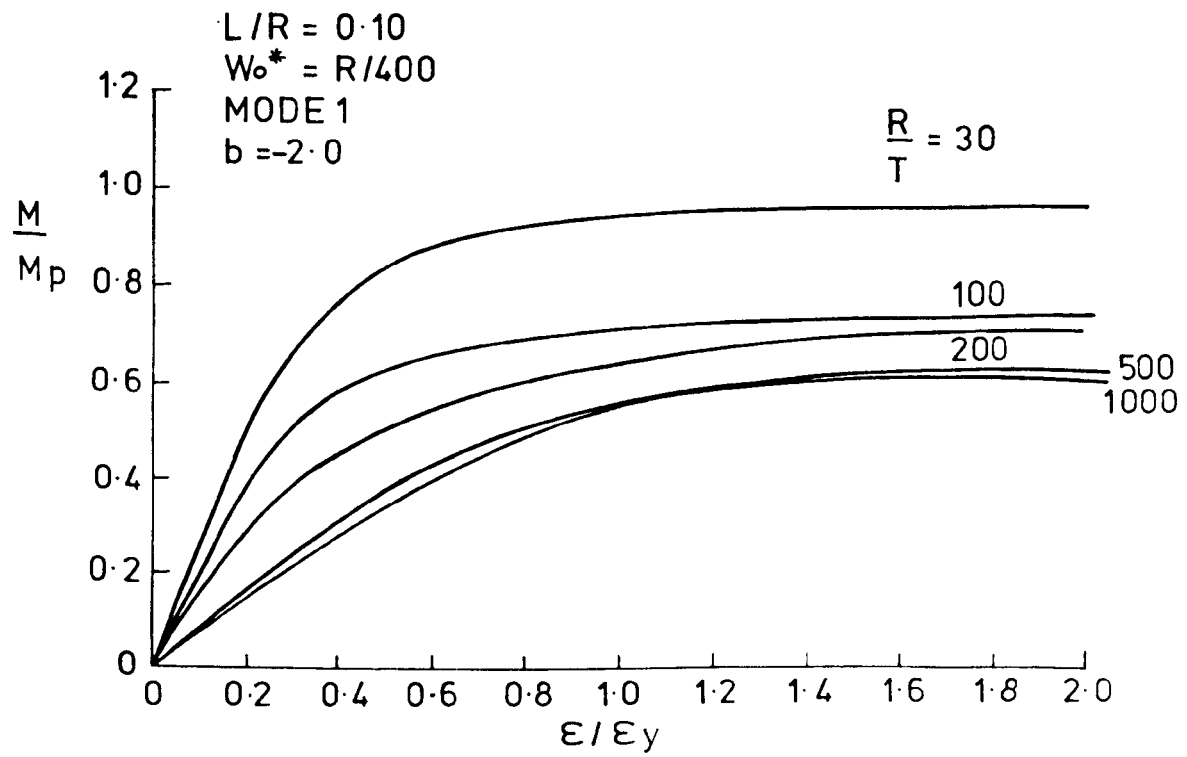

Fig. 6.52b

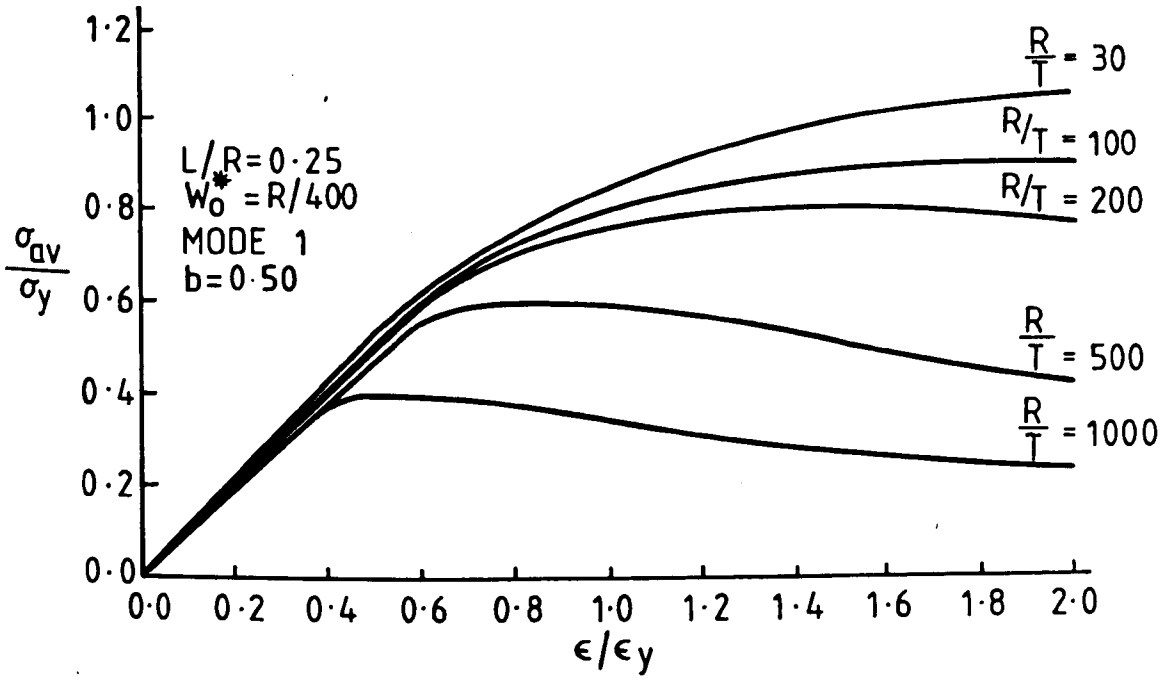

Fig. 6.53a

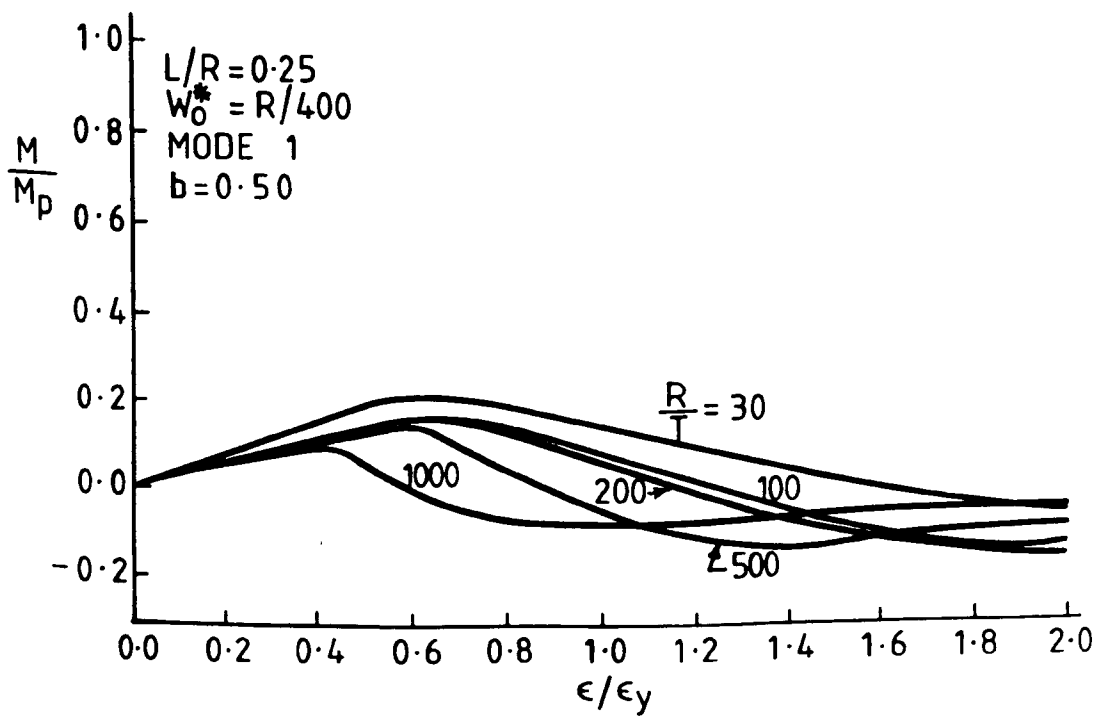

Fig. 6.53b

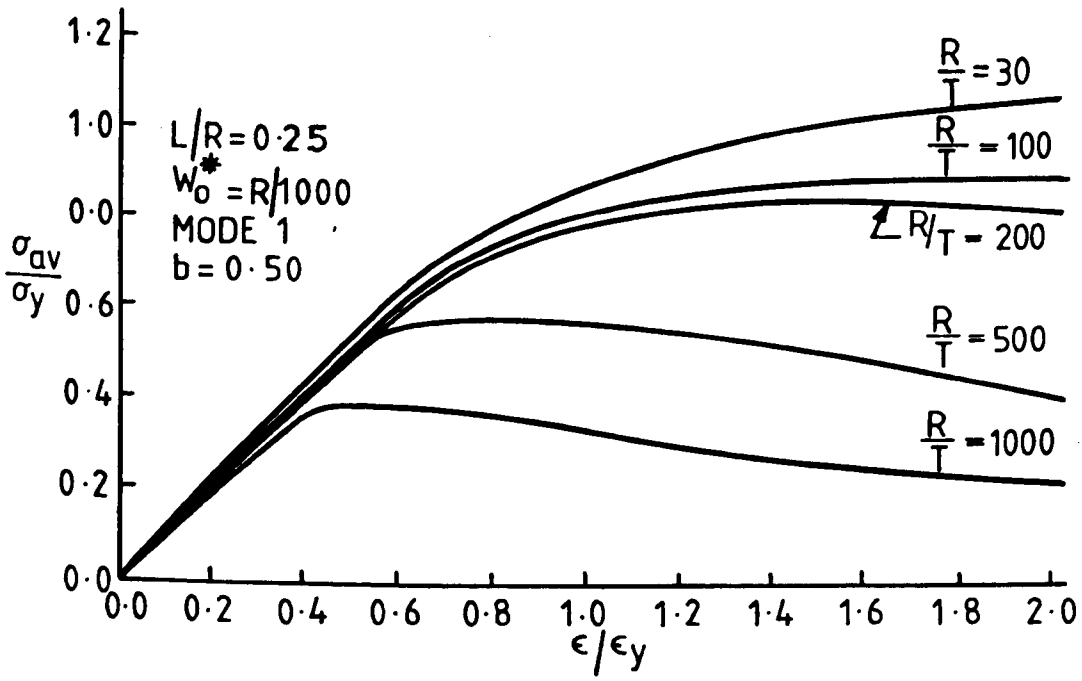

Fig. 6.54a

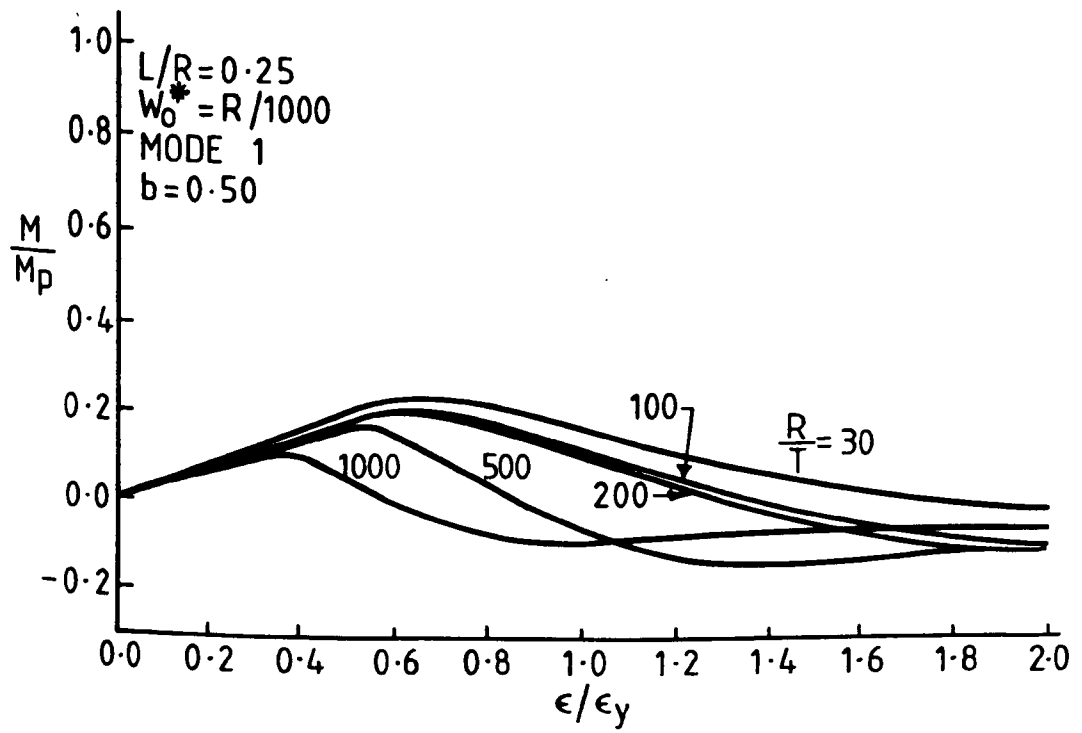

Fig. 6.54b

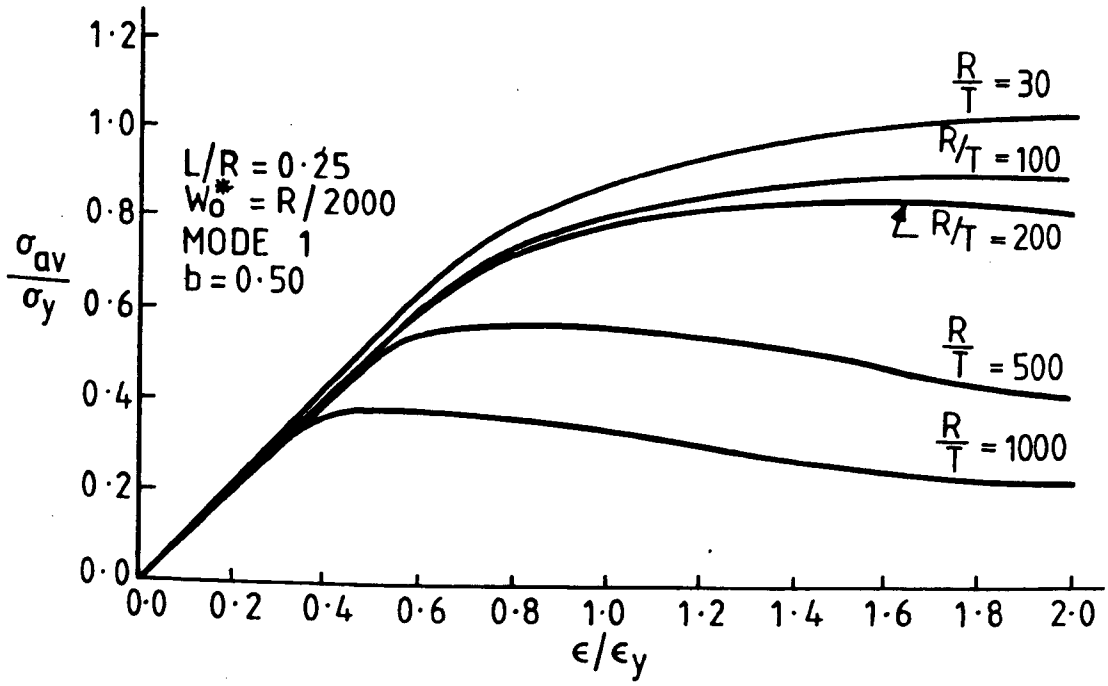

Fig. 6.55a

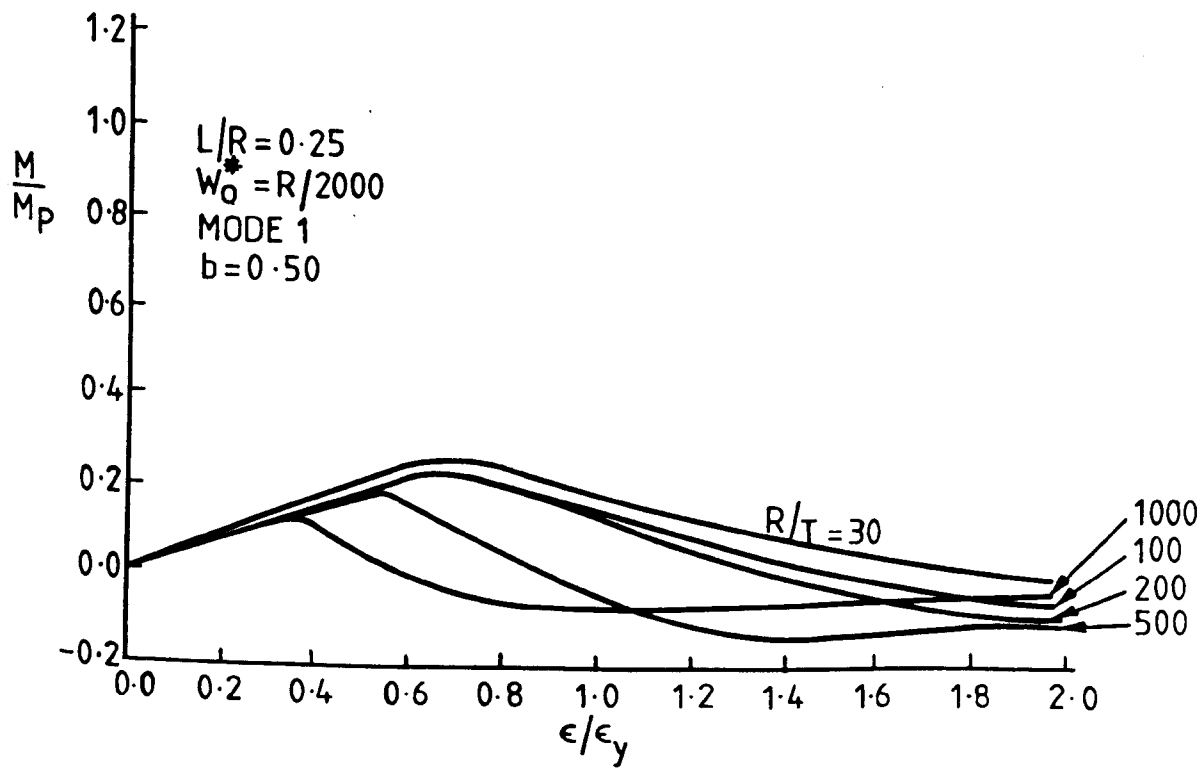

Fig. 6.55b

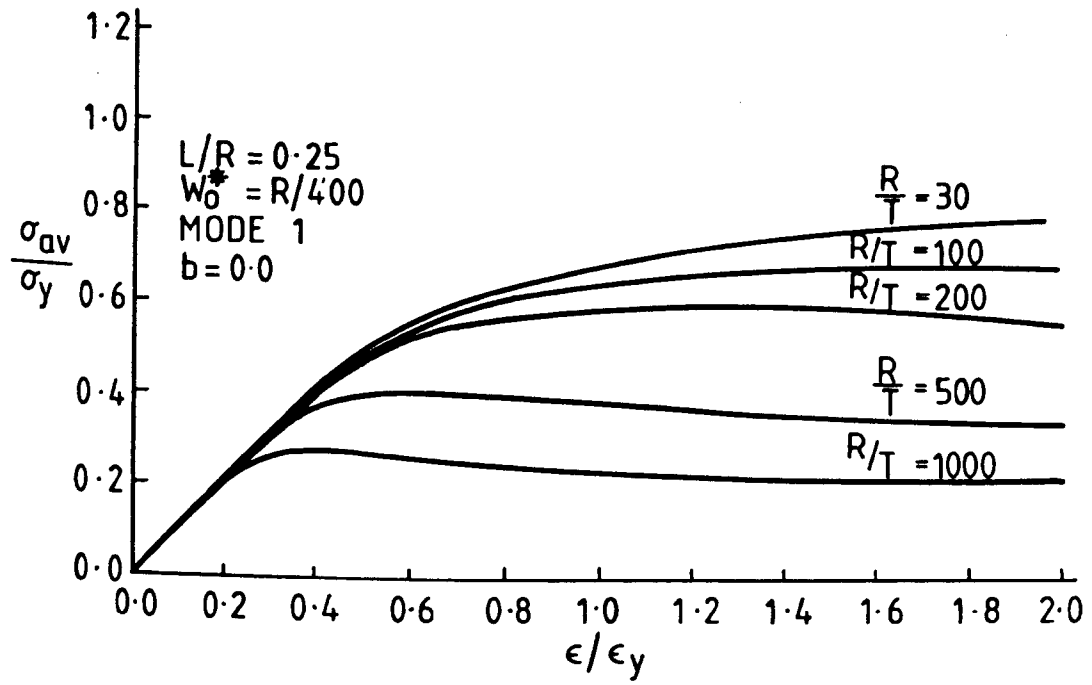

Fig. 6.56a

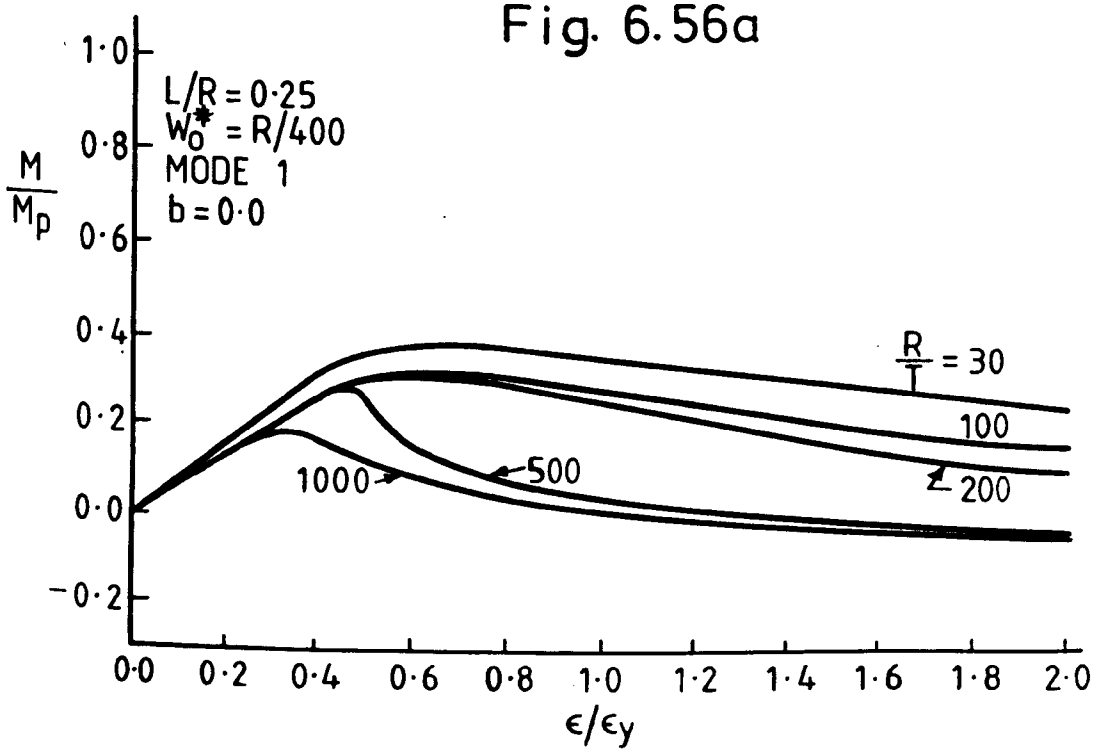

Fig. 6.56b

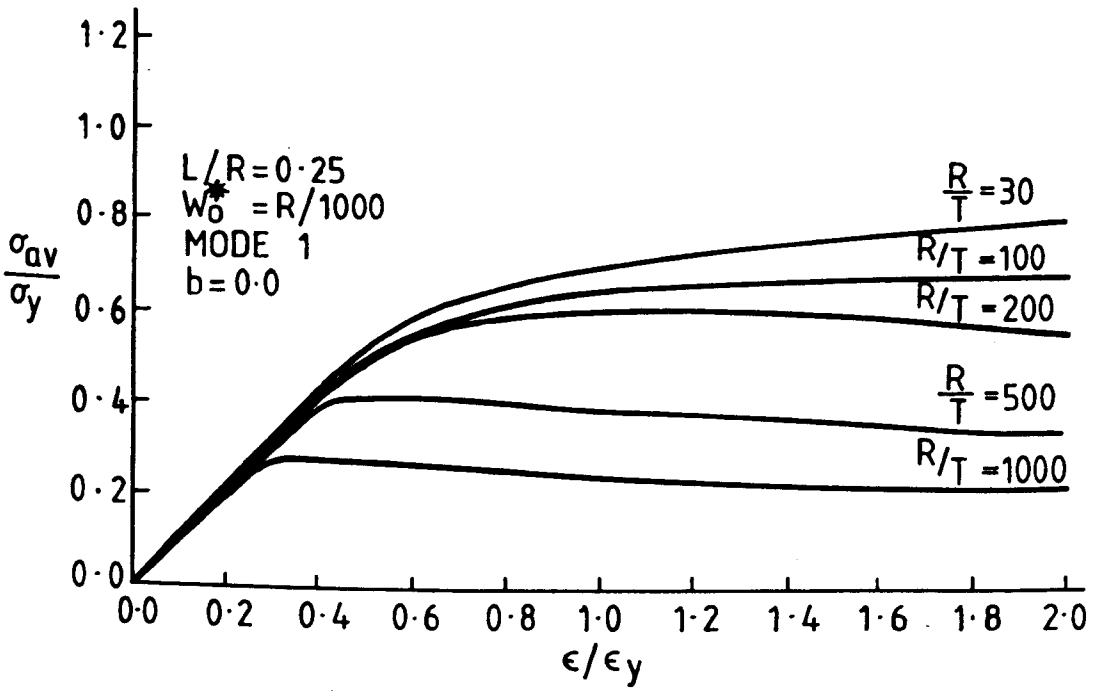

Fig. 6.57a

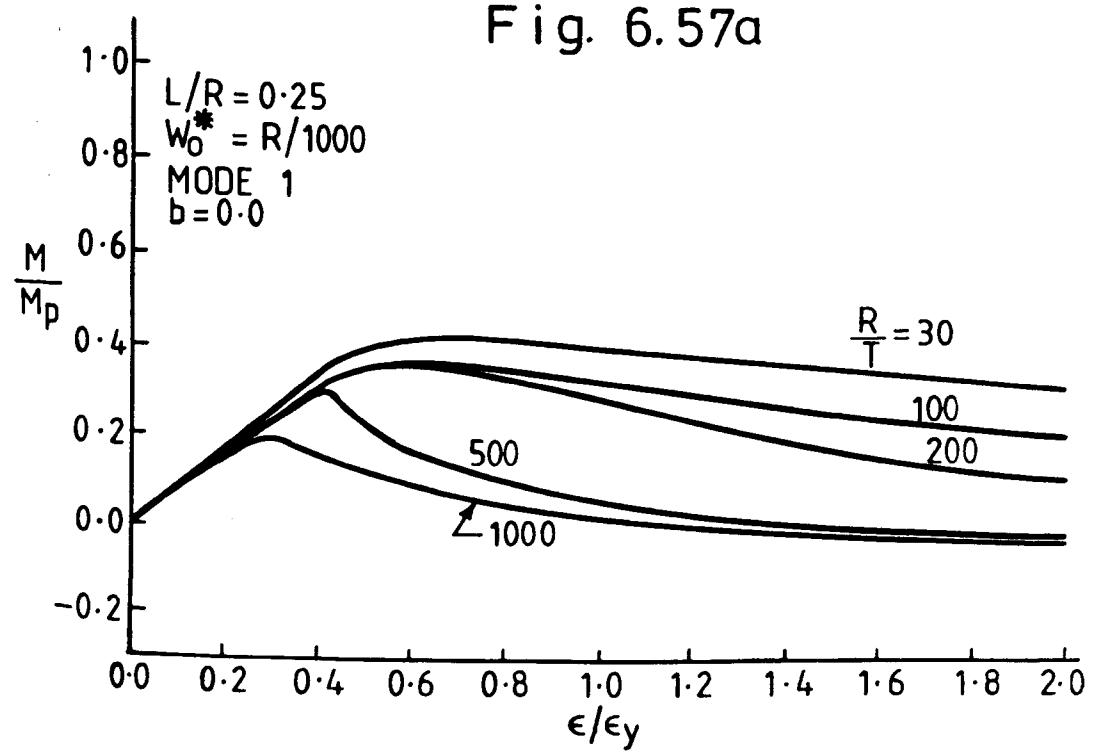

Fig. 6.57b

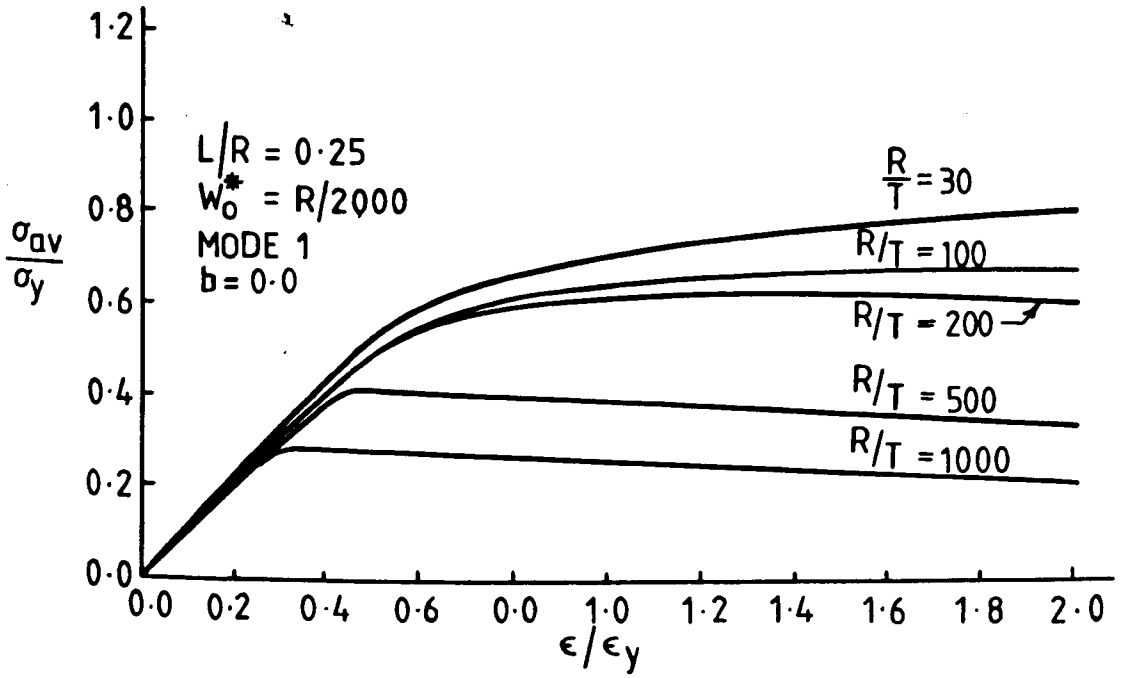

Fig. 6.58a

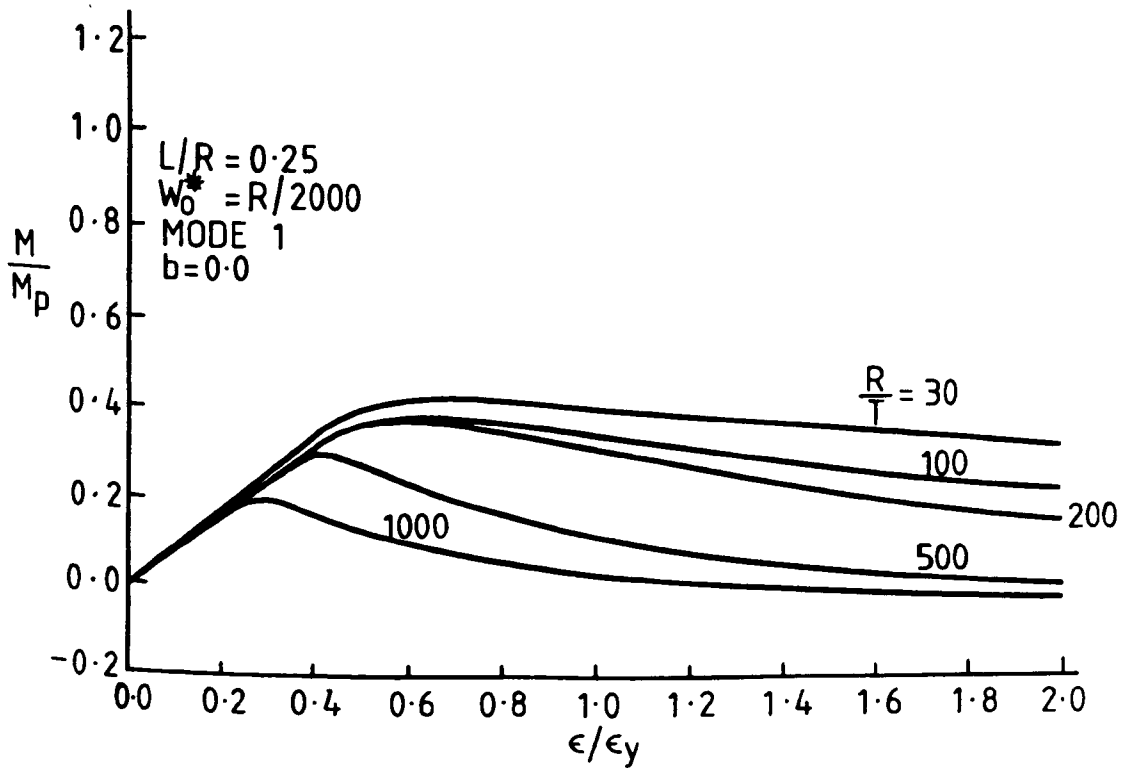

Fig. 6.58b

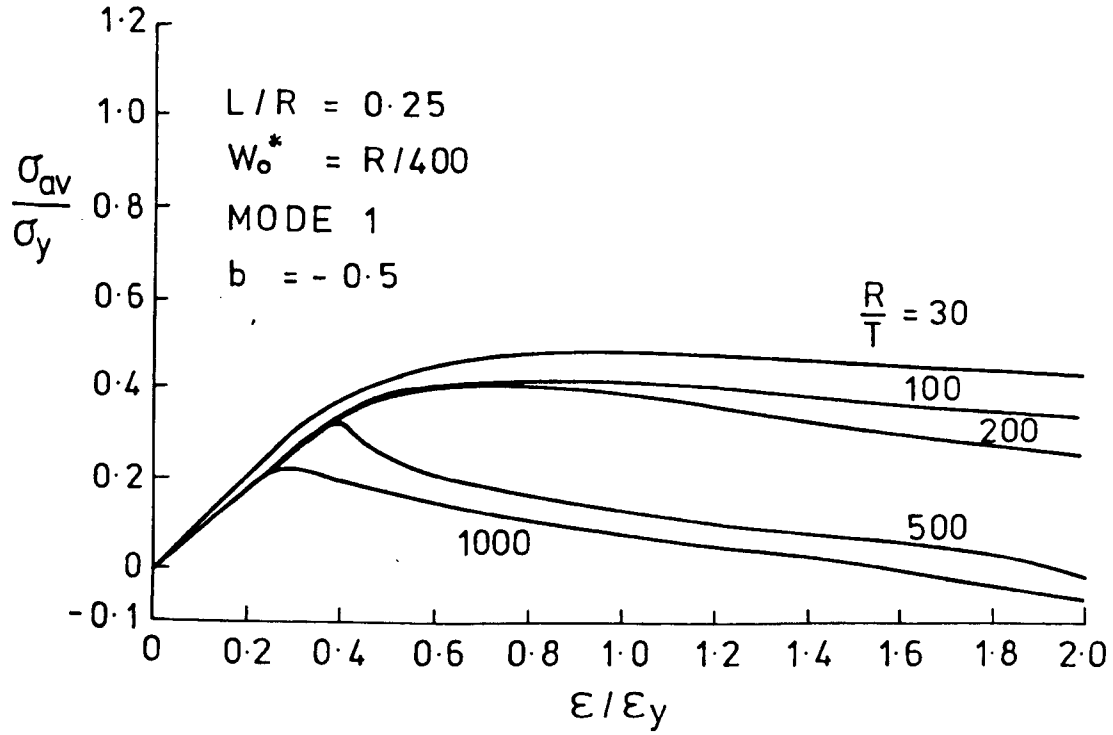

Fig. 6.59a

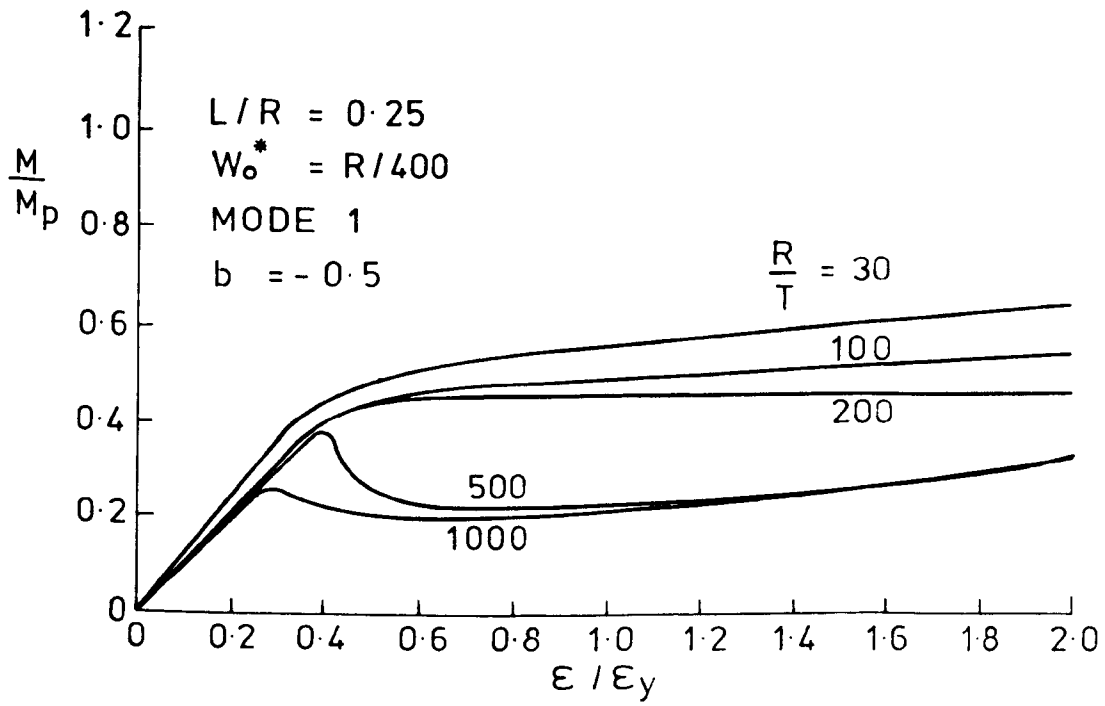

Fig. 6.59b

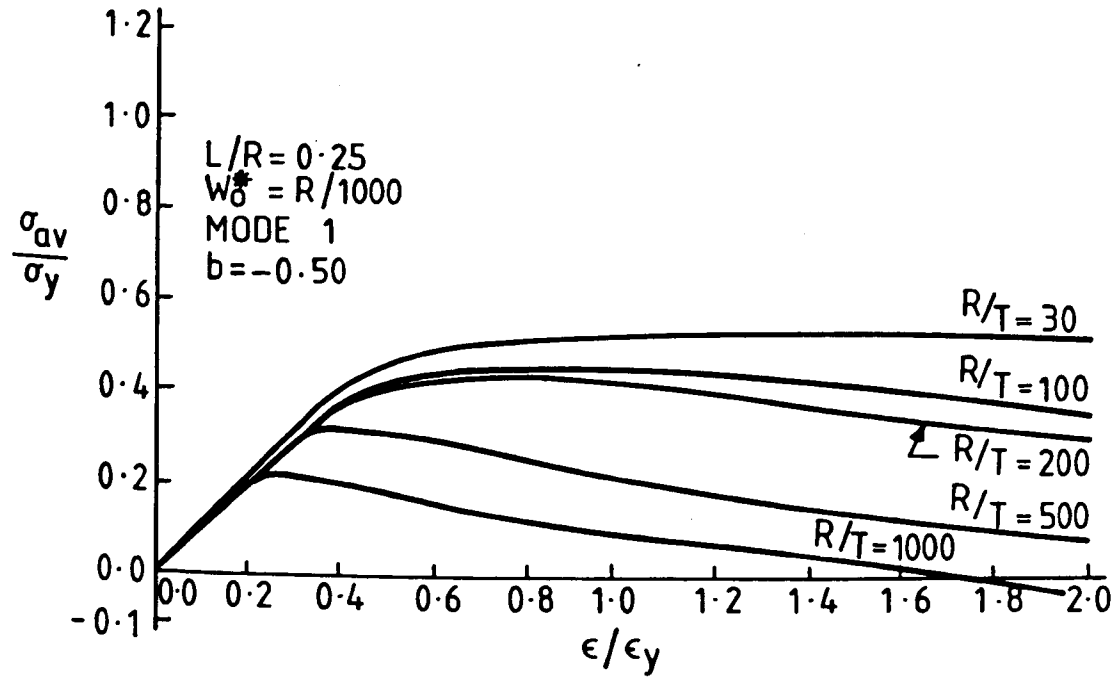

Fig. 6.60a

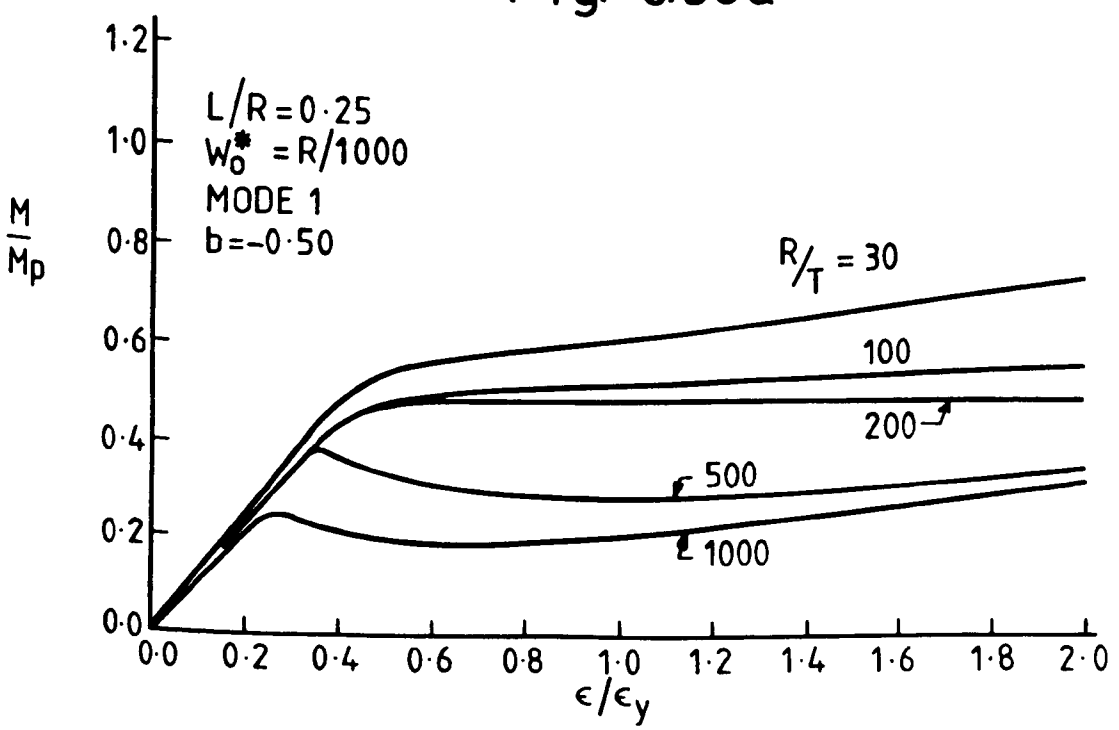

Fig. 6.60b

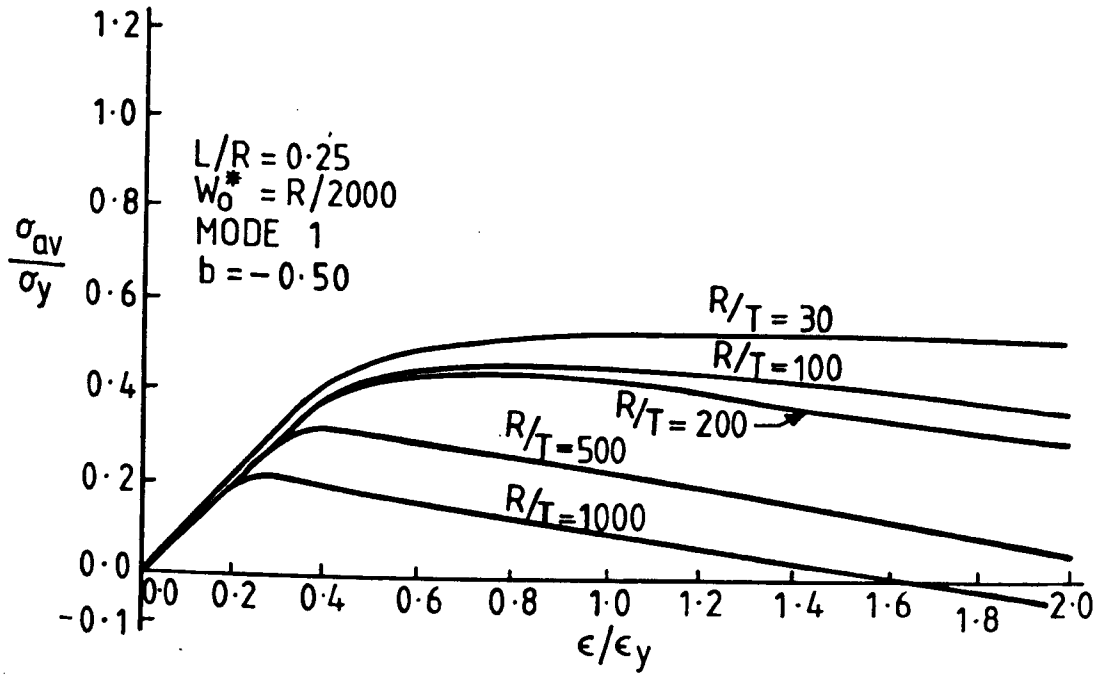

Fig. 6.61a

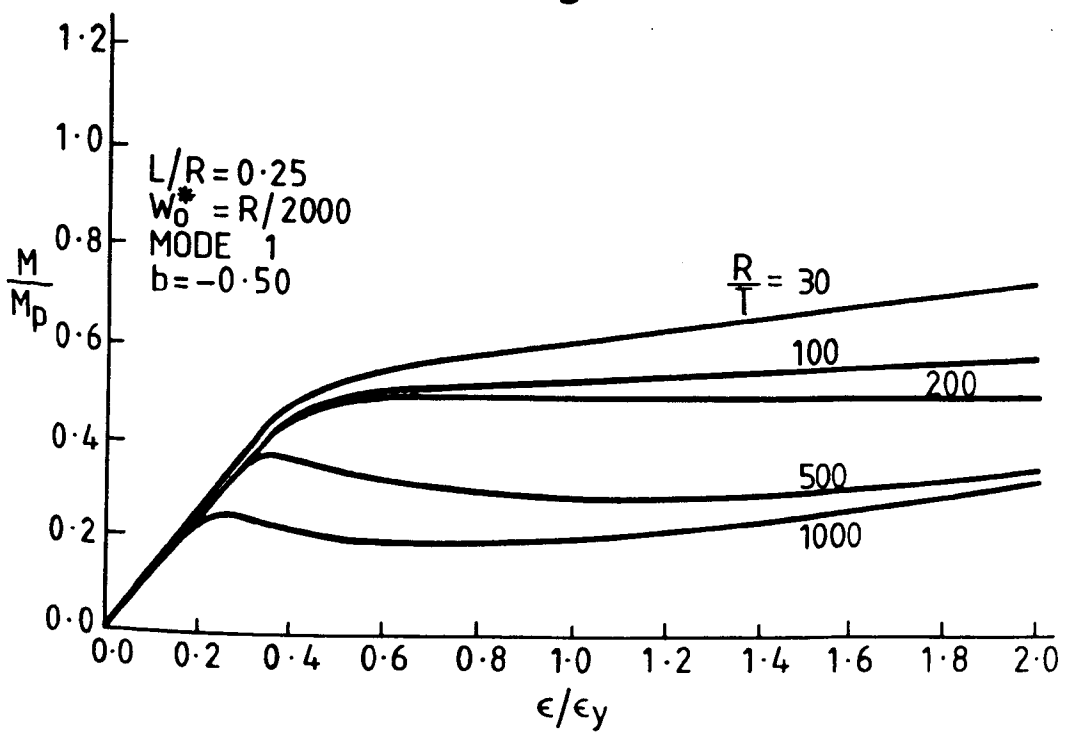

Fig. 6.61b

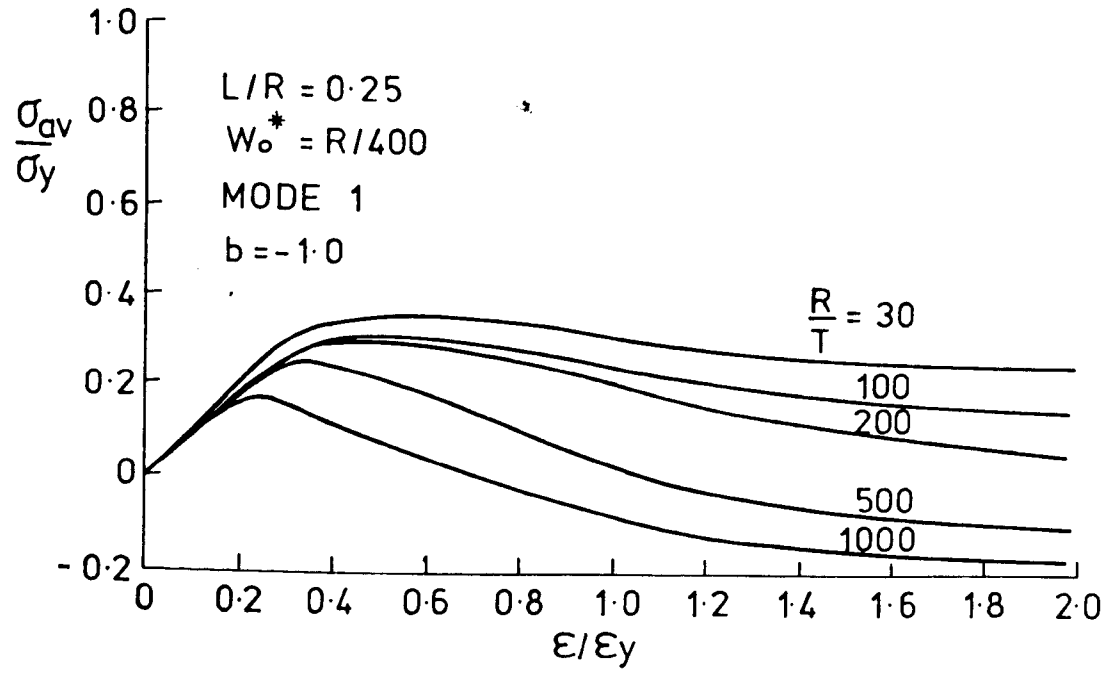

Fig. 6.62a

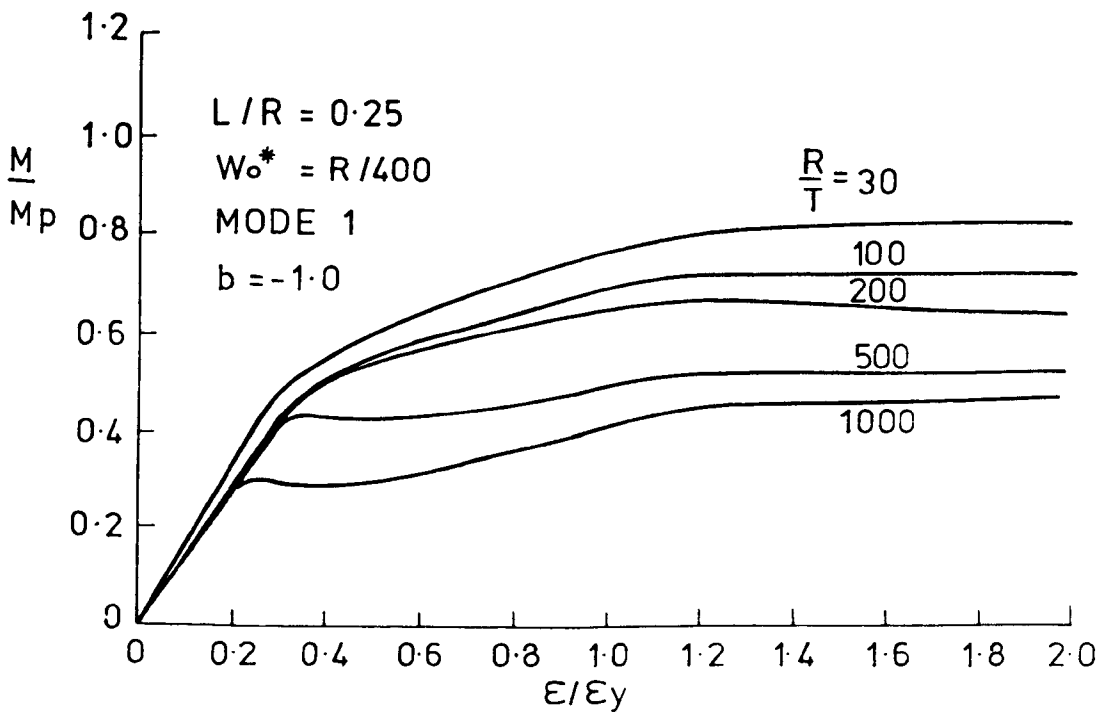

Fig. 6.62b

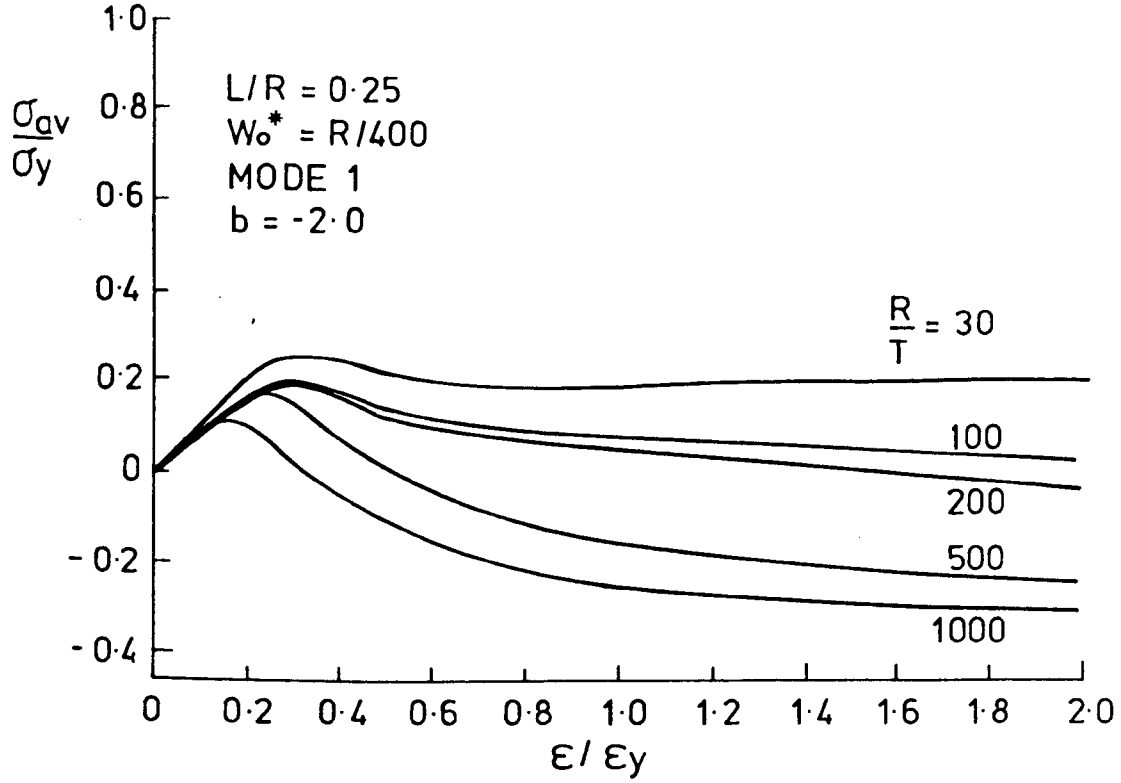

Fig.6.63a

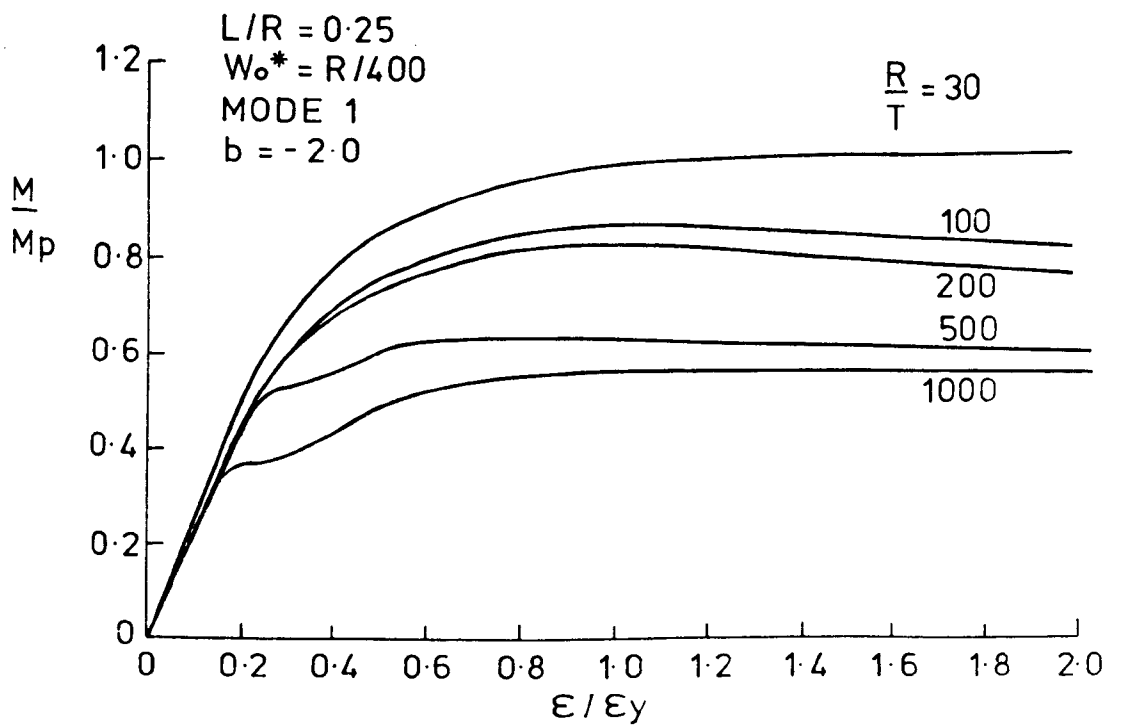

Fig. 6.63b

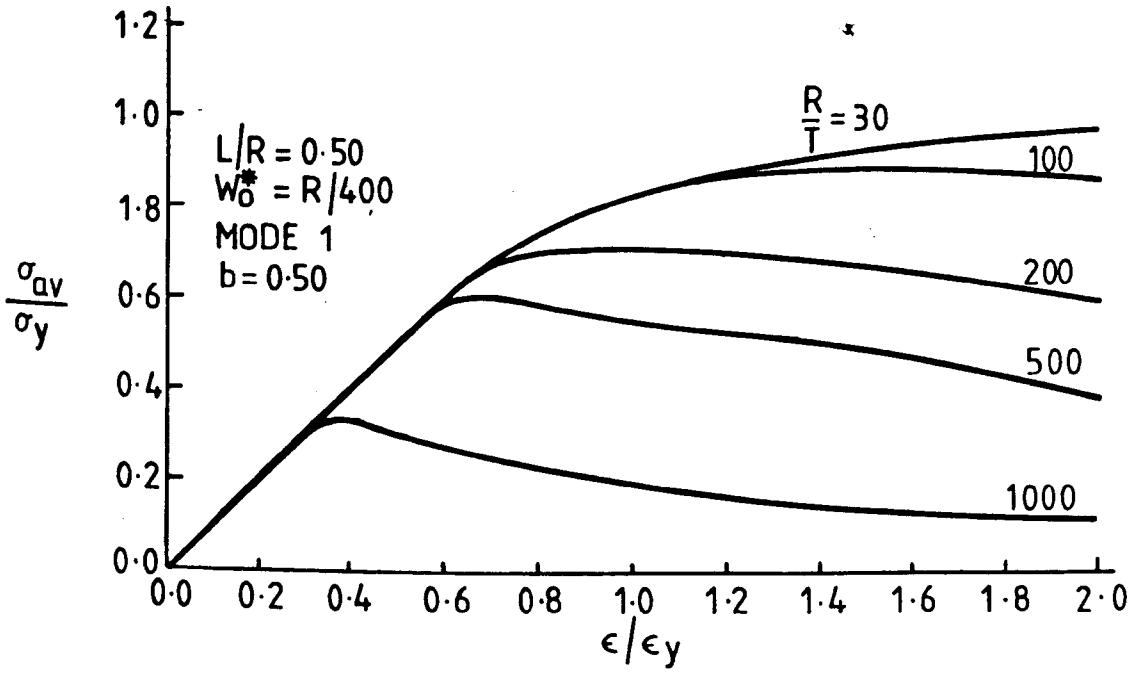

Fig. 6.64a

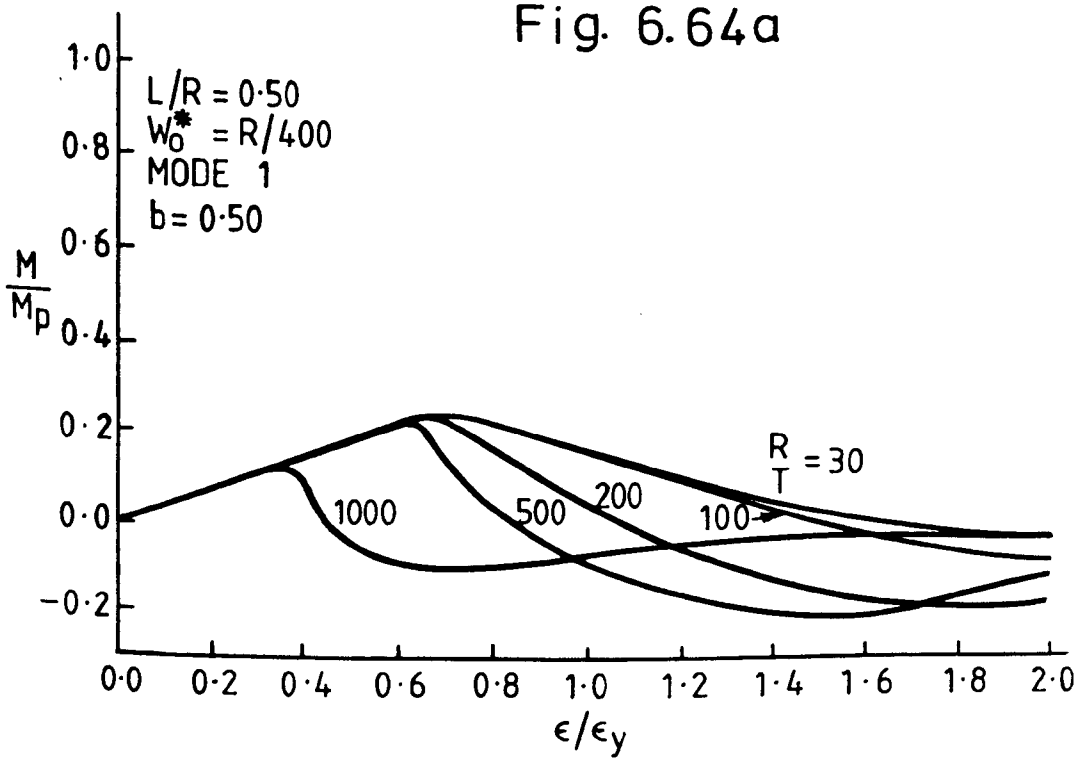

Fig. 6.64b

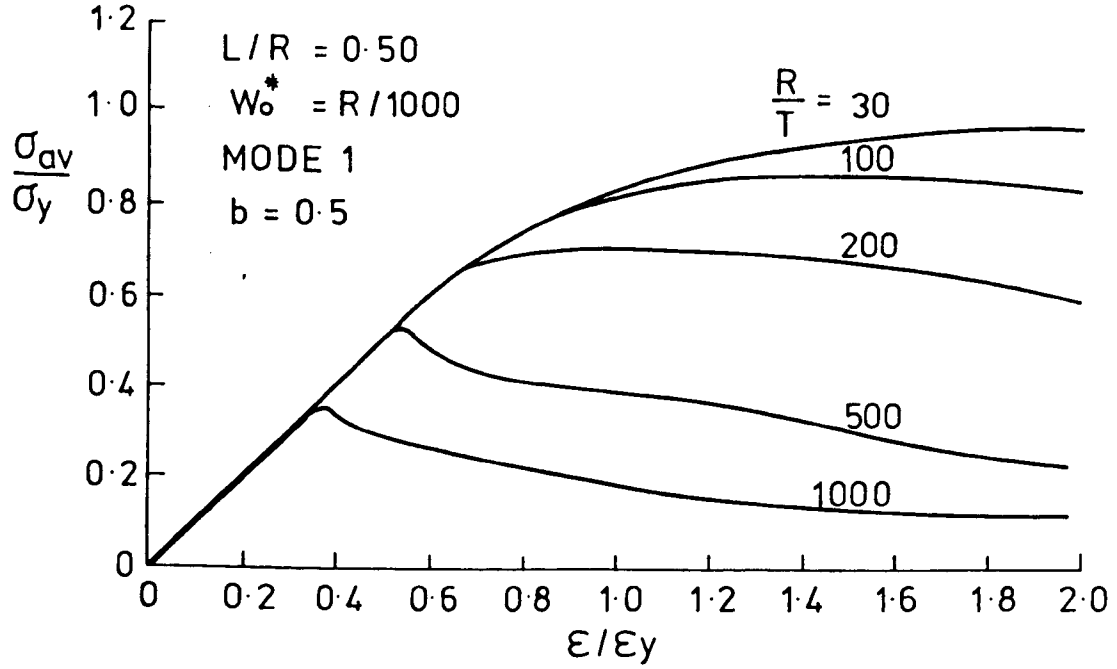

Fig. 6.65a

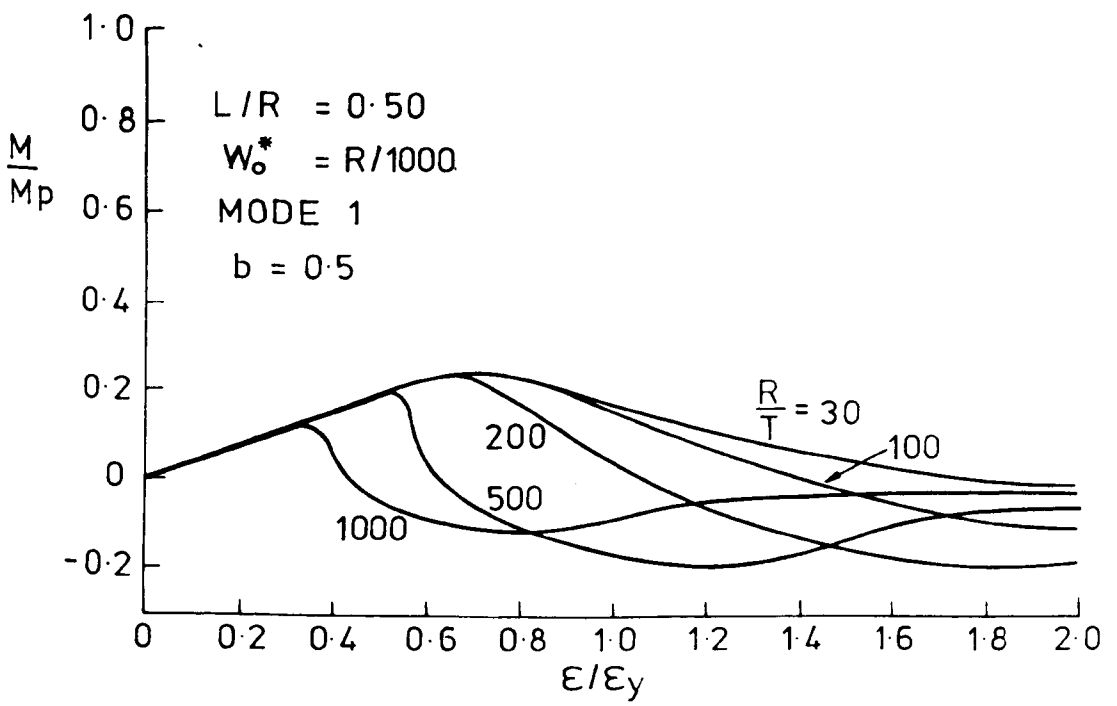

Fig. 6. 65b

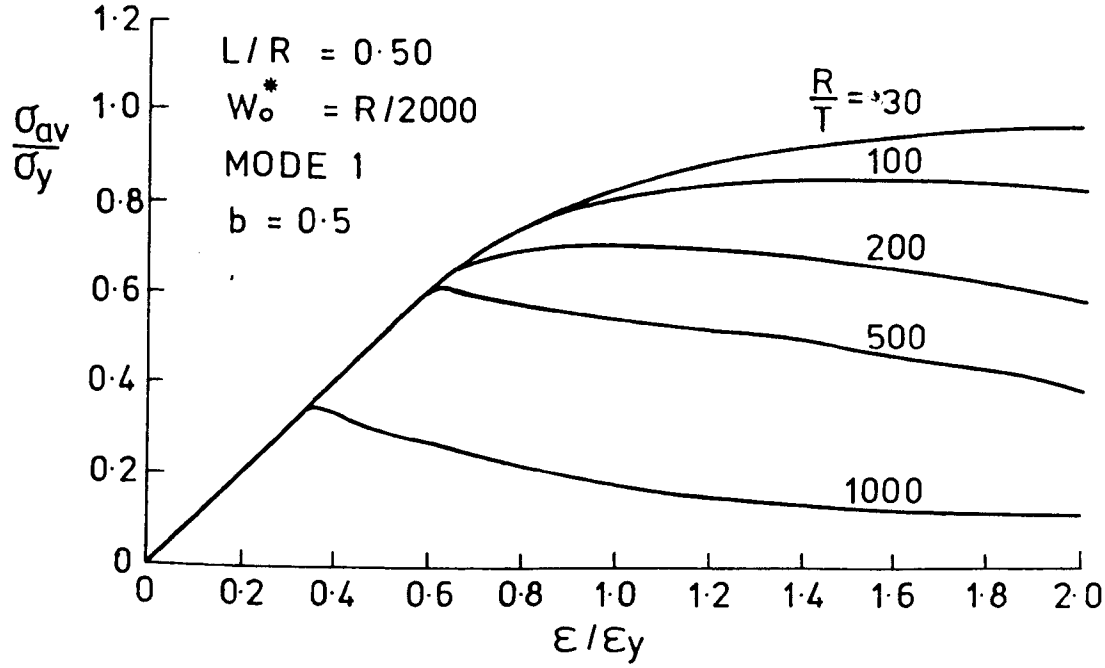

Fig. 6.66a

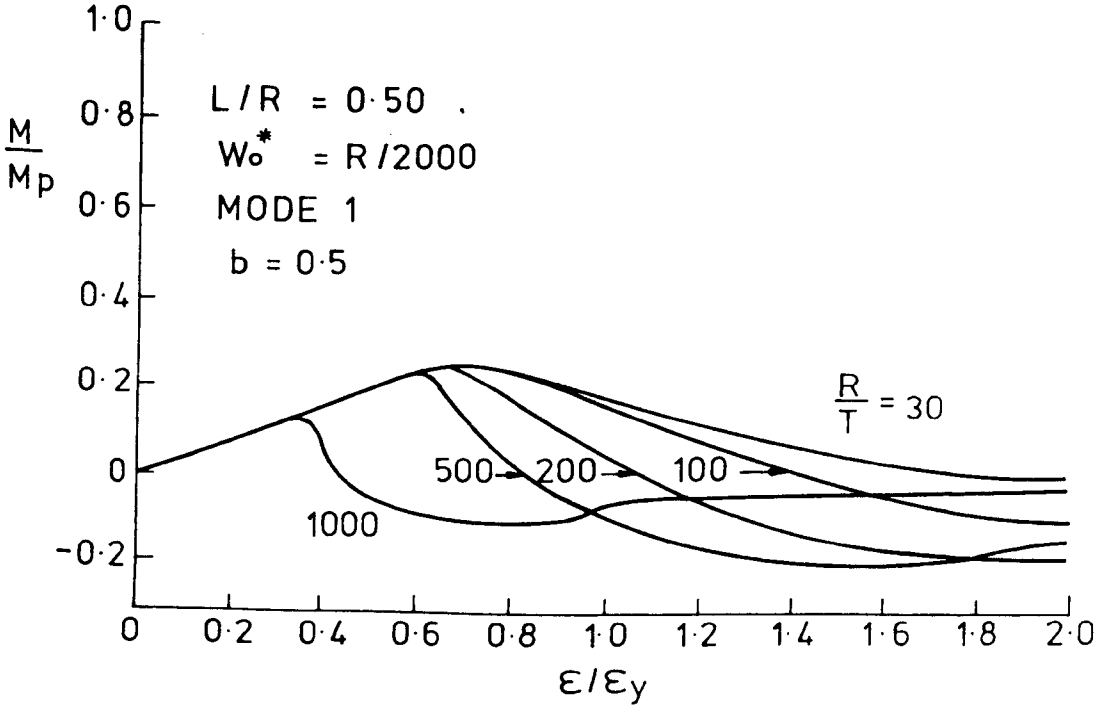

Fig. 6.66b

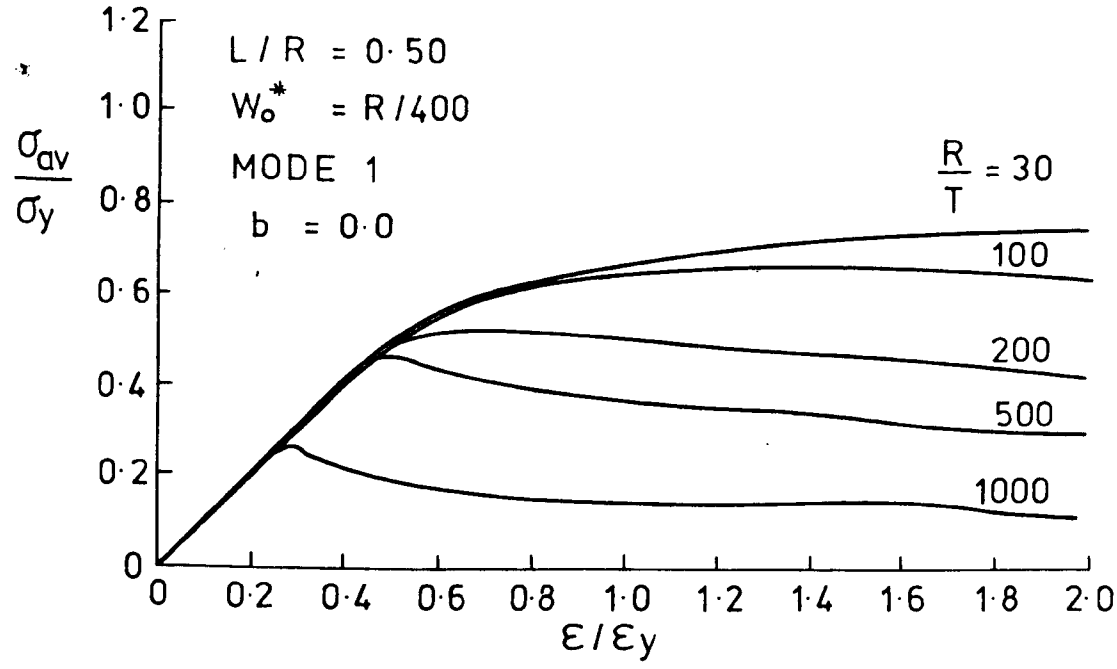

Fig. 6.67a

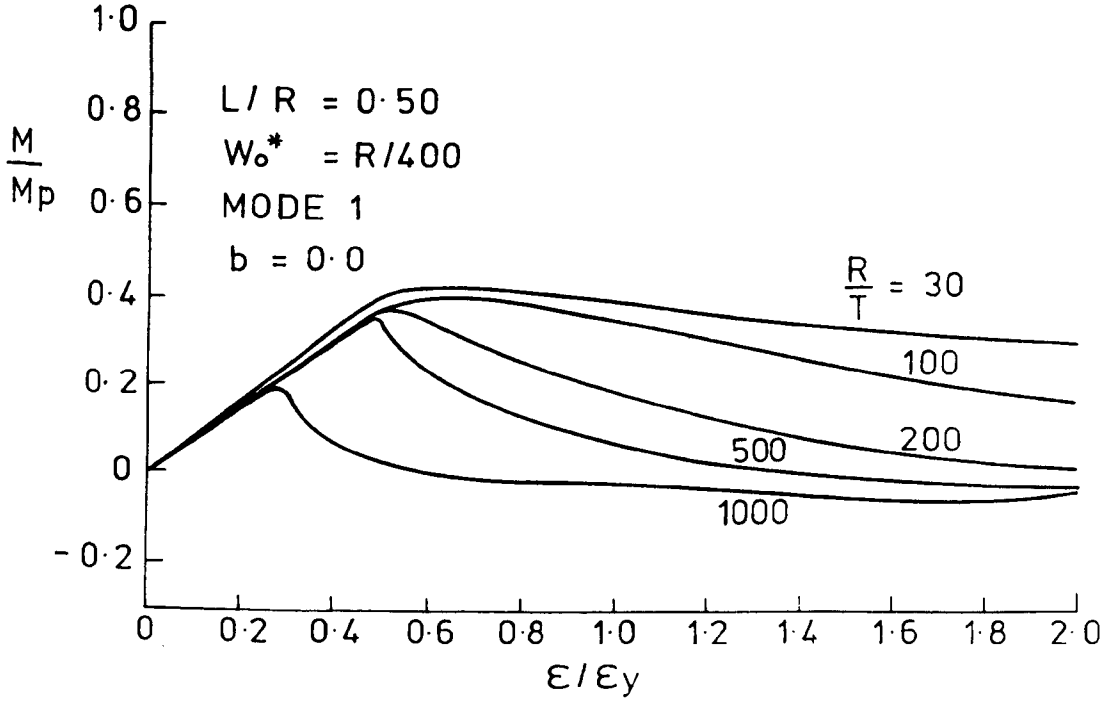

Fig. 6.67b

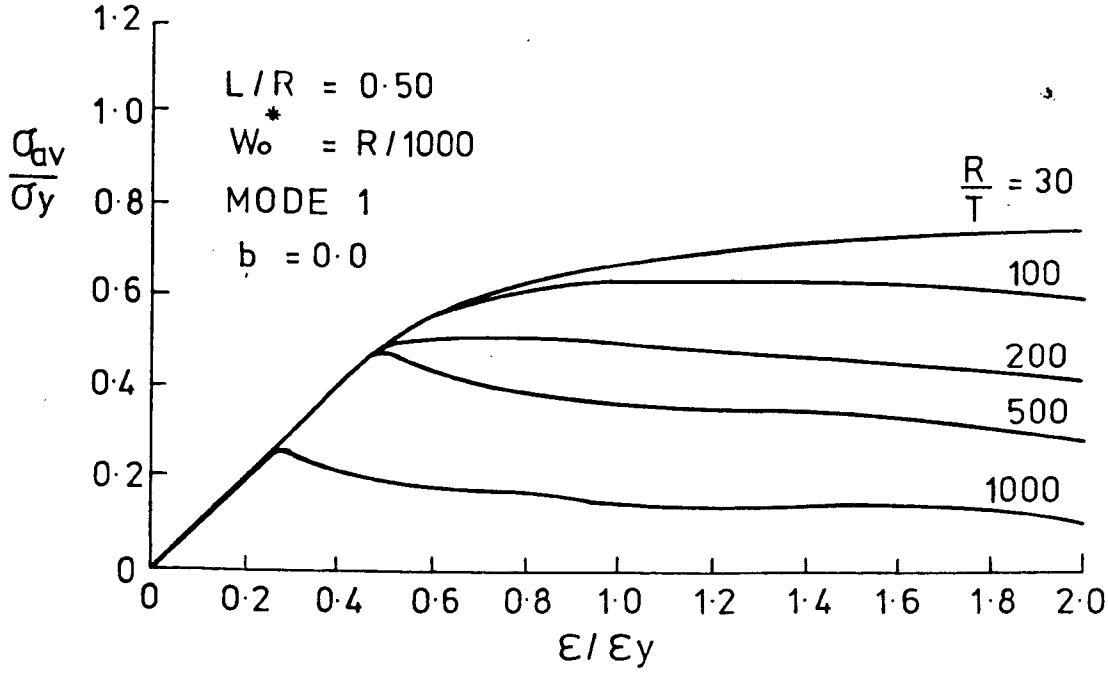

Fig. 6.68a

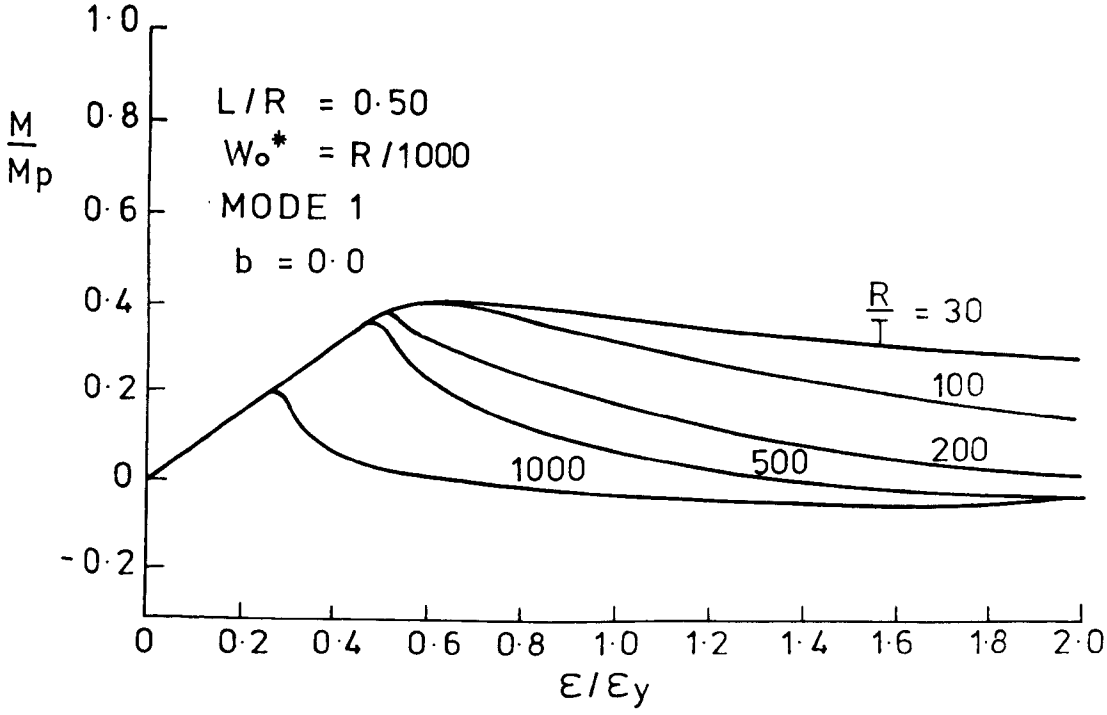

Fig. 6.68b

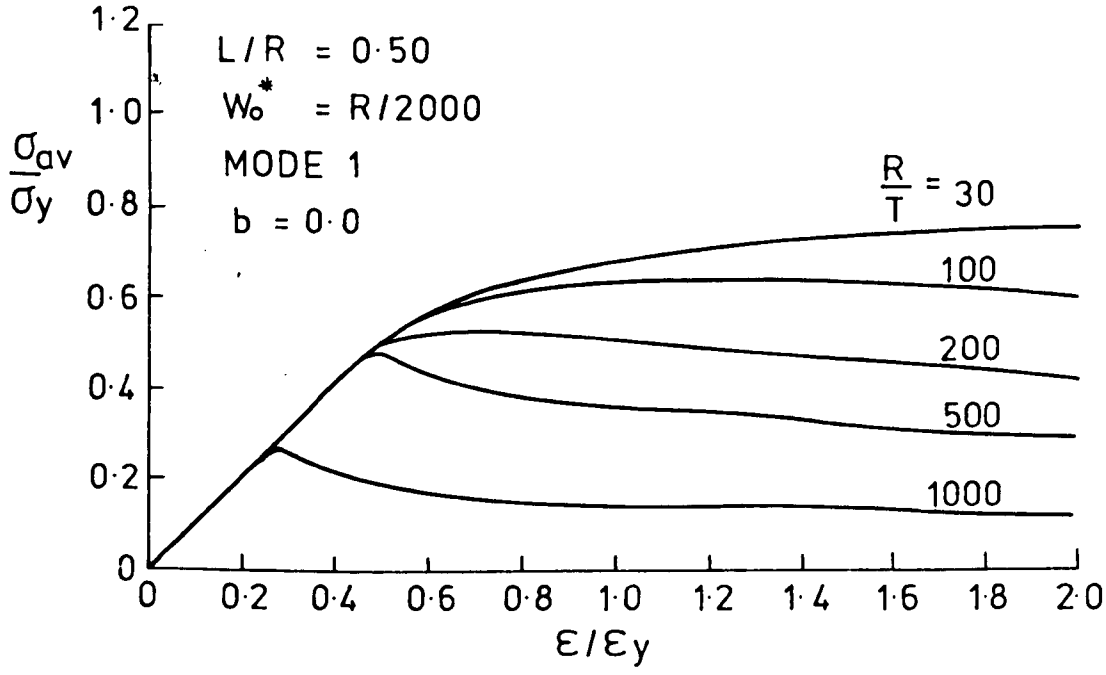

Fig. 6.69a

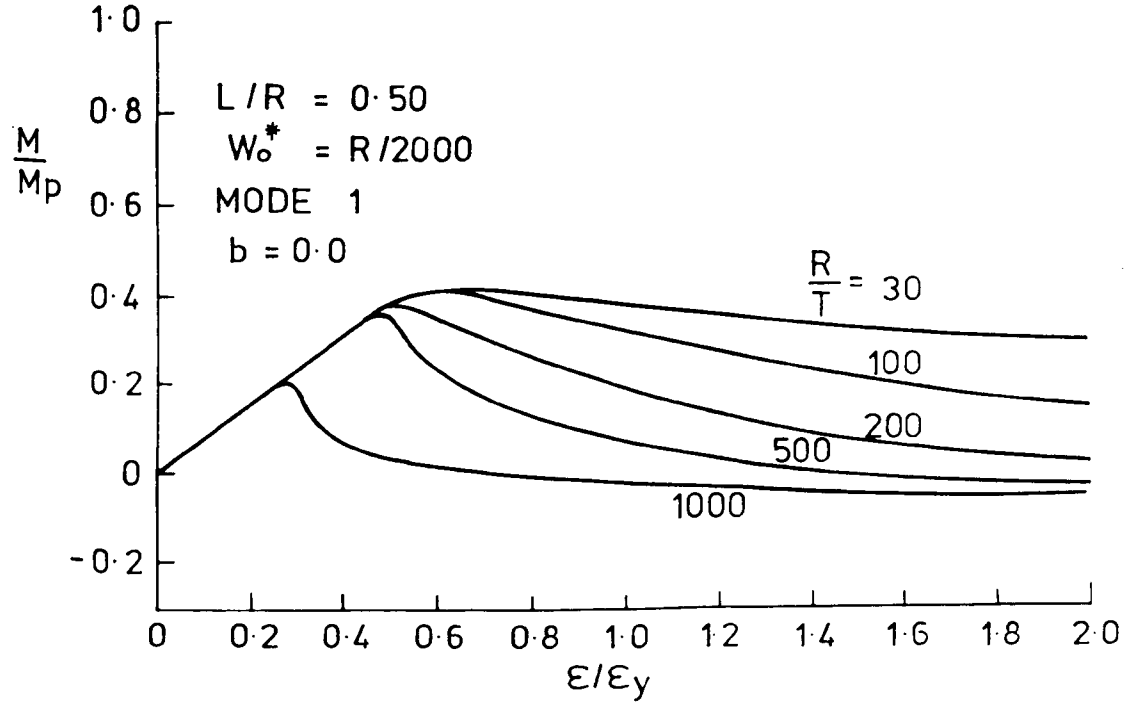

Fig. 6.69b

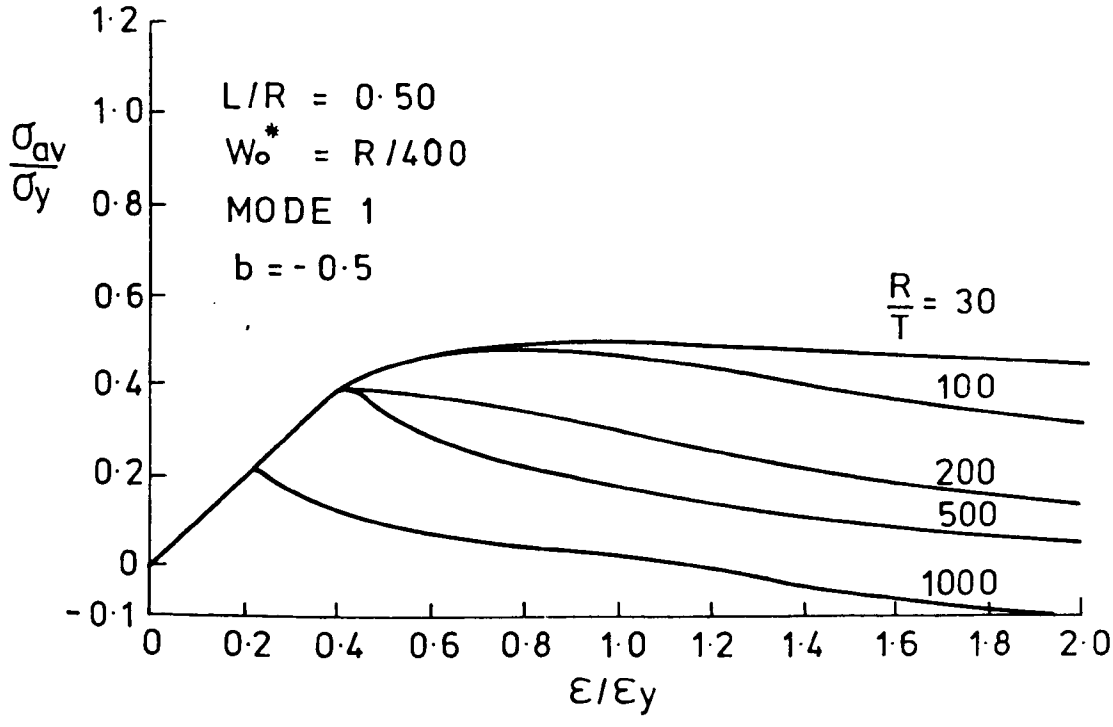

Fig. 6.70a

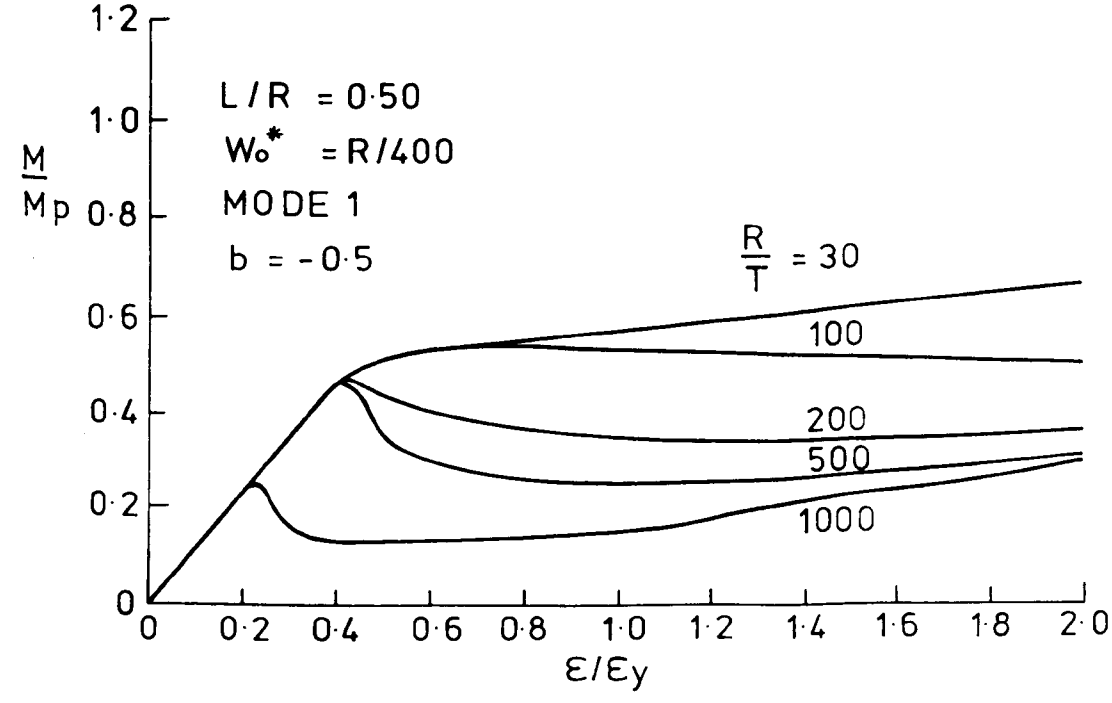

Fig. 6.70b

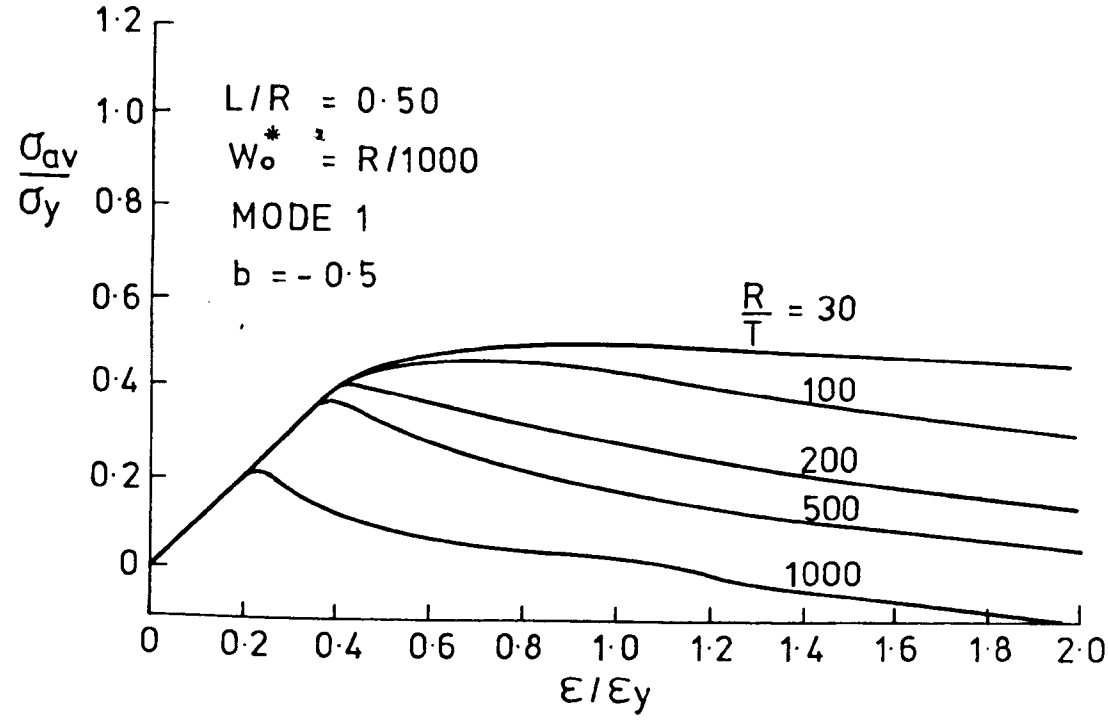

Fig. 6.71a

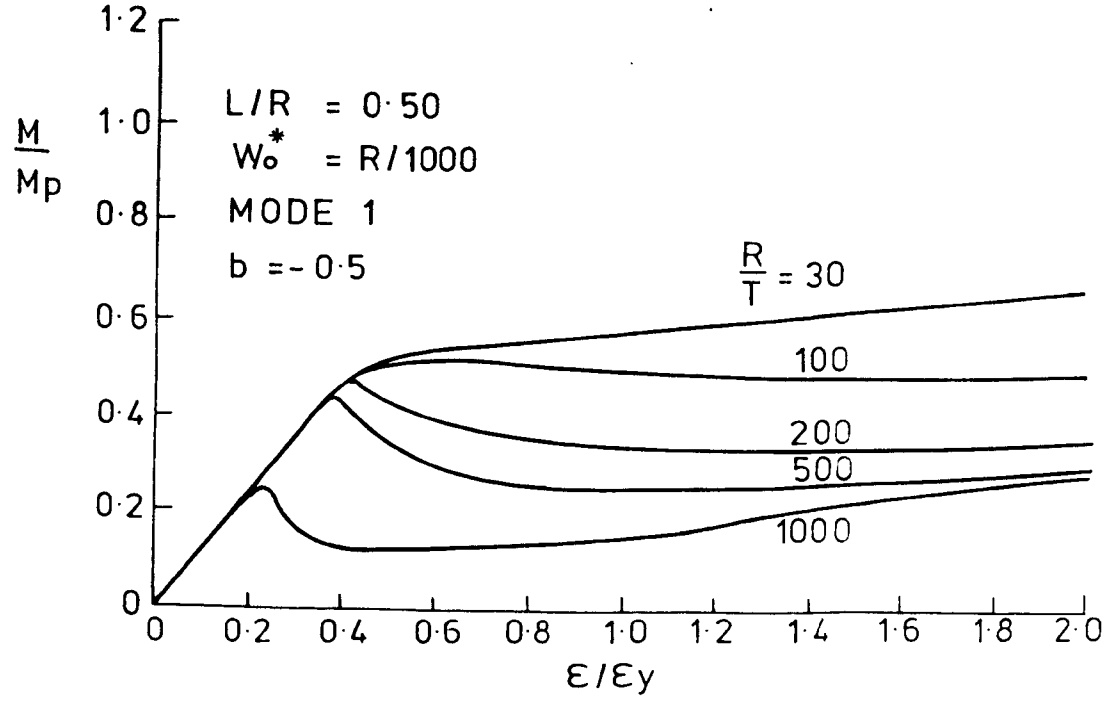

Fig. 6.71b

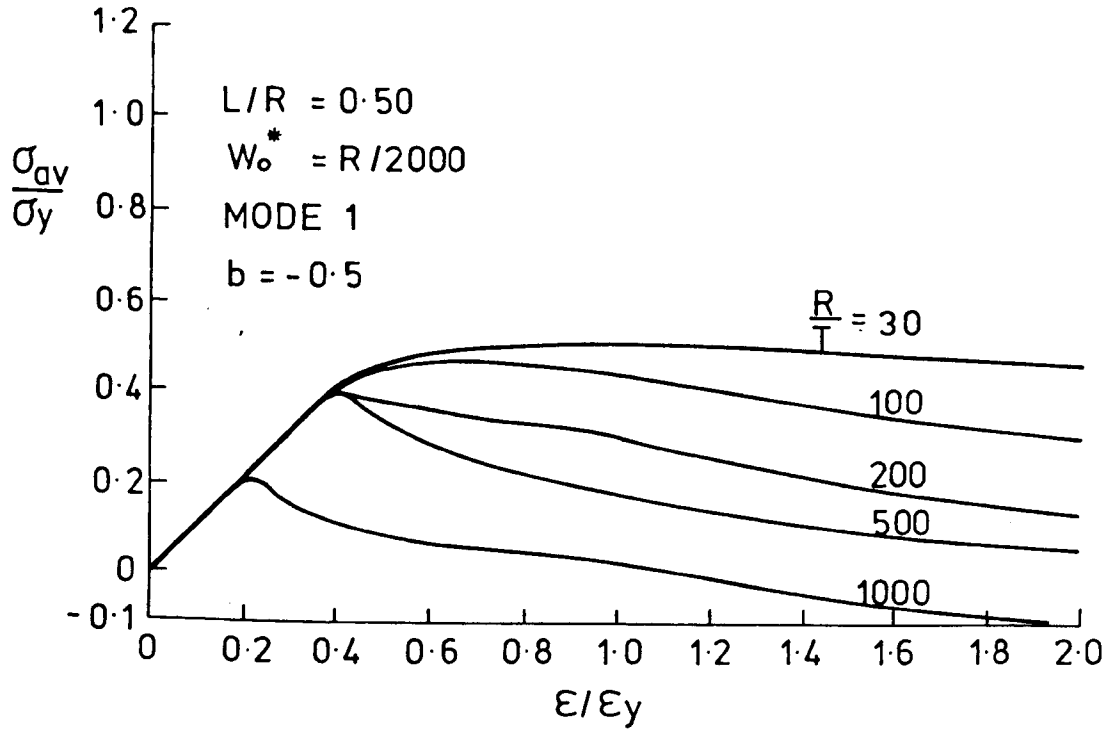

Fig. 6.72a

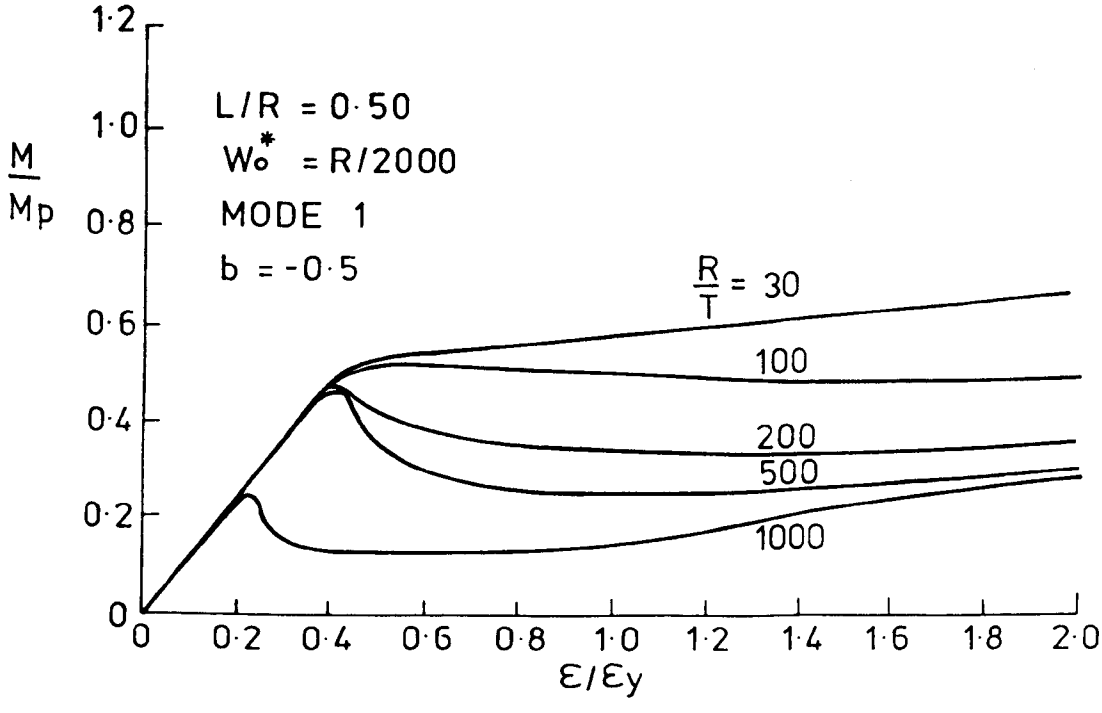

Fig. 6.72b

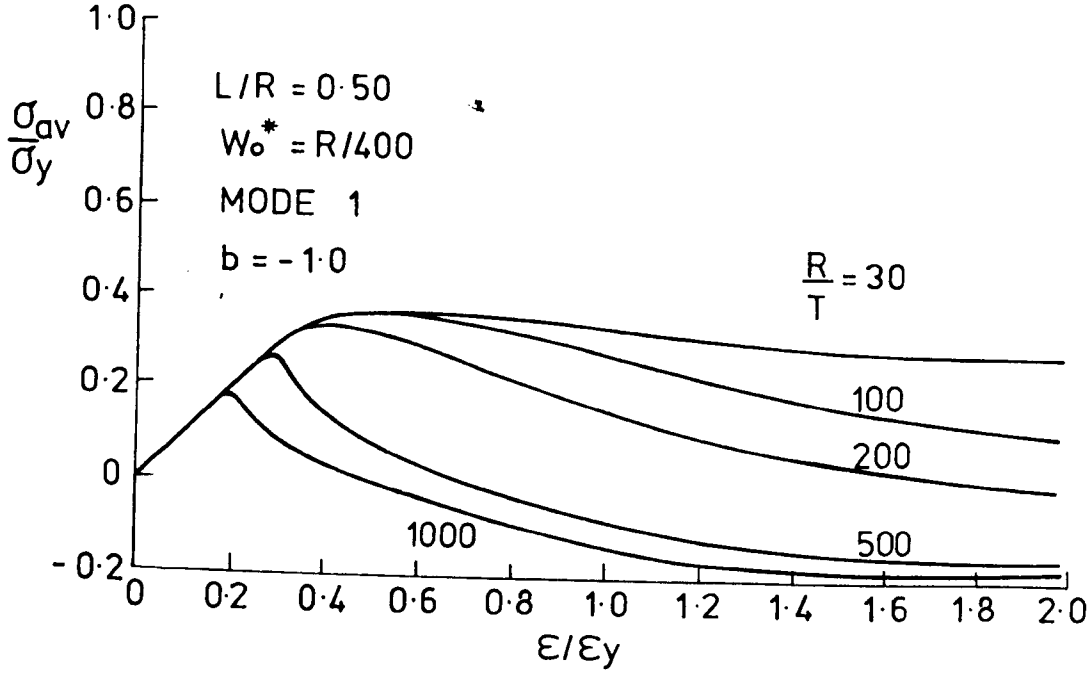

Fig 6 73a

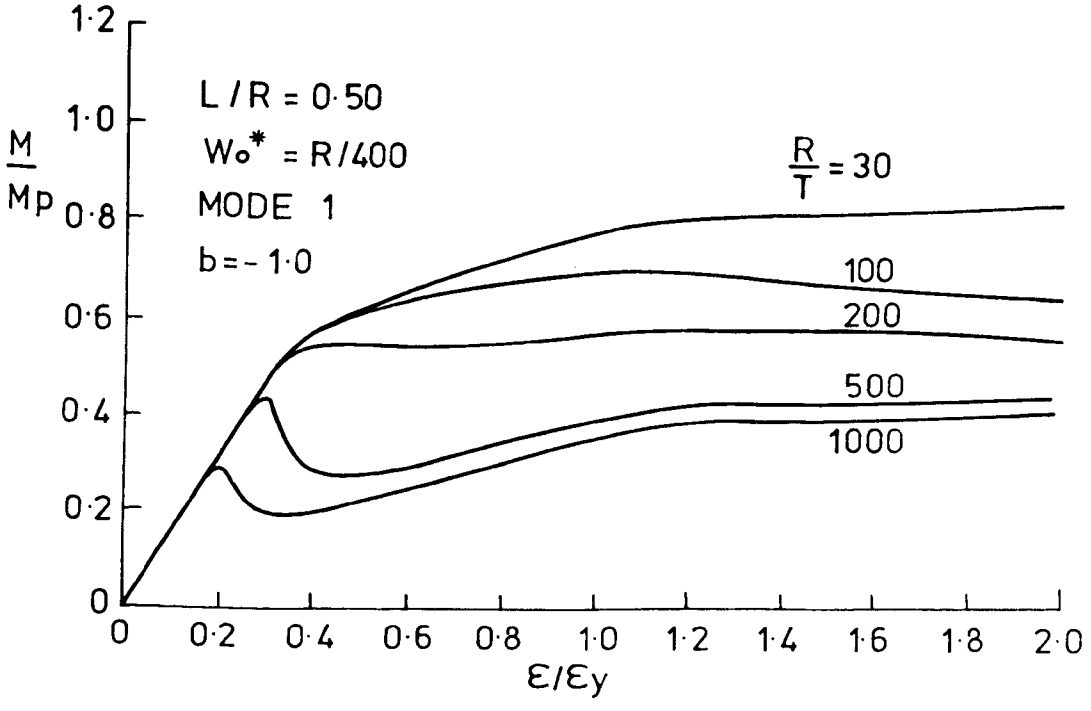

Fig. 6.73b

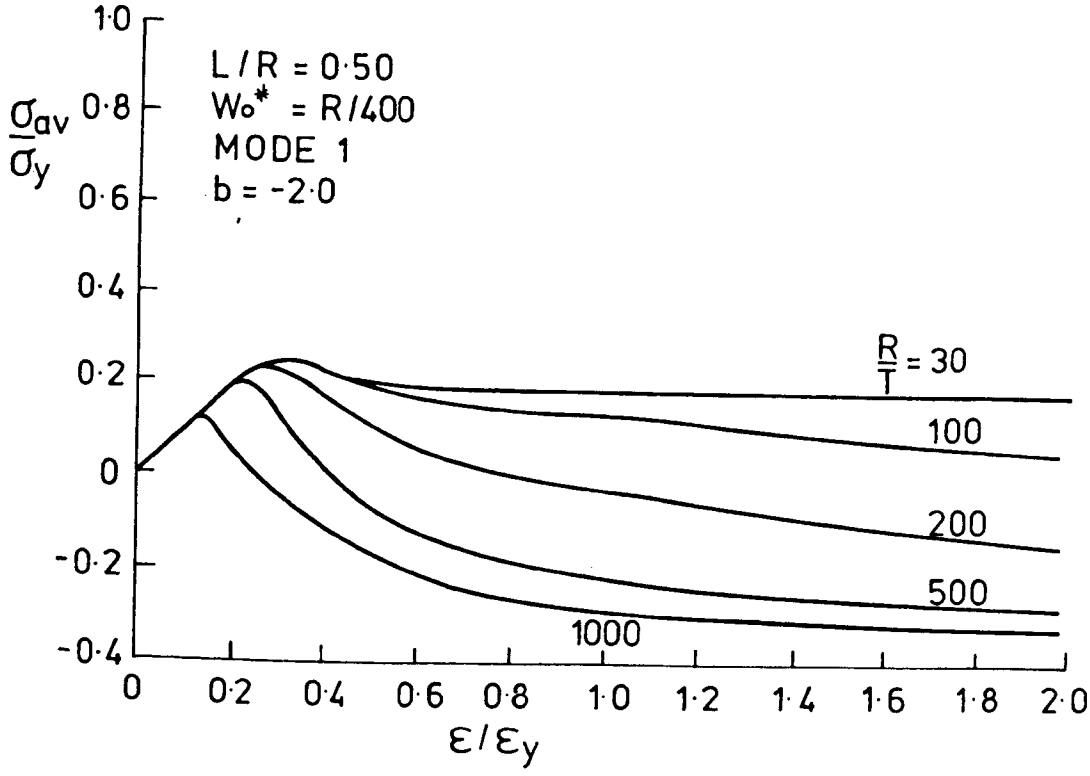

Fig. 6.74a

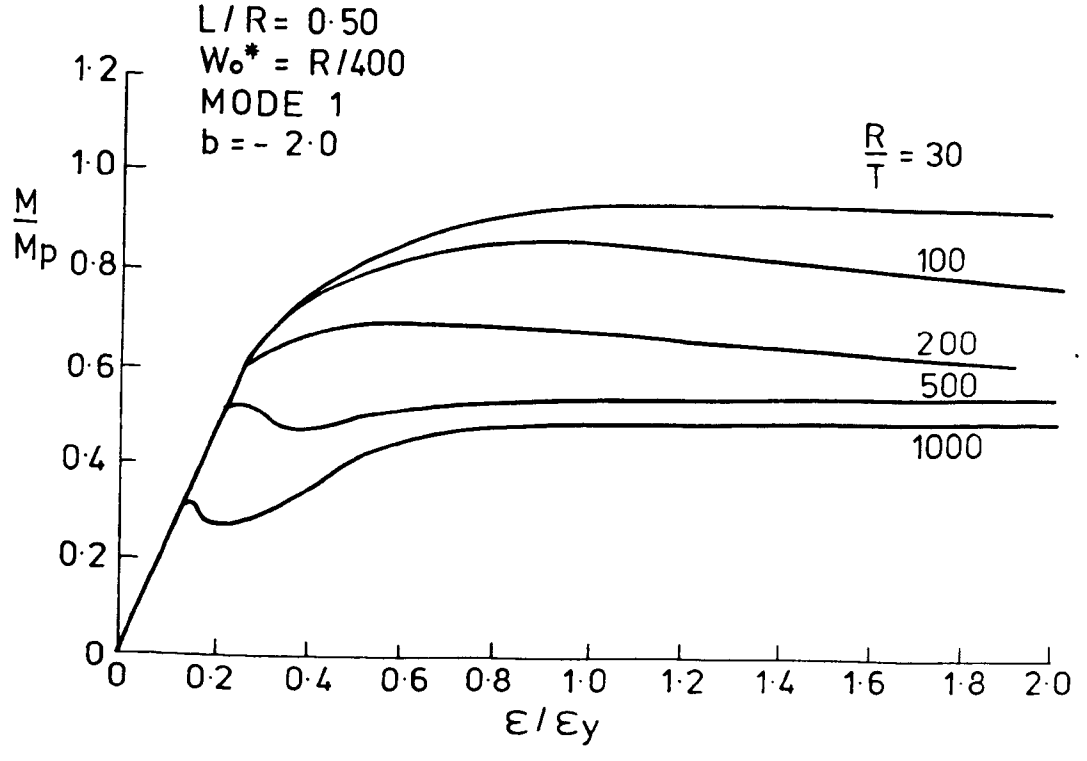

Fig. 6.74b

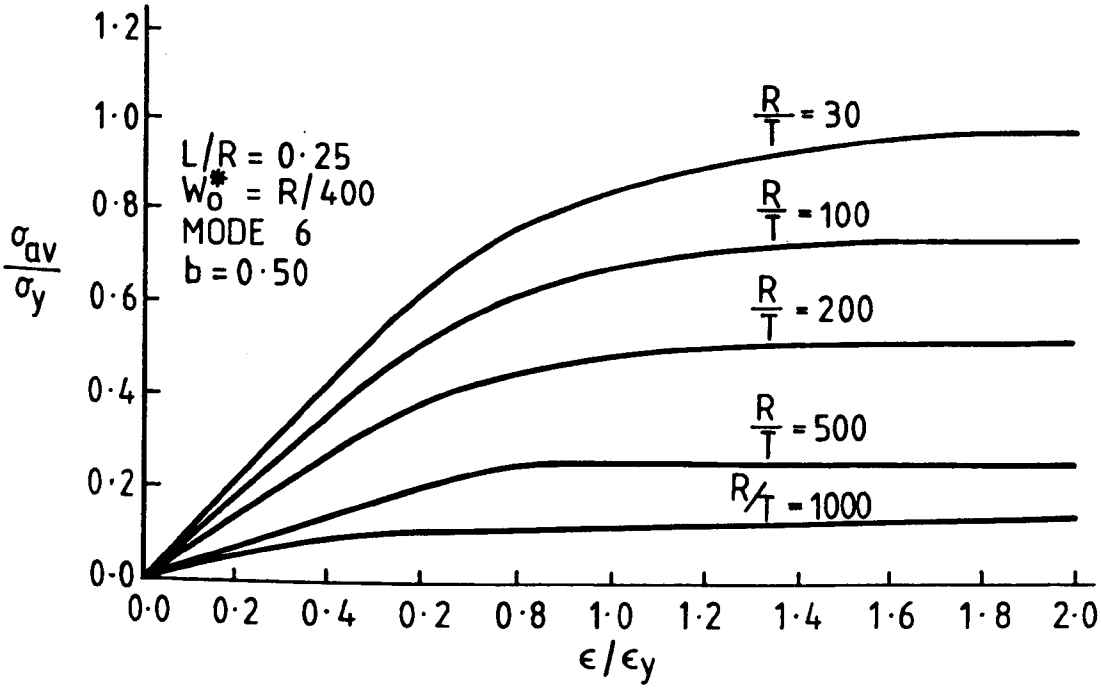

Fig. 6.75a

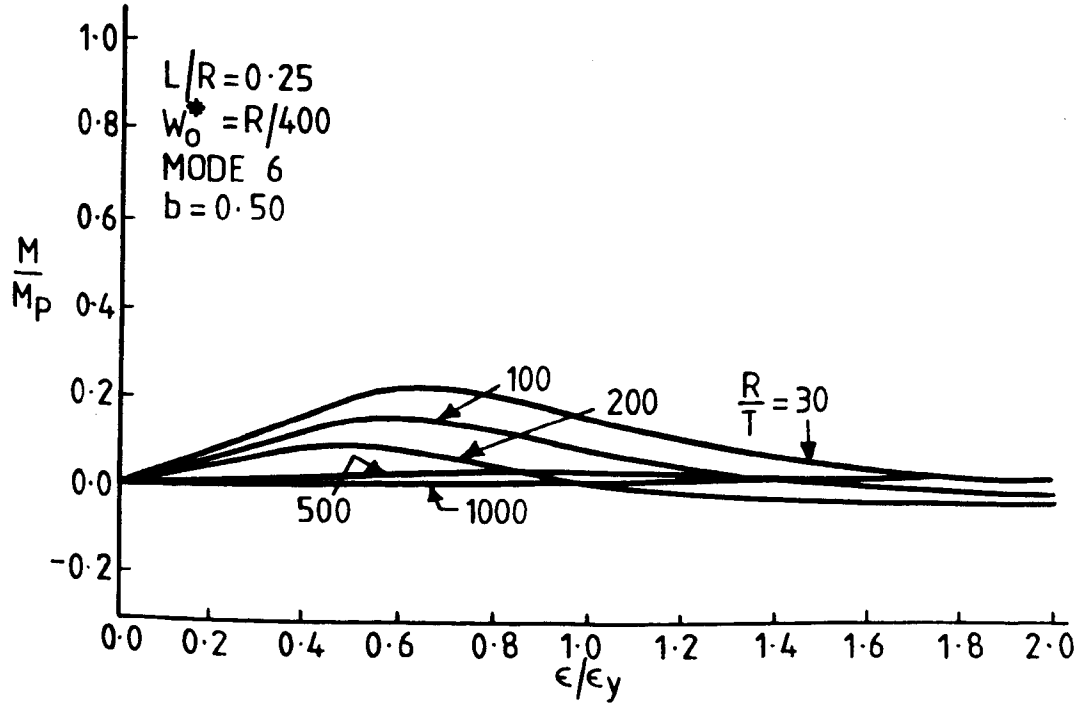

Fig. 6.76b

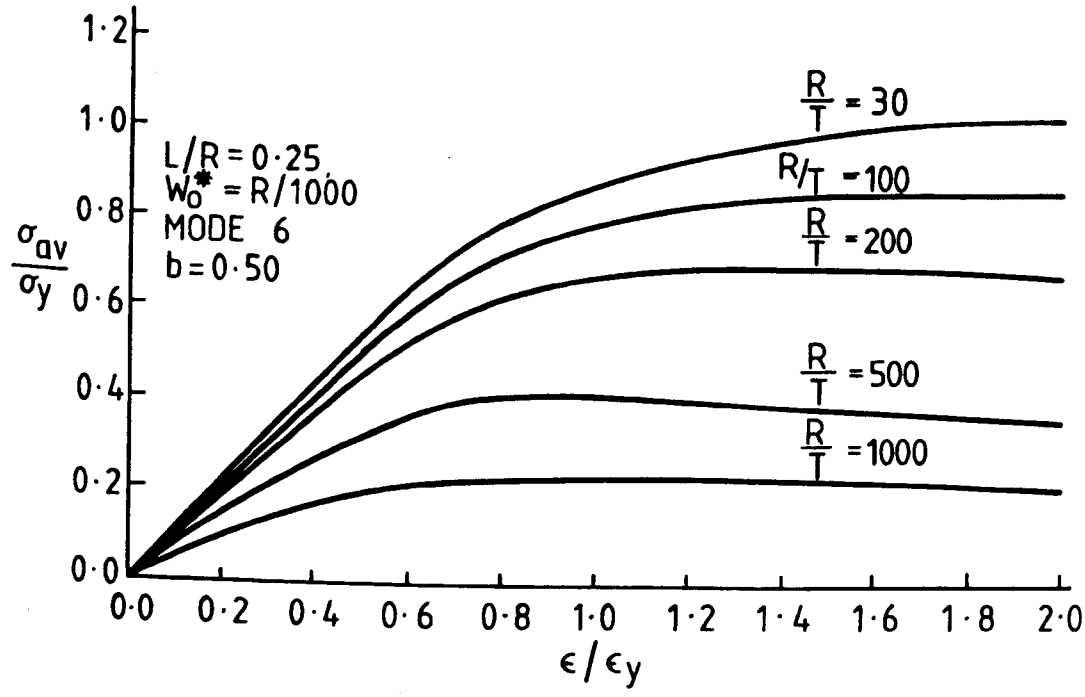

Fig. 6.77a

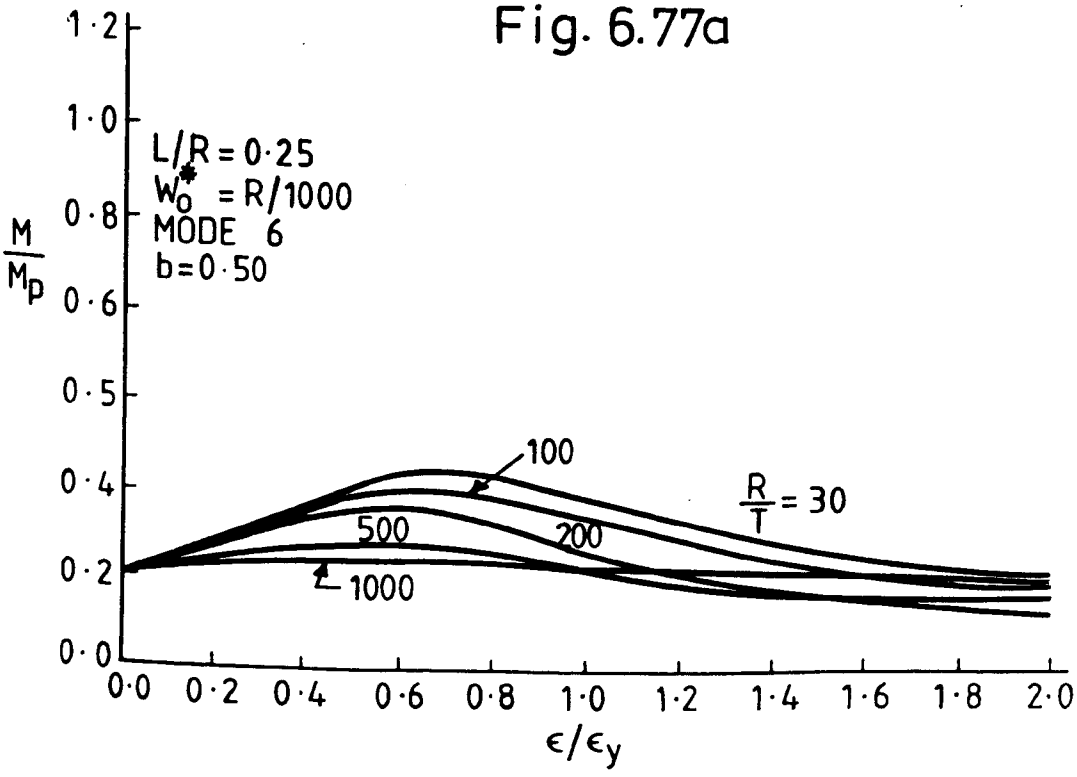

Fig. 6.77b

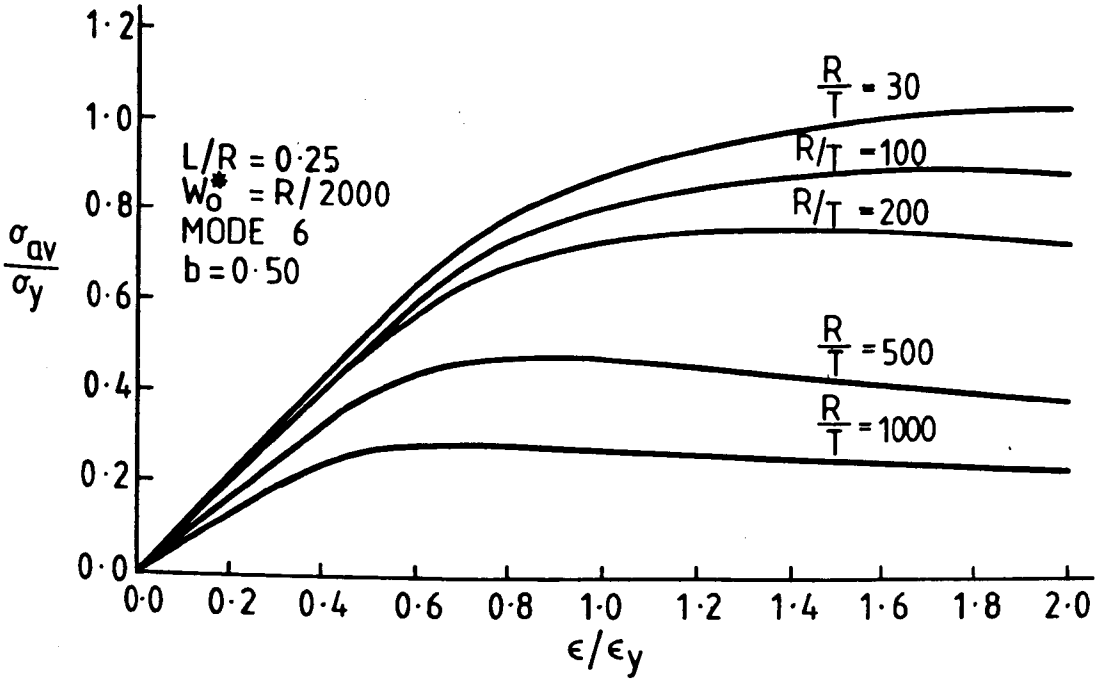

Fig. 6.78a

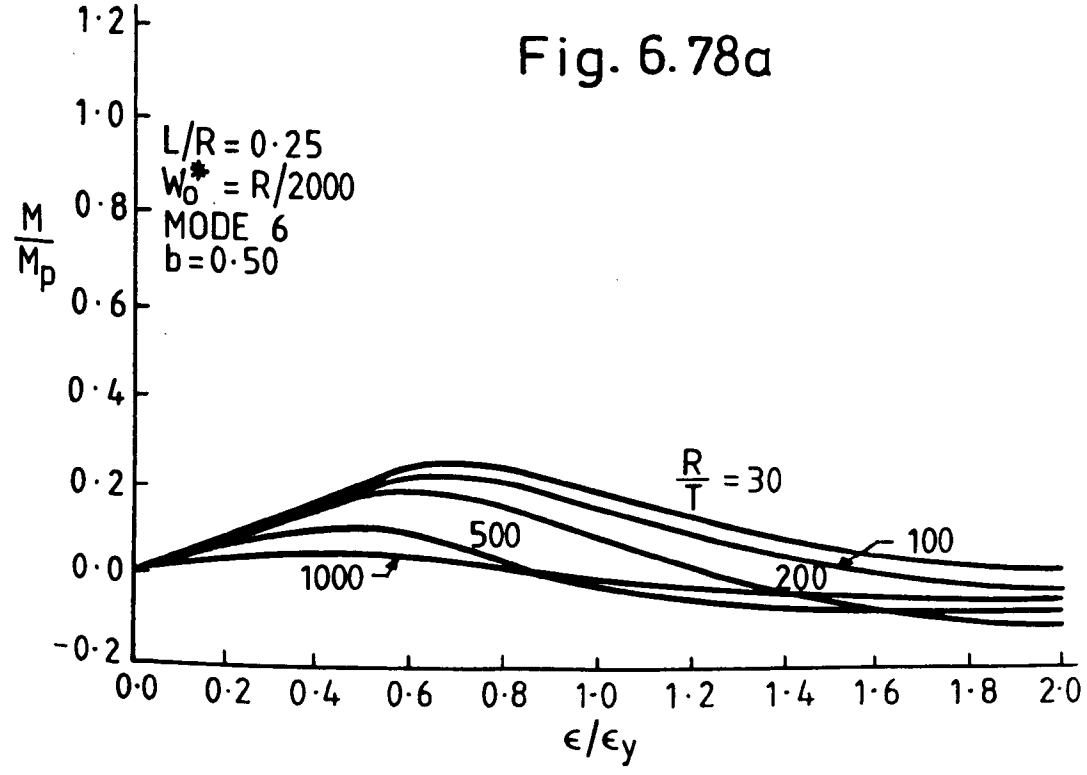

Fig. 6.78b

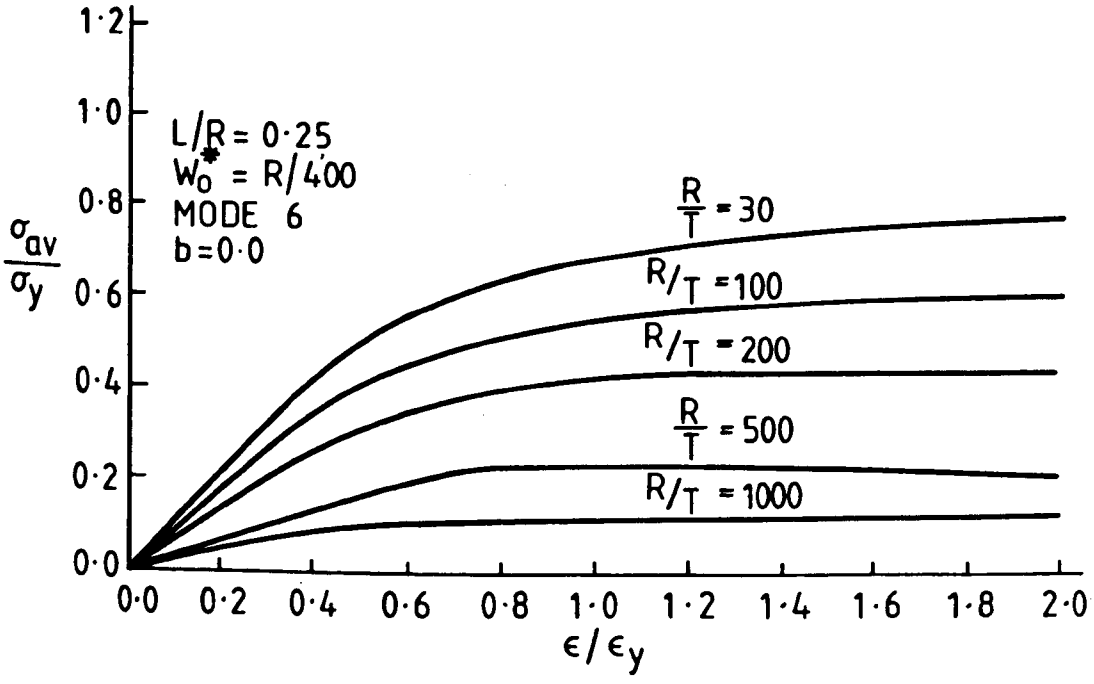

Fig. 6.79a

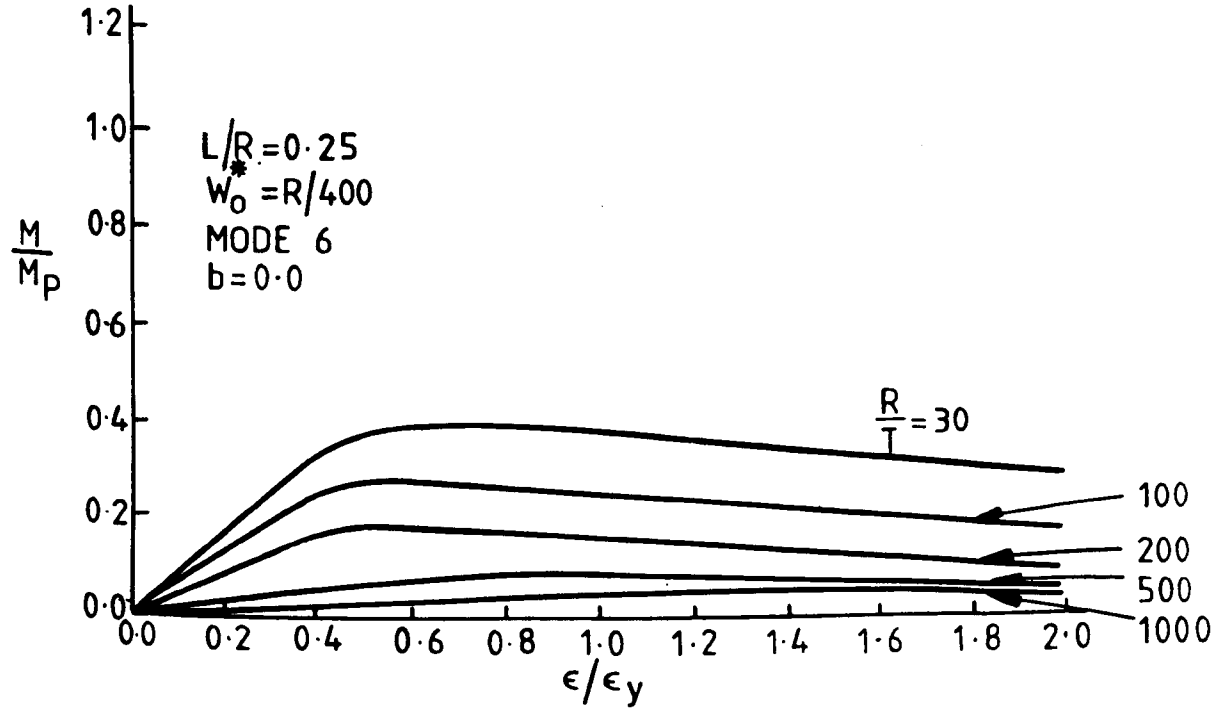

Fig. 6.79b

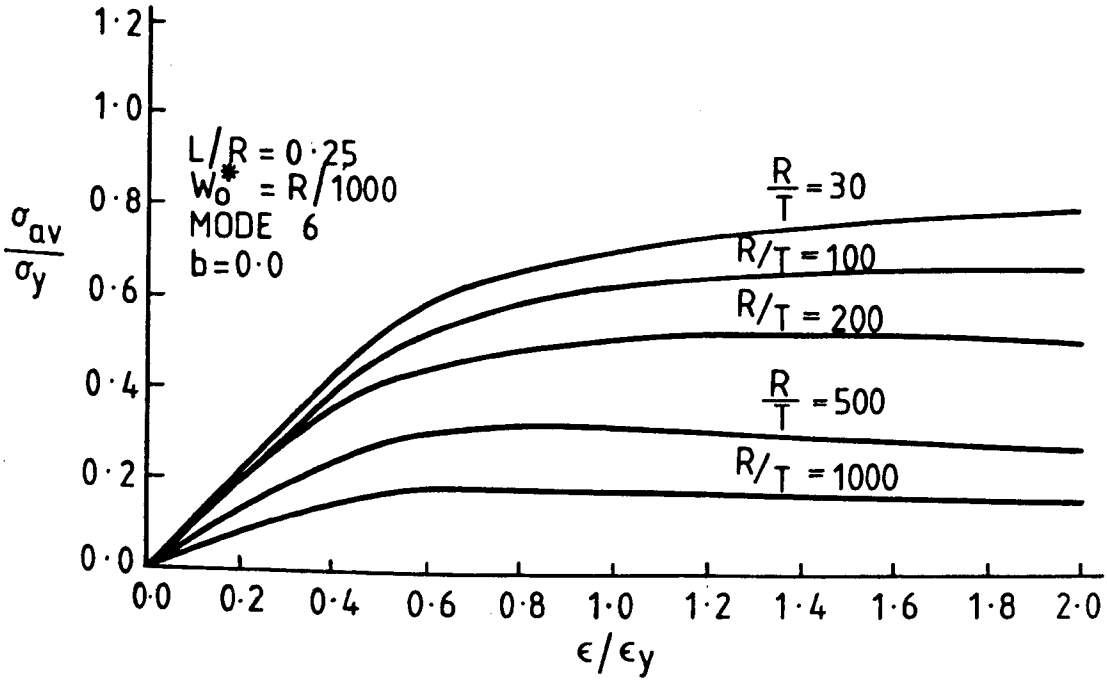

Fig. 6.80a

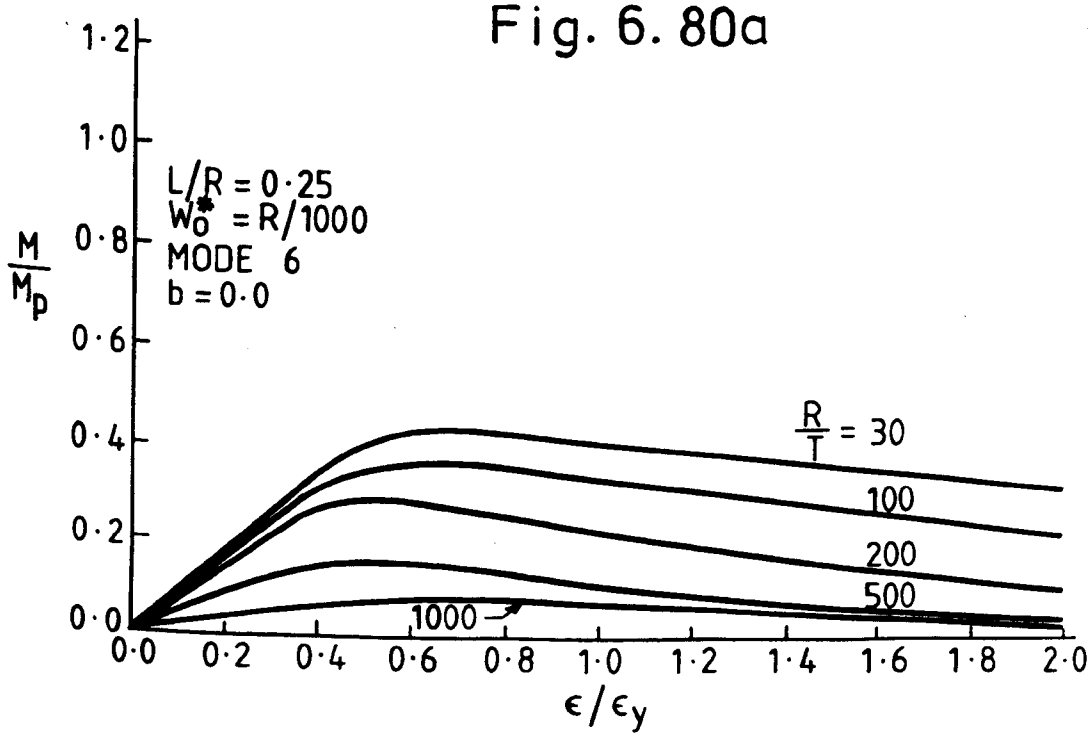

Fig. 6.80b

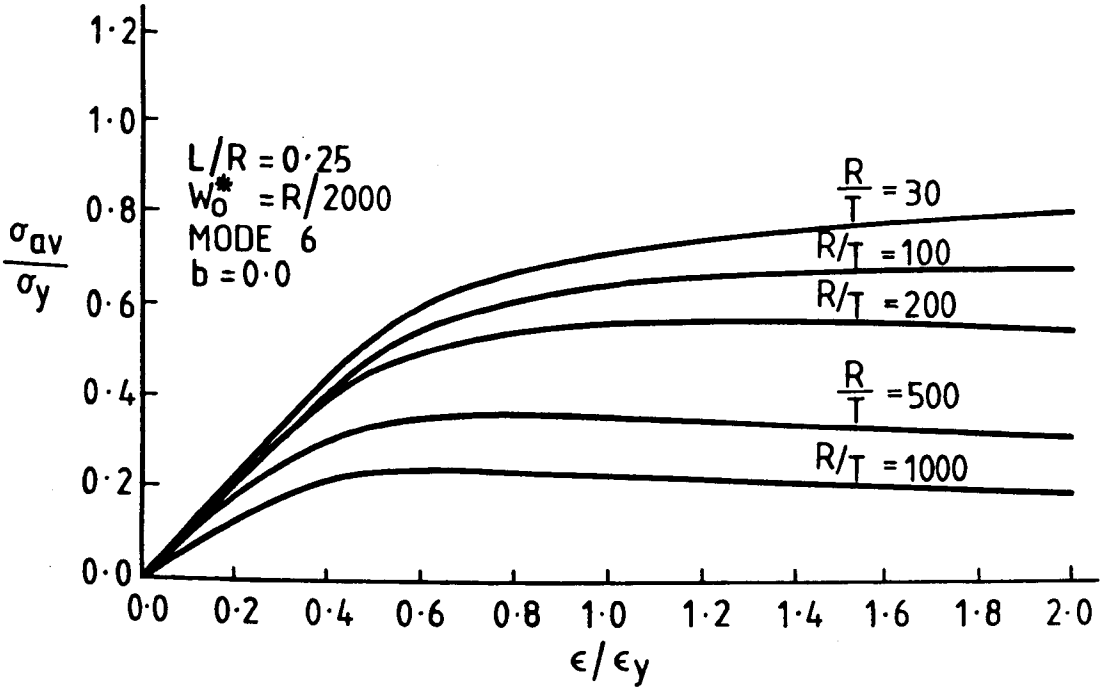

Fig. 6.81a

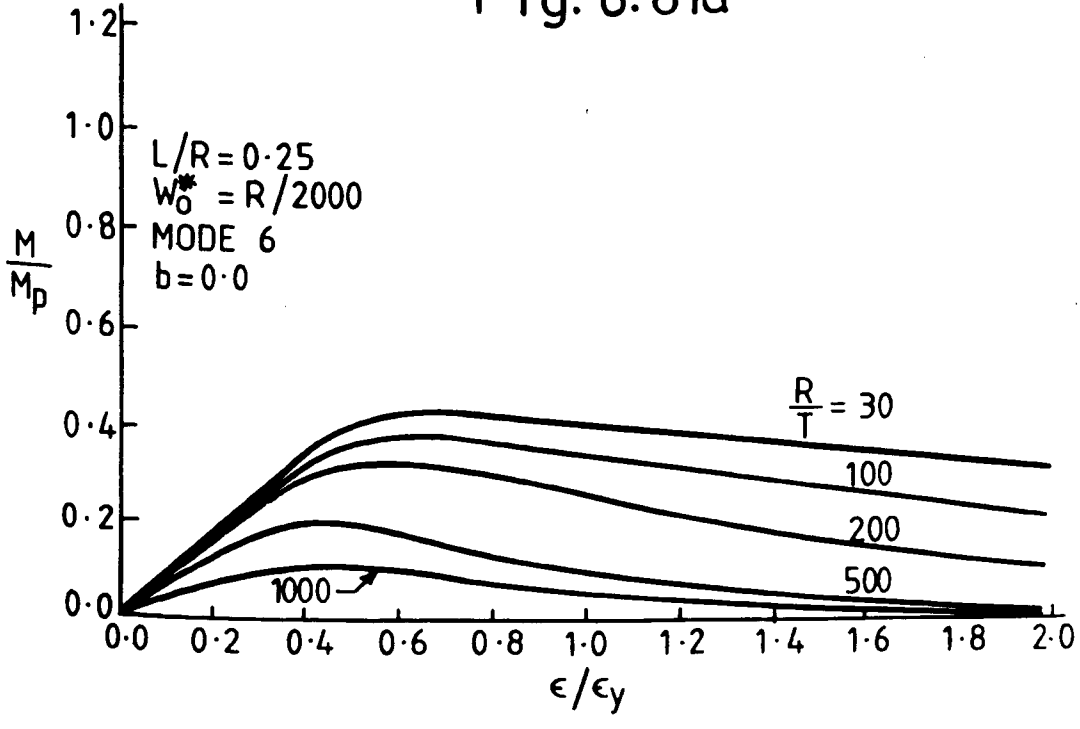

Fig. 6.81b

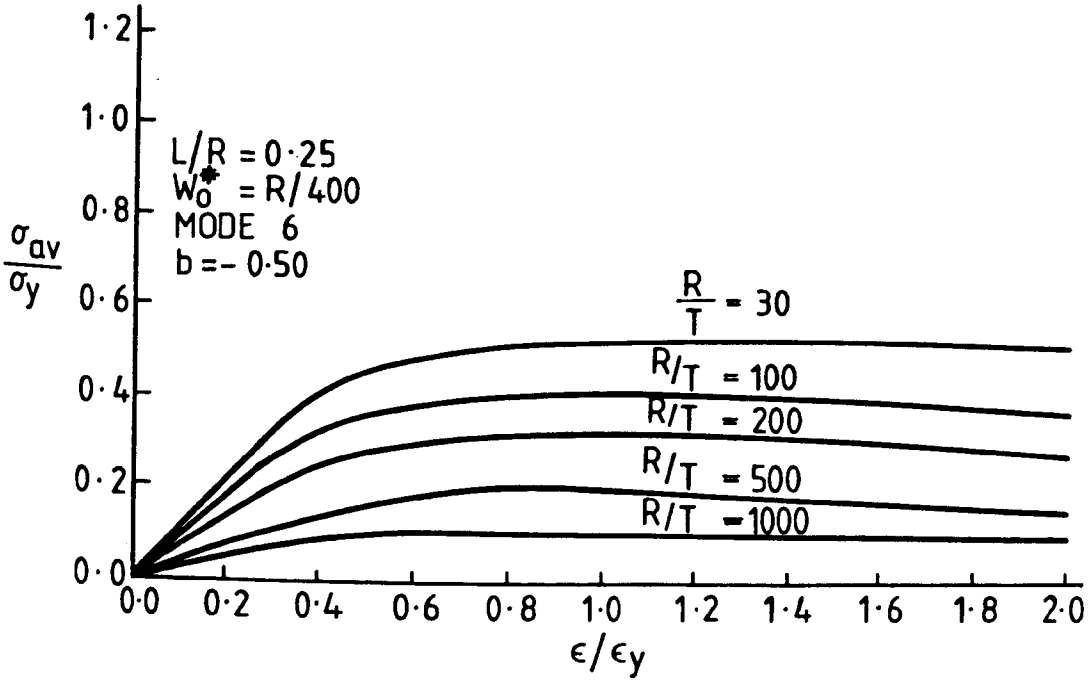

Fig. 6.82a

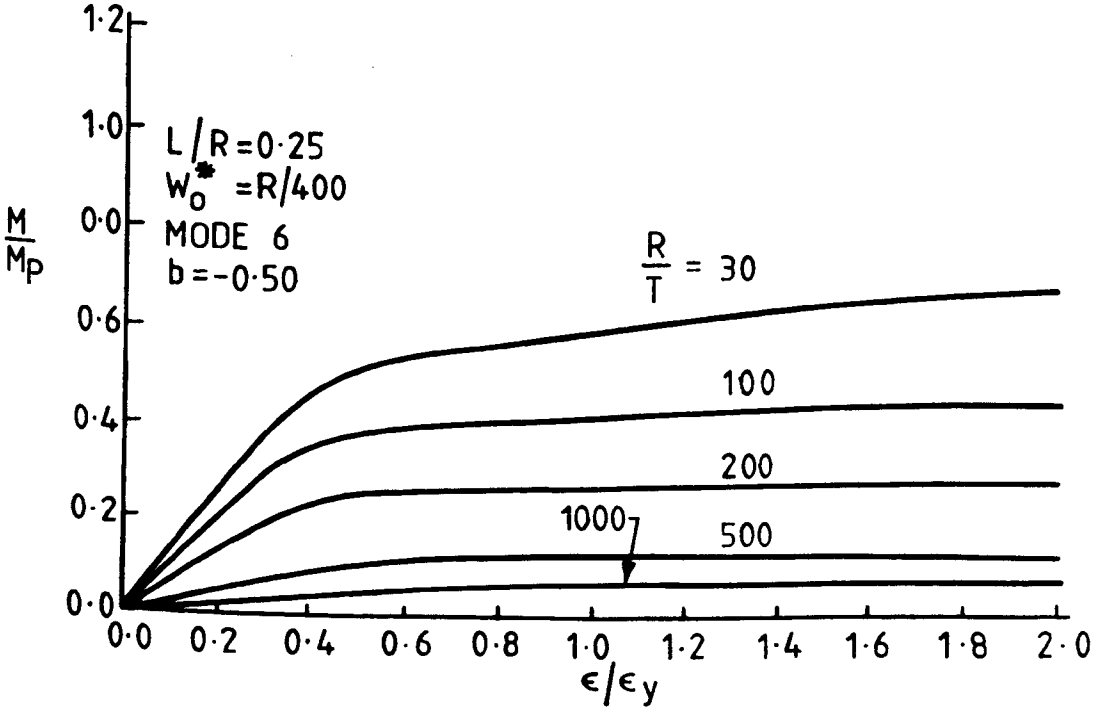

Fig. 6.82b

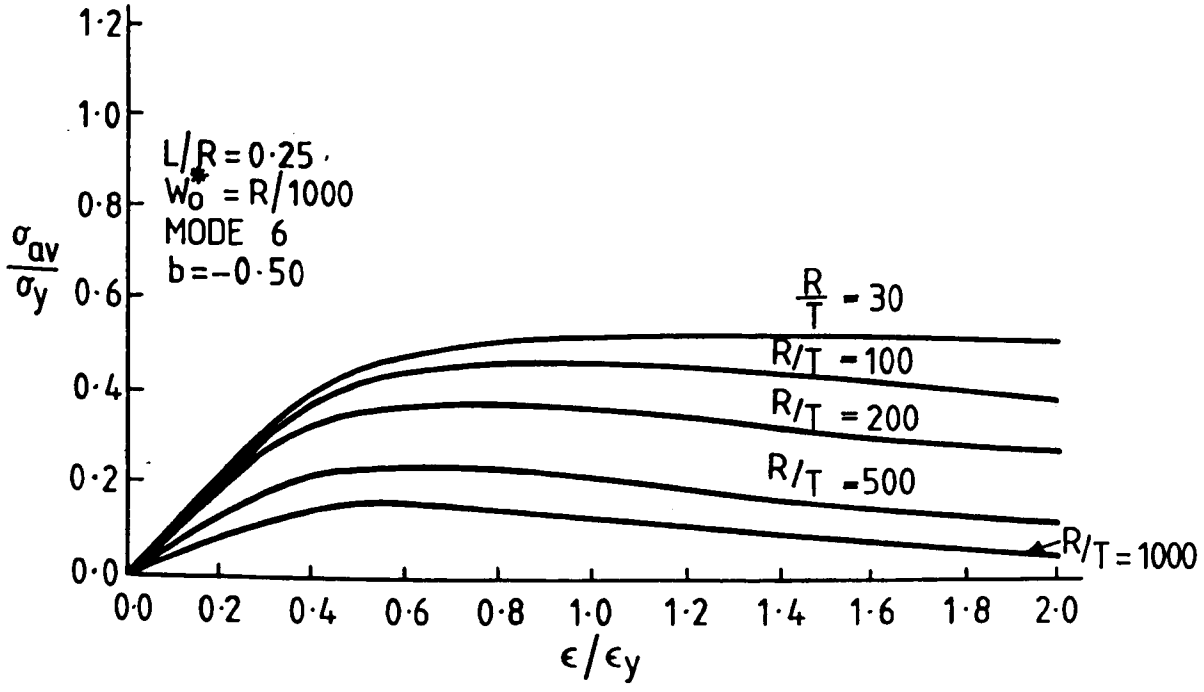

Fig. 6.83a

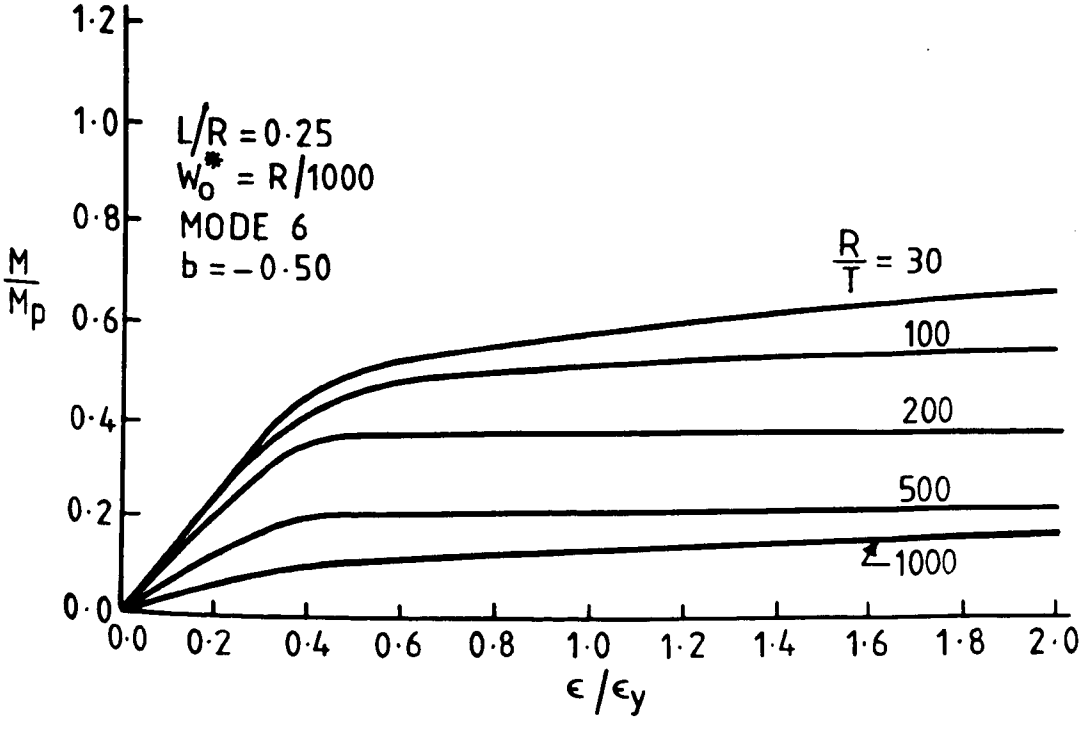

Fig. 6.83b

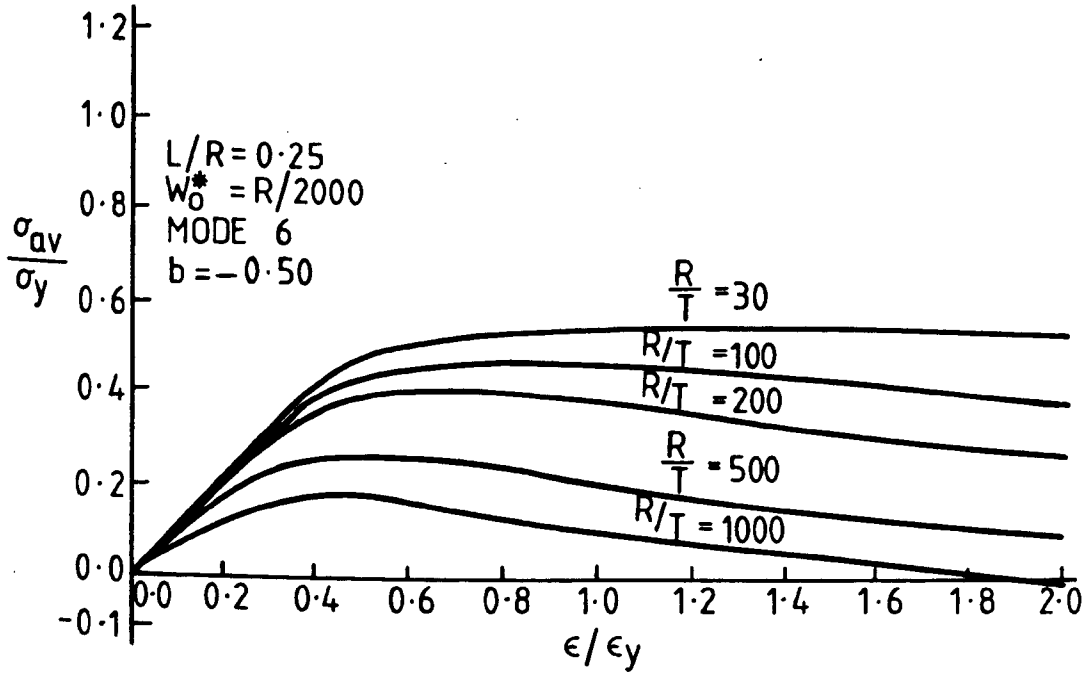

Fig. 6.84a

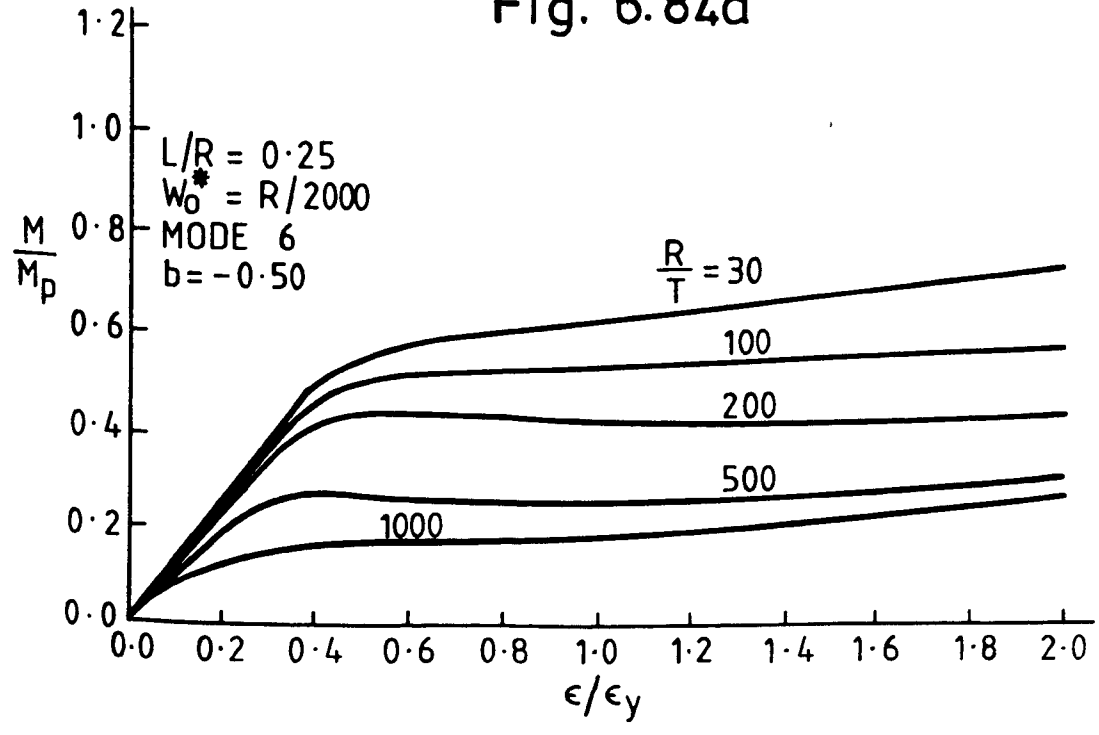

Fig. 6.84b

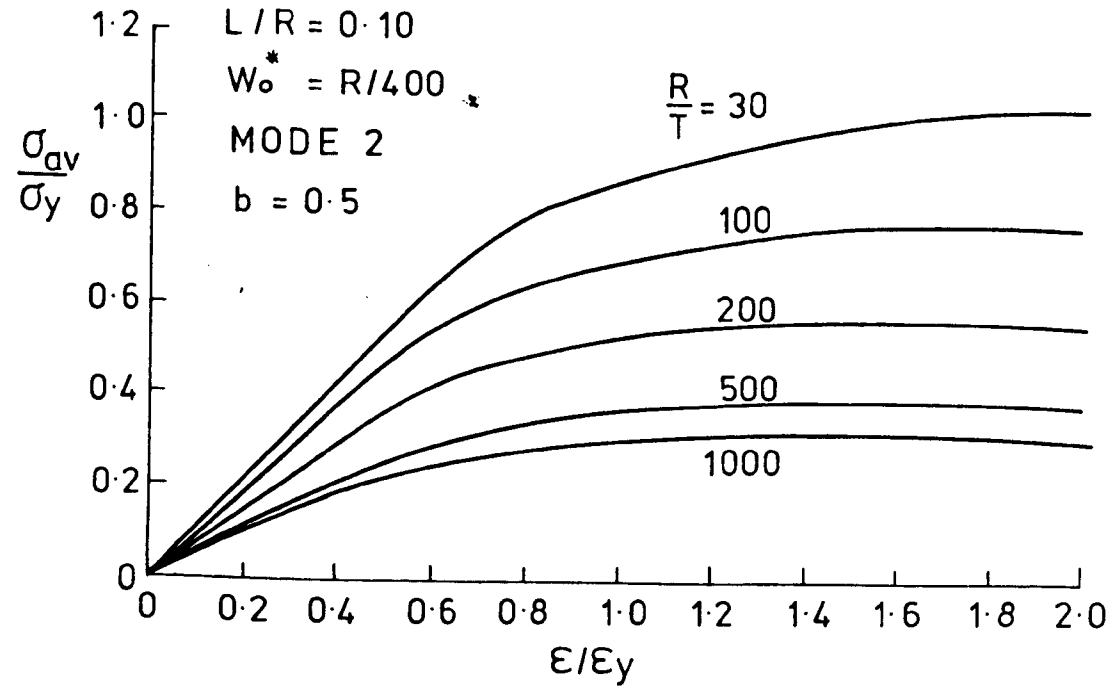

Fig. 6.85a

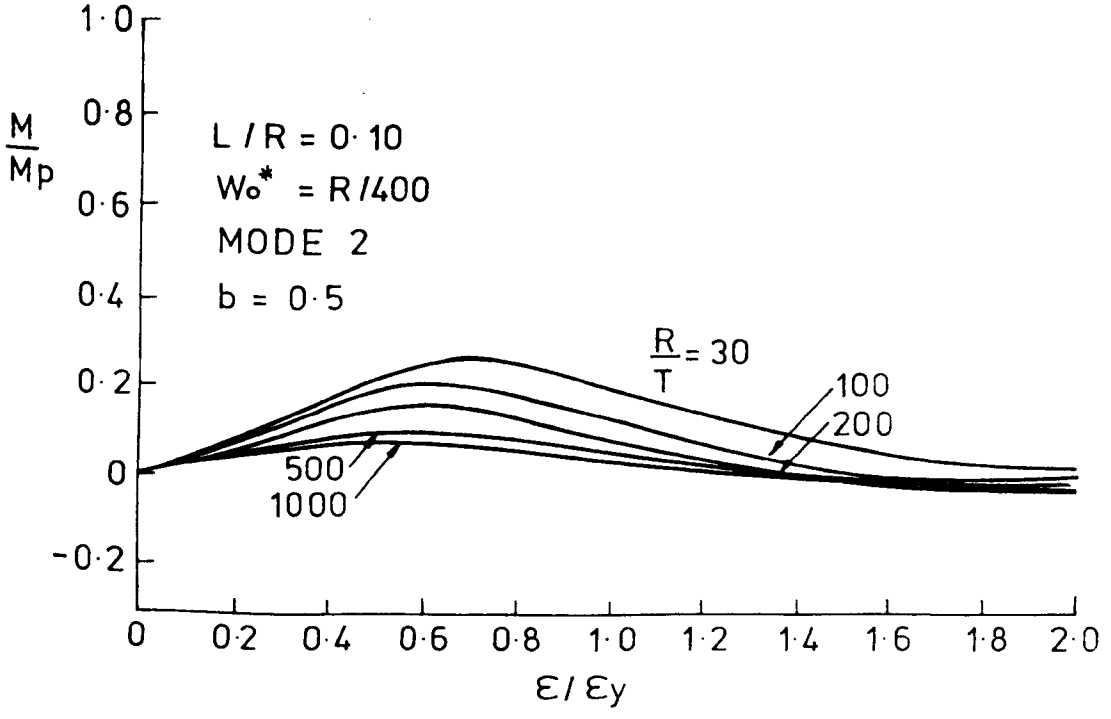

Fig. 6.85b

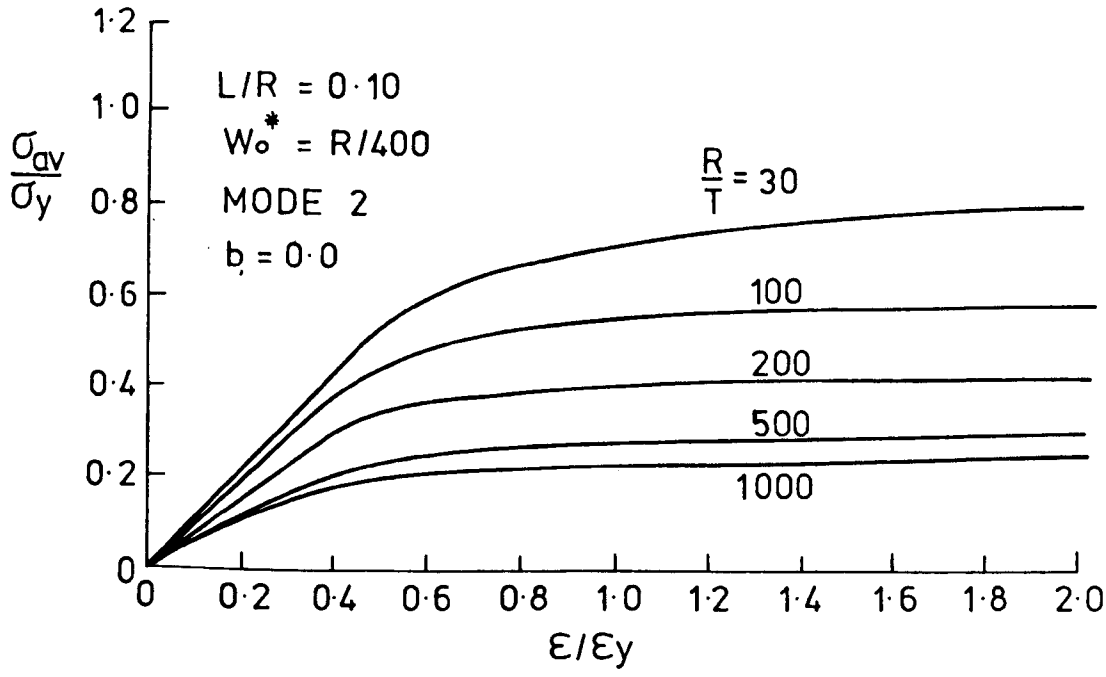

Fig. 6.86a

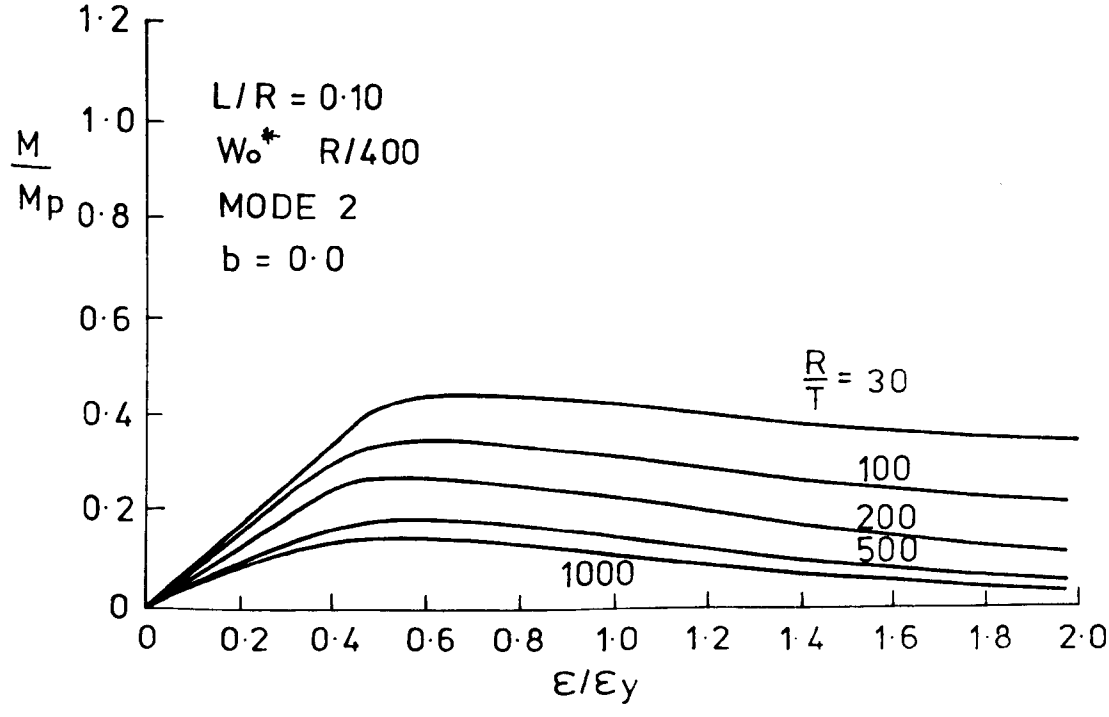

Fig. 6.86b

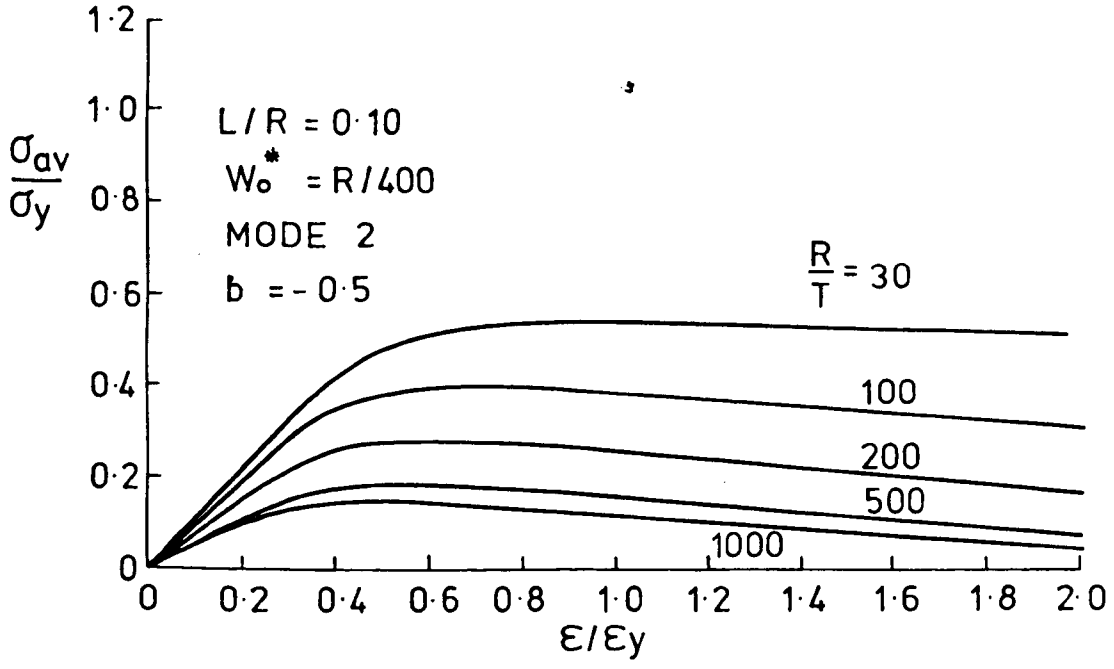

Fig. 6.87a

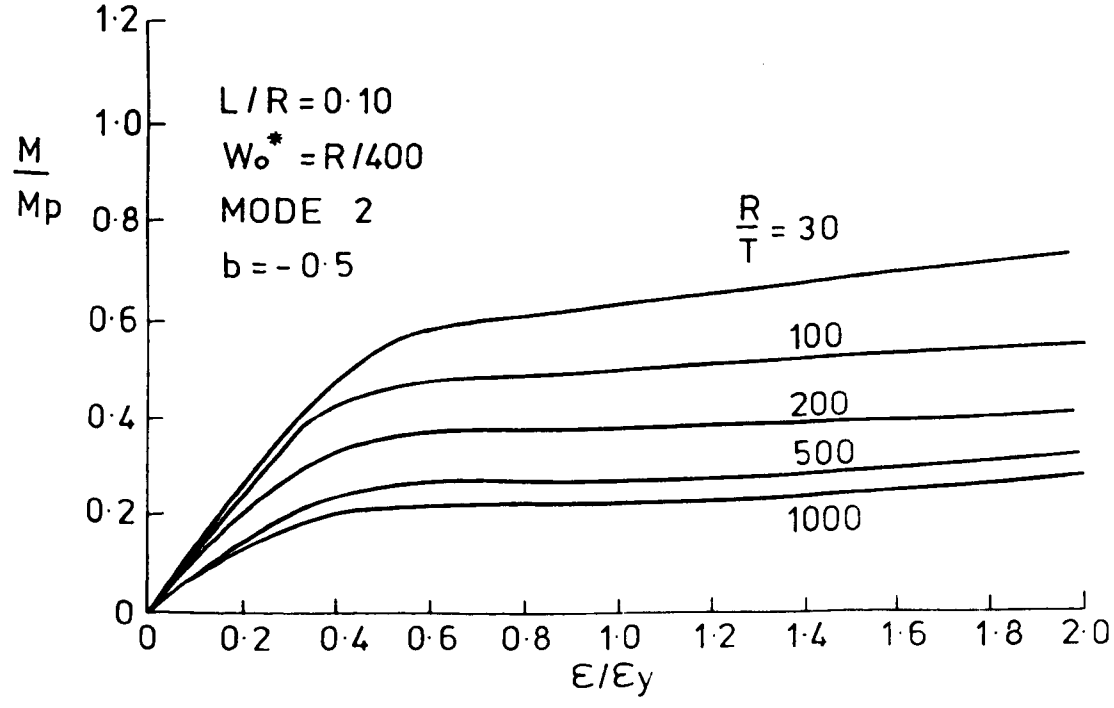

Fig. 6.87b

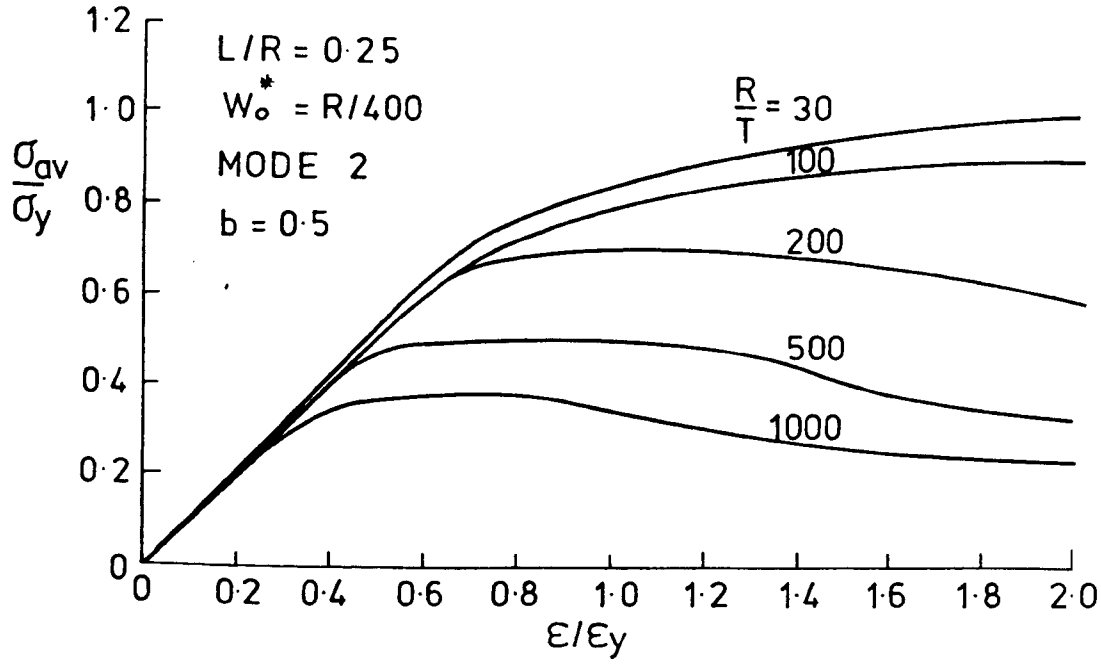

Fig. 6.88a

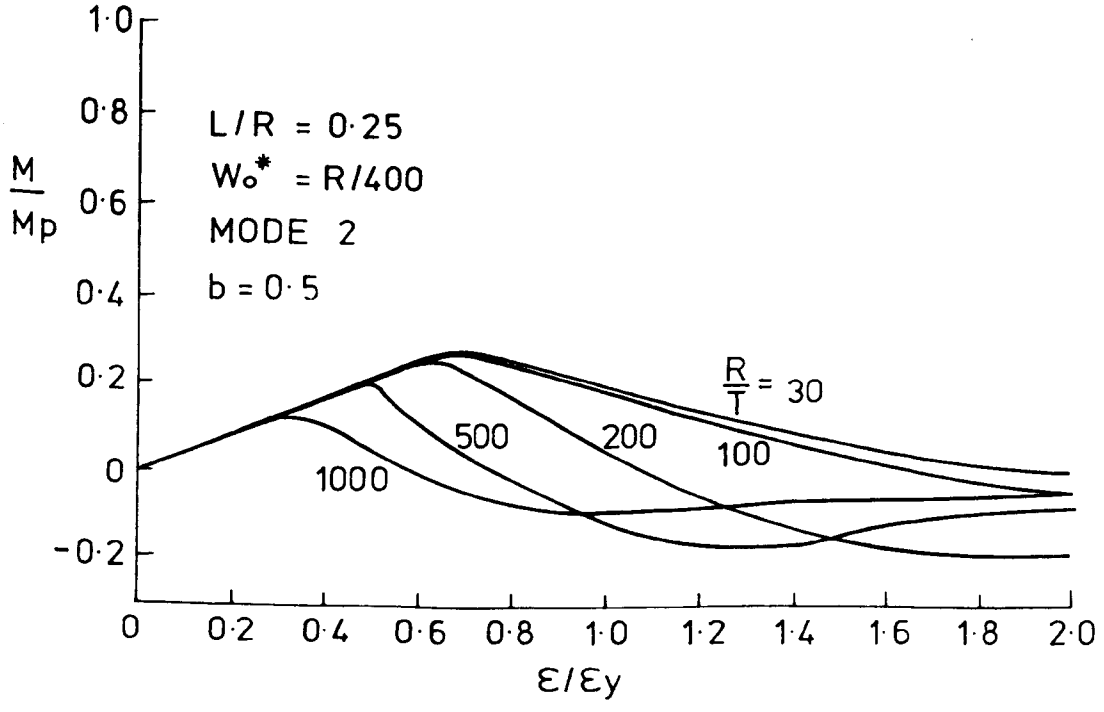

Fig. 6.88b

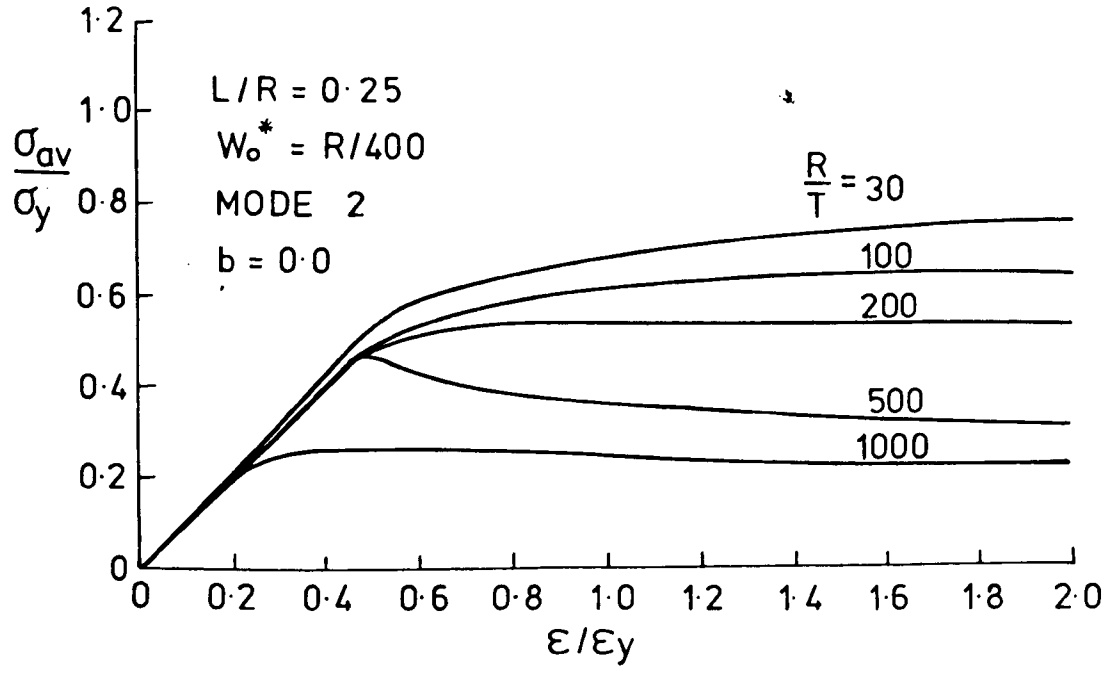

Fig. 6.89a

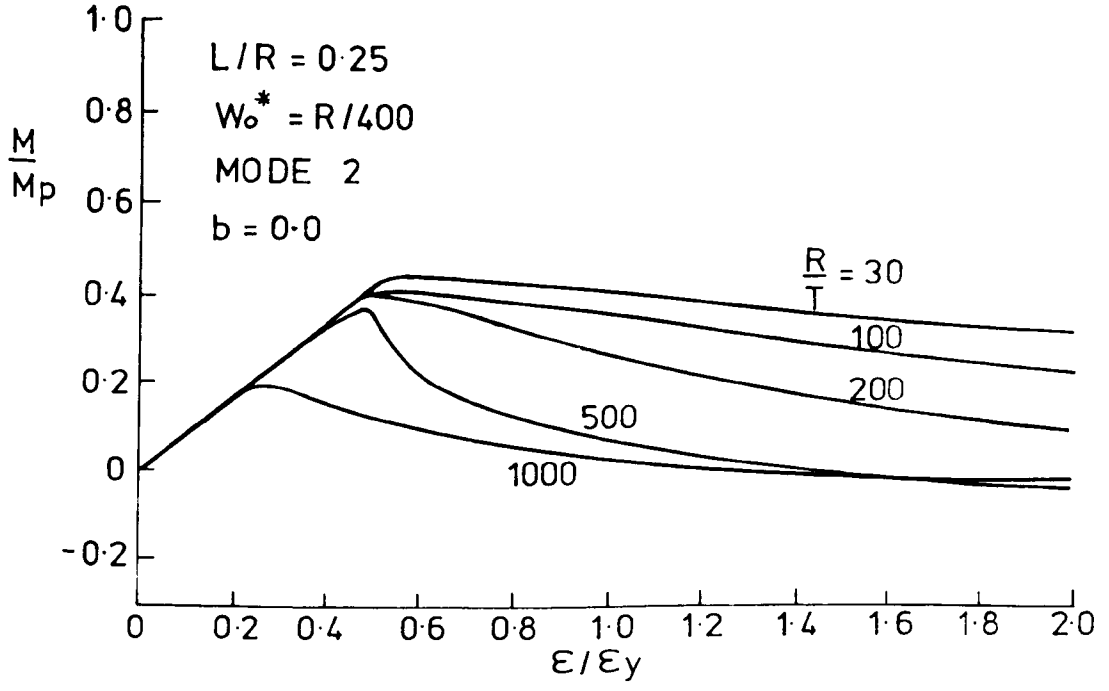

Fig. 6.89b

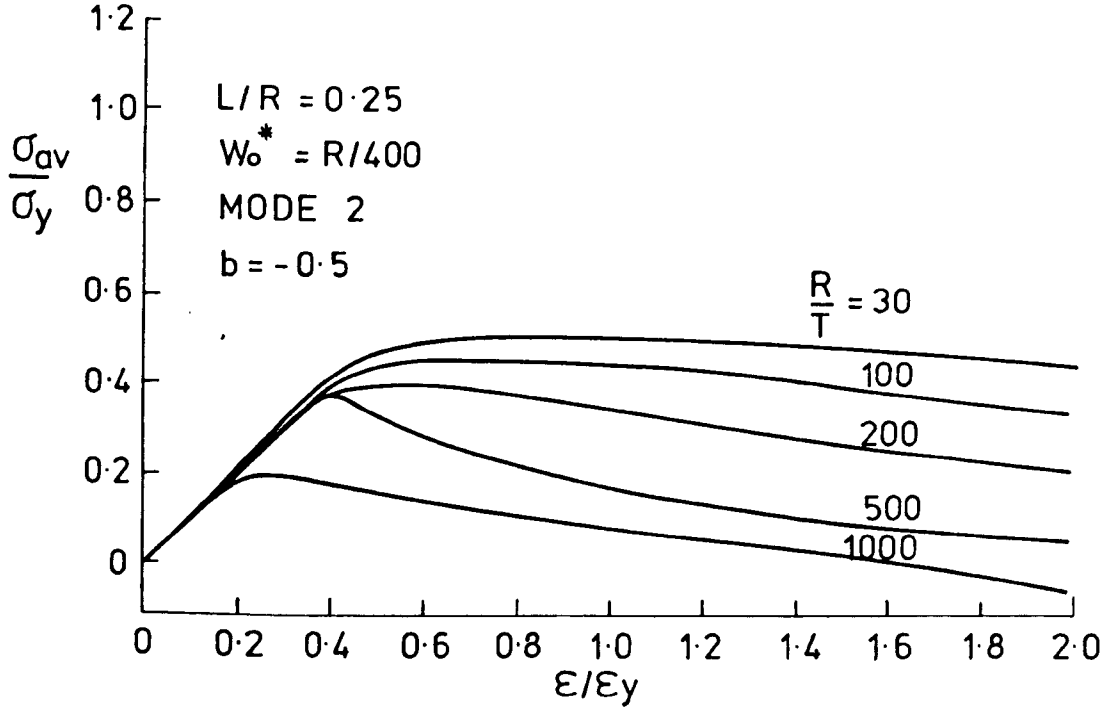

Fig. 6.90a

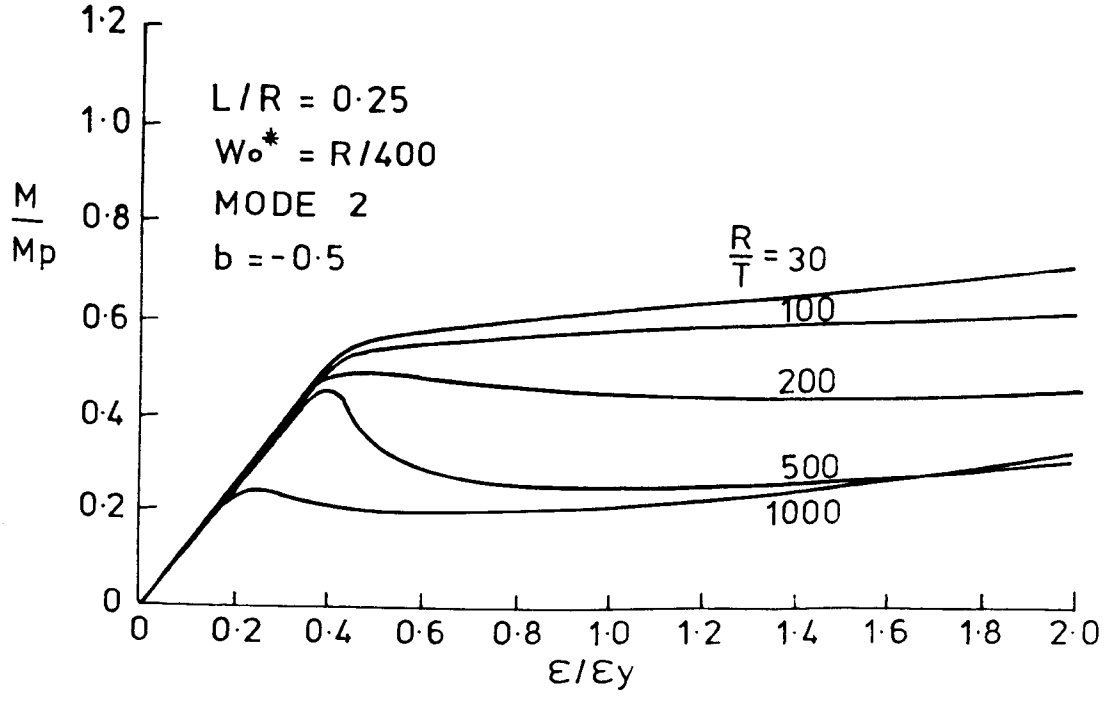

Fig. 6.90b

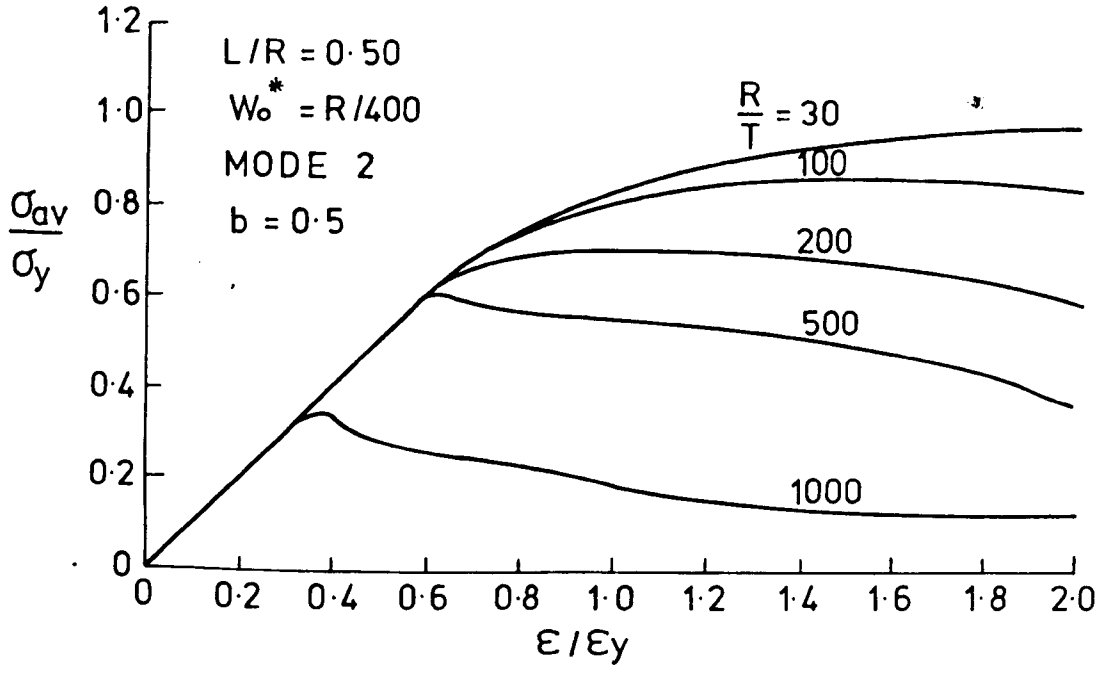

Fig. 6.91a

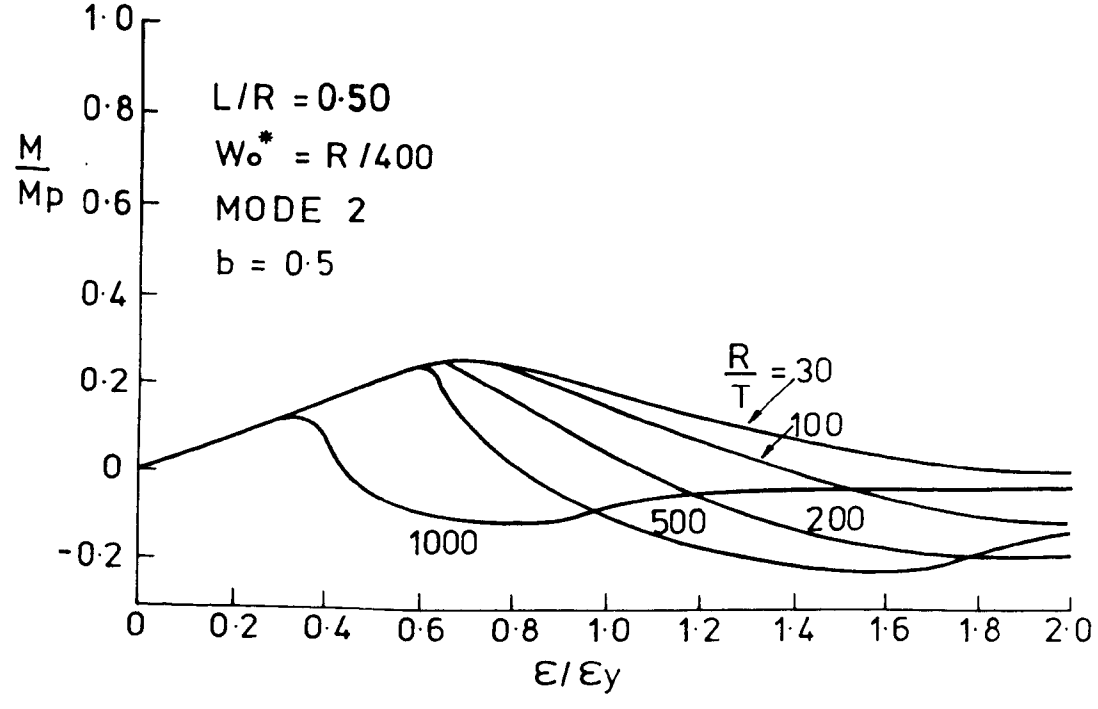

Fig. 6.91b

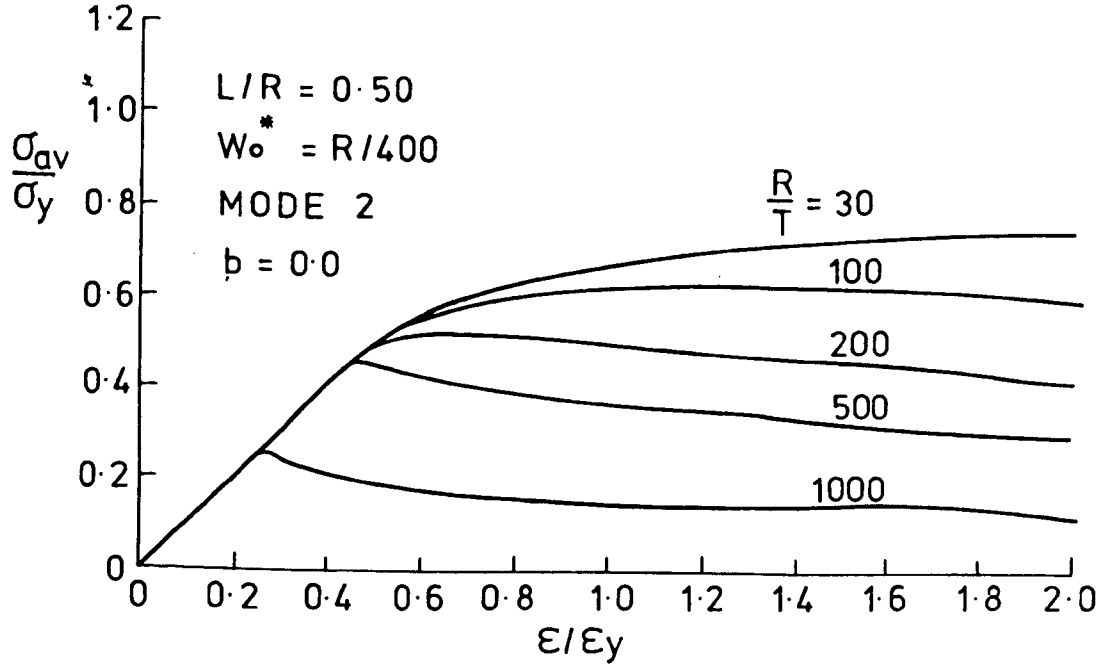

Fig. 6.92a

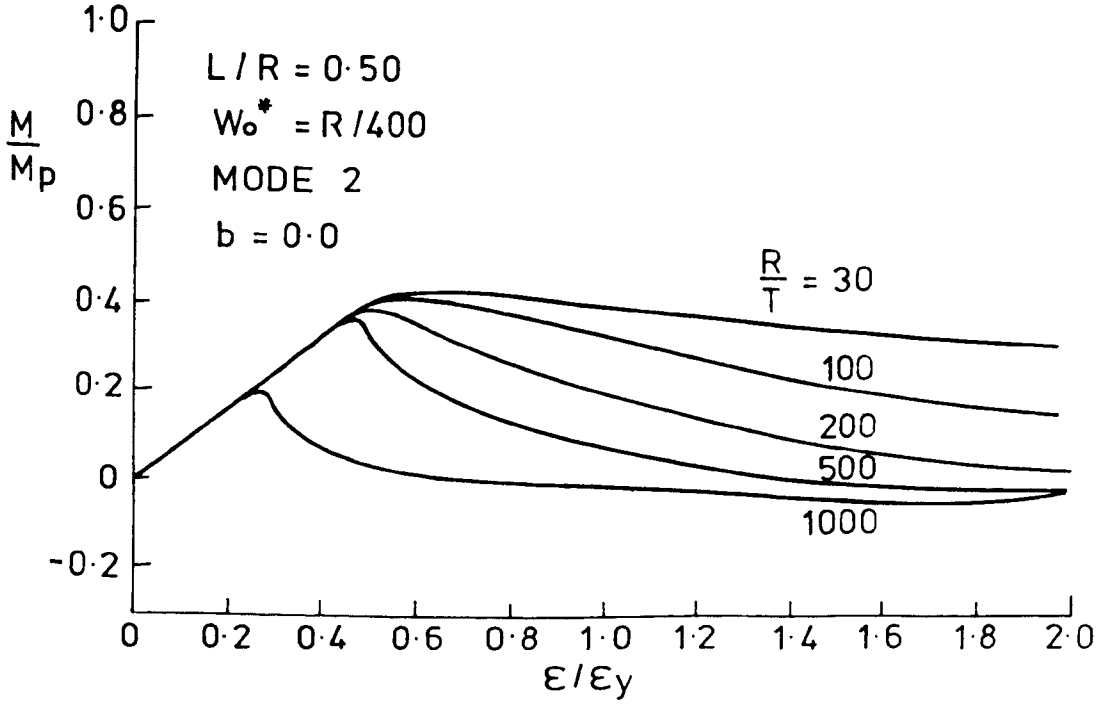

Fig. 6.92b

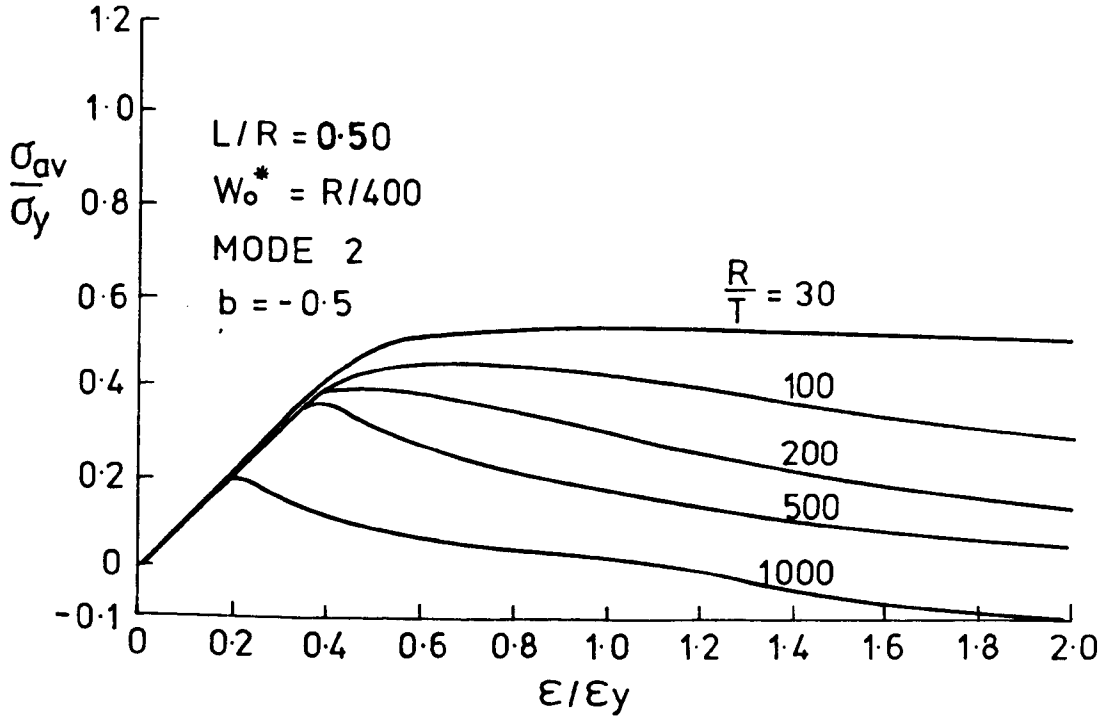

Fig. 6.93a

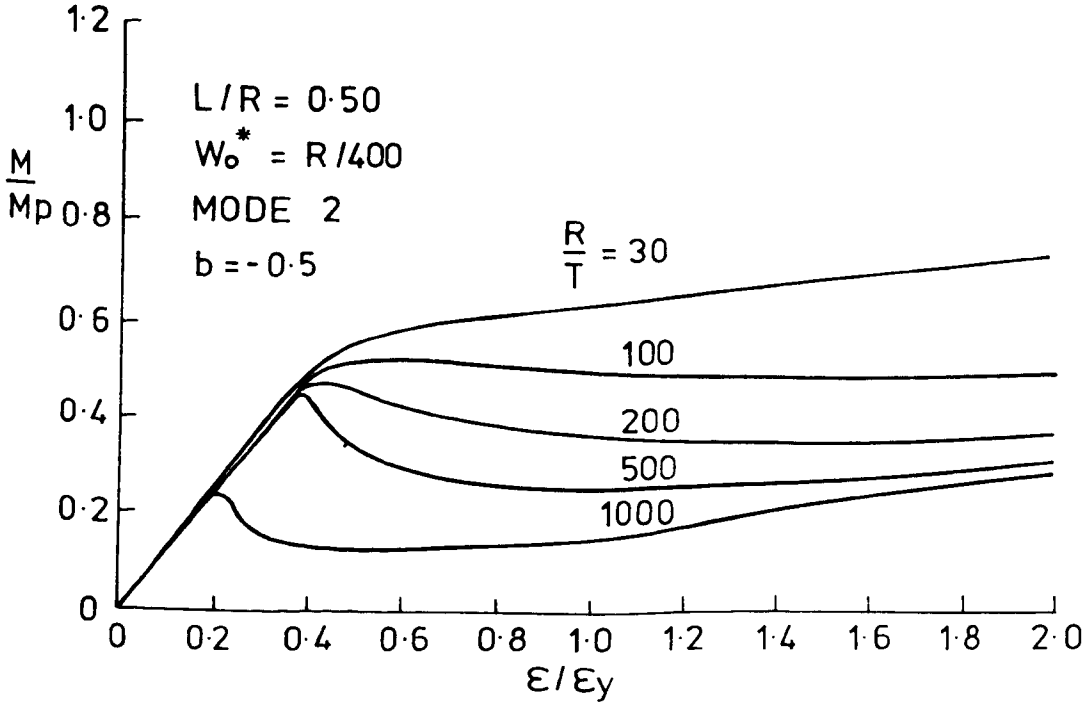

Fig. 6.93b

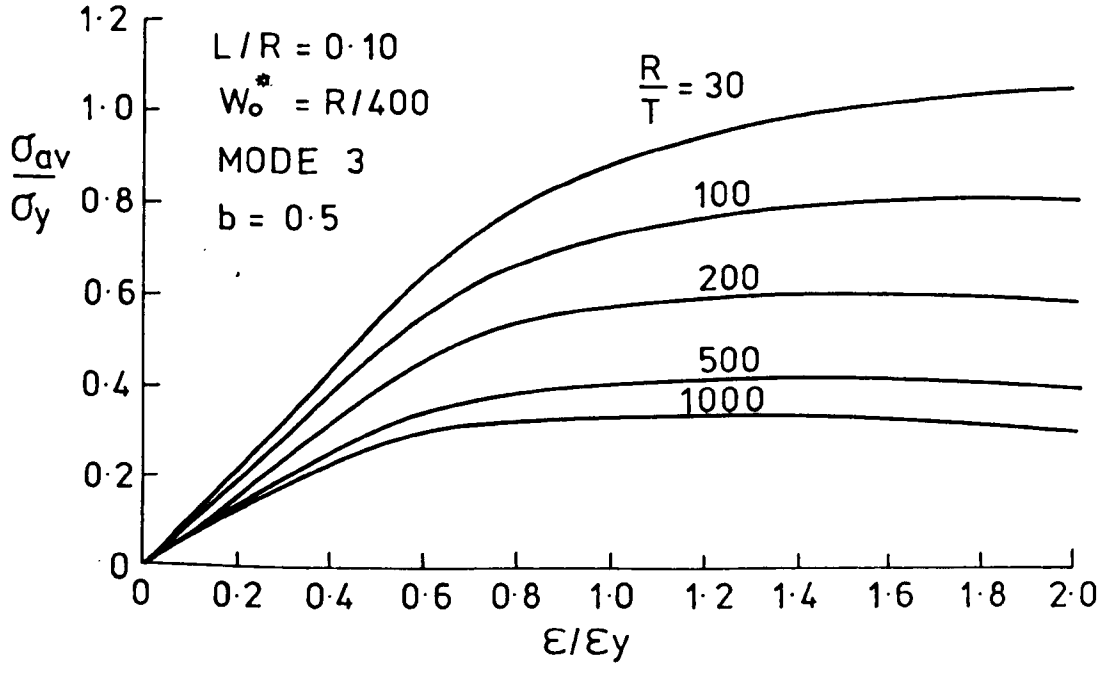

Fig. 6.94a

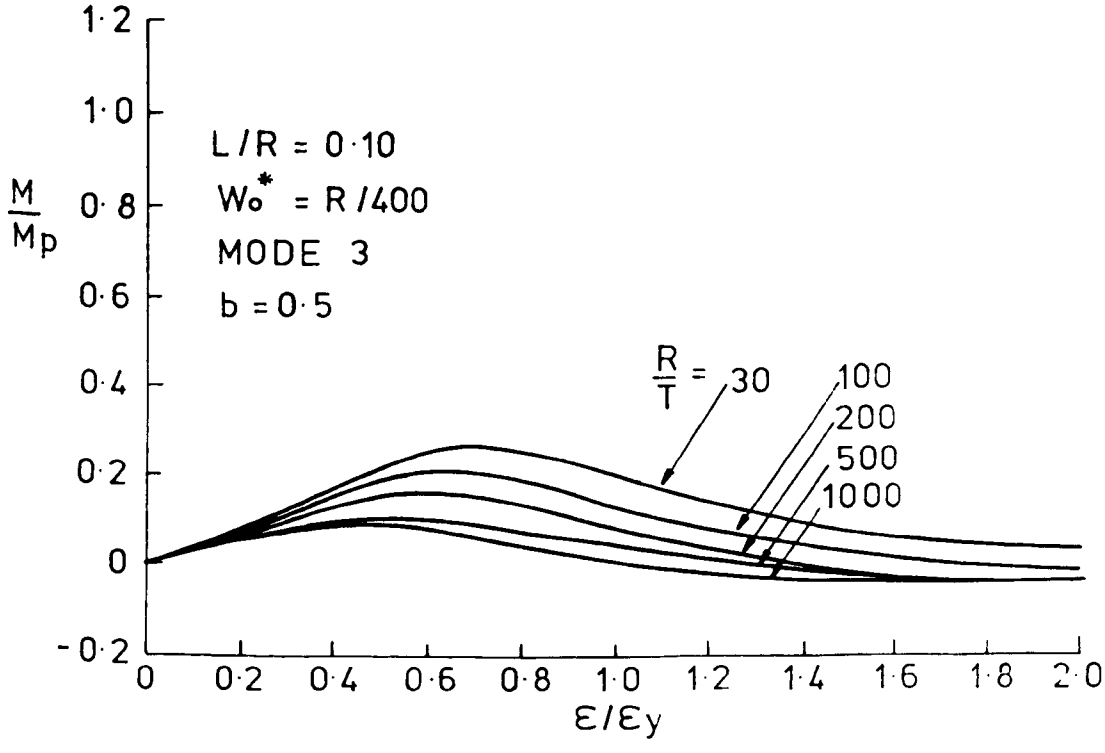

Fig. 6.94b

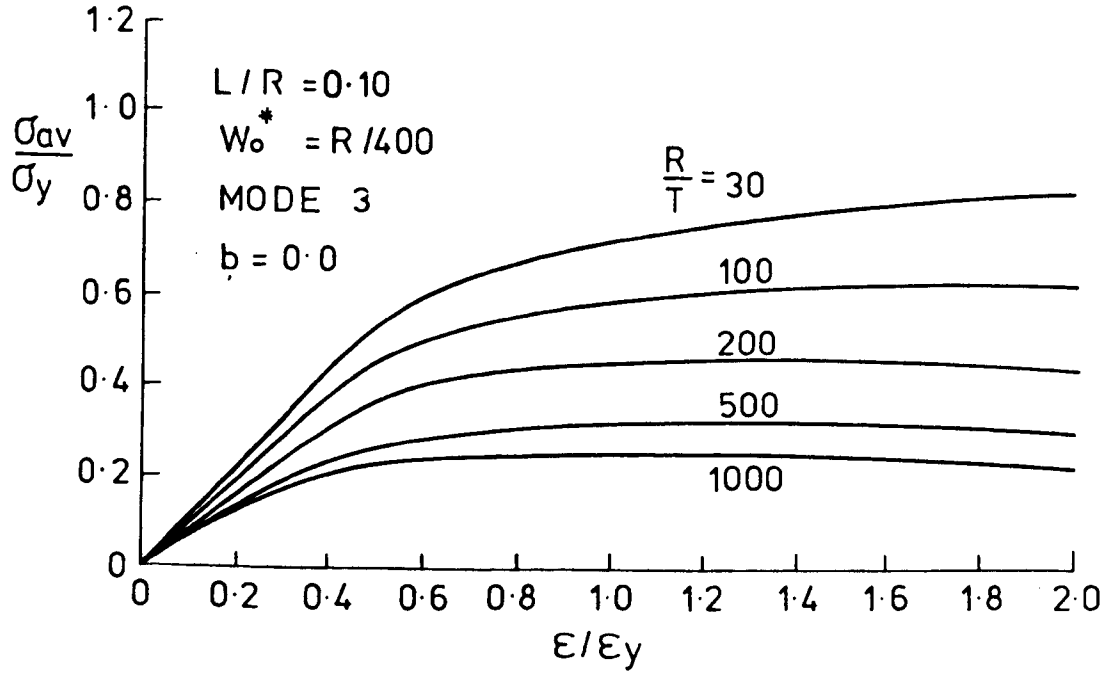

Fig. 6.95a

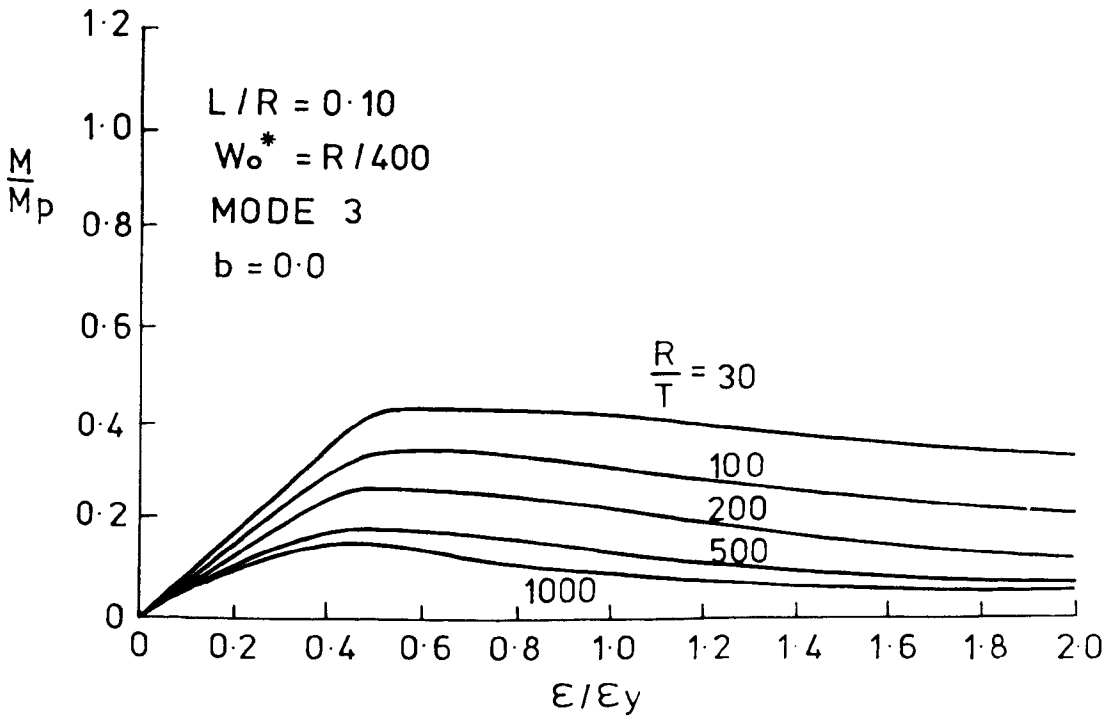

Fig. 6.95b

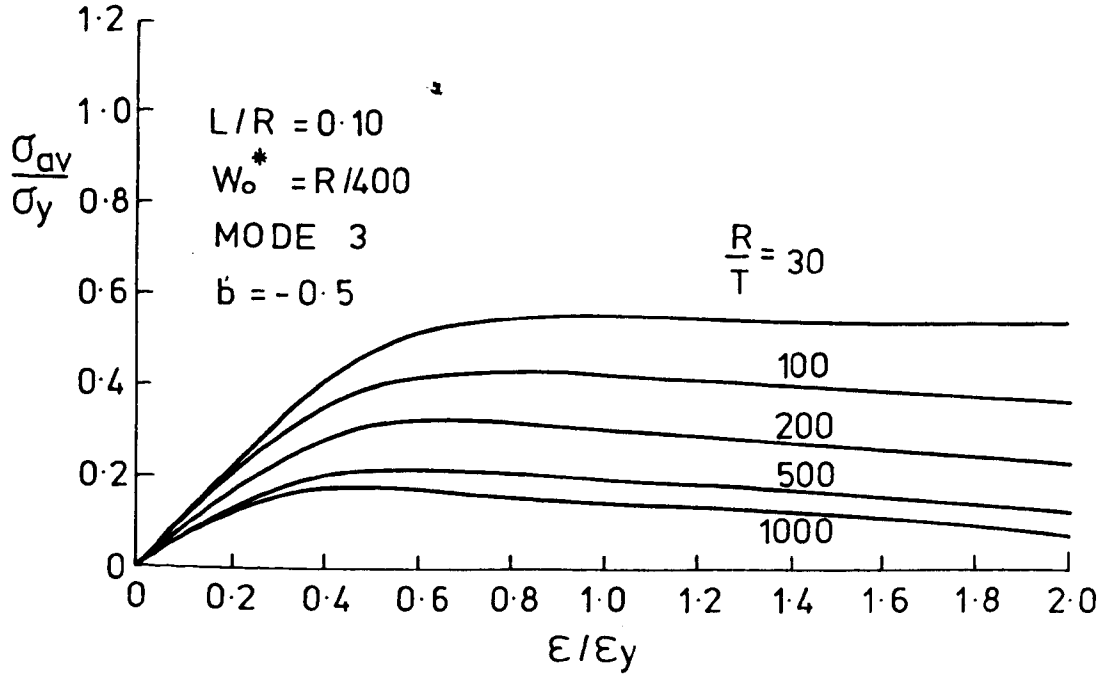

Fig. 6.96a

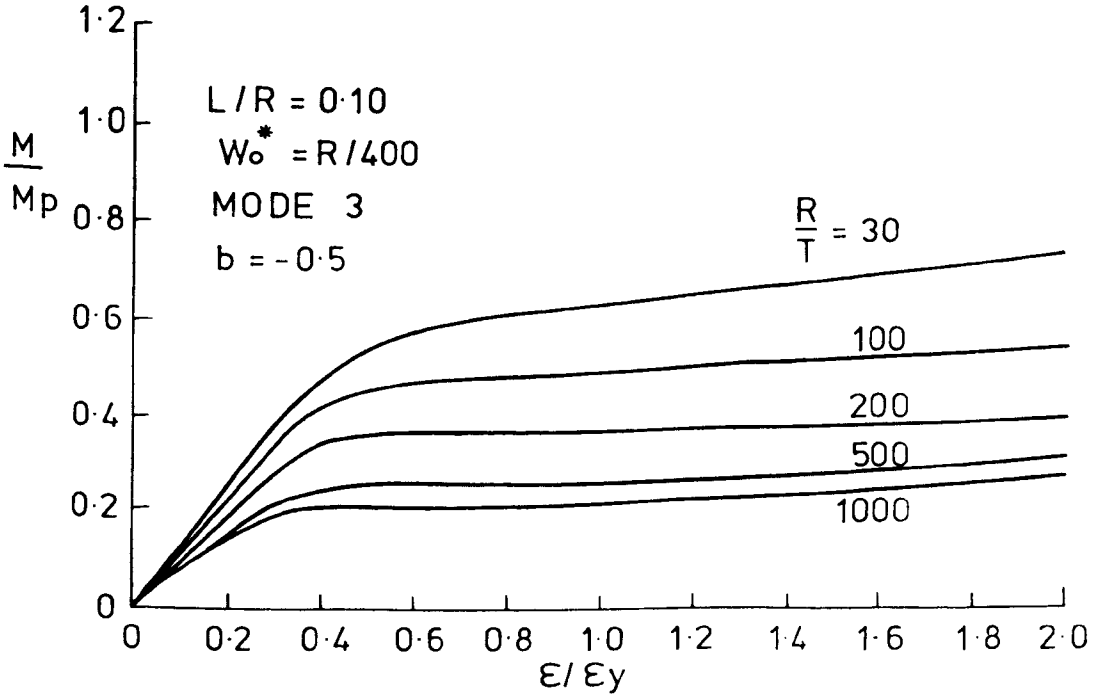

Fig. 6.96b

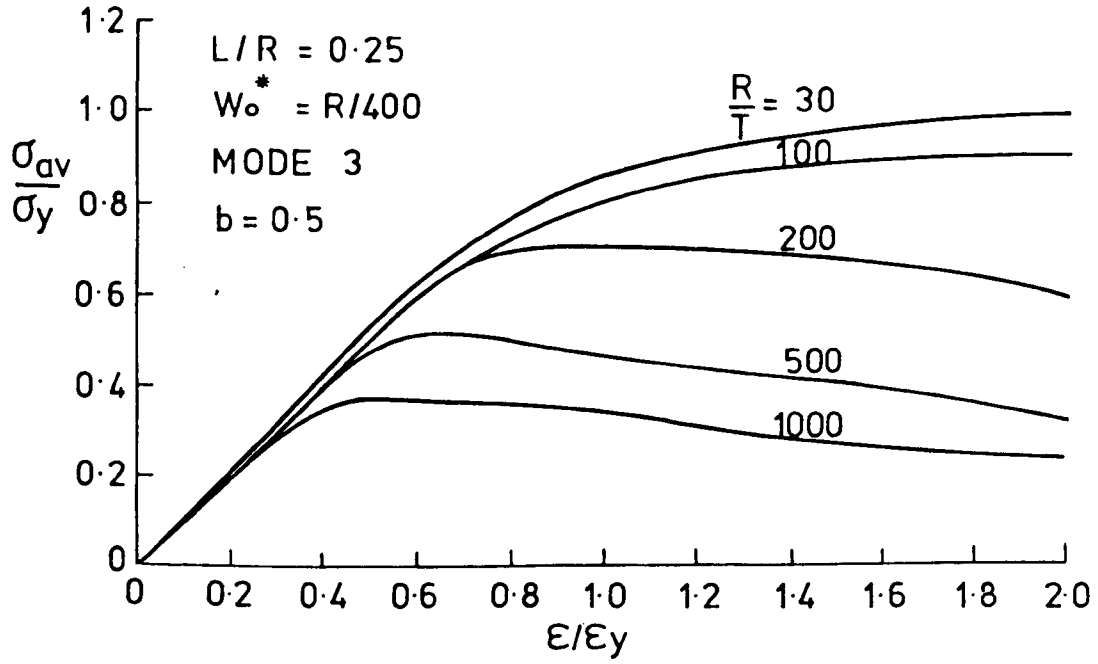

Fig. 6.97a

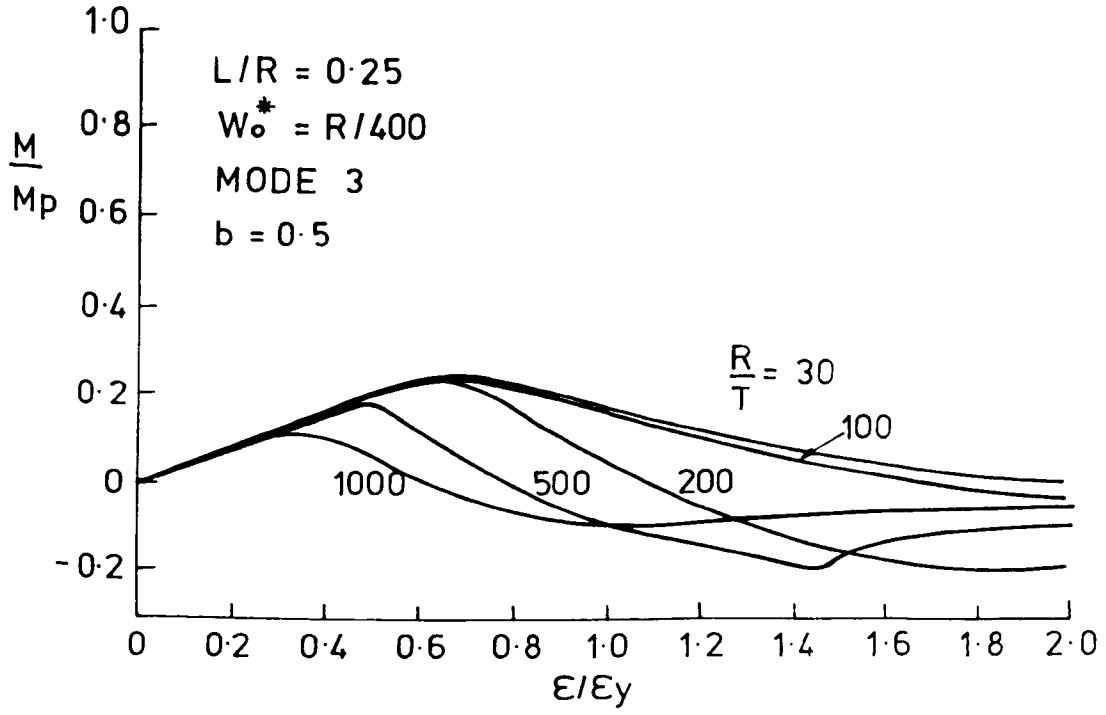

Fig. 6.97b

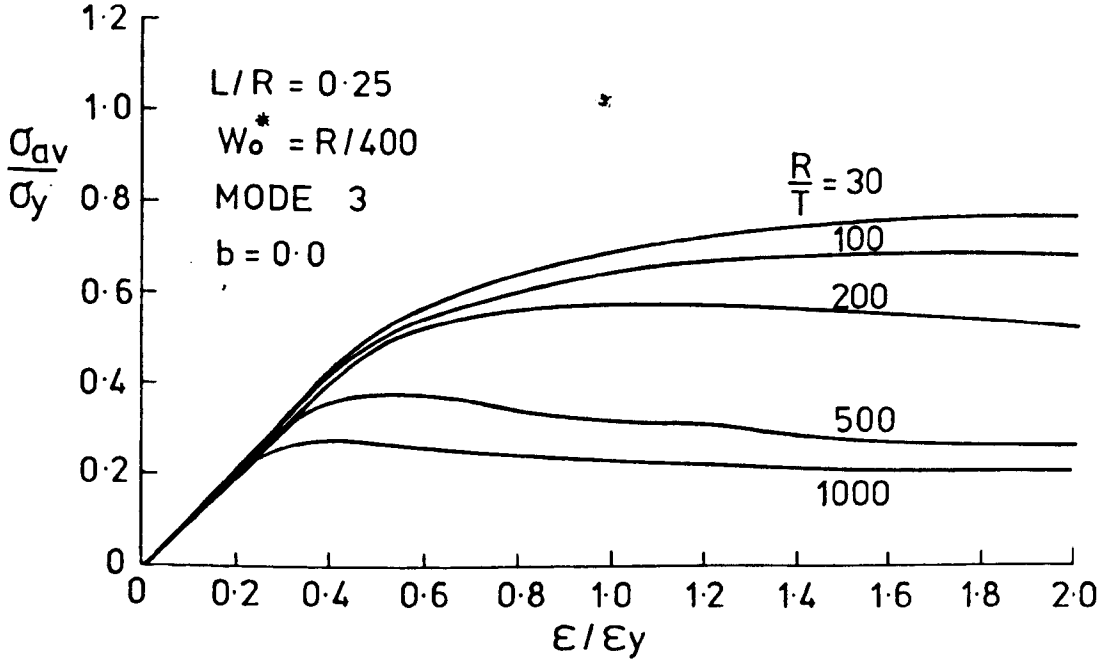

Fig. 6.98a

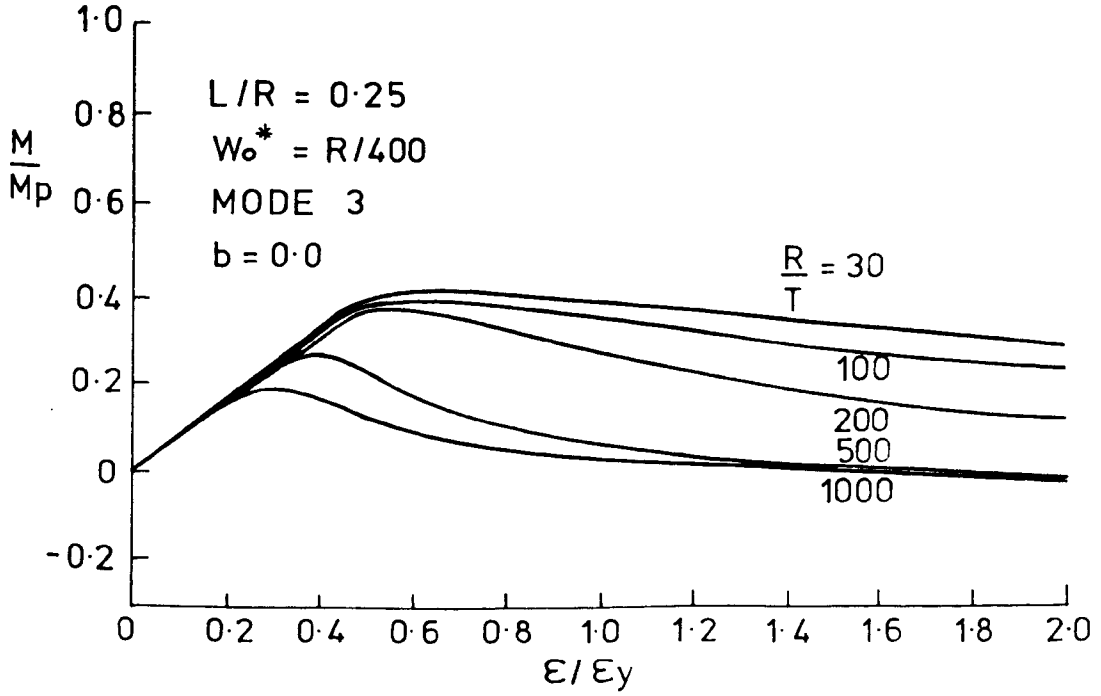

Fig. 6.98b

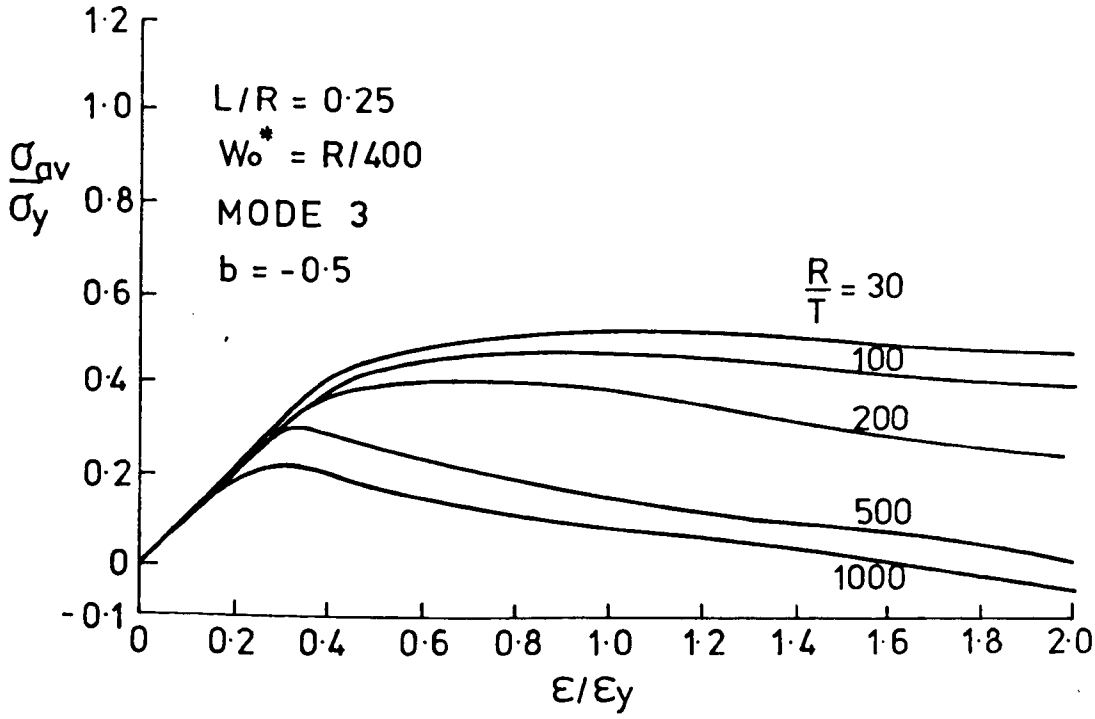

F ig. 6. 99a

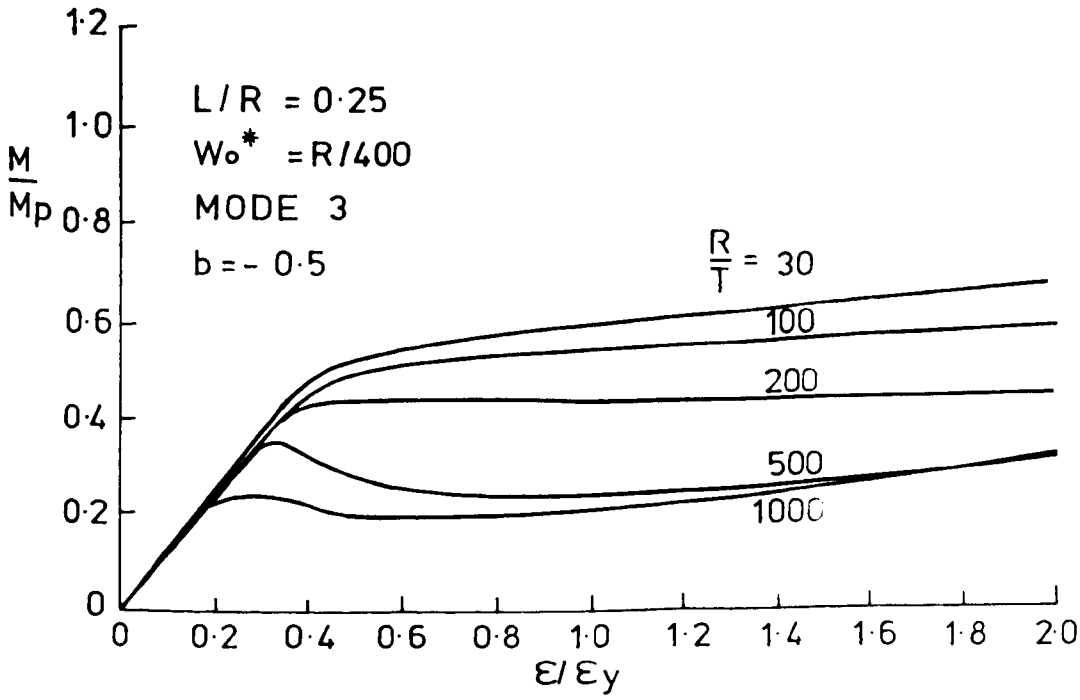

F ig. 6. 99b

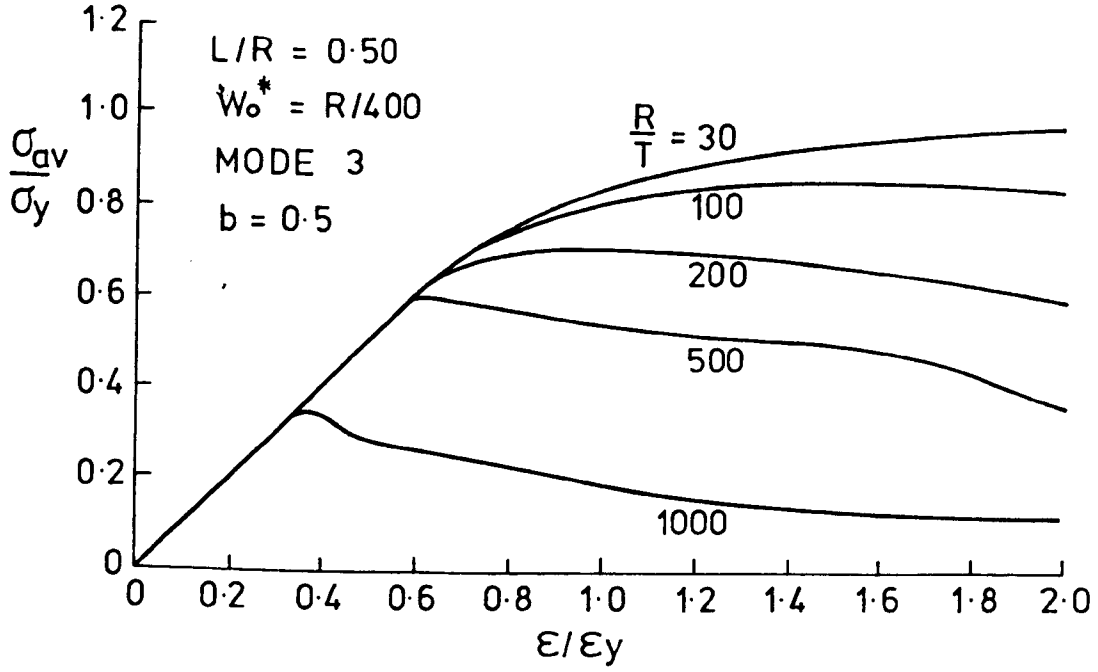

Fig. 6.100a

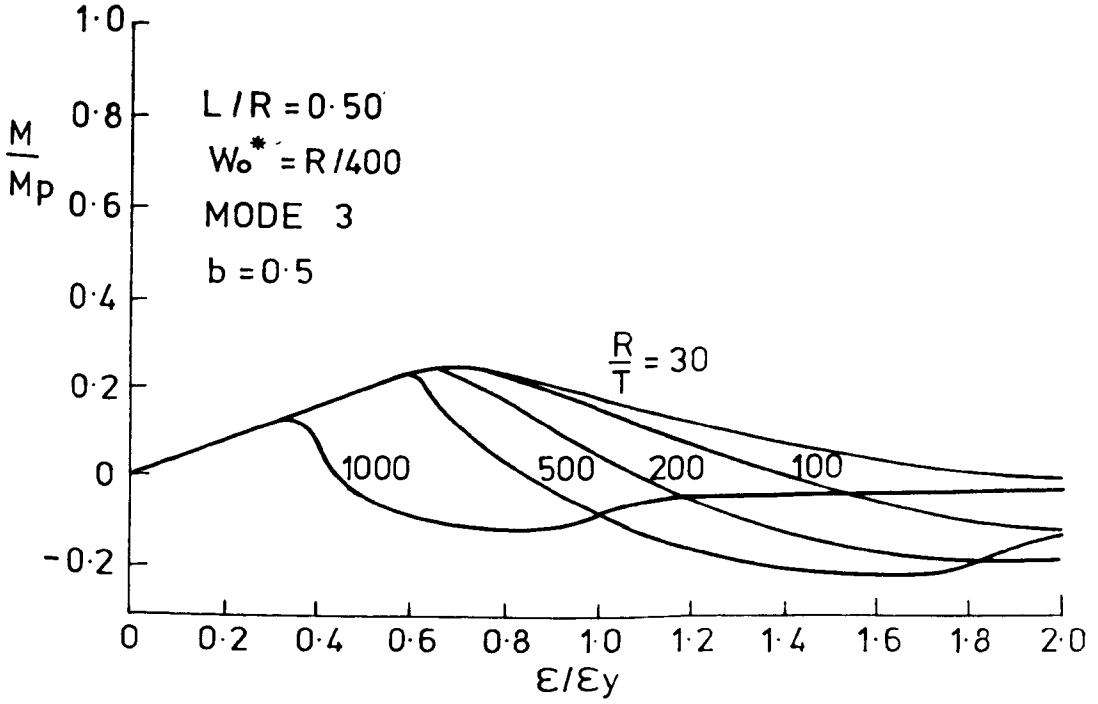

Fig. 6.100b

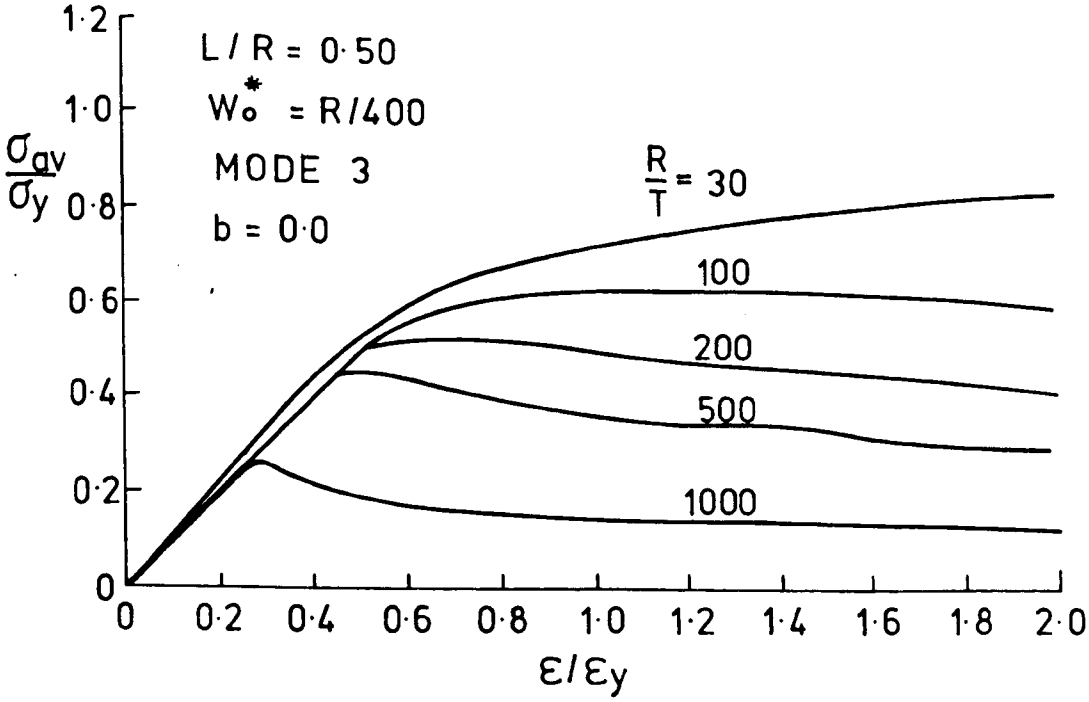

Fig. 6.101a

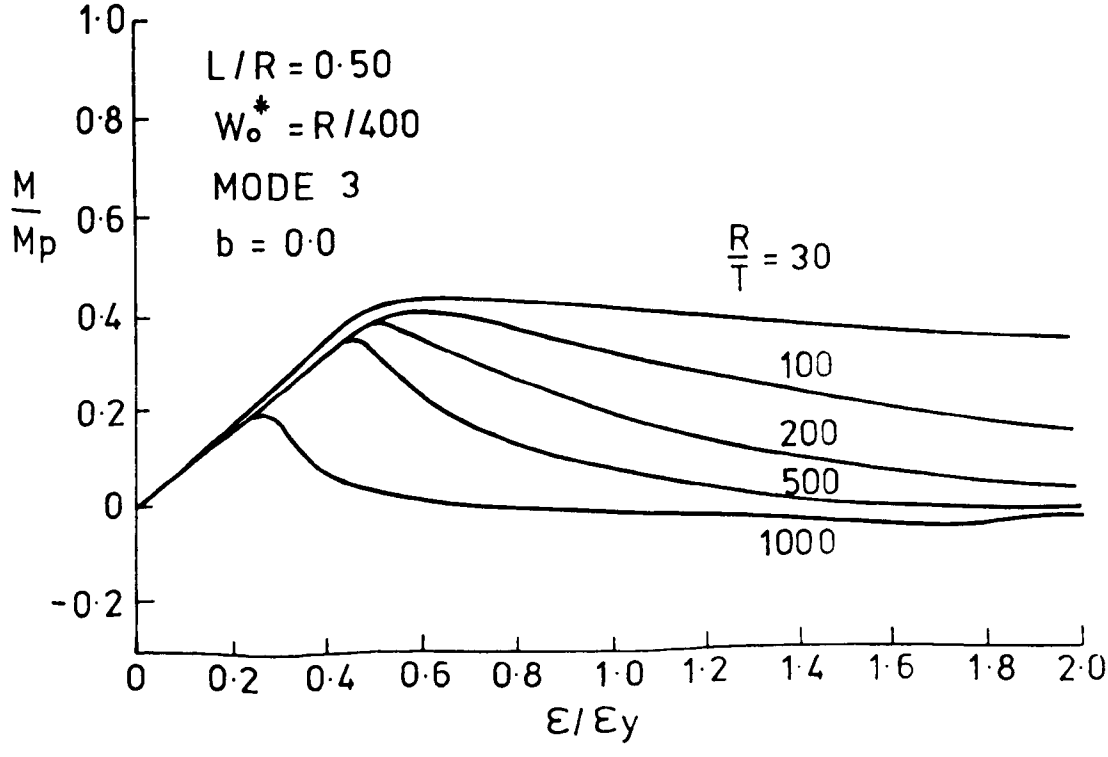

Fig. 6.101b

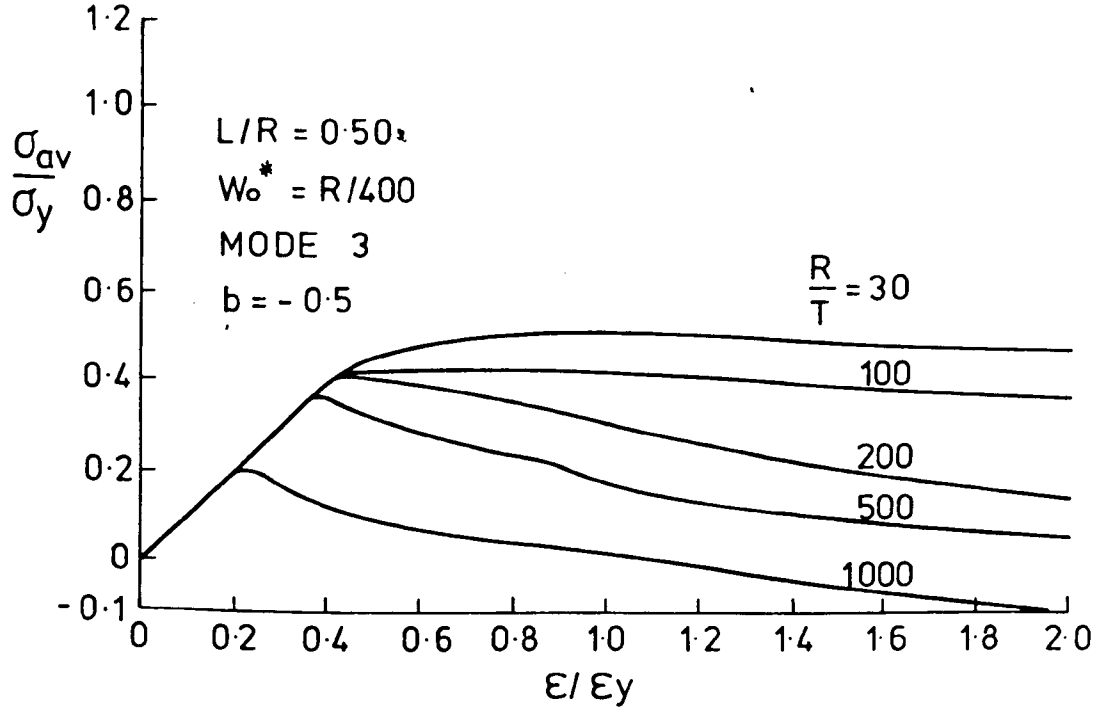

Fig. 6. 102a

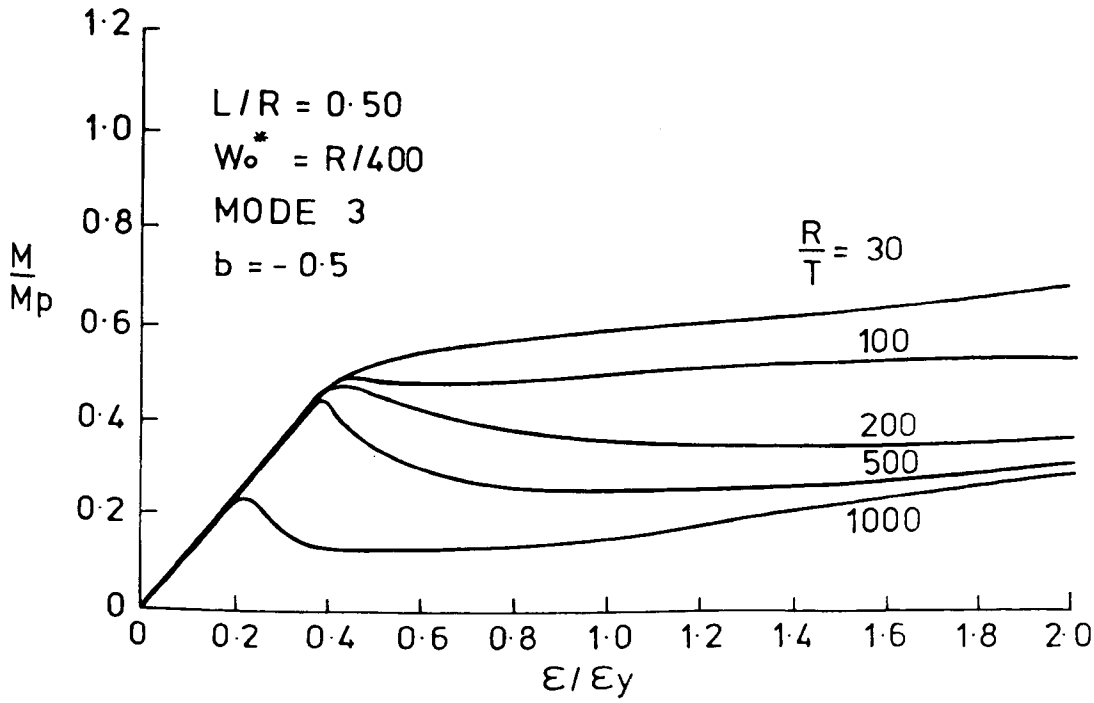

Fig. 6.102b

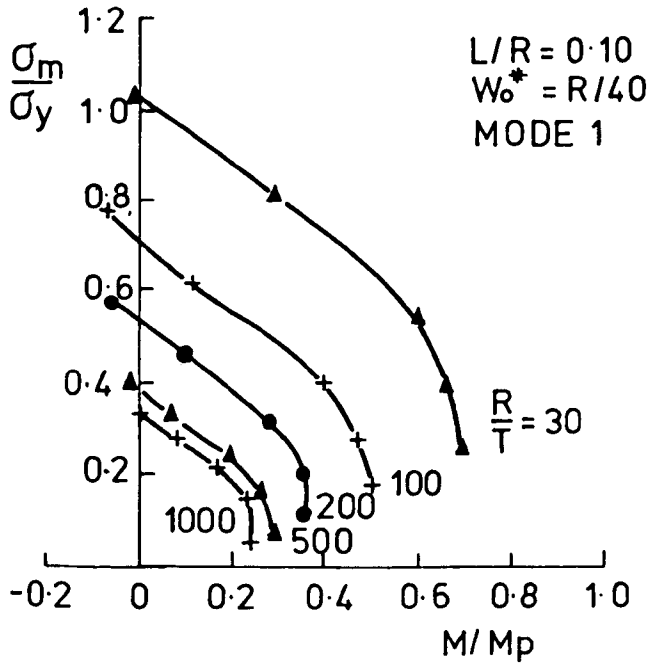

Fig. 6. 103

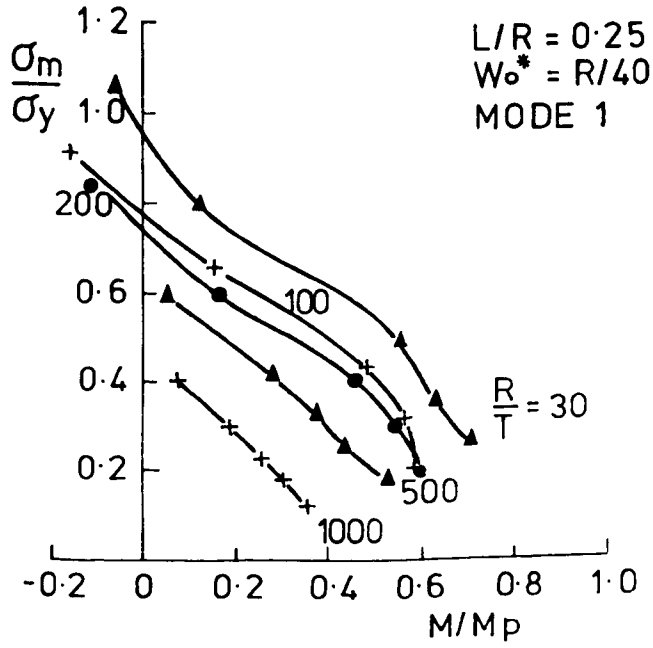

Fig. 6. 104

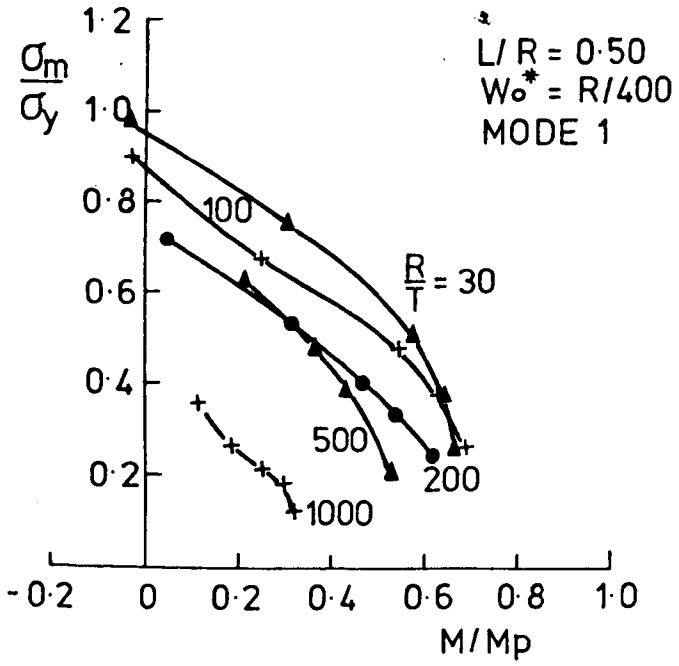

Fig. 6. 105

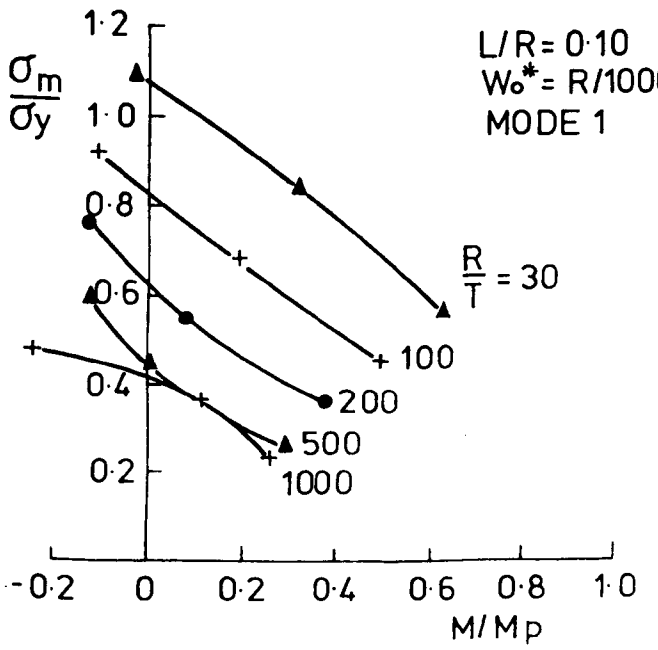

Fig. 6. 106

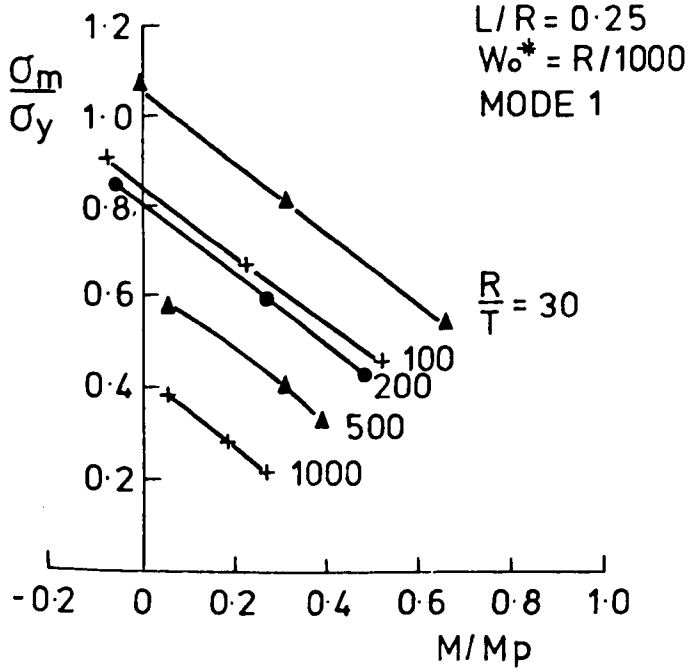

Fig. 6.107

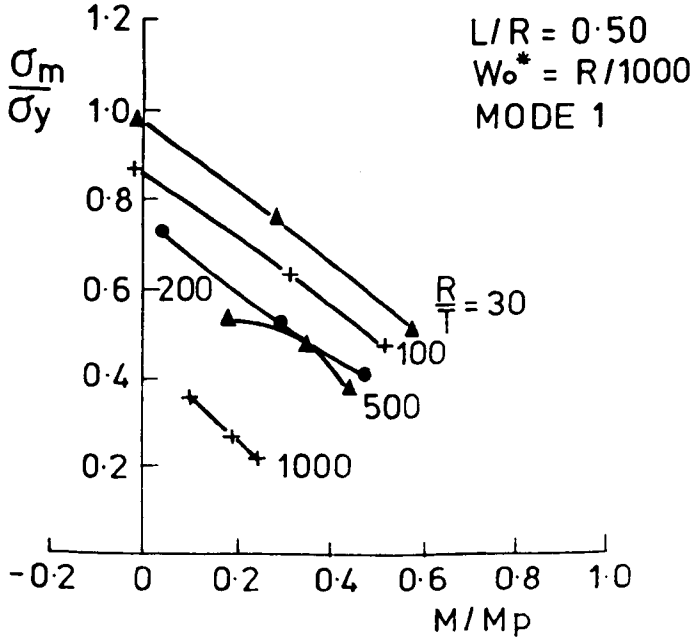

Fig. 6.108

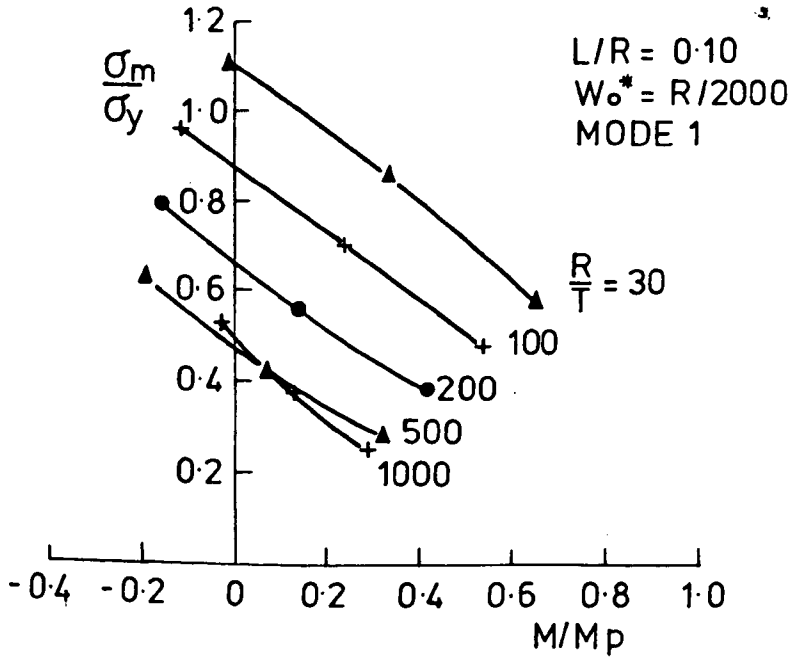

Fig. 6. 109

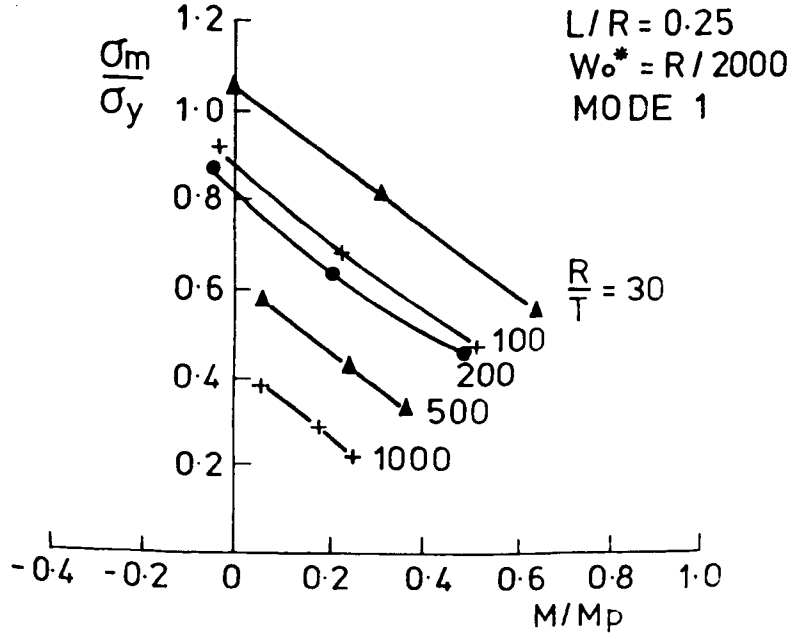

Fig. 6. 110

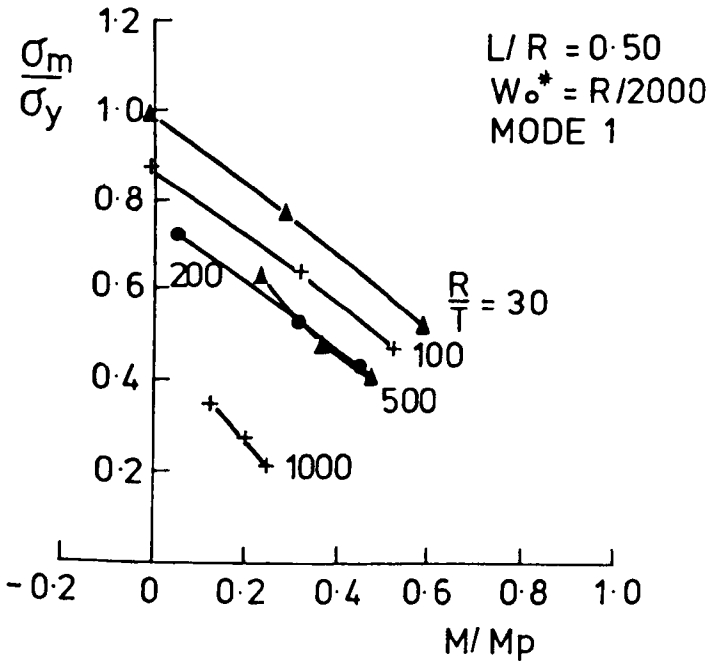

Fig. 6.111

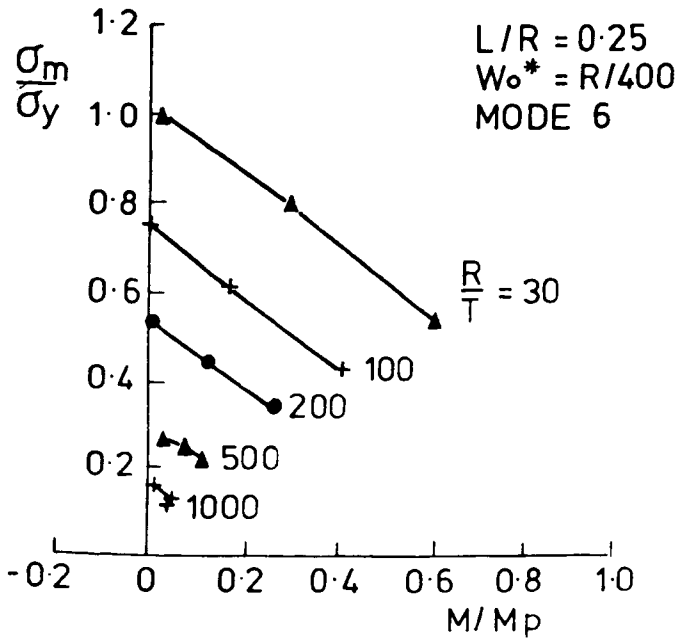

Fig. 6. 112

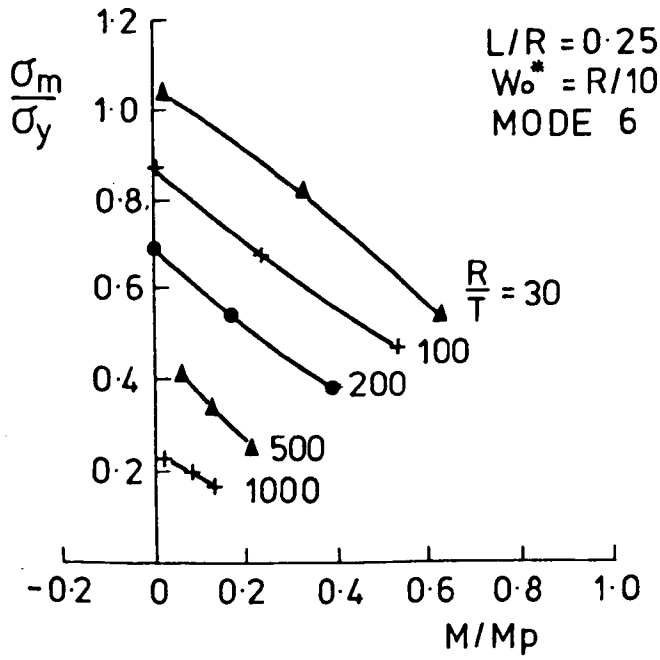

Fig. 6. 113

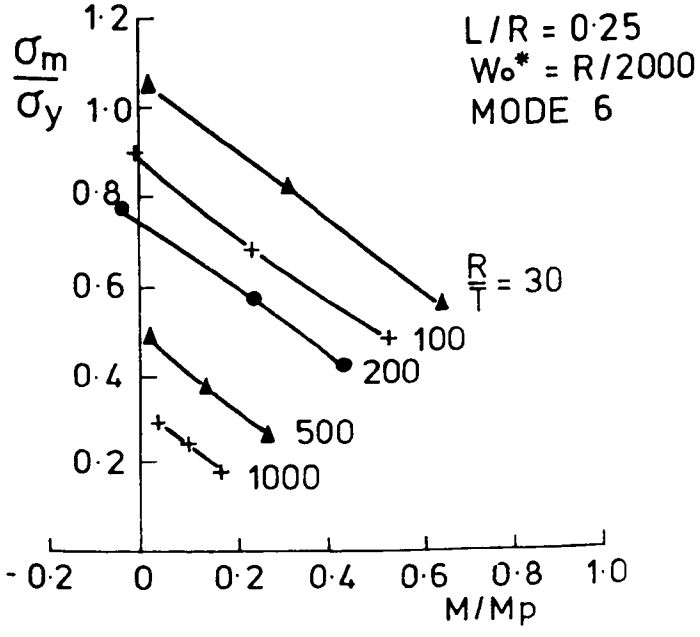

Fig. 6. 114

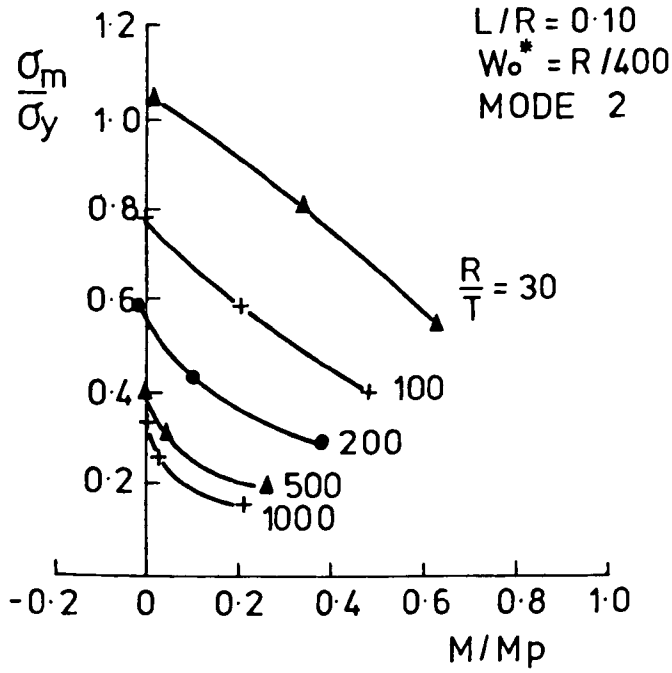

Fig. 6.115

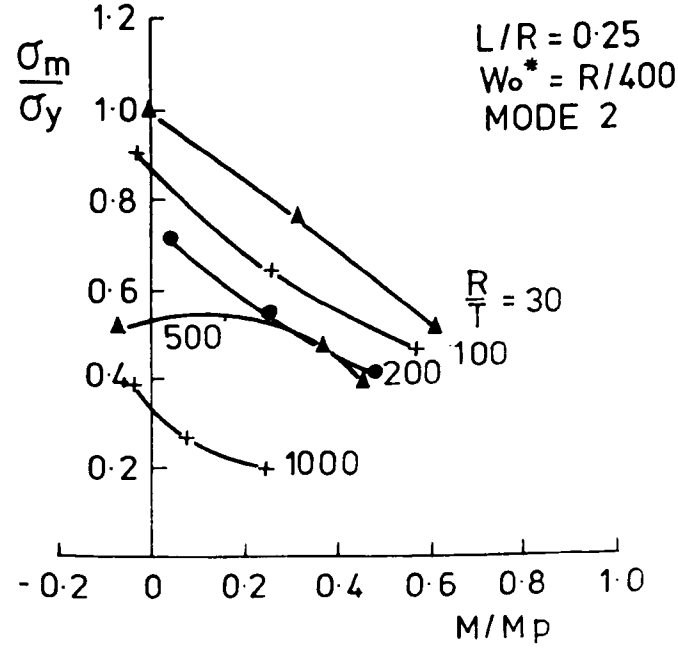

Fig. 6. 116

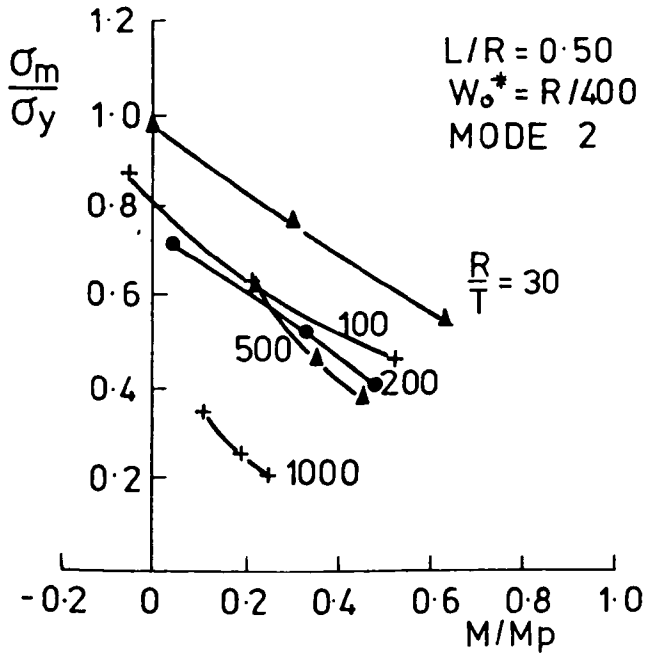

Fig. 6. 117

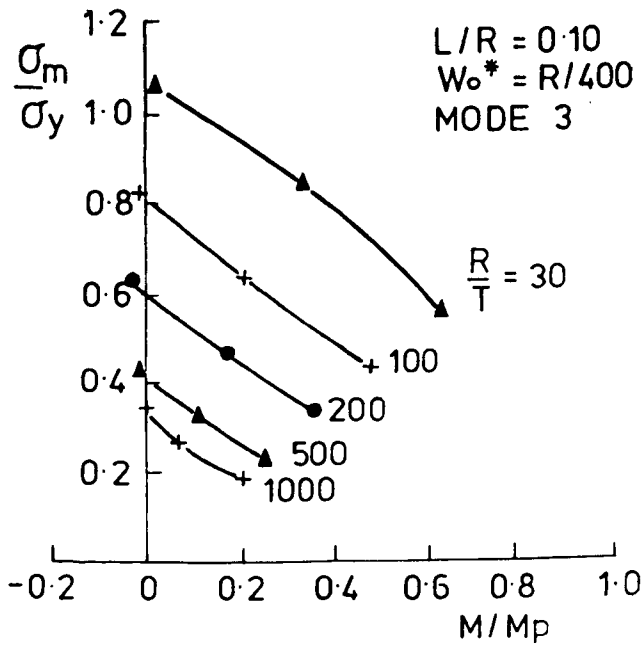

Fig. 6.118

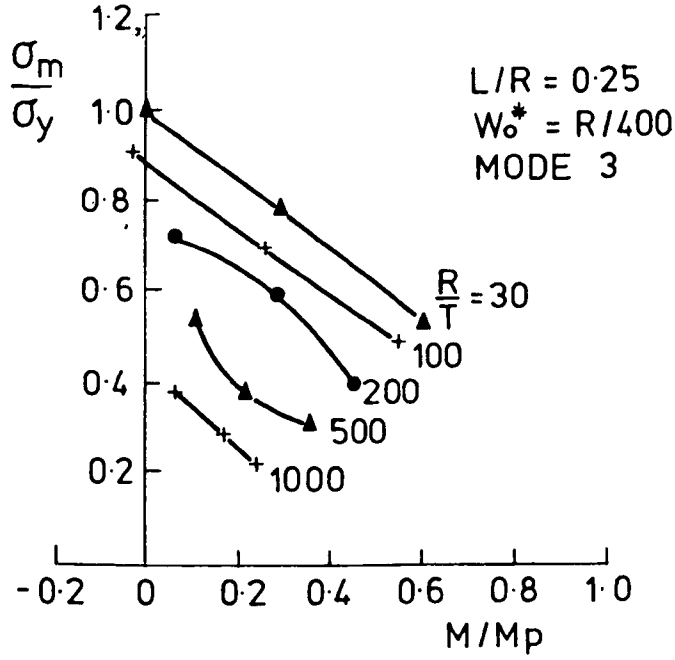

Fig. 6. 119

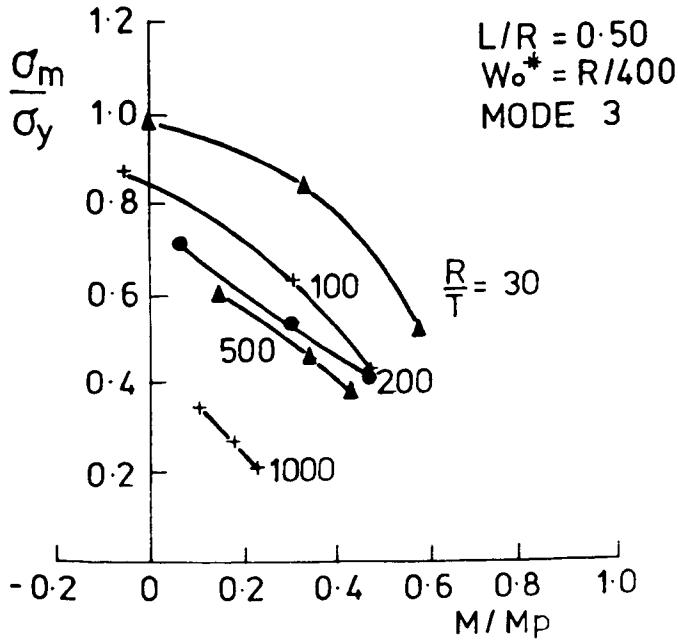

Fig. 6. 120

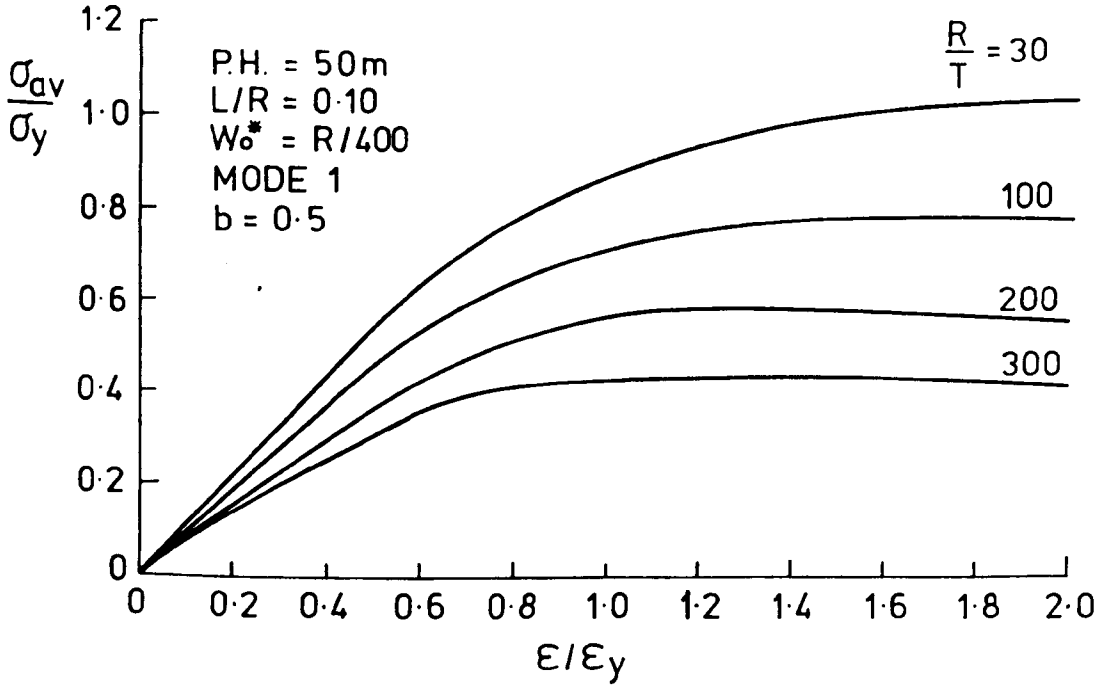

Fig. 6. 121a

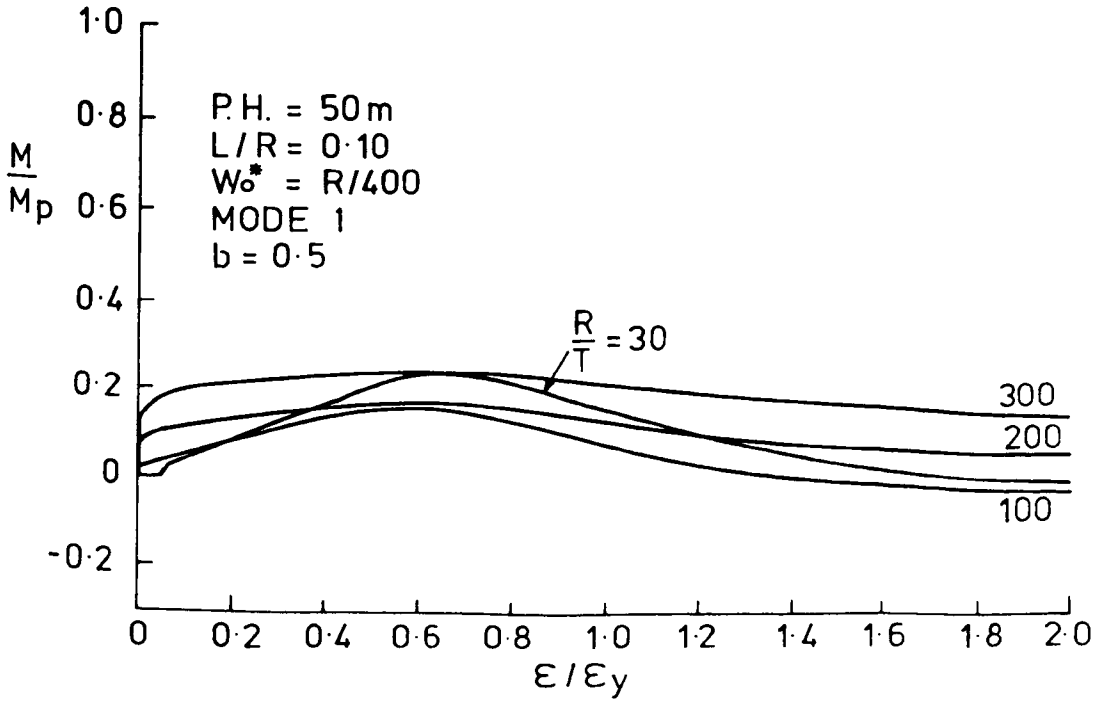

Fig. 6. 121b

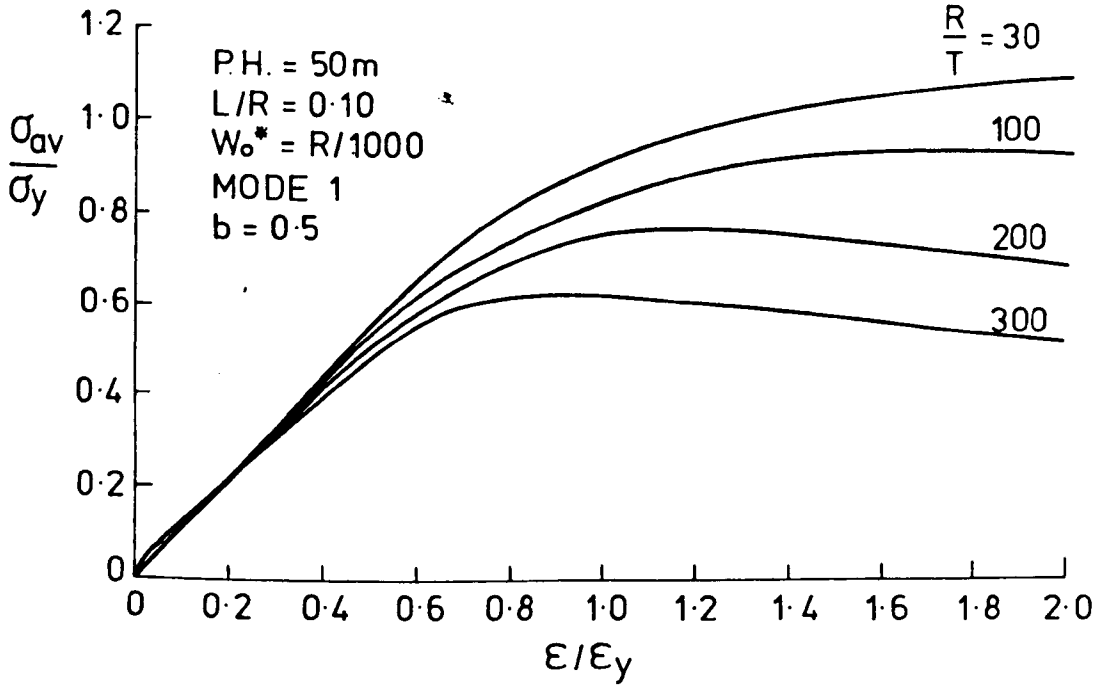

Fig. 6.122a

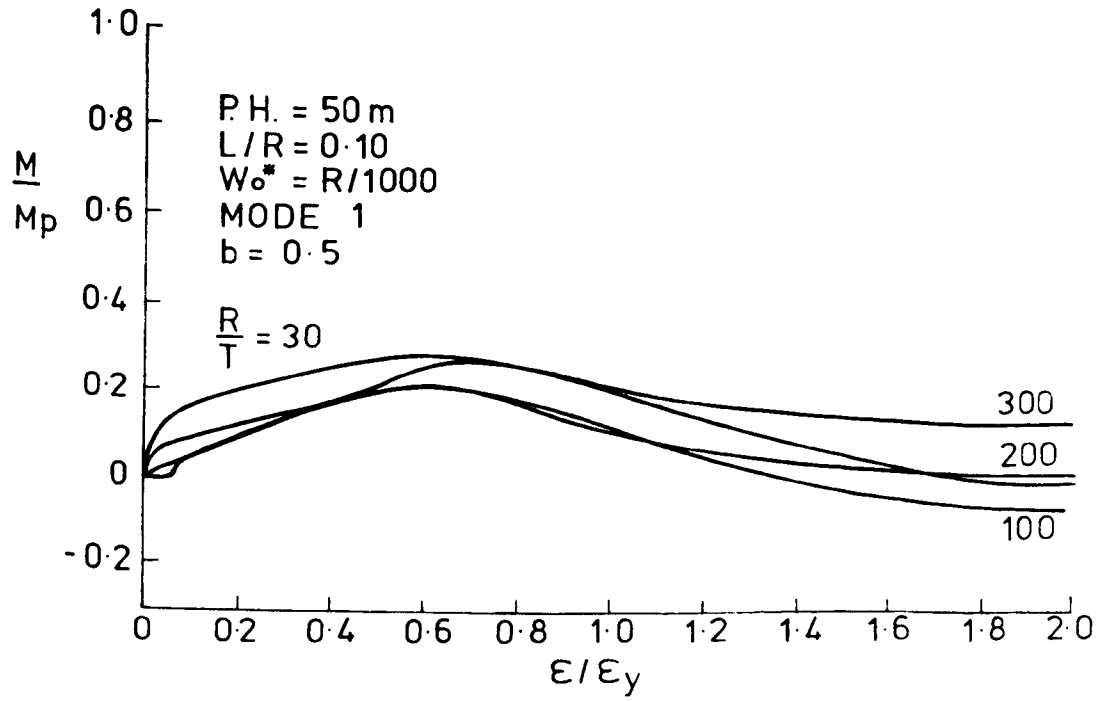

Fig. 6.122b

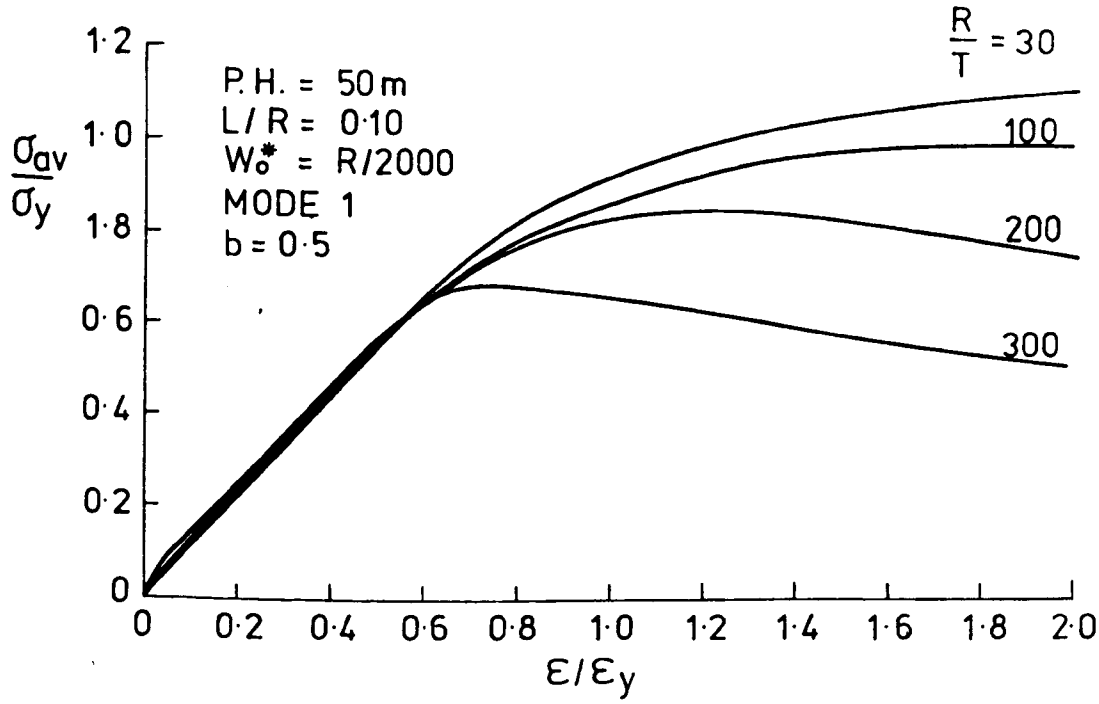

Fig. 6.123a

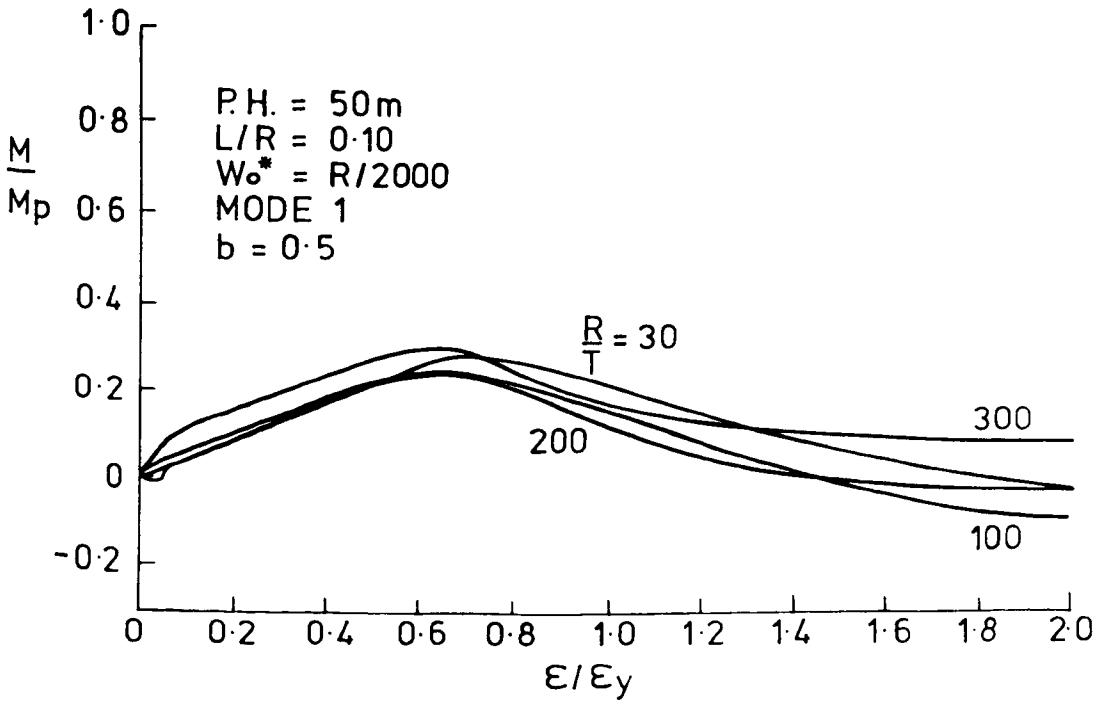

Fig. 6.123b

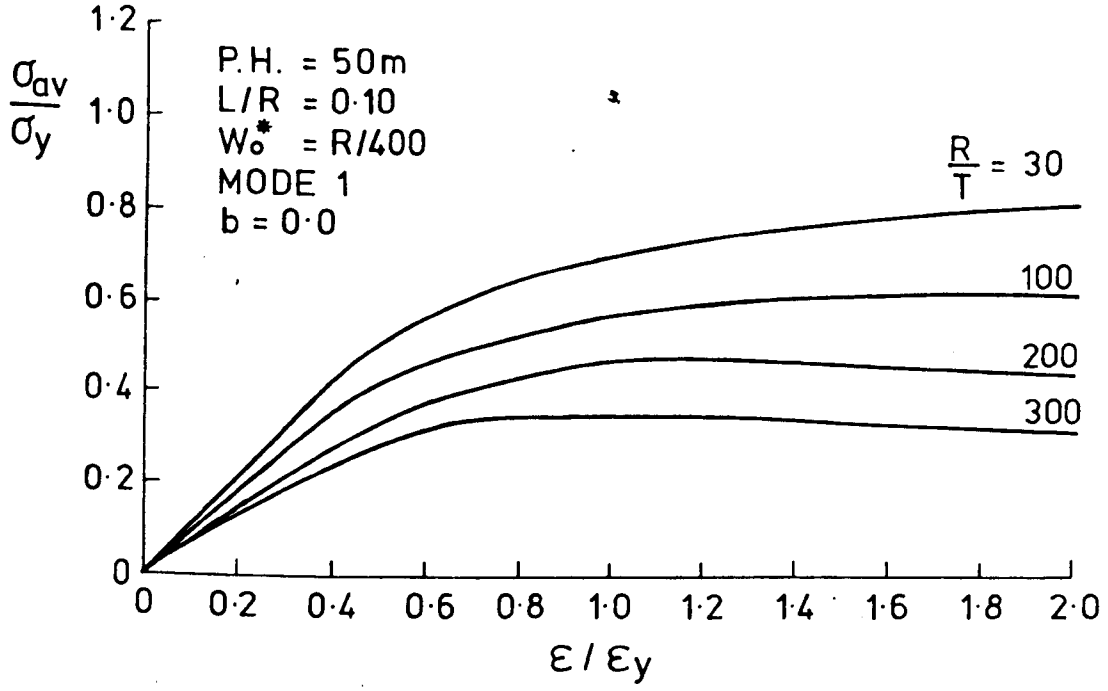

Fig. 6.124a

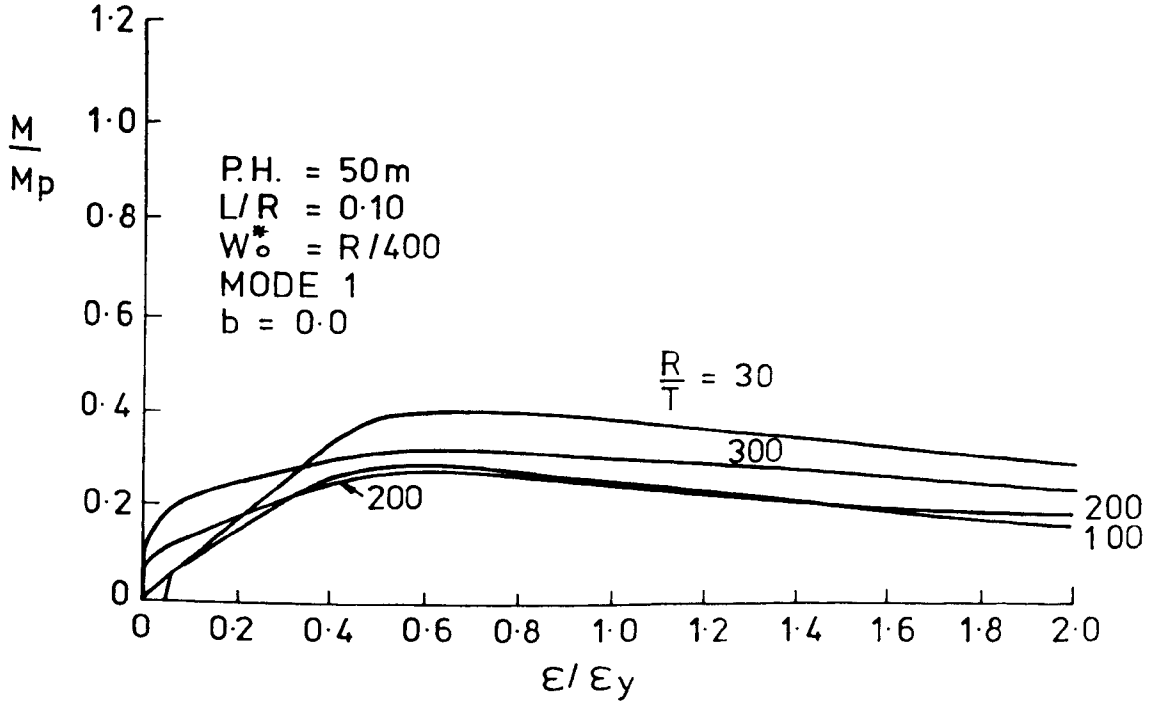

Fig. 6.124b

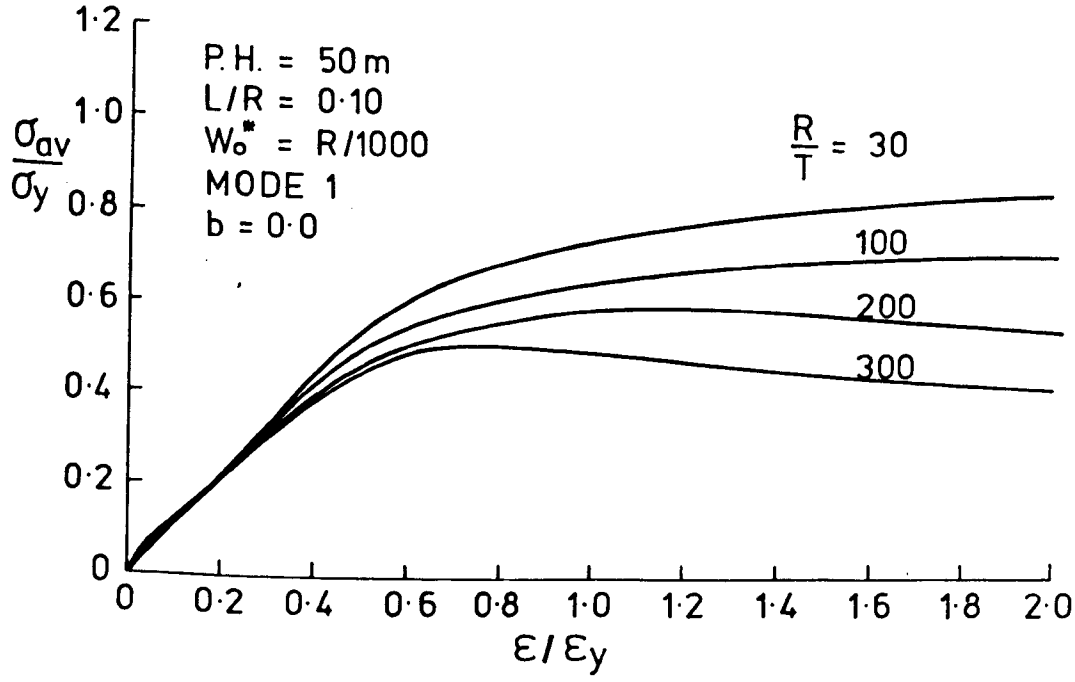

Fig. 6.125a

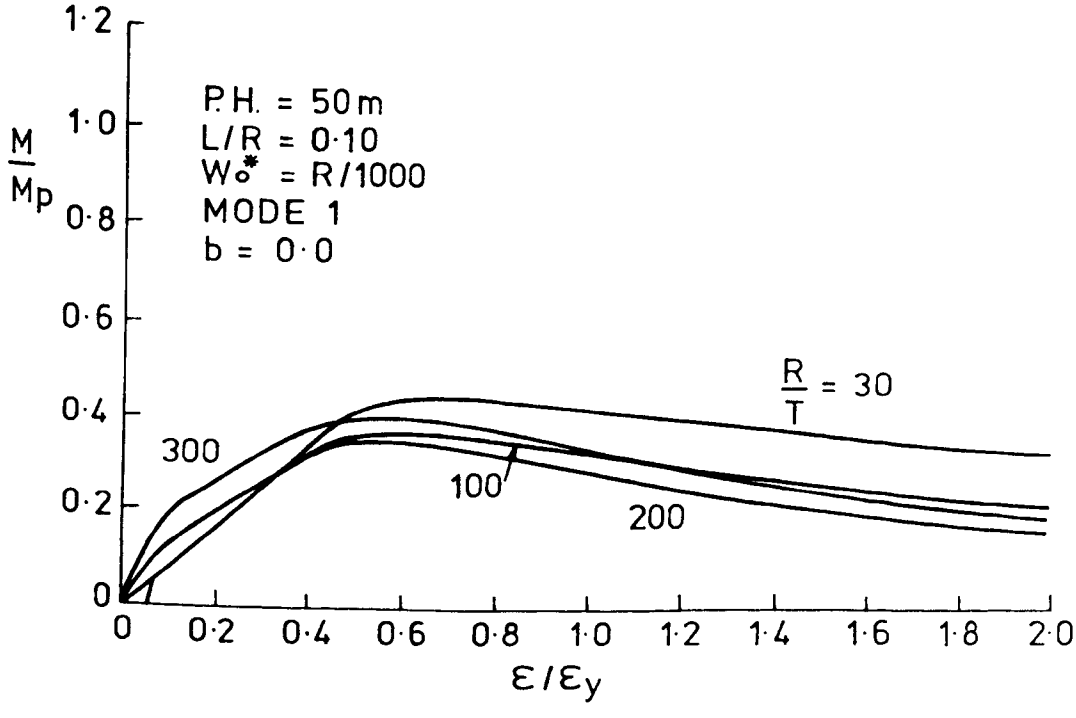

Fig. 6.125b

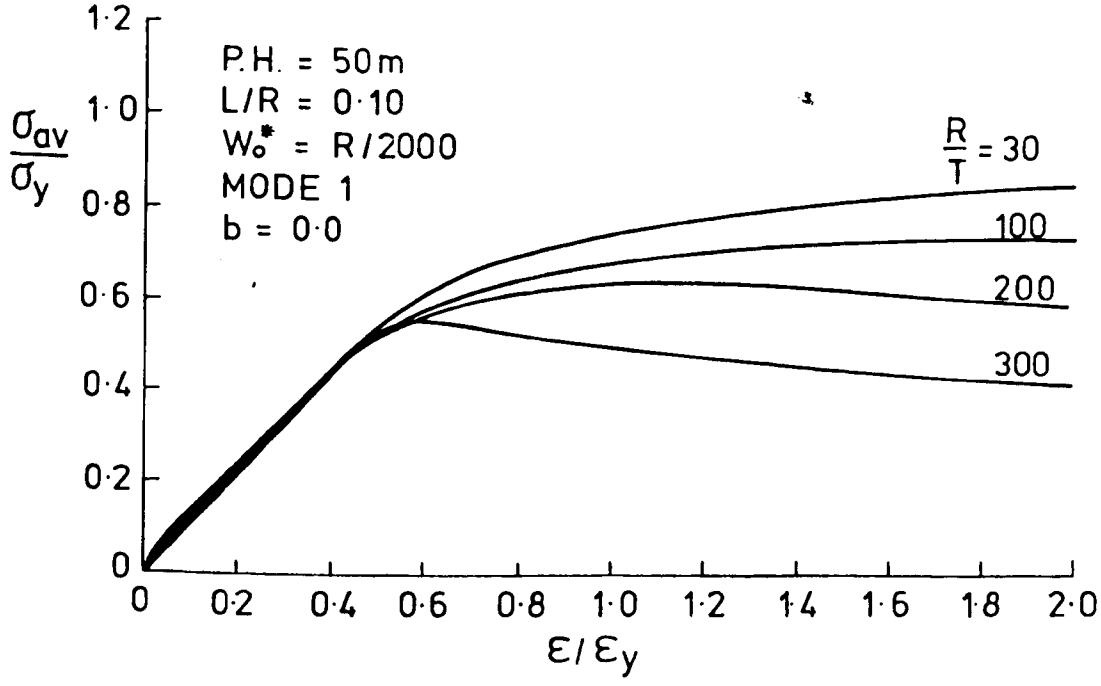

Fig. 6.126a

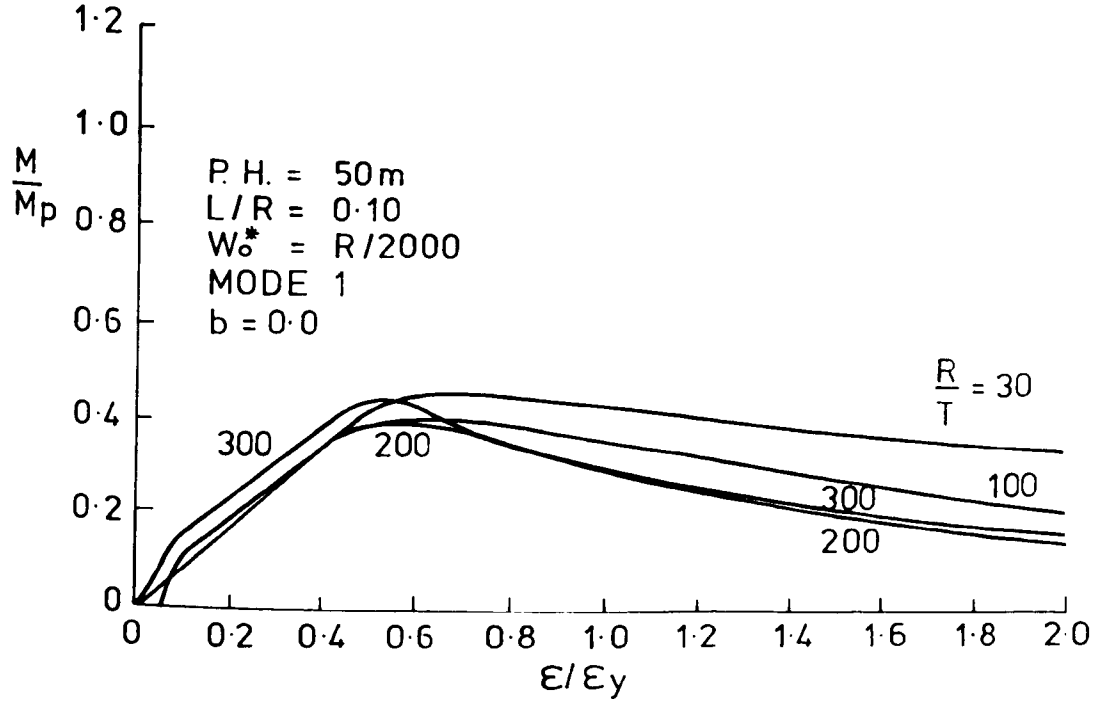

Fig. 6.126b

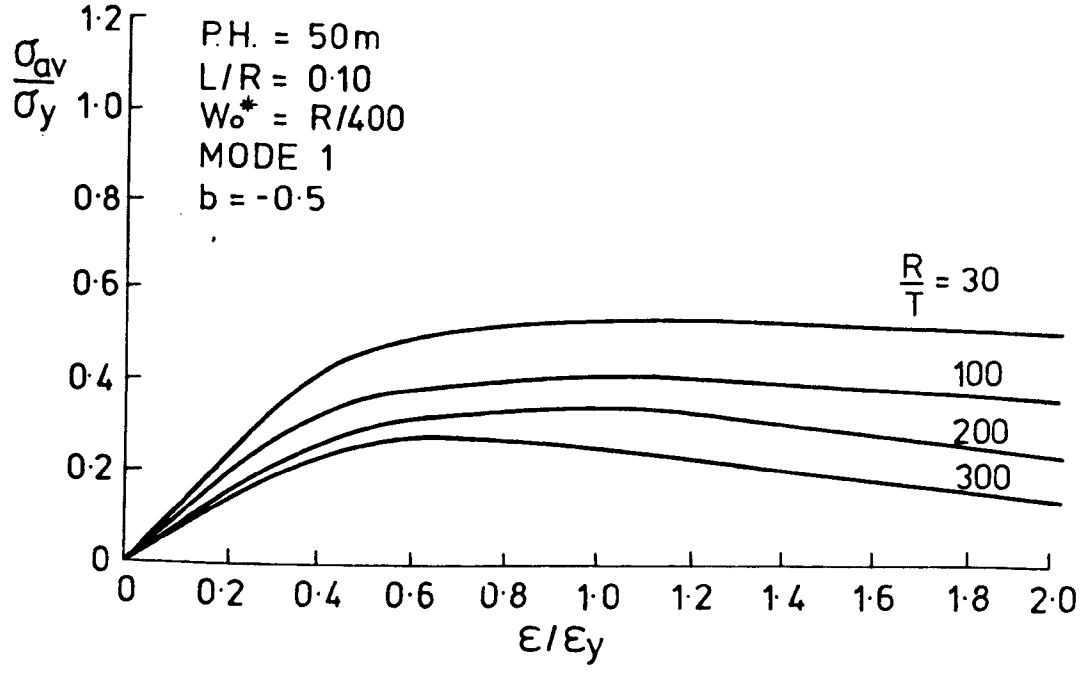

Fig. 6.127a

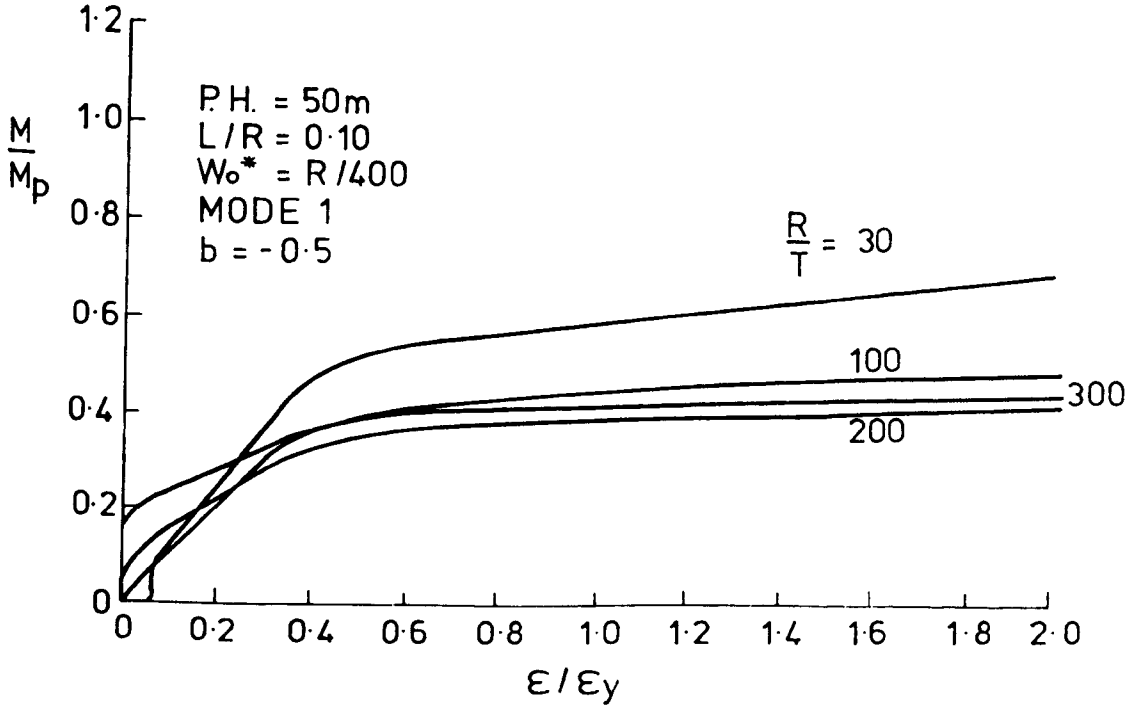

Fig. 6.127b

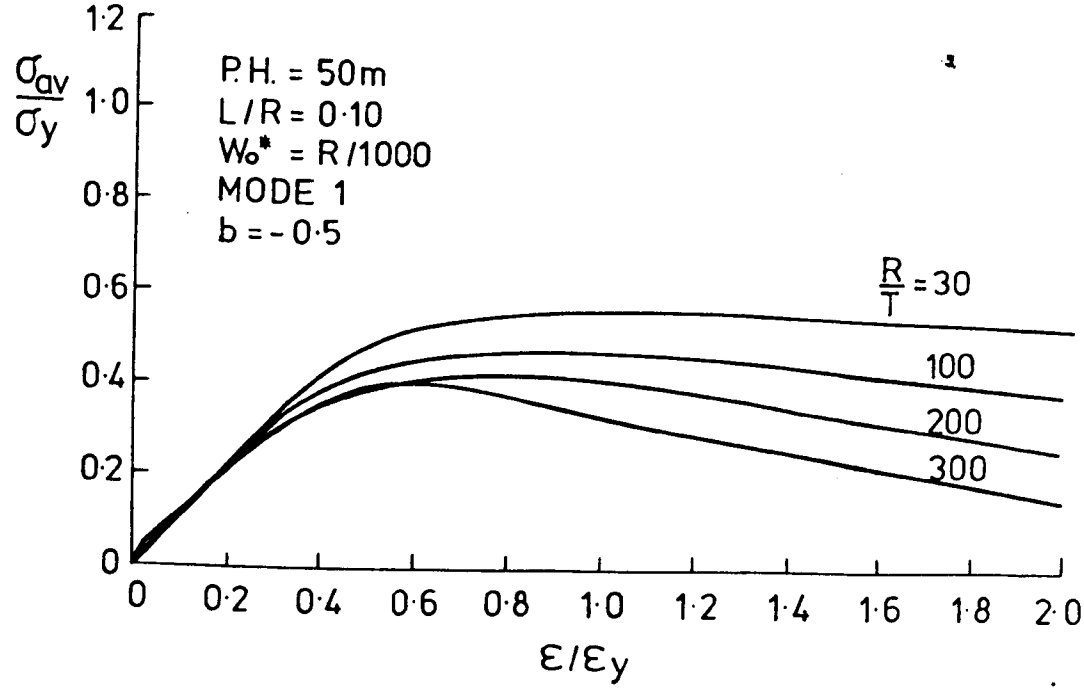

Fig. 6. 128a

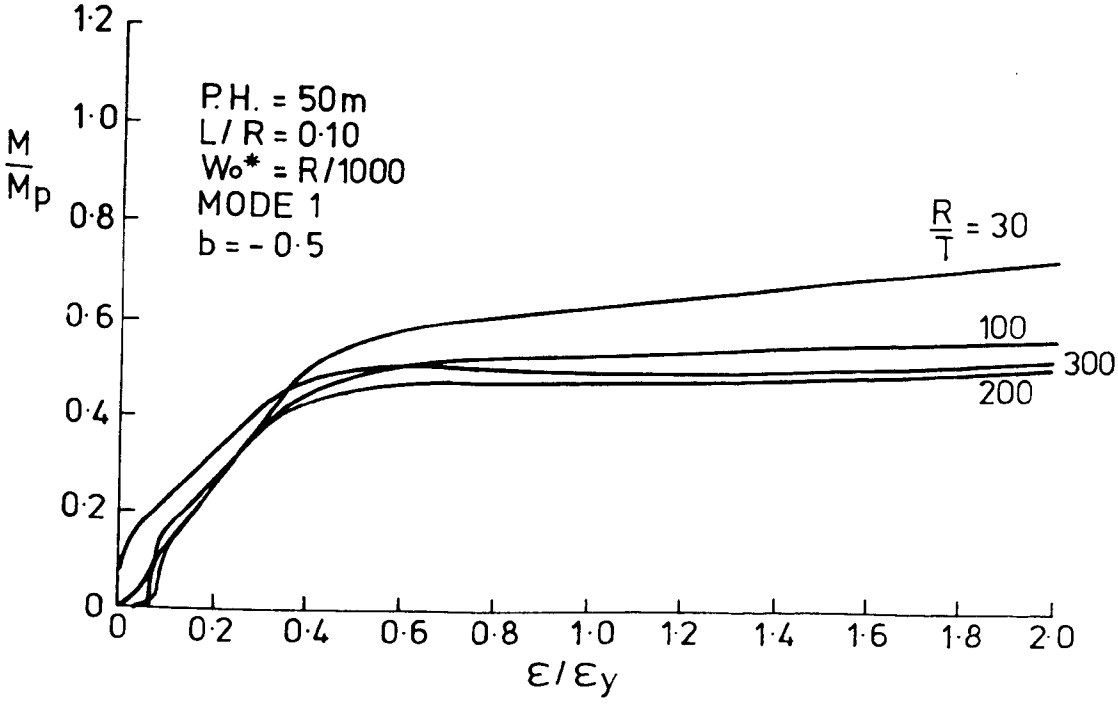

Fig. 6. 128b

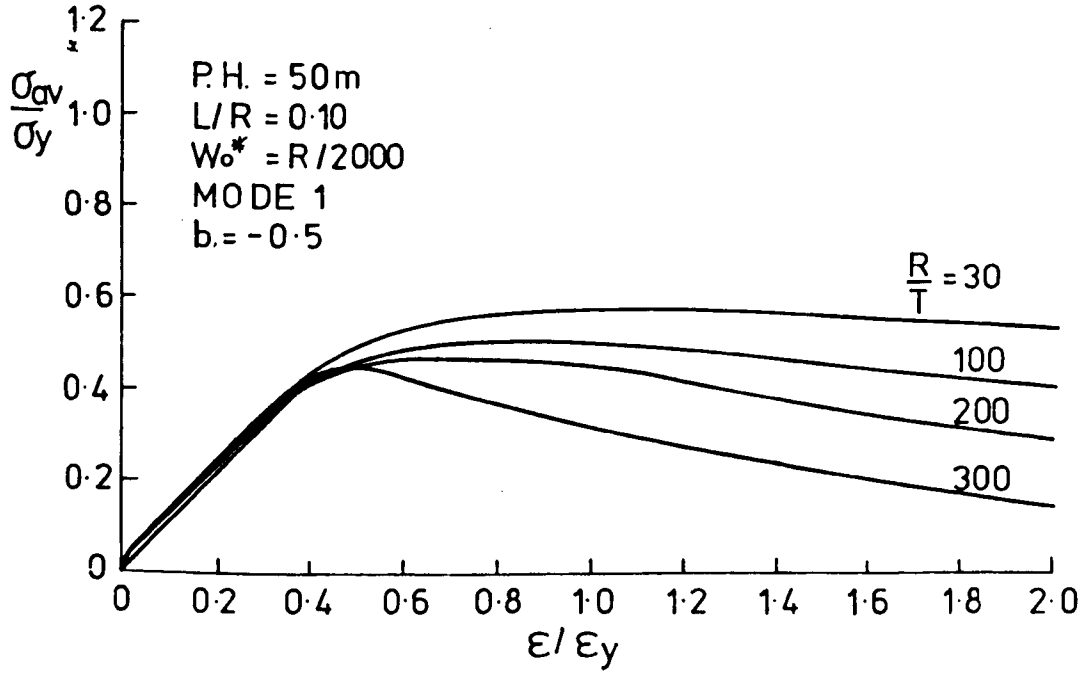

Fig. 6. 129a

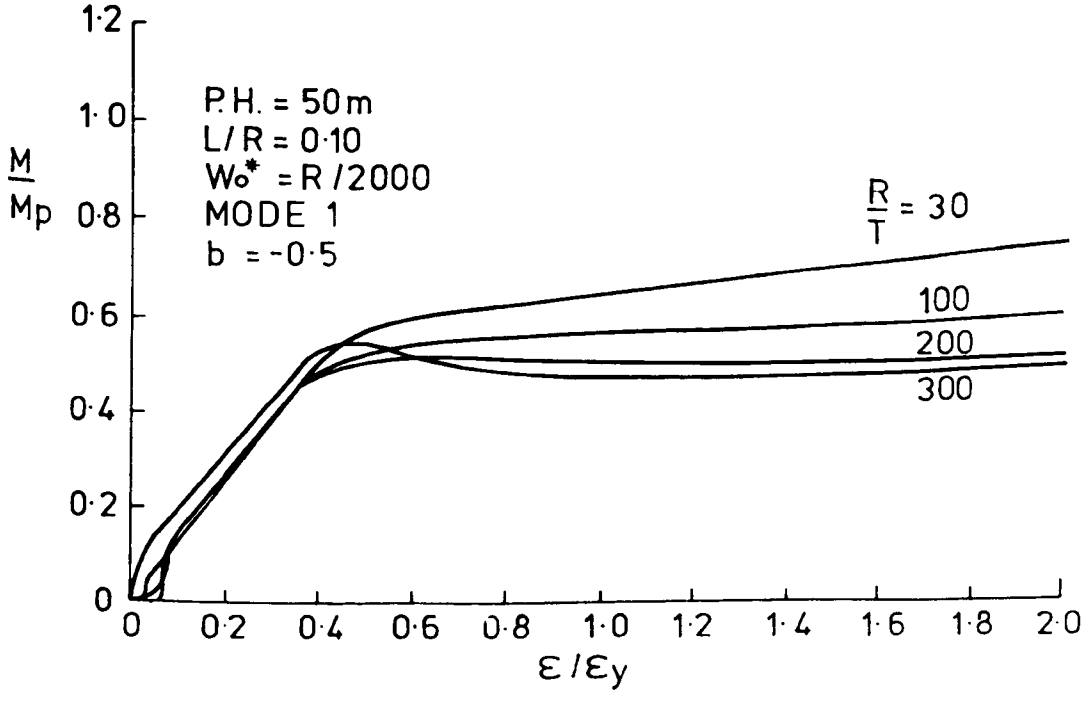

Fig. 6. 129b

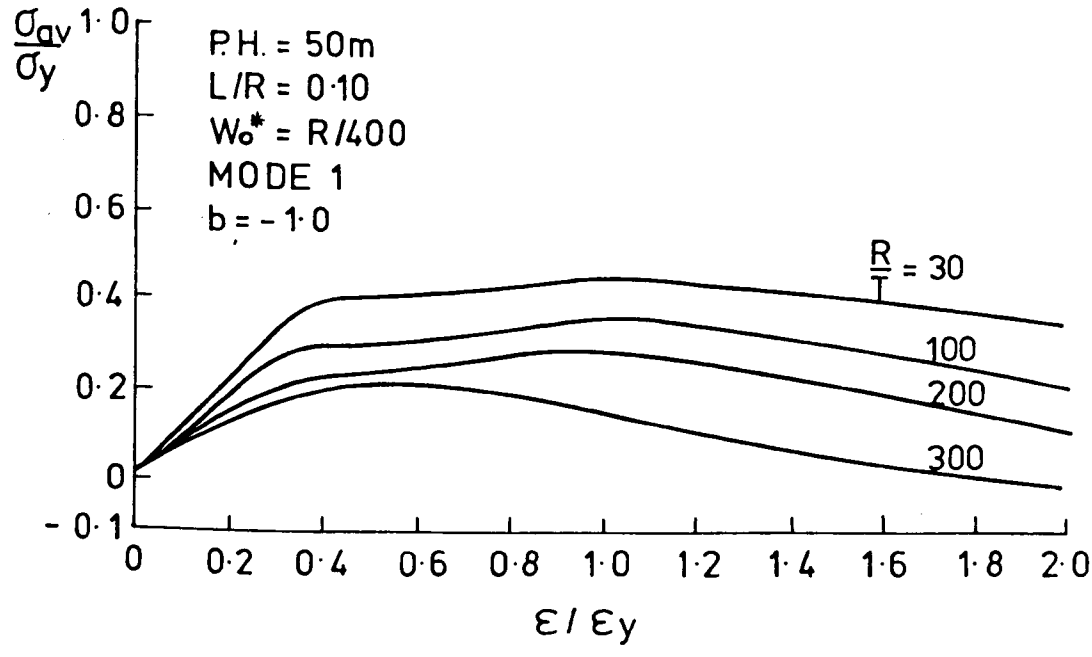

Fig. 6. 130a

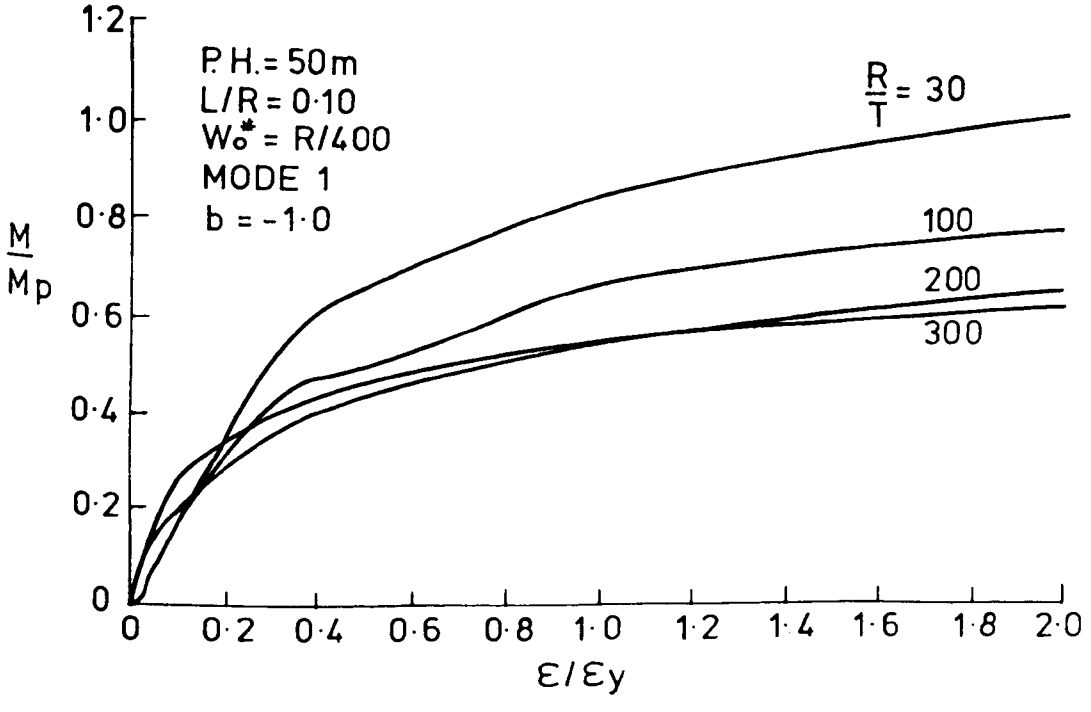

Fig. 6. 130b

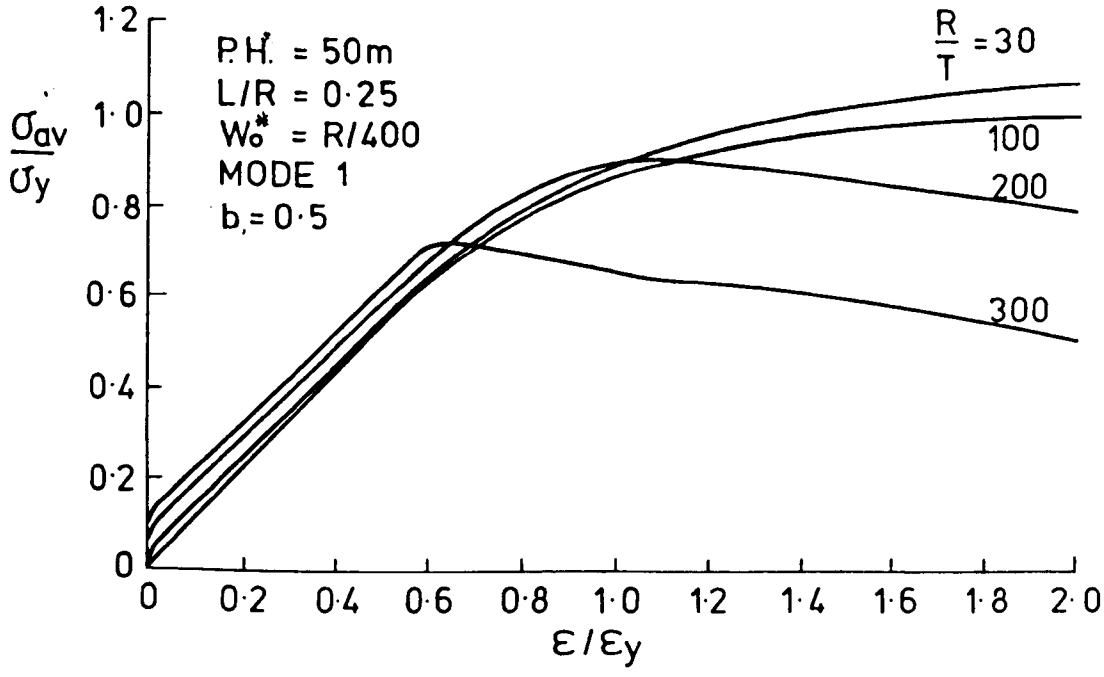

Fig.6. 131a

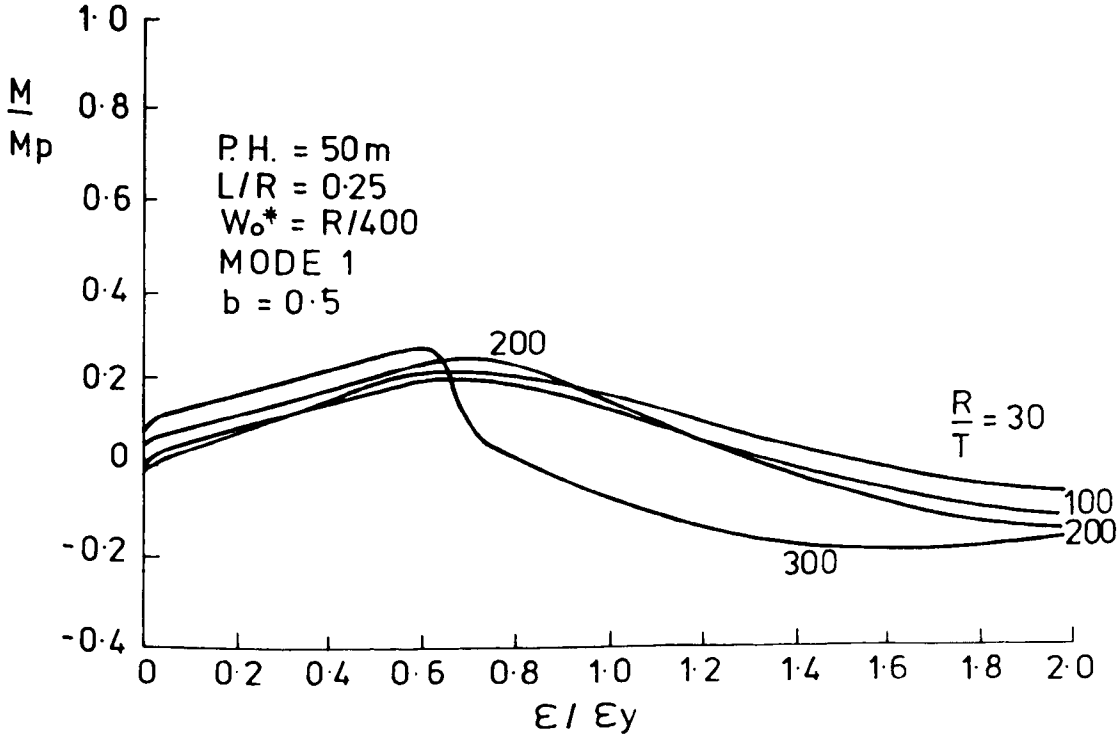

Fig. 6. 131b

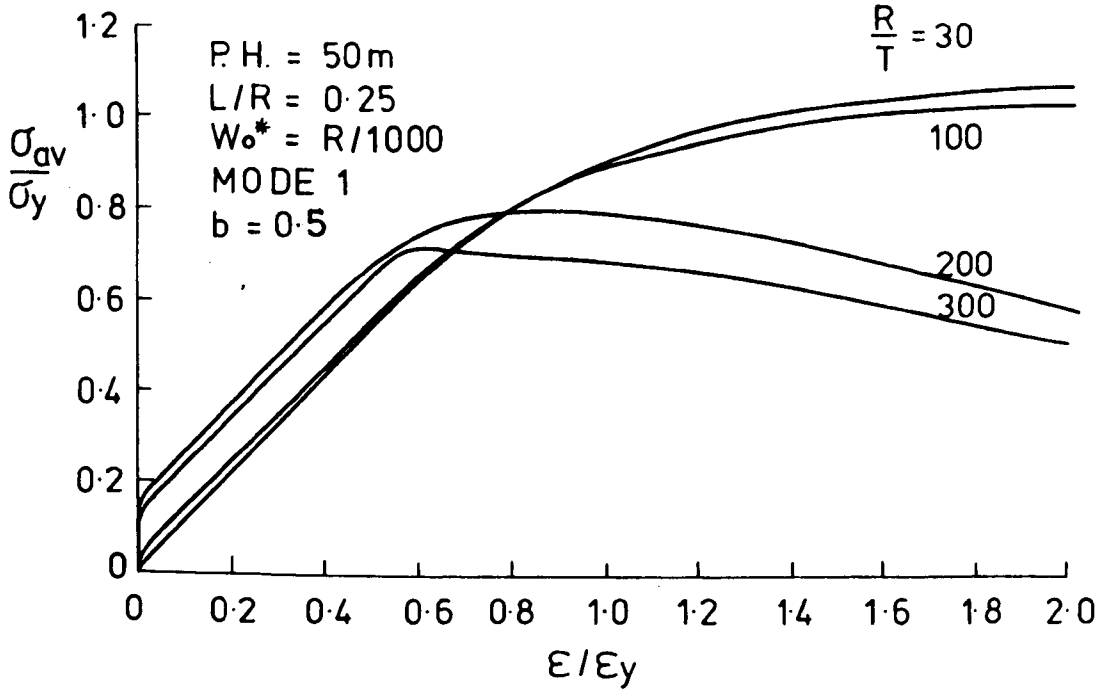

Fig. 6. 132a

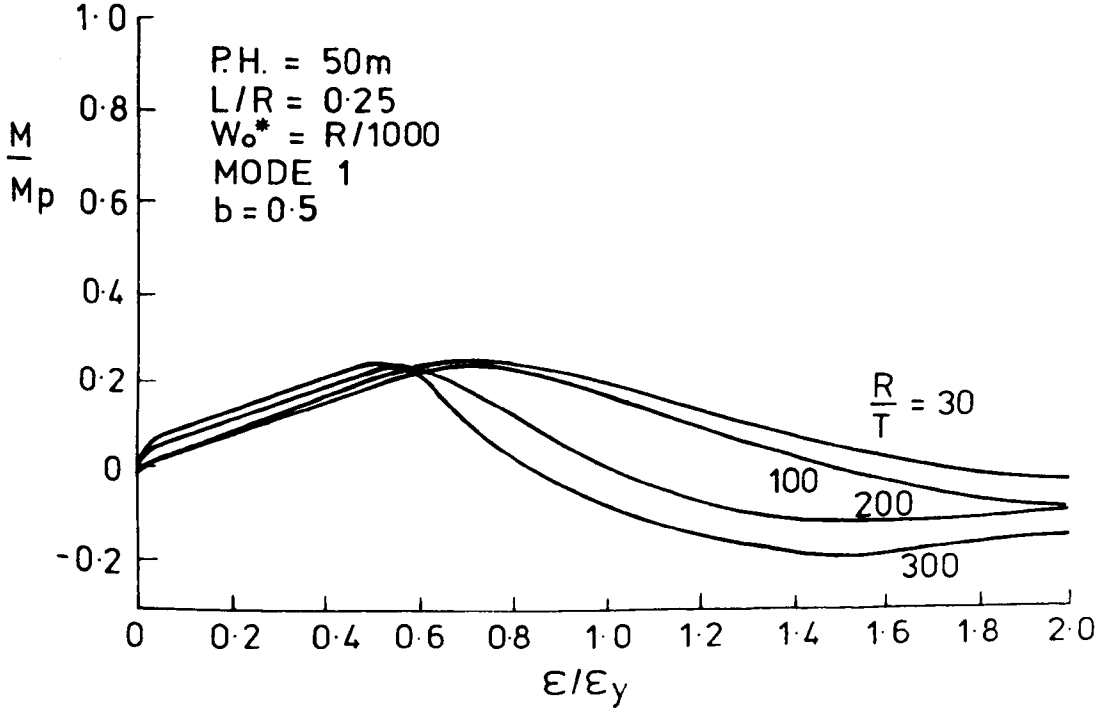

Fig. 6.132b

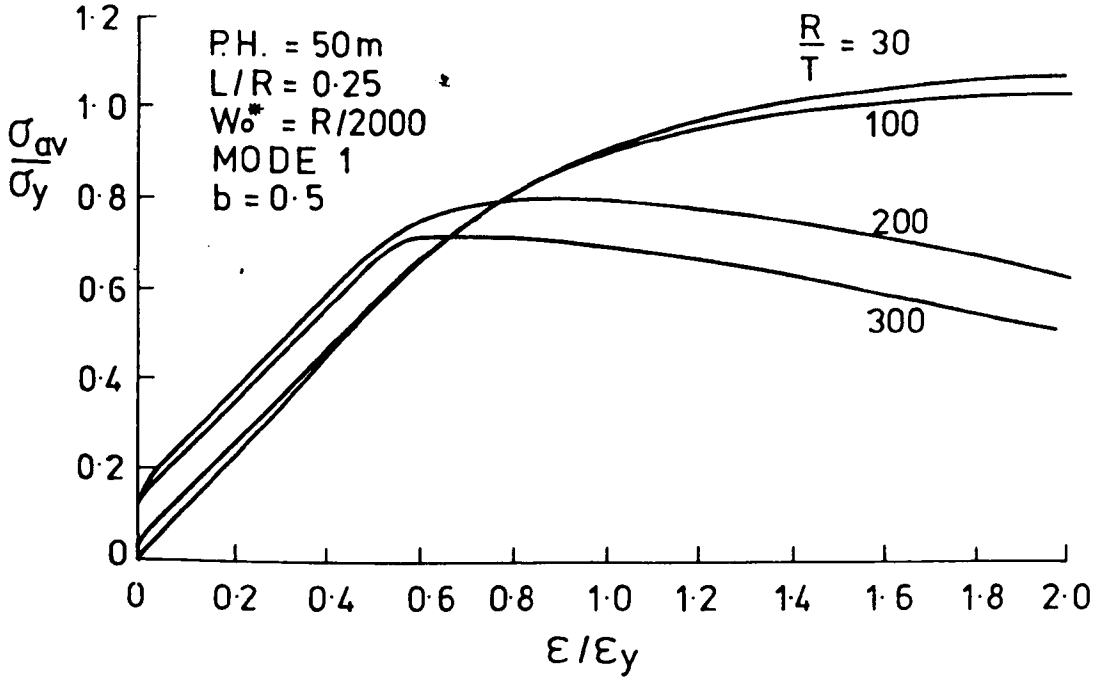

Fig. 6.133a

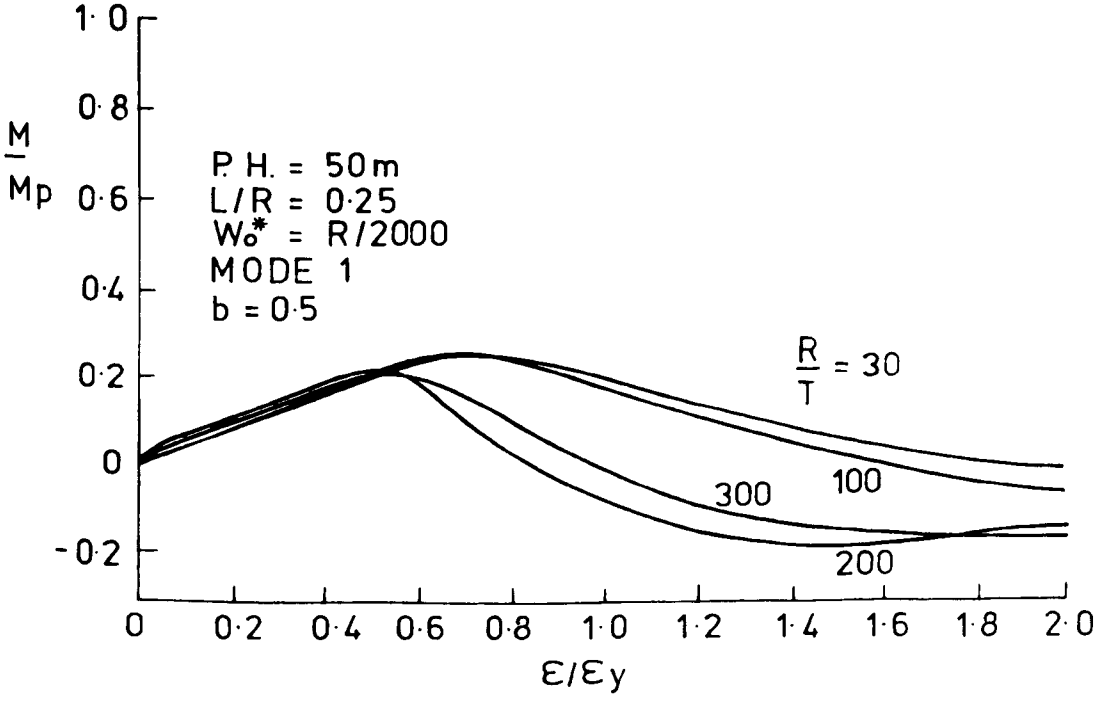

Fig. 6.133b

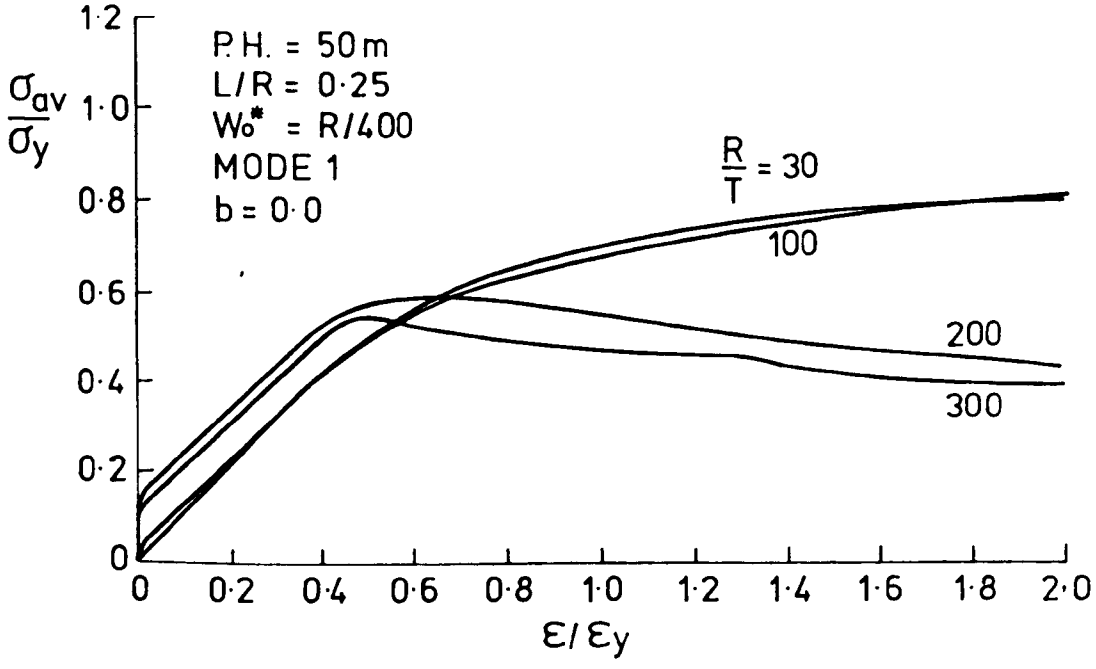

Fig. 6. 134a

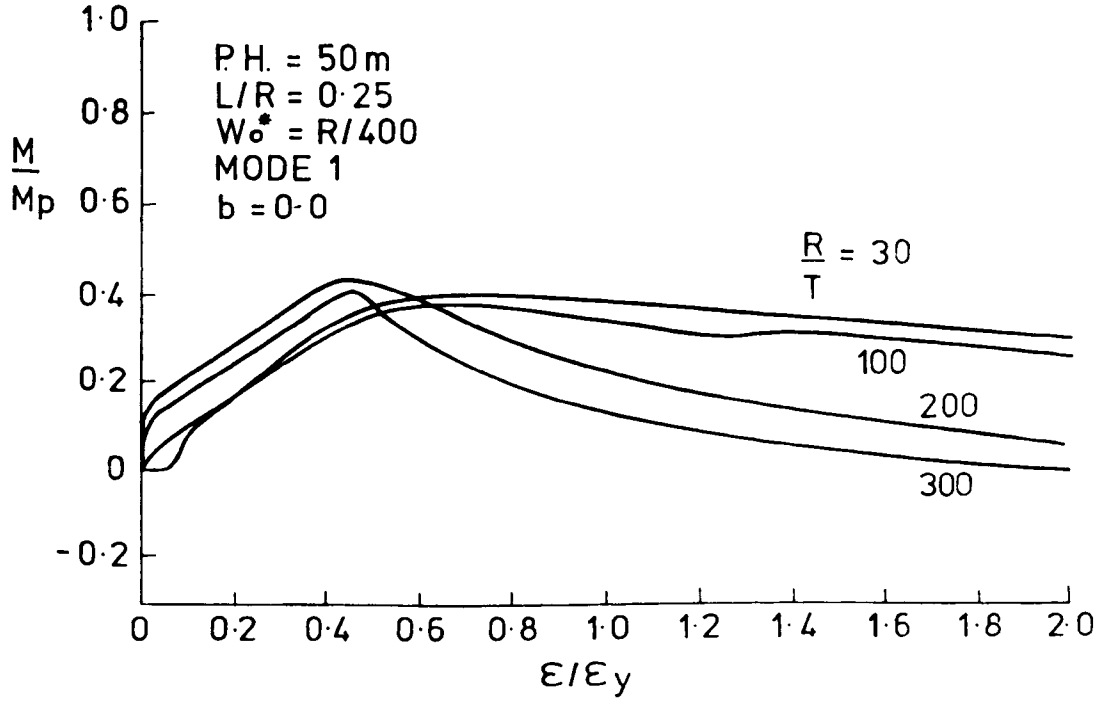

Fig. 6. 134b

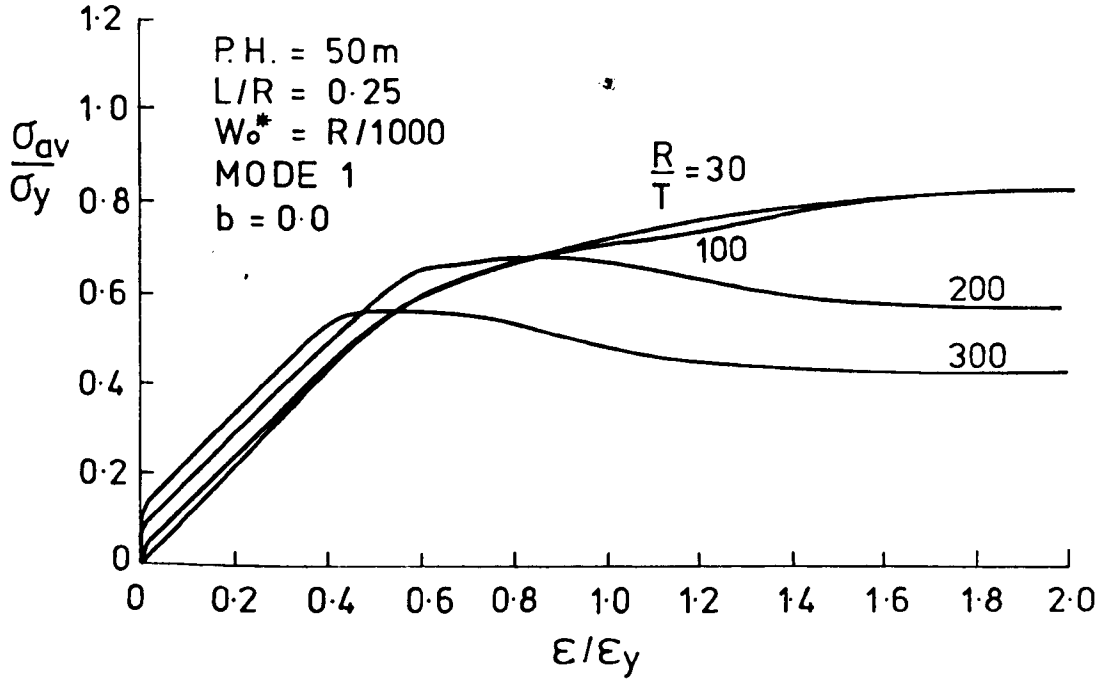

Fig.6.135a

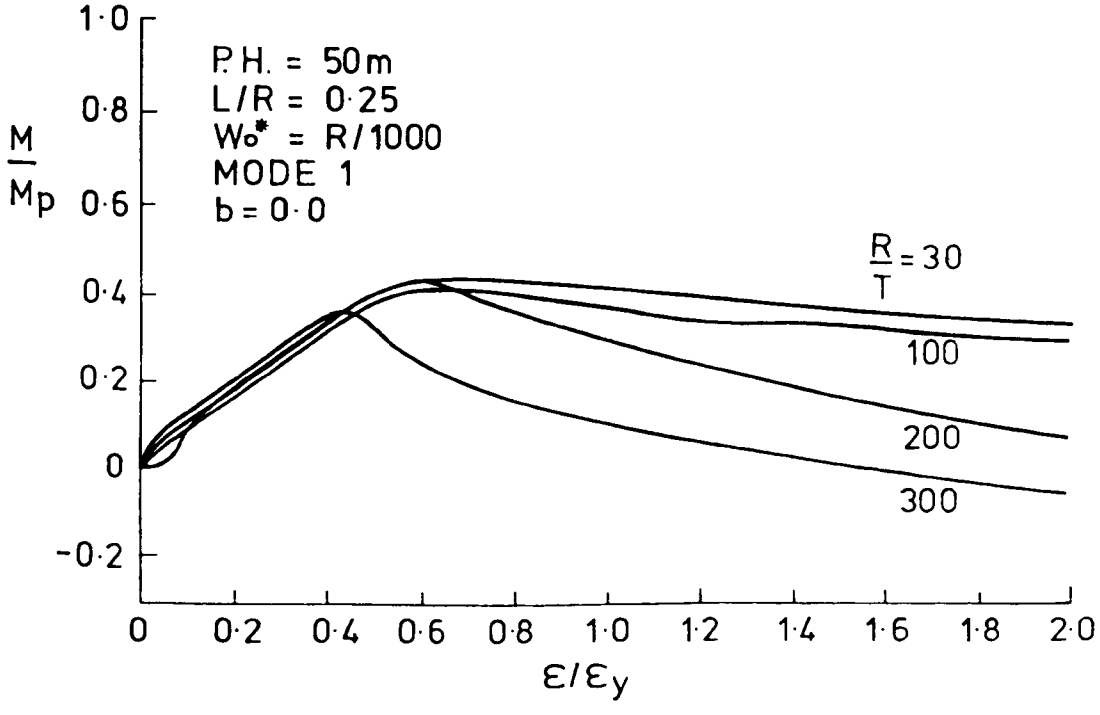

Fig. 6. 135b

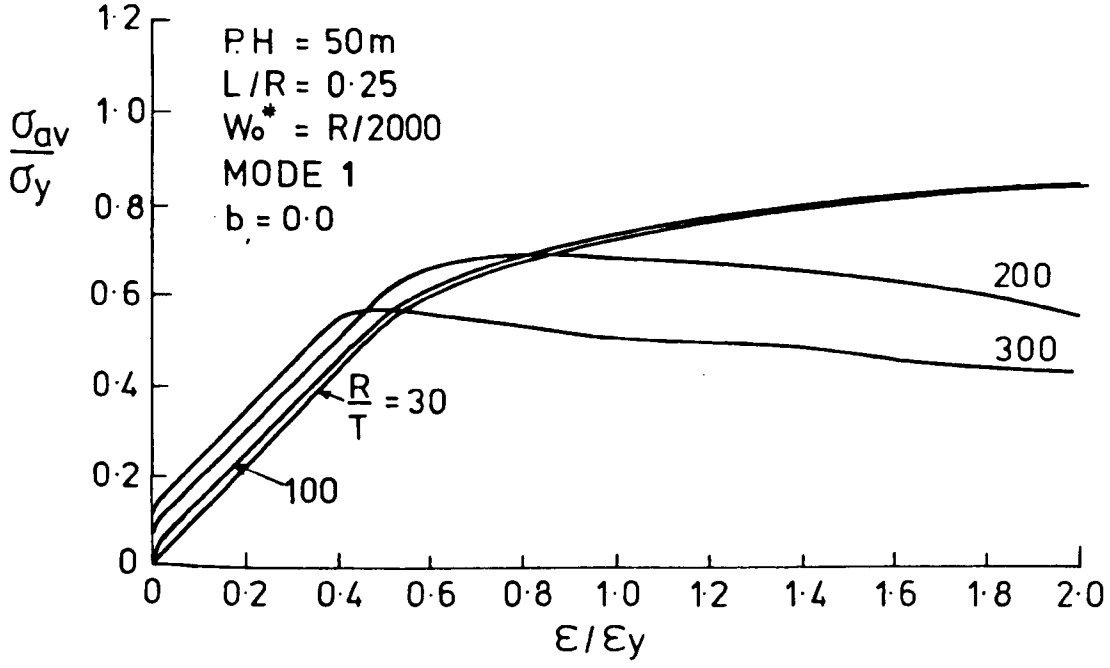

Fig. 6. 136a

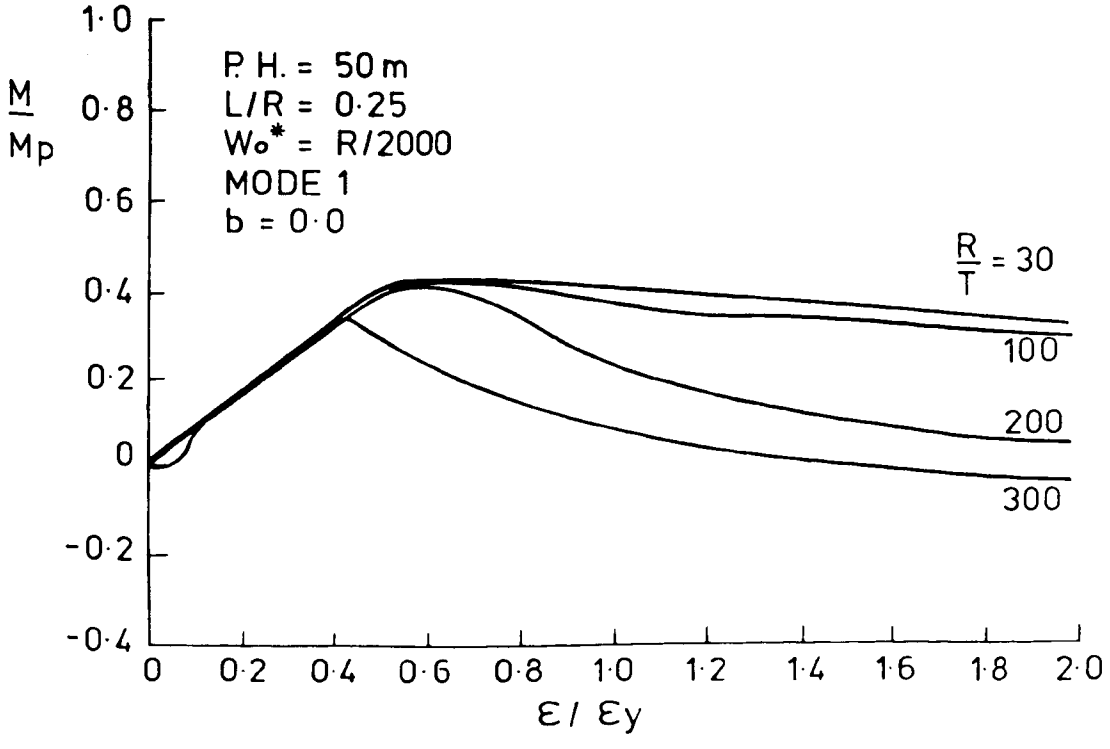

Fig. 6. 136b

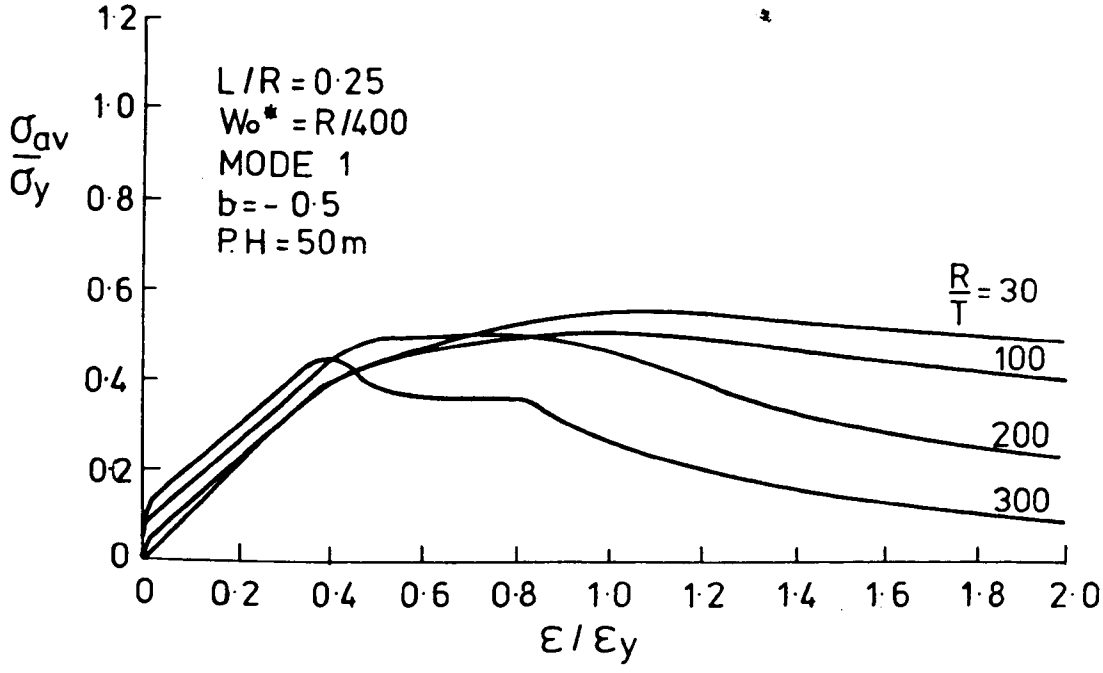

Fig. 6.137a

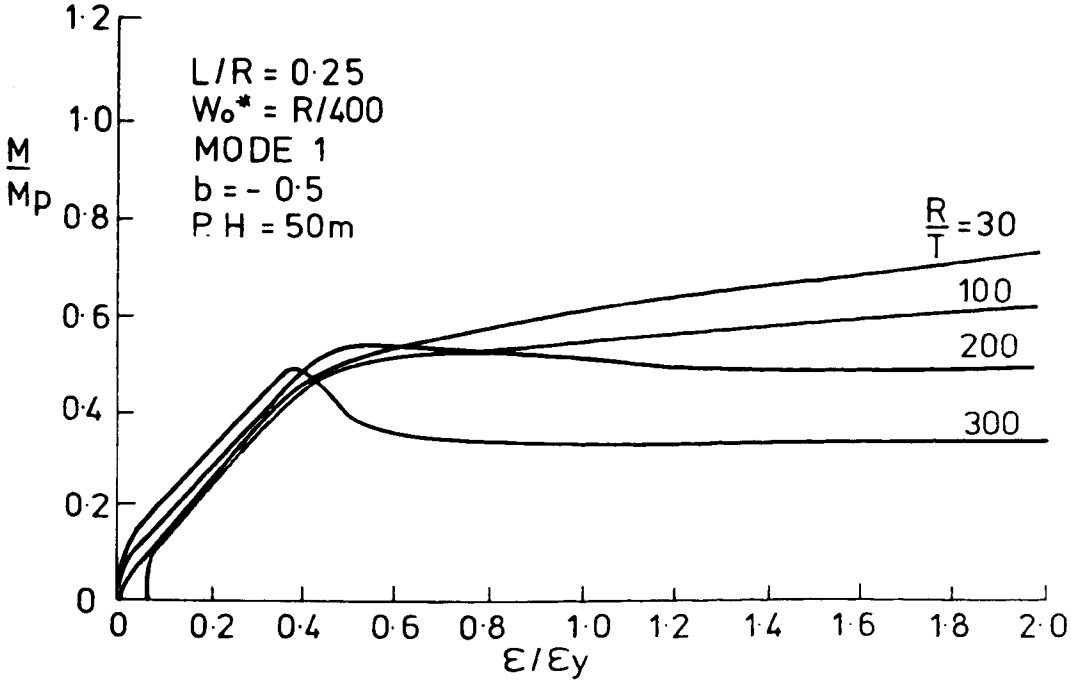

Fig. 6.137b

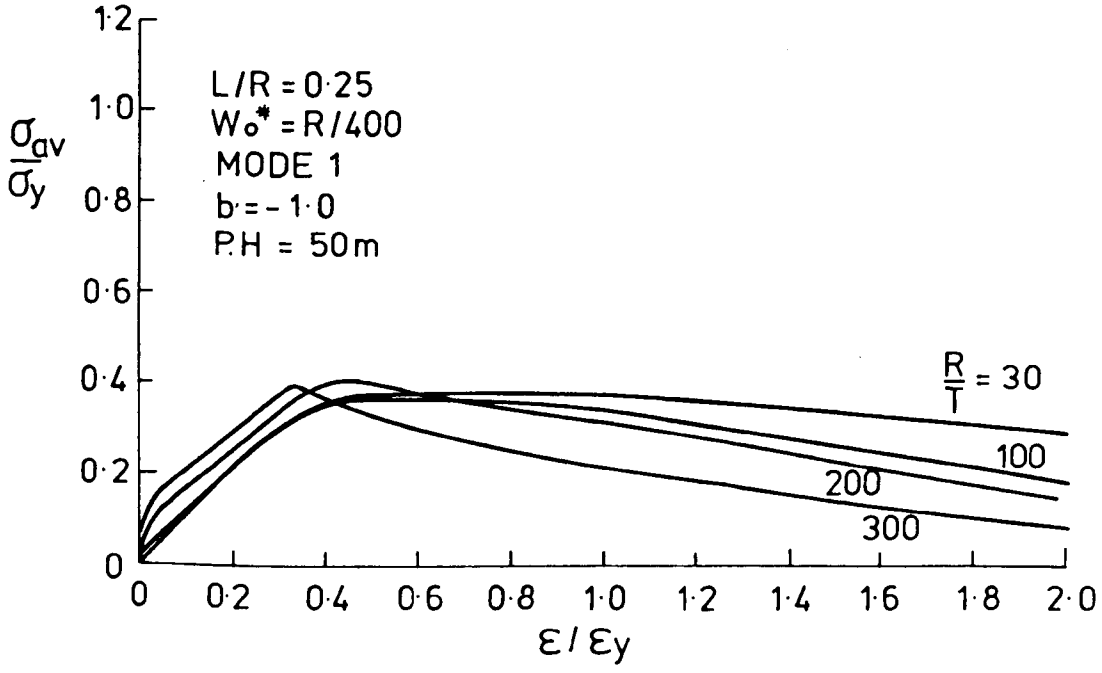

Fig. 6.138a

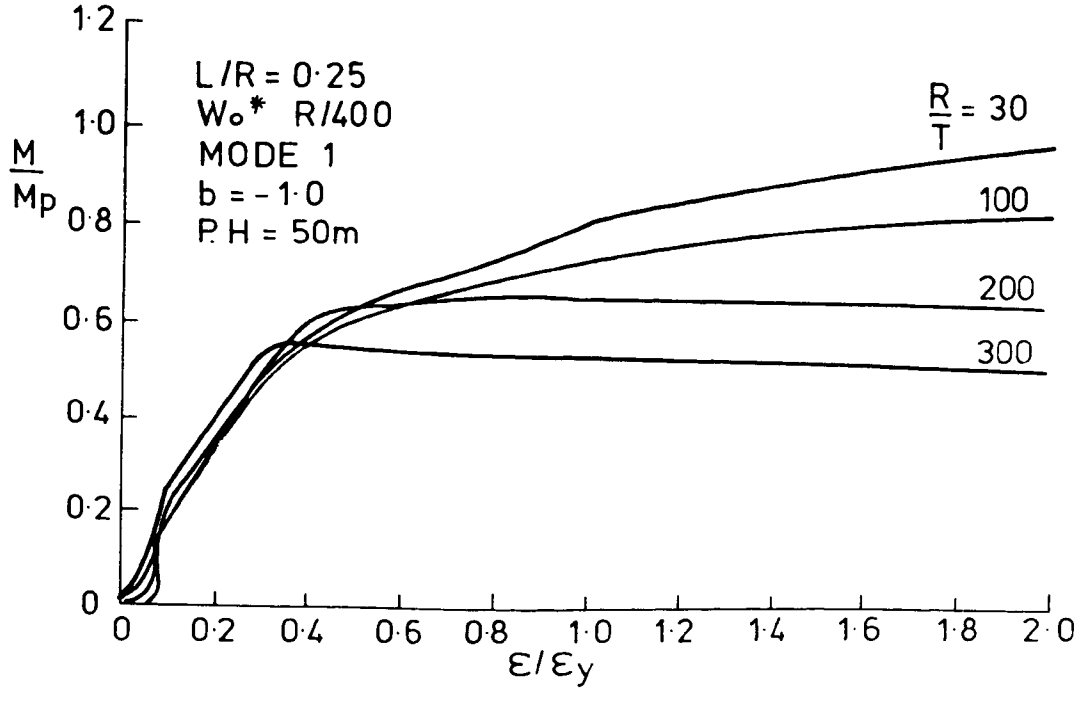

Fig. 6.138b

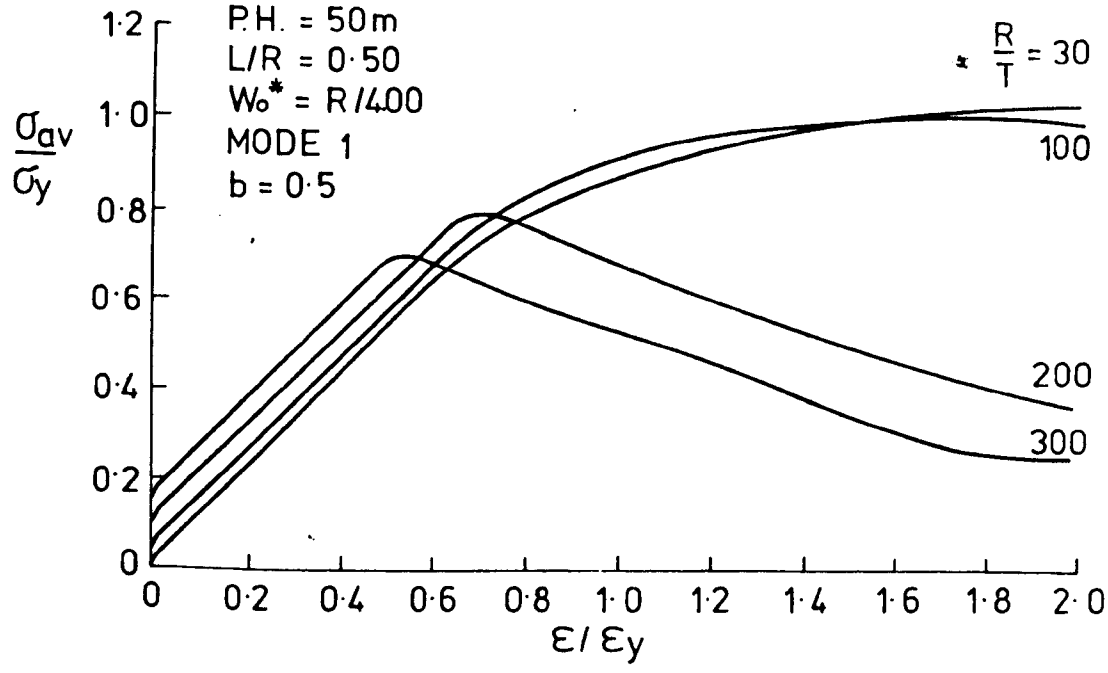

Fig. 6. 139a

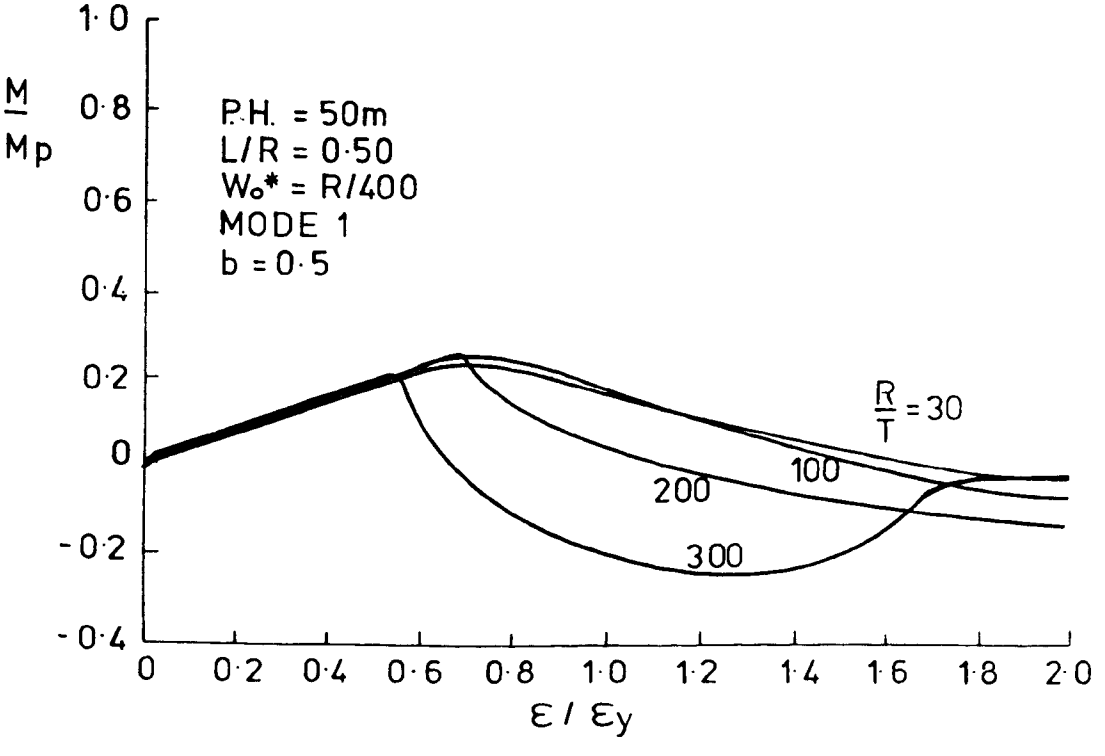

Fig.6. 139b

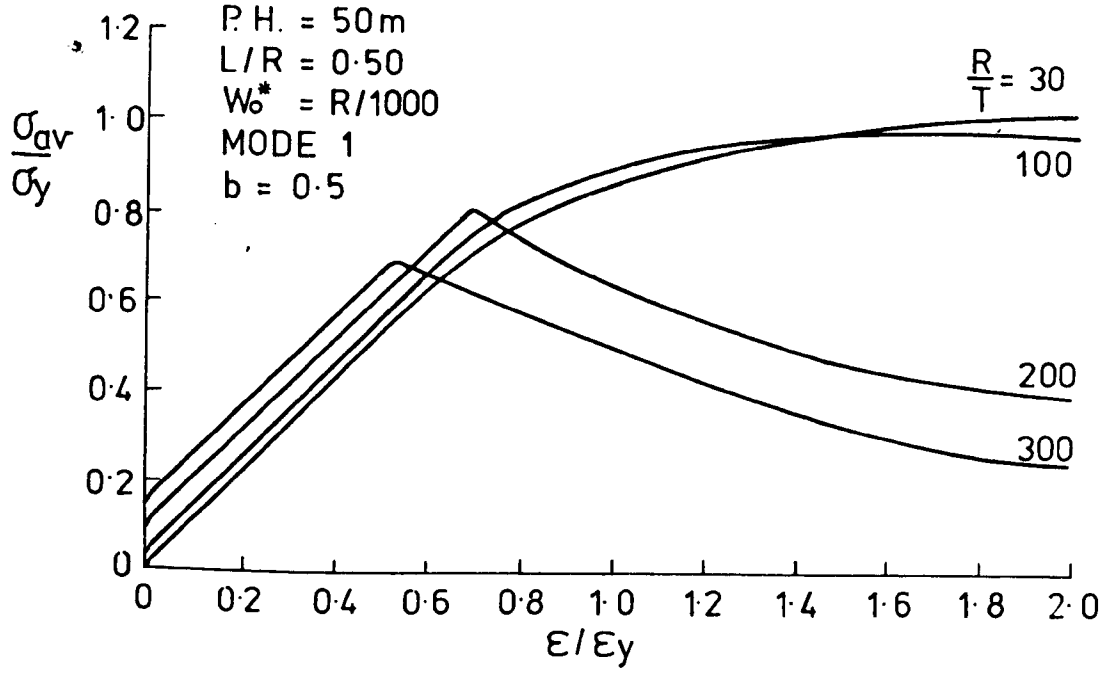

Fig. 6. 140a

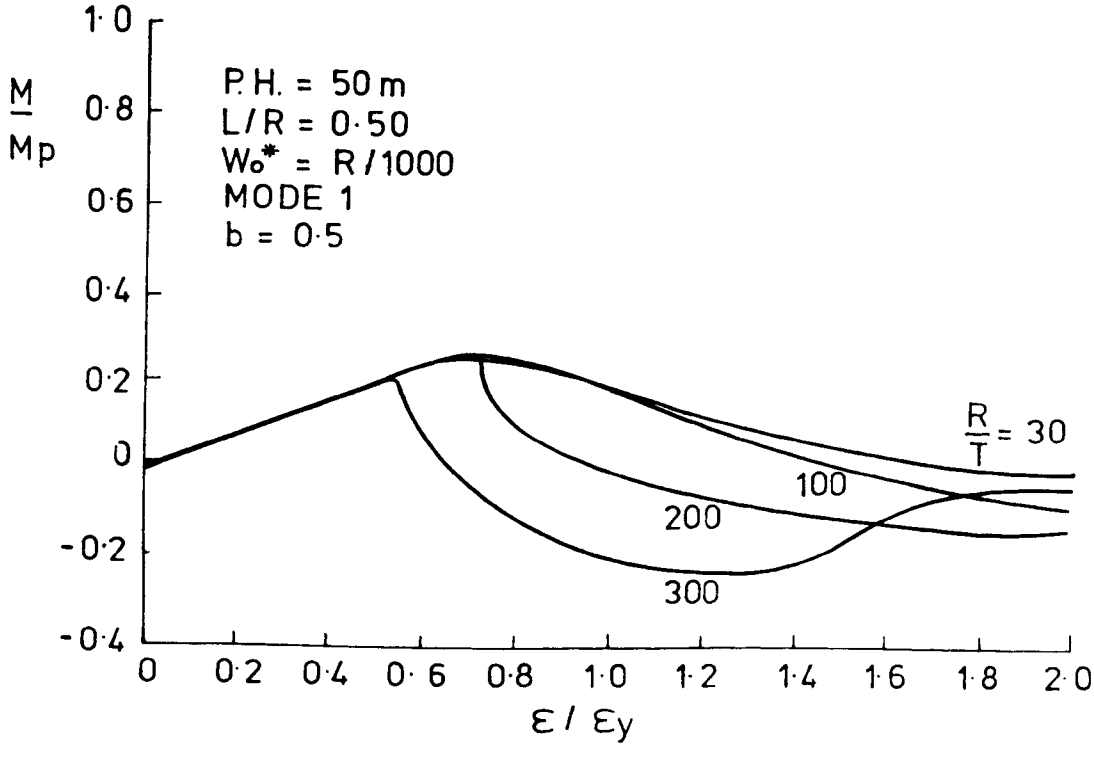

Fig. 6.140b

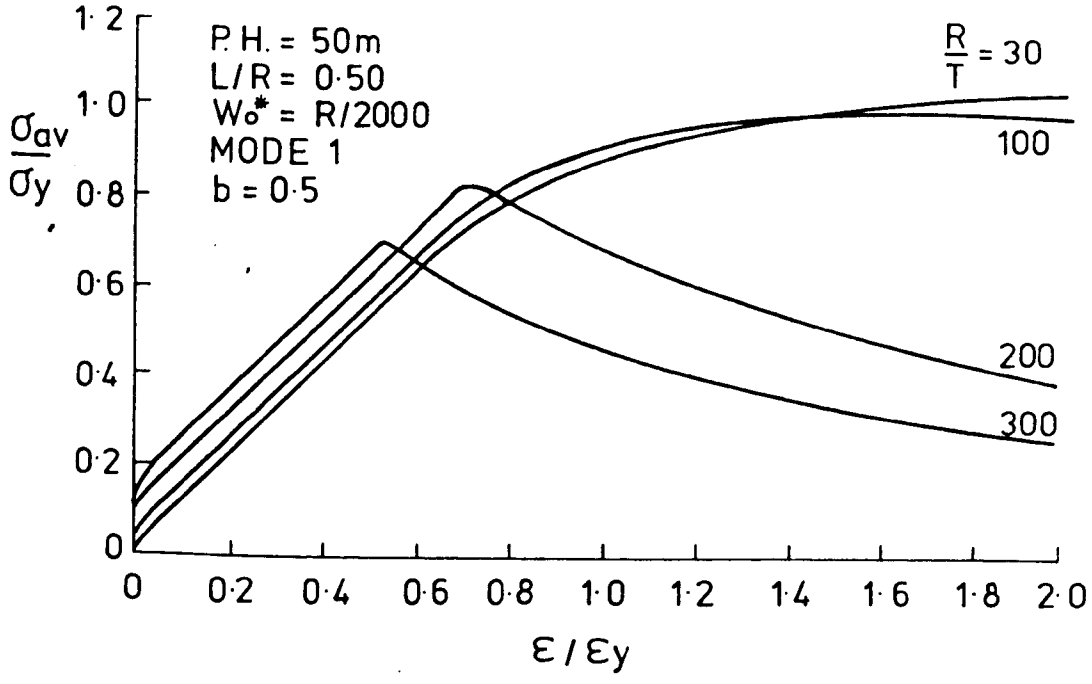

Fig. 6.141a

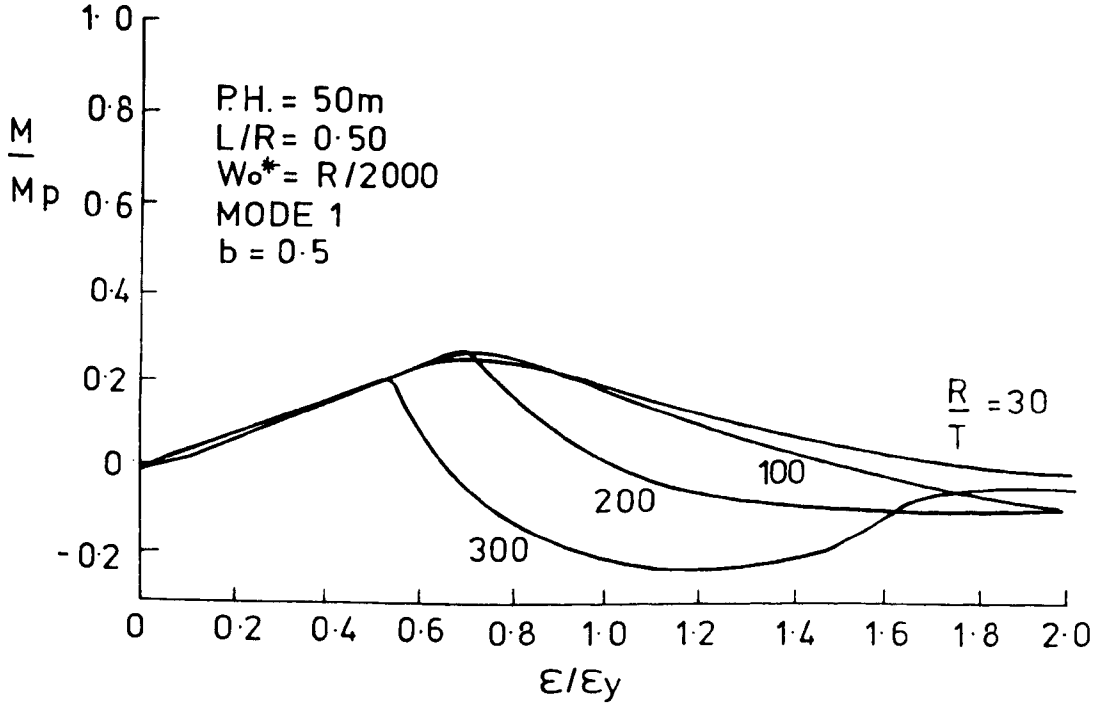

Fig. 6.141b

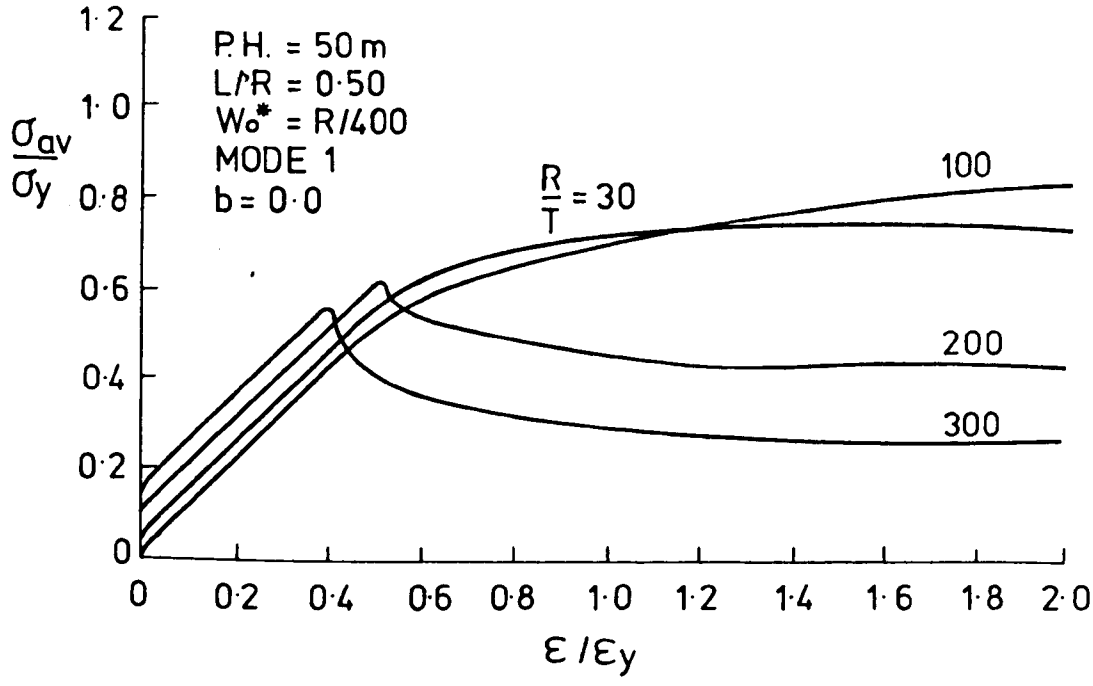

Fig. 6. 142a

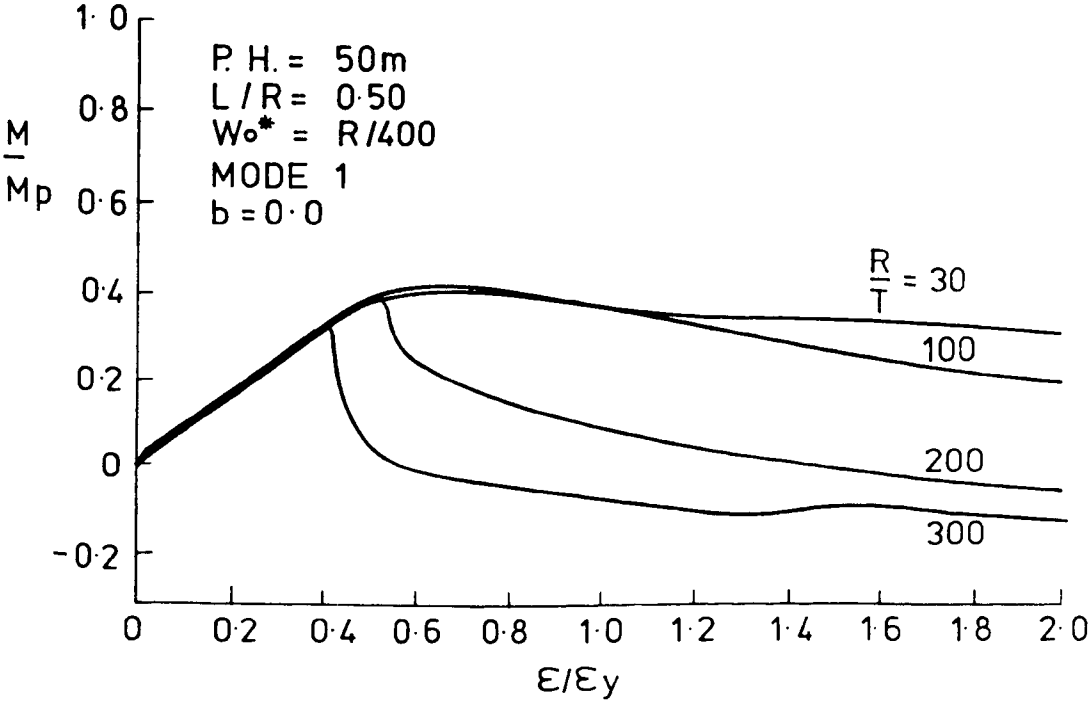

Fig. 6. 142b

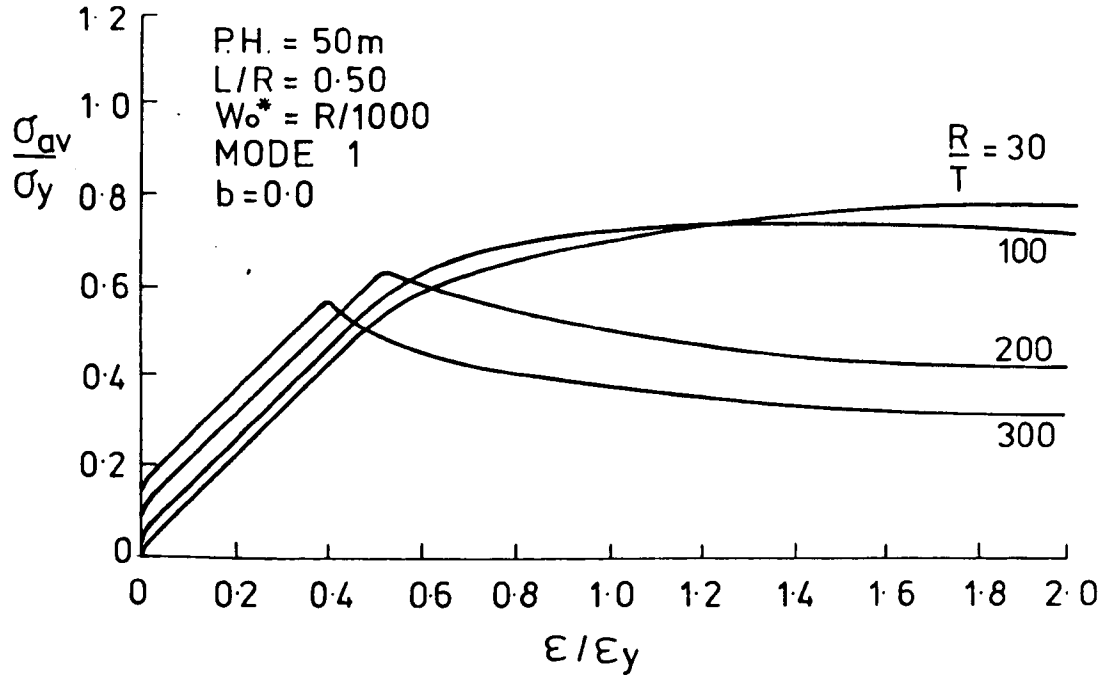

Fig. 6.143a

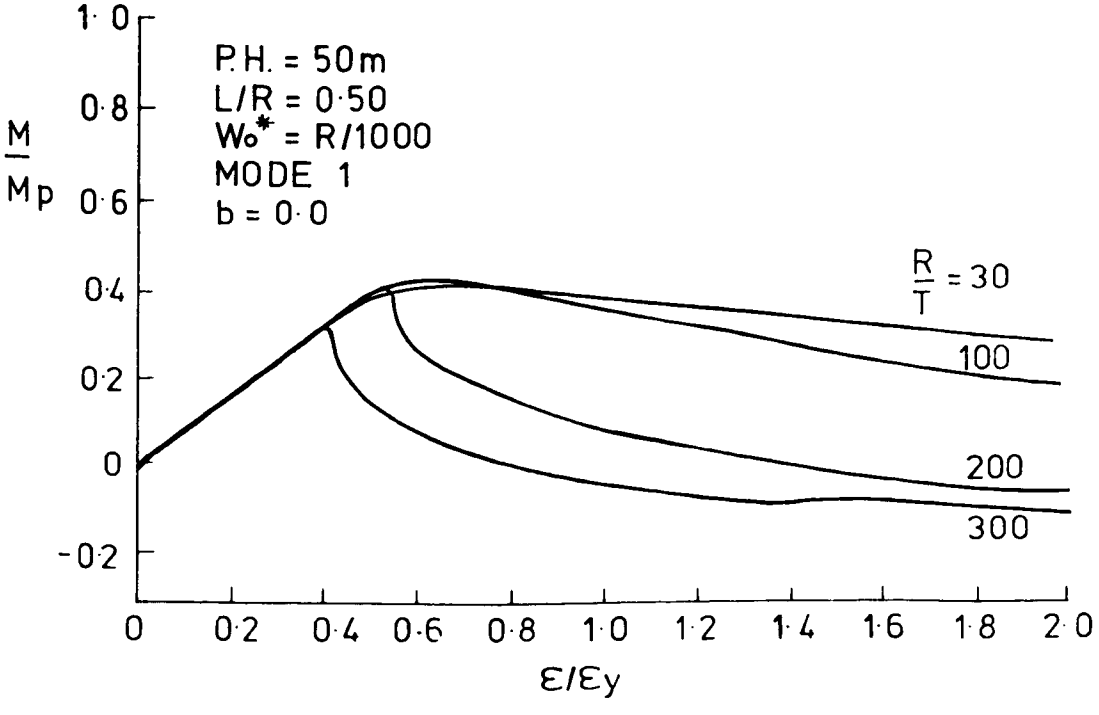

Fig. 6.143b

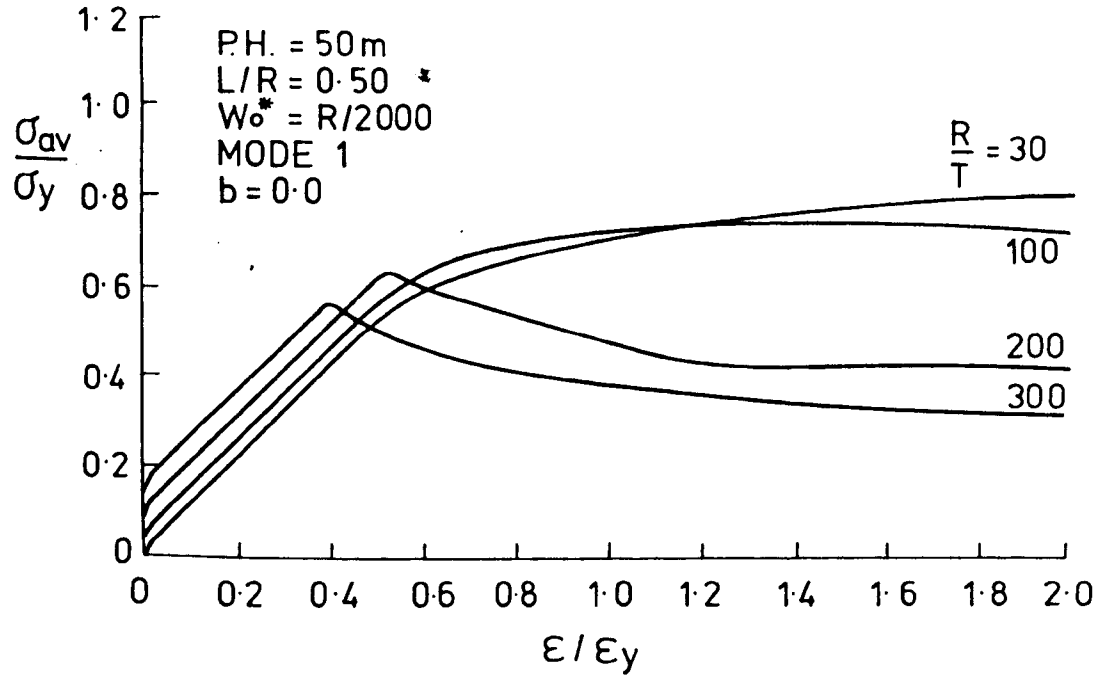

Fig. 6. 144a

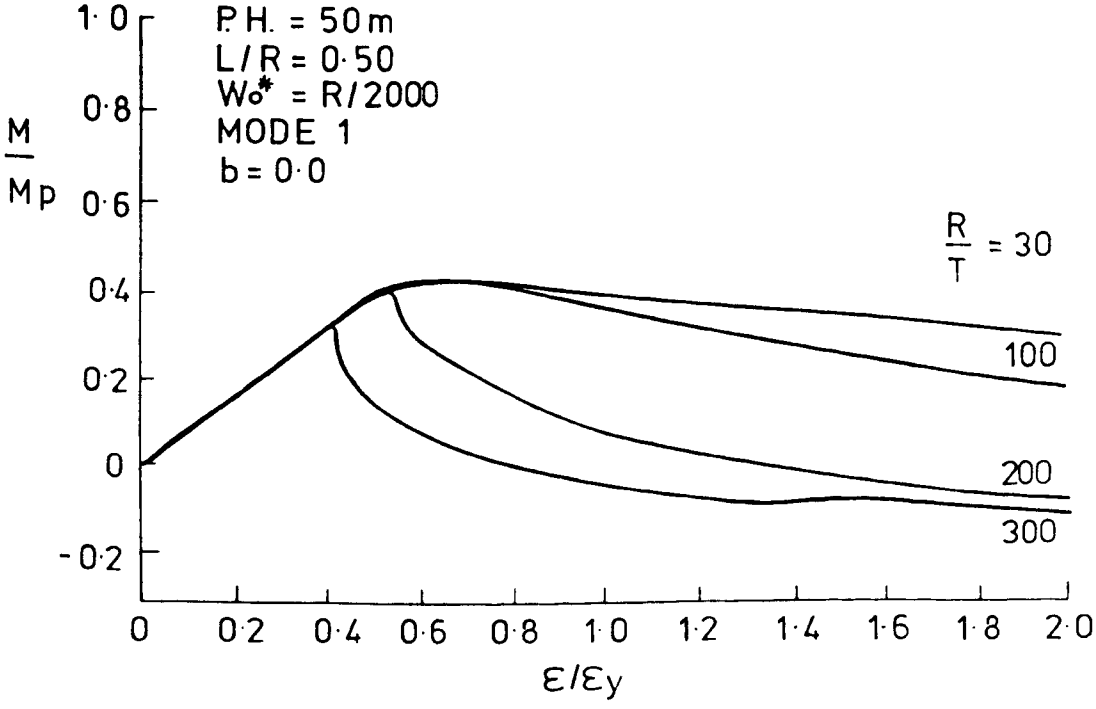

Fig. 6. 144b

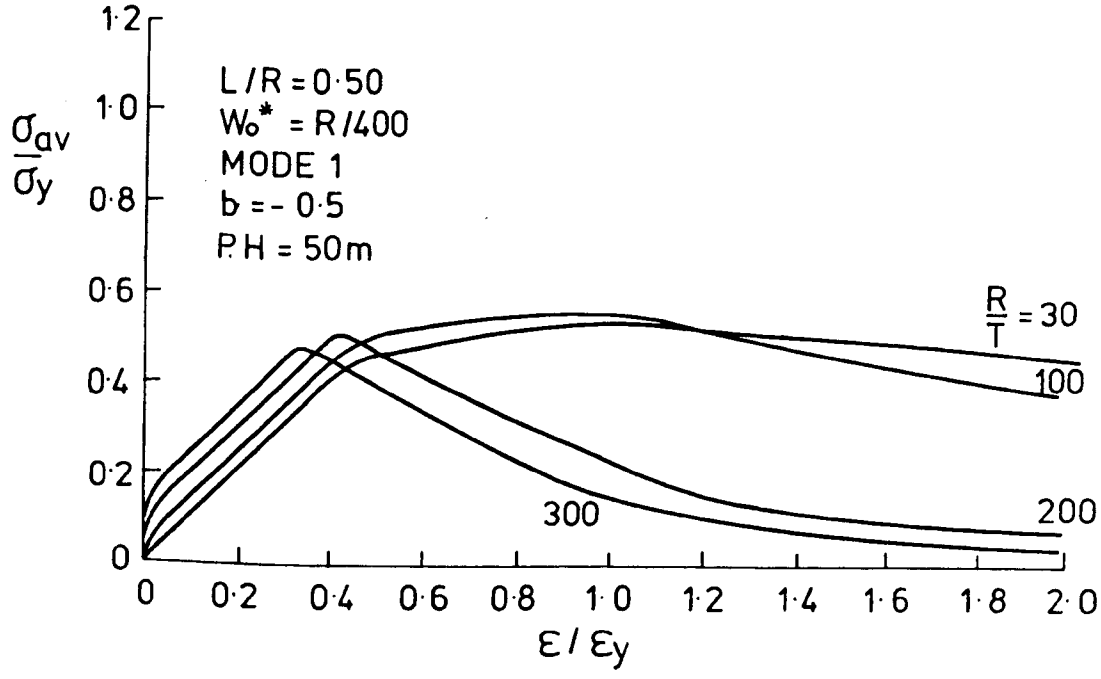

Fig. 6.145a

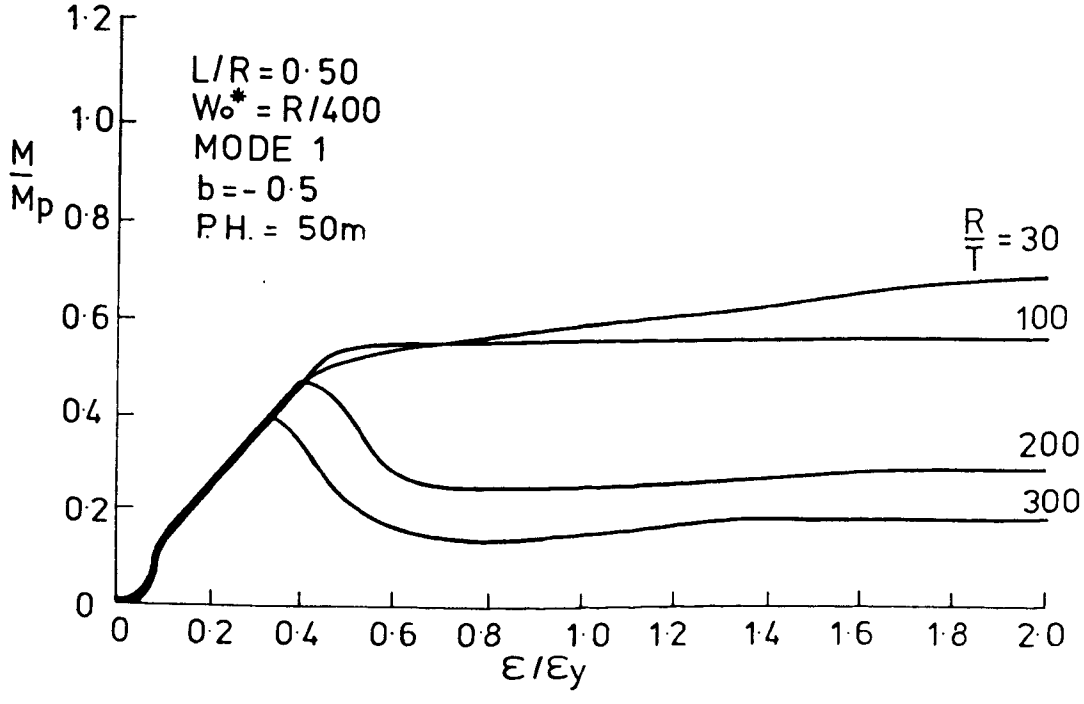

Fig. 6. 145b

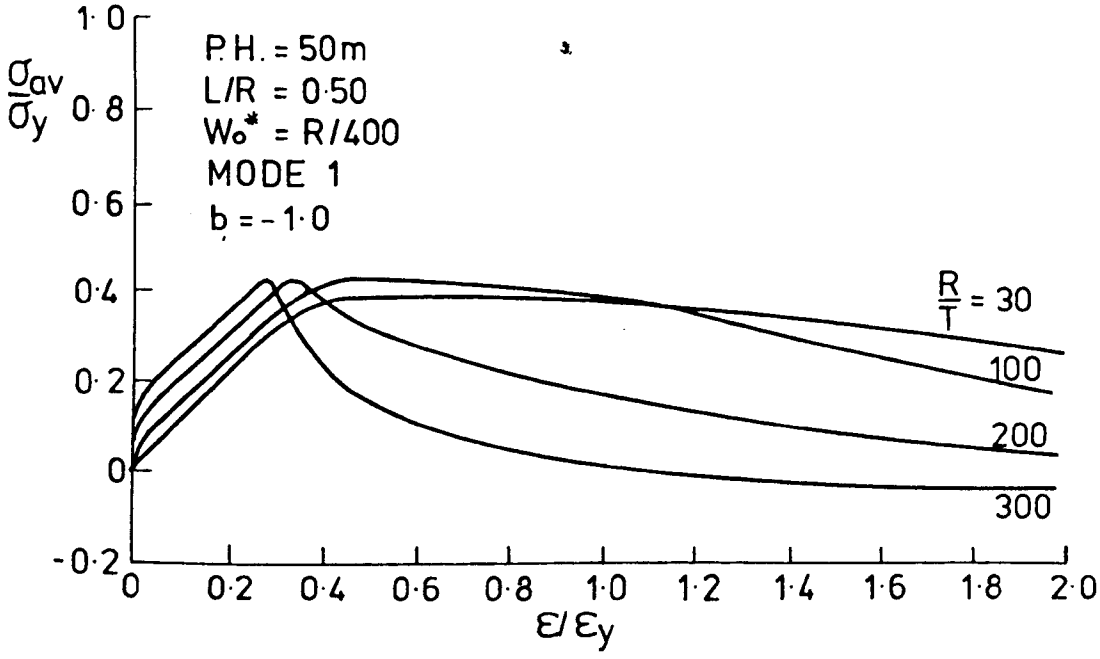

Fig. 6.146a

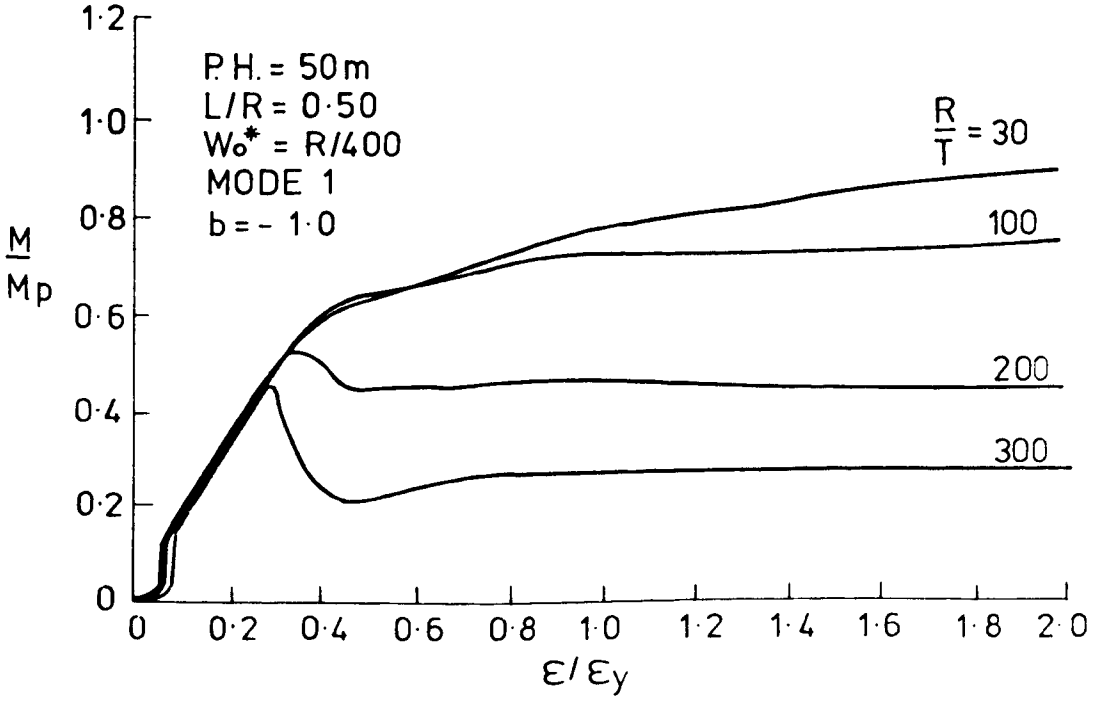

Fig. 6.146b

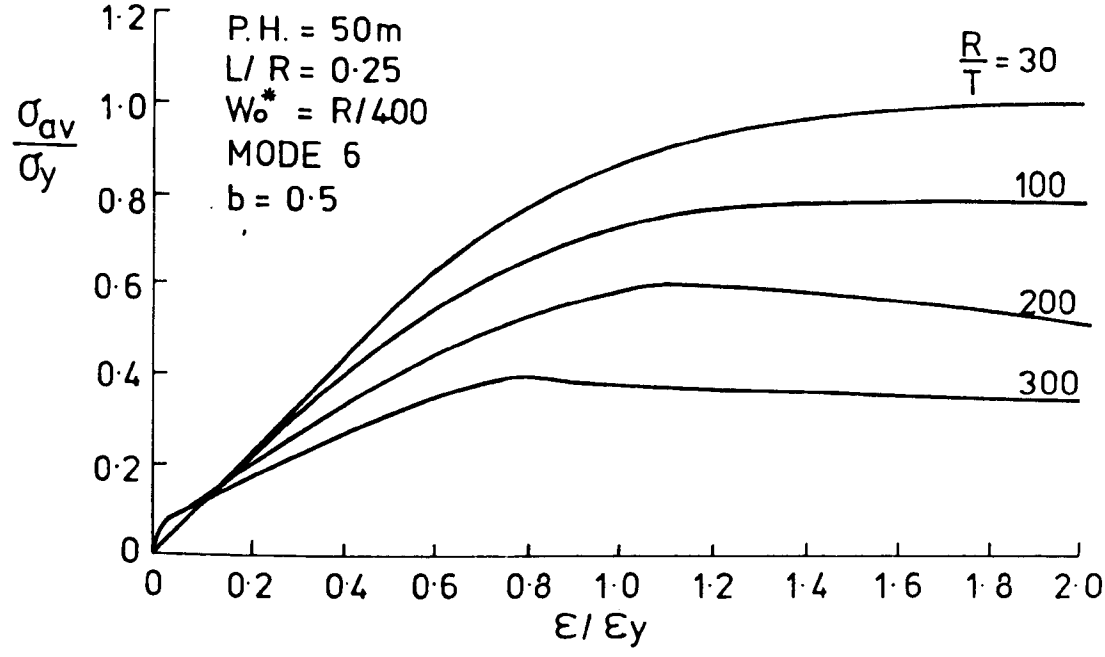

Fig. 6.147a

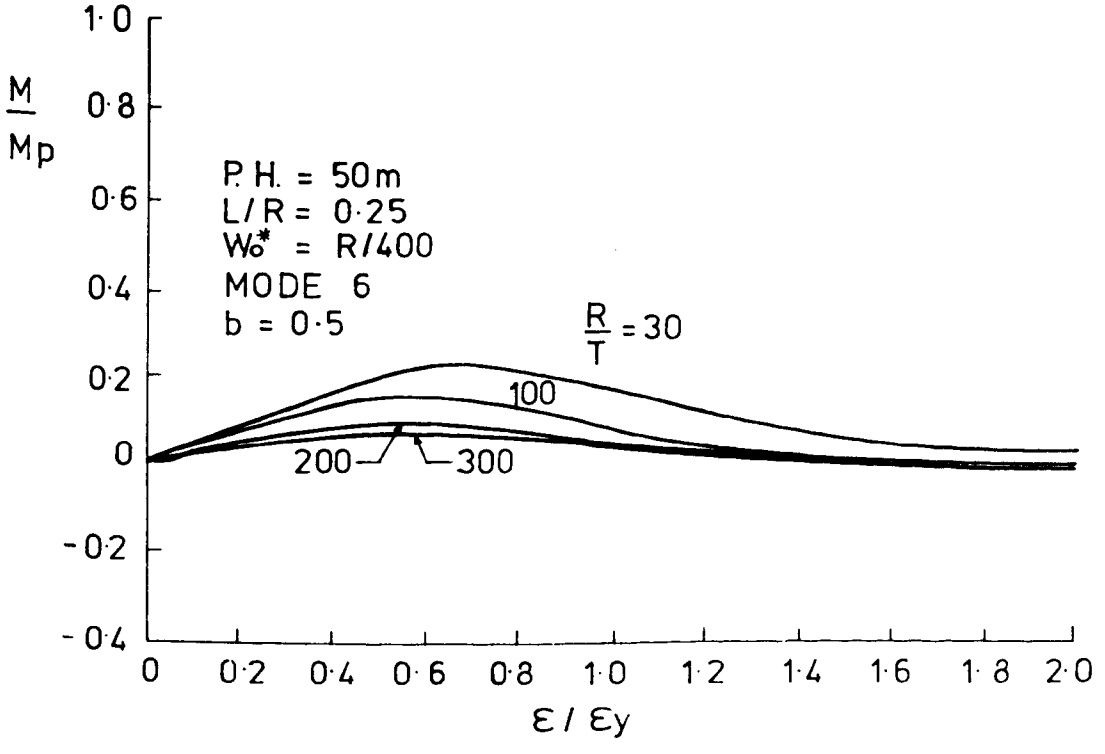

Fig. 6.147b

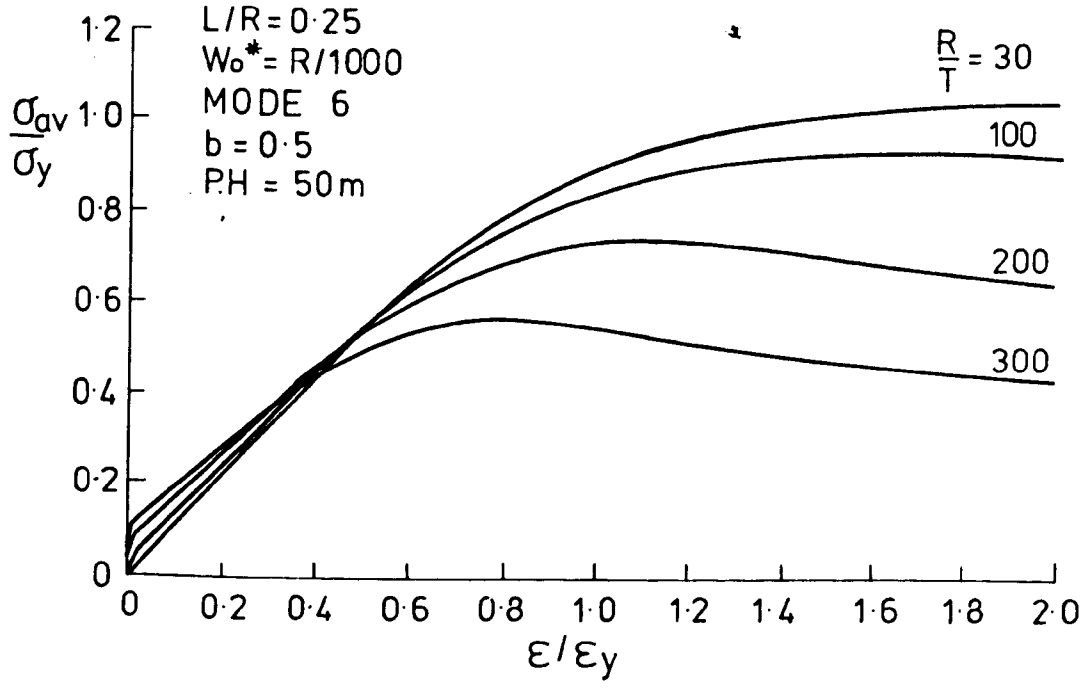

Fig. 6.148a

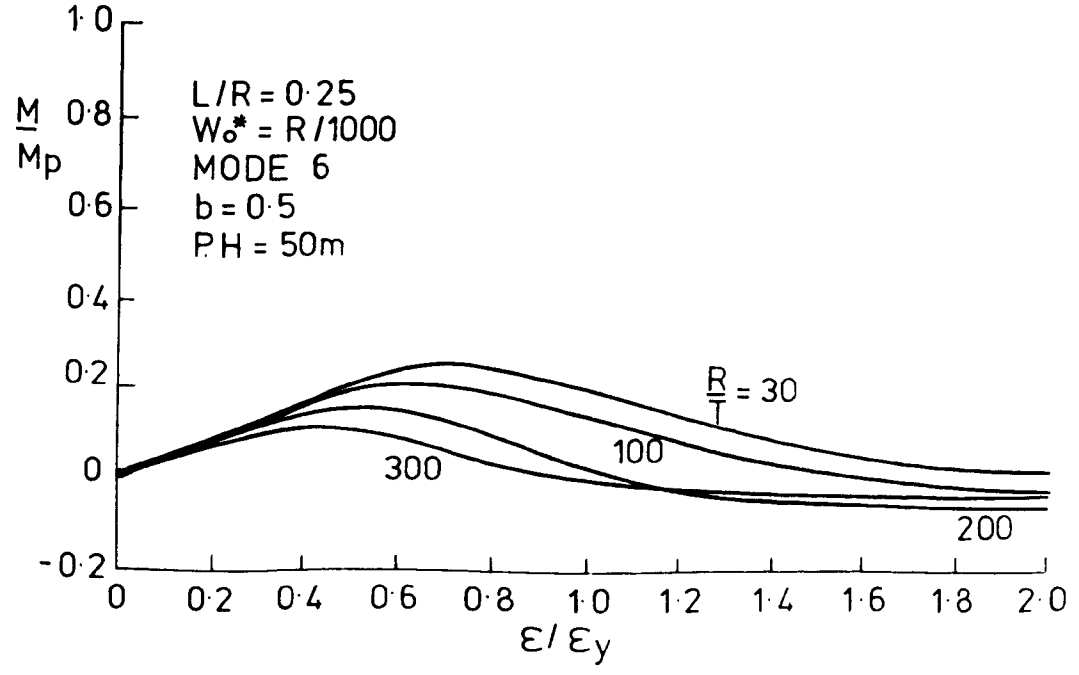

Fig. 6.148b

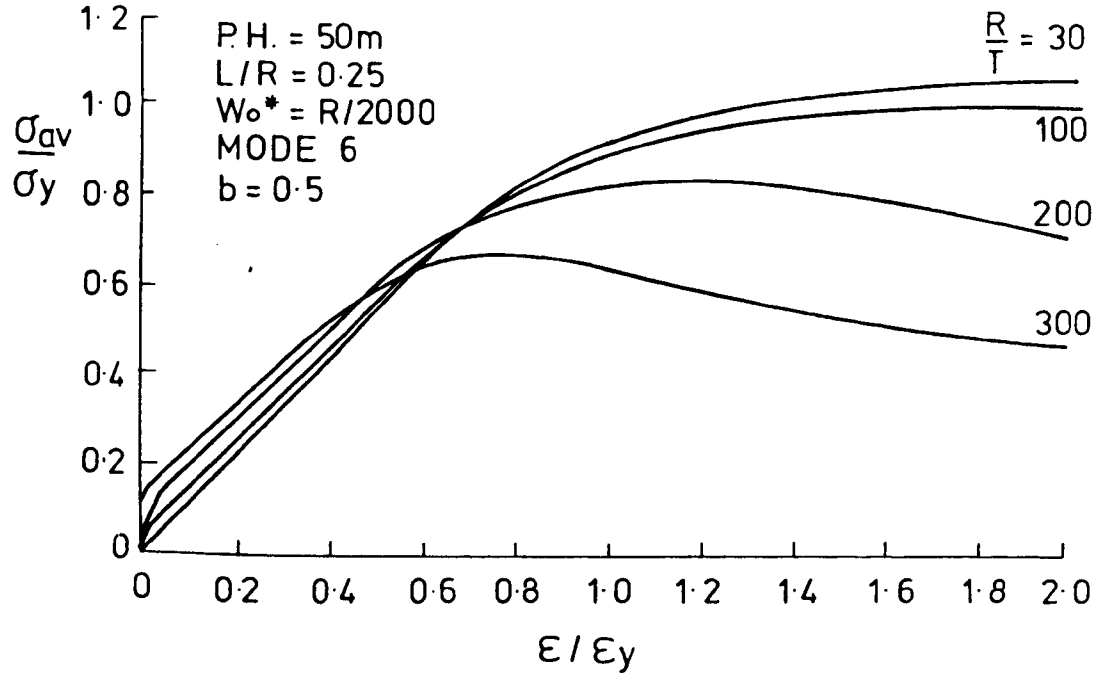

Fig. 6.149a

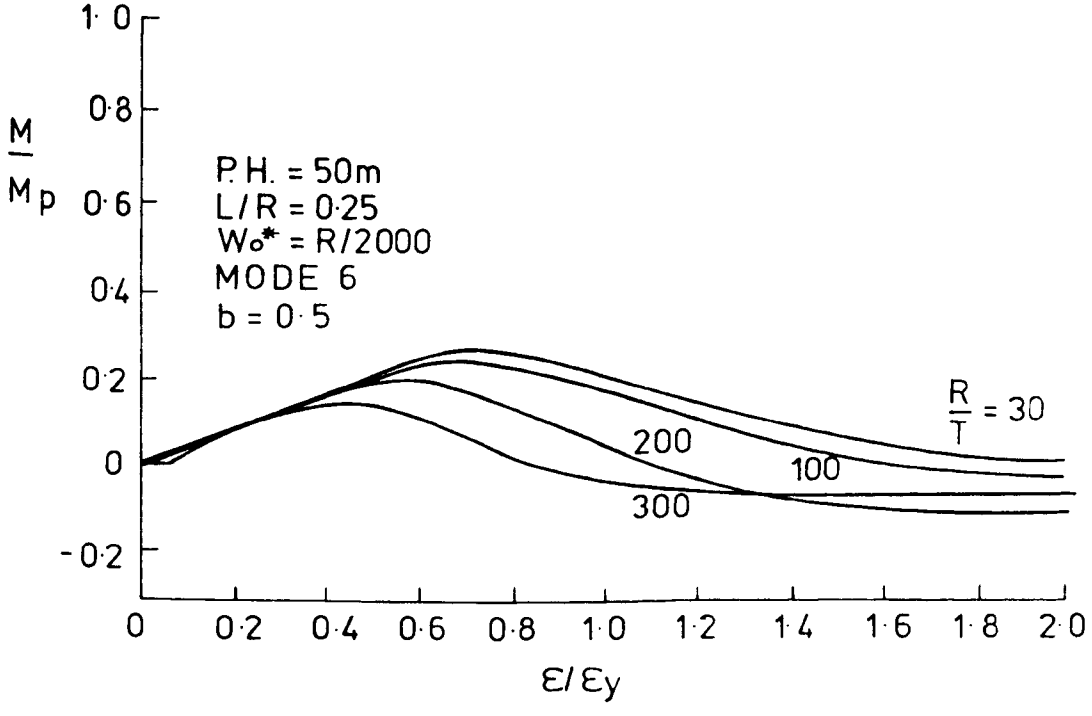

Fig. 6.149b

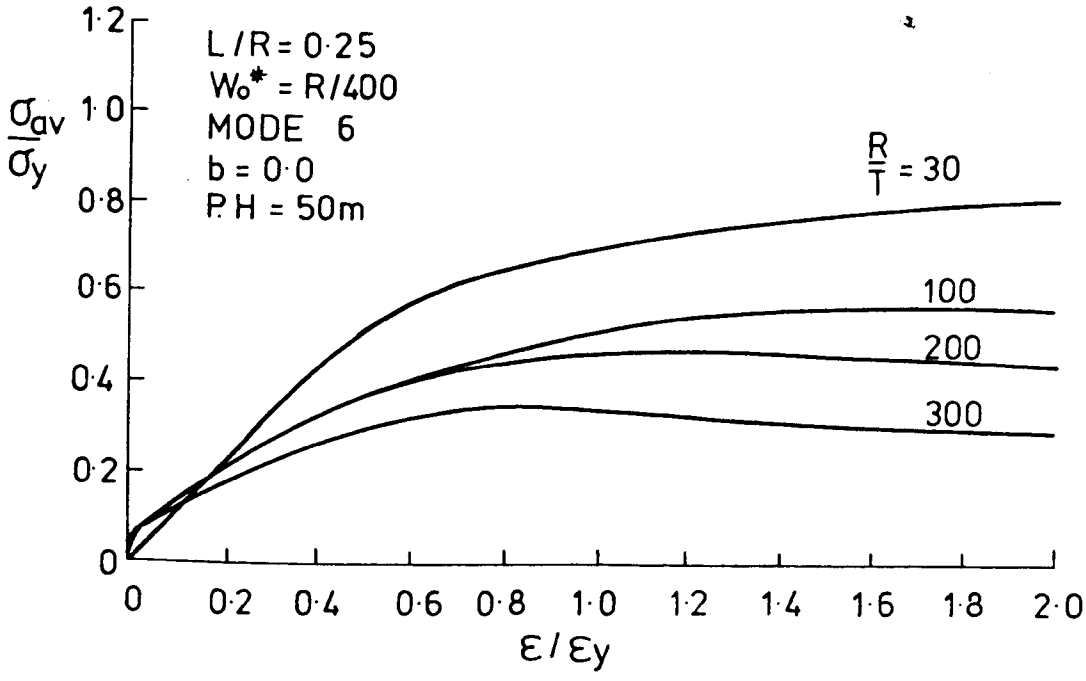

Fig. 6. 150a

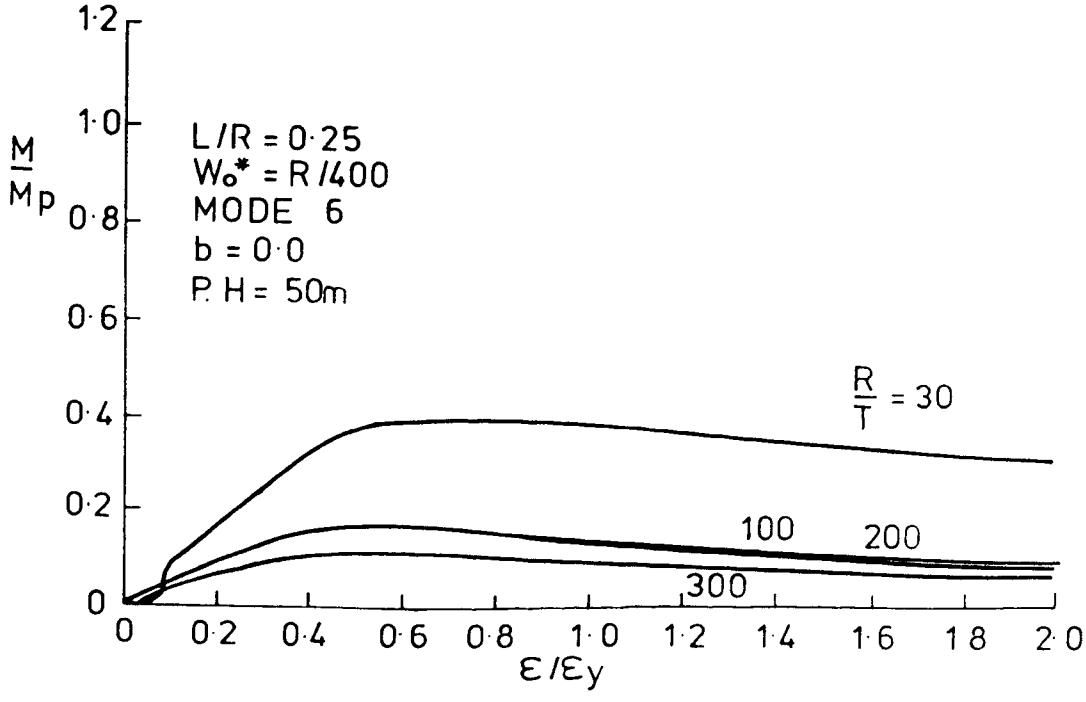

Fig. 6. 150b

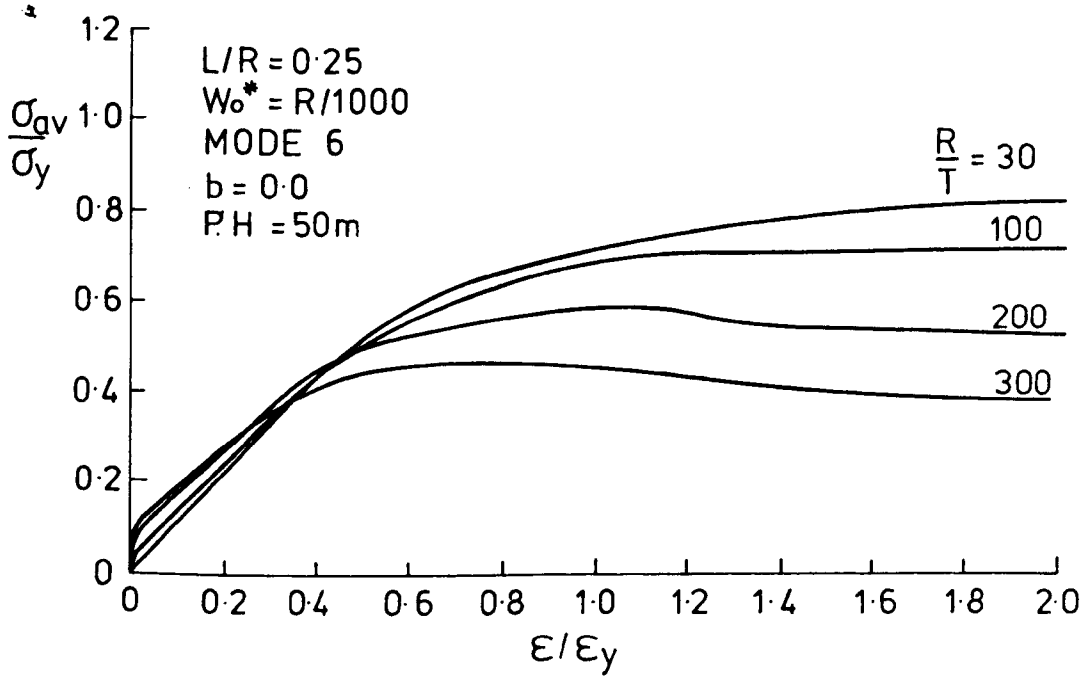

Fig. 6.151a

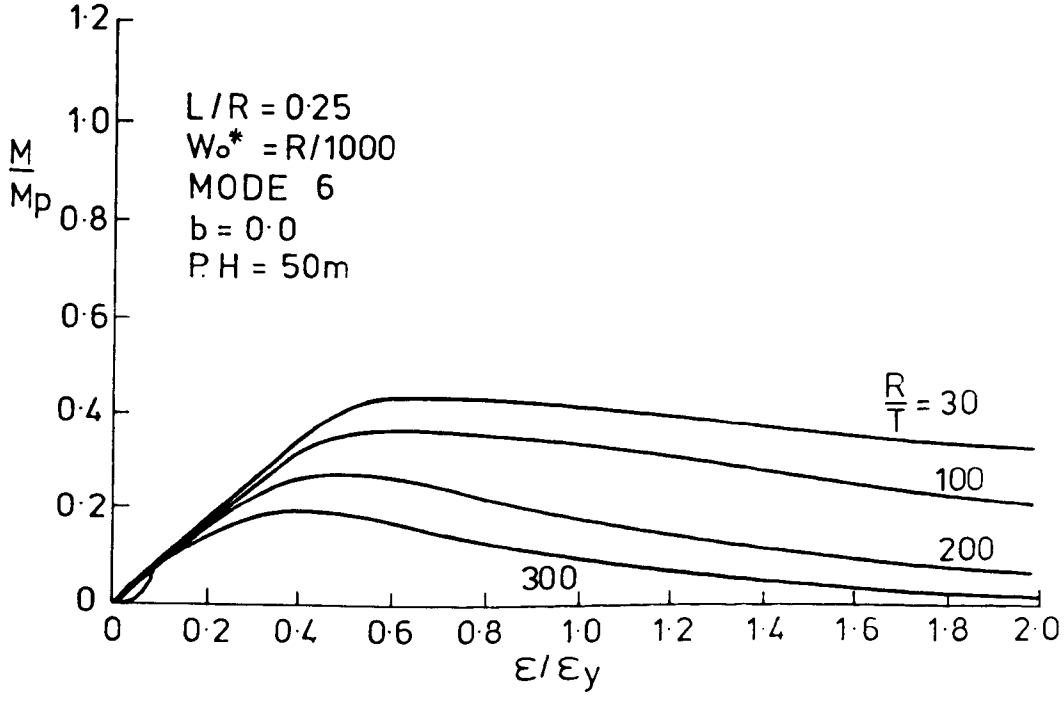

Fig. 6.151b

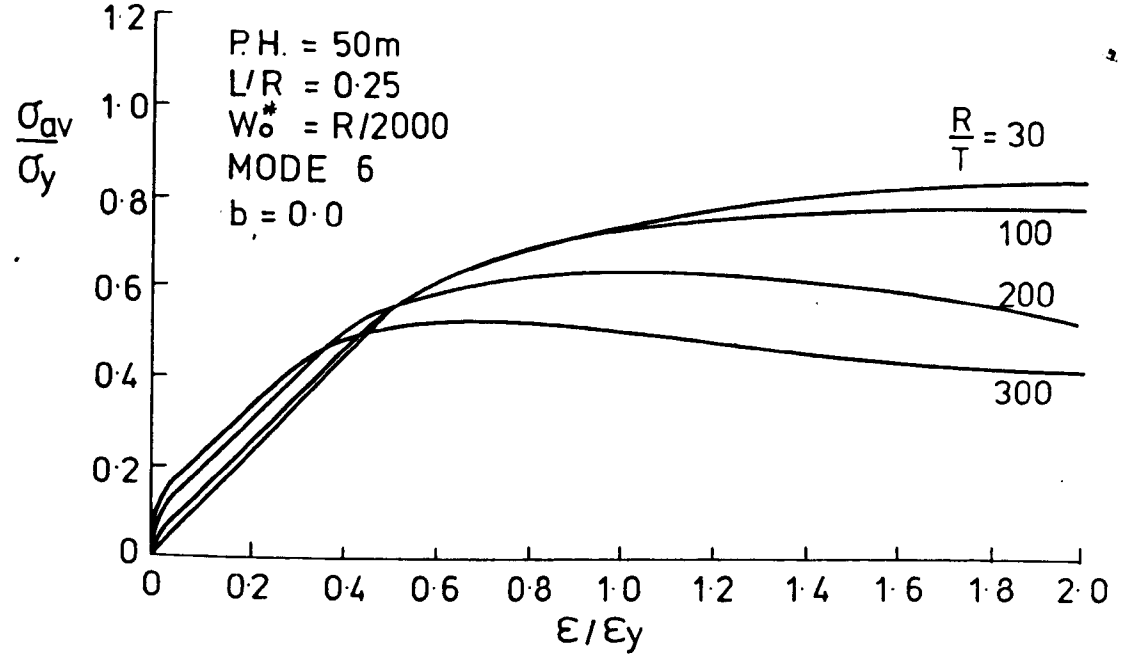

Fig. 6. 152a

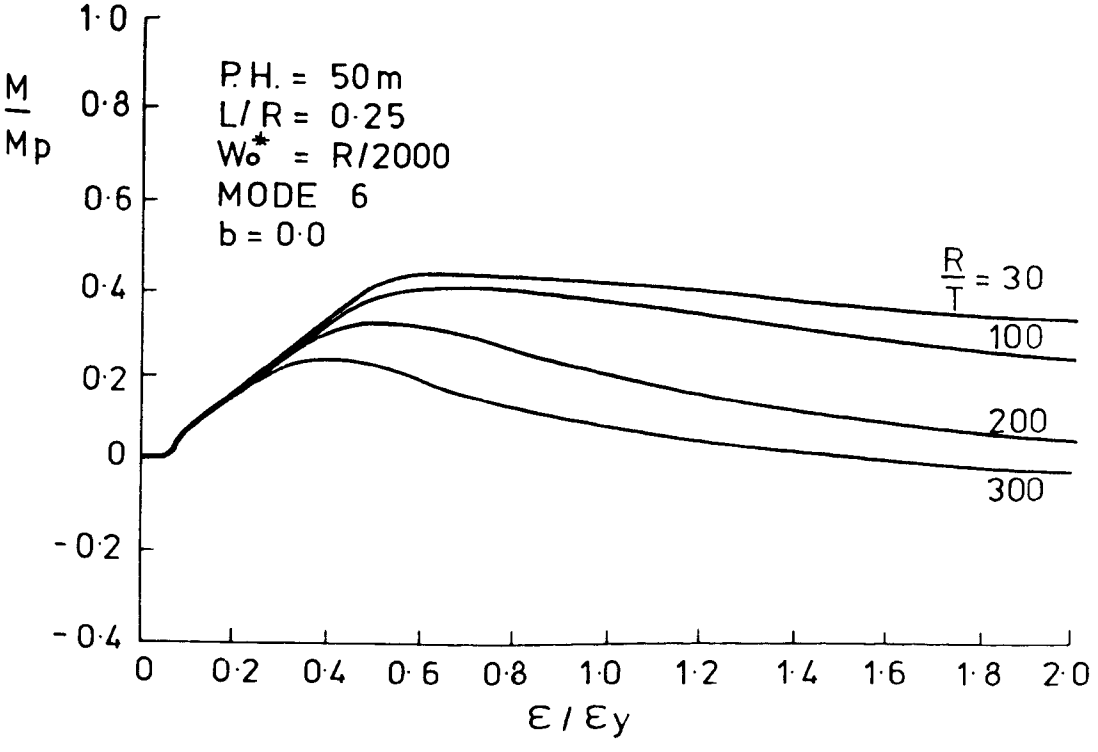

Fig. 6. 152b

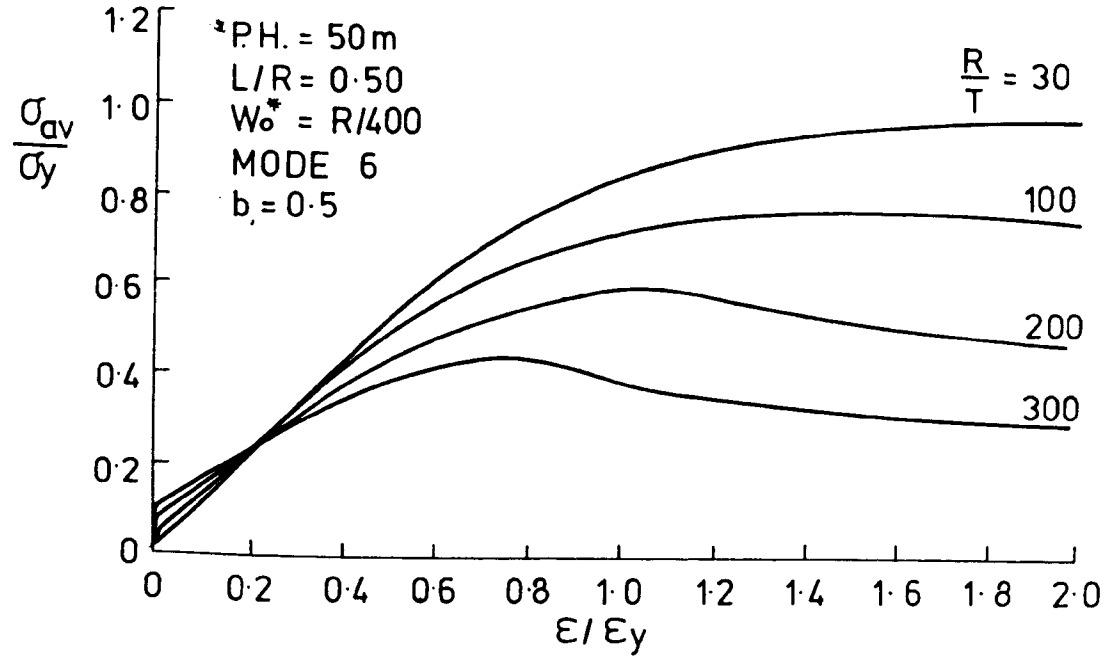

Fig. 6.153a

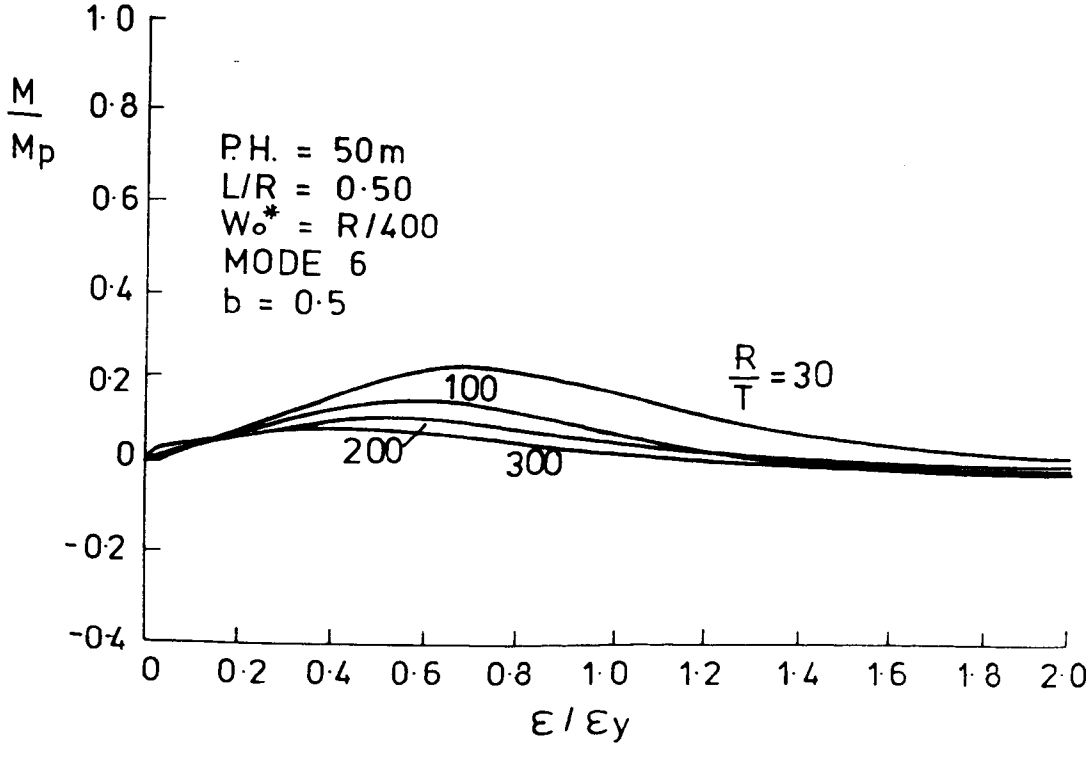

Fig. 6.153b

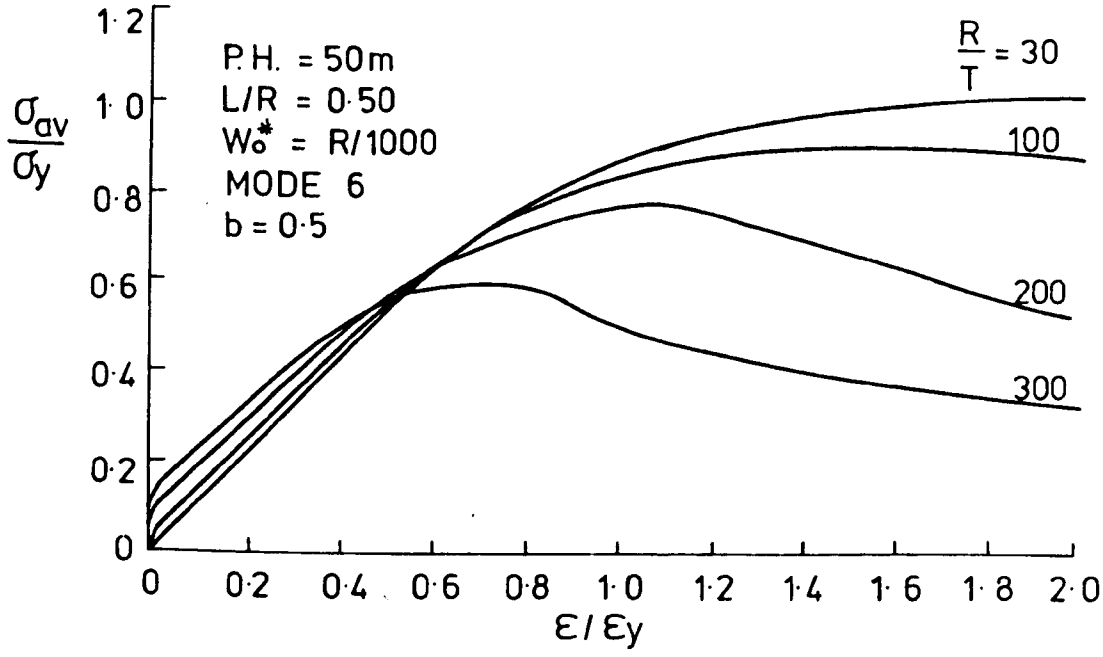

Fig. 6. 154a

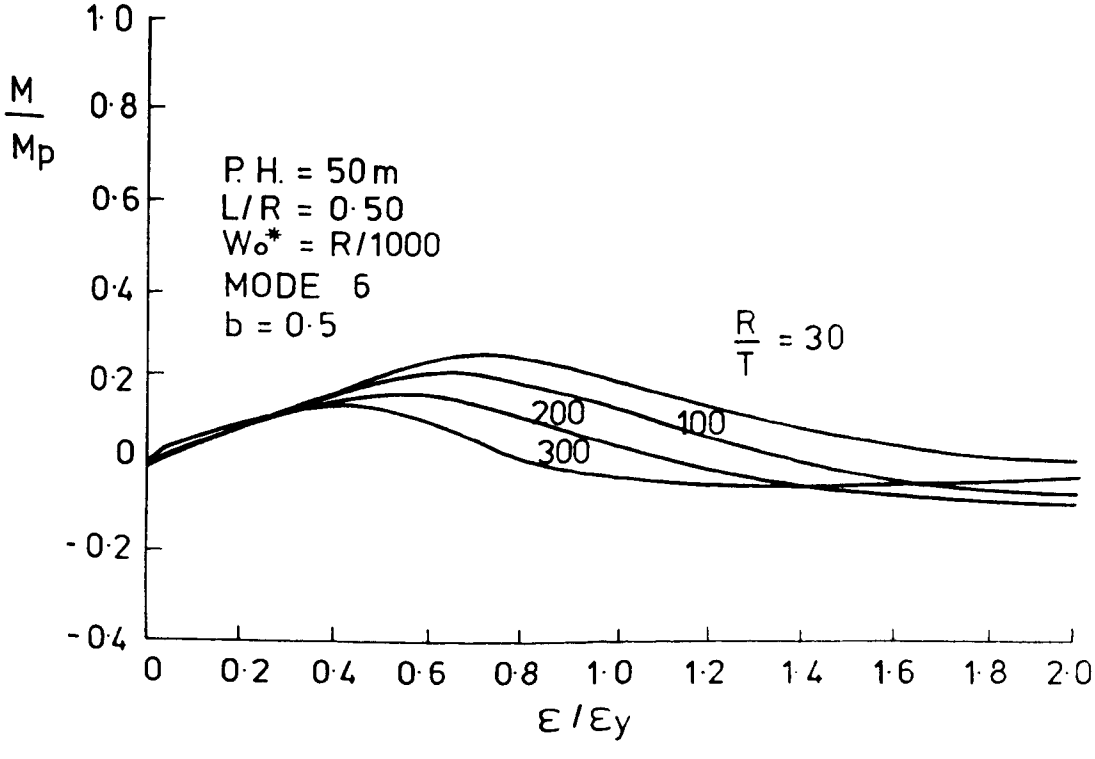

Fig. 6.154b

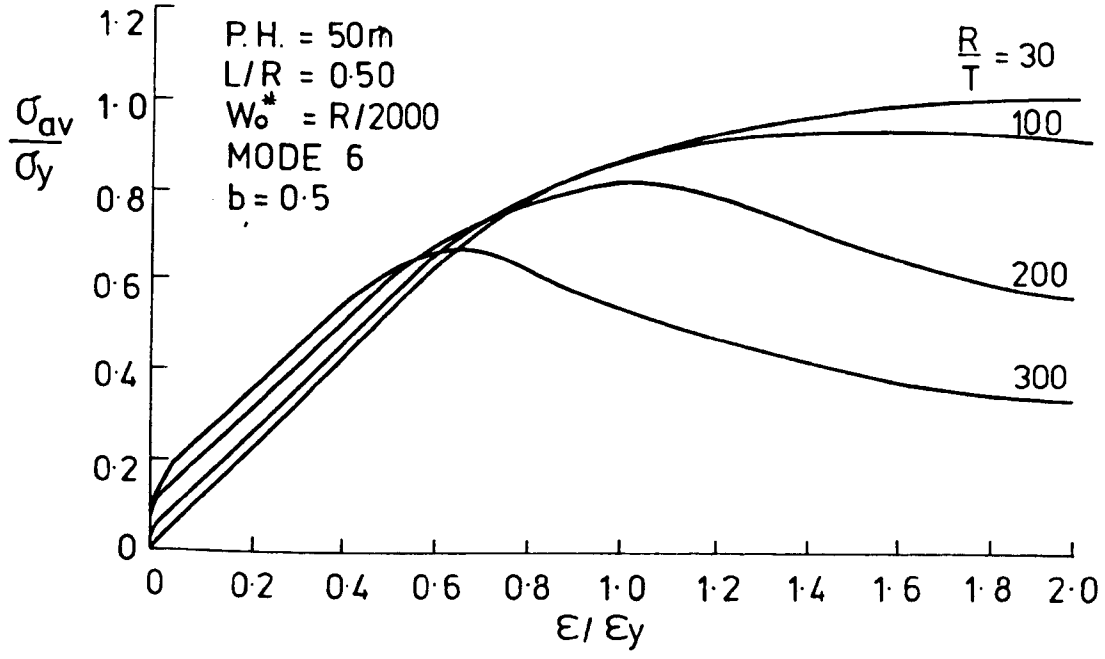

Fig. 6.155a

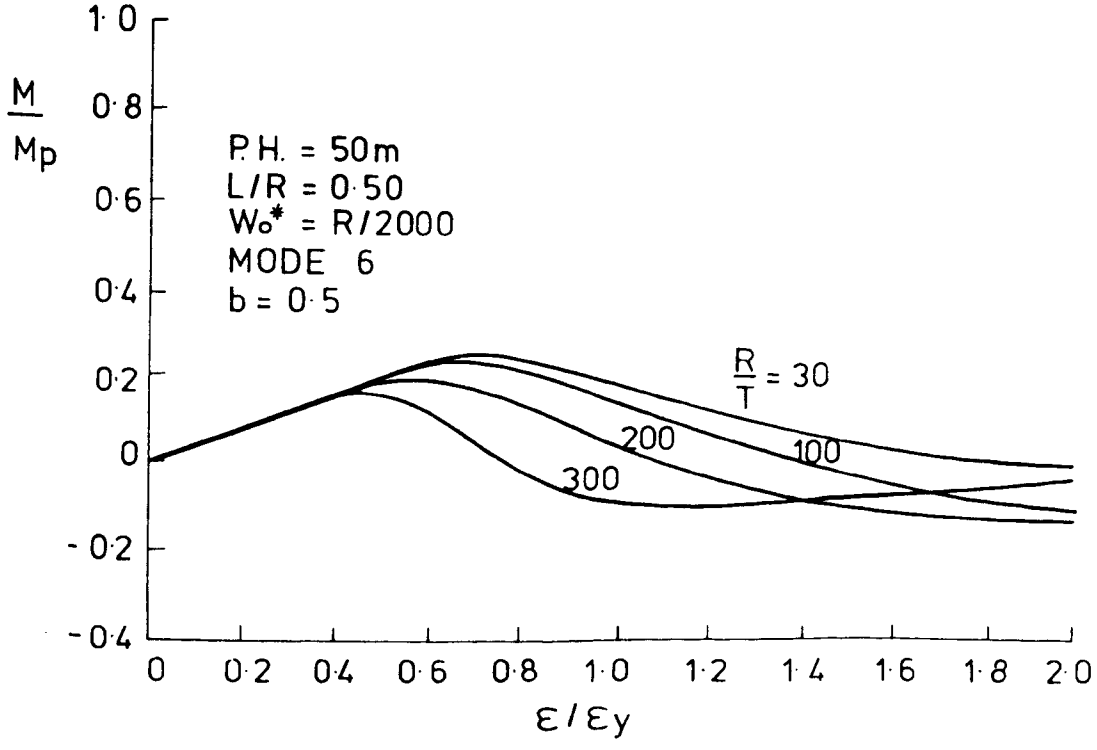

Fig. 6. 155b

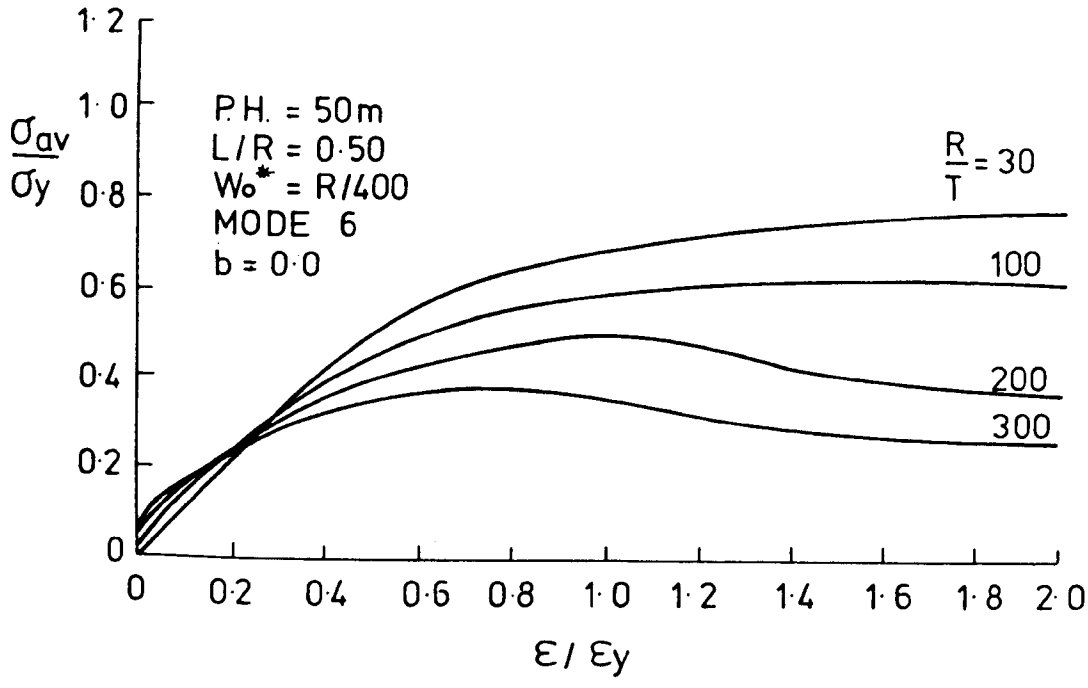

Fig. 6. 156a

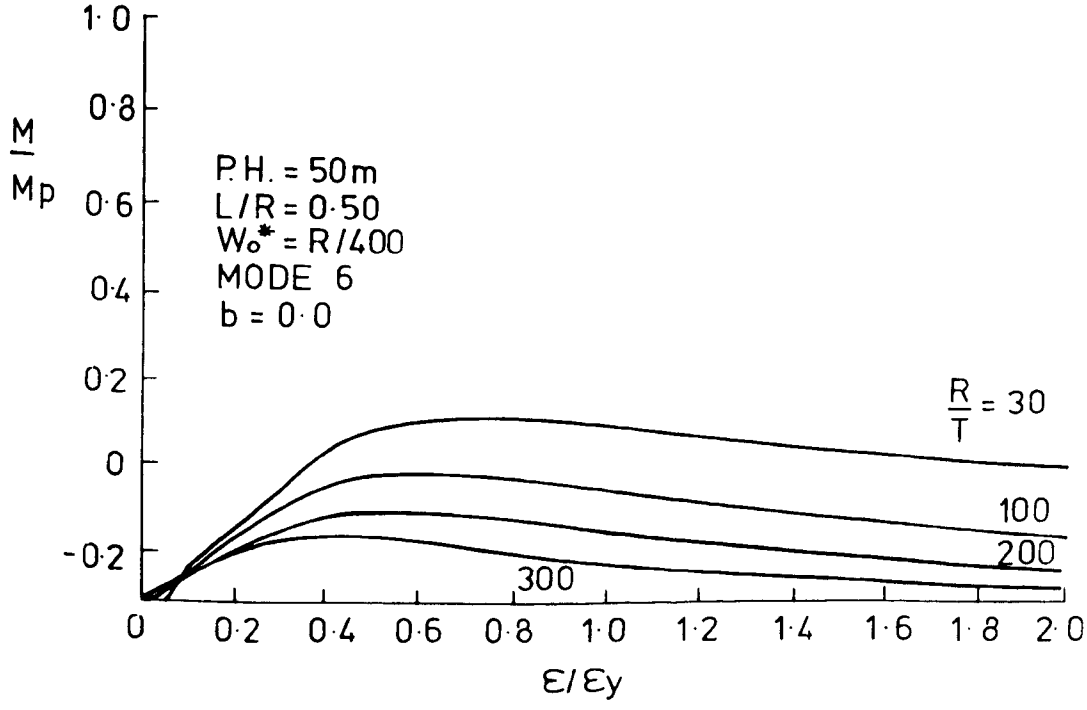

Fig. 6. 156b

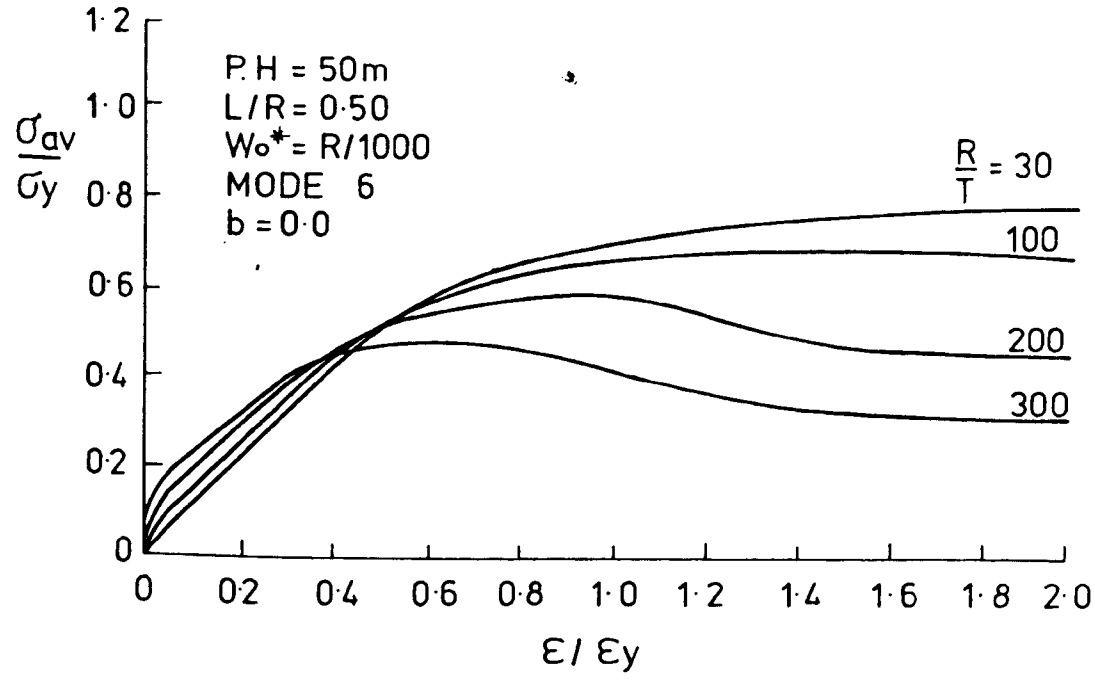

Fig. 6. 157a

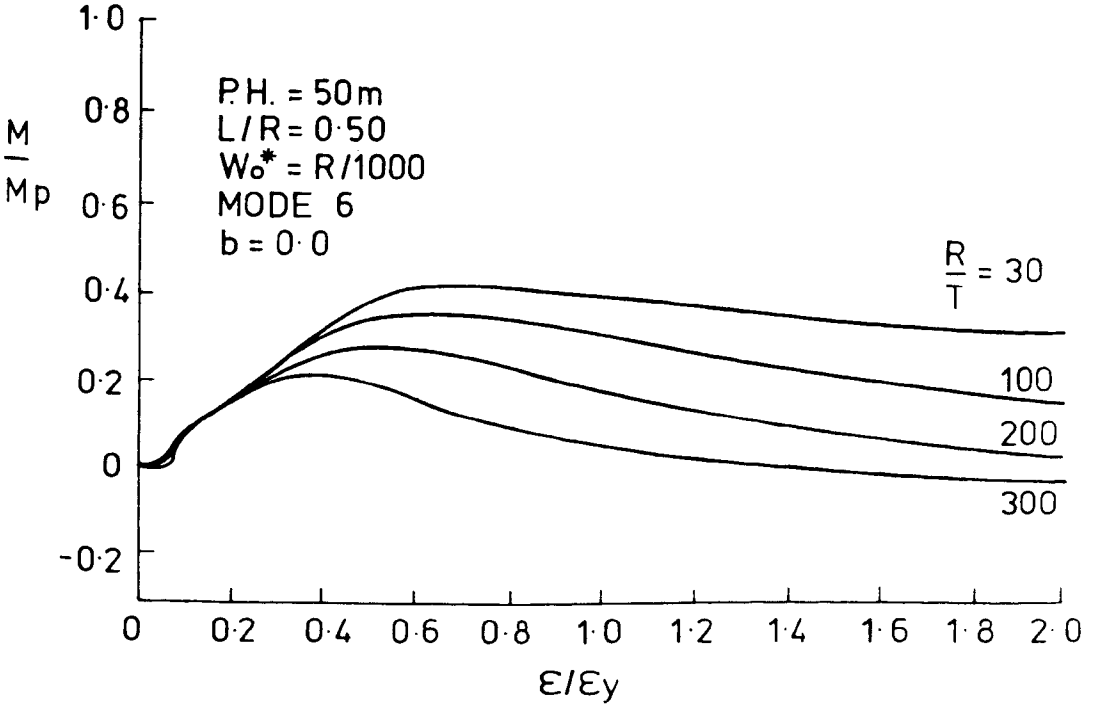

Fig. 6. 157b

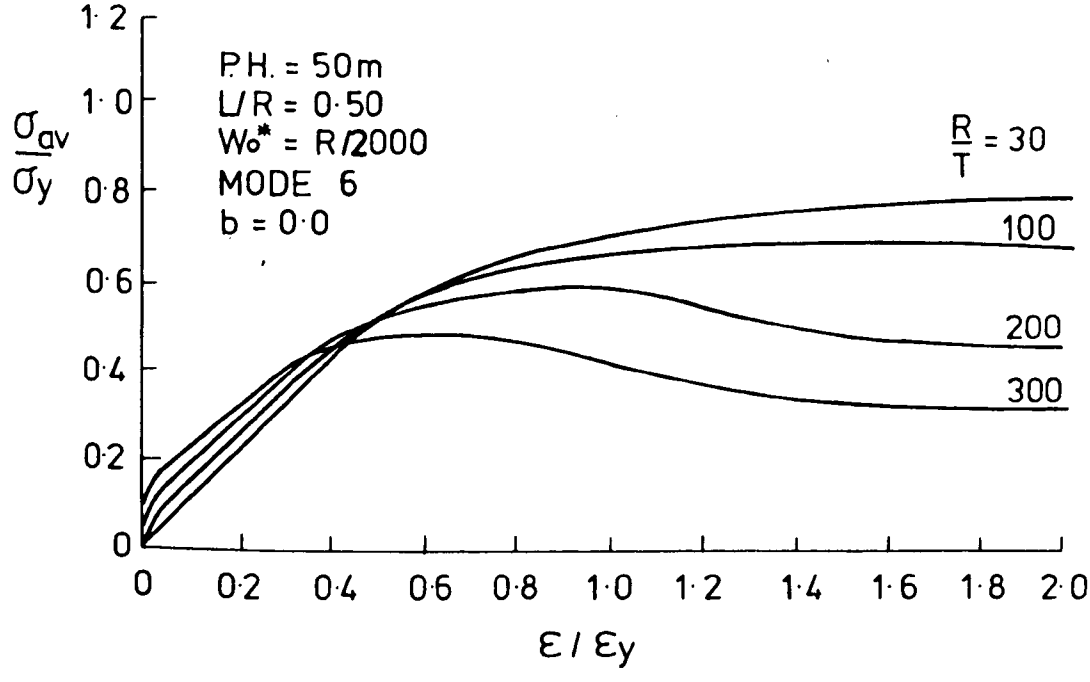

Fig. 6.158a

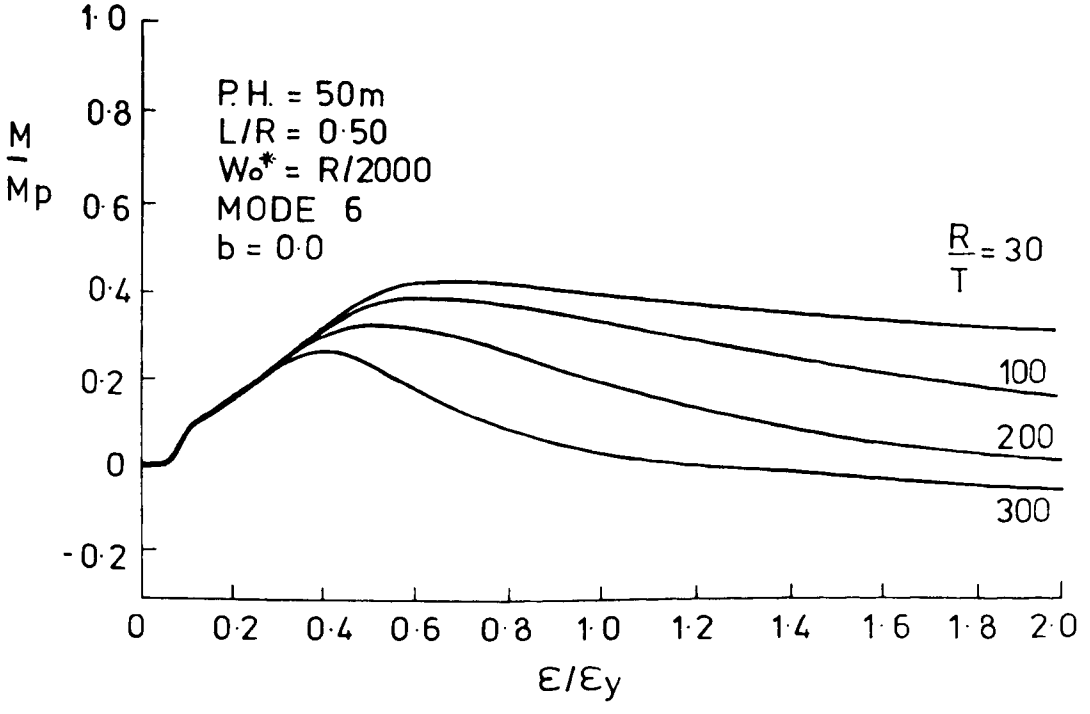

Fig. 6.158b

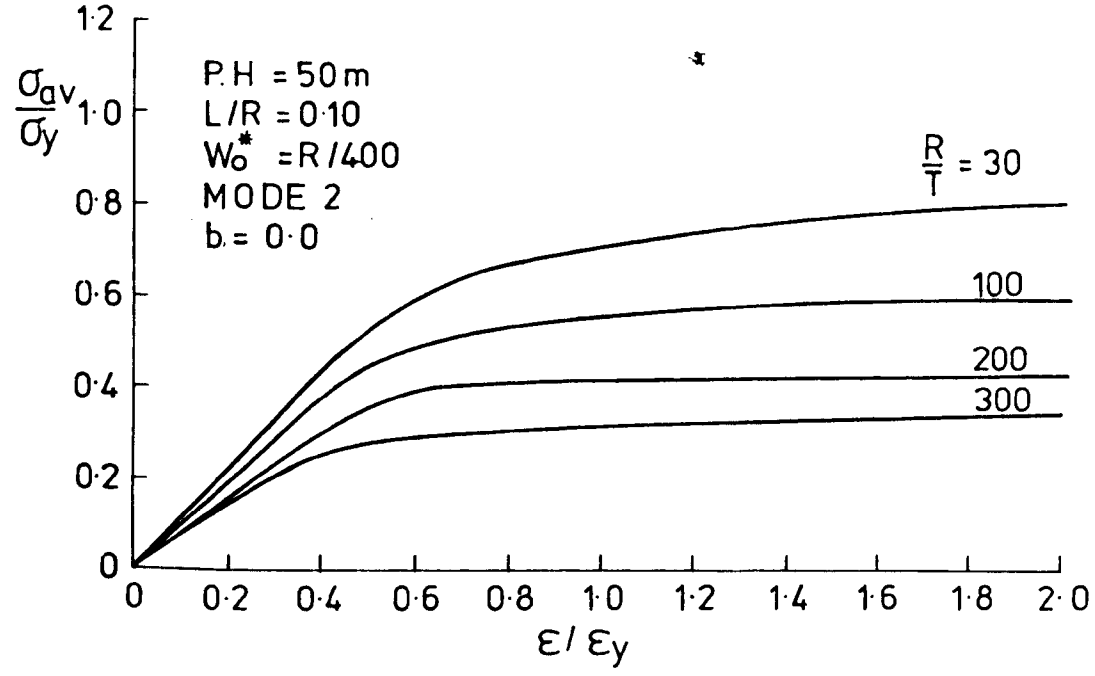

Fig.6.159a

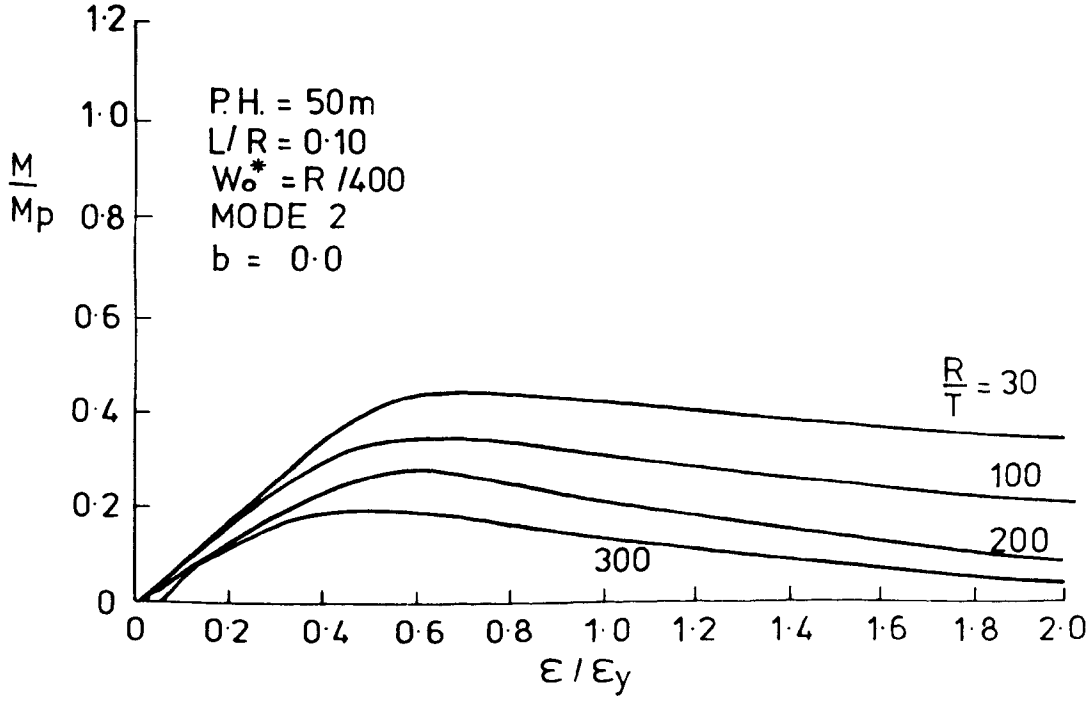

Fig. 6.159b

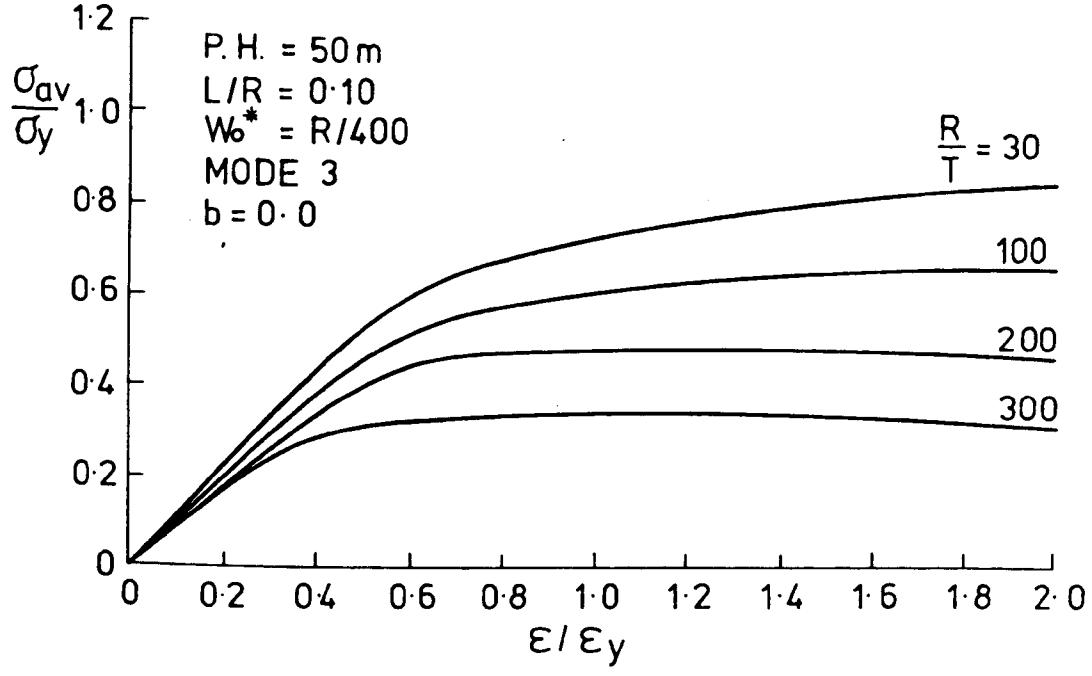

Fig. 6. 160a

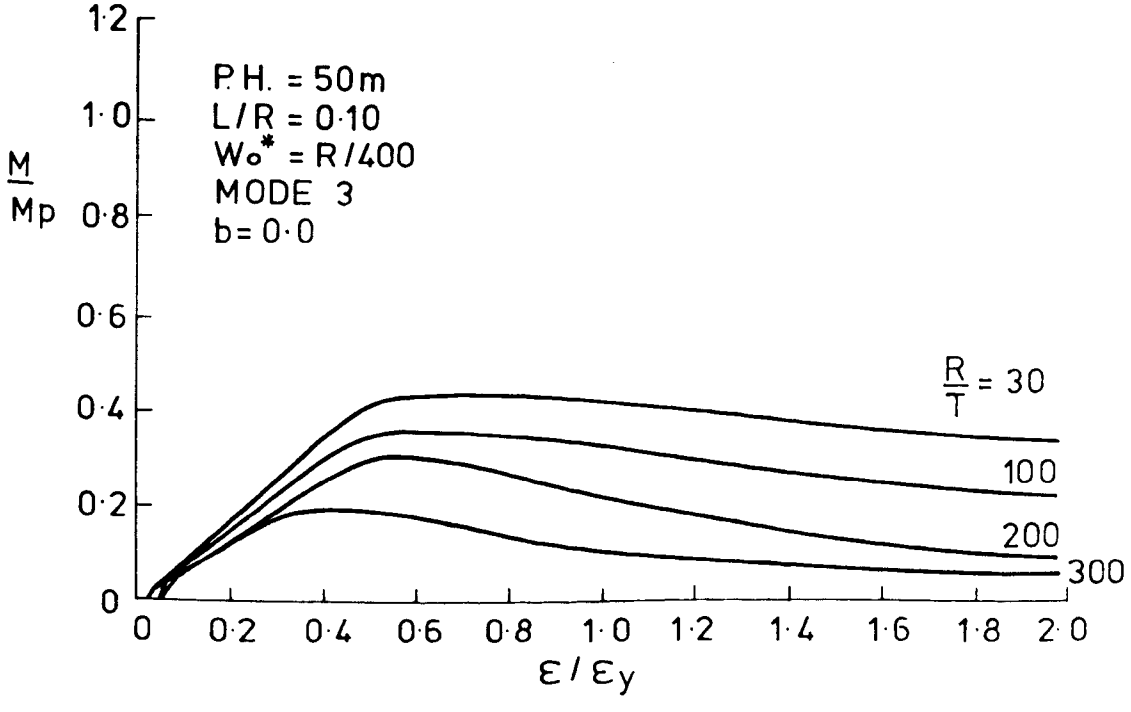

Fig. 6. 160b

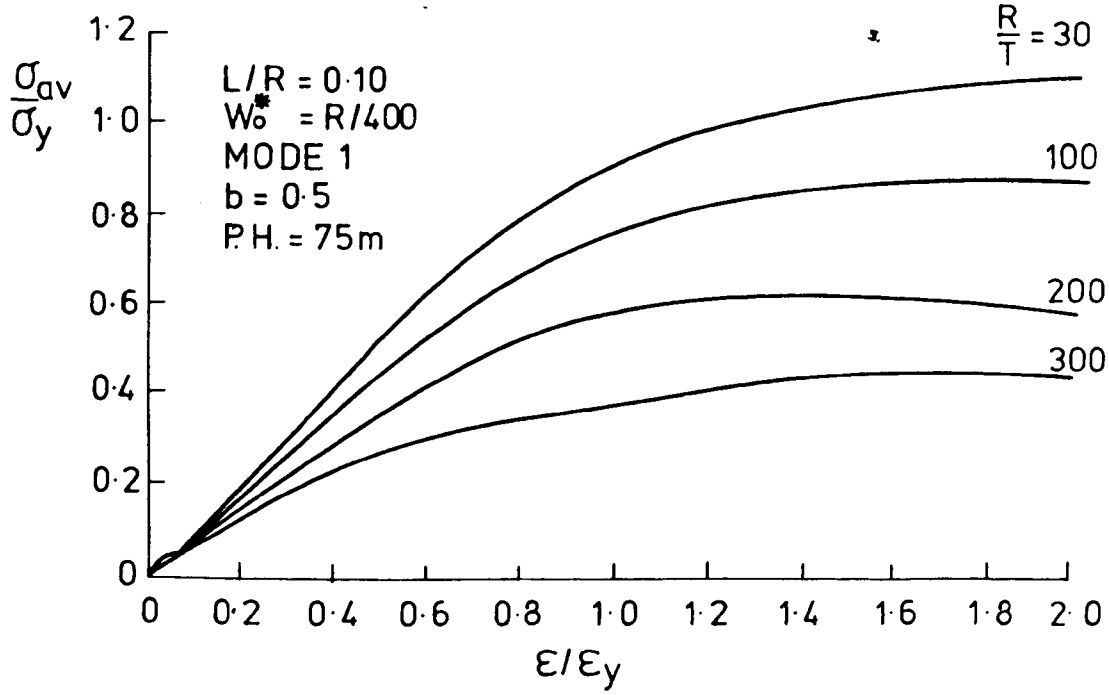

Fig.6. 161a

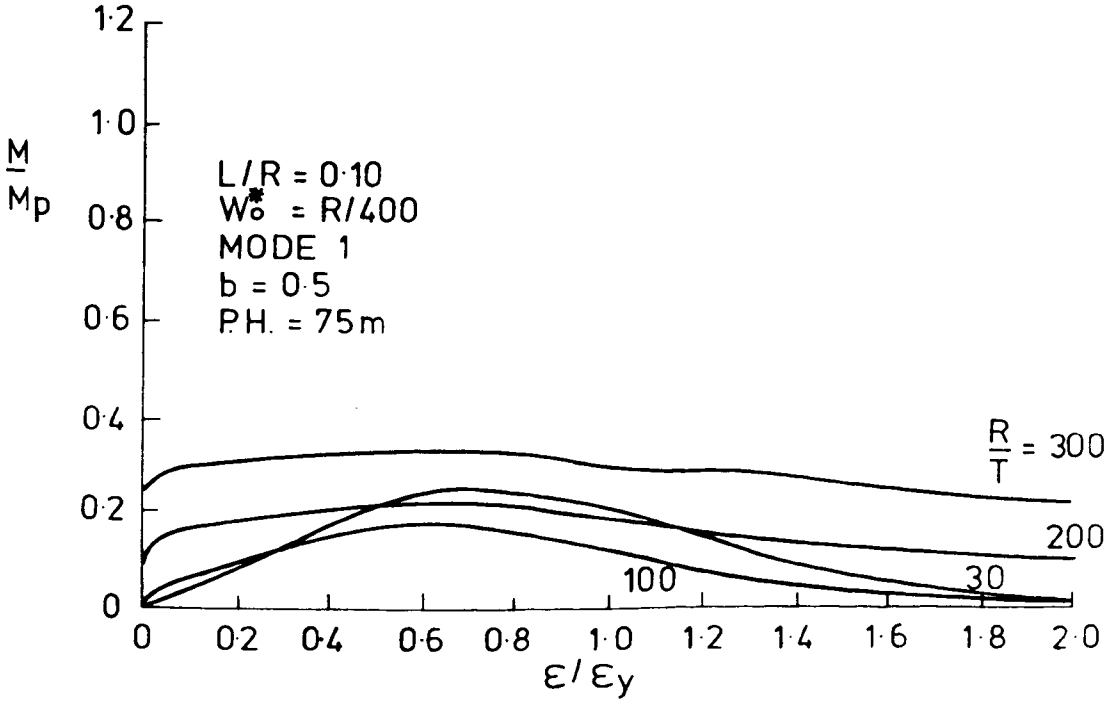

Fig. 6. 161b

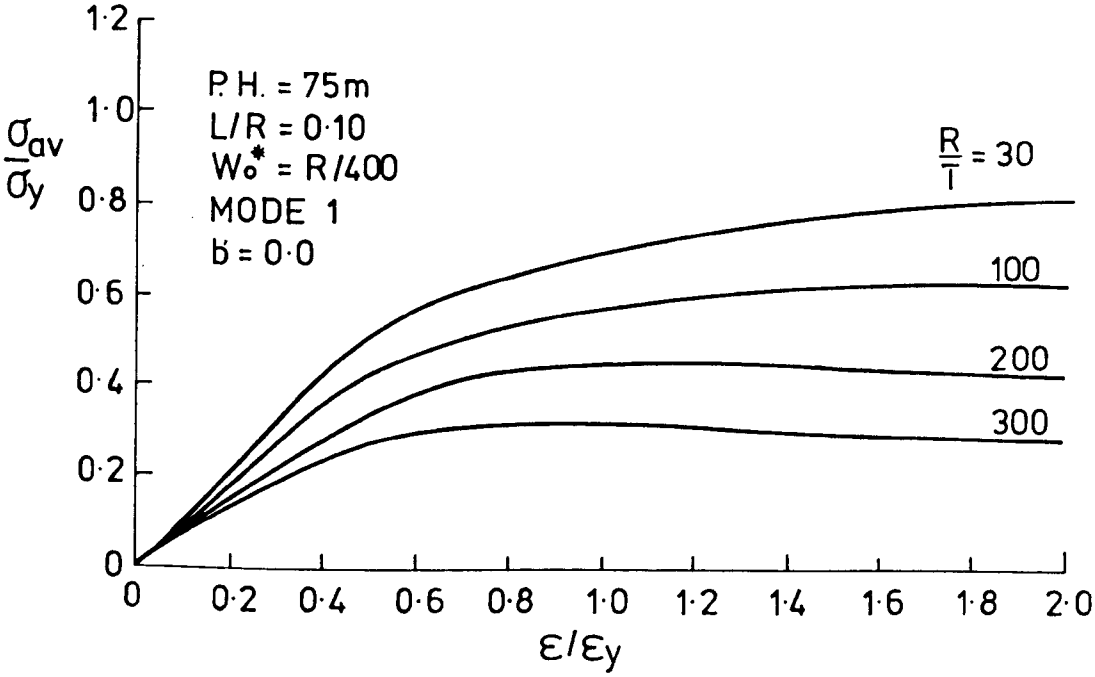

Fig. 6. 162a

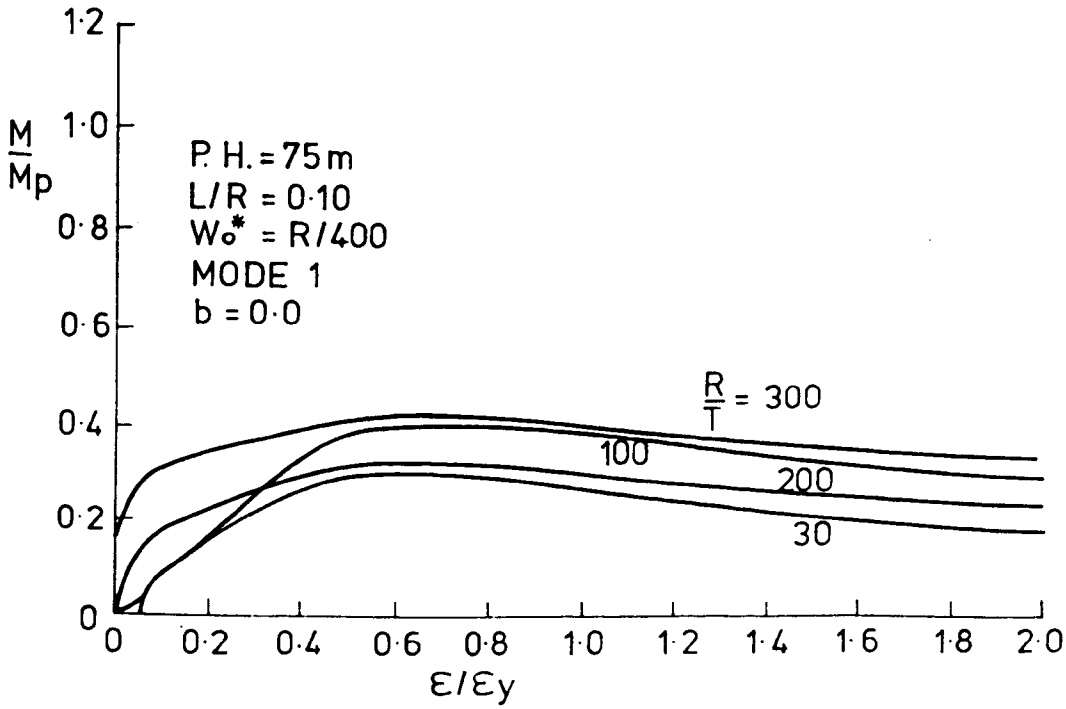

Fig. 6. 162b

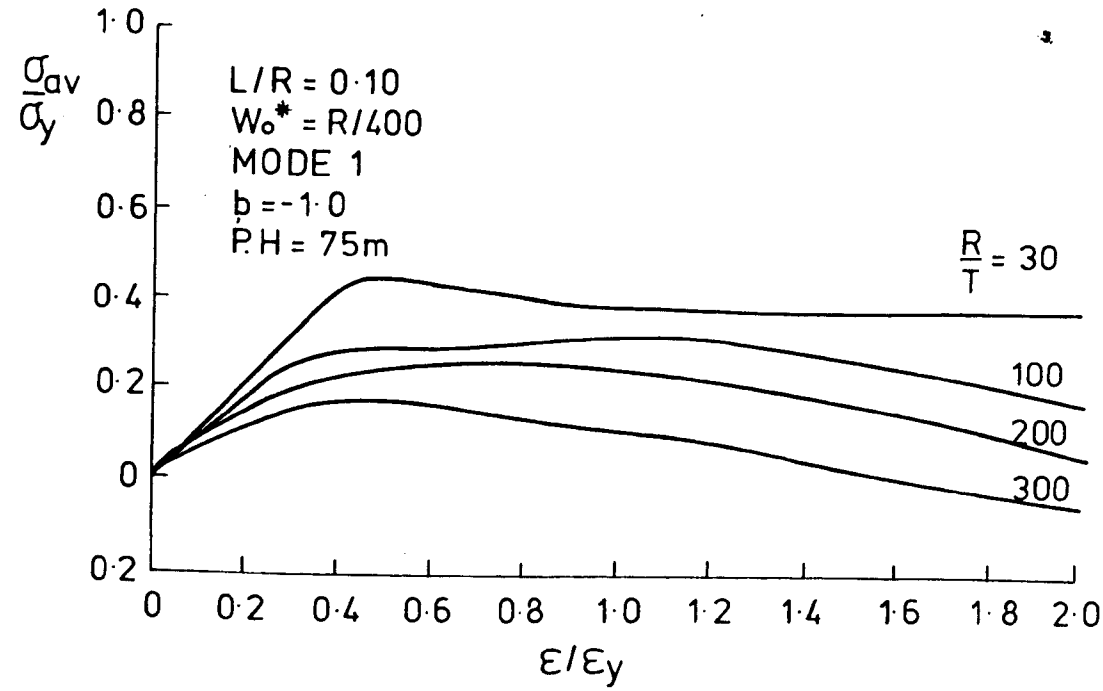

Fig 6 163a

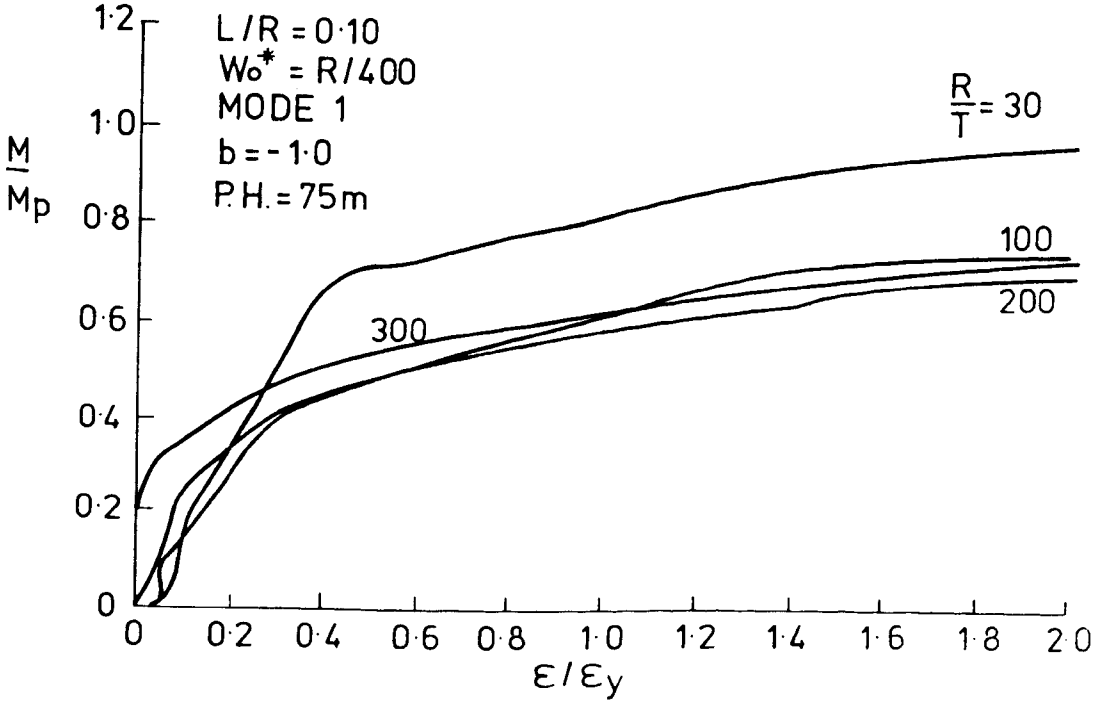

Fig. 6. 163b

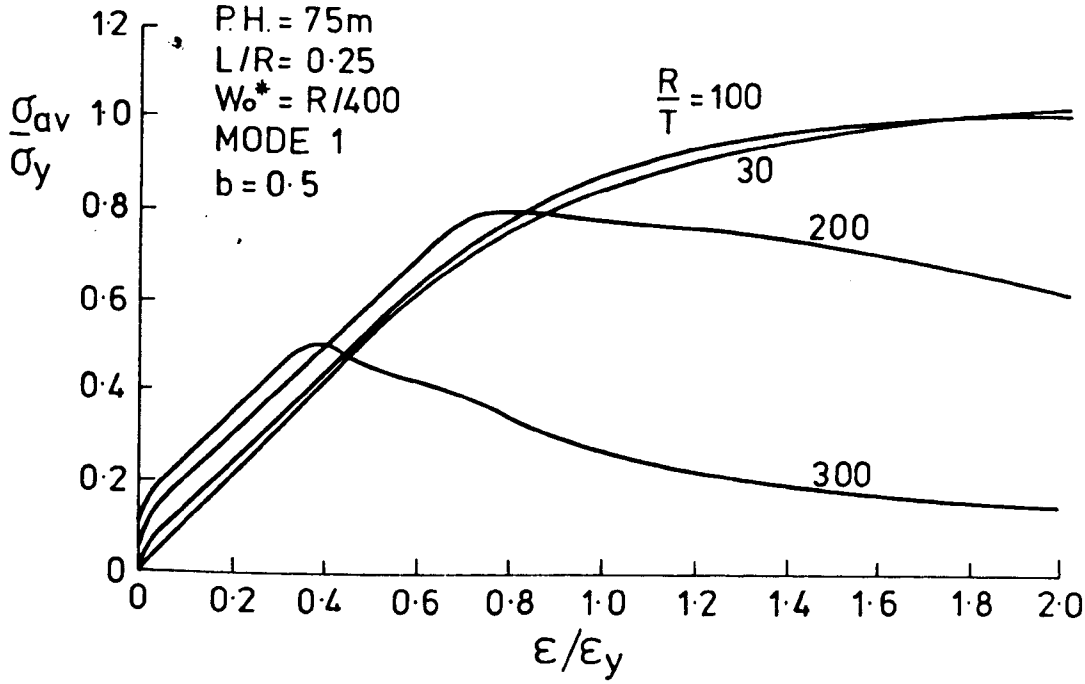

Fig. 6. 164a

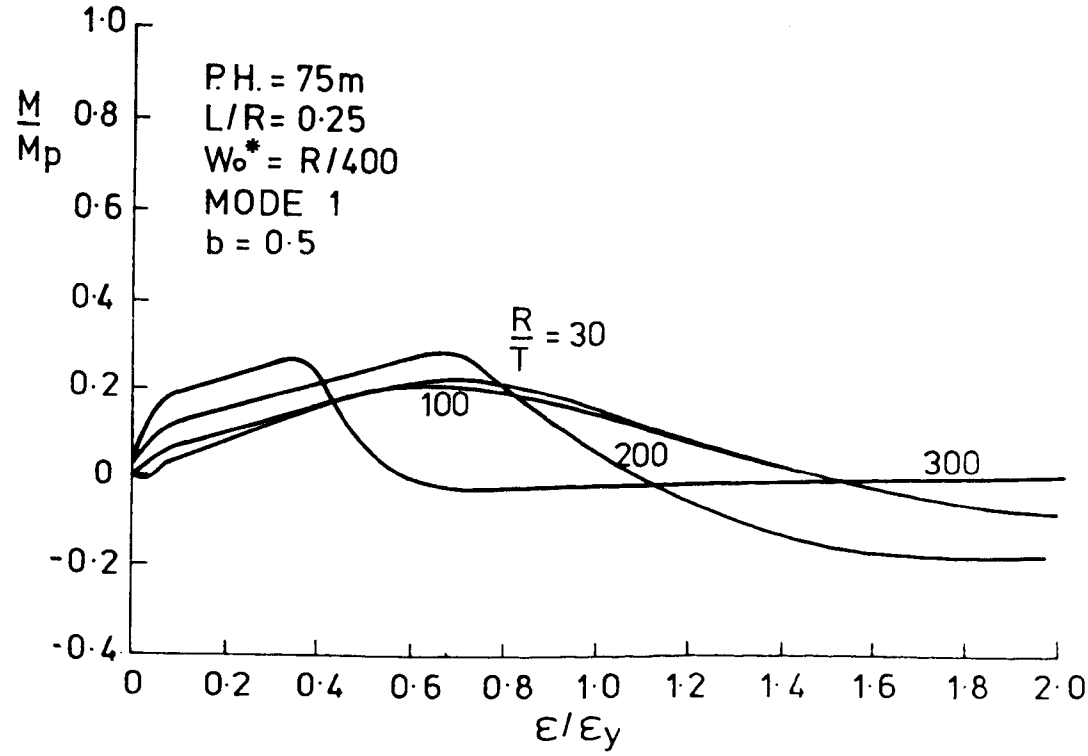

Fig. 6.164b

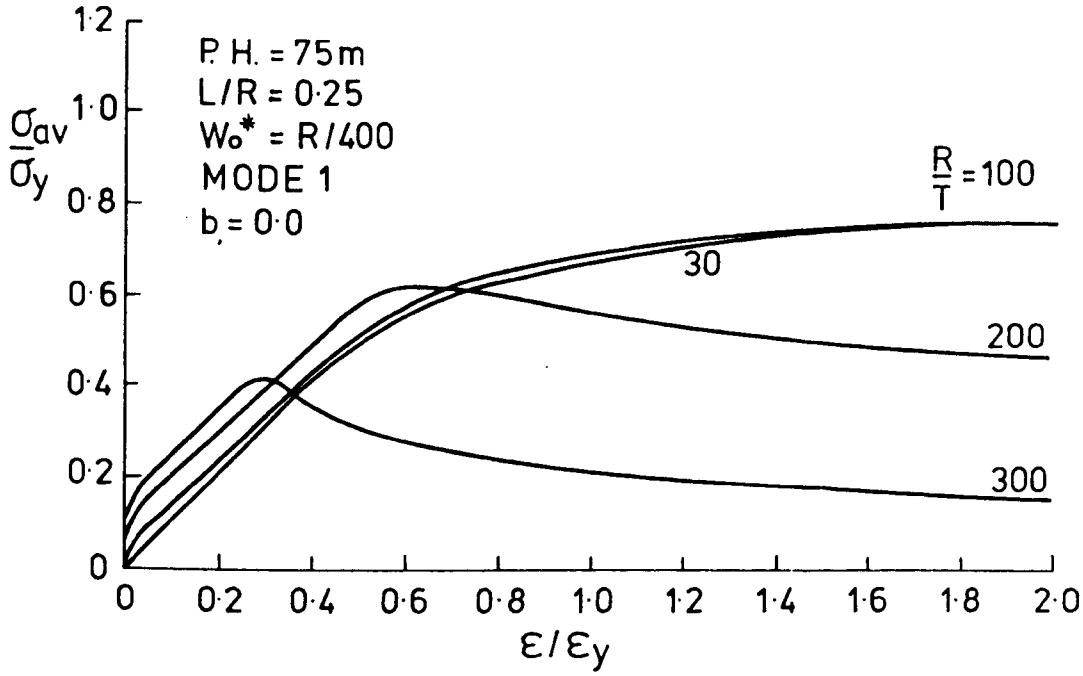

Fig. 6.165a

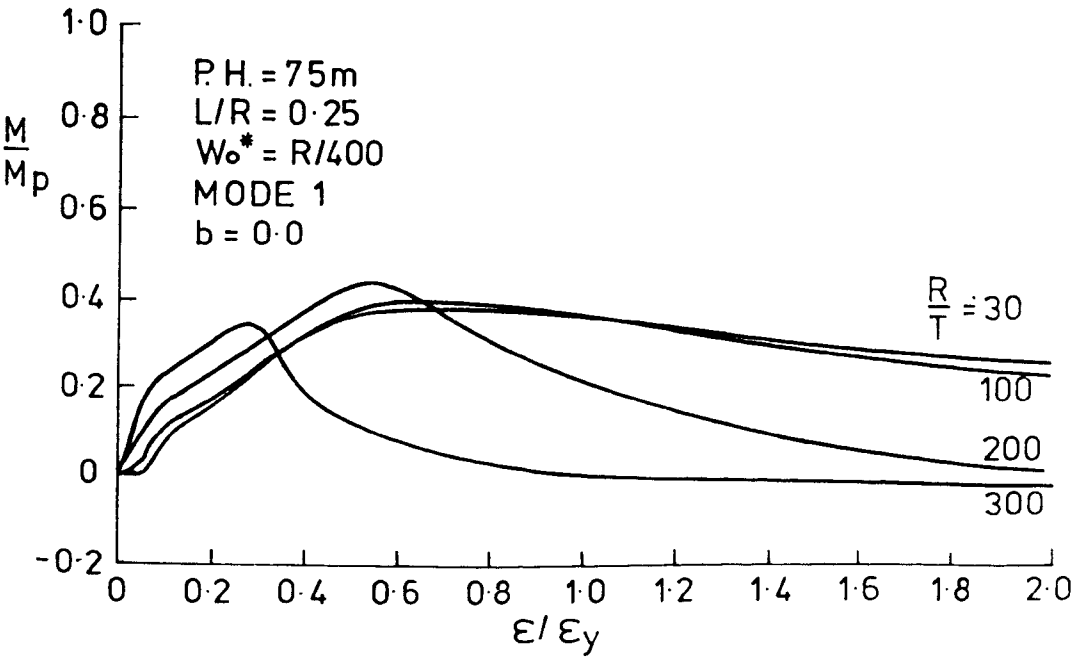

Fig. 6.165b

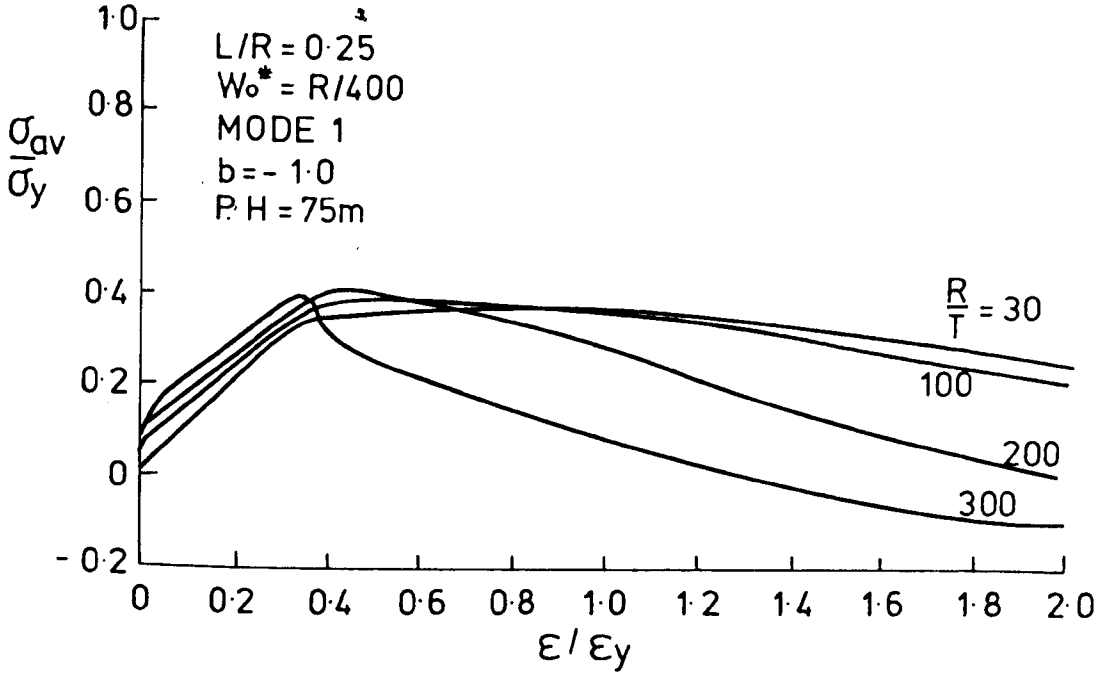

Fig. 6. 166a

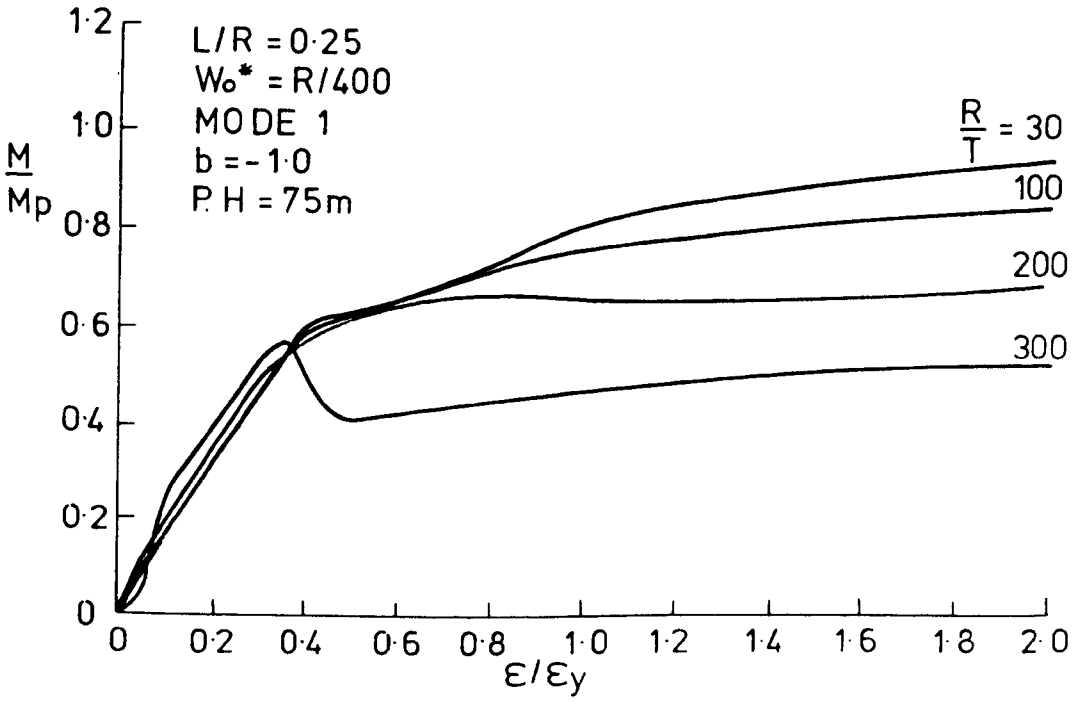

Fig. 6. 166b

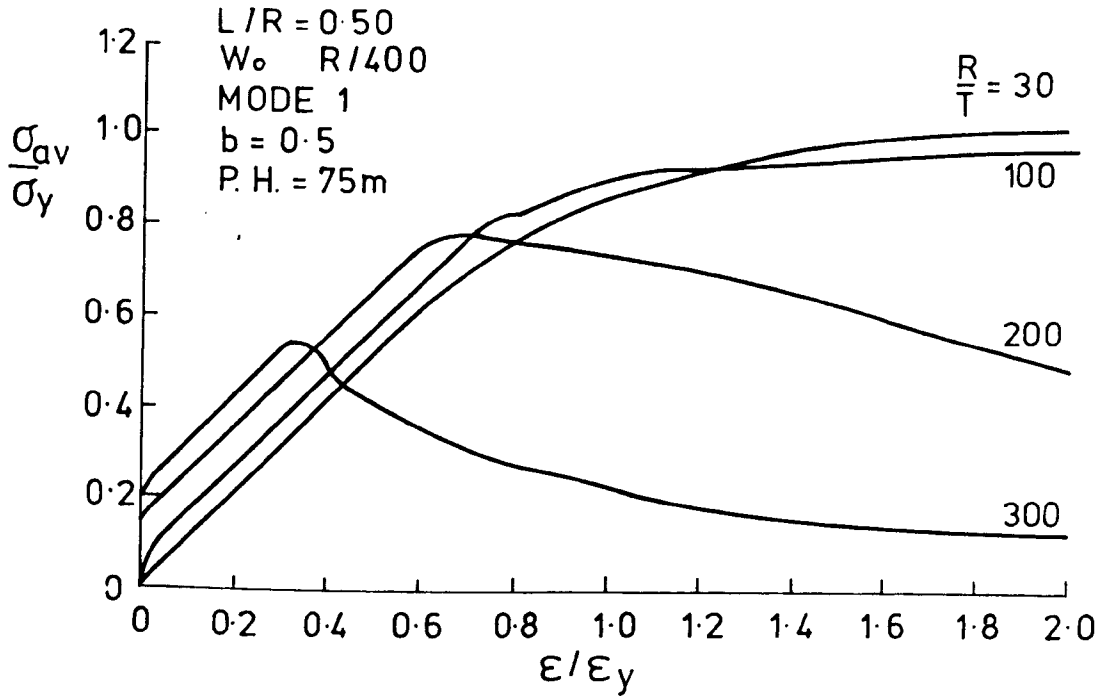

Fig.6. 167a

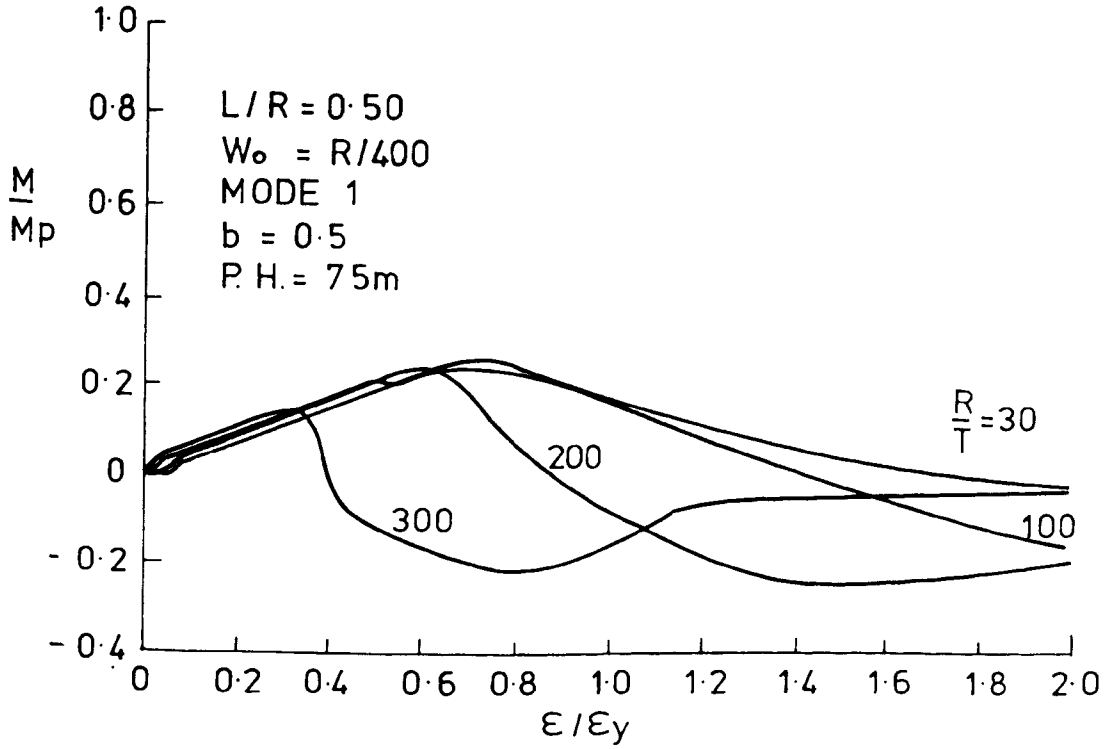

Fig. 6.167b

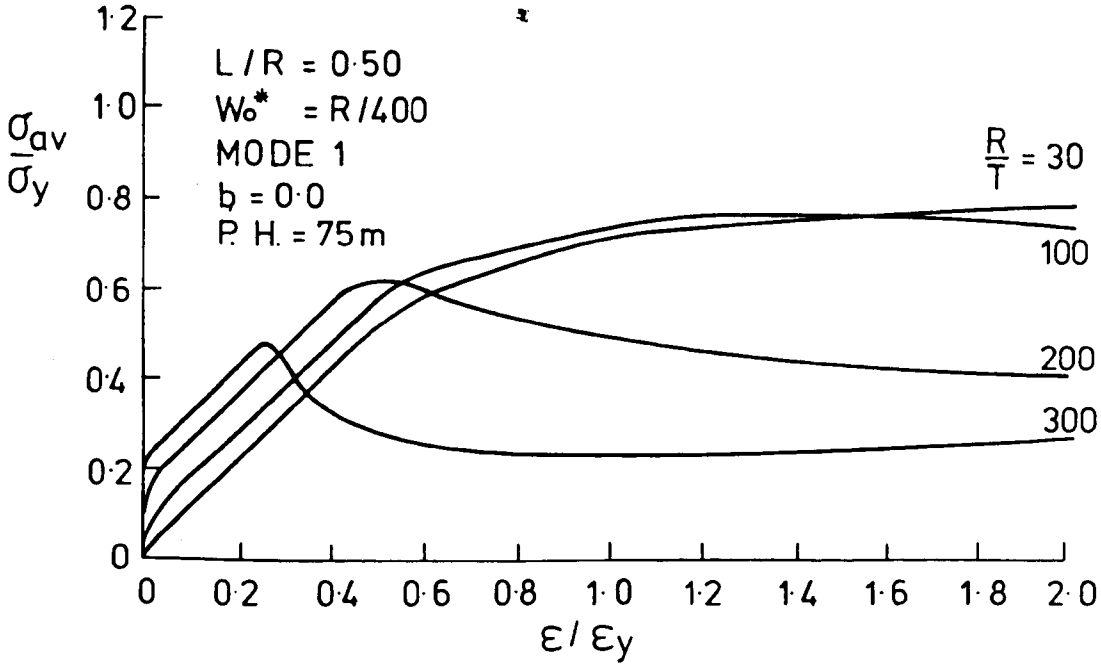

Fig. 6.168a

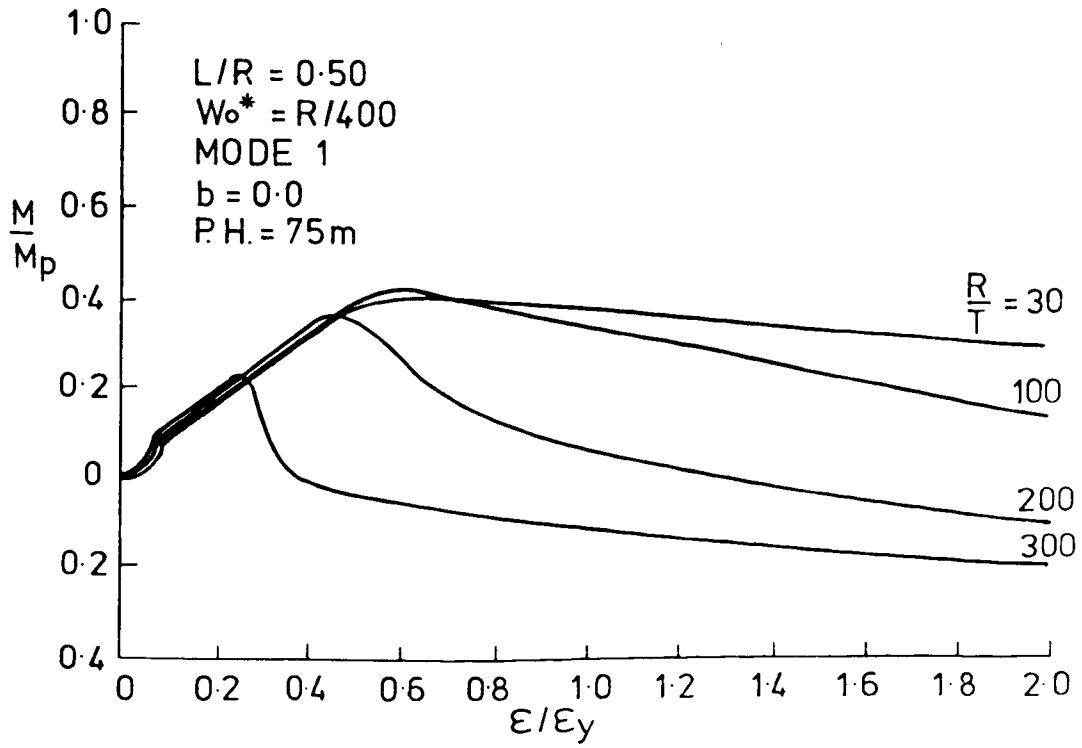

Fig. 6.168b

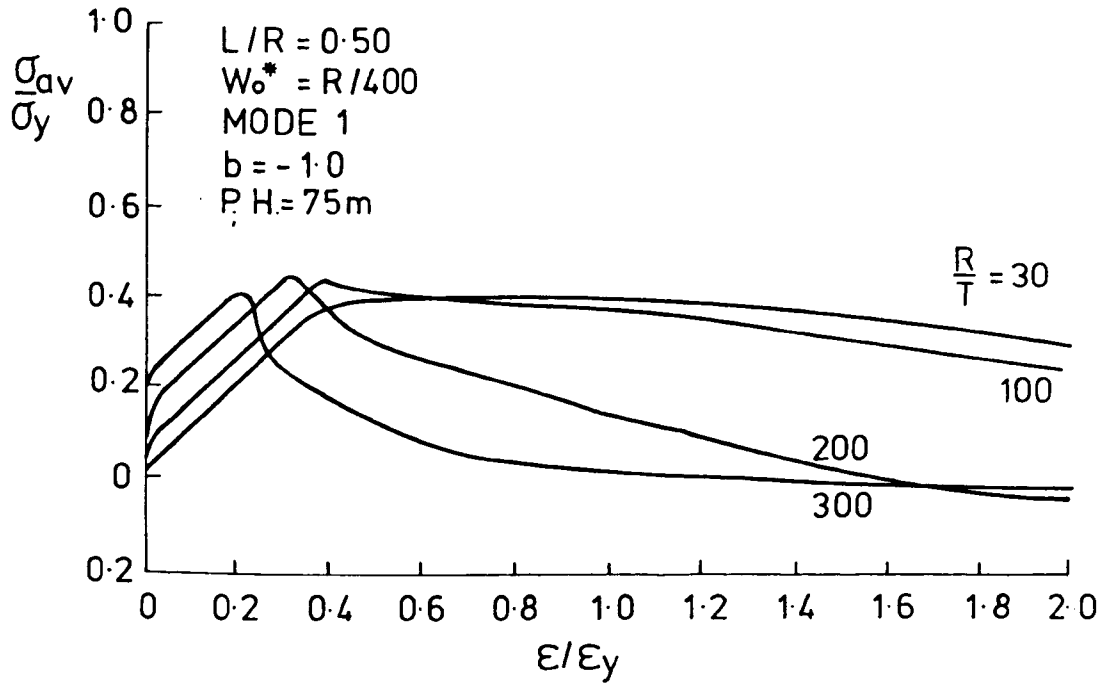

Fig. 6.169a

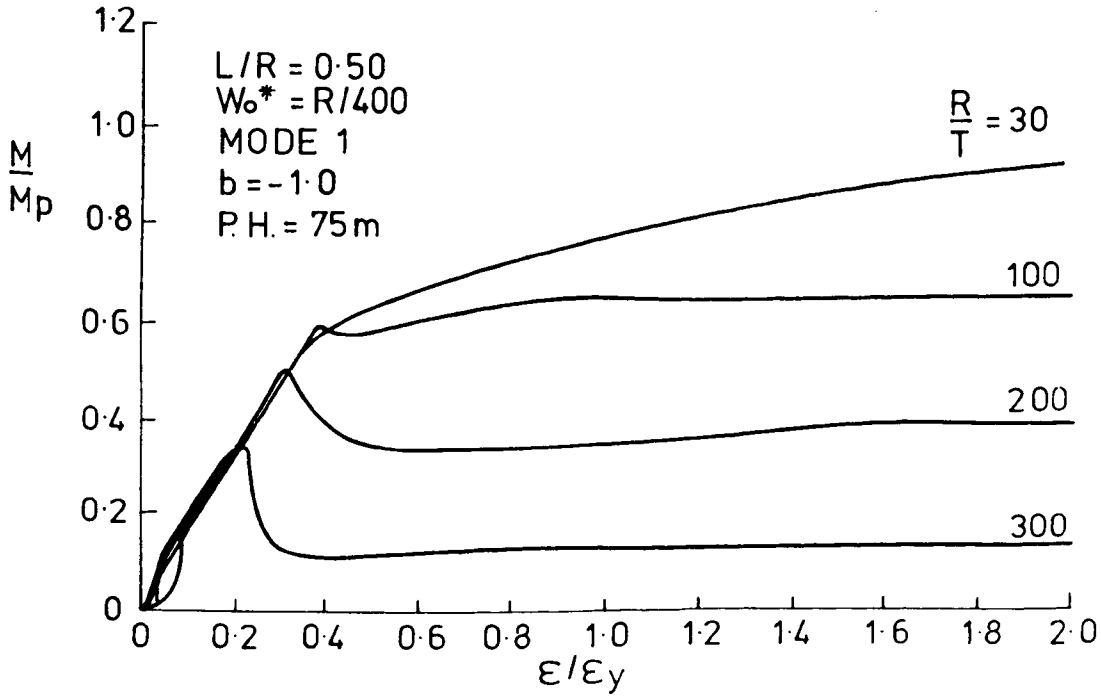

Fig. 6.169b

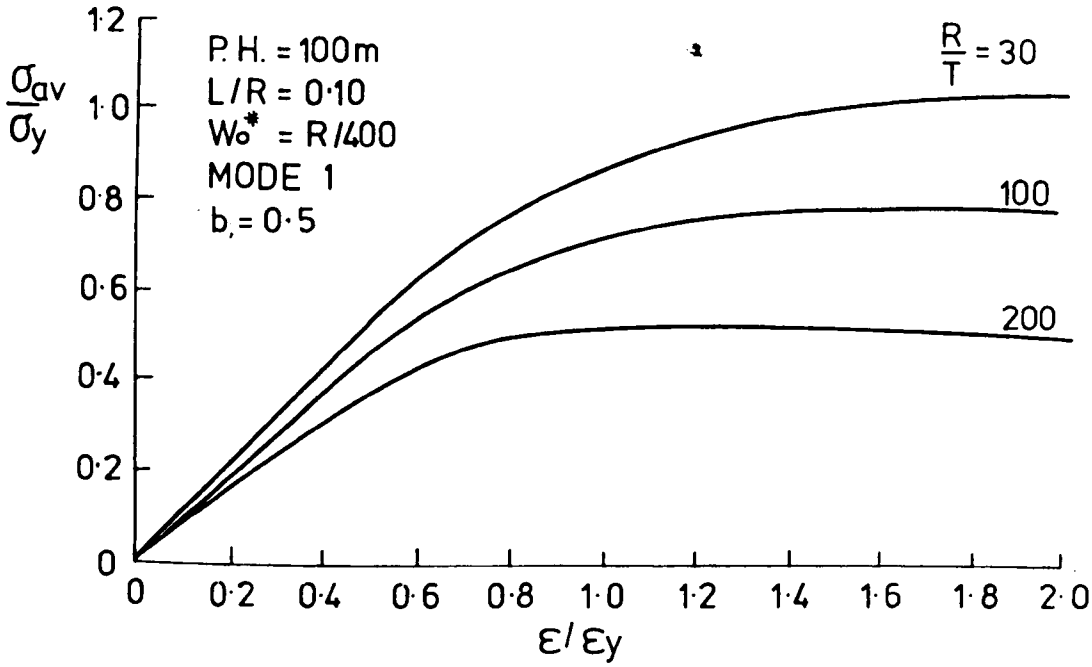

Fig. 6. 170a

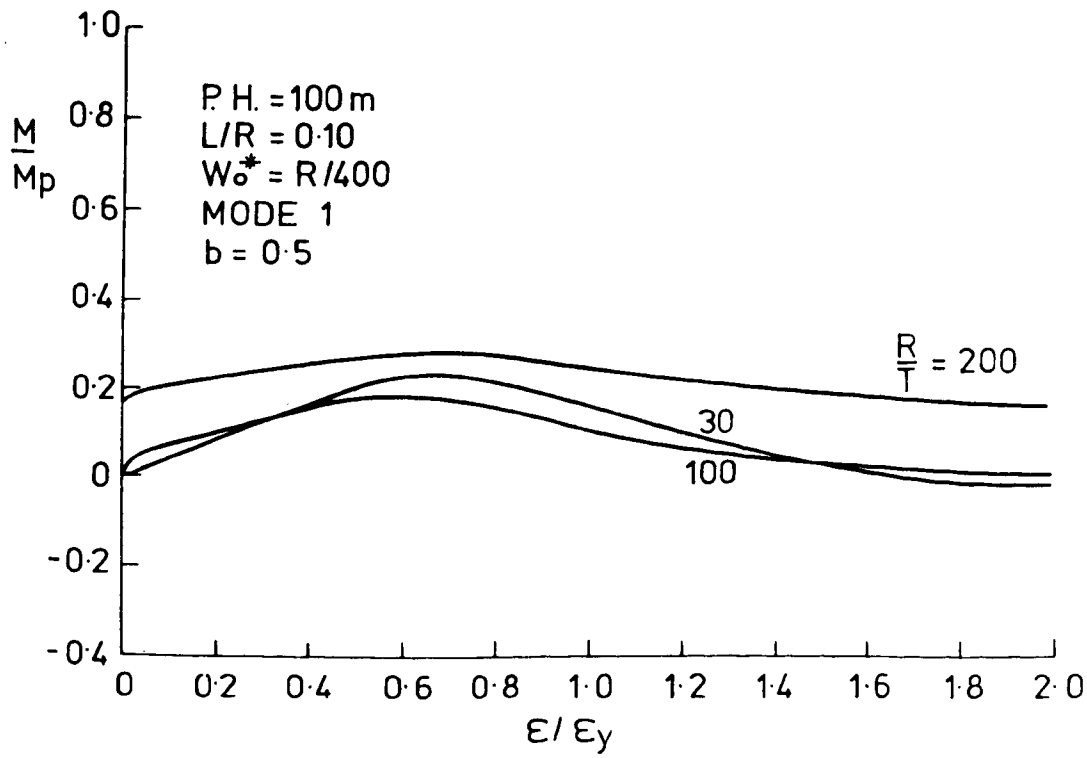

Fig. 6.170b

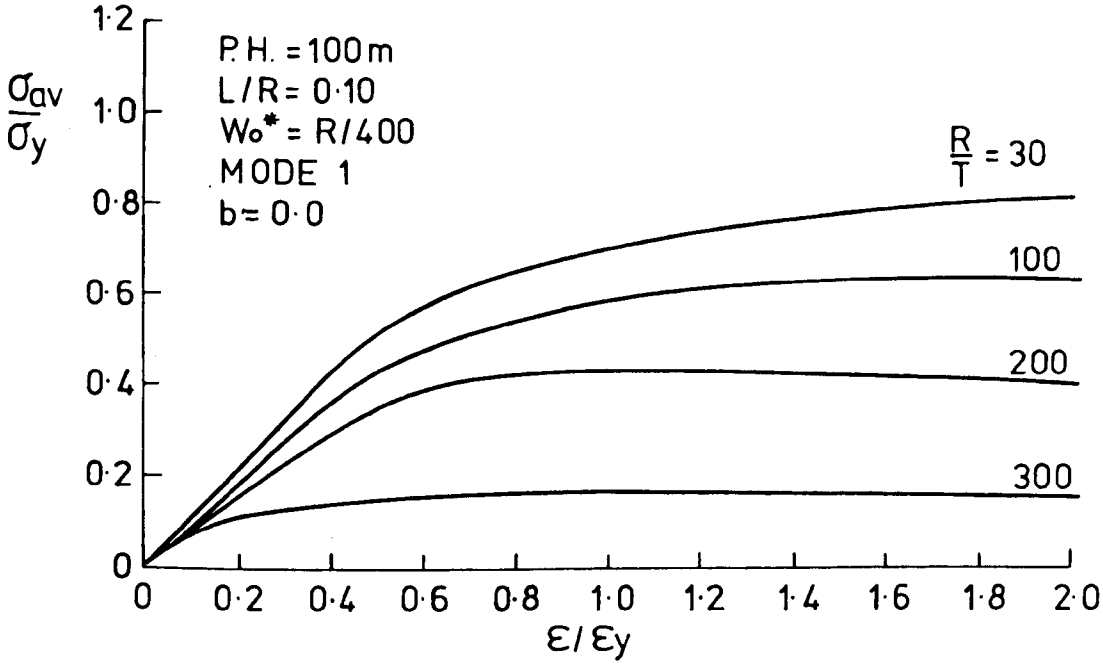

Fig. 6. 171a

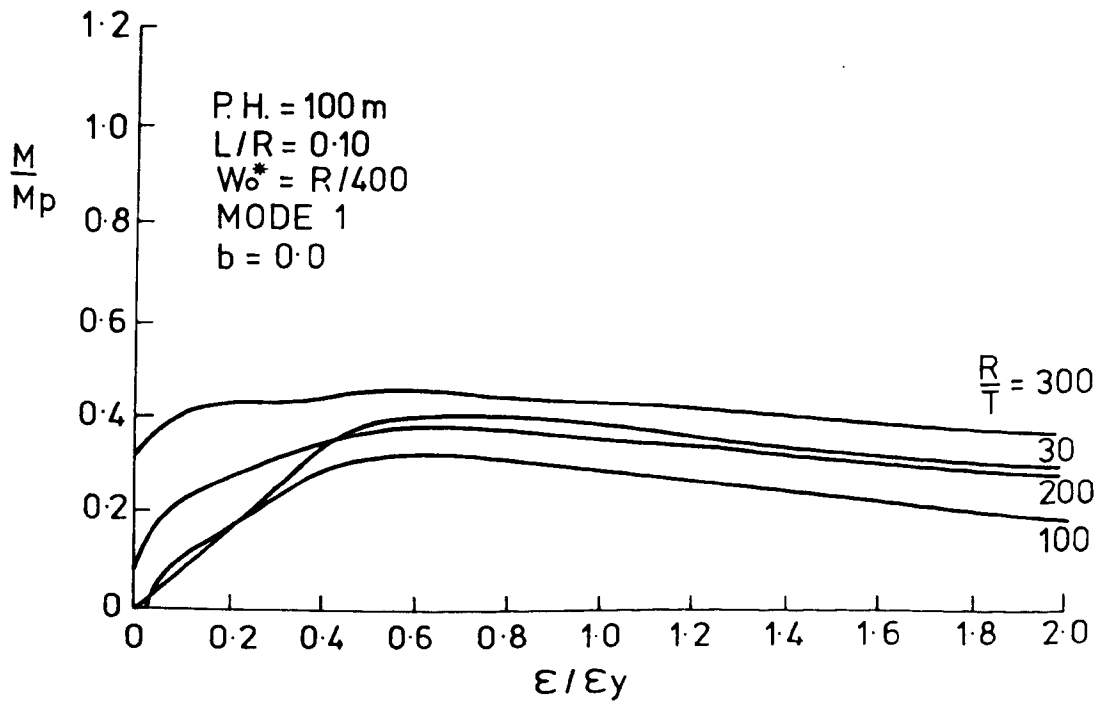

Fig. 6. 171b

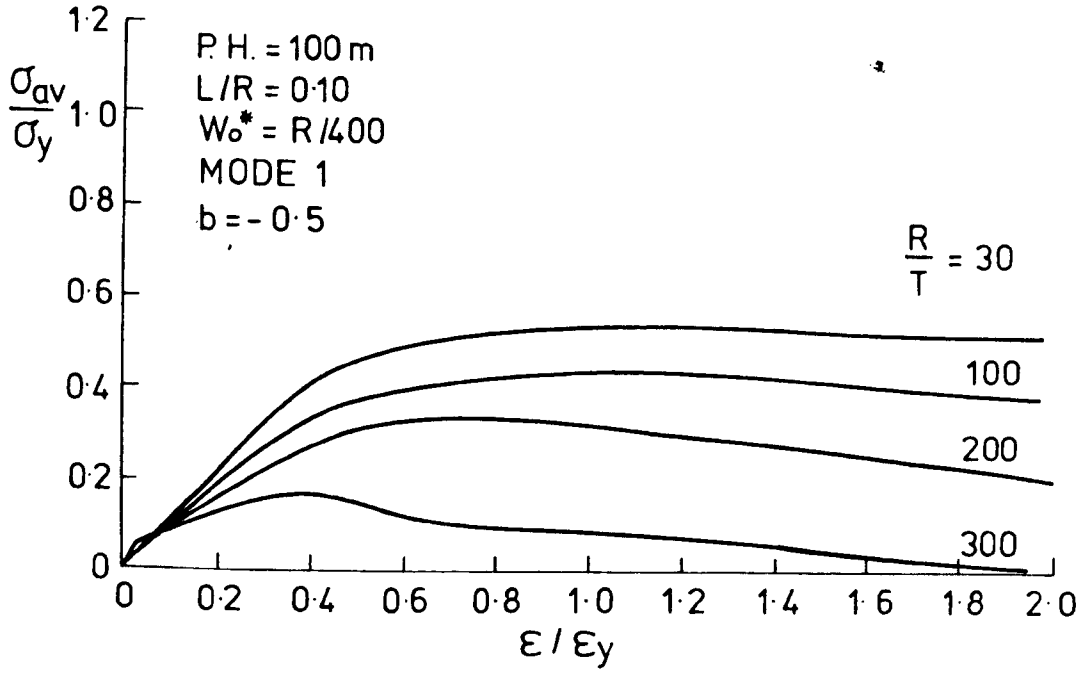

Fig. 6.172a

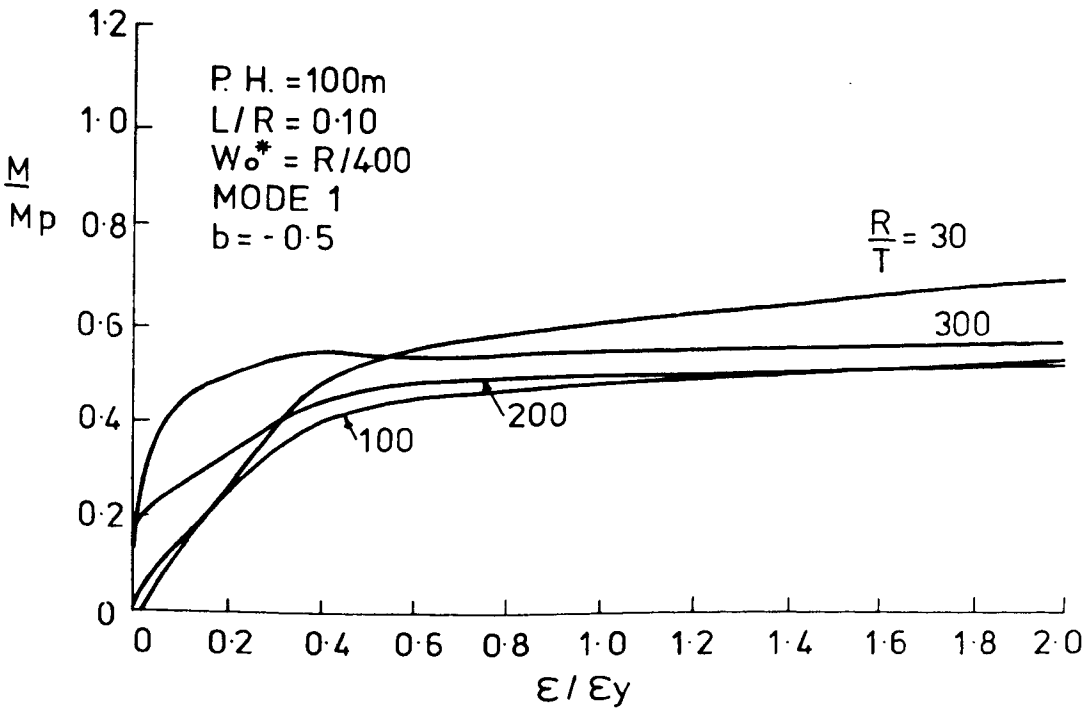

Fig. 6.172b

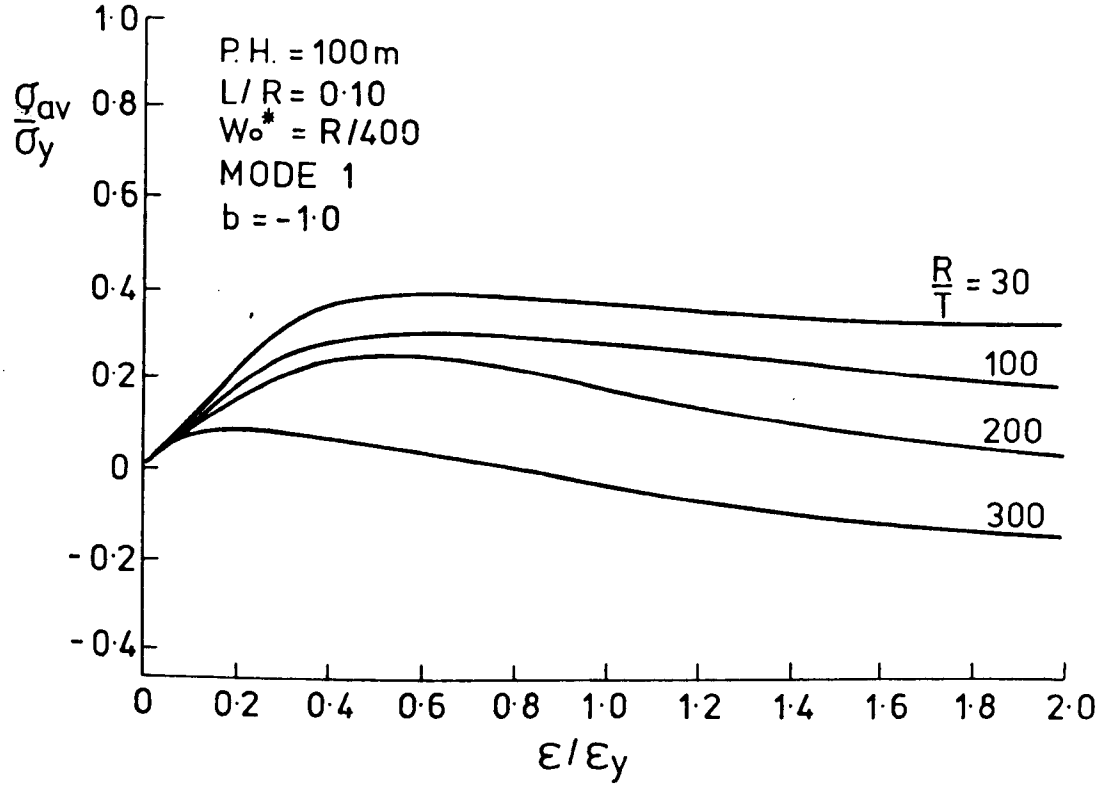

Fig. 6.173a

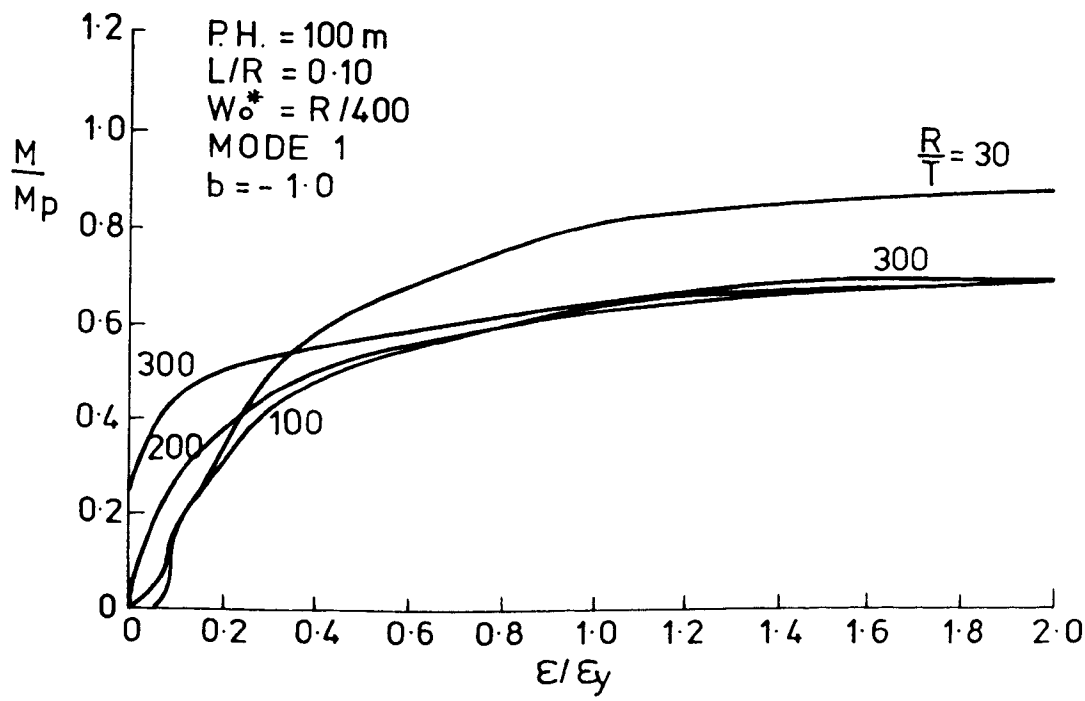

Fig. 6.173b

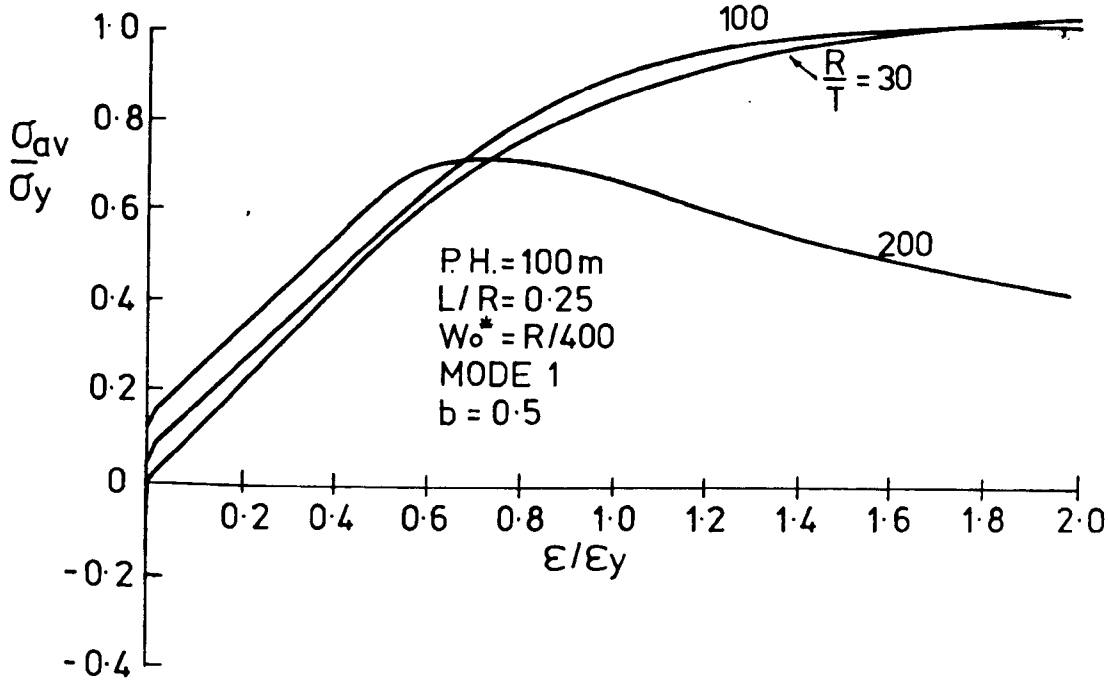

Fig. 6. 174a

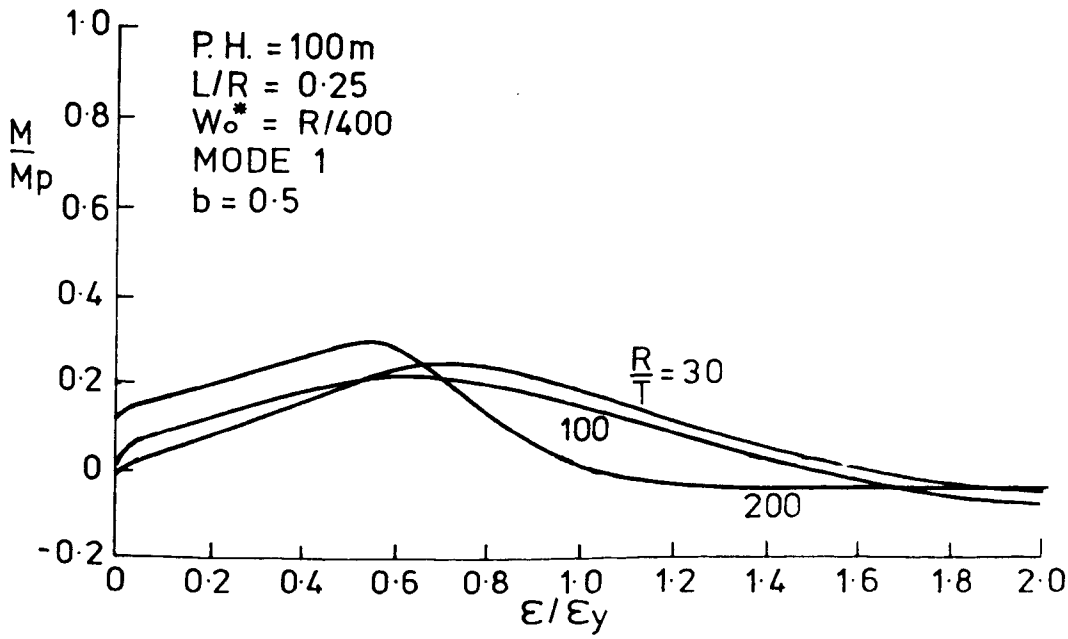

Fig. 6. 174b

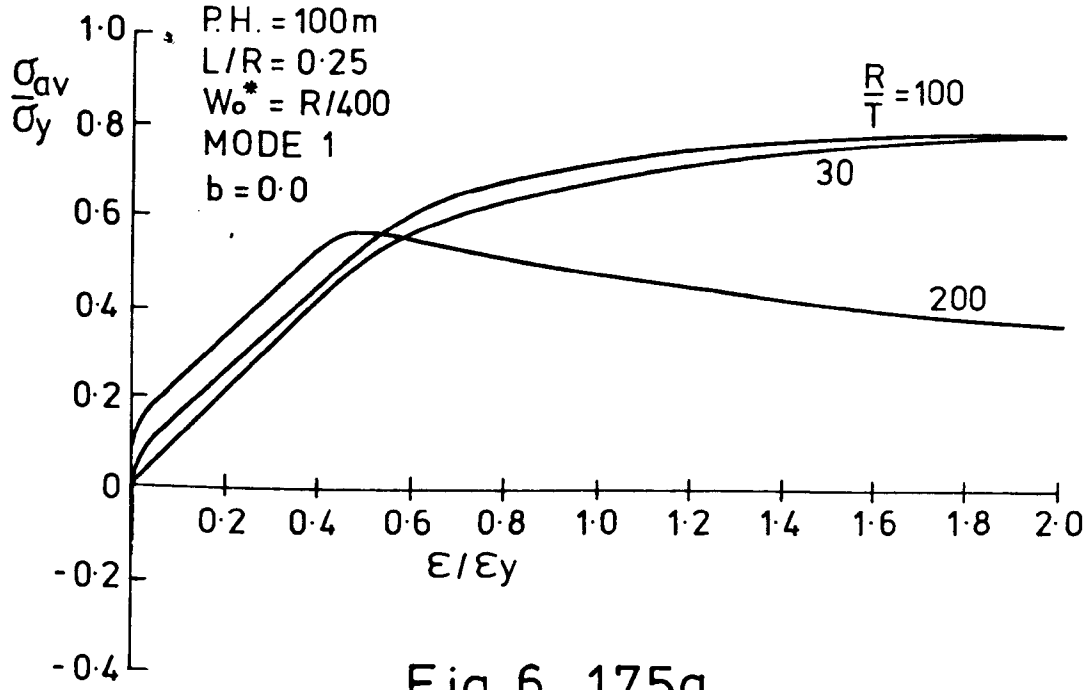

Fig. 6. 175a

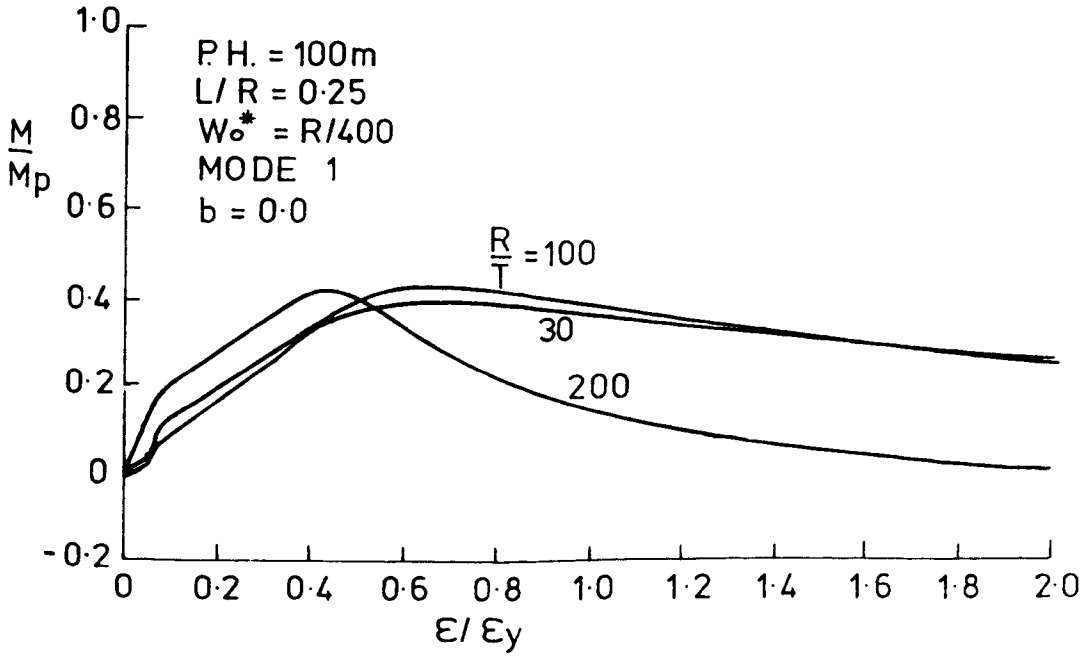

Fig. 6.175b

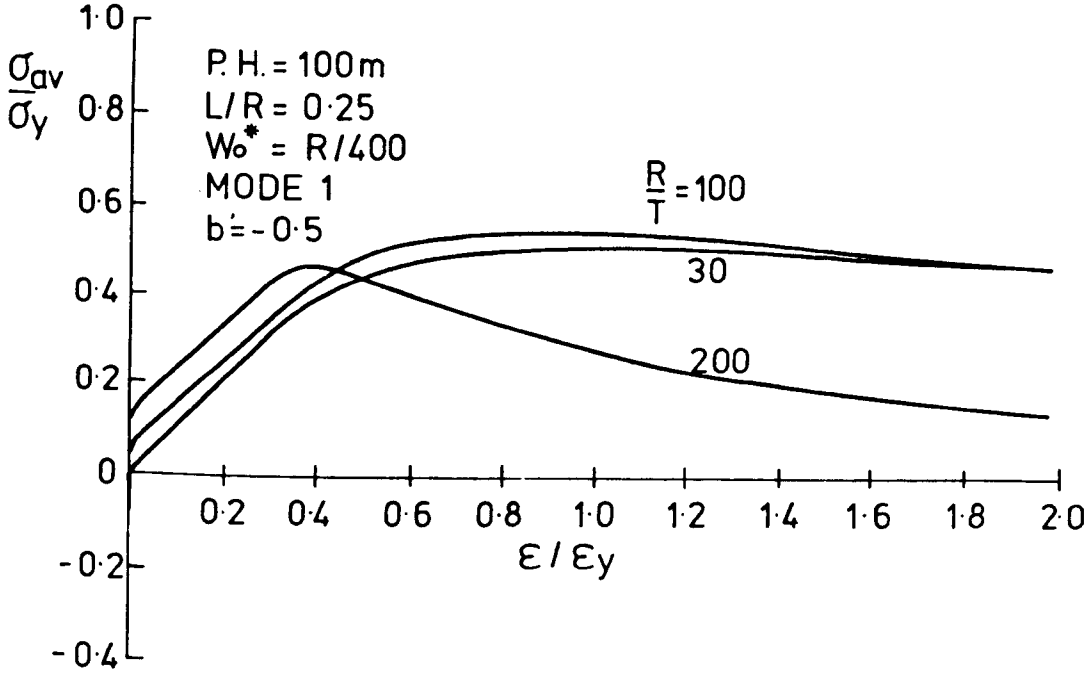

Fig. 6. 176a

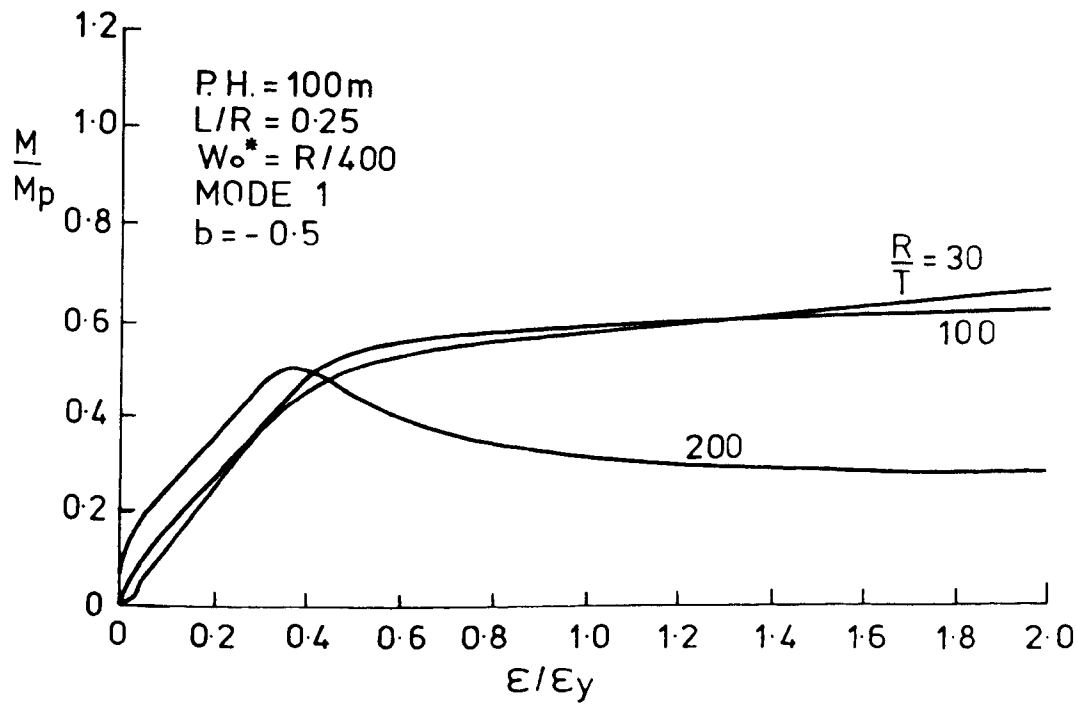

Fig. 6. 176b

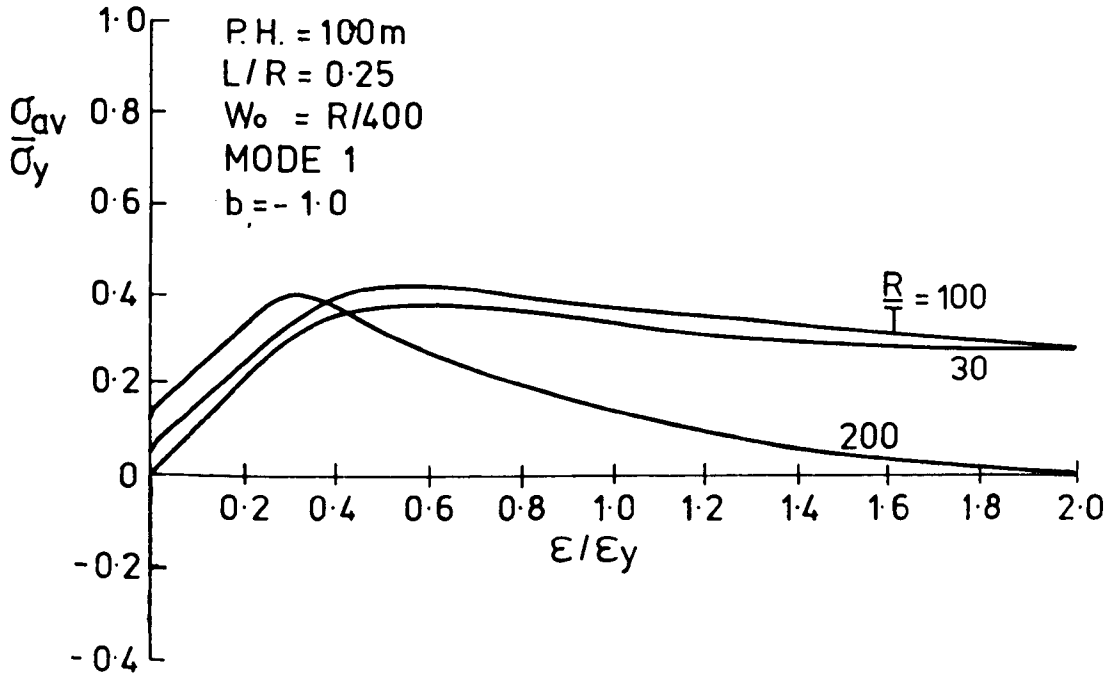

Fig. 6.177a

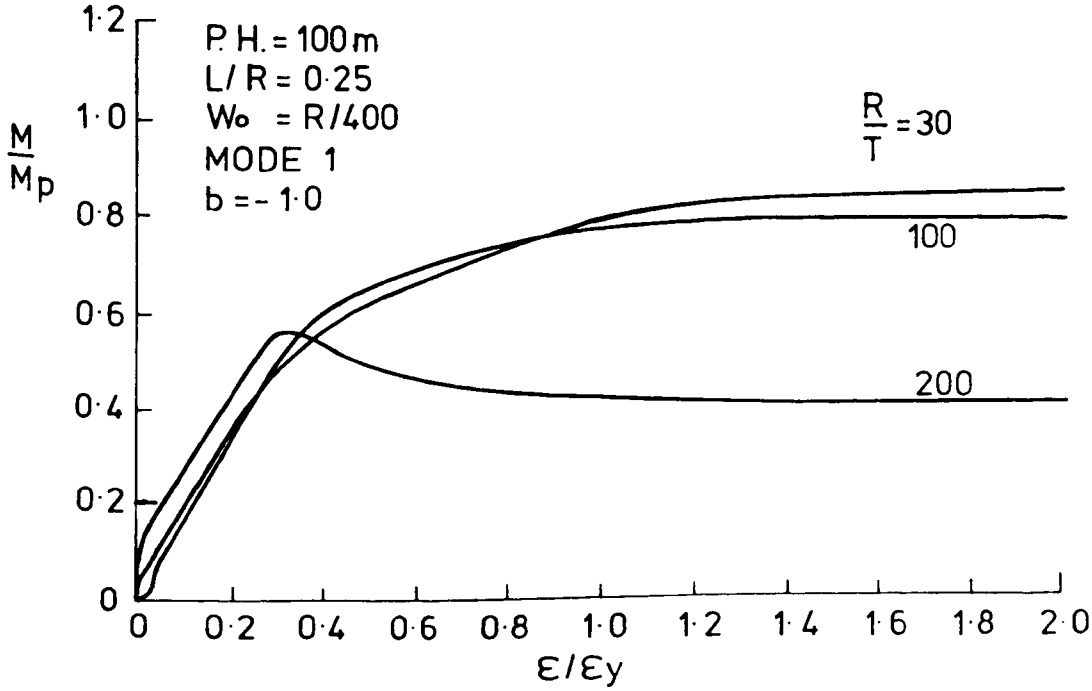

Fig. 6.177b

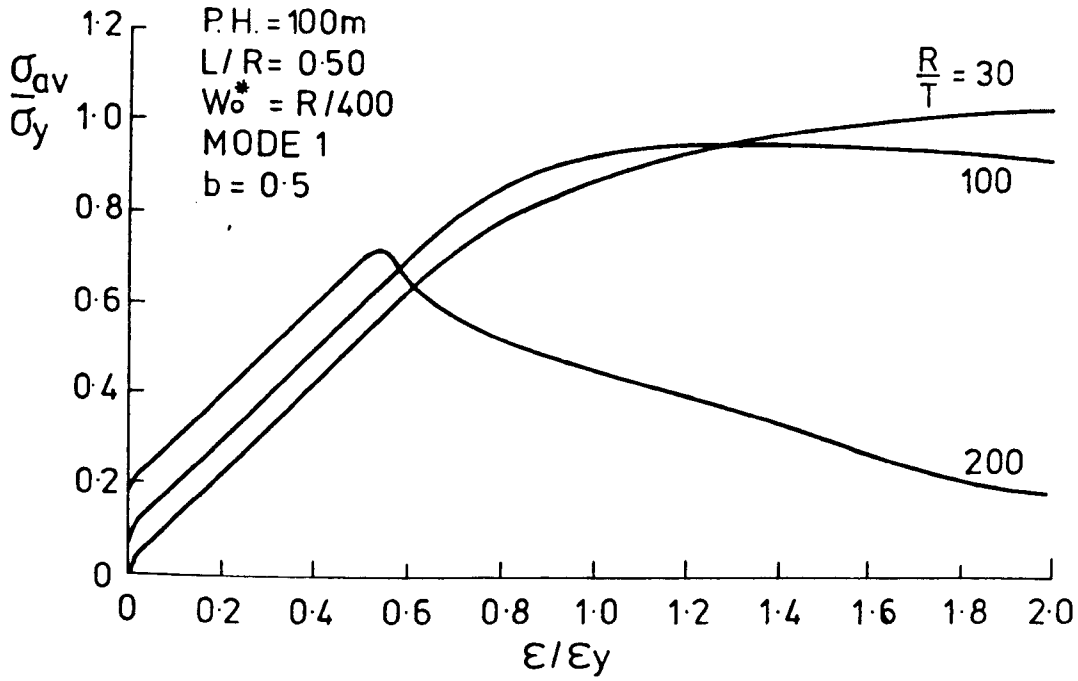

Fig. 6.178a

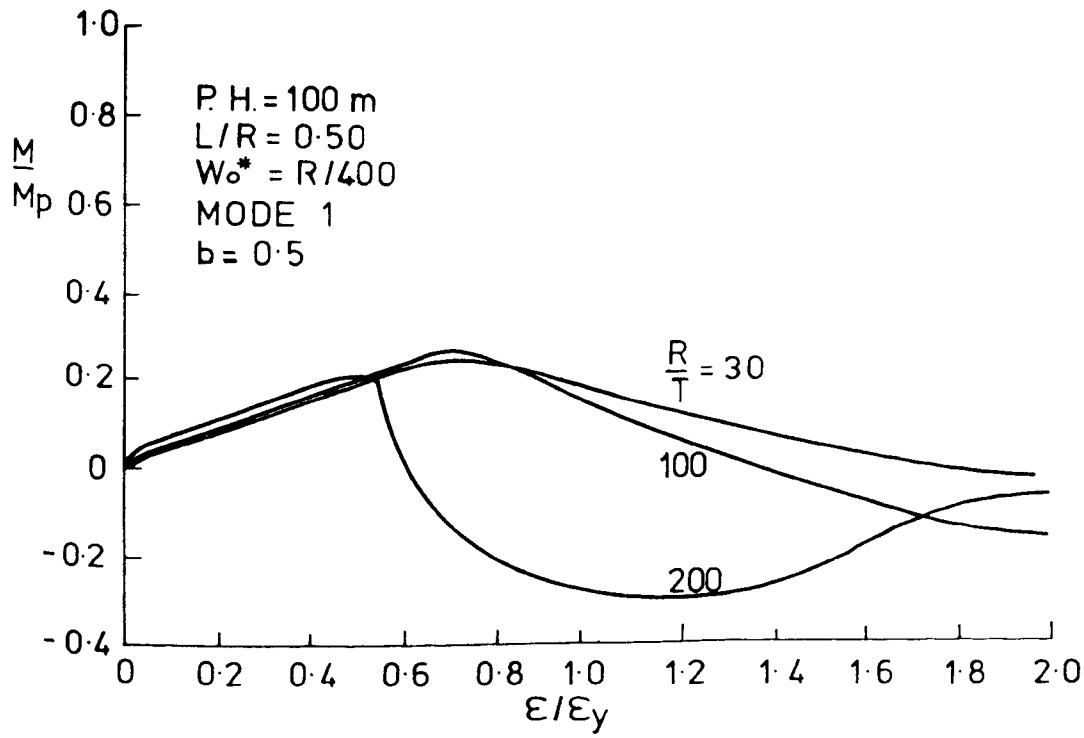

Fig. 6. 178b

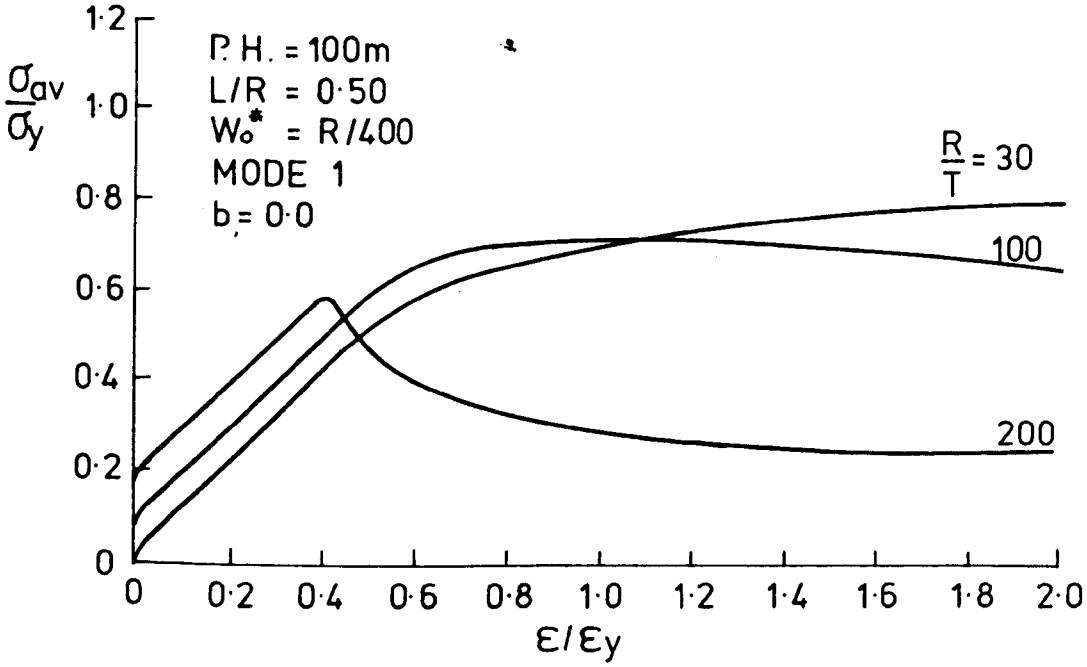

Fig. 6. 179a

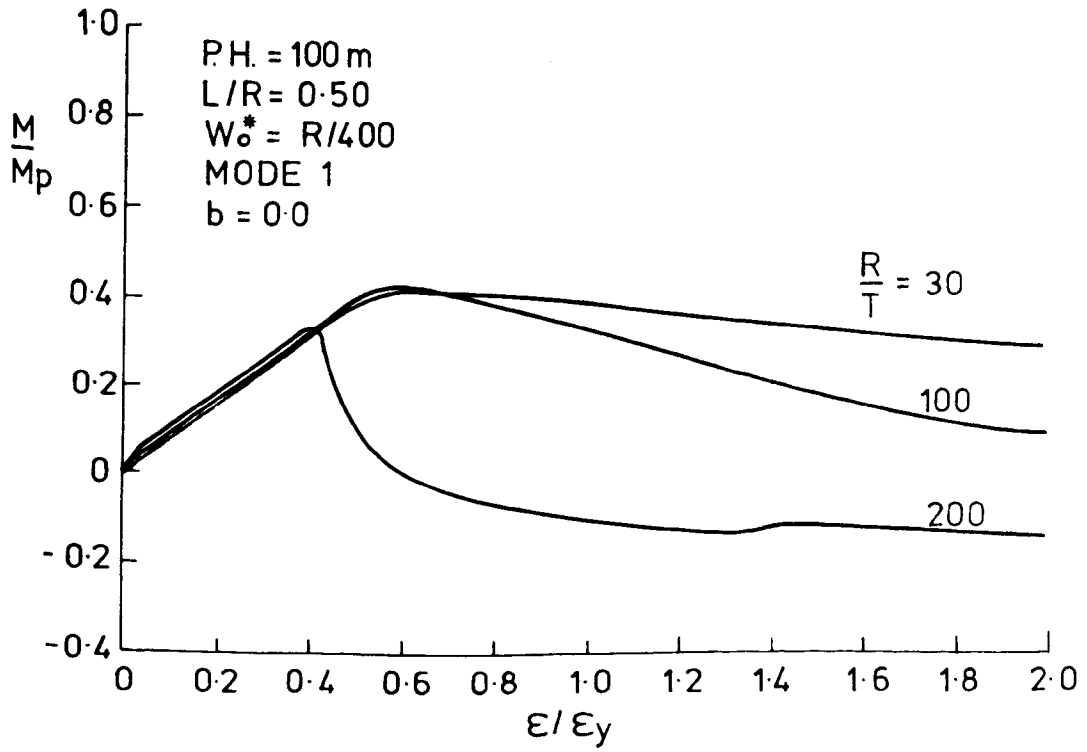

Fig. 6. 179b

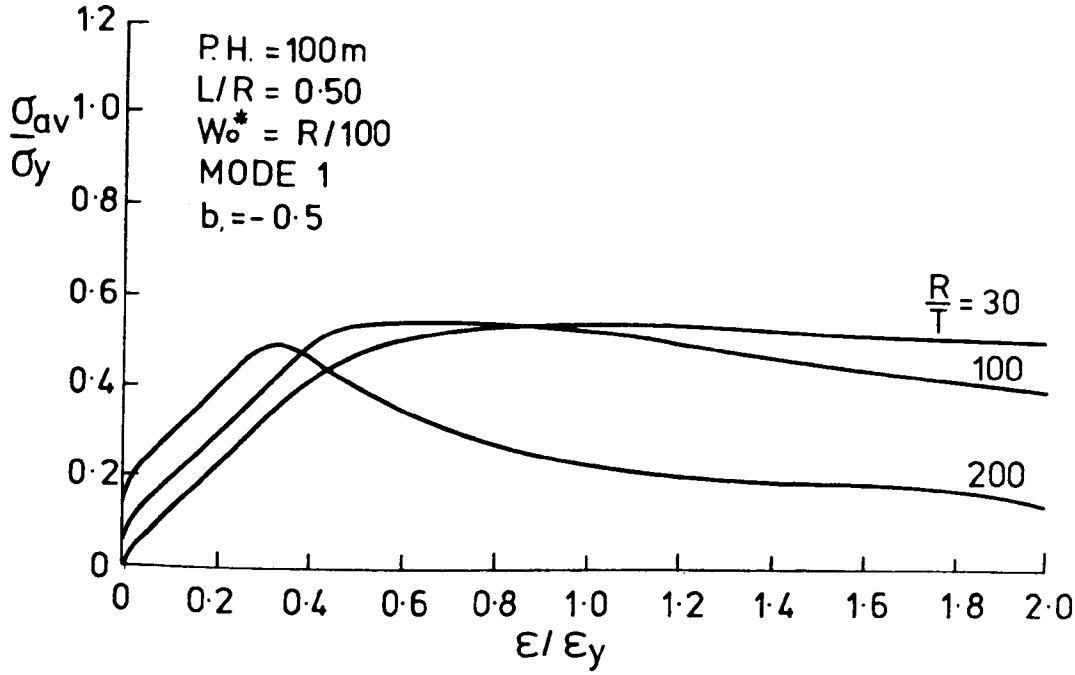

Fig. 6. 180a

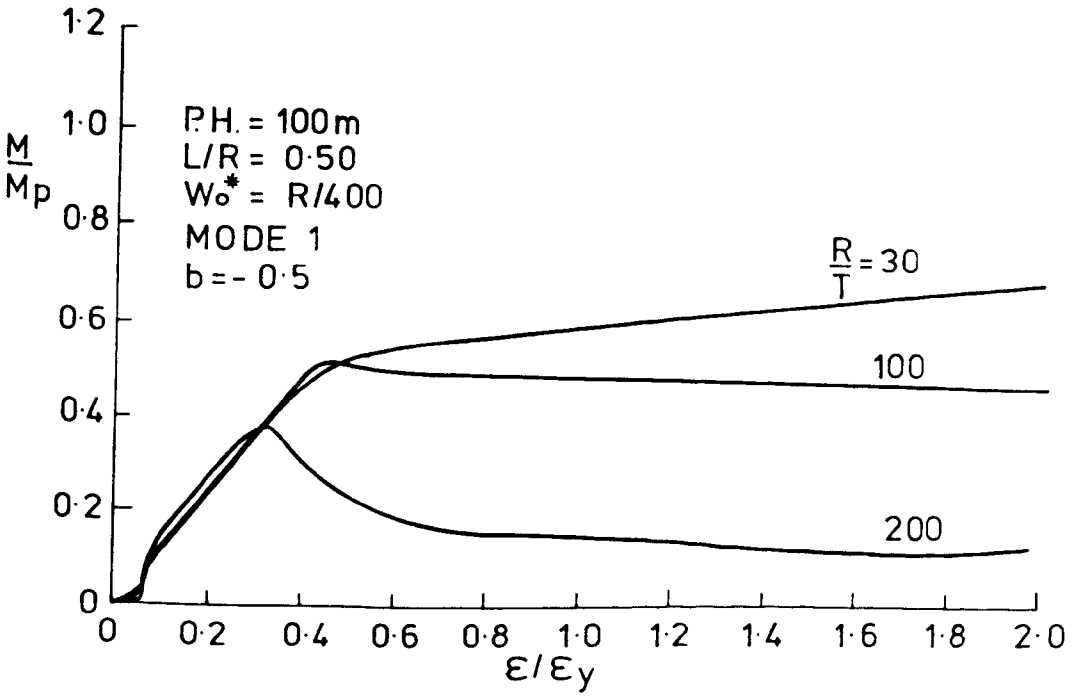

Fig. 6. 180b

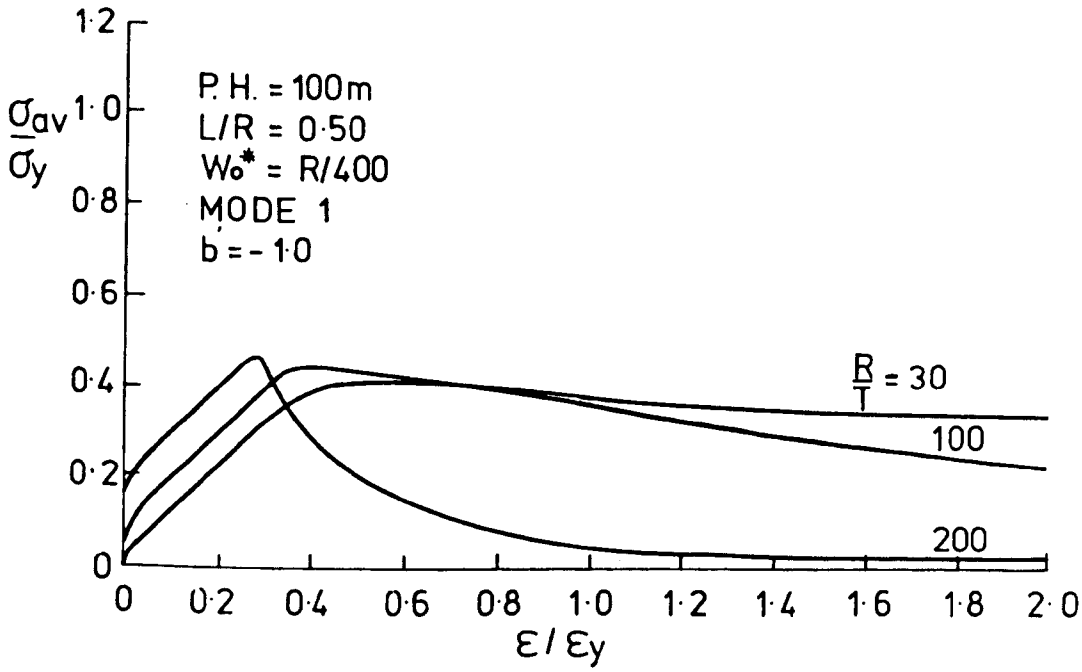

Fig. 6. 181a

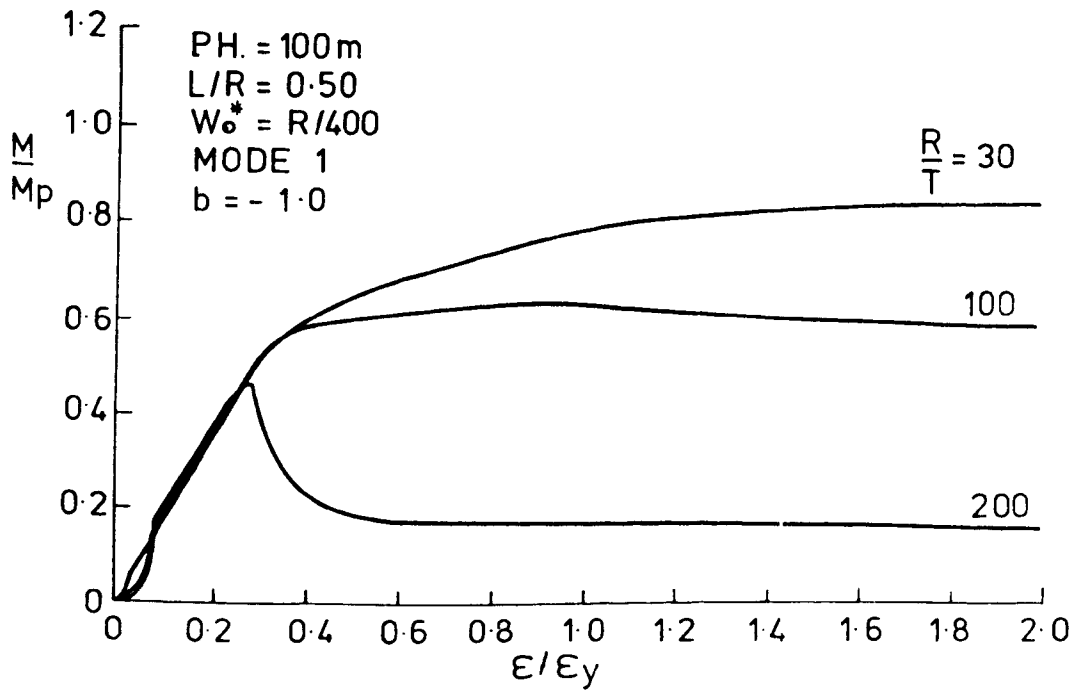

Fig. 6. 181b

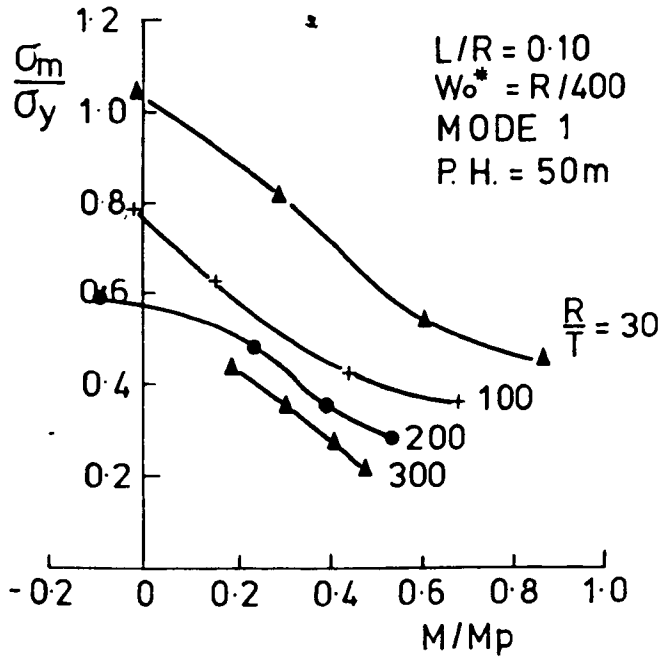

Fig. 6. 182

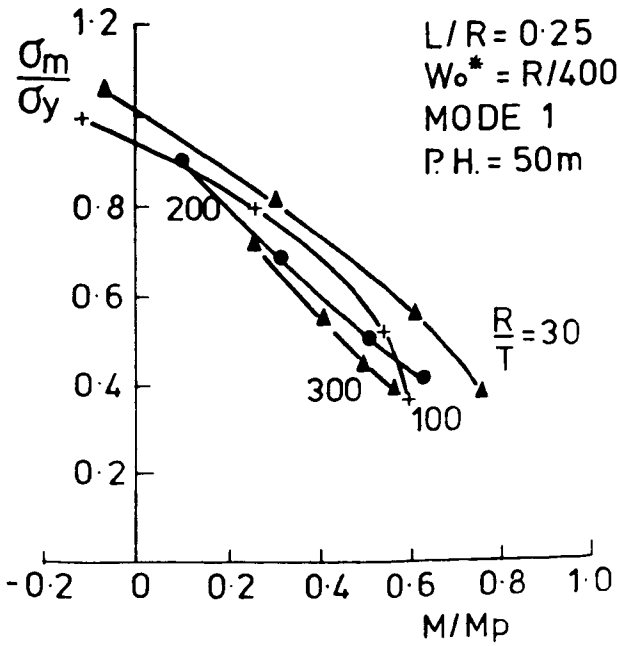

Fig. 6. 183

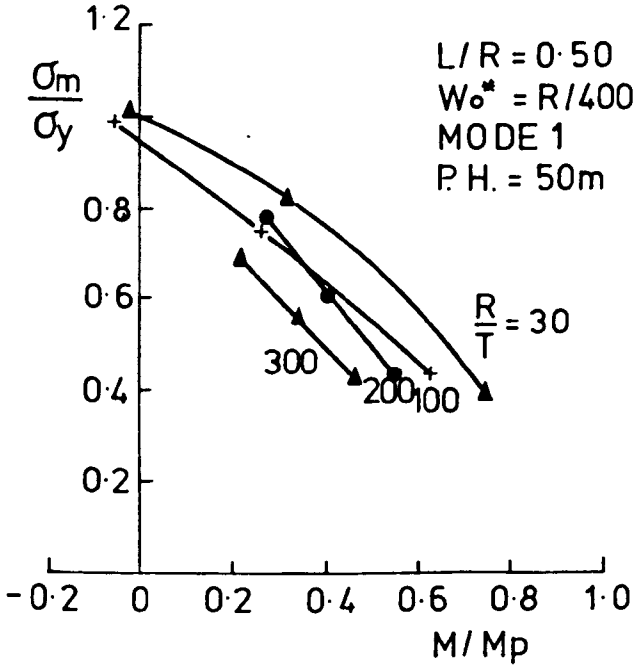

Fig. 6. 184

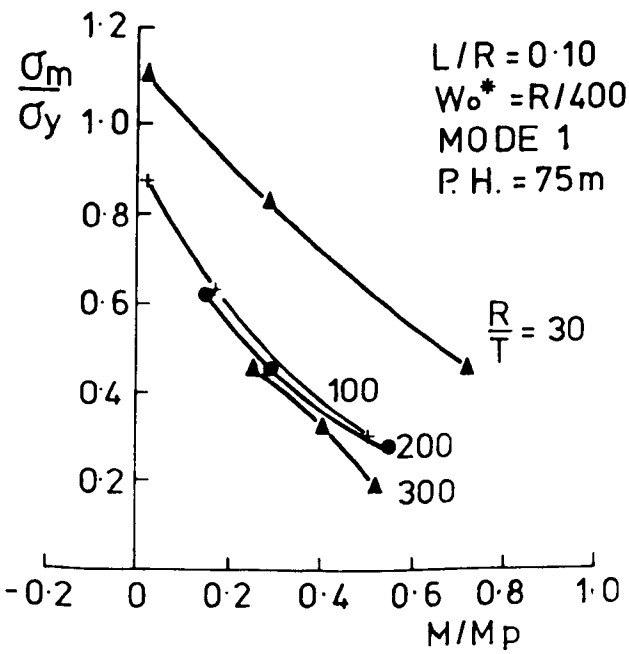

Fig.6. 185

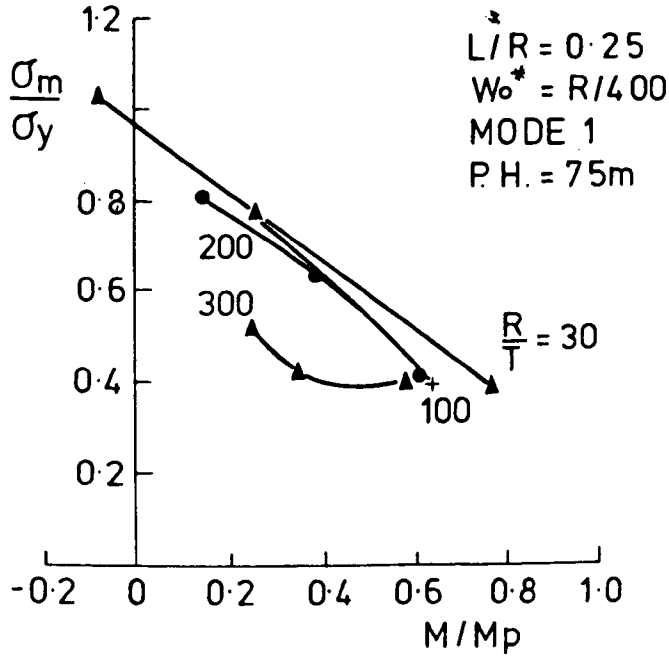

Fig. 6.186

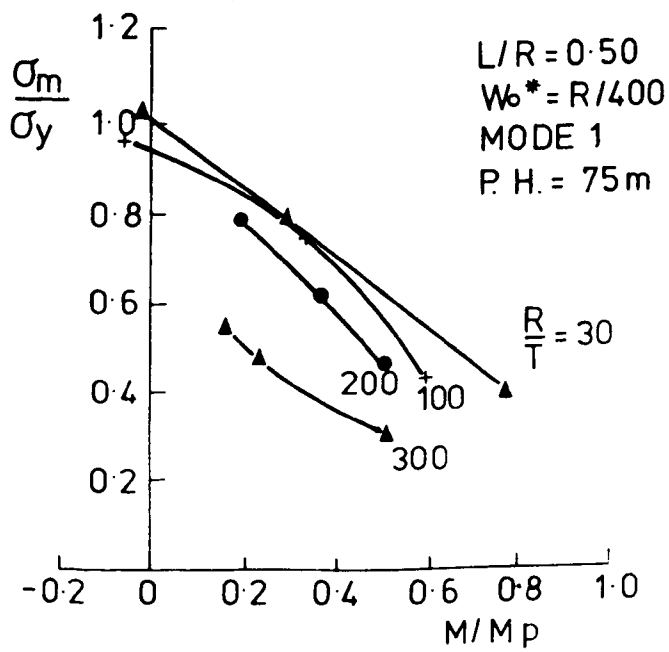

Fig. 6.187

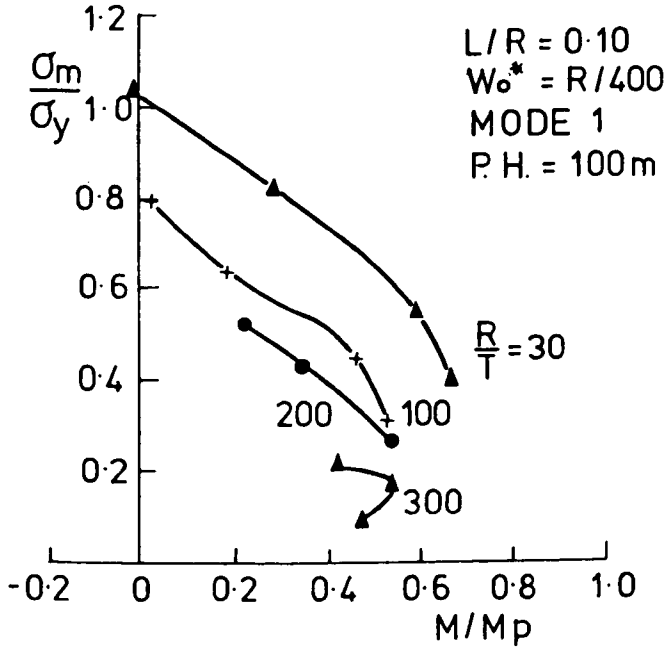

Fig.6.188

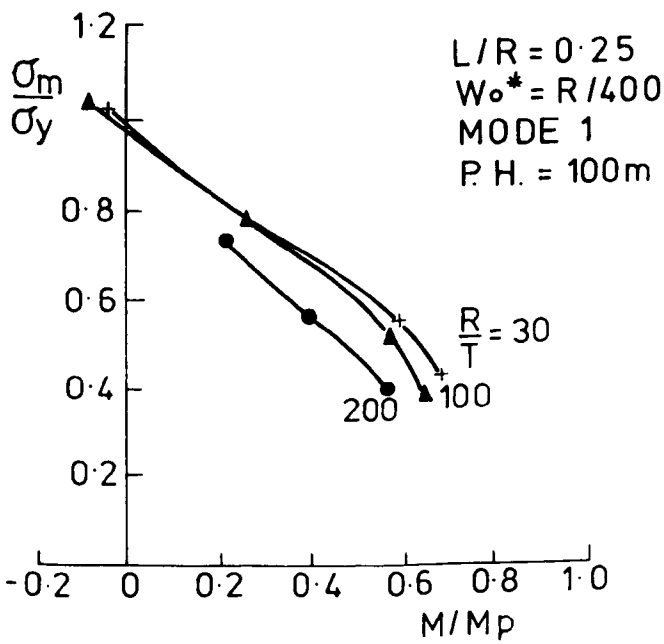

Fig. 6. 189

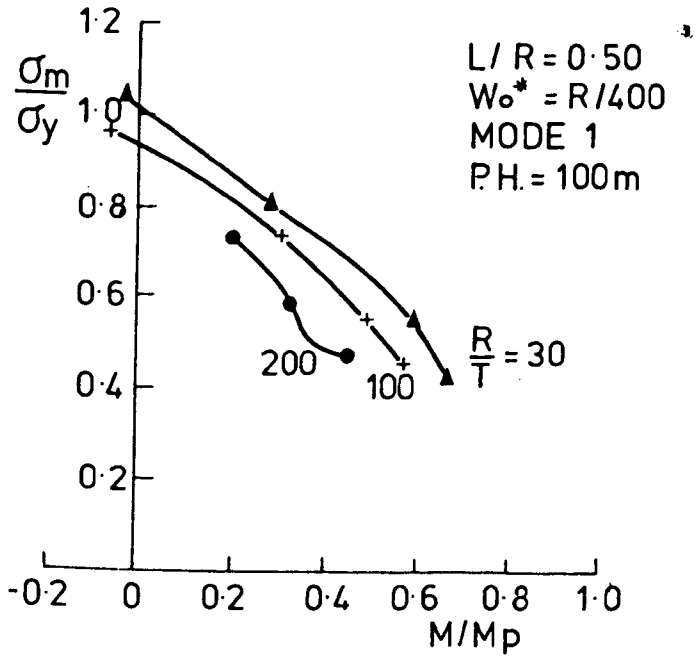

Fig. 6. 190

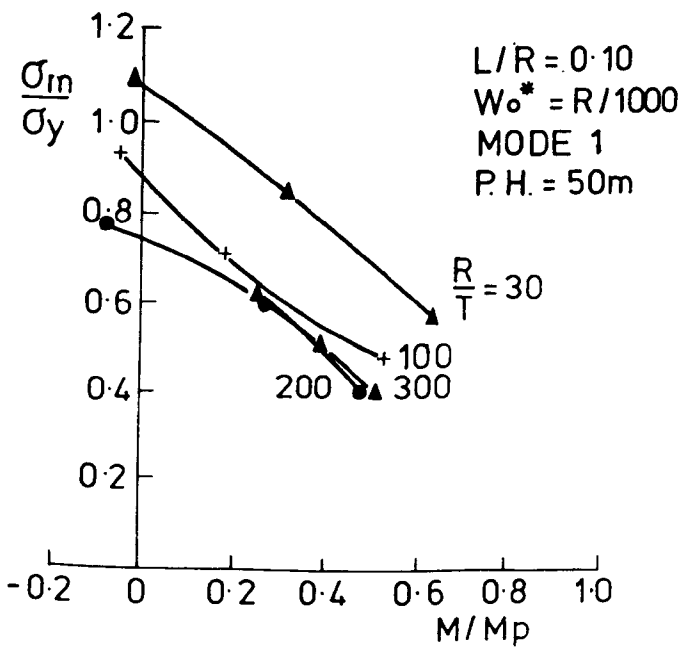

Fig. 6. 191

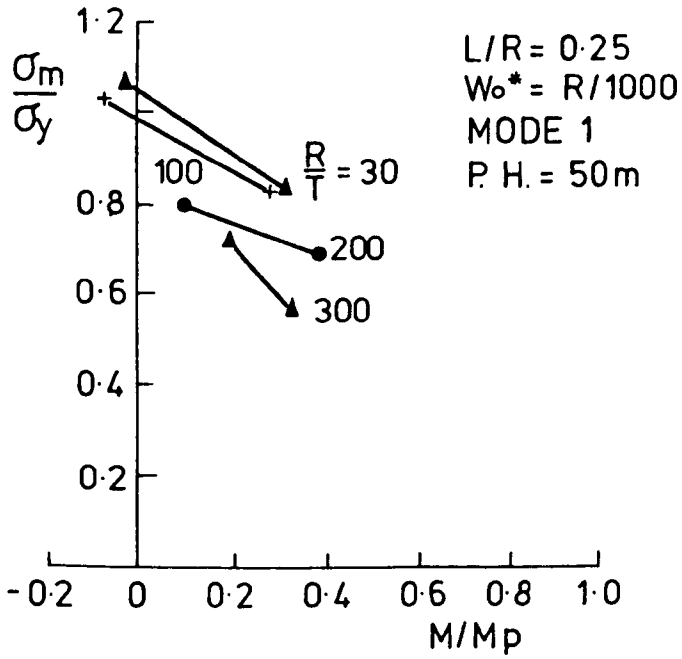

Fig. 6.192

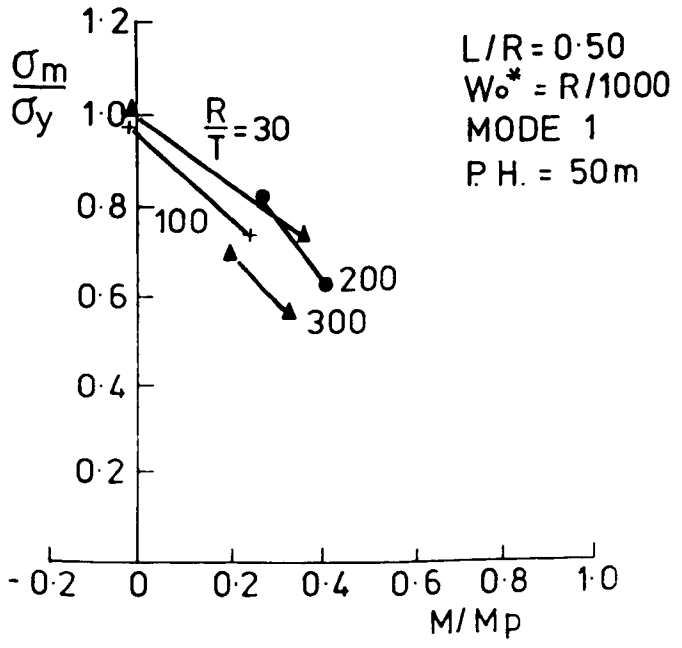

Fig. 6.193

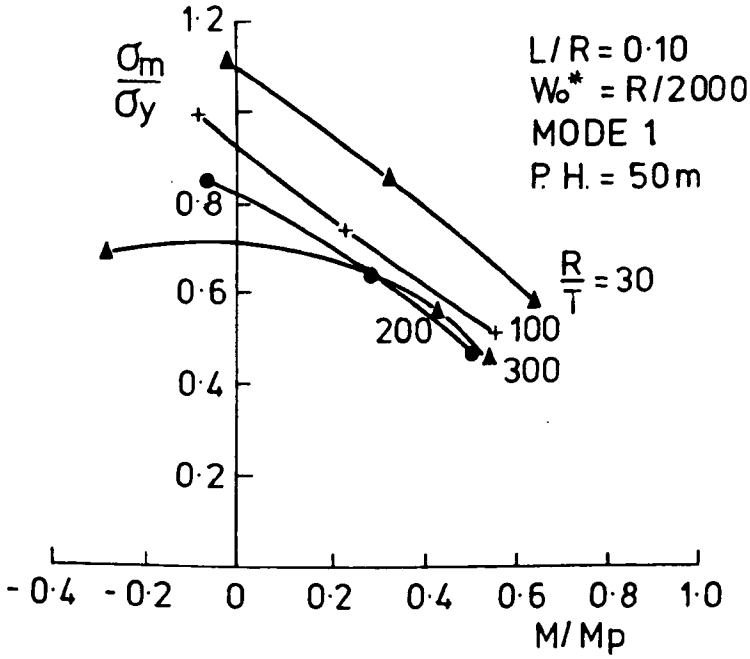

Fig. 6.194

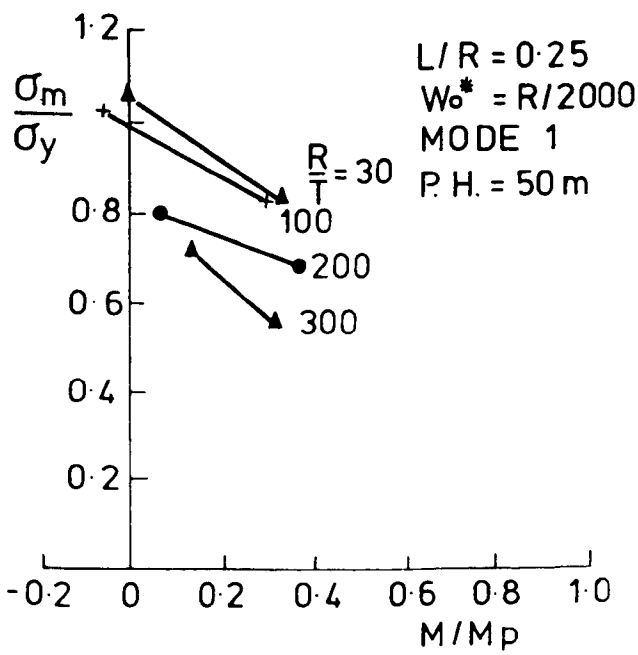

Fig. 6.195

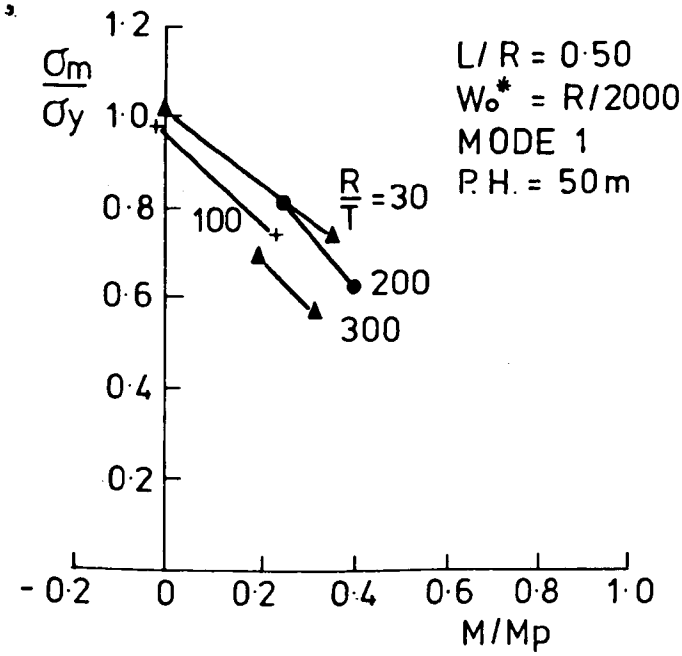

Fig.6. 196

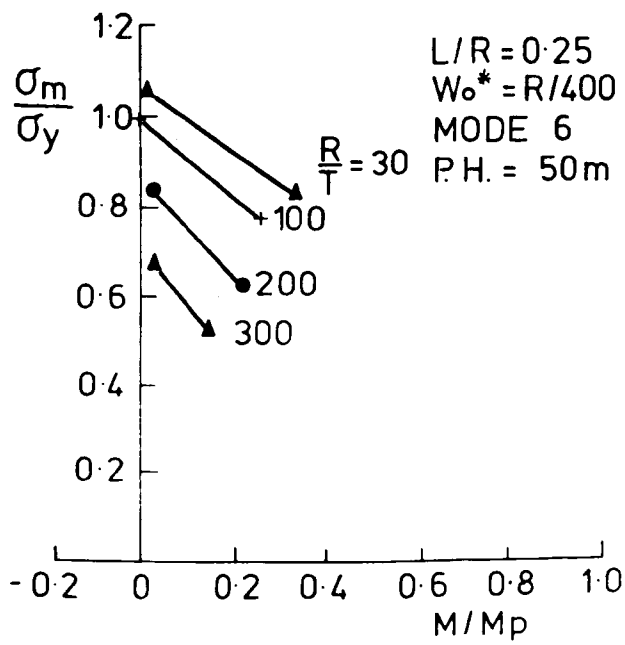

Fig. 6.197

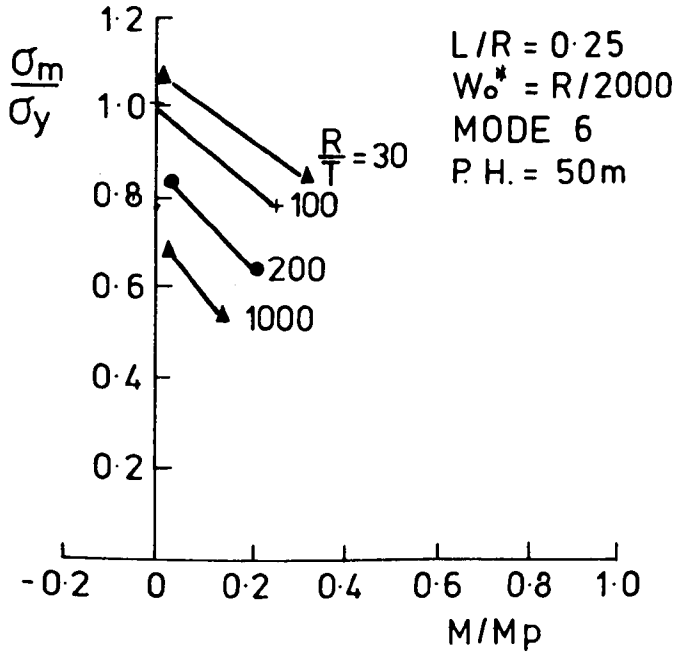

Fig. 6.198

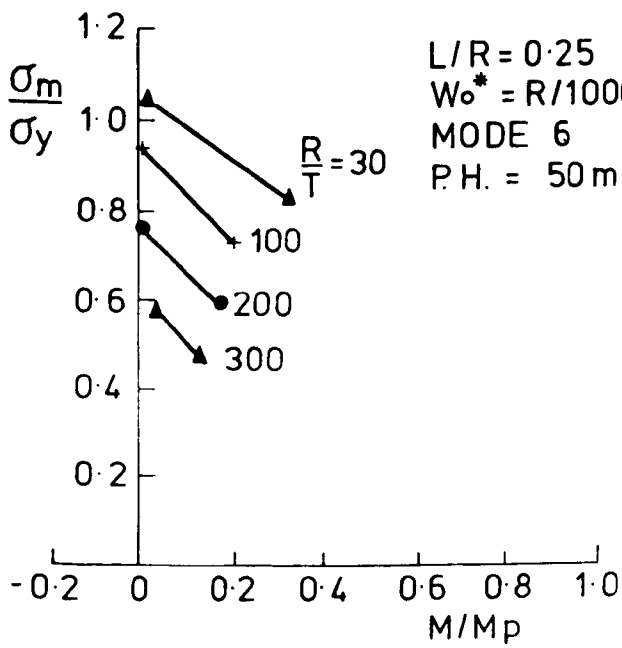

Fig. 6.199

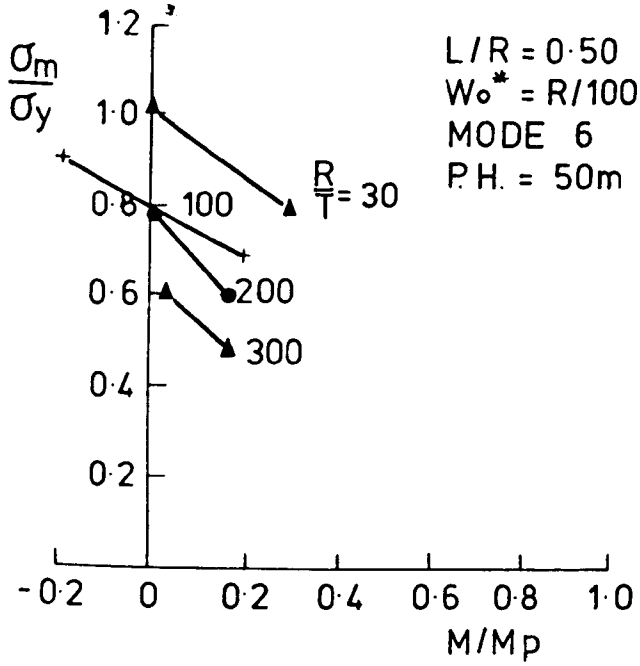
σm/σy
1·2
1·0
0·8
0·6
0·4
0·2
-0·2
0
0·2
0·4
0·6
0·8
1·0
M/Mp
R/T = 30
100
200
300
L/R = 0·50
Wo* = R/1000
MODE 6
P.H. = 50m

Fig.6.200

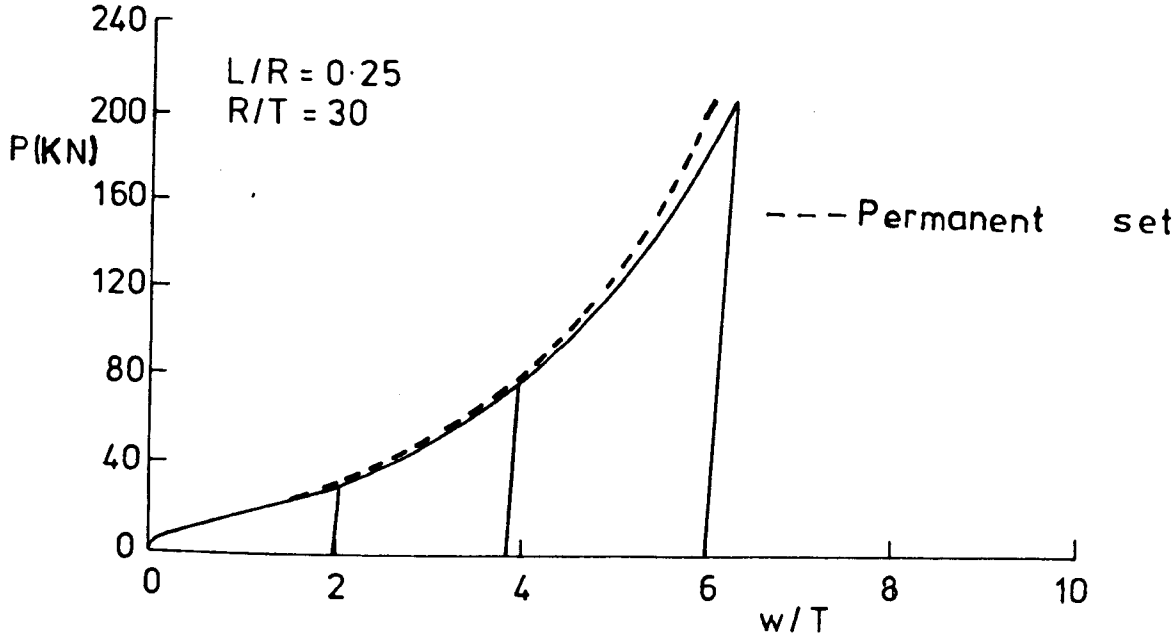

Fig. 6. 201a

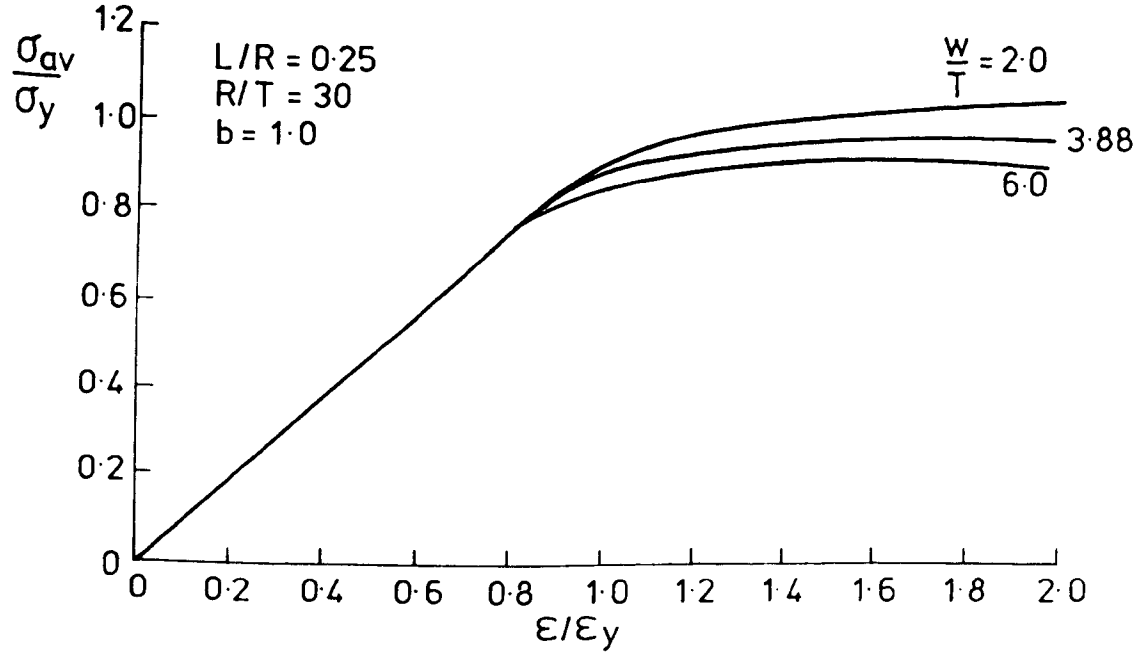

Fig. 6. 201b

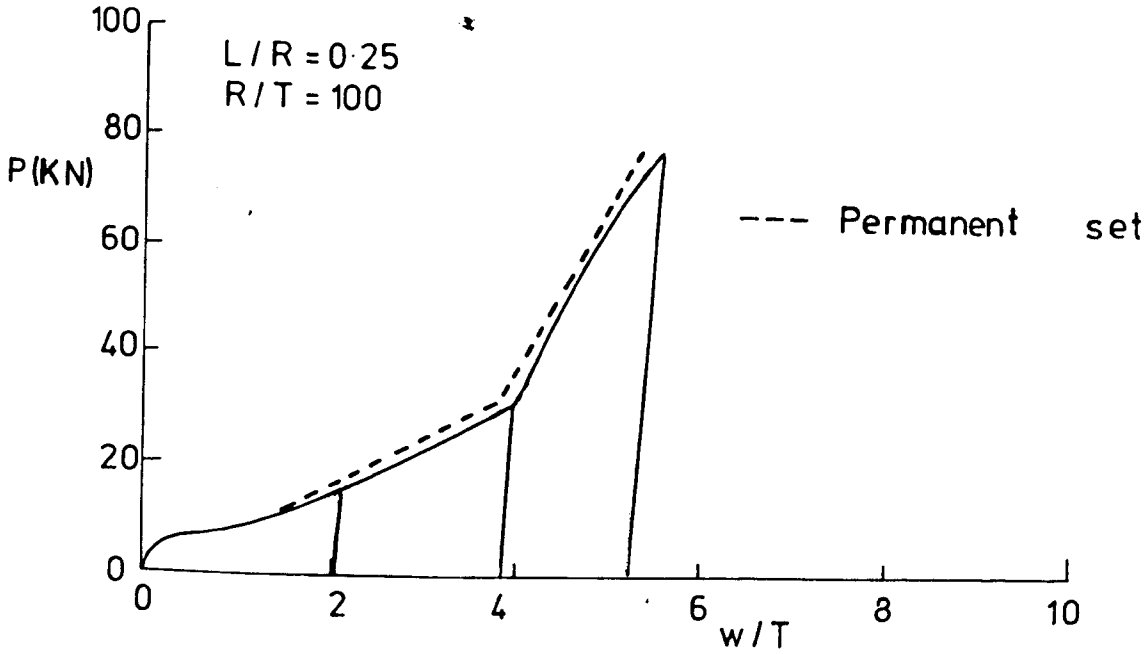

Fig. 6. 202a

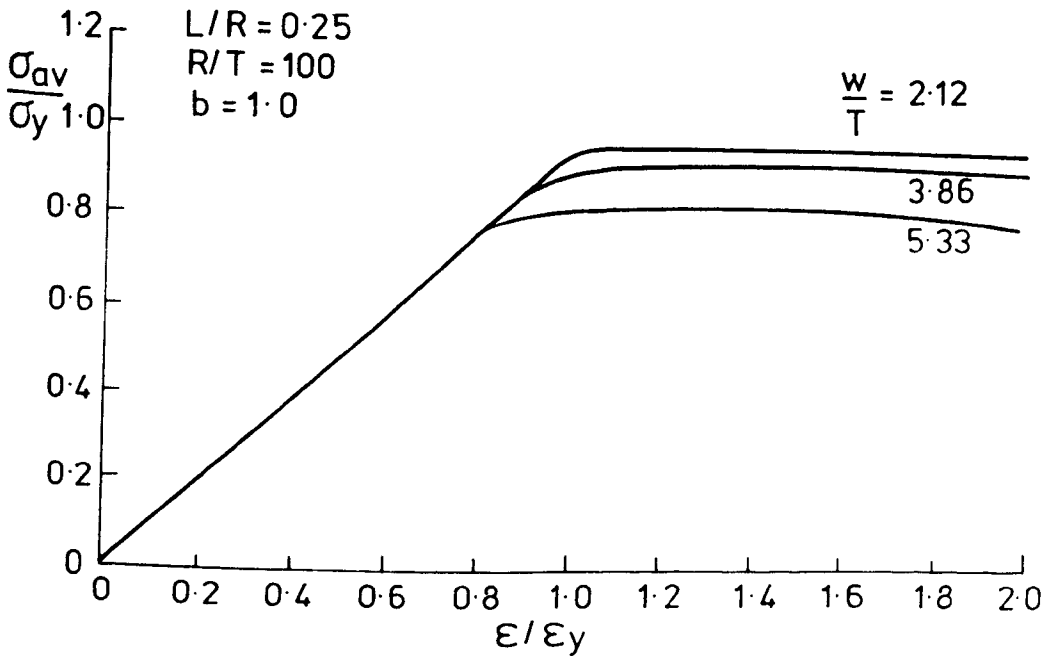

Fig. 6. 202b

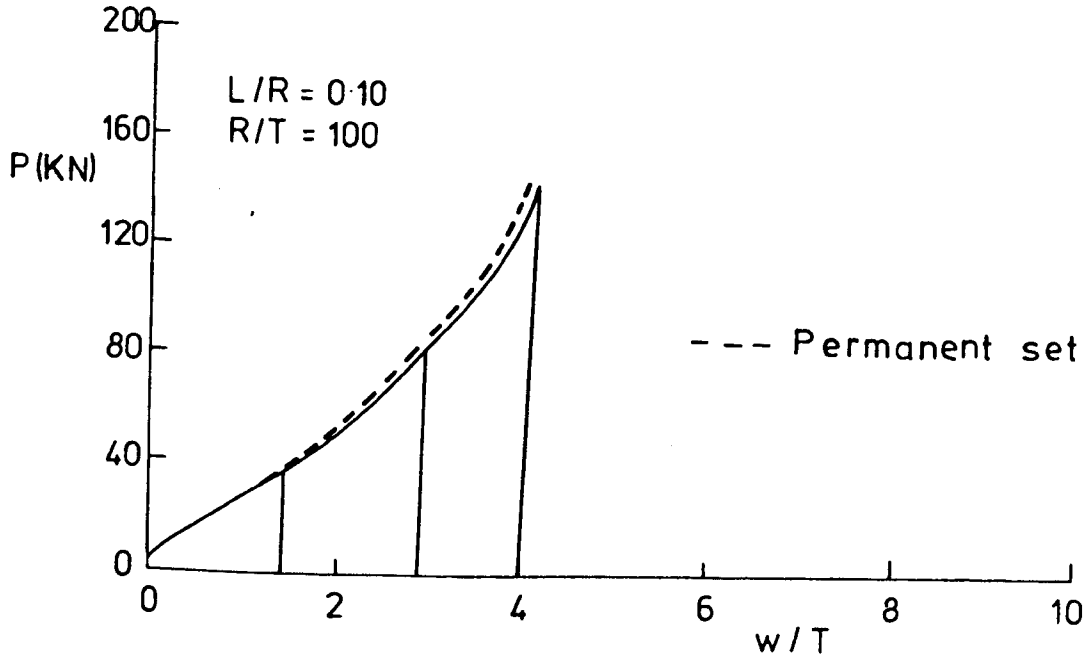

Fig. 6. 203a

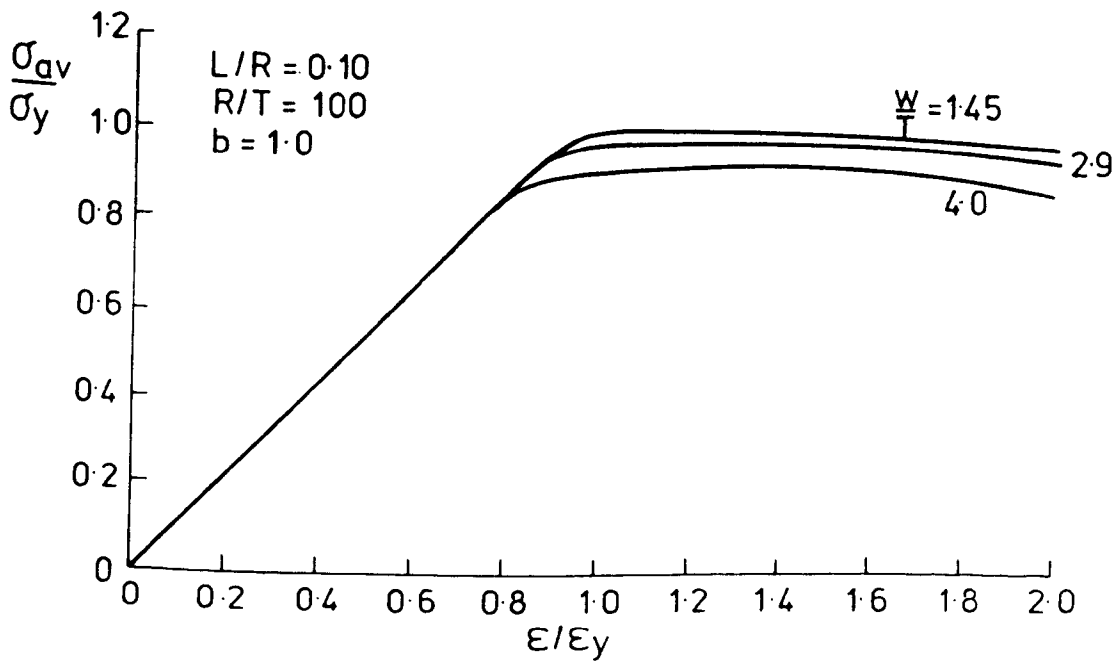

Fig. 6. 203b

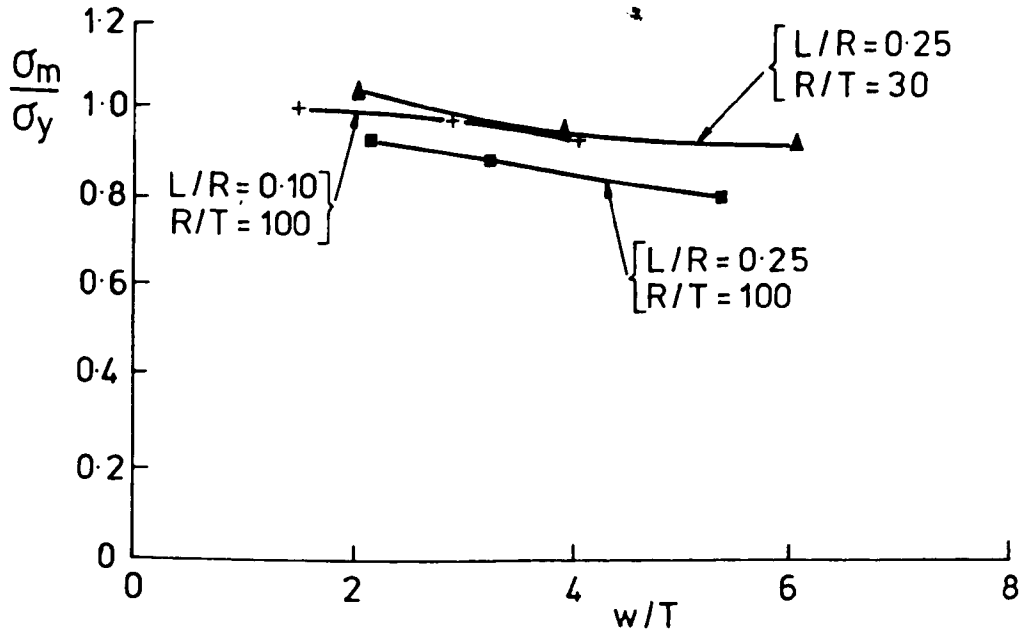
σm/σy
1·2
1·0
0·8
0·6
0·4
0·2
0
0
2
4
6
8
w/T
L/R = 0·25
R/T = 30
L/R = 0·10
R/T = 100
L/R = 0·25
R/T = 100

Fig. 6. 204

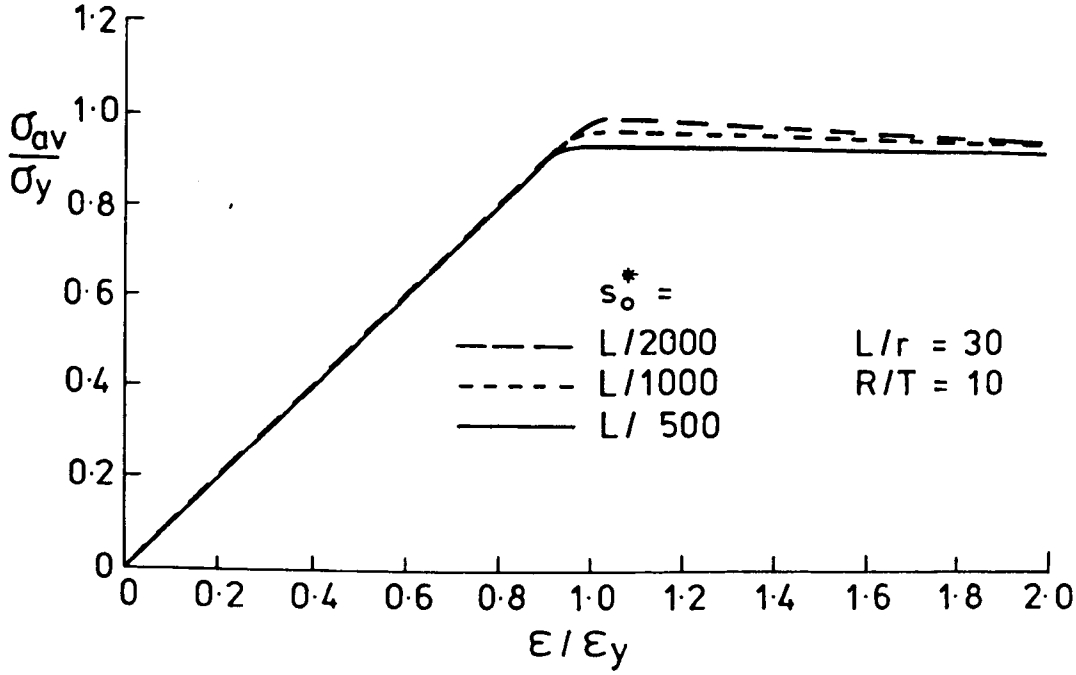

Fig. 6. 205a

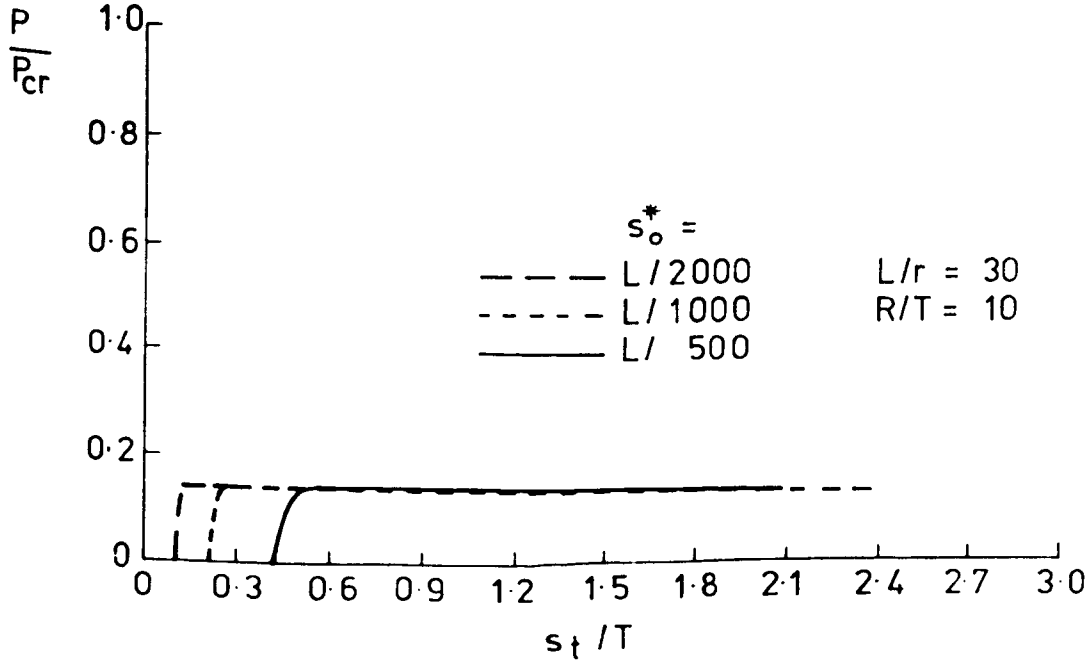

Fig. 6. 205b

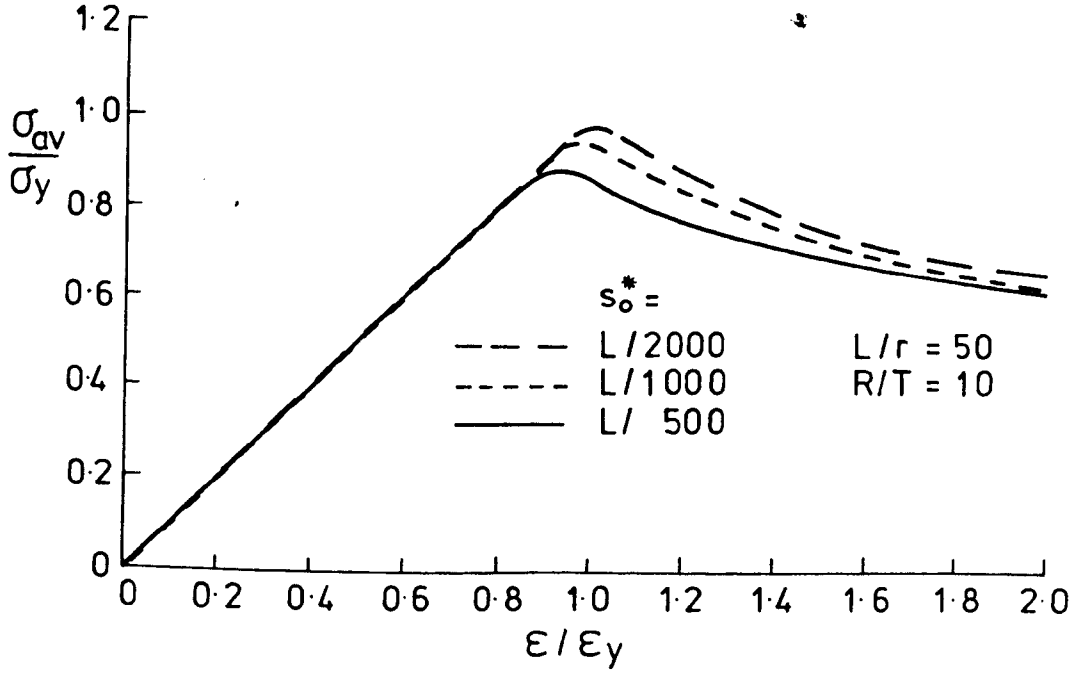

Fig. 6. 206a

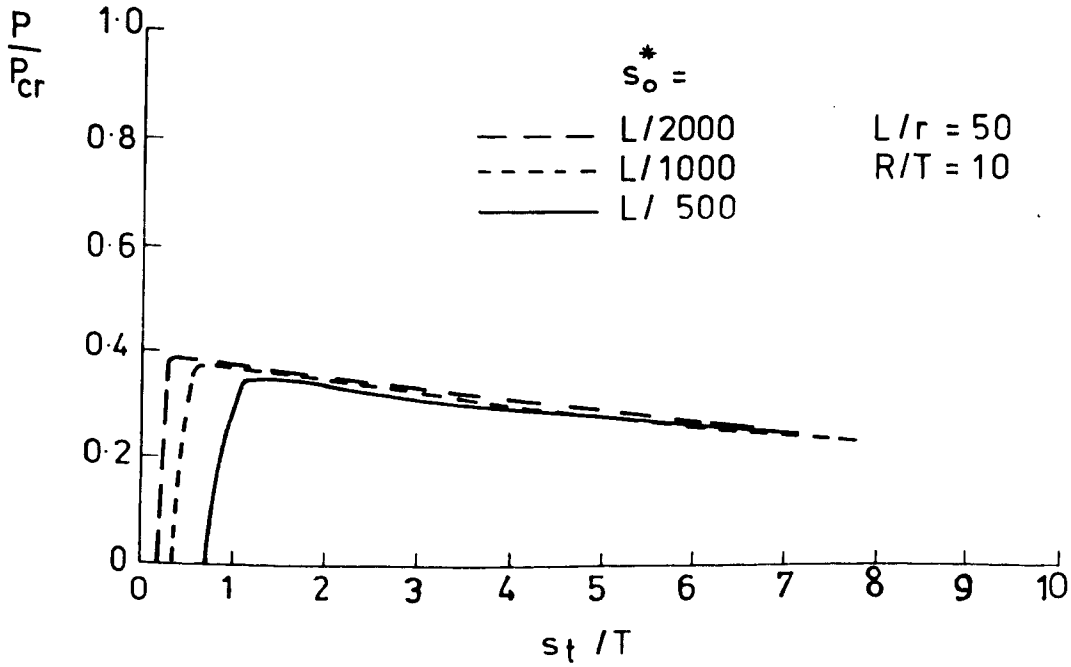

Fig. 6. 206b

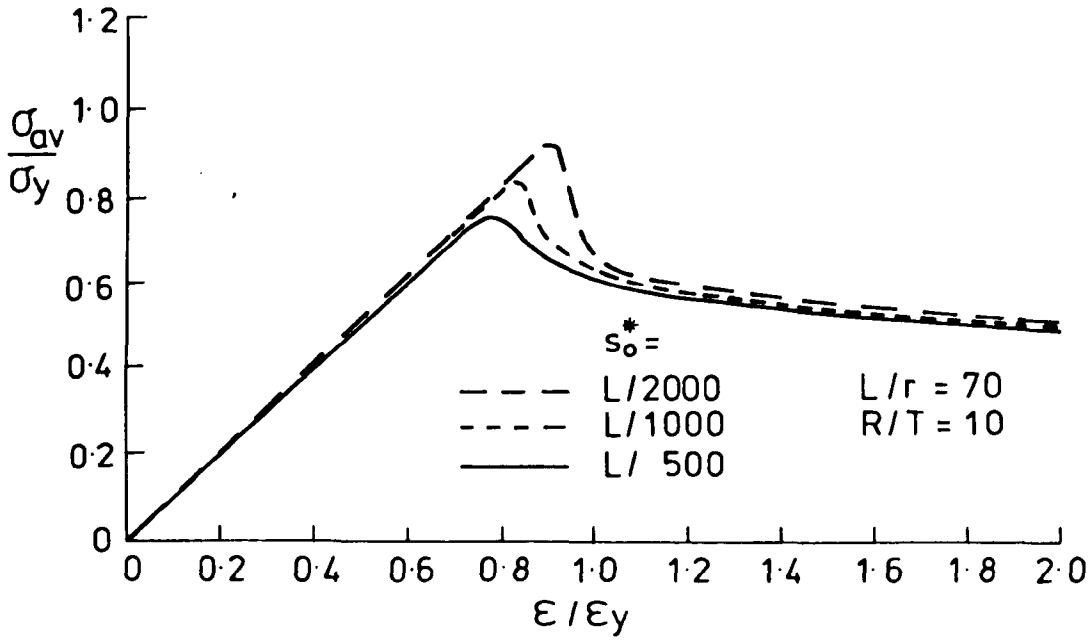

Fig. 6. 207a

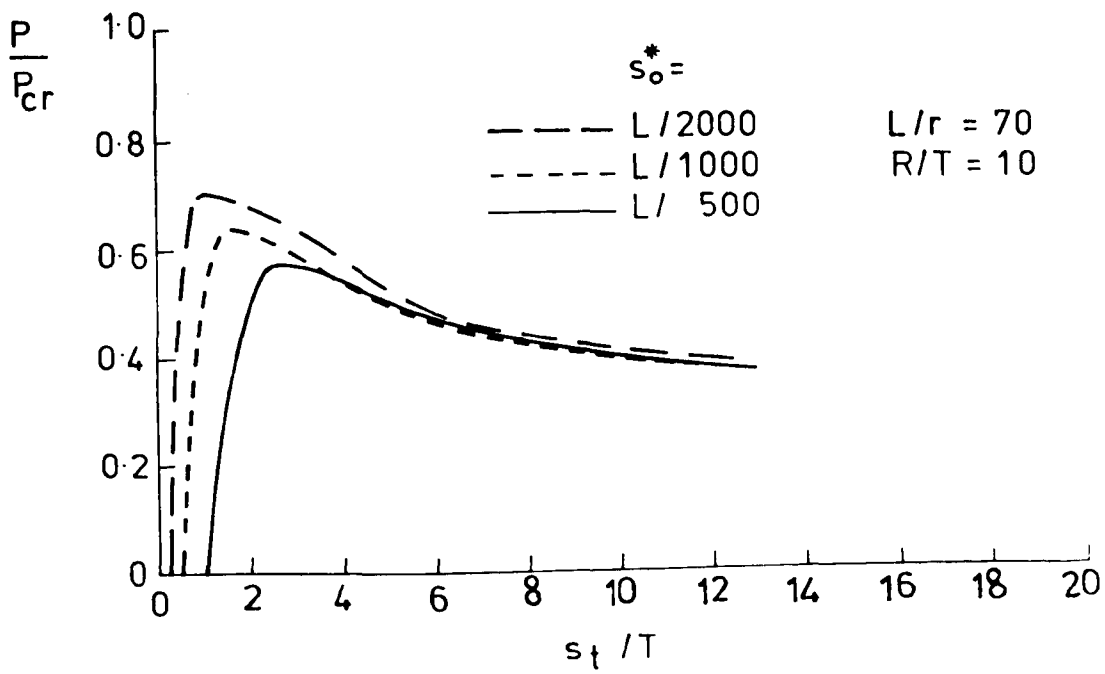

Fig. 6. 207b

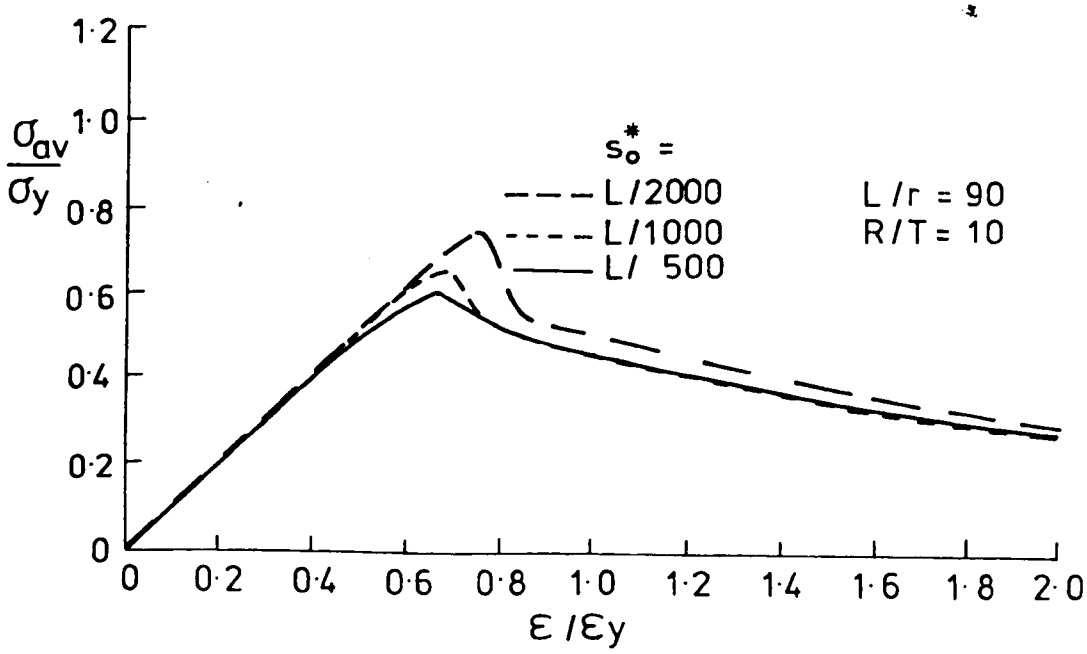

Fig. 6.208a

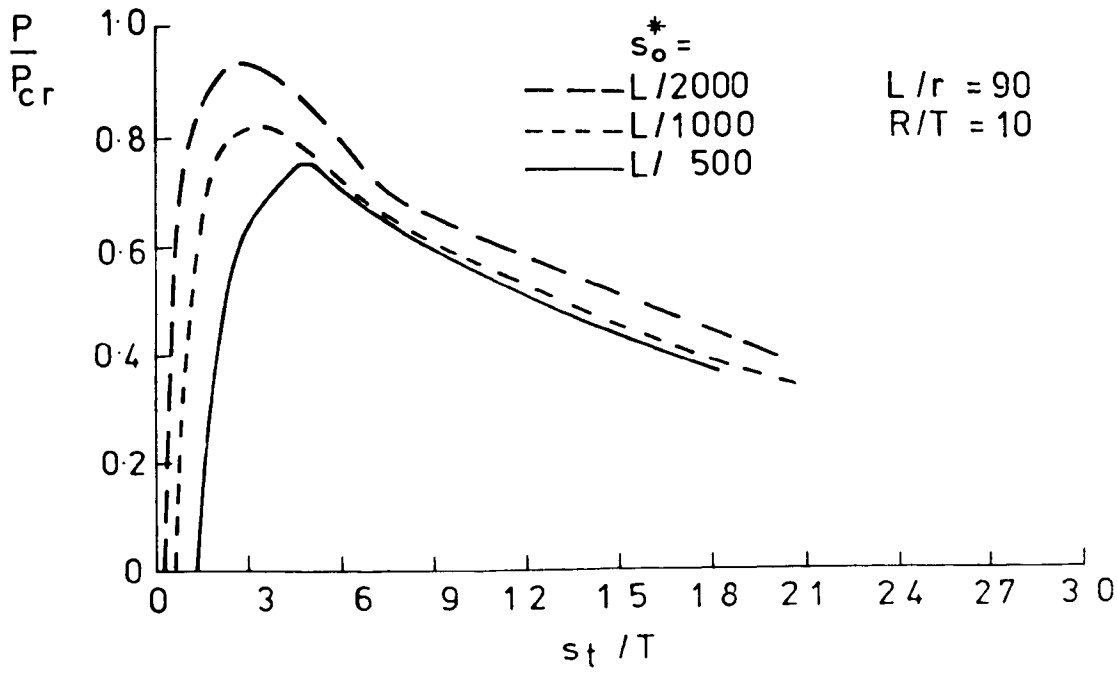

Fig. 6. 208b

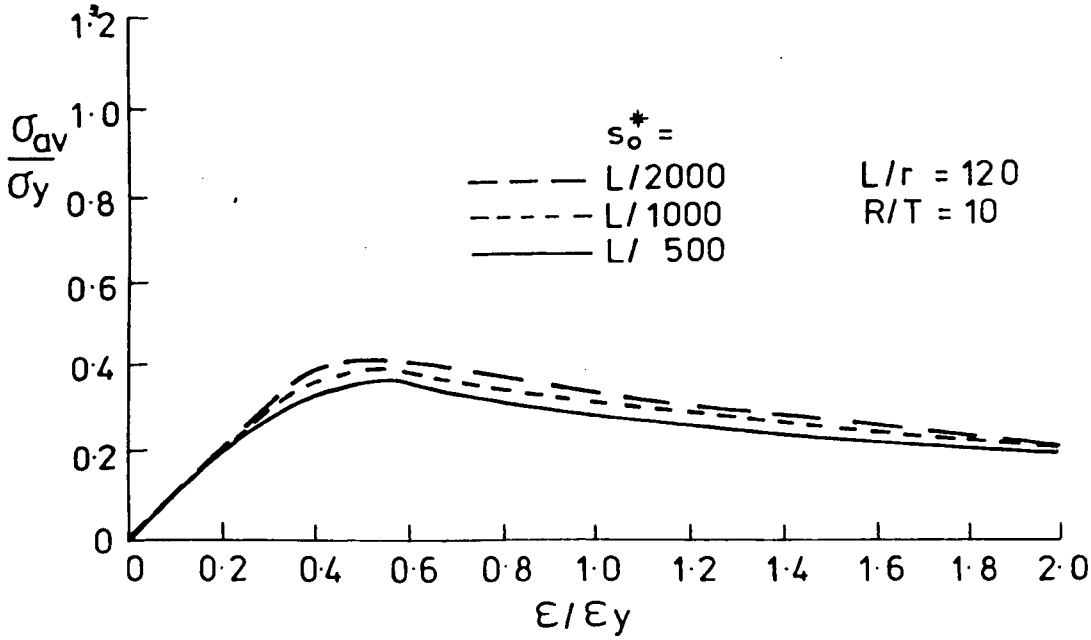

Fig. 6.209a

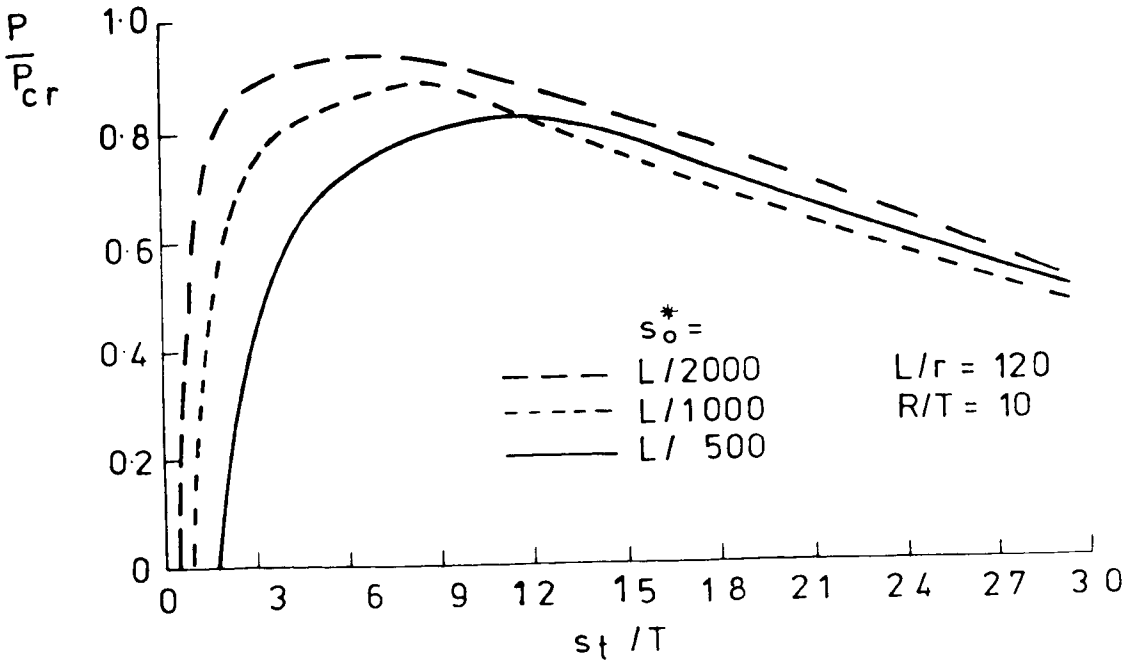

Fig. 6.209b

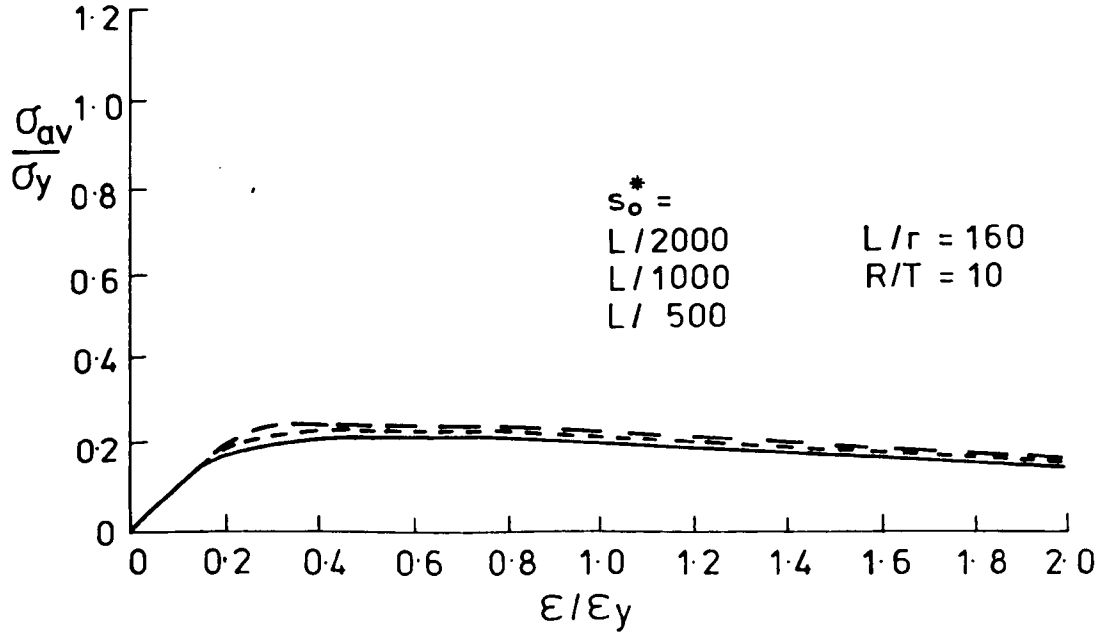

Fig. 6. 210a

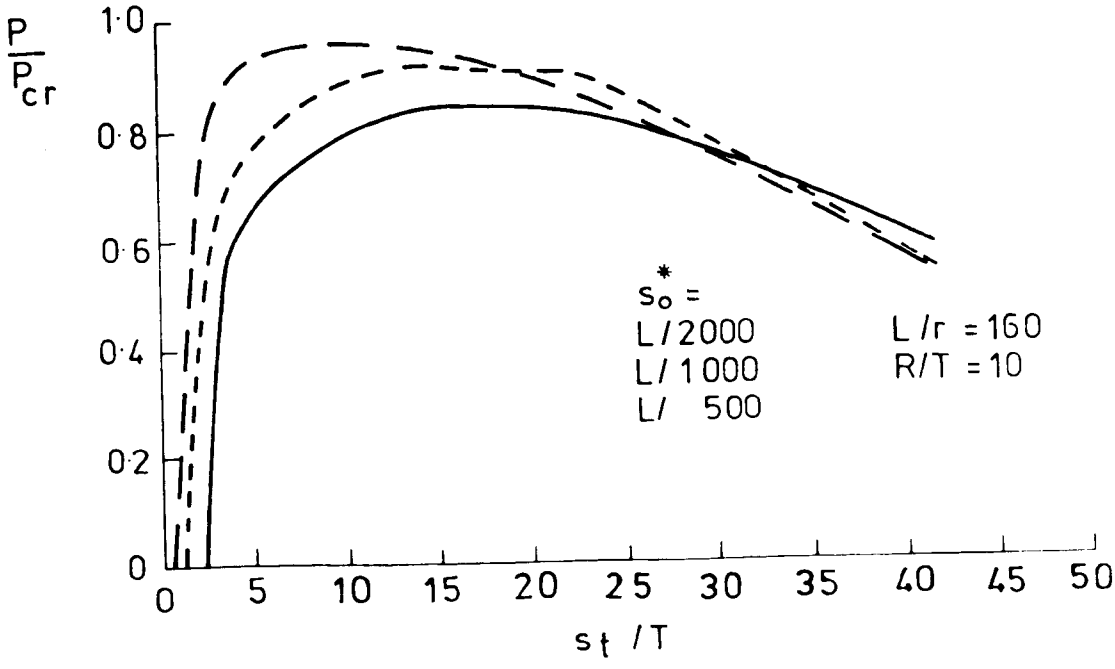

Fig. 6. 210b

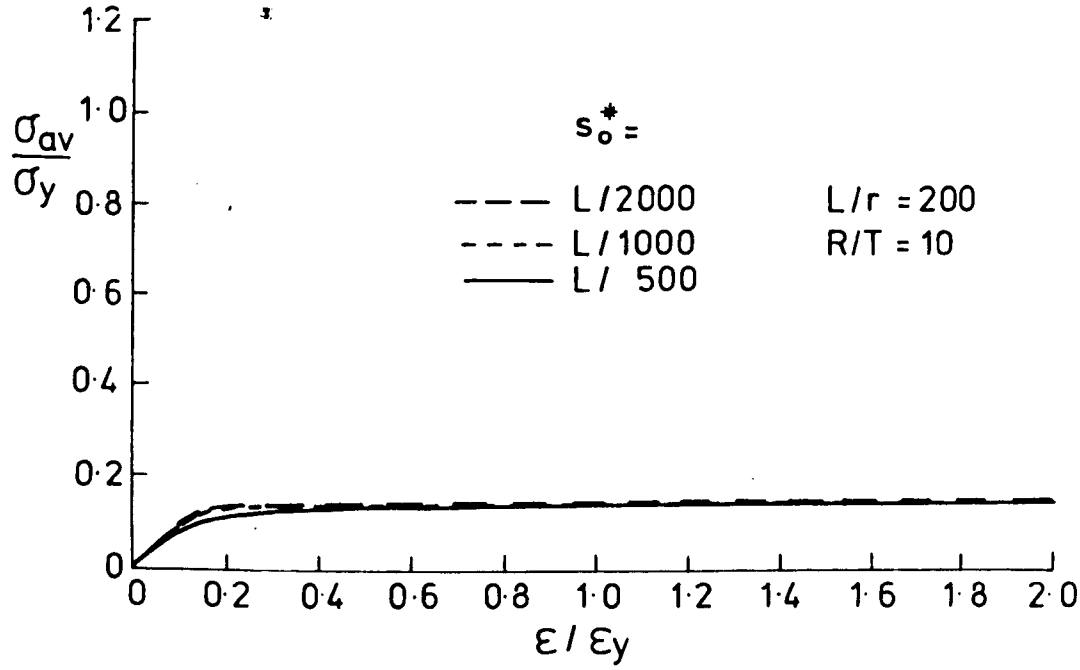

Fig. 6. 211a

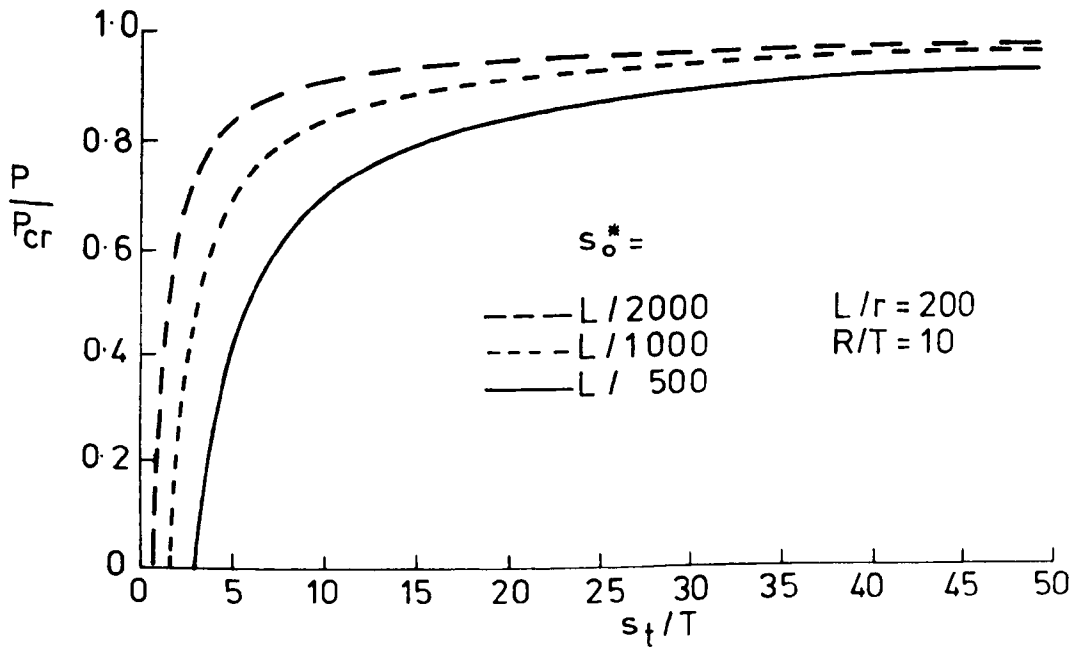

Fig. 6. 211b

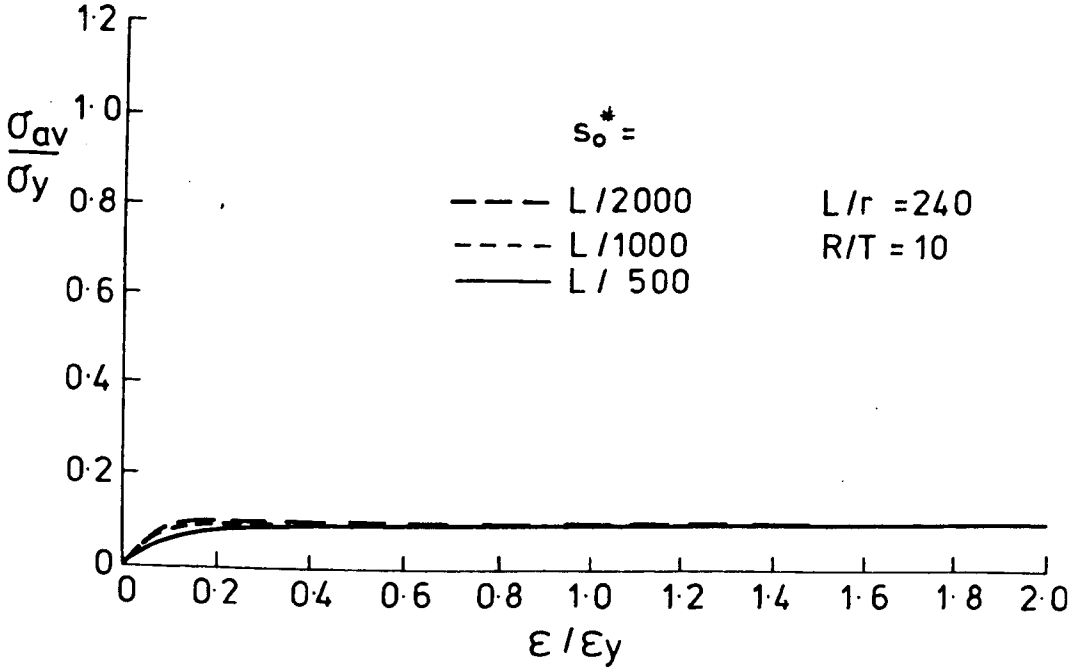

Fig. 6. 212a

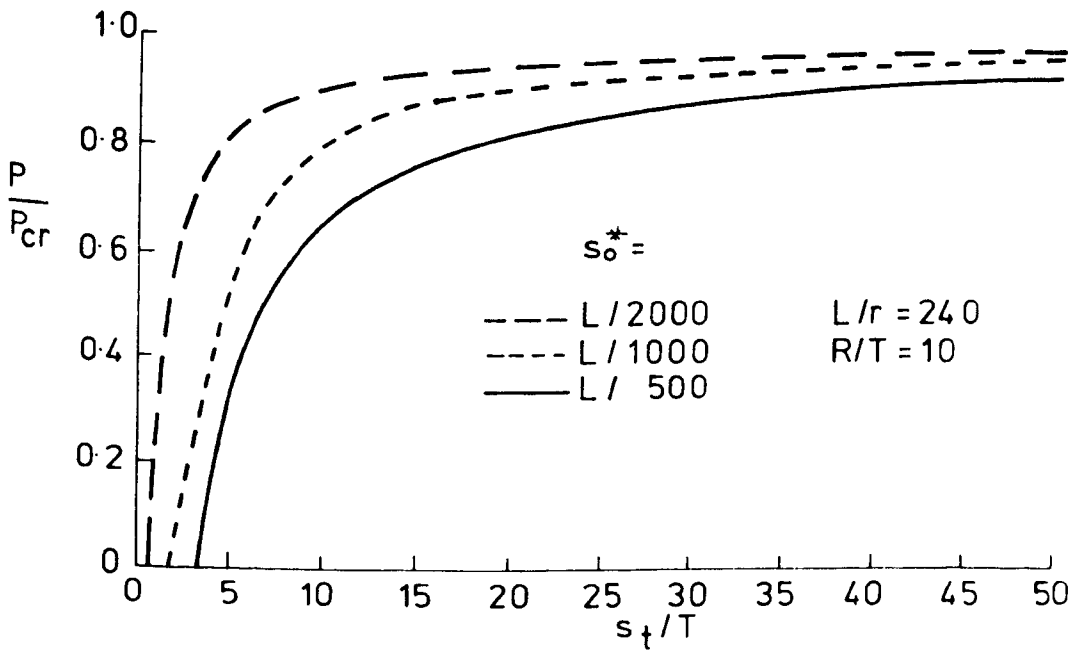

Fig. 6. 212b

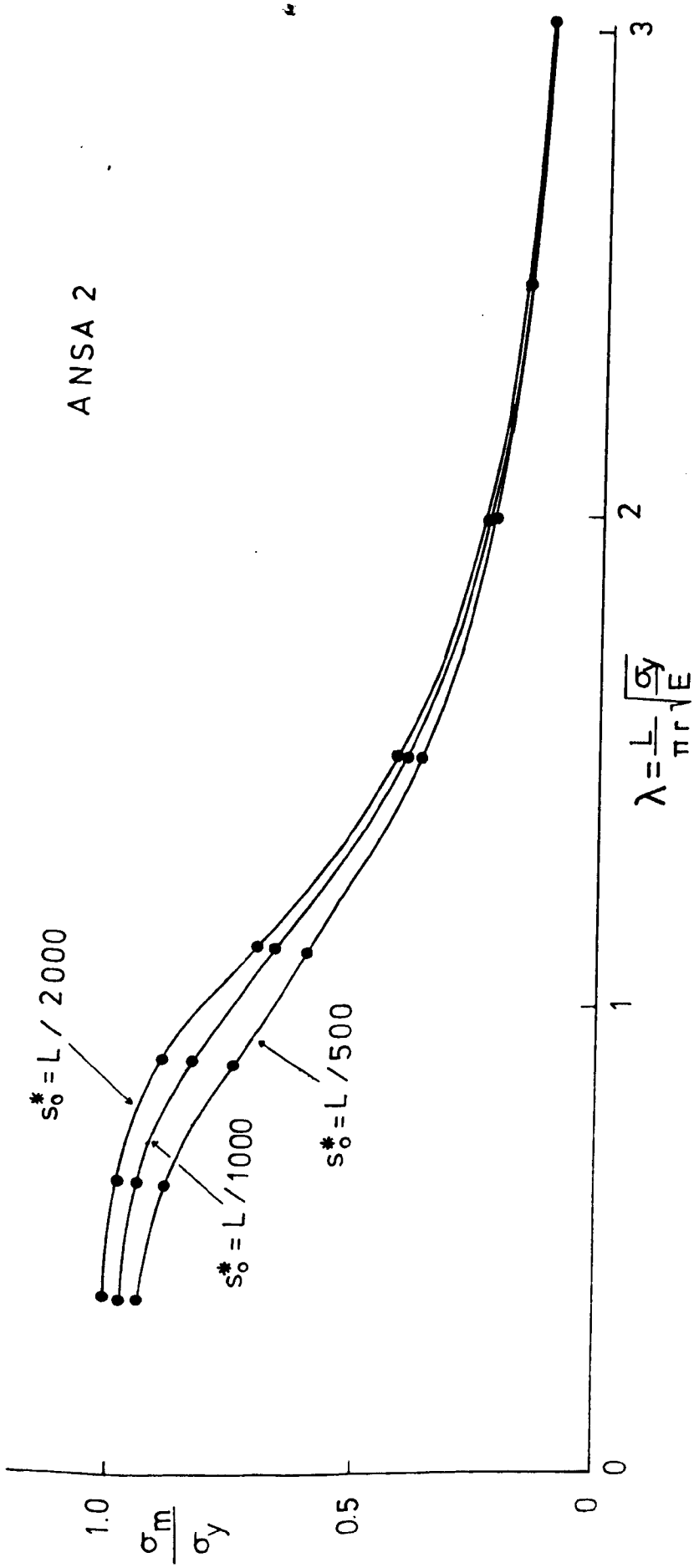
ANSA 2
$s_o^* = L/2000$
$s_o^* = L/1000$
$s_o^* = L/500$
$\frac{\sigma_m}{\sigma_y}$
1.0
0.5
0
0
1
2
3
$\lambda = \frac{L}{\pi r}\sqrt{\frac{\sigma_y}{E}}$

Fig. 6. 213

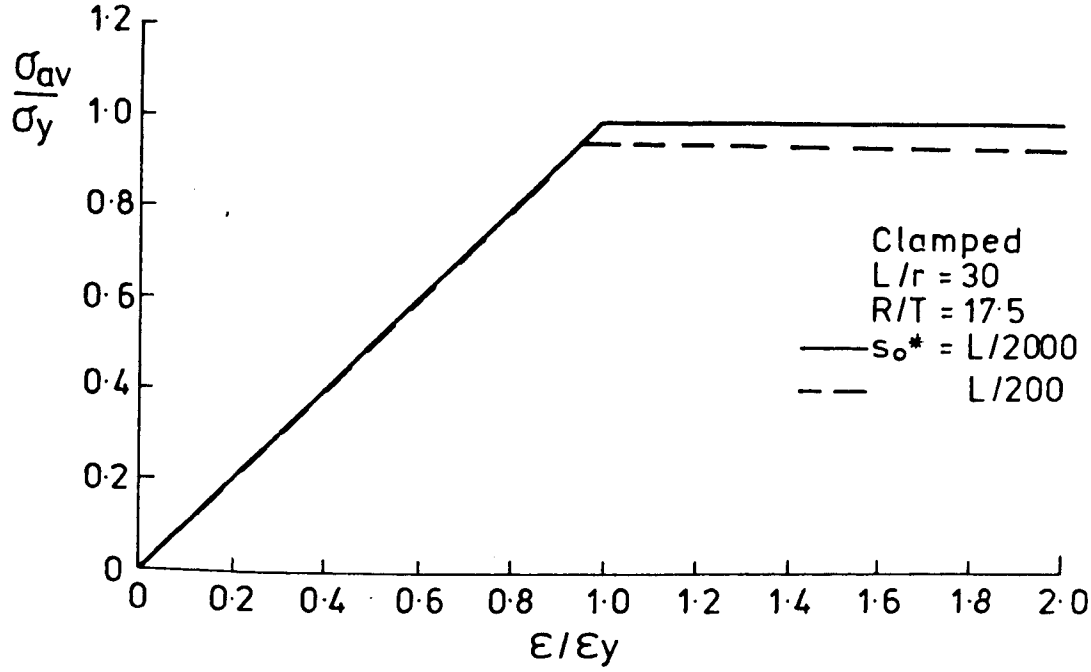

Fig. 6. 214a

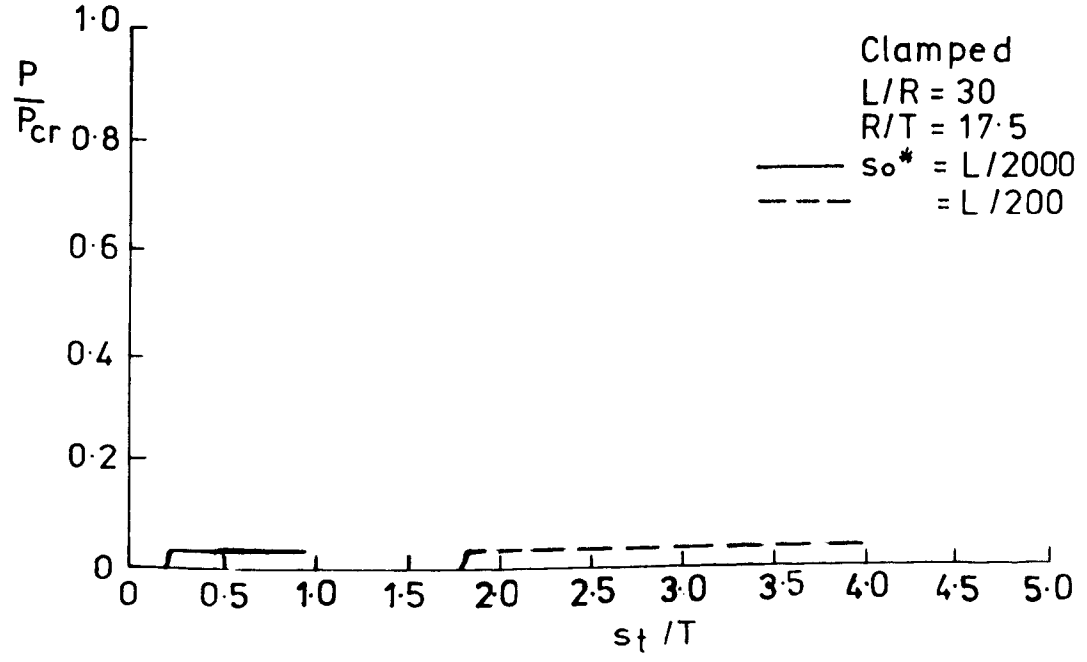

Fig. 6. 214b

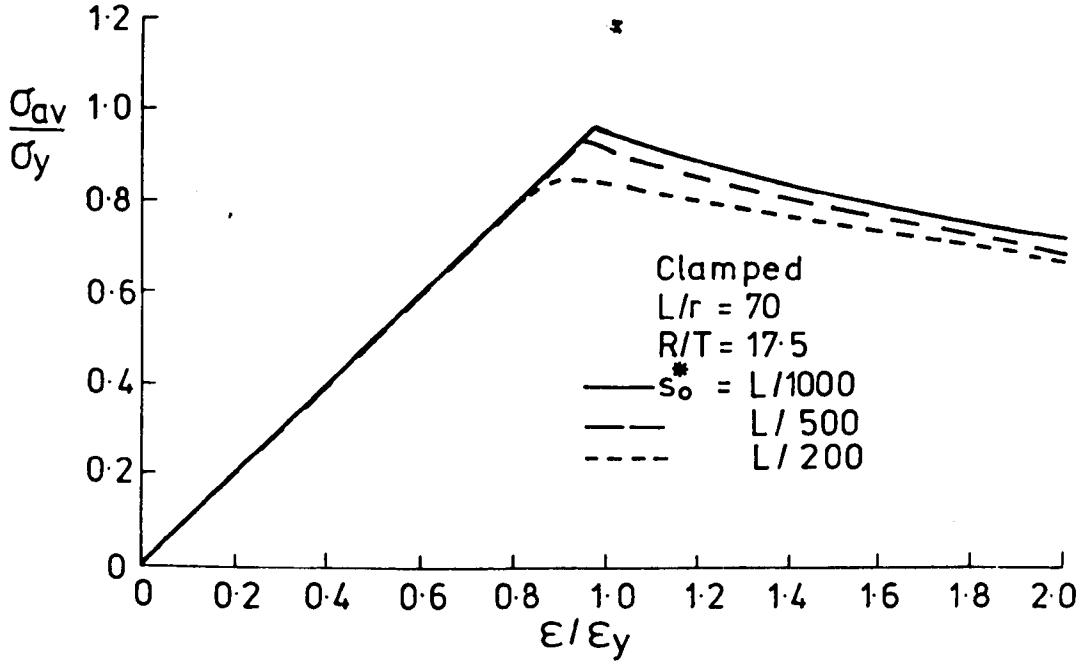

Fig. 6. 215a

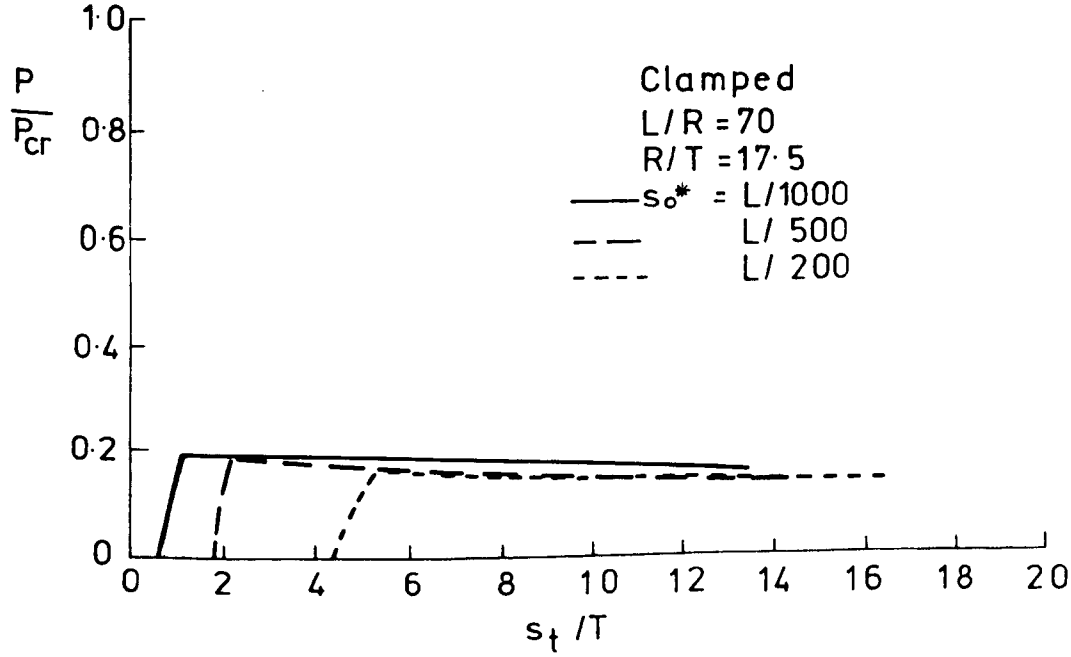

Fig. 6. 215b

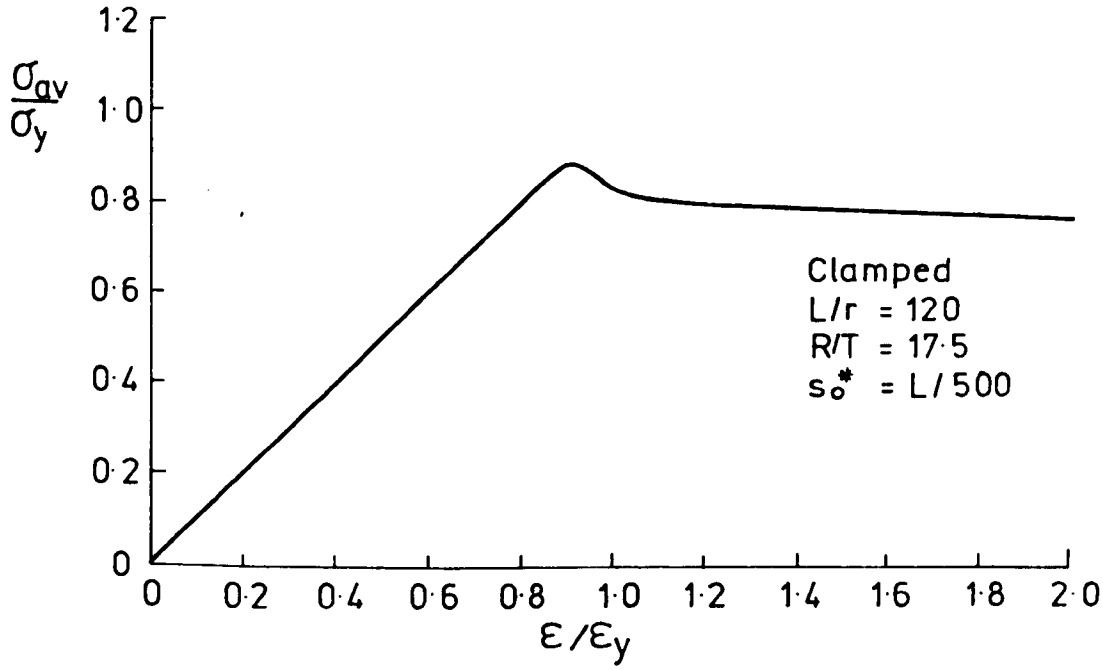

Fig. 6. 216a

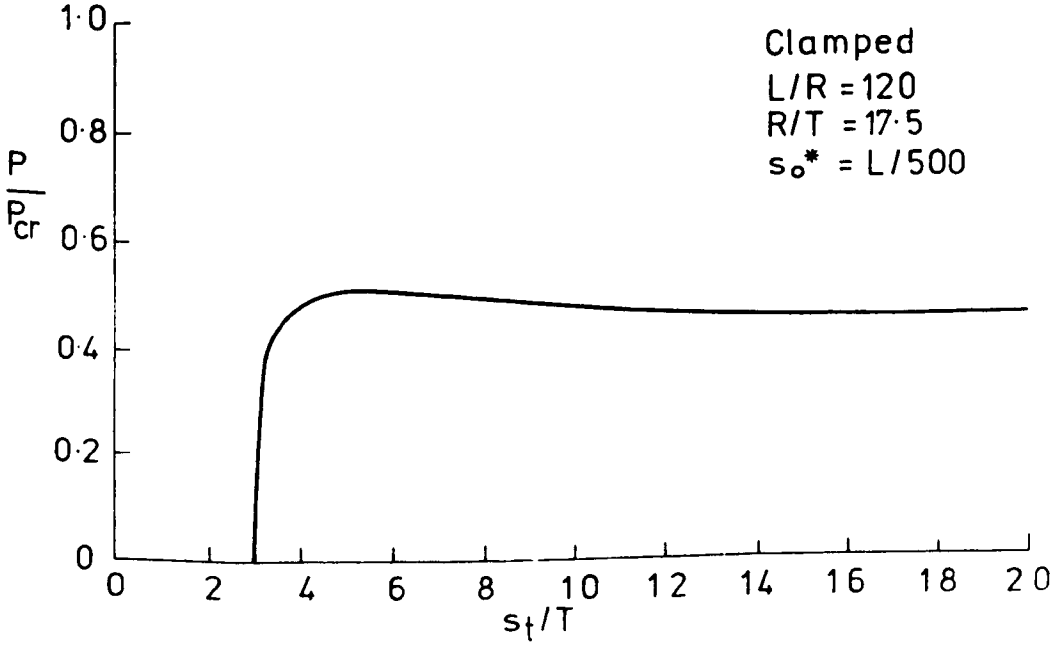

Fig. 6.216b

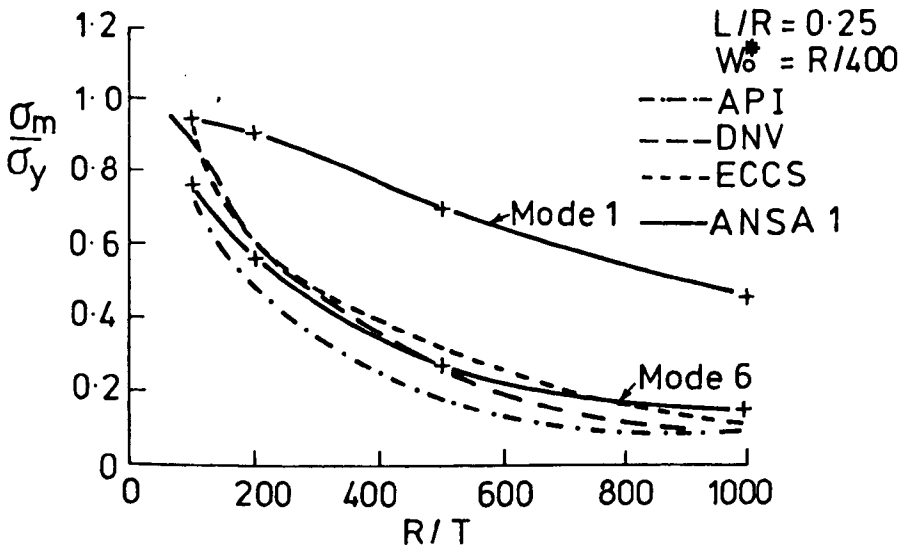

Fig. 6·217

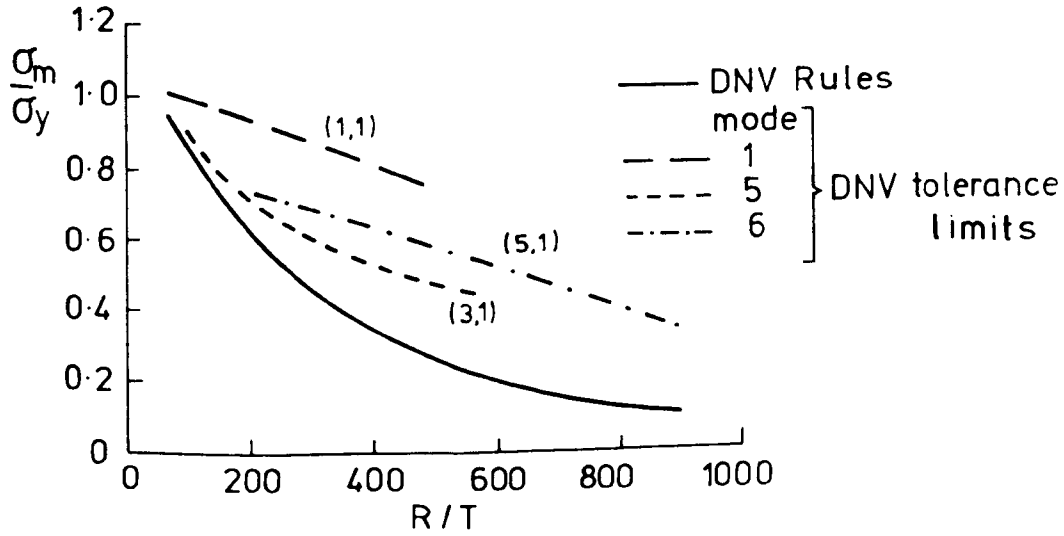

Fig. 6. 218

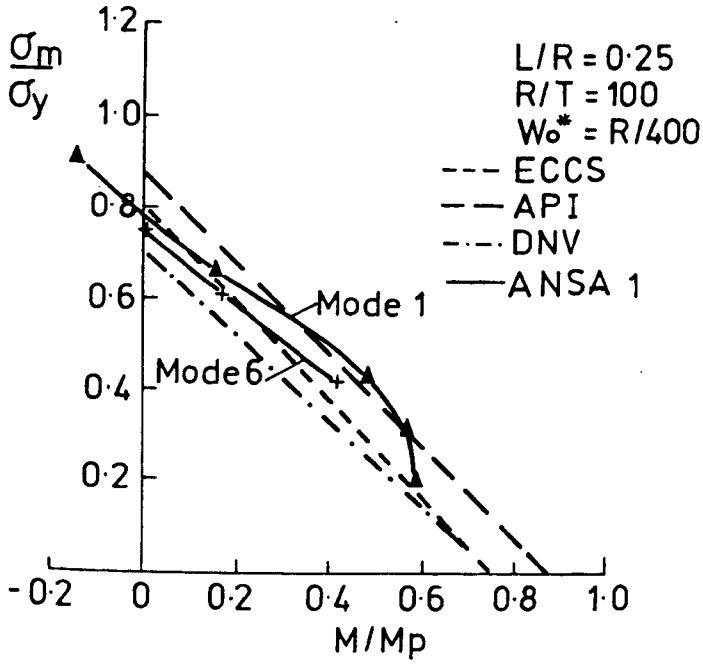

Fig. 6.219

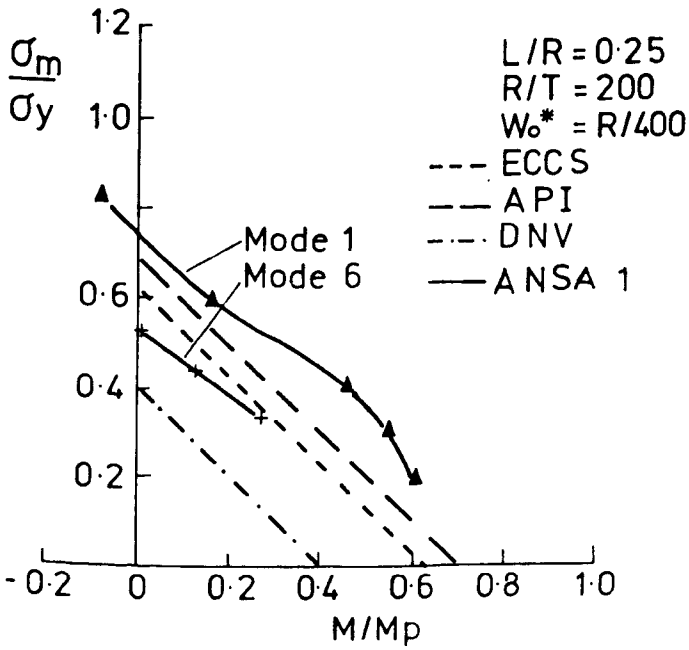

Fig. 6.220

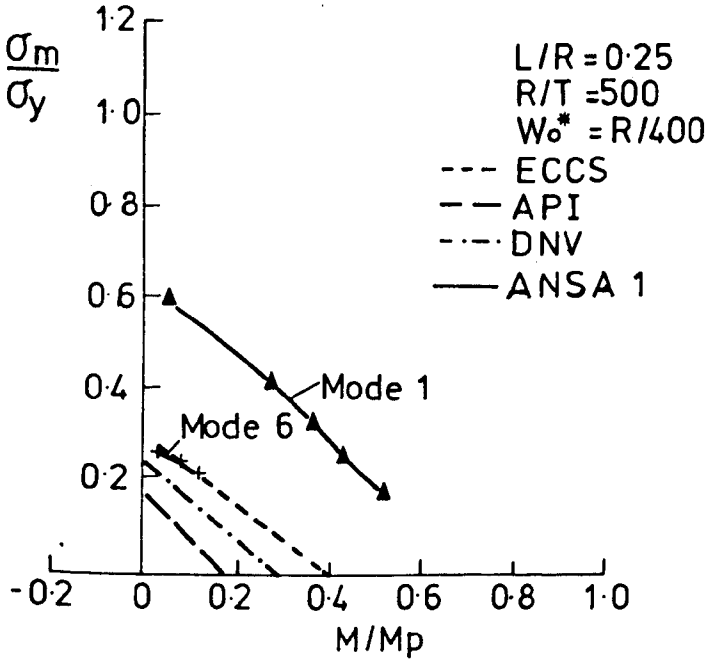

Fig. 6.221

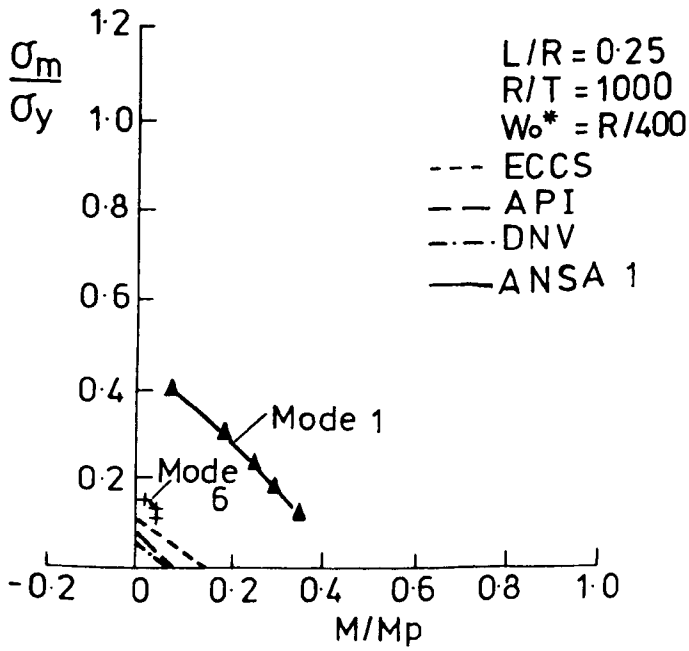

Fig. 6.222

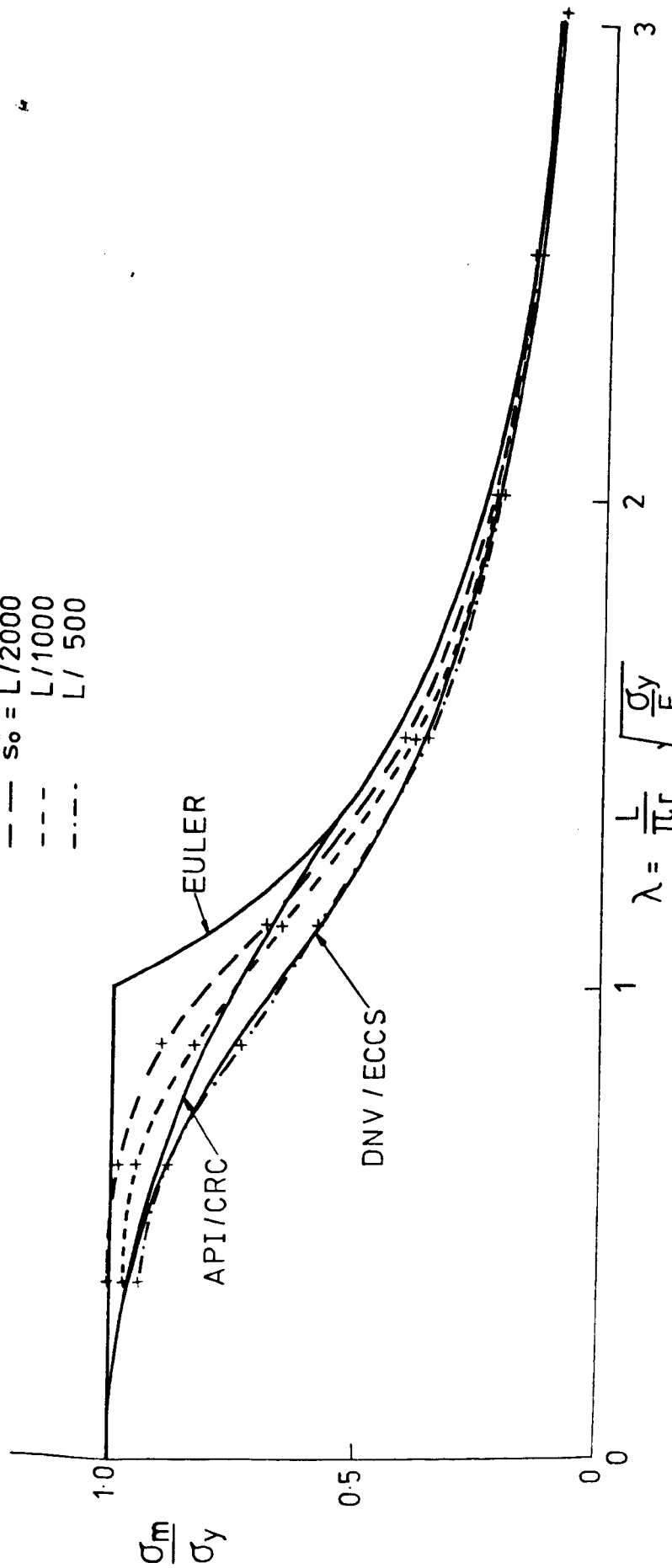
ANSA 2
$s_o^* = L/2000$
L/1000
L/ 500
EULER
API/CRC
DNV / ECCS
$\frac{\sigma_m}{\sigma_y}$
1·0
0·5
0
0
1
2
3
$\lambda = \frac{L}{\pi r}\sqrt{\frac{\sigma_y}{E}}$

Fig. 6.223

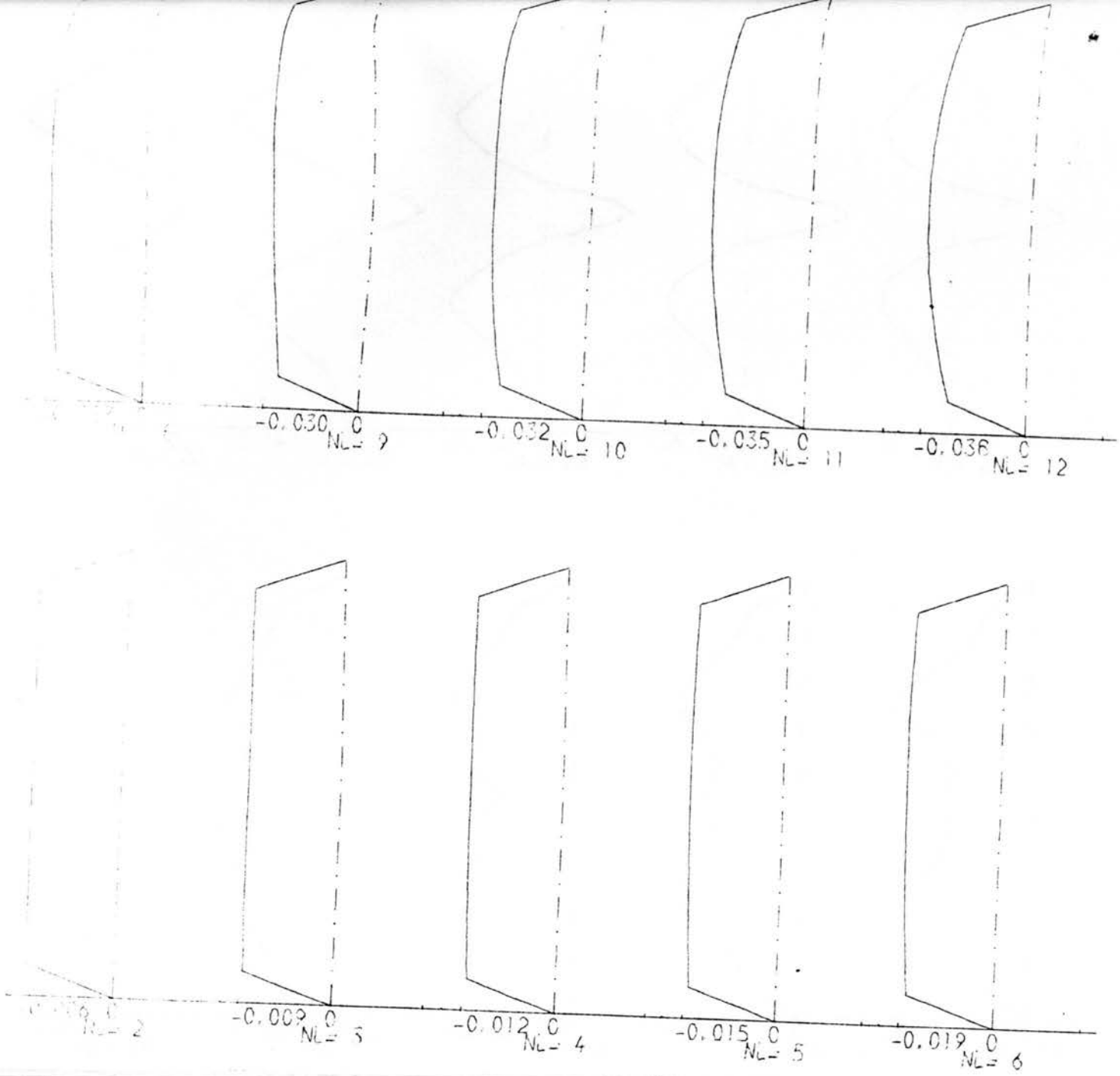

ANSA 2

L / r = 68.40

R / T = 43.65

T = 1.02

Fig. 6.224

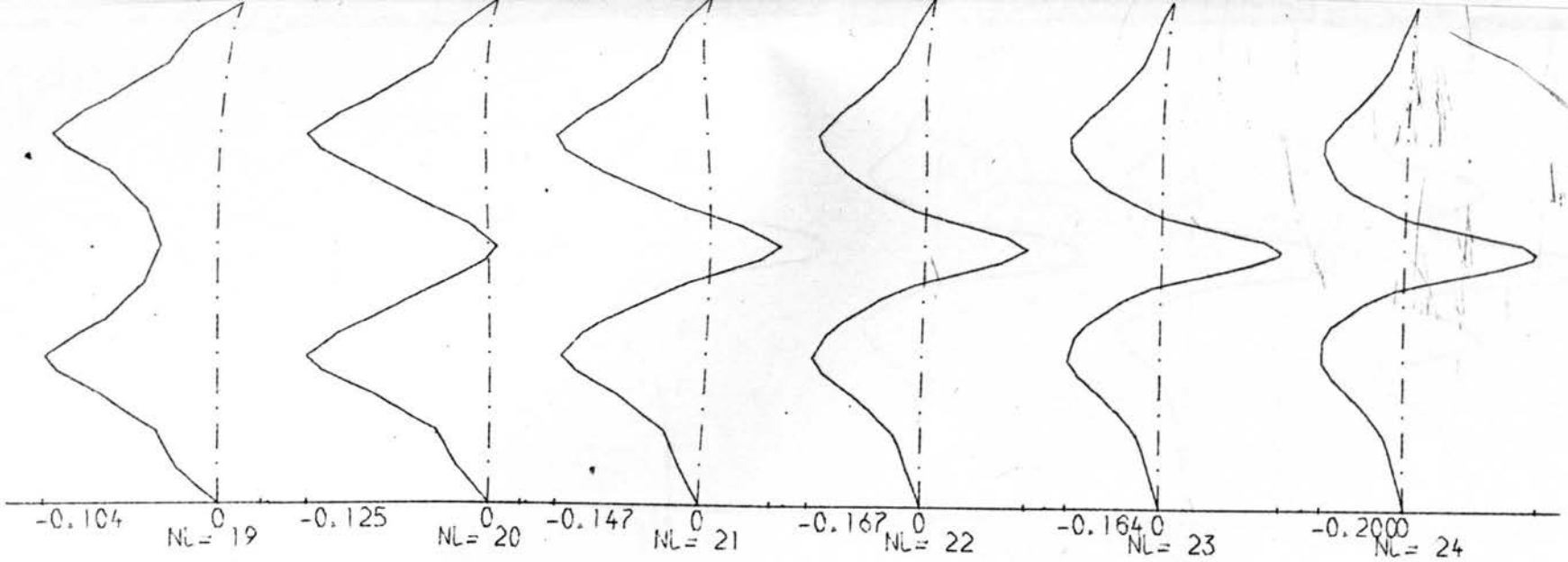
-0.104
0
NL= 19
-0.125
0
NL= 20
-0.147
0
NL= 21
-0.167
0
NL= 22
-0.164
0
NL= 23
-0.2000
NL= 24

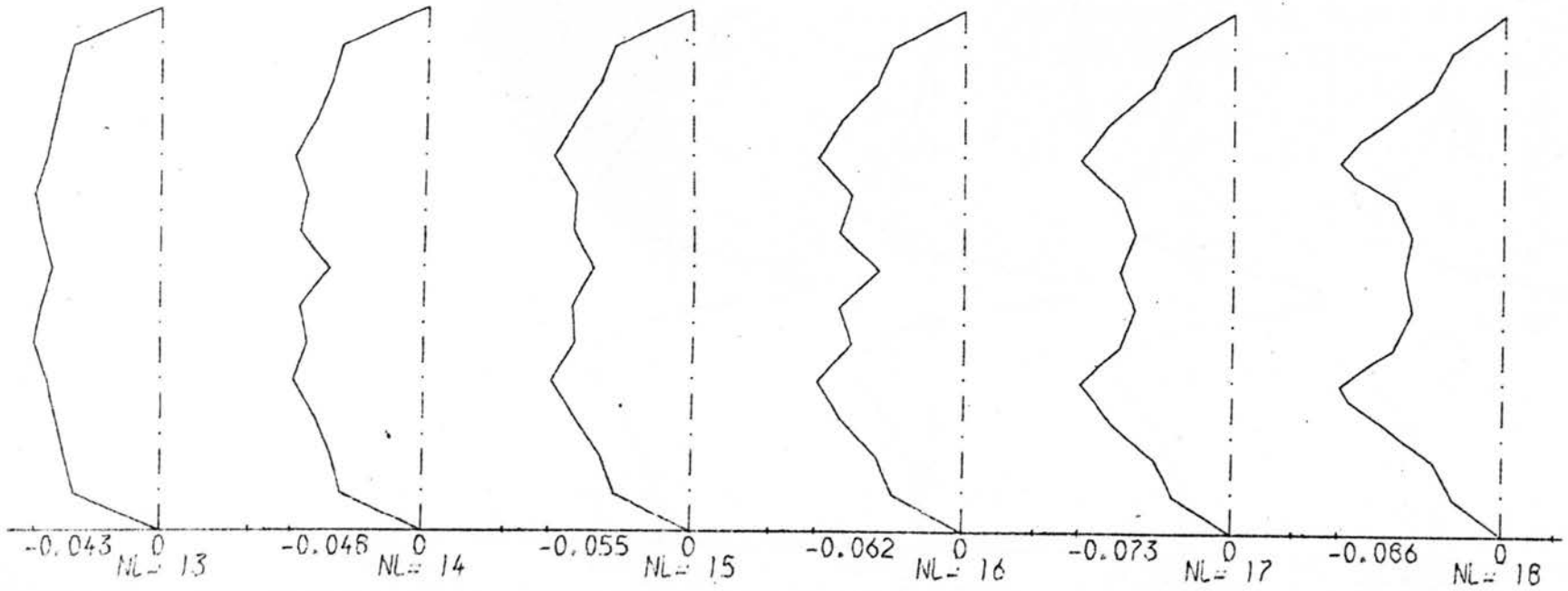
-0.043
0
NL= 13
-0.048
0
NL= 14
-0.055
0
NL= 15
-0.062
0
NL= 16
-0.073
0
NL= 17
-0.066
0
NL= 18

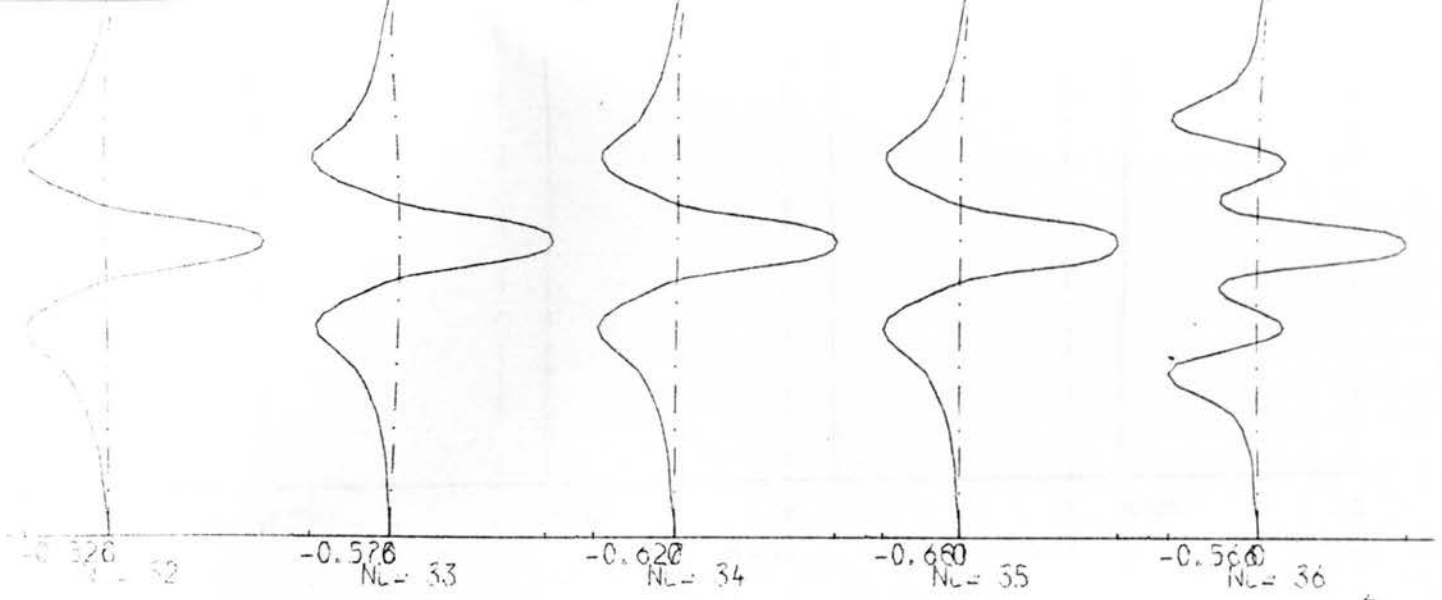
-0.520
NL= 33
-0.620
NL= 34
-0.680
NL= 35
-0.560
NL= 36

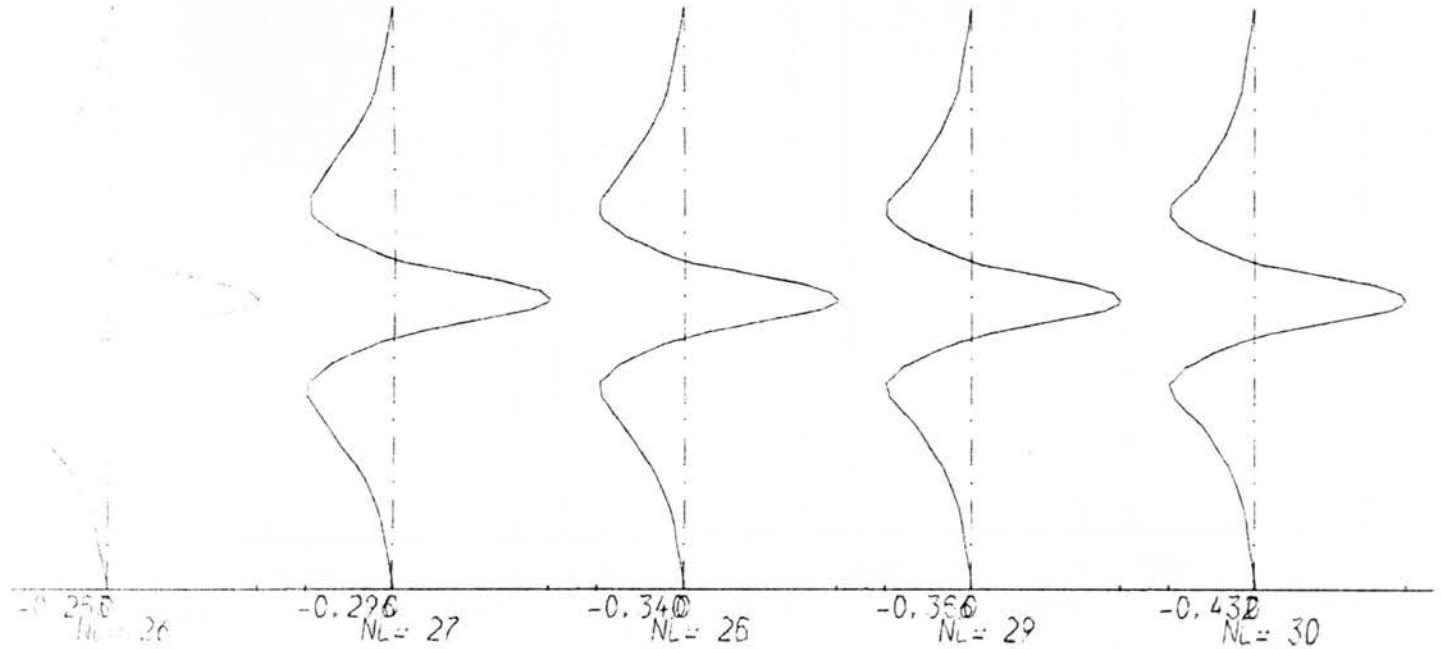
-0.220
NL= 27
-0.340
NL= 28
-0.360
NL= 29
-0.430
NL= 30

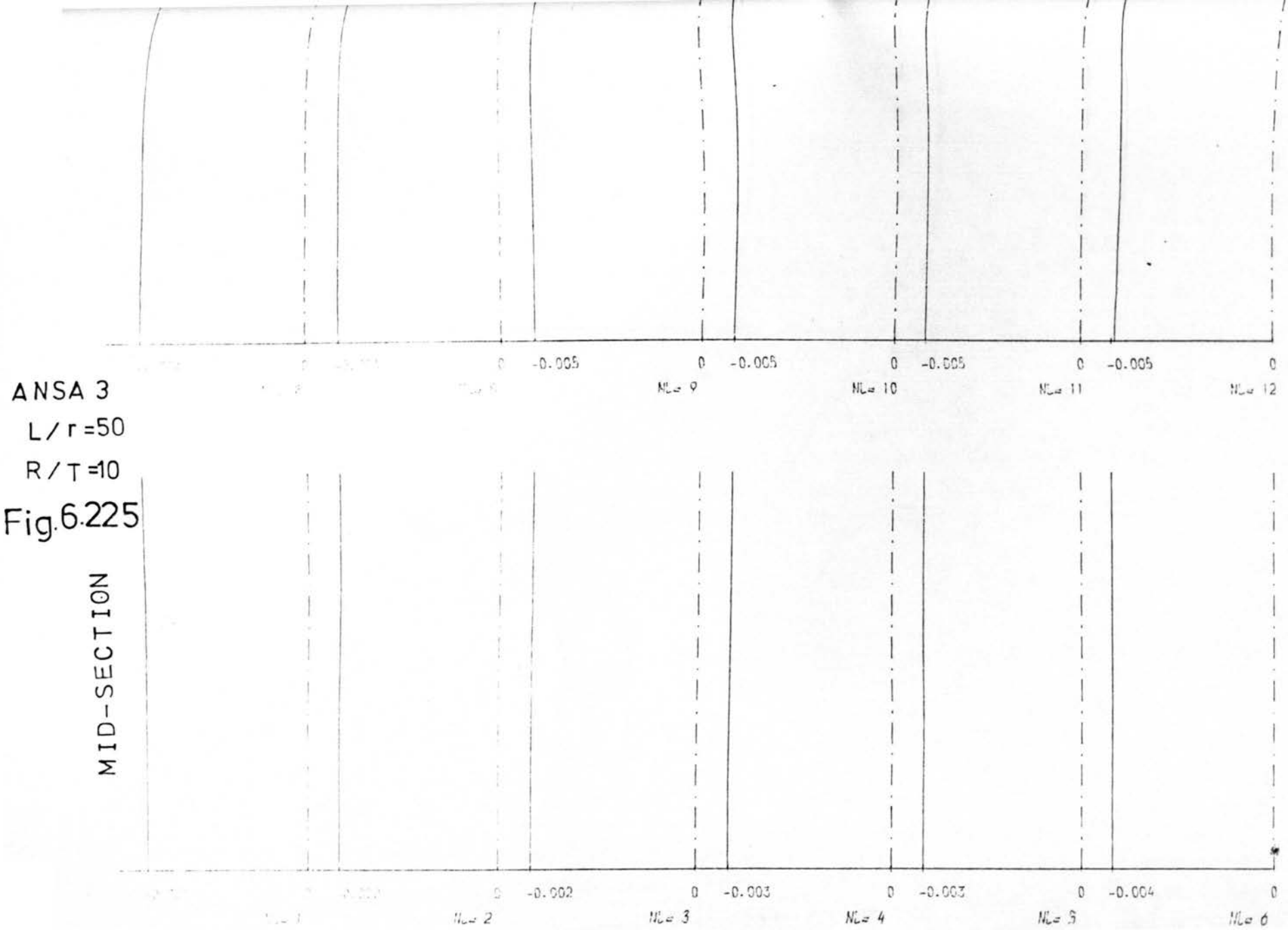

ANSA 3

L / r =50

R / T =10

Fig.6.225

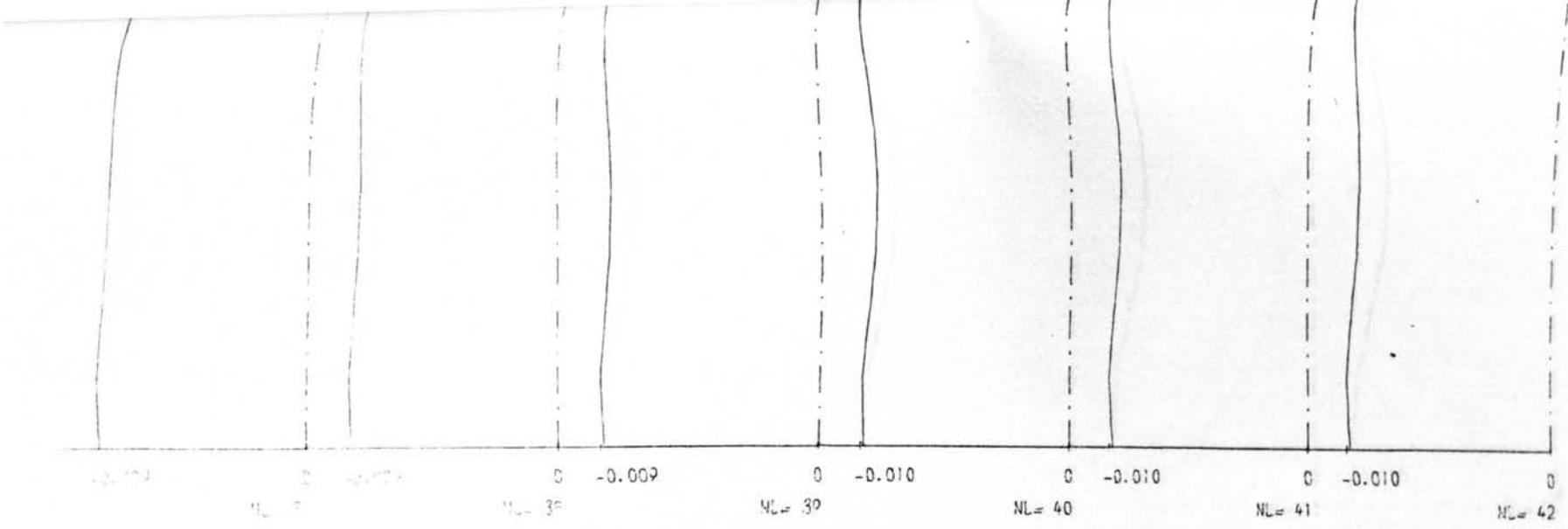
0
-0.009
0
-0.010
0
-0.010
0
-0.010
0
NL= 39
NL= 40
NL= 41
NL= 42

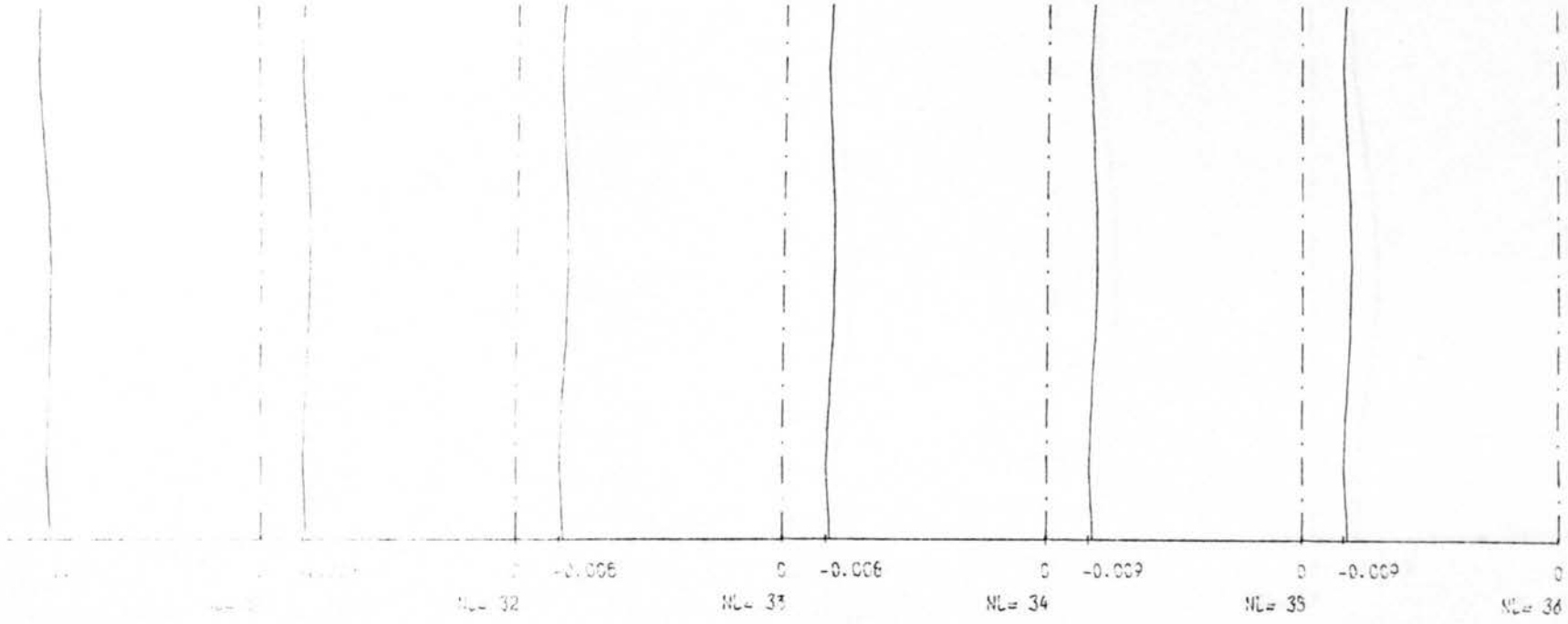
-0.006
0
-0.006
0
-0.009
0
-0.009
0
NL= 32
NL= 33
NL= 34
NL= 35
NL= 36

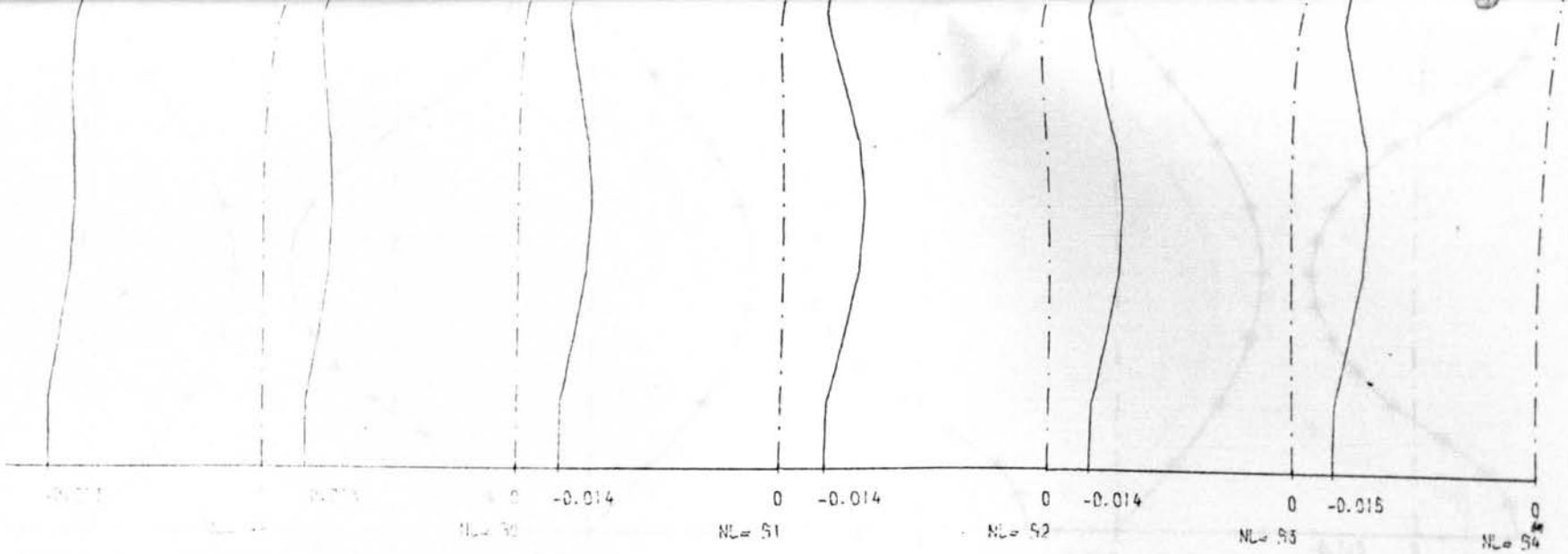
0
-0.014
0
-0.014
0
-0.014
0
-0.015
0
NL= 51
NL= 52
NL= 53
NL= 54

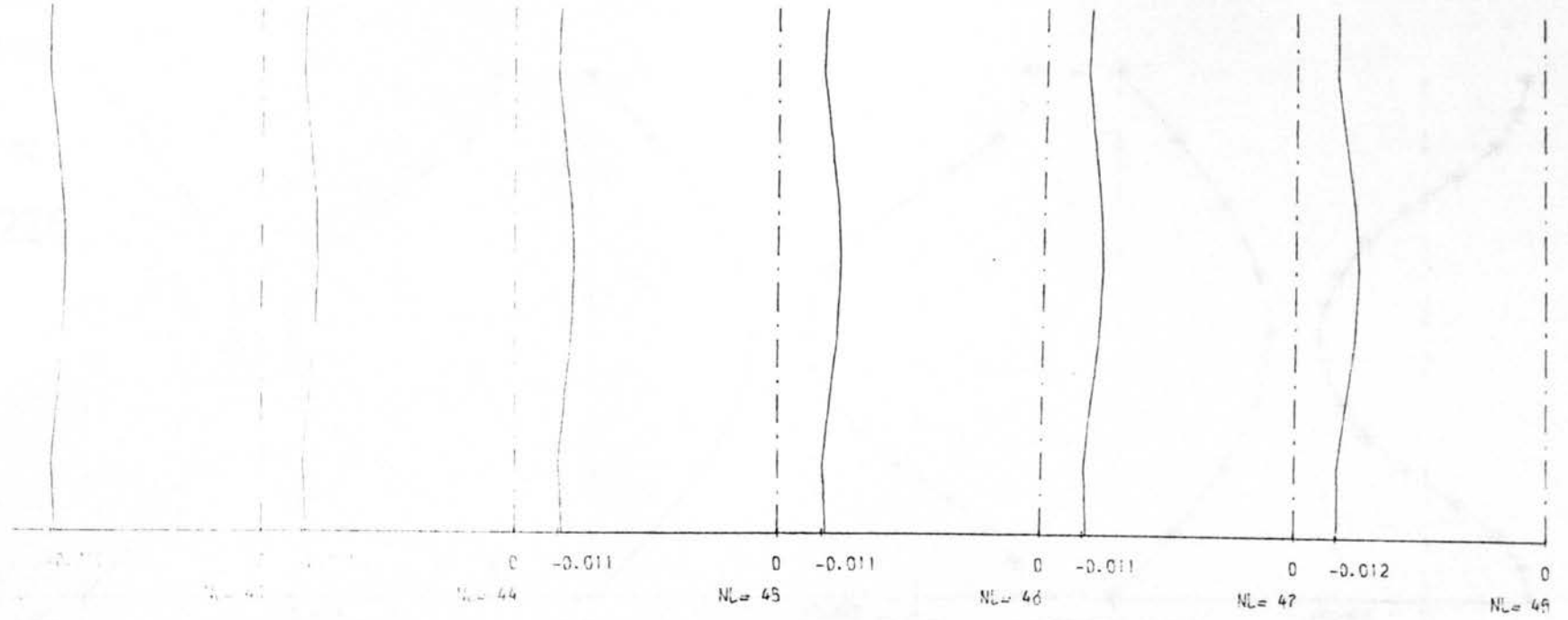
0
-0.011
0
-0.011
0
-0.011
0
-0.012
0
NL= 44
NL= 45
NL= 46
NL= 47
NL= 48

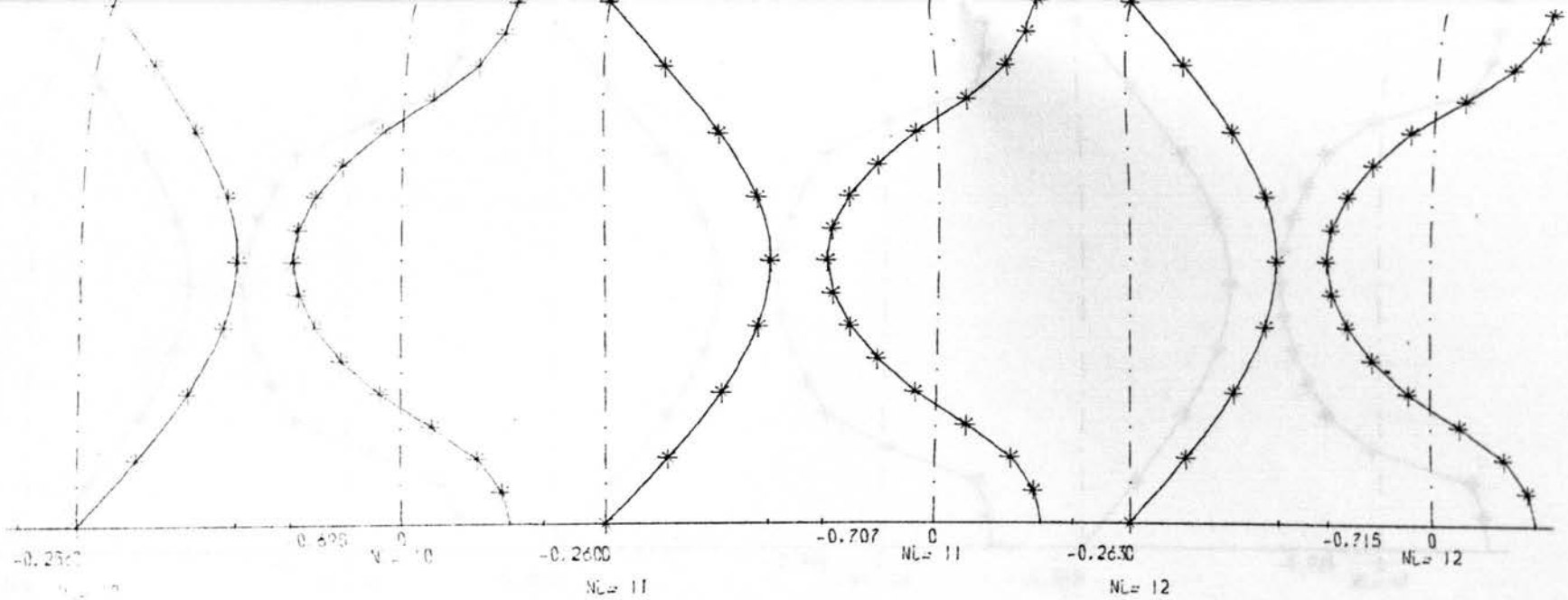

L / R = 0.10

R / T = 500

b = 1.0

$w_0^* = R/1000$

Fig.6.226

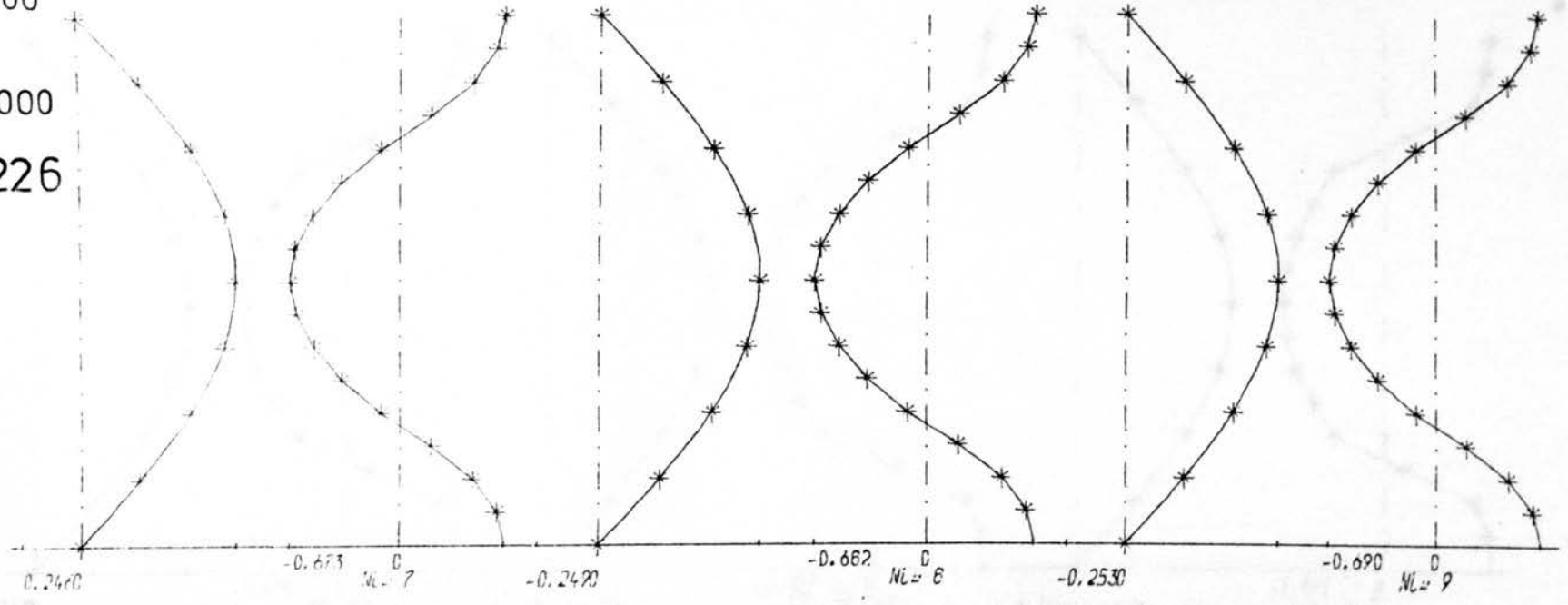

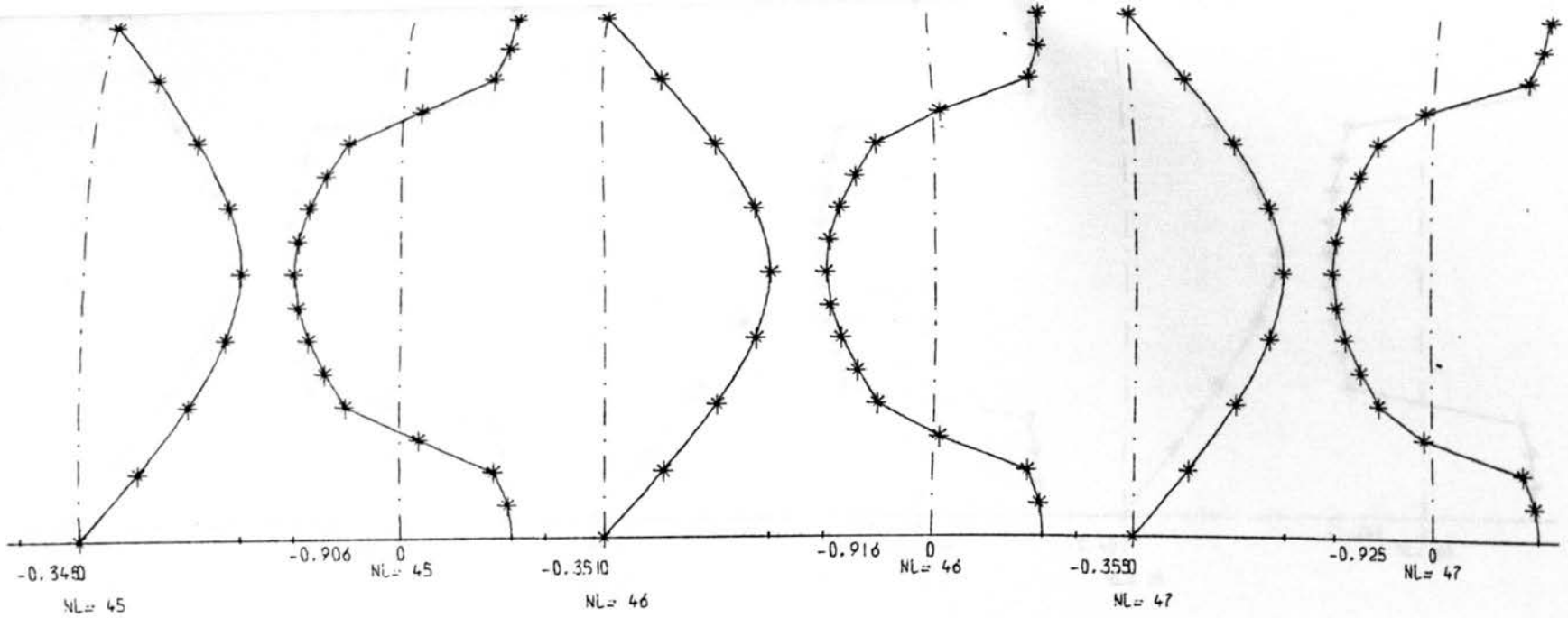
-0.3490
NL= 45
-0.906
0
NL= 45
-0.3510
NL= 46
-0.916
0
NL= 46
-0.3590
NL= 47
-0.925
0
NL= 47

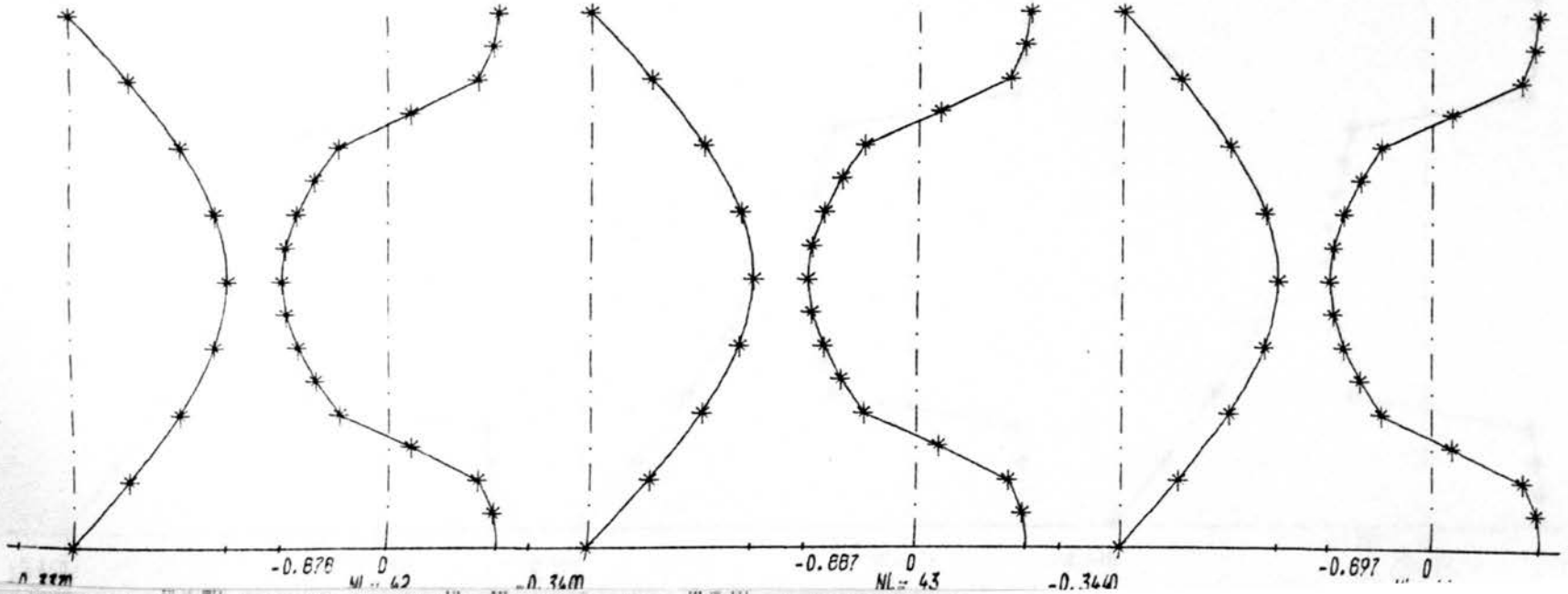
-0.878
0
-0.3400
-0.887
0
NL= 43
-0.3440
-0.897
0

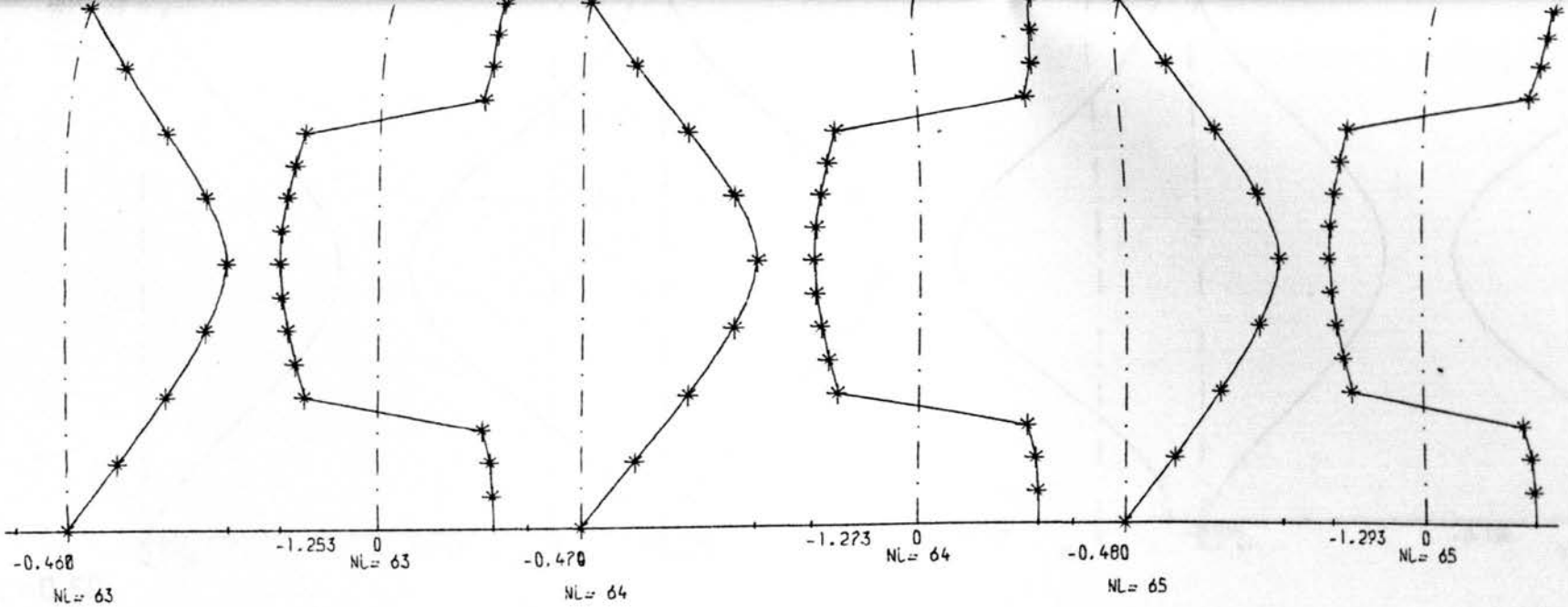
-0.468
NL= 63
-1.253
0
NL= 63
-0.470
NL= 64
-1.273
0
NL= 64
-0.480
NL= 65
-1.293
0
NL= 65

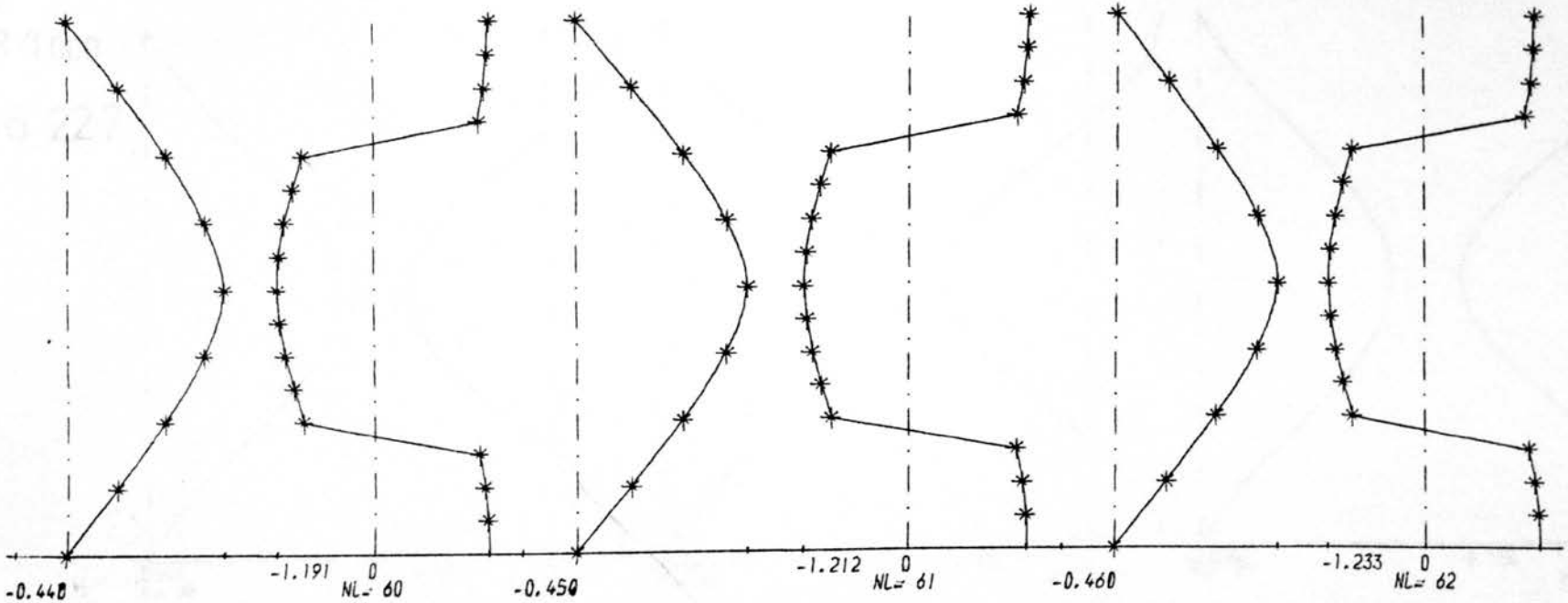
-0.440
-1.191
0
NL= 60
-0.450
-1.212
0
NL= 61
-0.460
-1.233
0
NL= 62

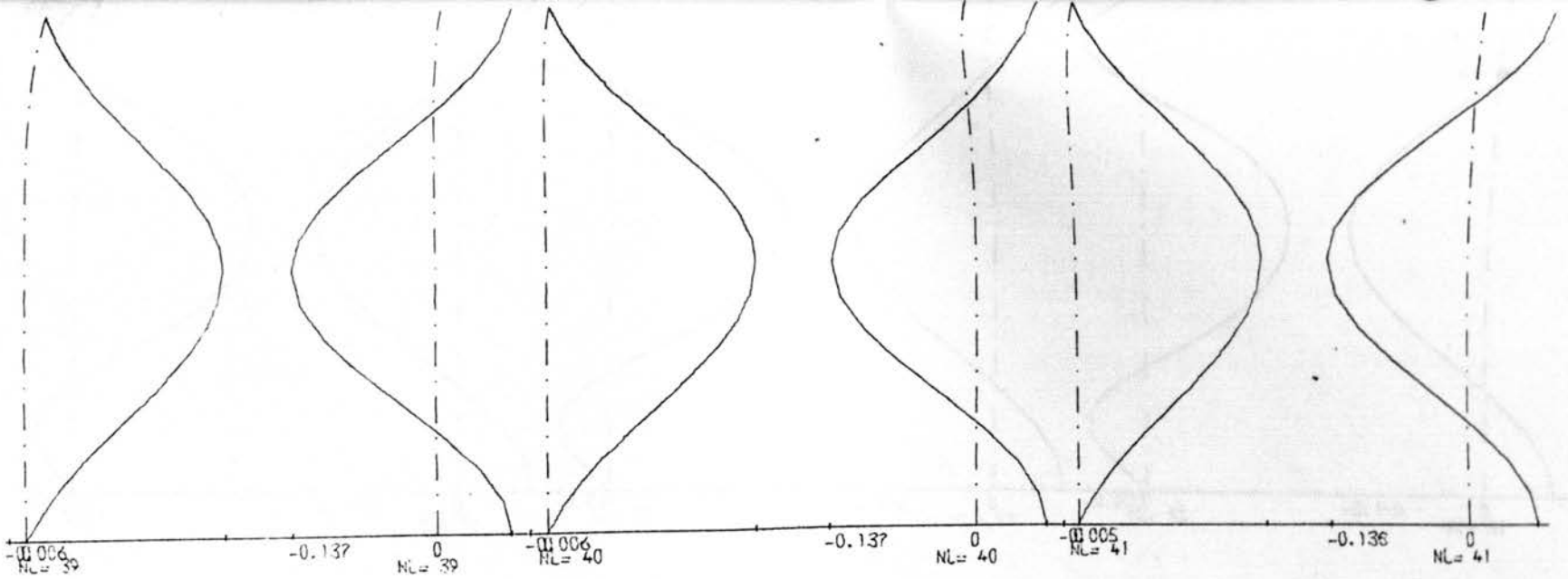

L/R =0.50

R/T =1000

b=1.0

$w_o^* = R/1000$

Fig.6.227

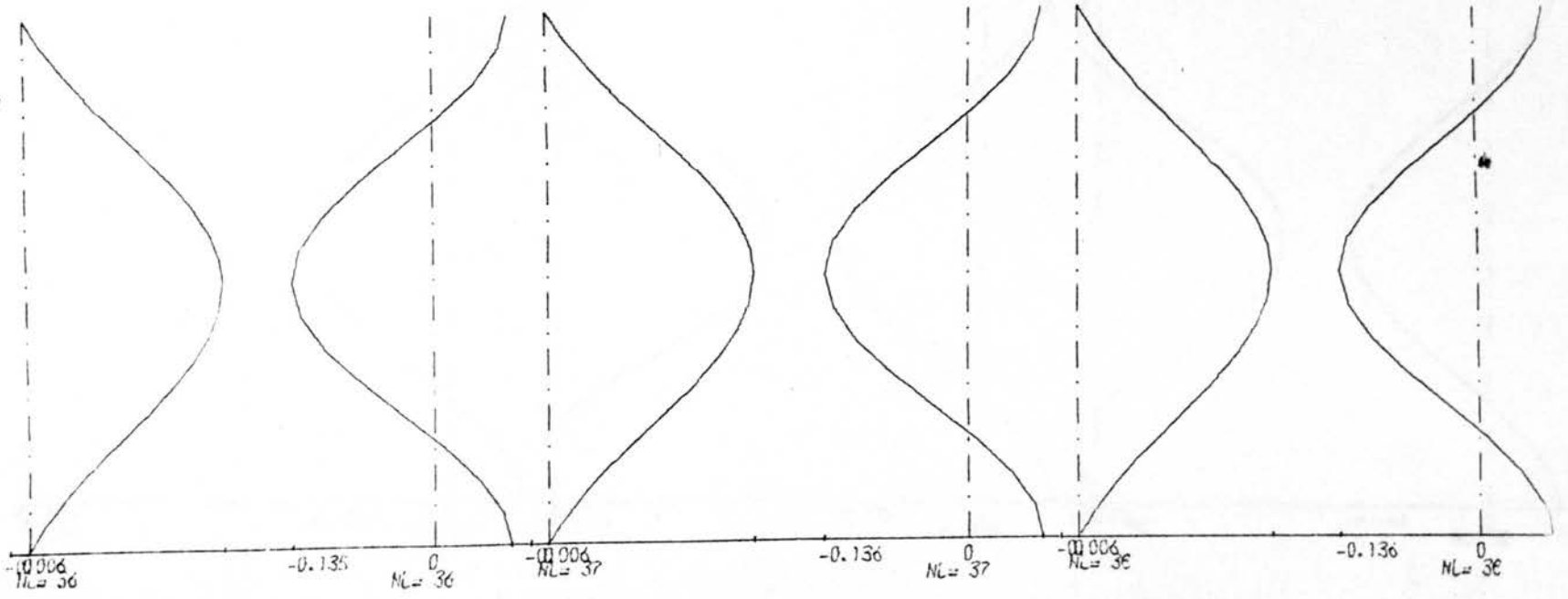

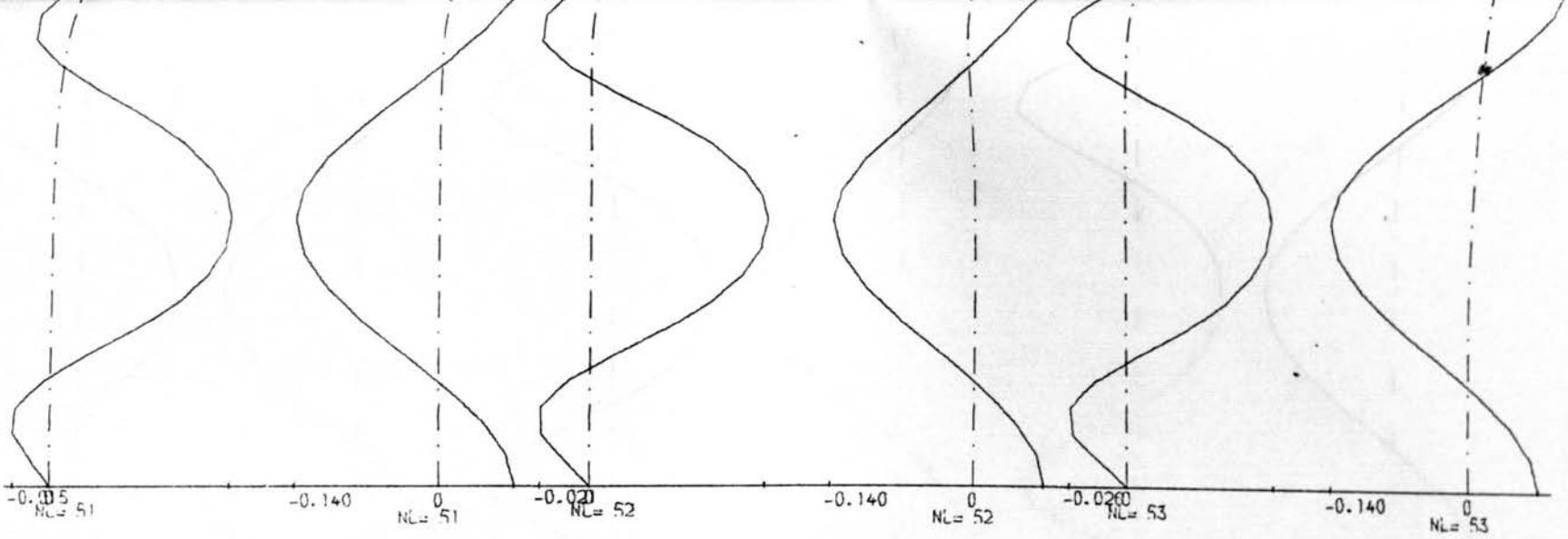
-0.140
0
NL= 51
-0.140
0
NL= 52
-0.140
0
NL= 53

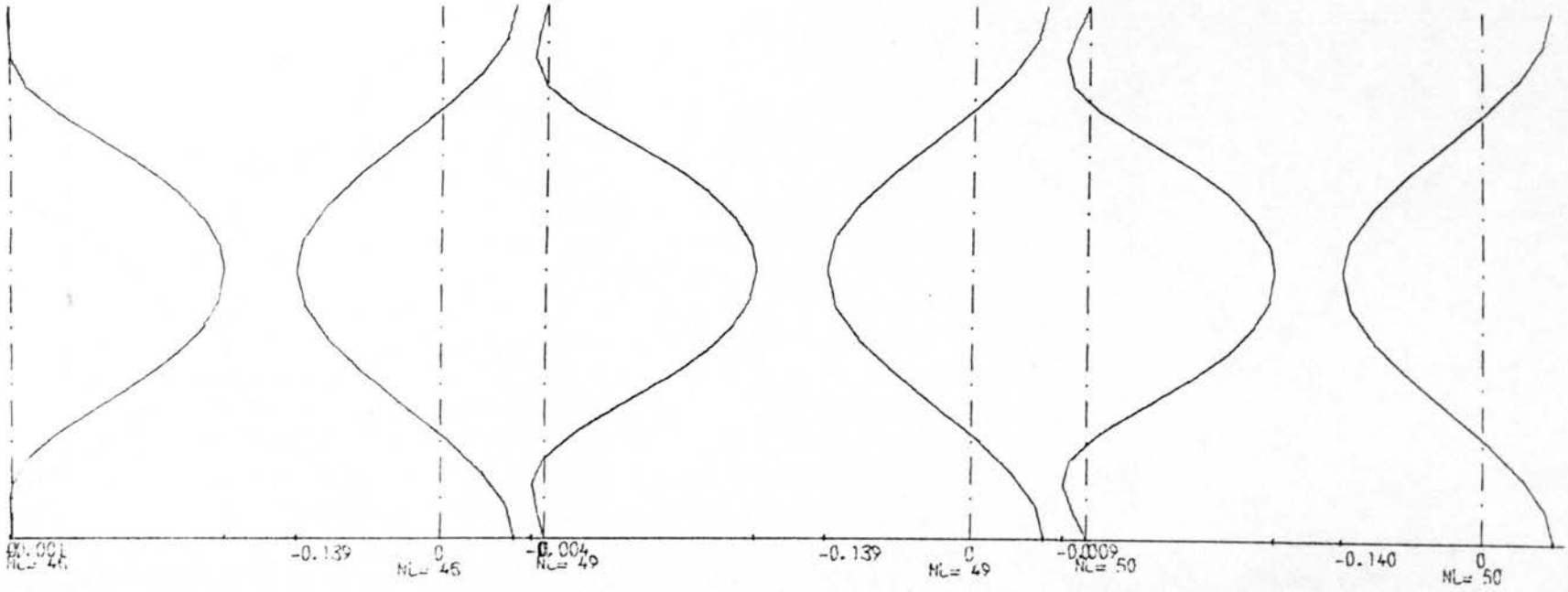
-0.139
0
NL= 48
-0.139
0
NL= 49
-0.140
0
NL= 50

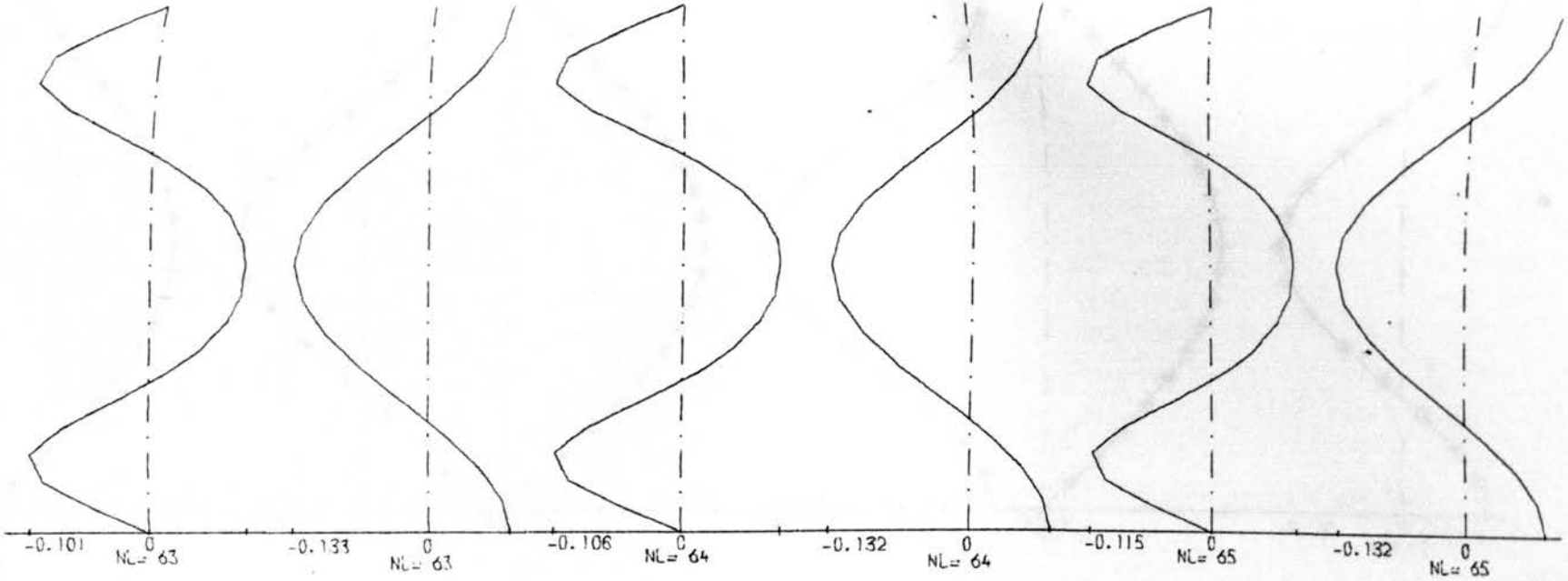
-0.101
0
NL= 63
-0.133
0
NL= 63
-0.106
0
NL= 64
-0.132
0
NL= 64
-0.115
0
NL= 65
-0.132
0
NL= 65

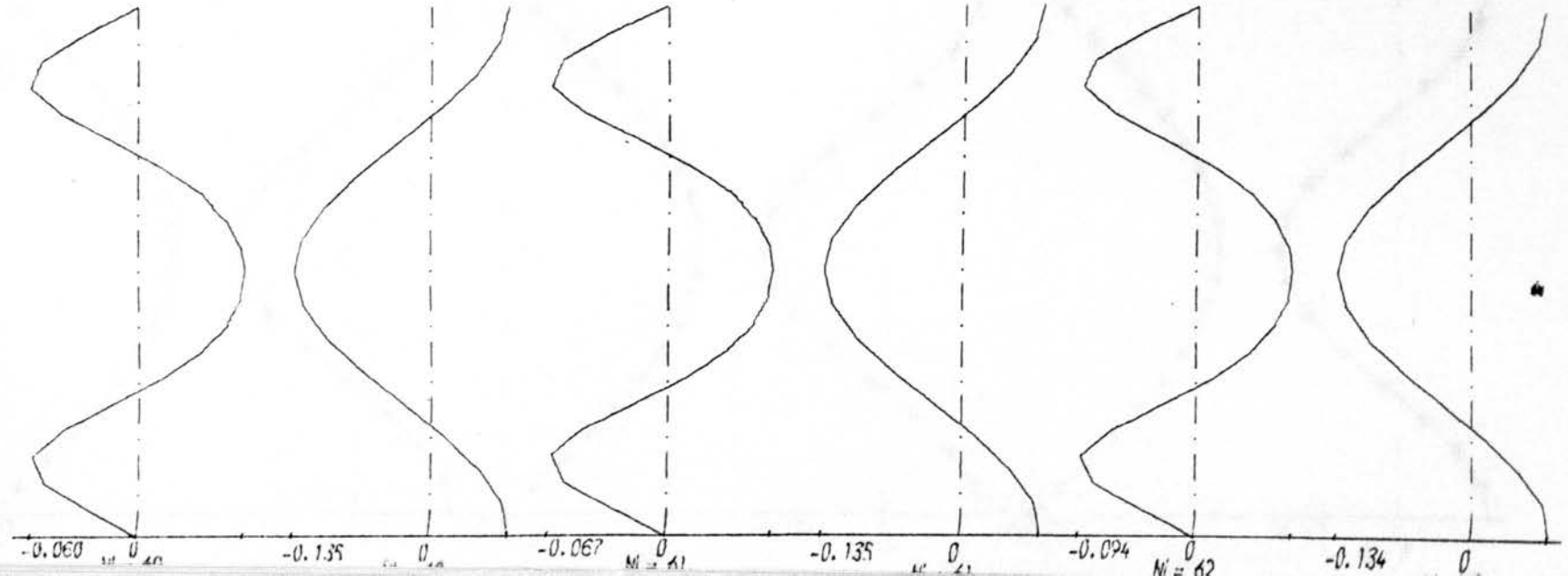
-0.060
0
-0.135
0
-0.067
0
NL= 61
-0.135
0
-0.094
0
NL= 62
-0.134
0

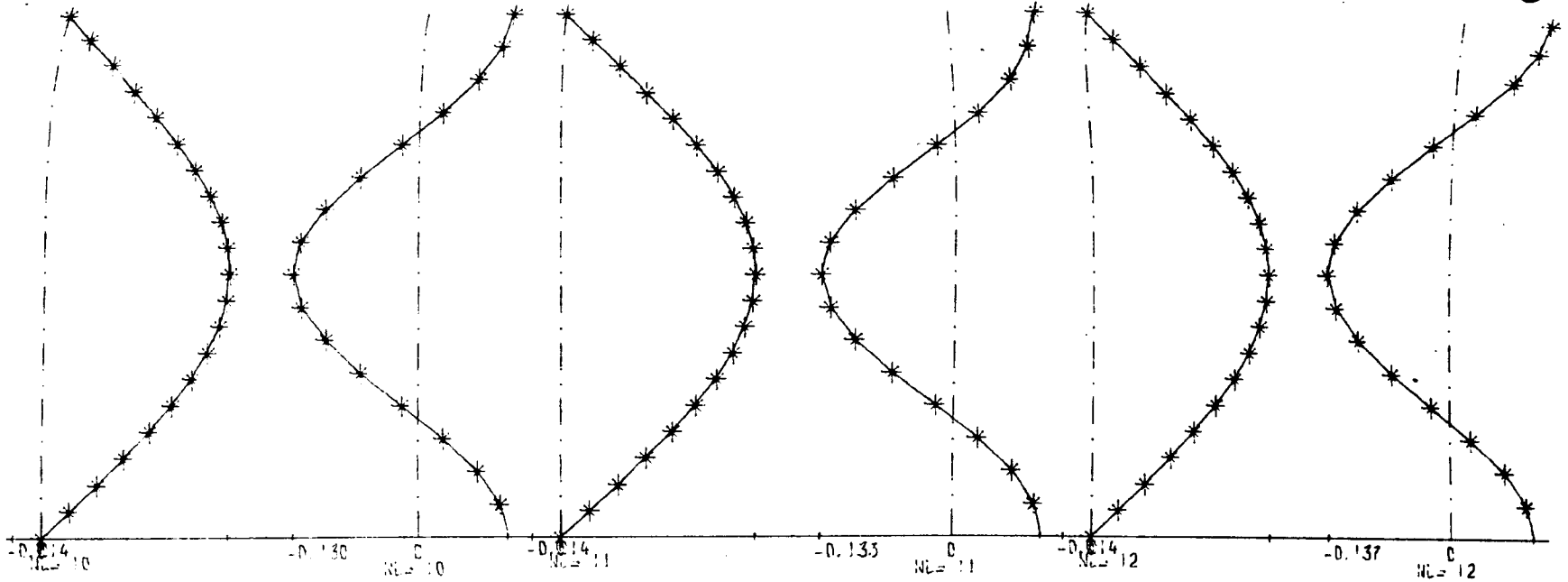

L/R=0.25
R/T=200
b=0.5
w_0^*=R/2000

Fig.6.228

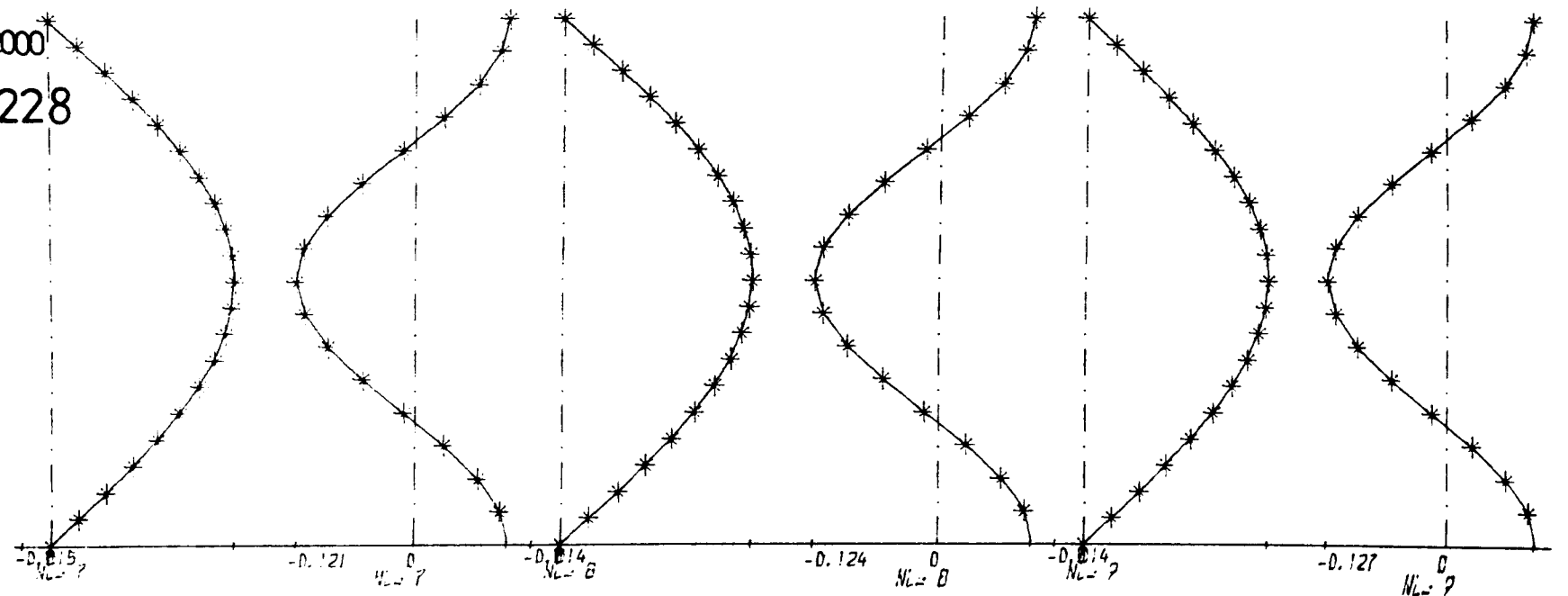

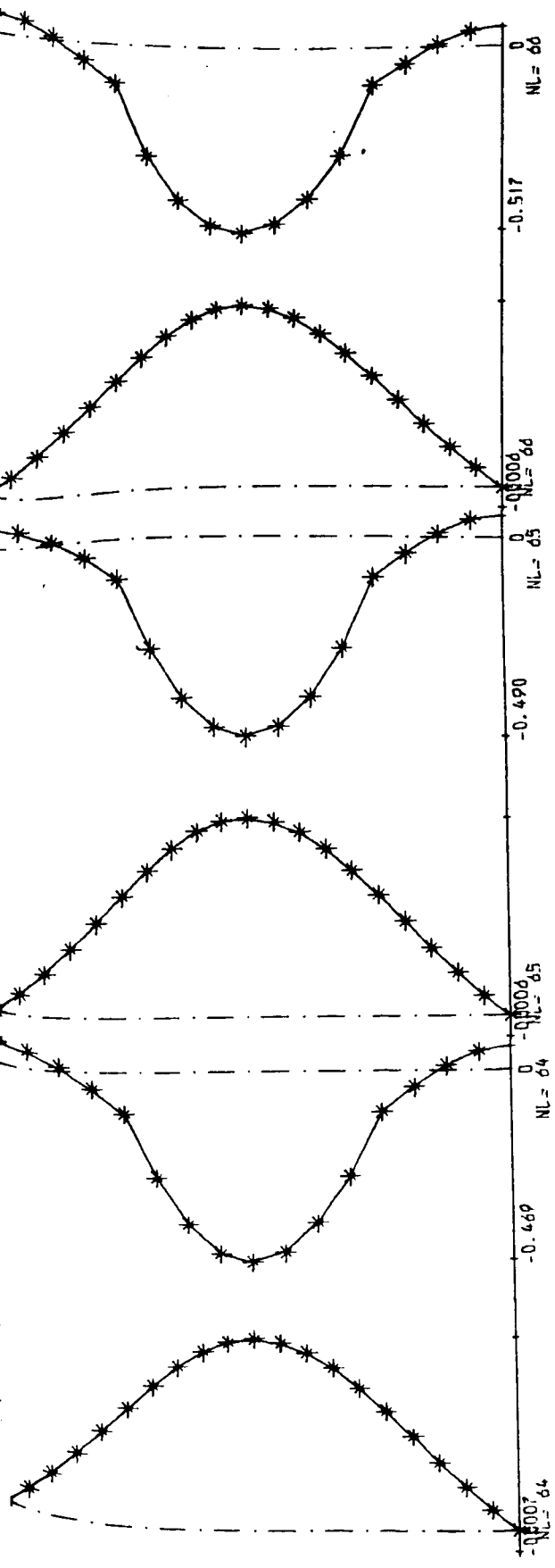
0
NL= 66
-0.517
-0.0006
NL= 66
0
NL= 65
-0.490
-0.0006
NL= 65
0
NL= 64
-0.469
-0.0007
NL= 64

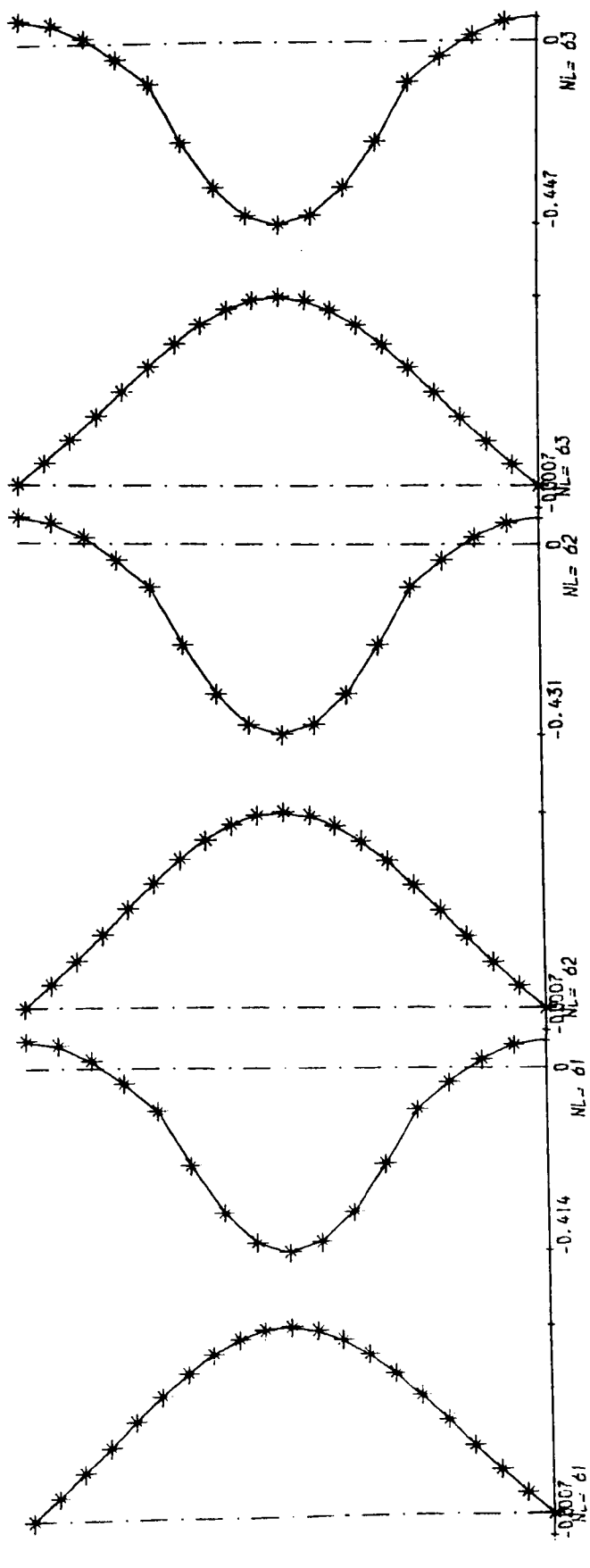
0
NL= 63
-0.447
-0.0007
NL= 63
0
NL= 62
-0.431
-0.0007
NL= 62
0
NL= 61
-0.414
-0.0007
NL= 61

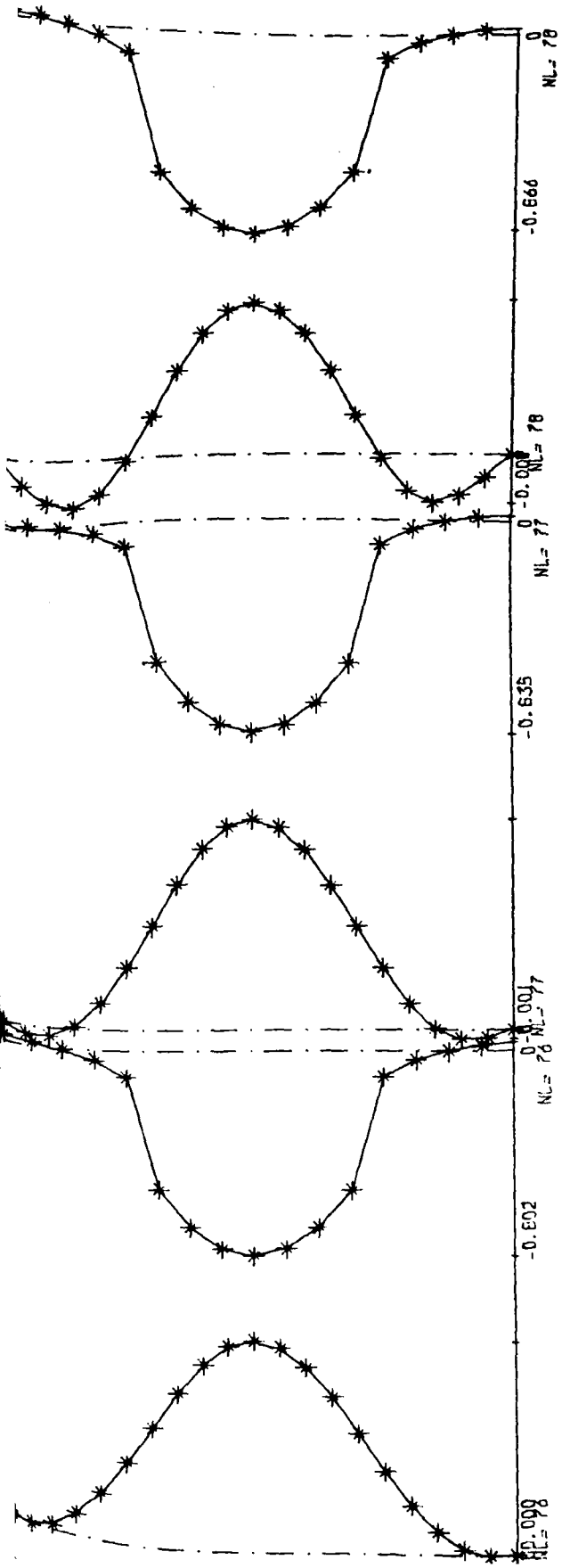
NL= 78
-0.666
NL= 78
-0.635
NL= 77
-0.602
NL= 77

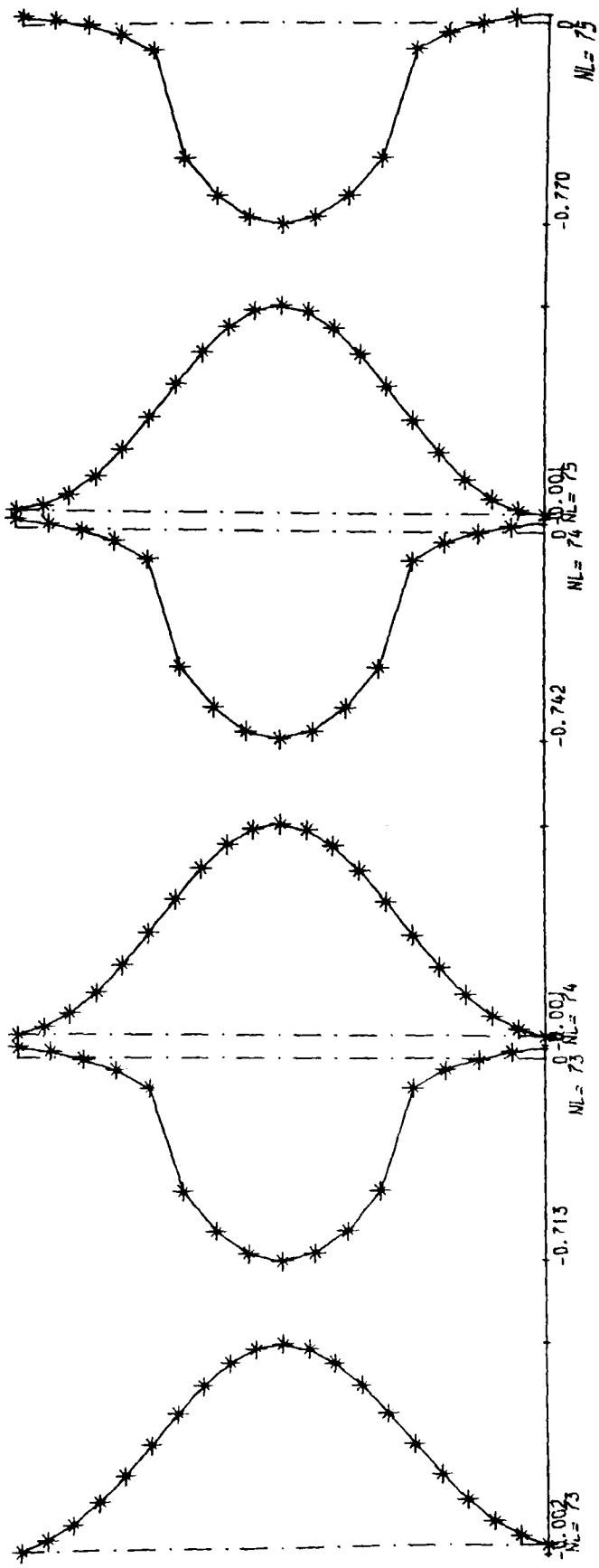
NL= 75
-0.770
NL= 75
-0.742
NL= 74
-0.713
NL= 74

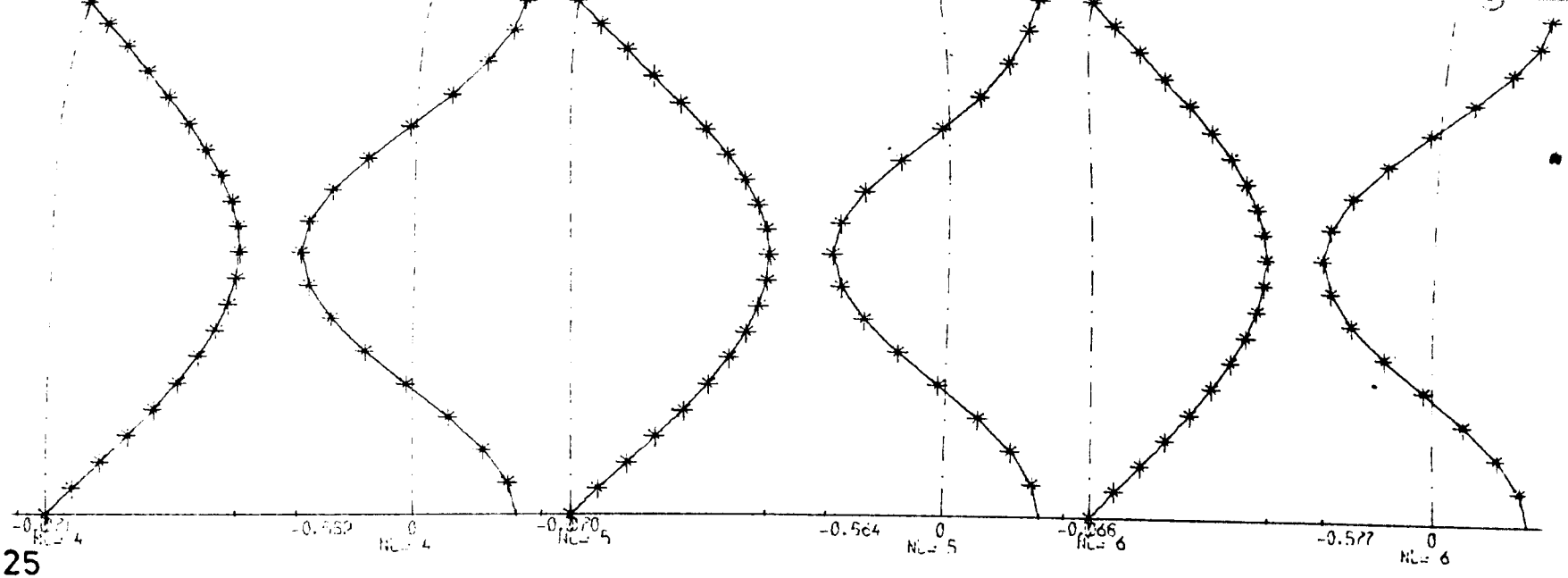

L/R=0.25
R/T=1000
b=0,5
w_o^*=R/2000

Fig.6.229

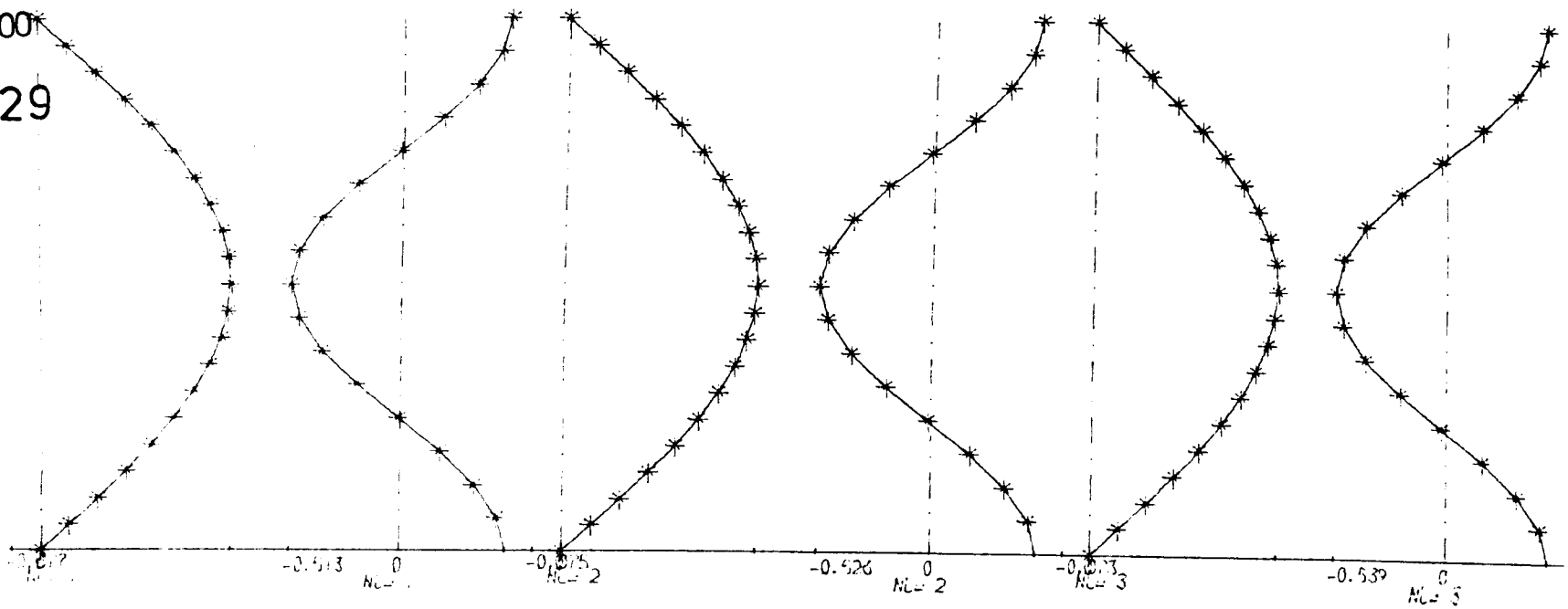

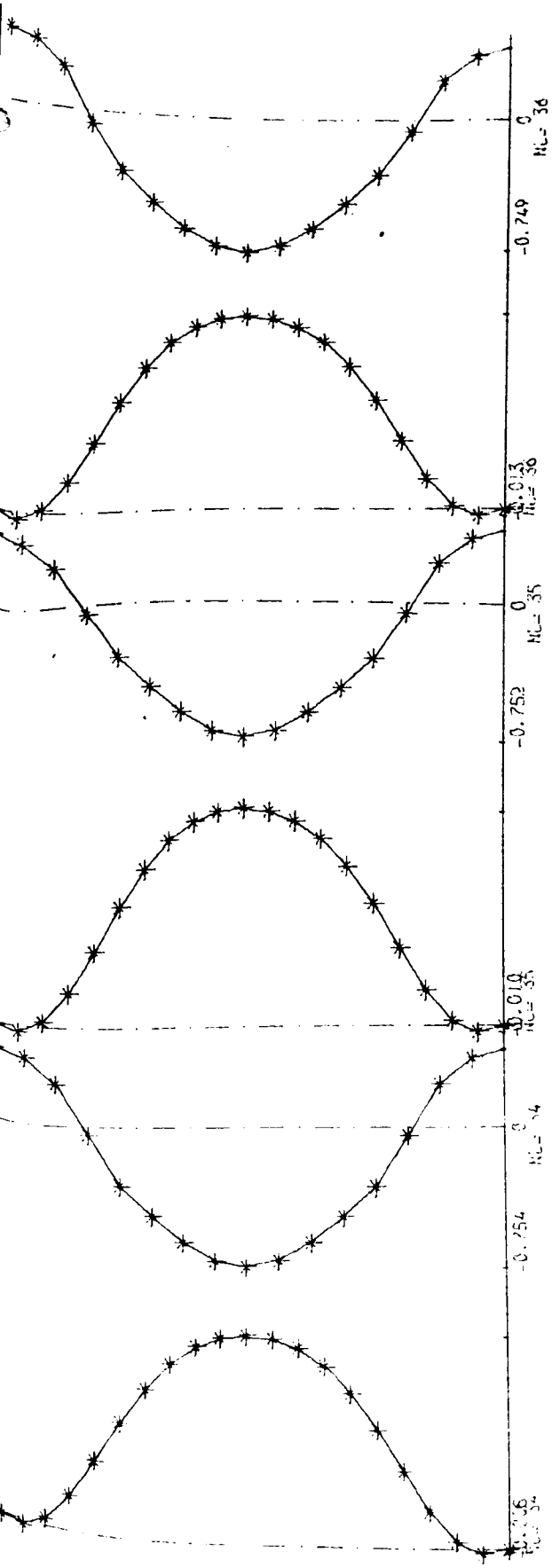
-0.749
-0.752
-0.754

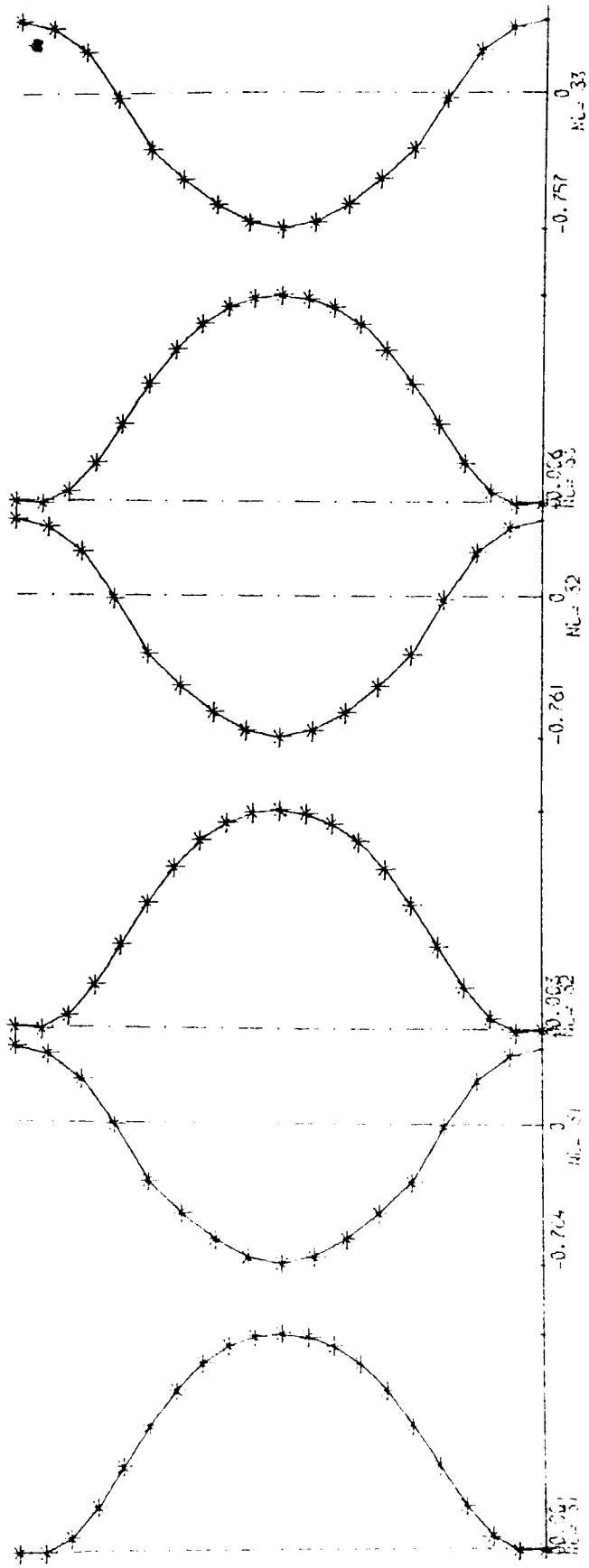
-0.757
-0.761
-0.764

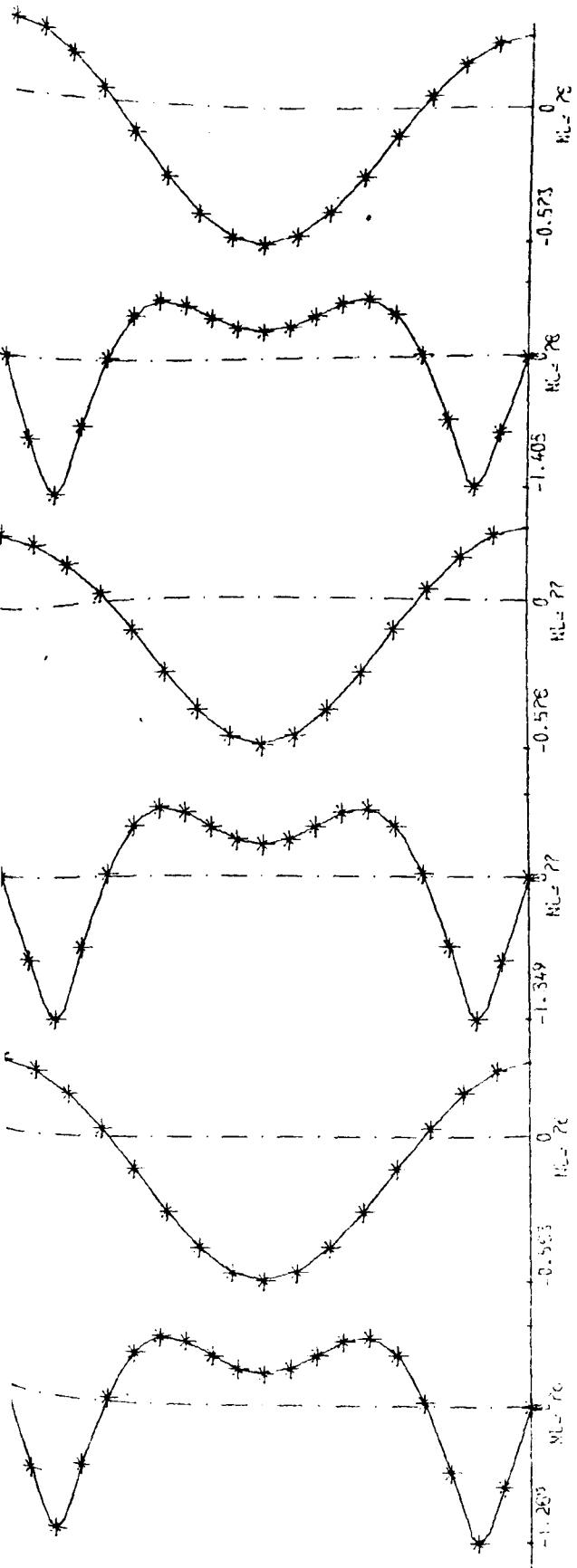
0
-0.573
0
-1.405
0
-0.578
0
-1.349
0
-0.553

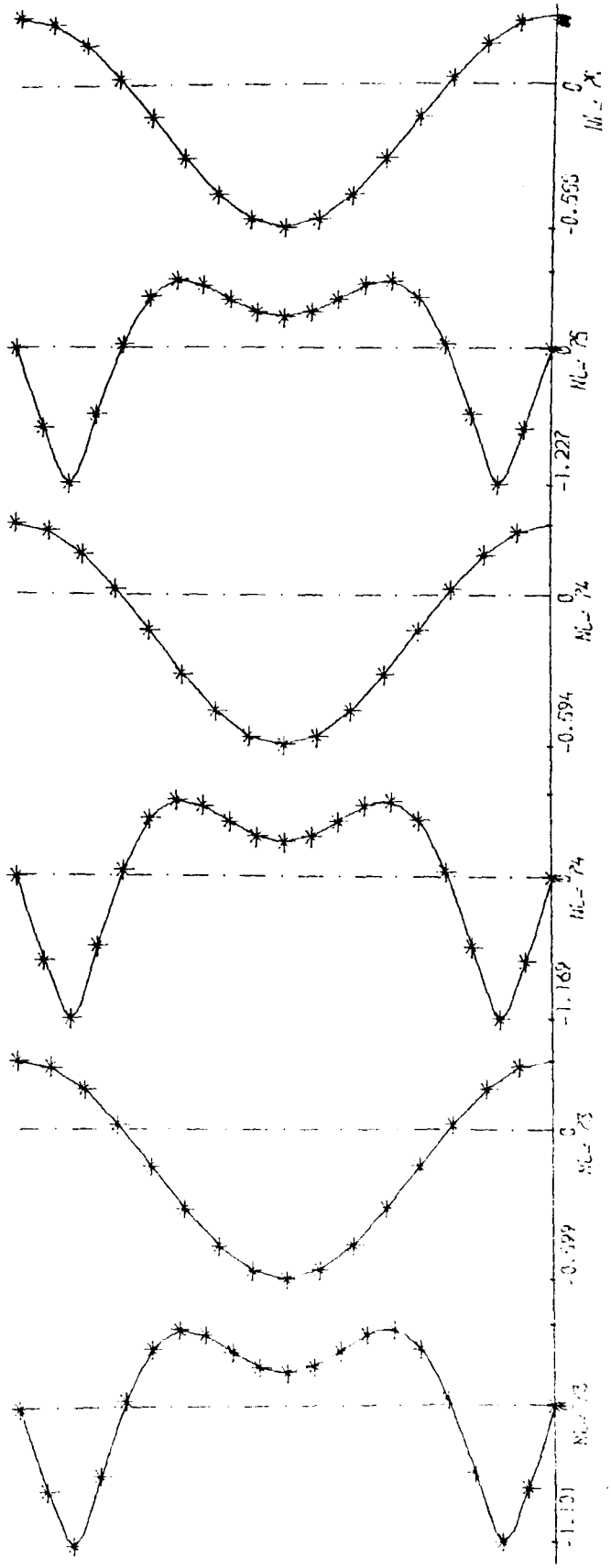
0
-0.555
0
-1.227
0
-0.594
0
-1.169
0
-0.599

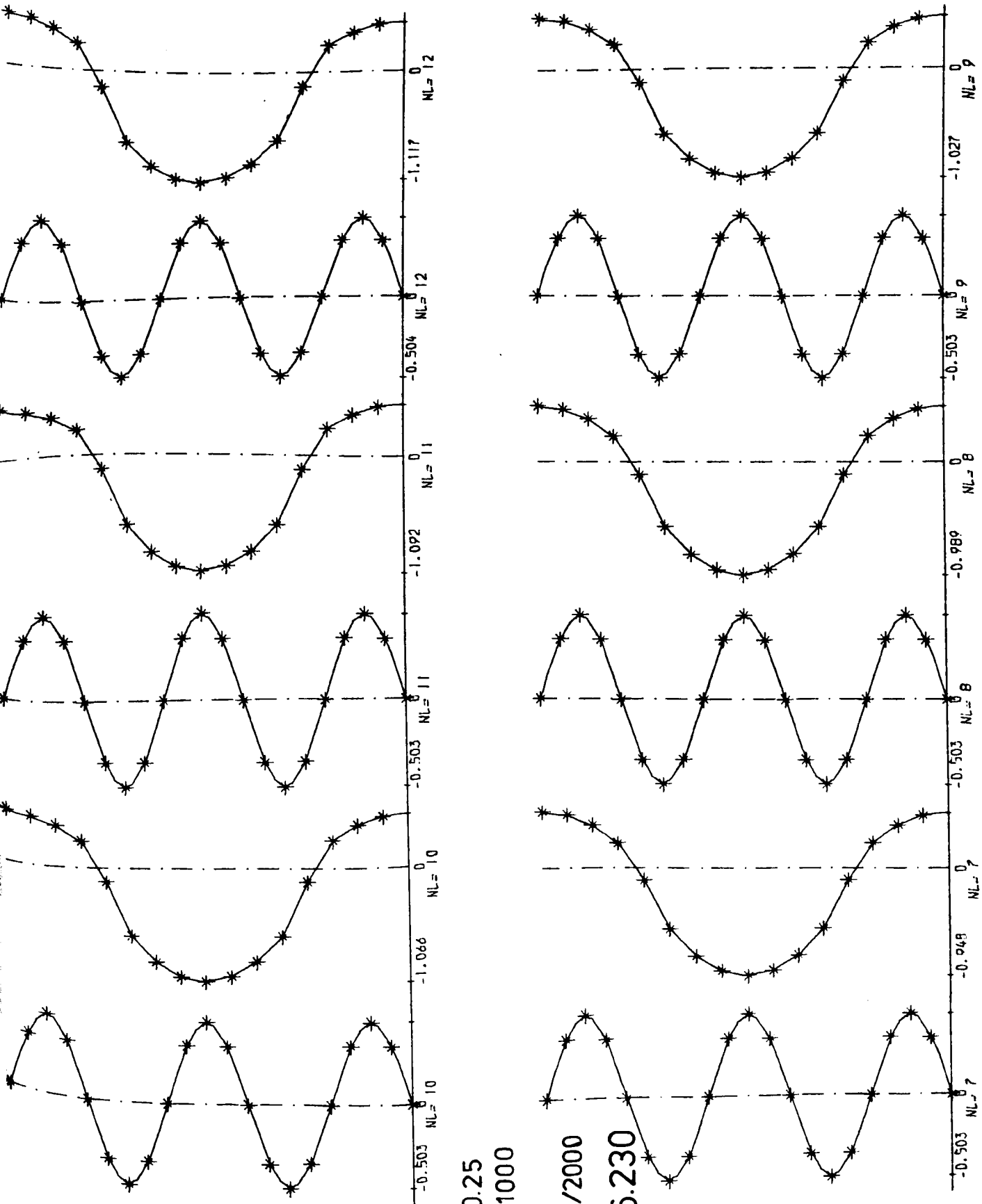

L/R=0.25
R/T=1000
b=0.0
$w_o^* = R/2000$

Fig.6.230

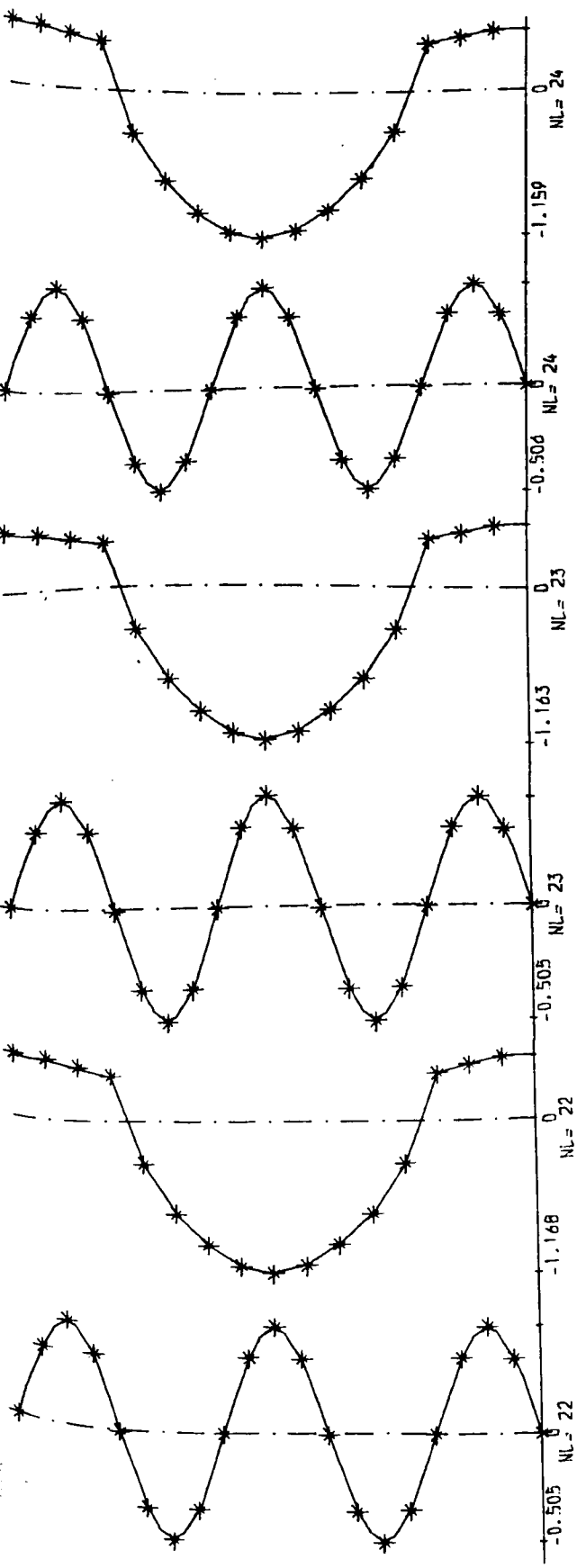
NL= 24
-1.159
NL= 24
-0.506
NL= 23
-1.163
NL= 23
-0.505
NL= 22
-1.168
NL= 22
-0.505

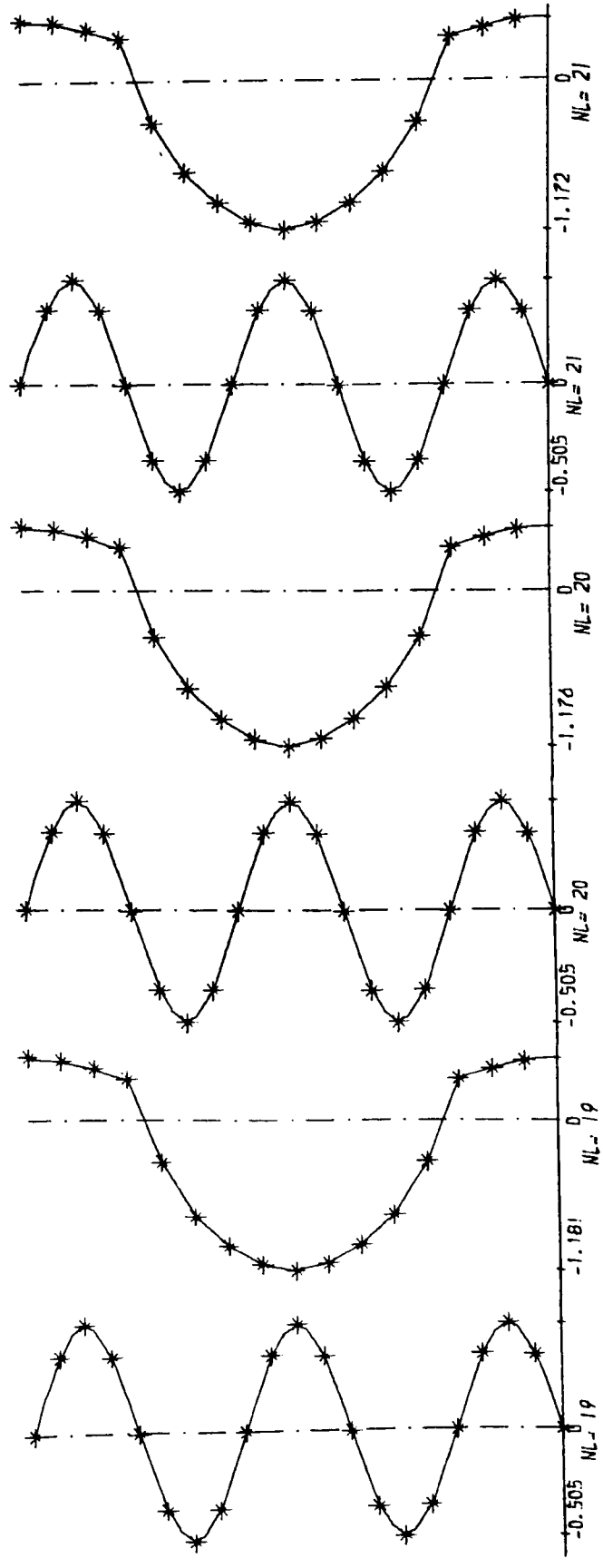
NL= 21
-1.172
NL= 21
-0.505
NL= 20
-1.176
NL= 20
-0.505
NL= 19
-1.181
NL= 19
-0.505

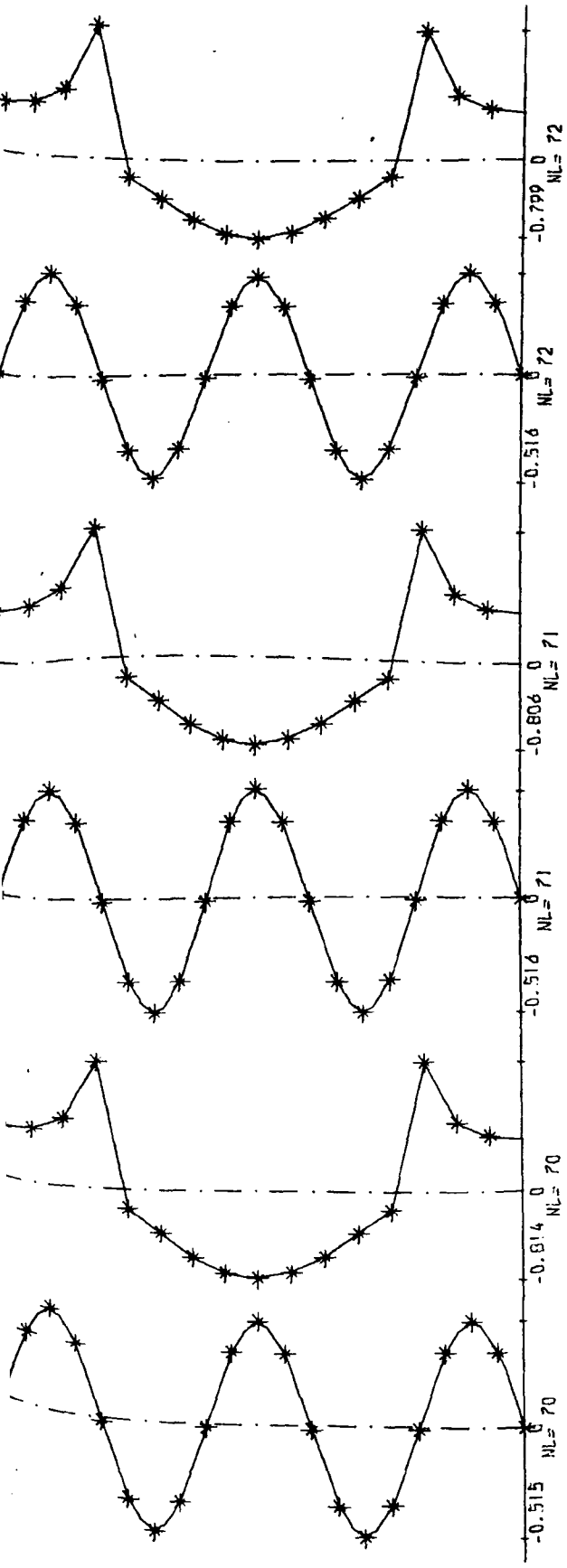
-0.515
0
NL= 70
-0.814
0
NL= 70
-0.516
0
NL= 71
-0.806
0
NL= 71
-0.516
0
NL= 72
-0.799
0
NL= 72

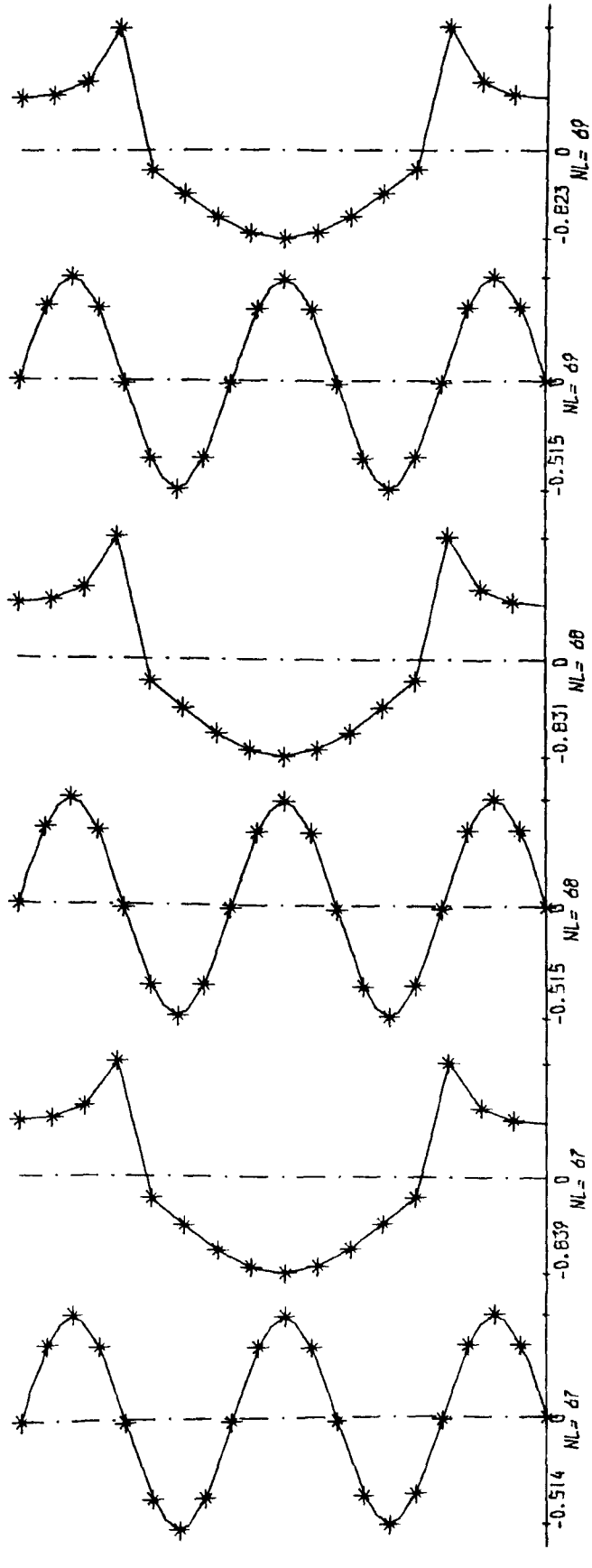
-0.514
0
NL= 67
-0.839
0
NL= 67
-0.515
0
NL= 68
-0.831
0
NL= 68
-0.515
0
NL= 69
-0.823
0
NL= 69

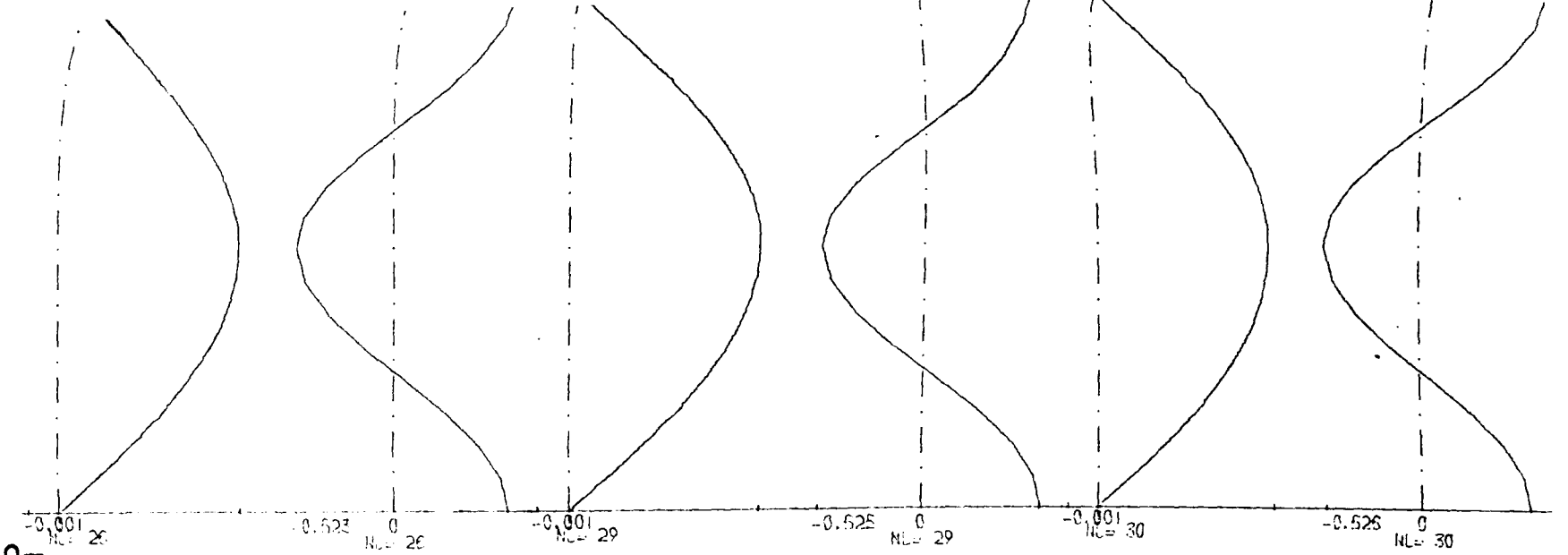

P.H.=50m
L/R=0.25
R/T=200
b=0.5
w_o^*=R/400

Fig.6.231

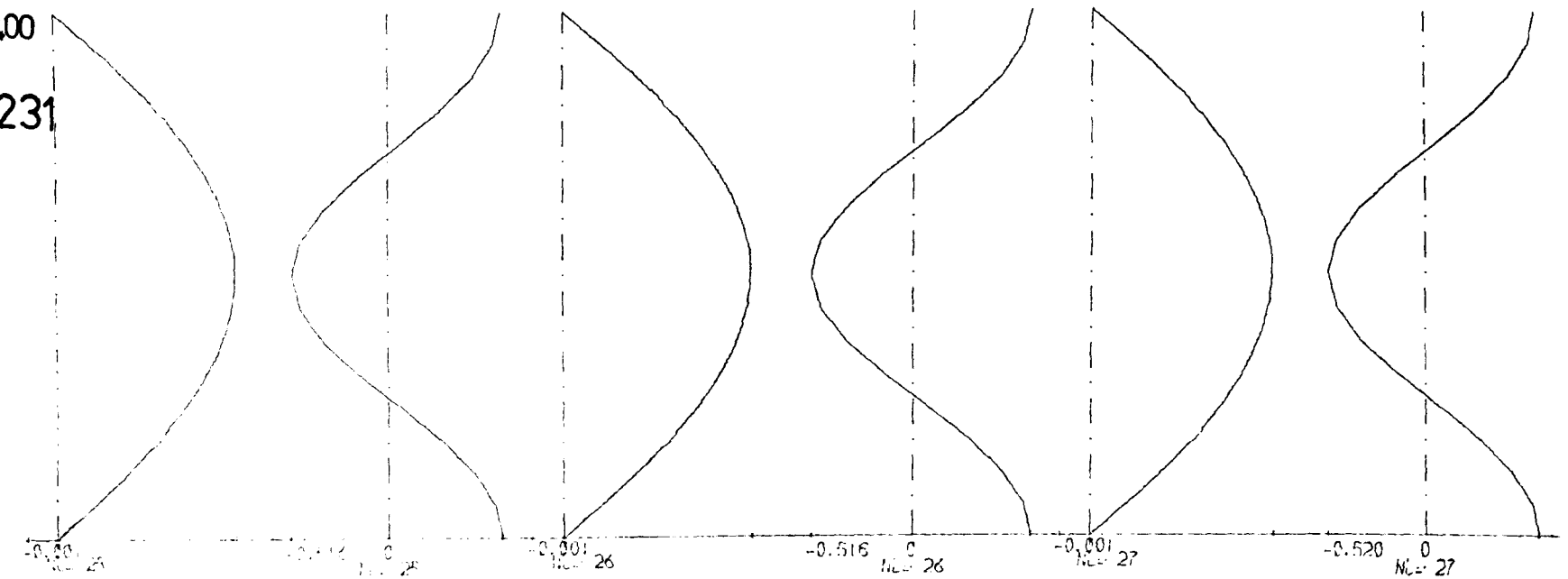

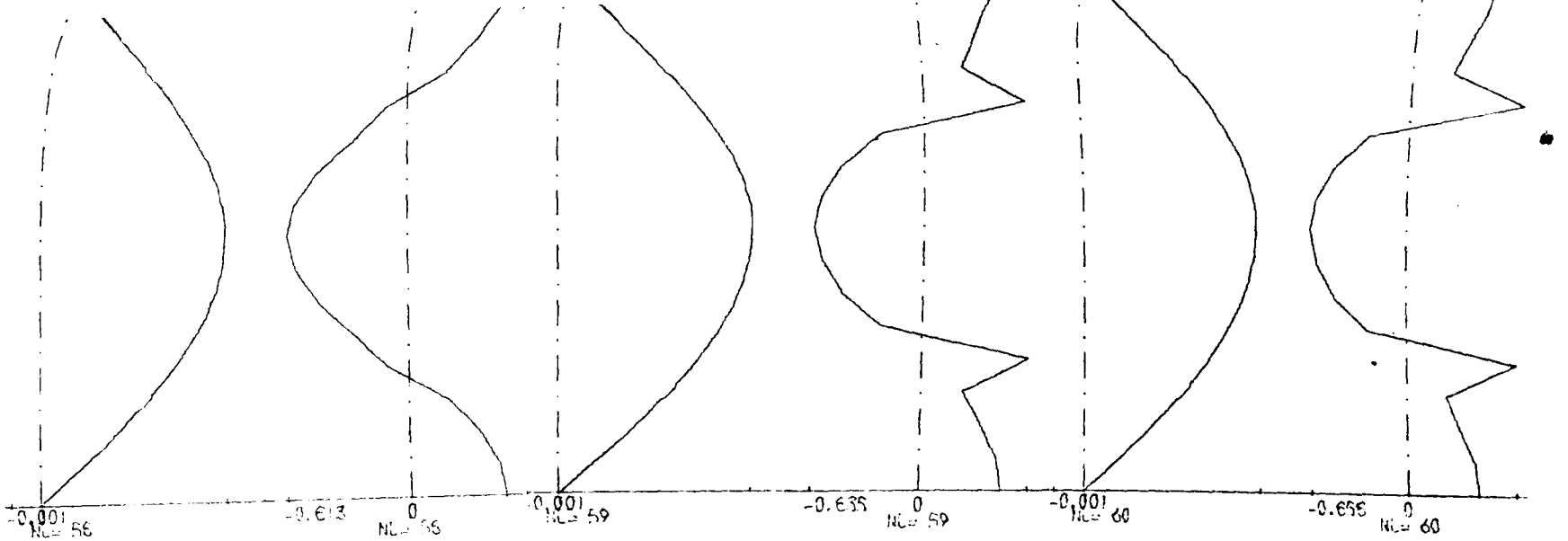
-0.001
NL= 56
-0.613
0
NL= 56
-0.001
NL= 59
-0.635
0
NL= 59
-0.001
NL= 60
-0.656
0
NL= 60

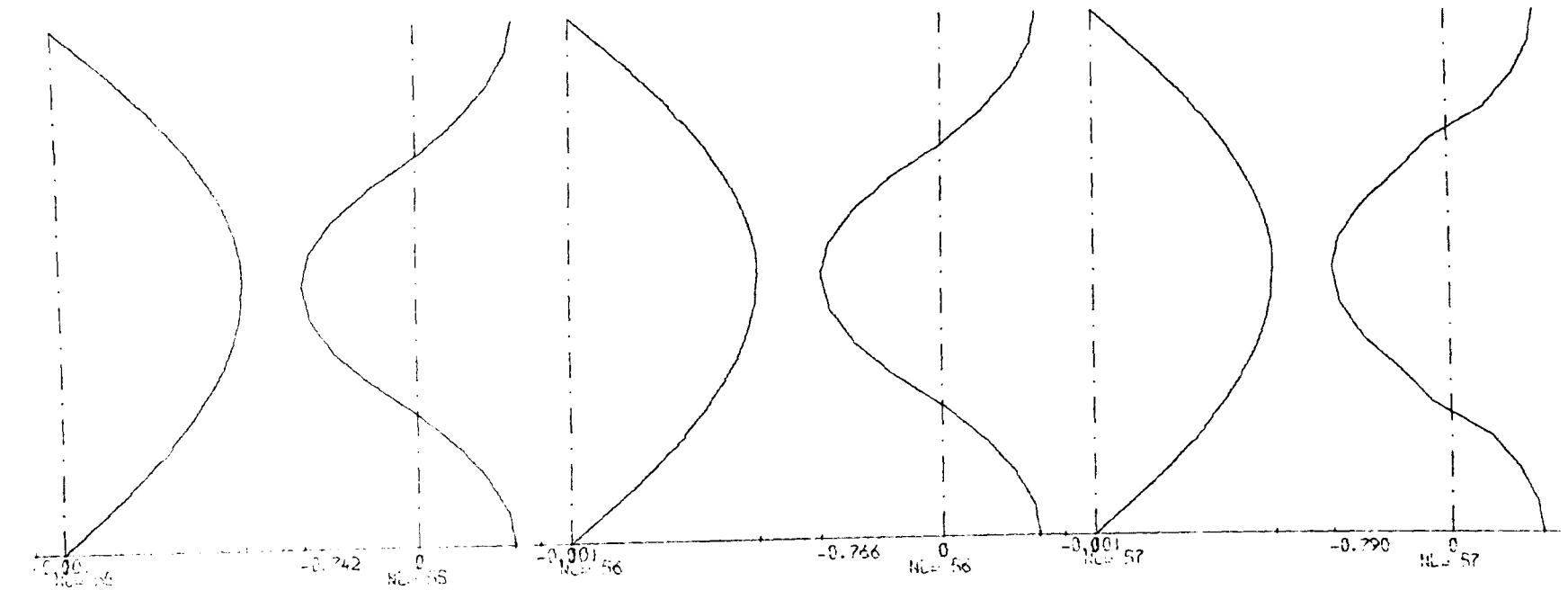
-0.001
NL= 56
-0.766
0
NL= 56
-0.001
NL= 57
-0.790
0
NL= 57

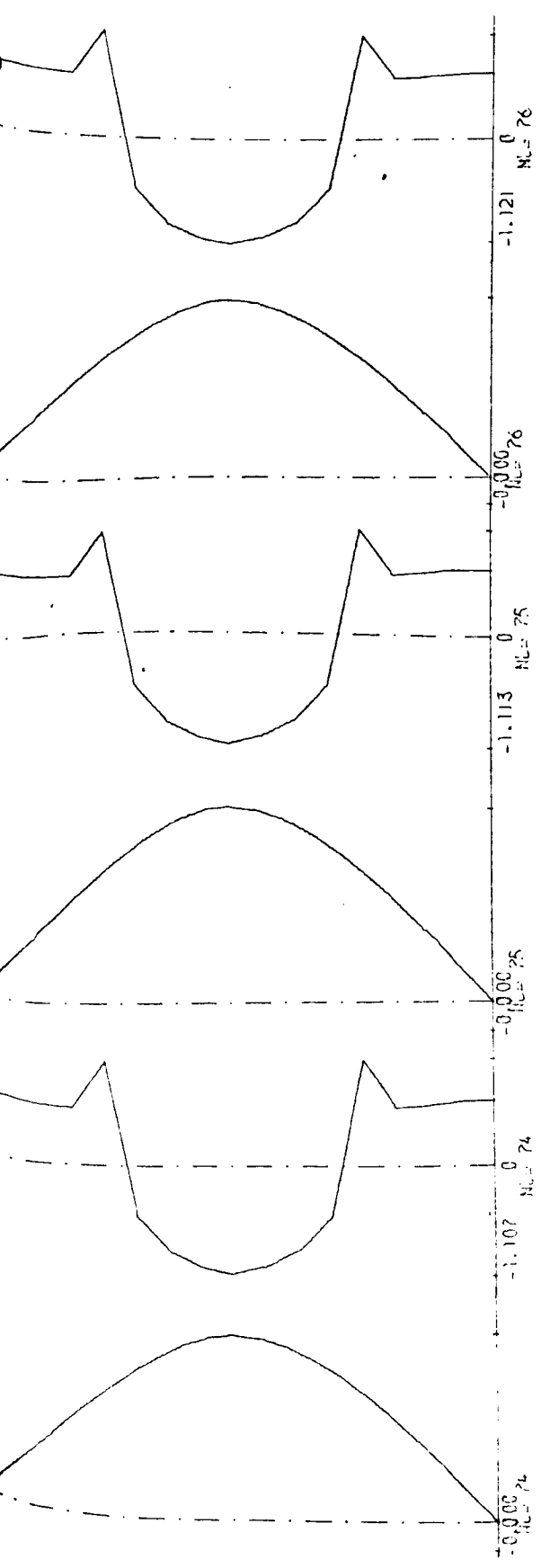
-1.121
-0.000
-1.113
-0.000
-1.107
-0.000

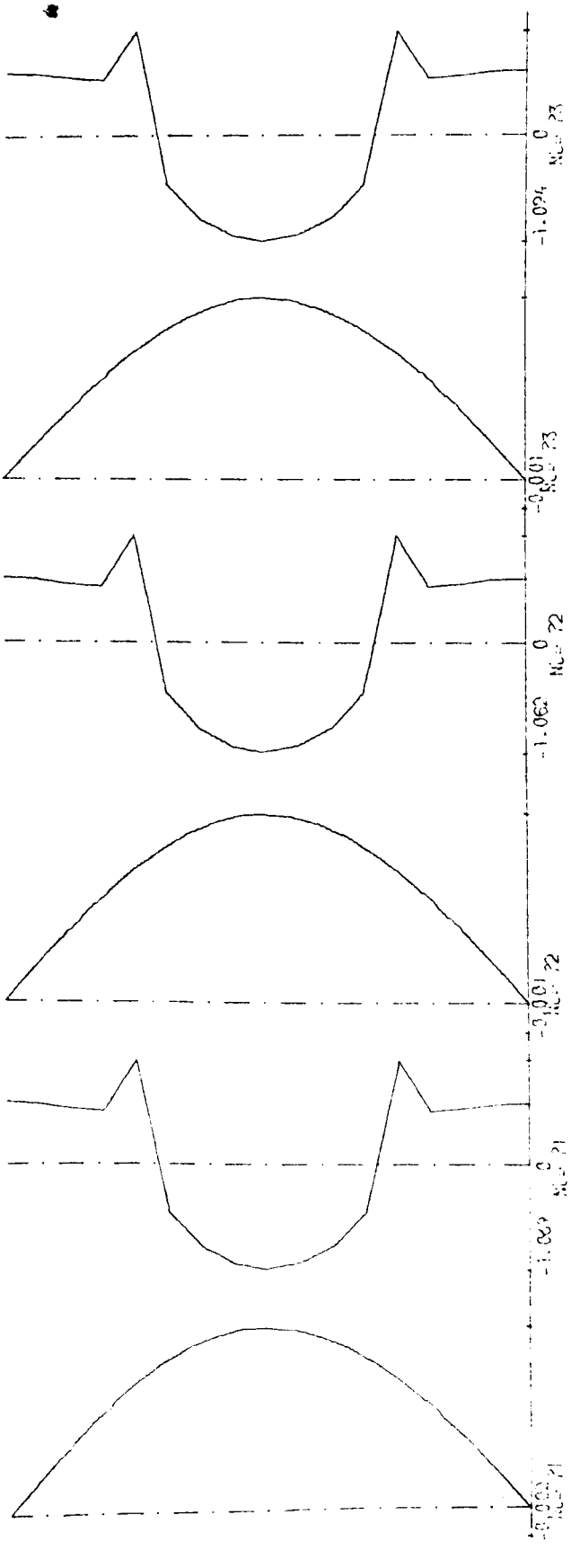
-1.094
-0.001
-1.062
-0.001

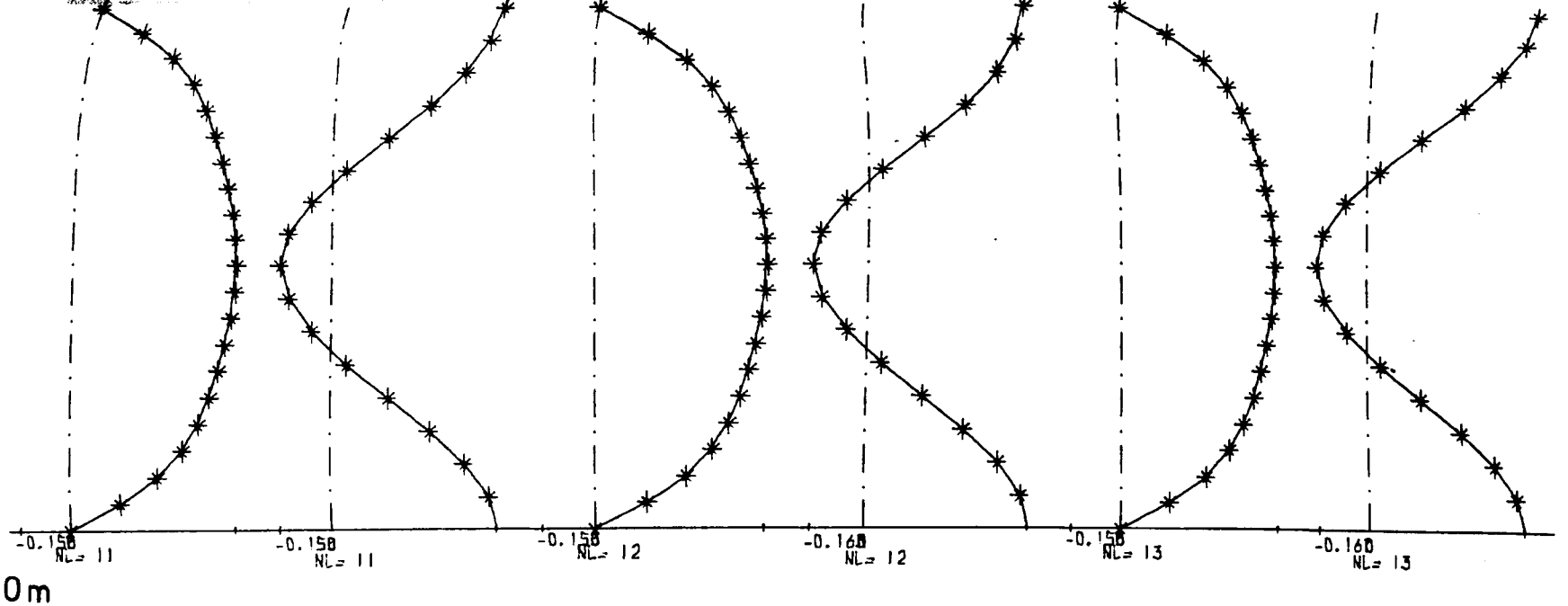

P. H.= 50 m
L/R=0.50
b=0.0
w_o^*=R/1000
R/T=300

Fig.6.232

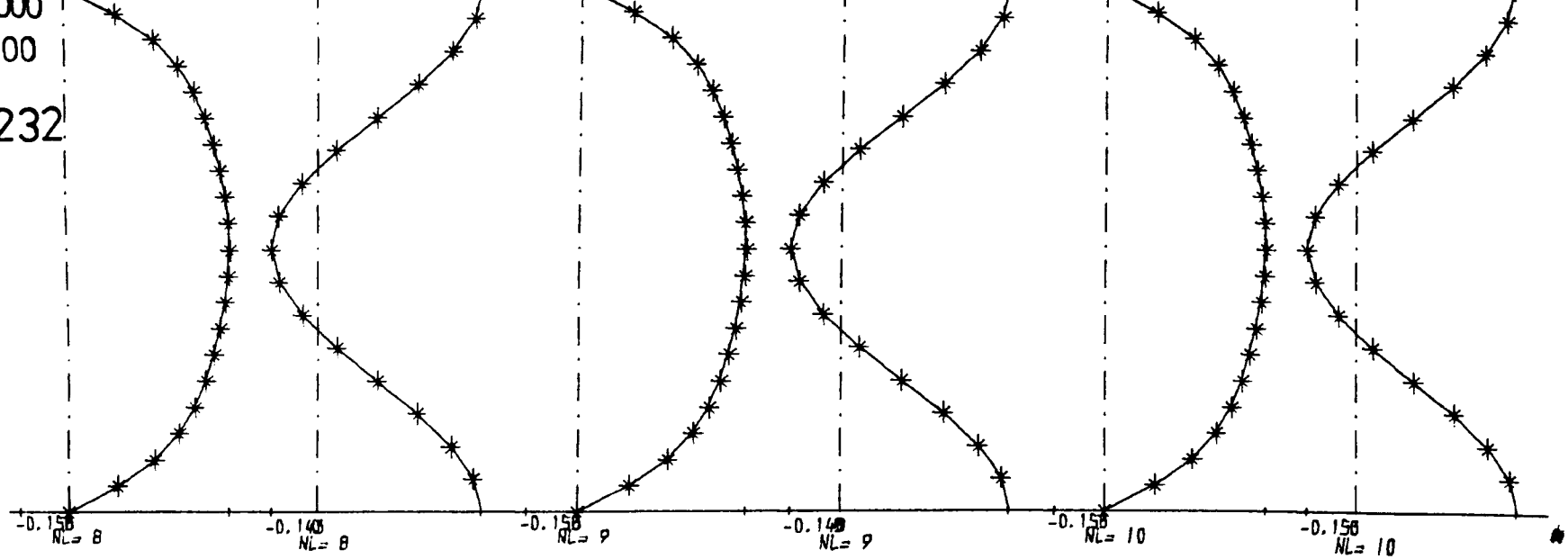

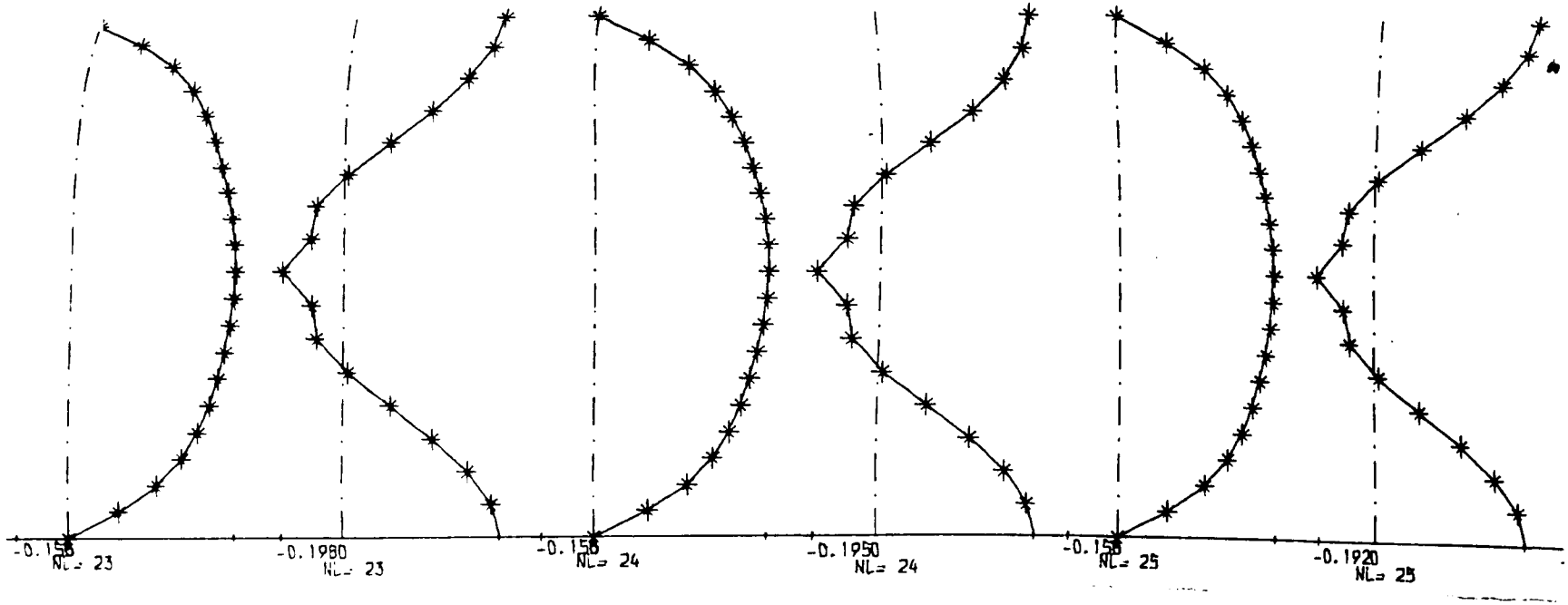
-0.1980
NL= 23
-0.1950
NL= 24
-0.1920
NL= 25

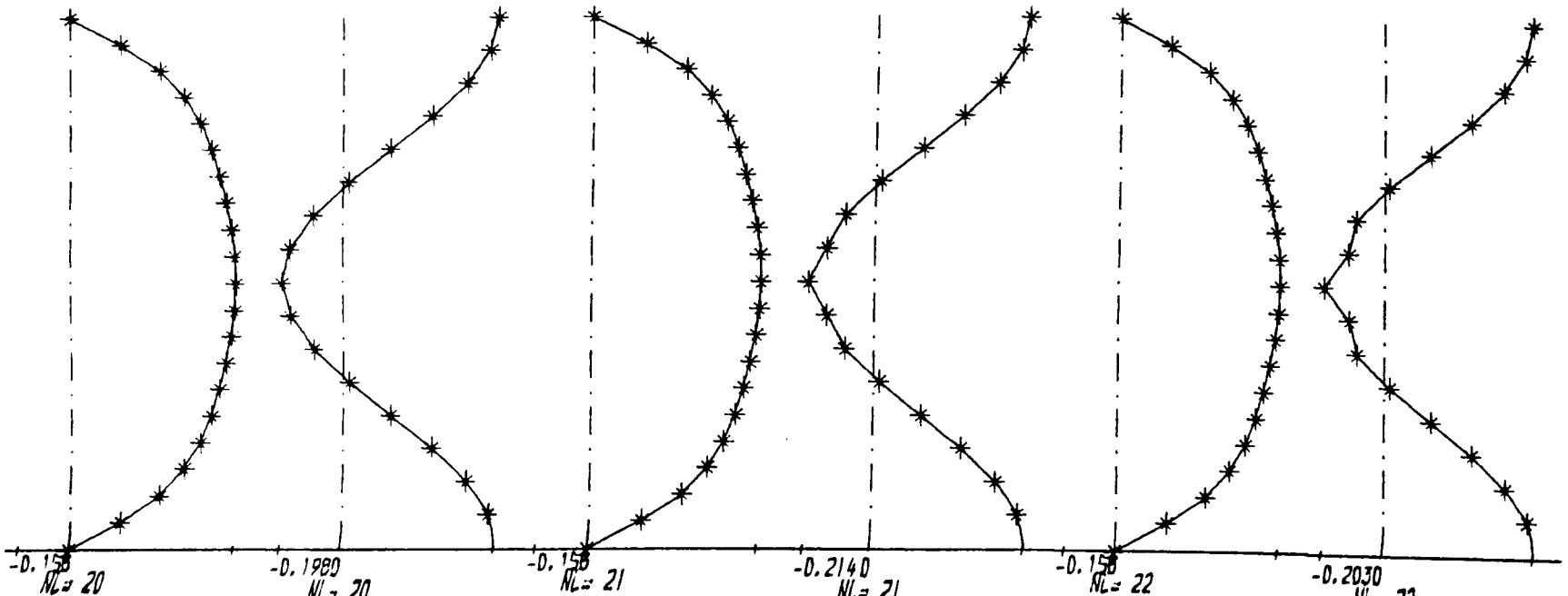
-0.1980
NL= 20
-0.2140
NL= 21
-0.2030

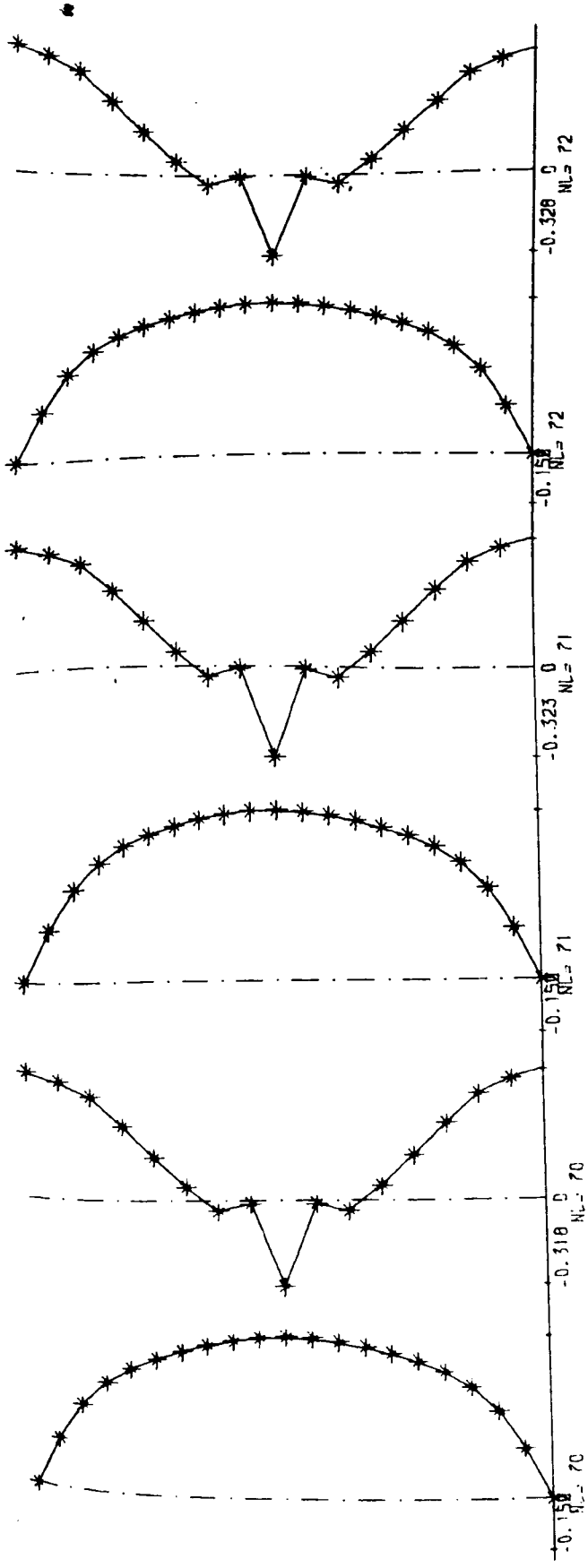
-0.328 0
NL= 72
-0.323 0
NL= 71
-0.318 0
NL= 70

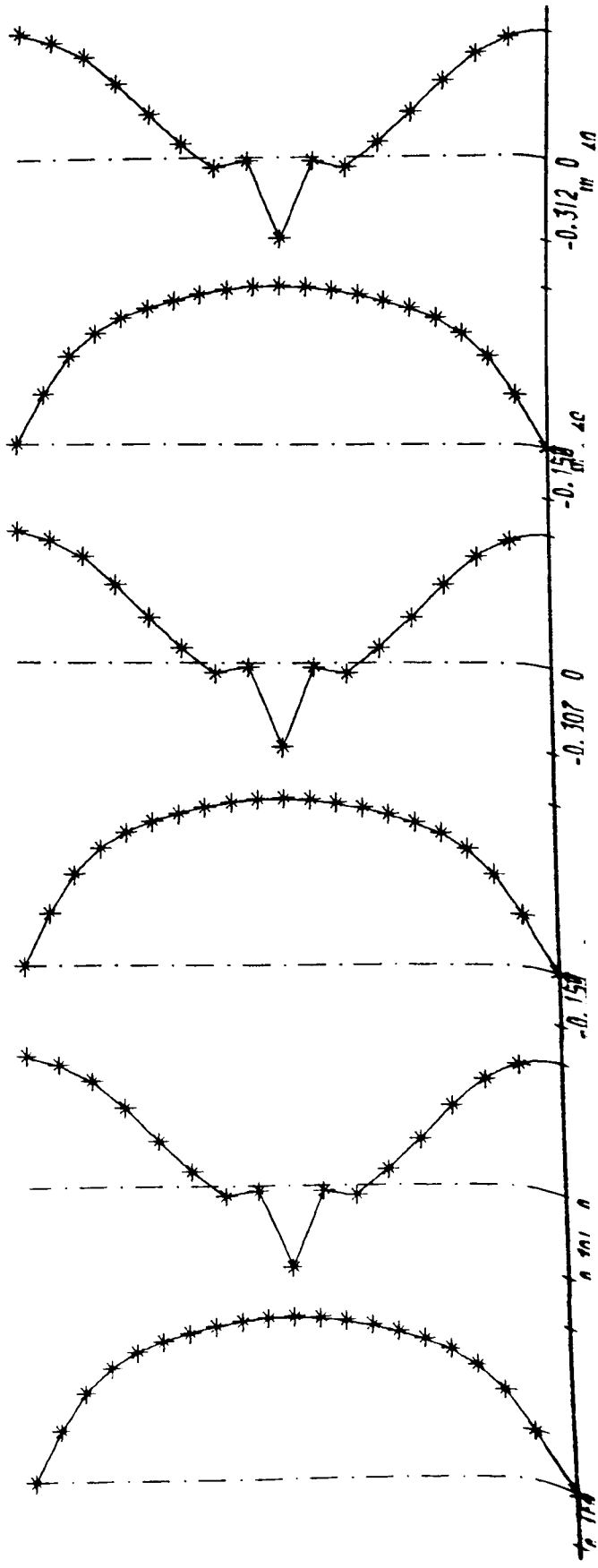
-0.312 0
-0.107 0

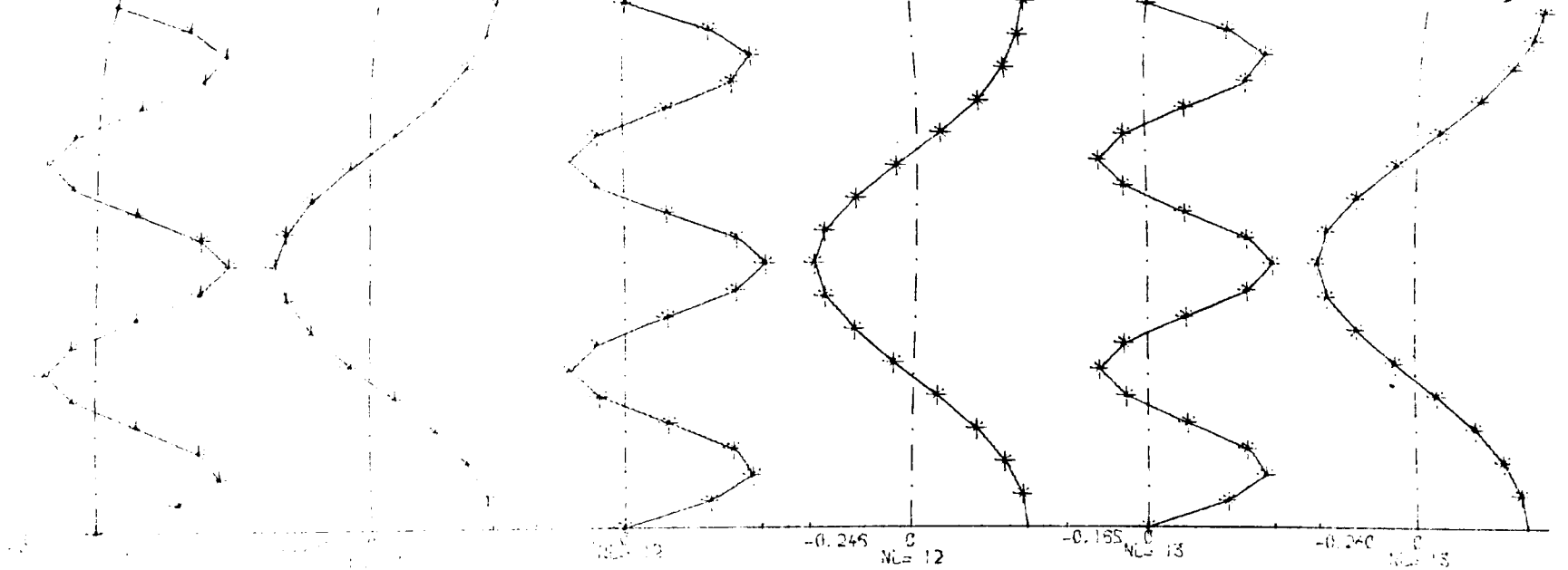

P.H. =50m
L/R =0.50
R/T =200
b =0.0
$w_o^* = R/1000$

Fig.6.233

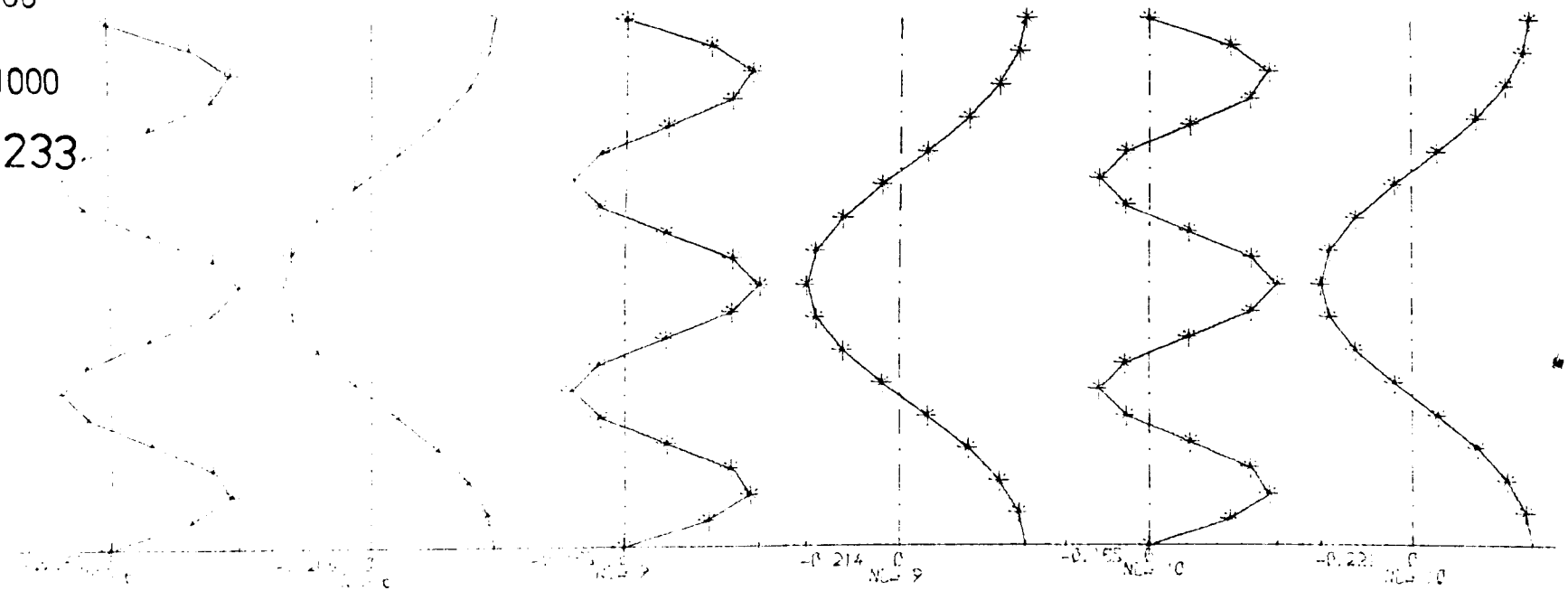

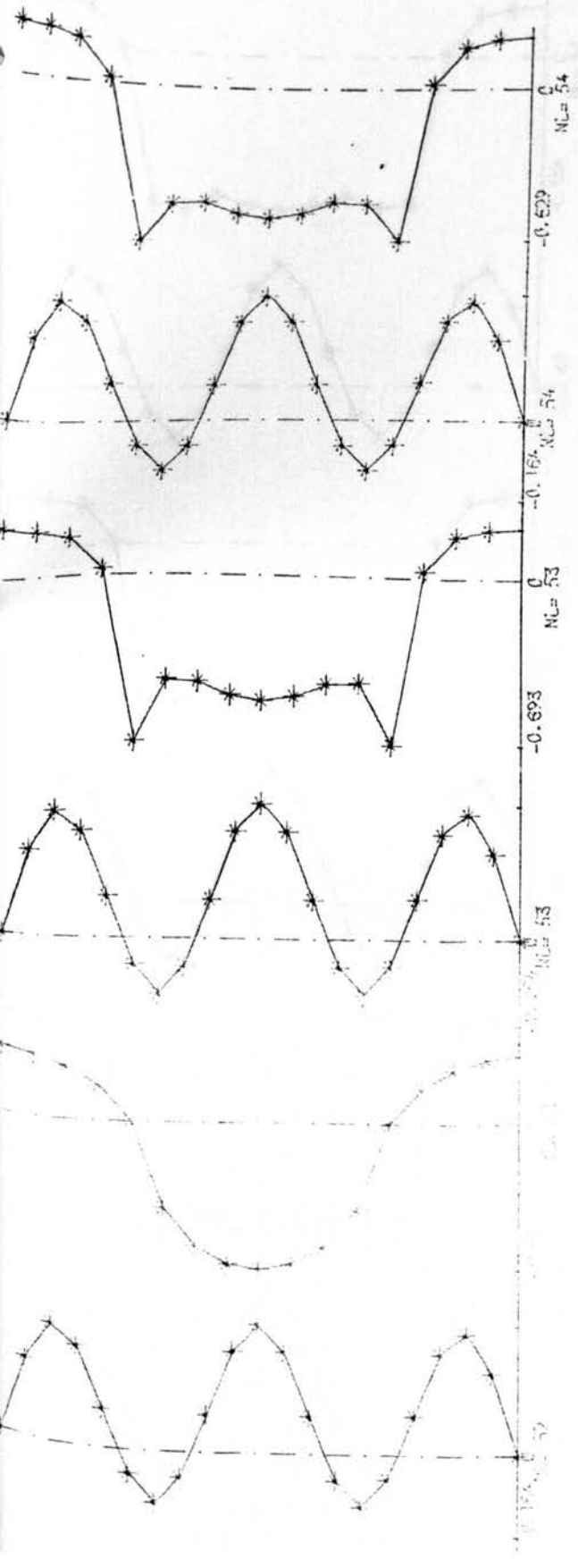
-0.629
-0.693

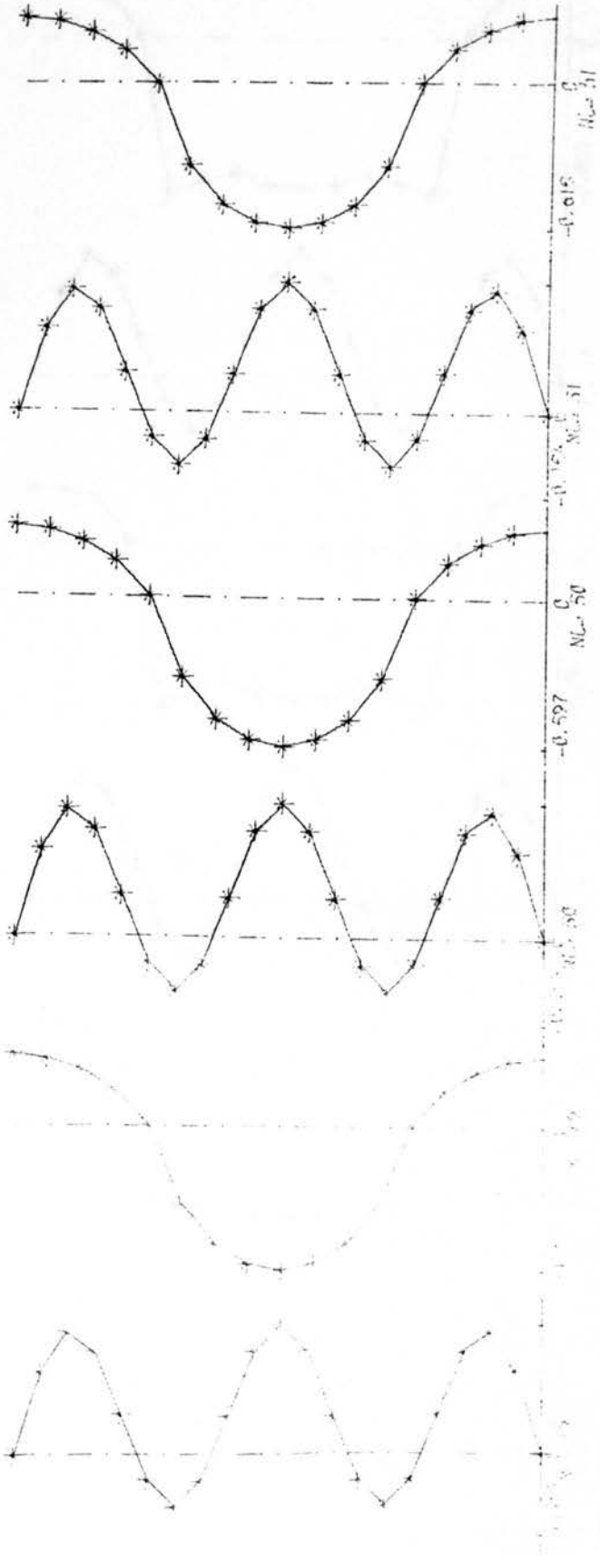

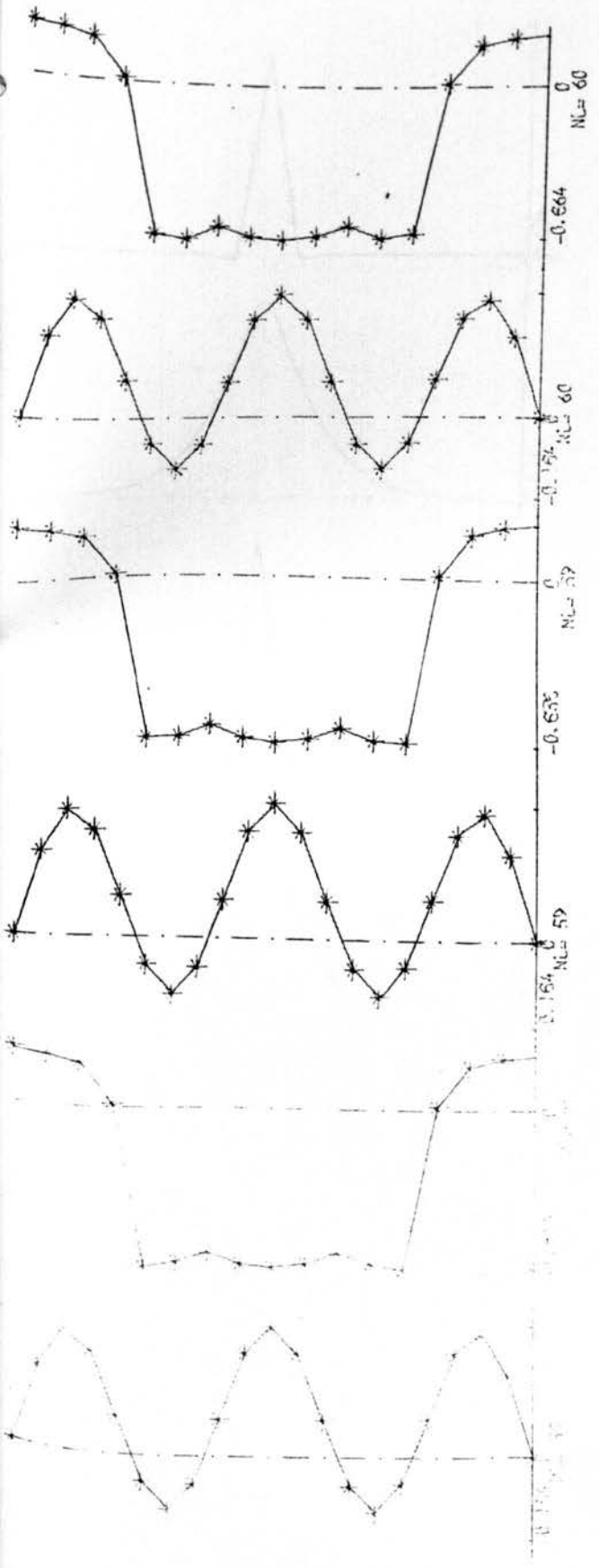
0
-0.664
0
-0.635

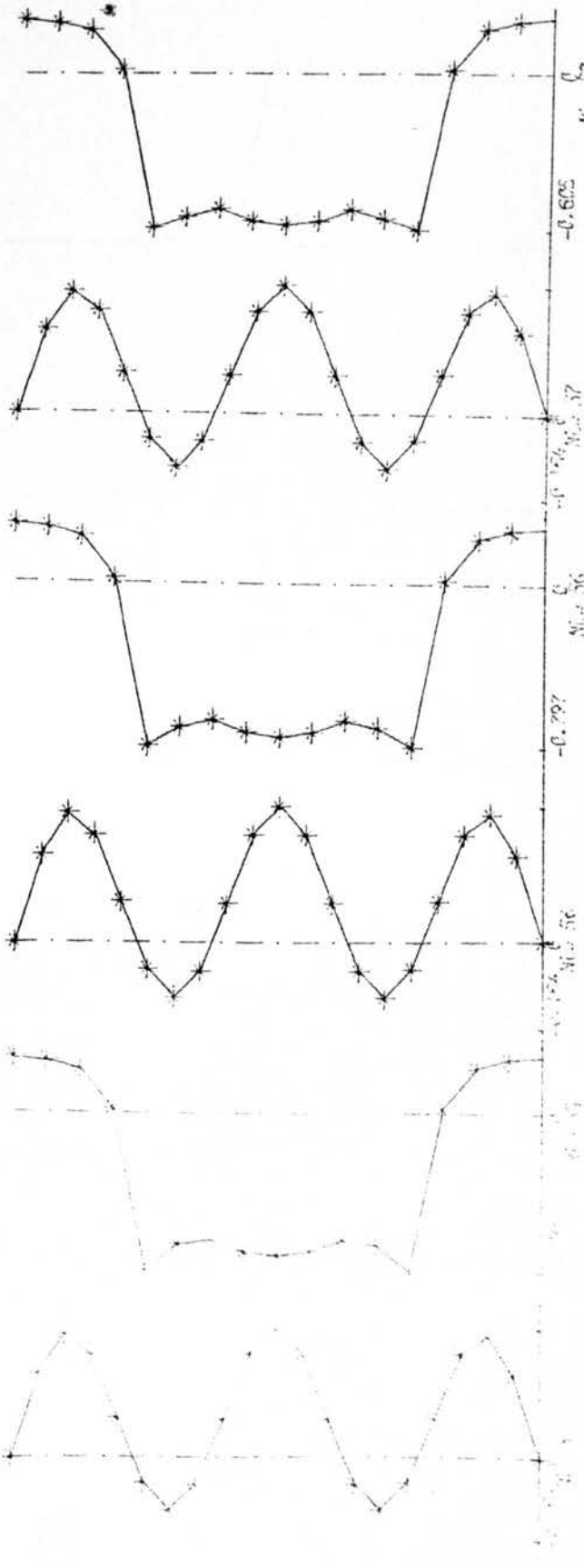
0
-0.625
0
-0.797

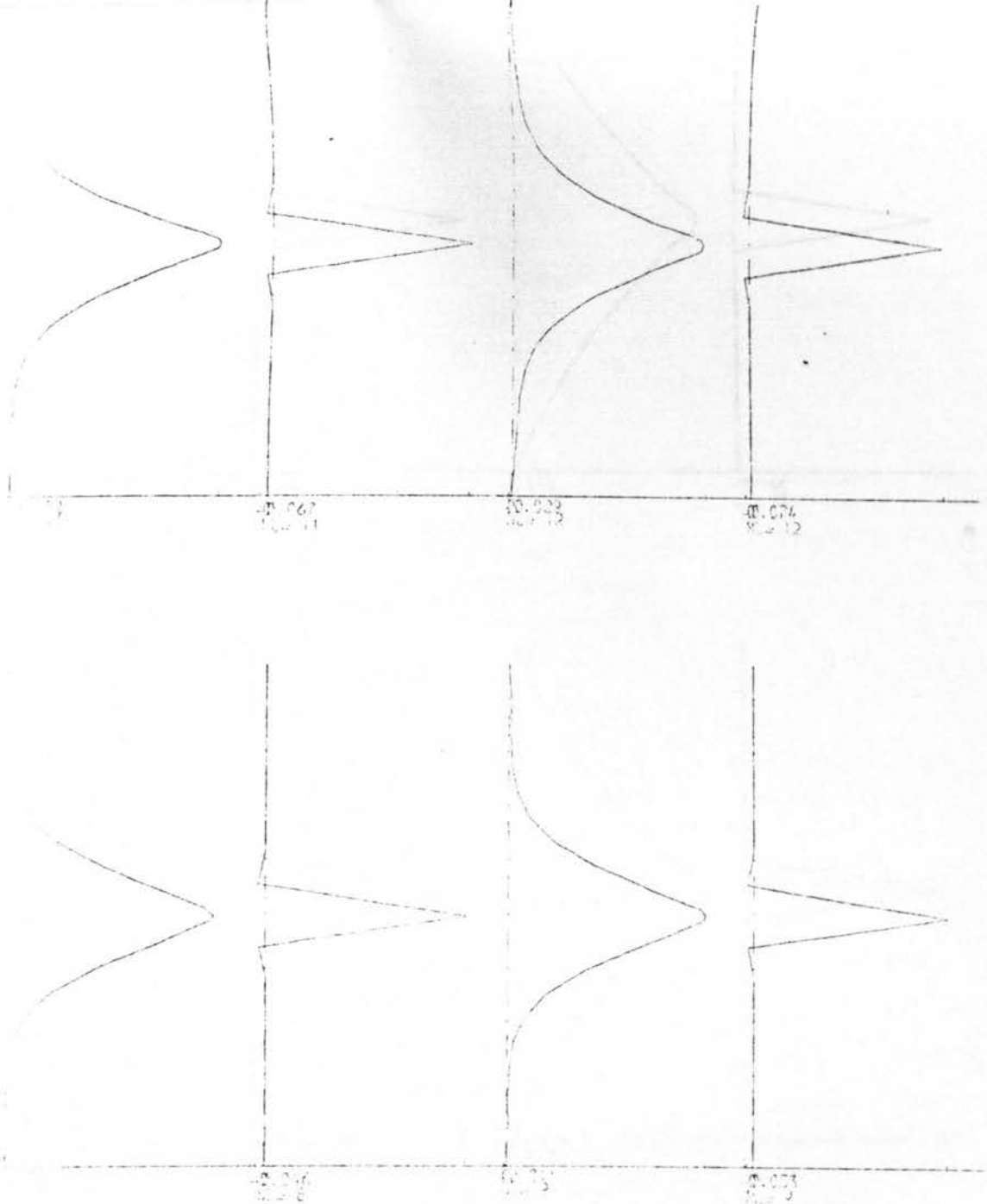

POINT LOAD
L / R = 0·25
R / T = 100

Fig.6.234

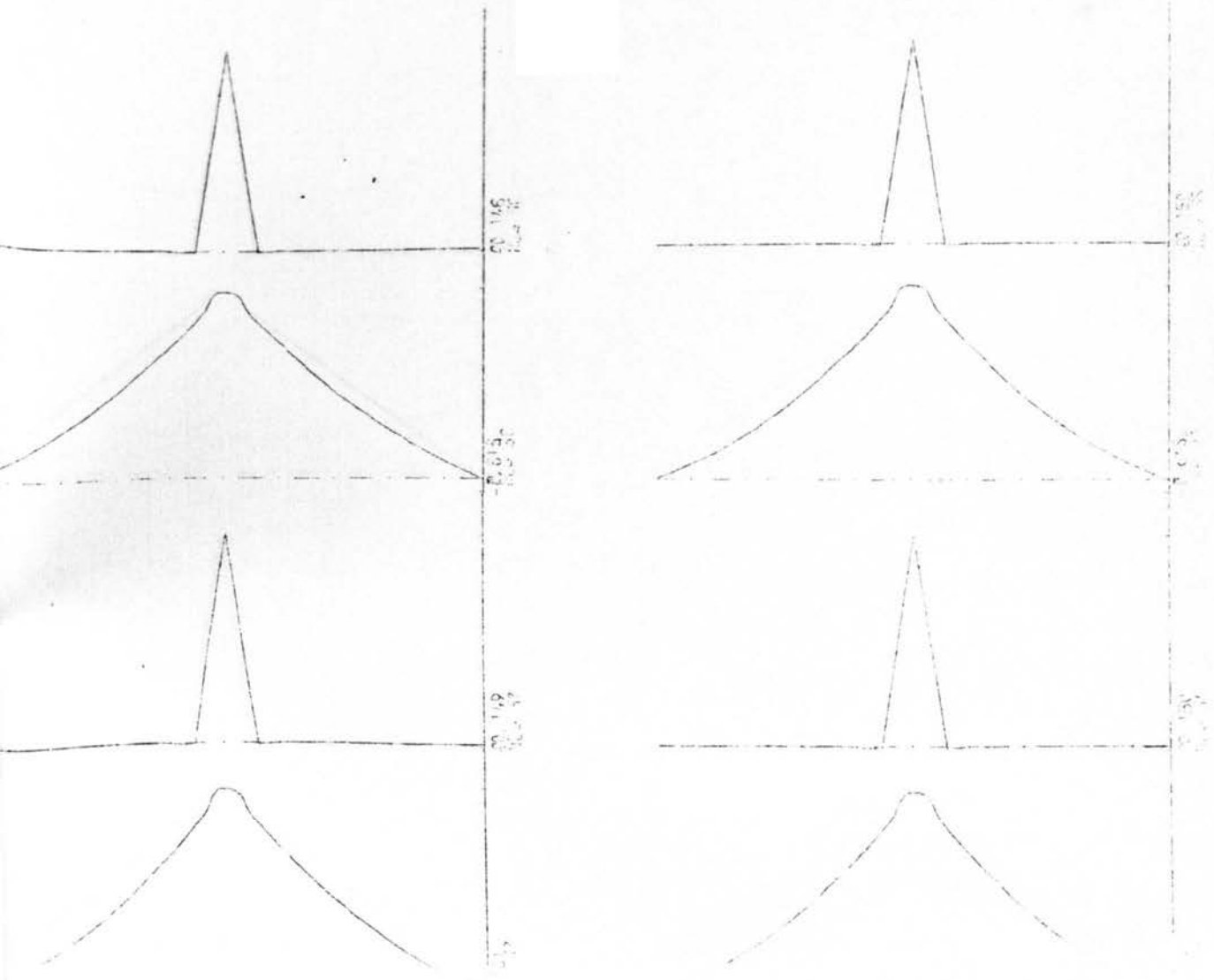

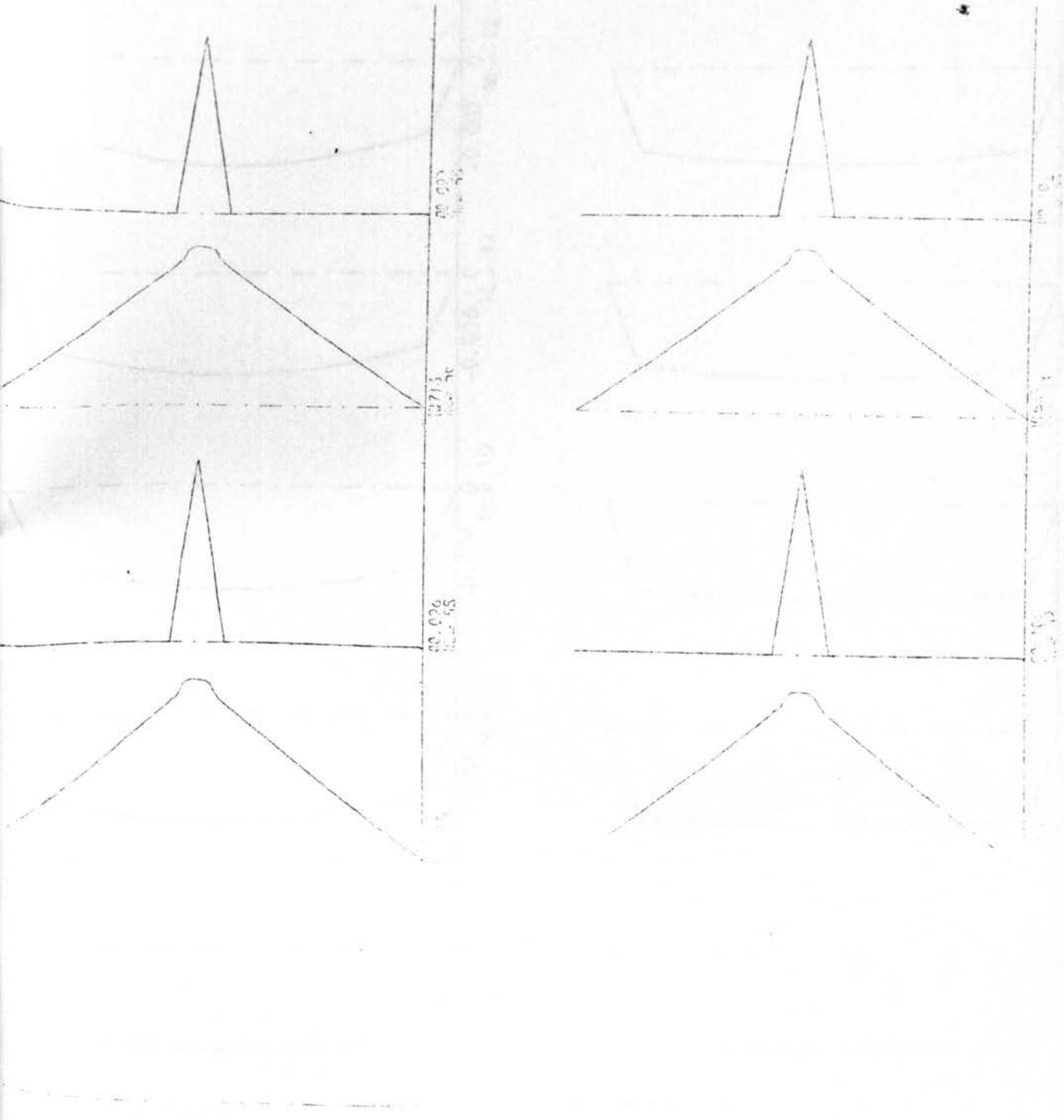

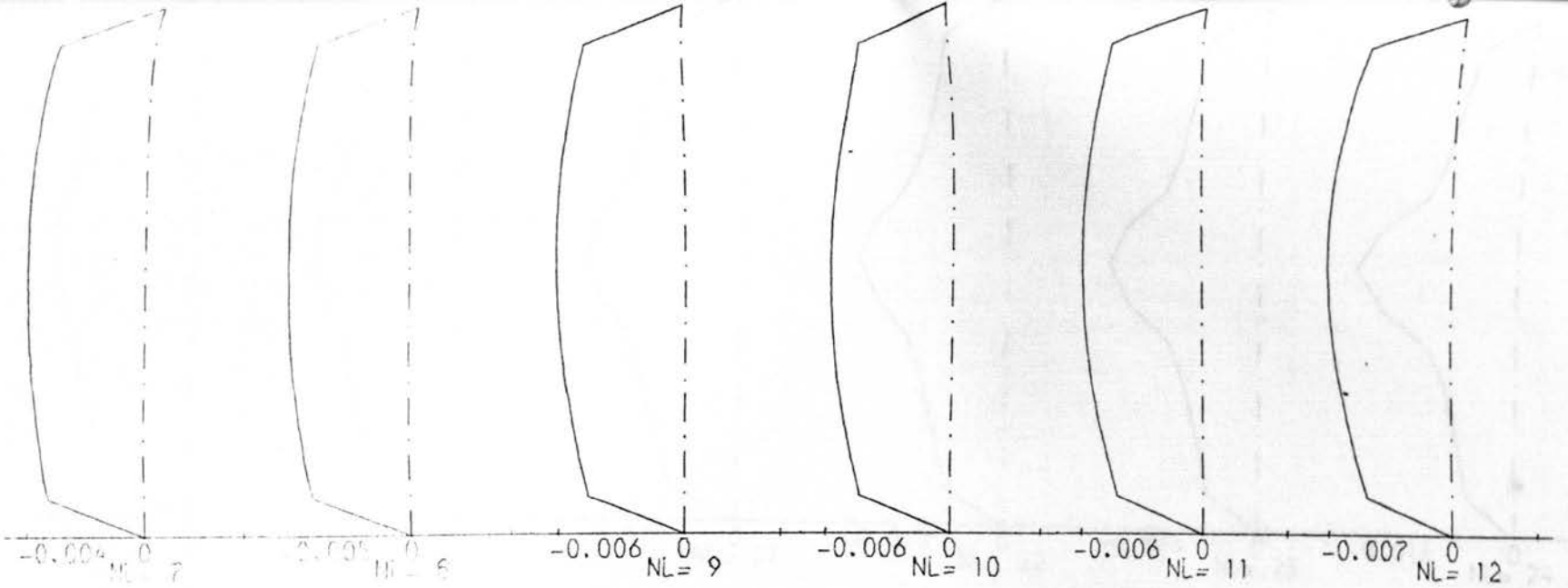

L/r=50
R/T=10
S.S.

Fig.6.235

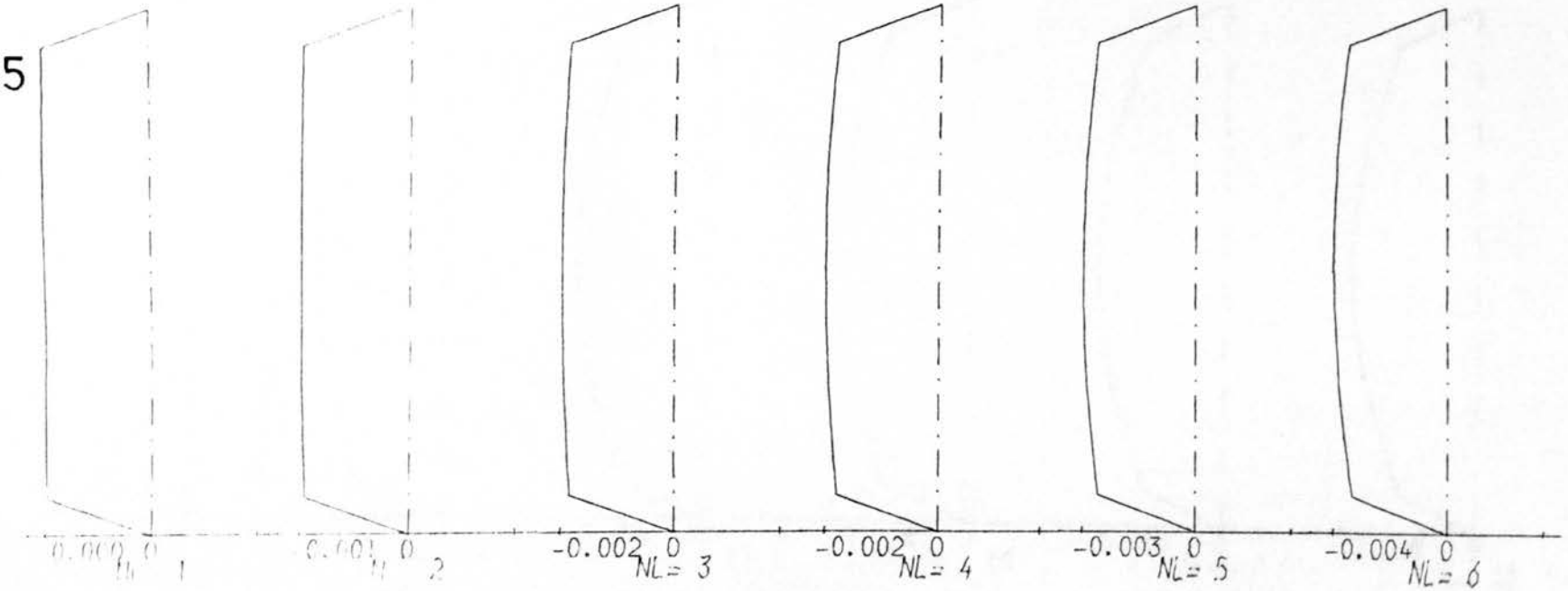

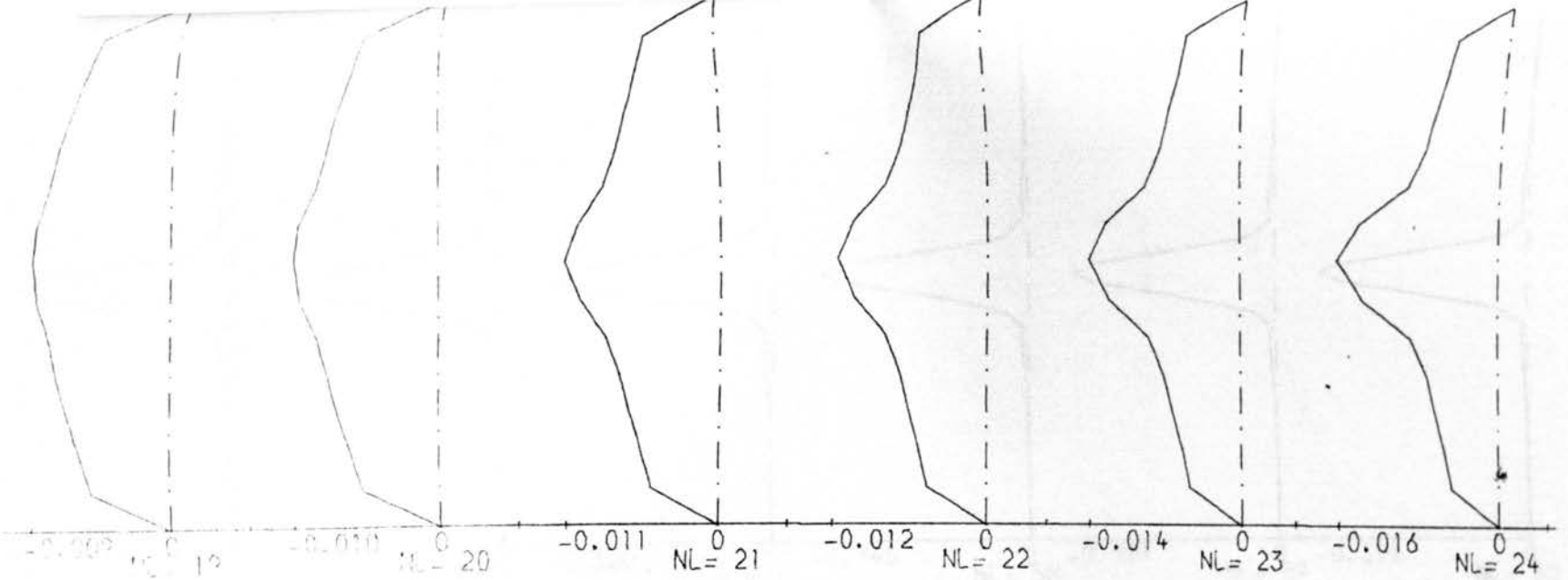
-0.011
0
NL= 21
-0.012
0
NL= 22
-0.014
0
NL= 23
-0.016
0
NL= 24

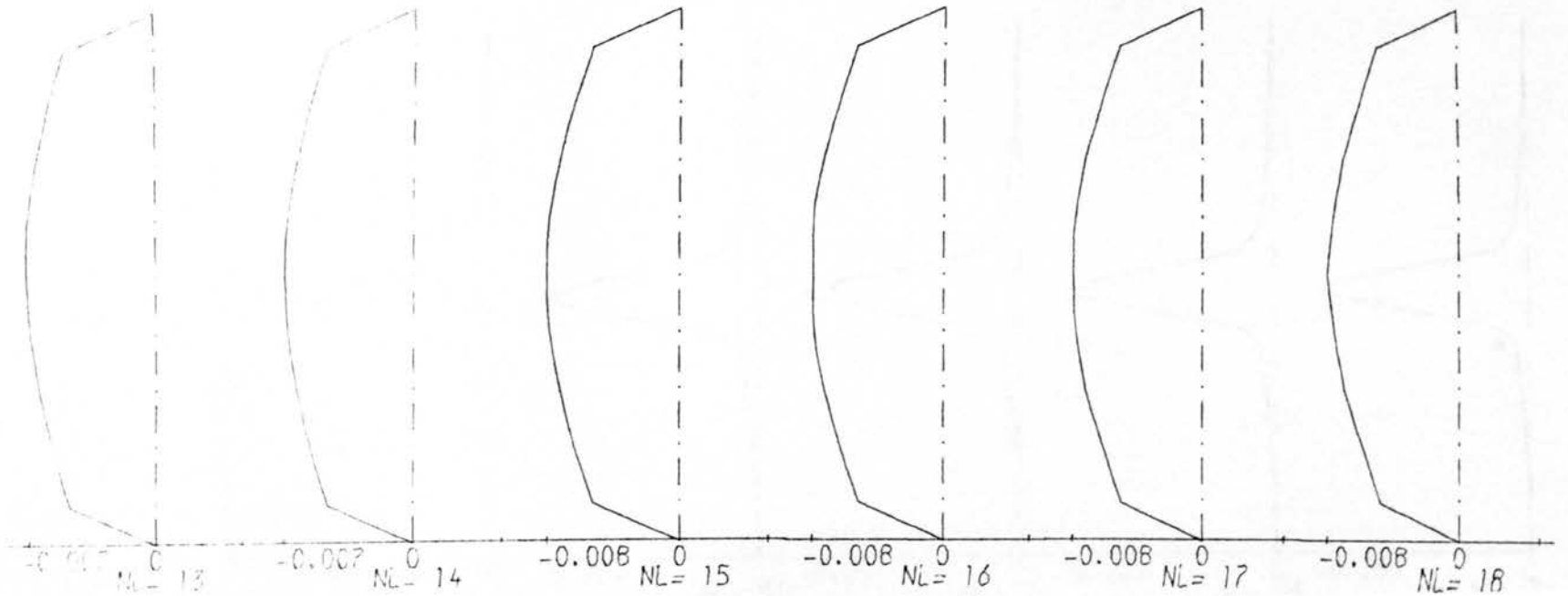
-0.007
0
NL= 14
-0.008
0
NL= 15
-0.008
0
NL= 16
-0.008
0
NL= 17
-0.008
0
NL= 18

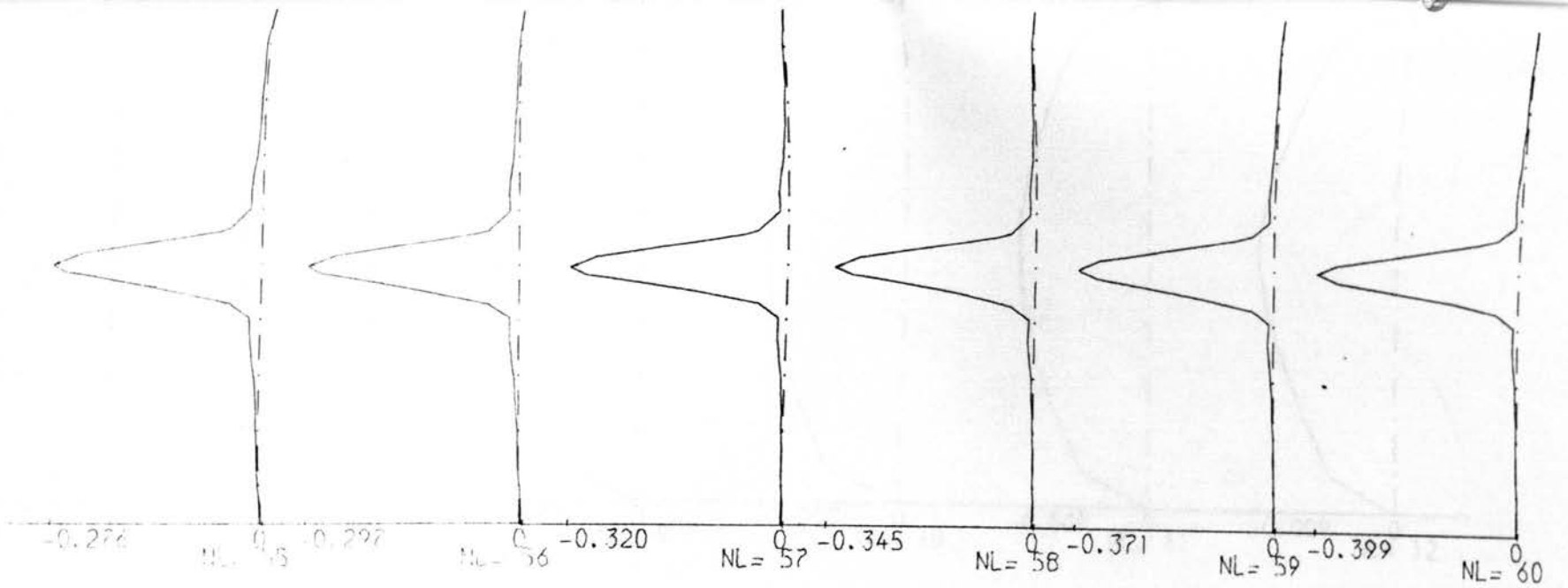
-0.320
NL= 57
-0.345
NL= 58
-0.371
NL= 59
-0.399
NL= 60

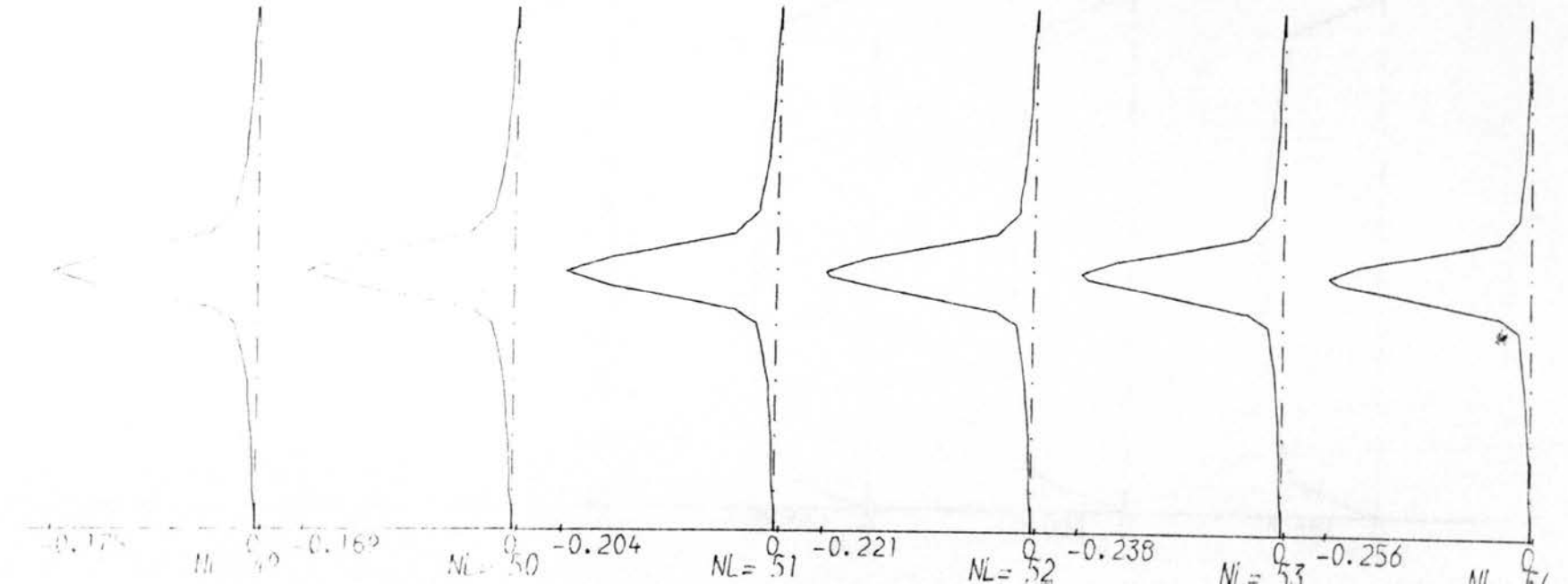
-0.204
NL= 51
-0.221
NL= 52
-0.238
-0.256

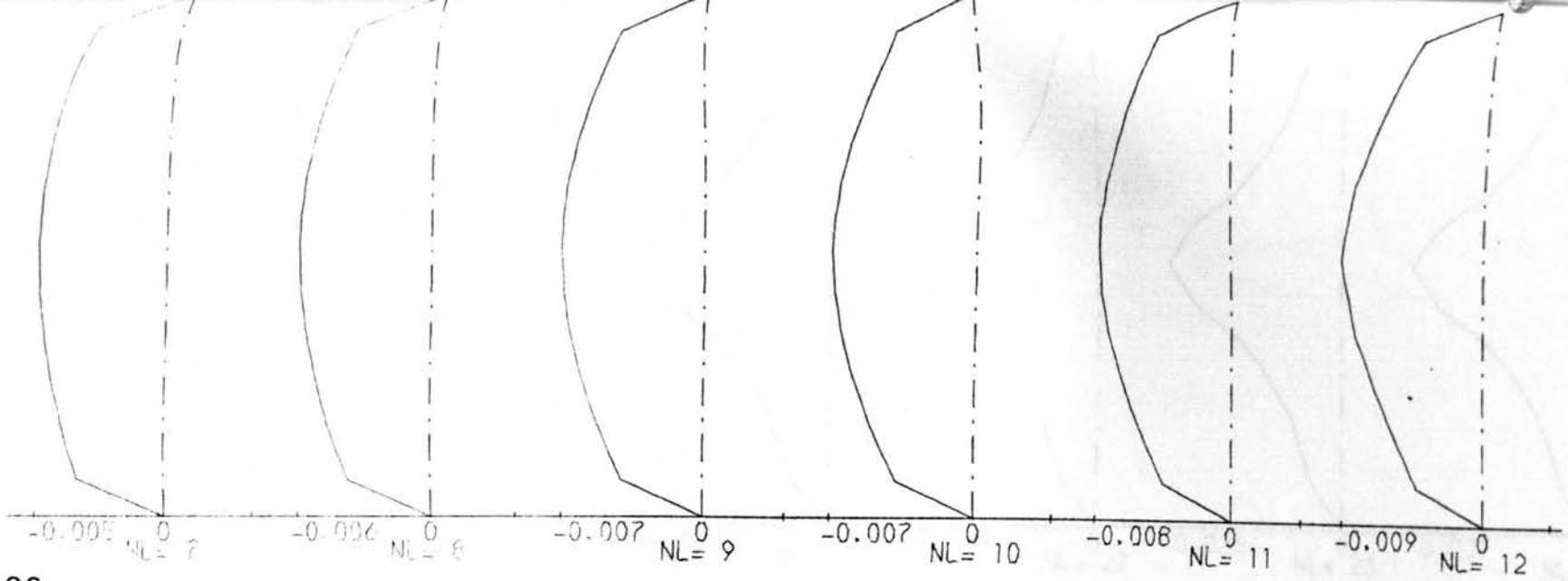

L/r = 90

R/T = 10

S.S.

Fig.6.23b

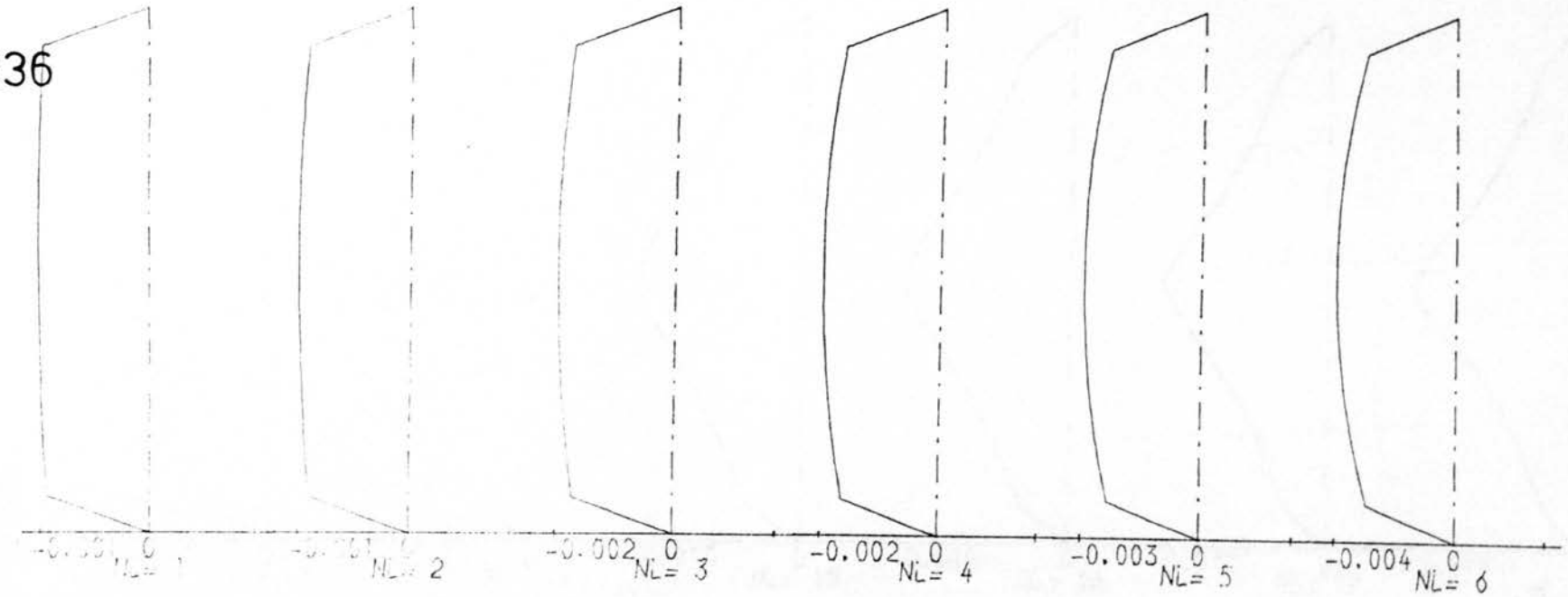

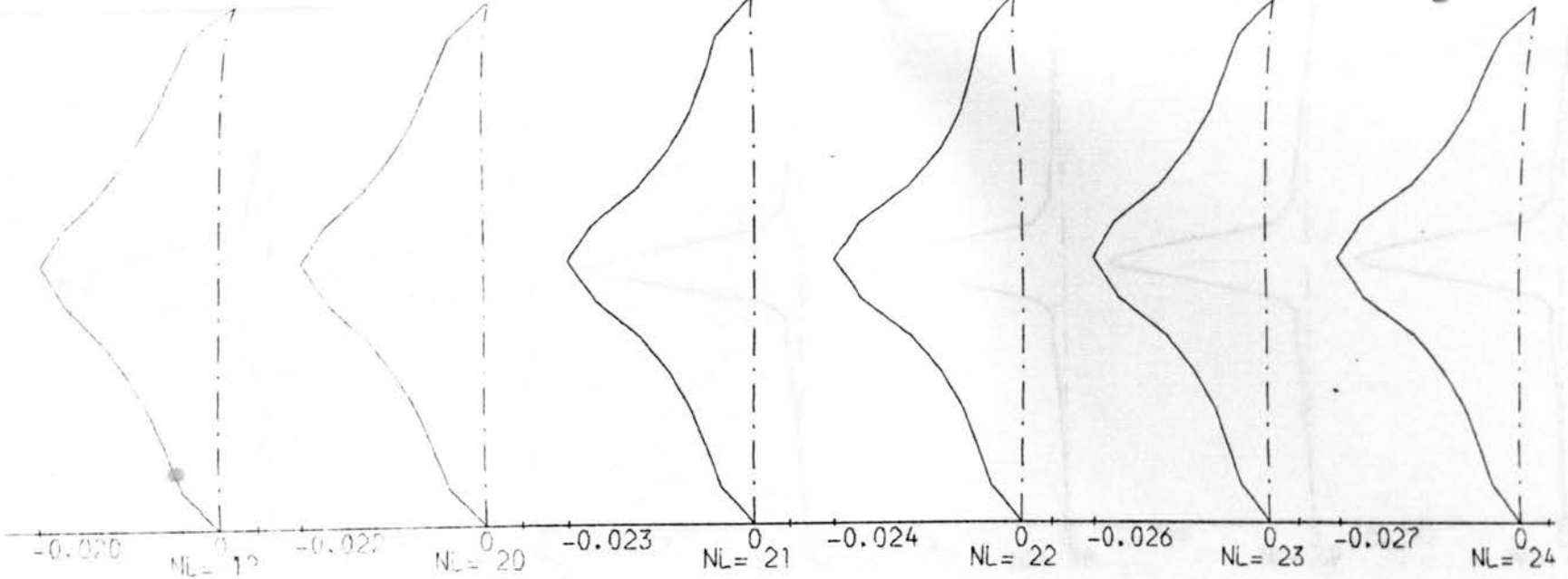
-0.020
0
NL= 19
-0.022
0
NL= 20
-0.023
0
NL= 21
-0.024
0
NL= 22
-0.026
0
NL= 23
-0.027
0
NL= 24

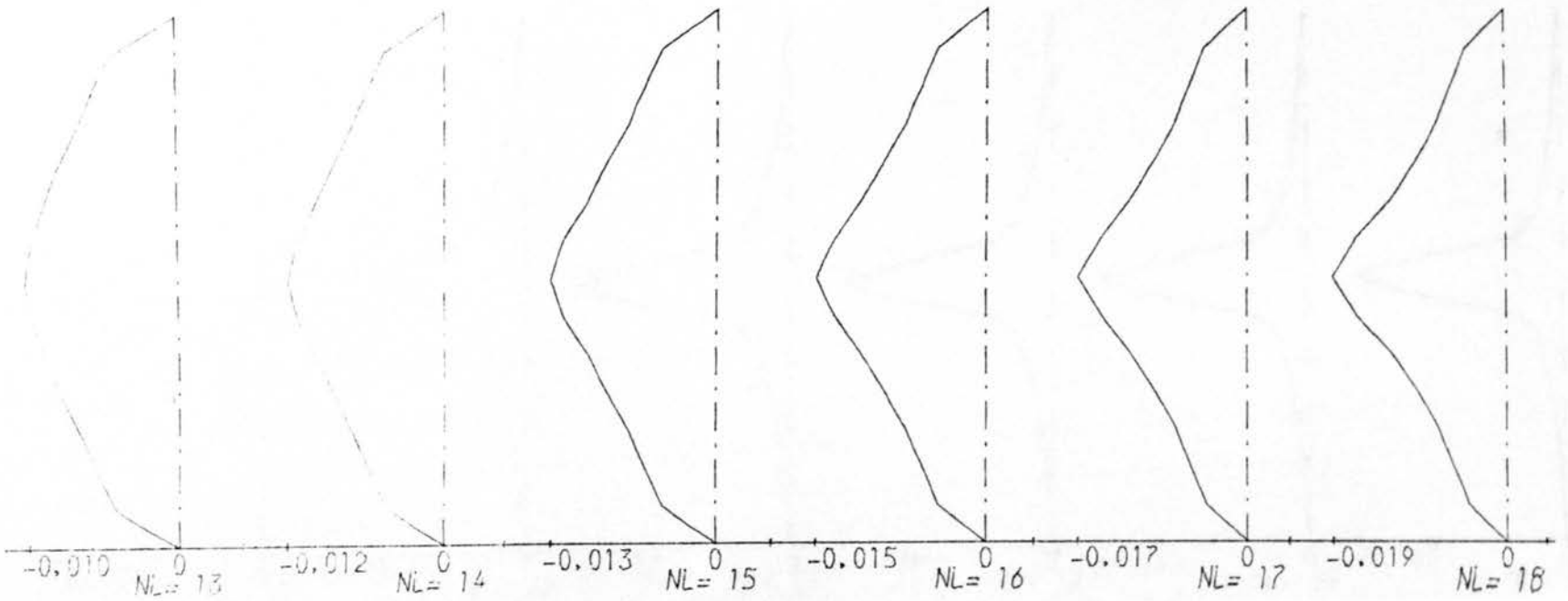
-0.010
0
NL= 13
-0.012
0
NL= 14
-0.013
0
NL= 15
-0.015
0
NL= 16
-0.017
0
NL= 17
-0.019
0
NL= 18

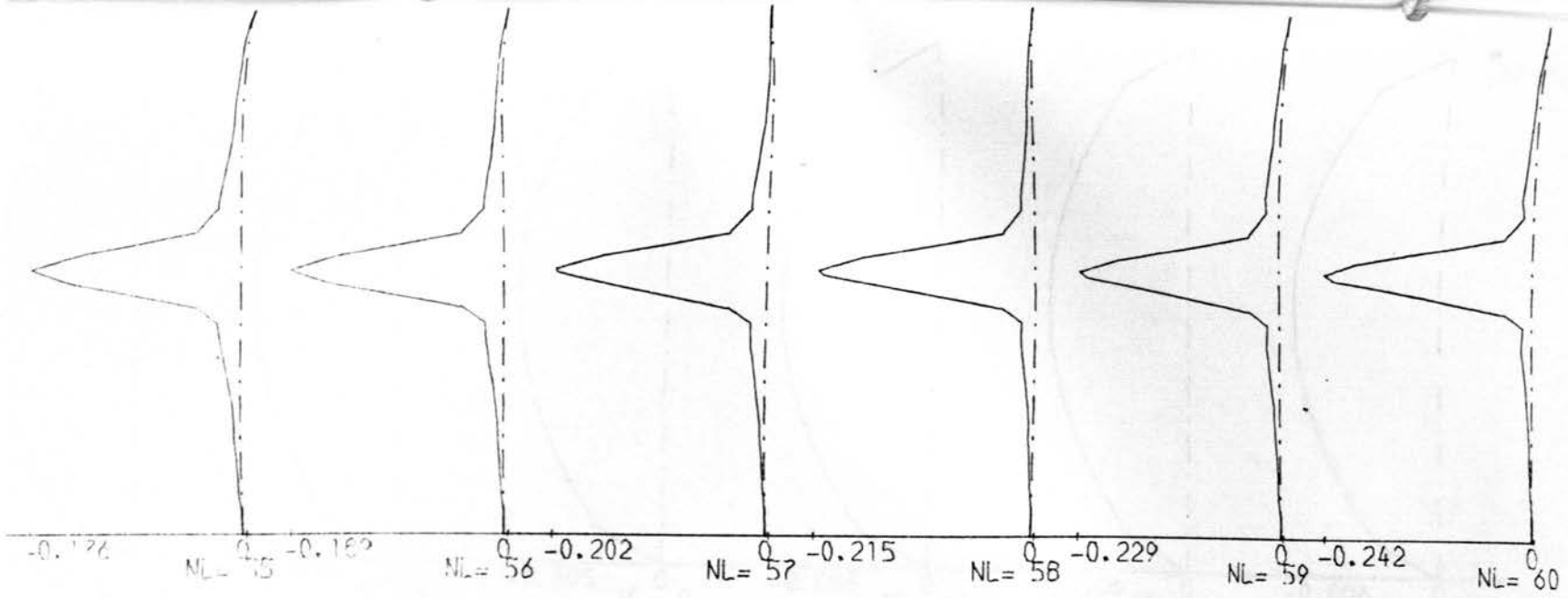
-0.176
0
NL= 55
-0.189
0
NL= 56
-0.202
0
NL= 57
-0.215
0
NL= 58
-0.229
0
NL= 59
-0.242
0
NL= 60

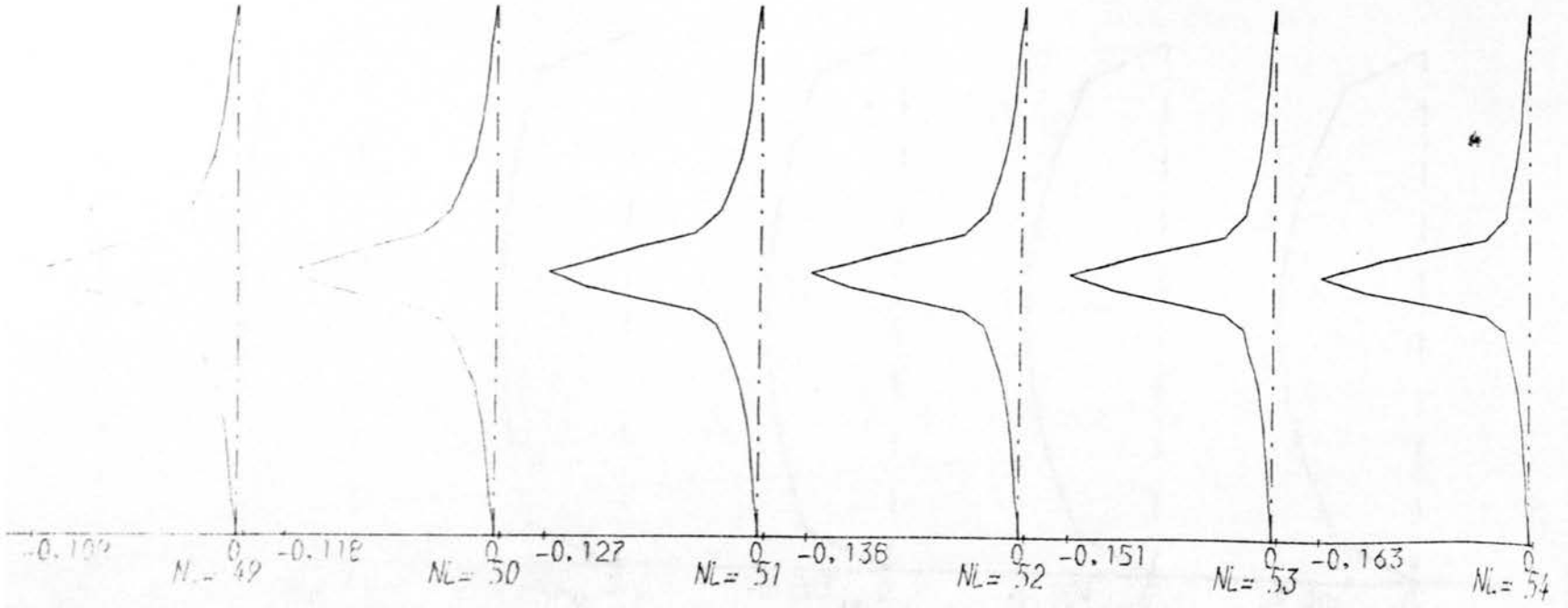
-0.103
0
NL= 49
-0.116
0
NL= 50
-0.127
0
NL= 51
-0.136
0
NL= 52
-0.151
0
NL= 53
-0.163
0
NL= 54

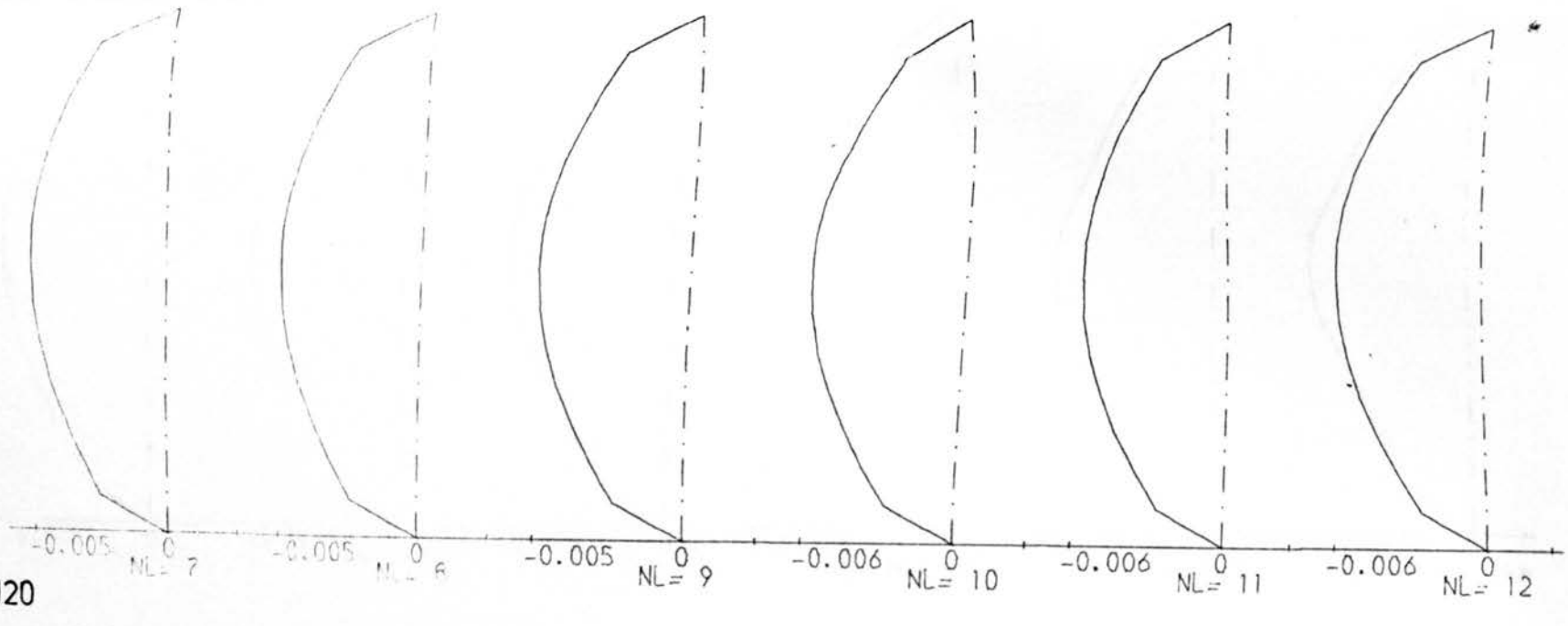

L/r =120

R/T =10

S.S.

Fig.6.237

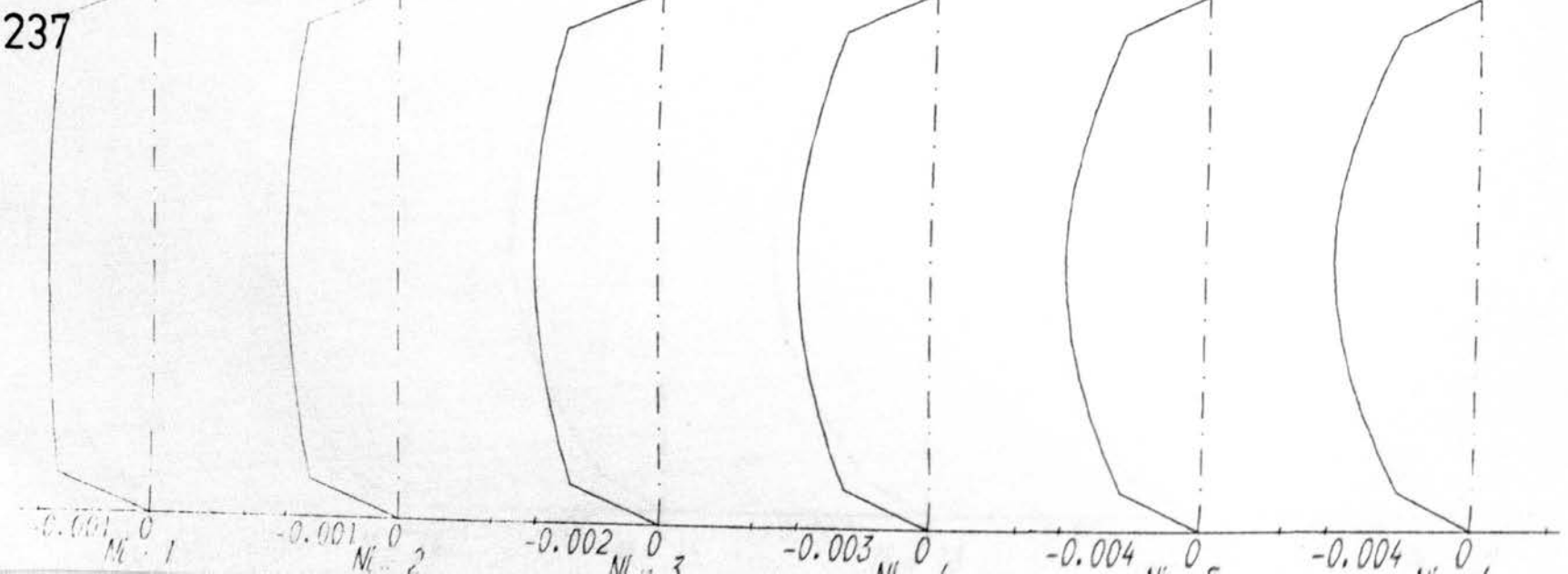

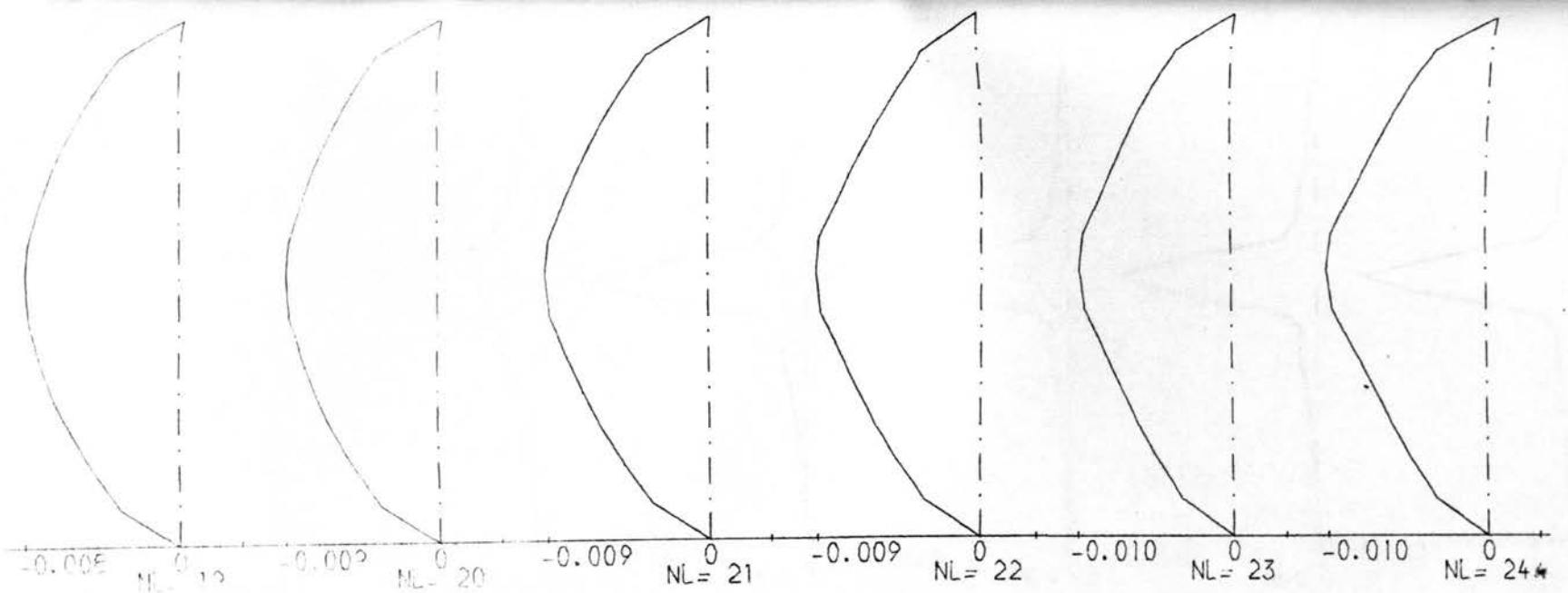
-0.009
0
NL= 21
-0.009
0
NL= 22
-0.010
0
NL= 23
-0.010
0
NL= 24

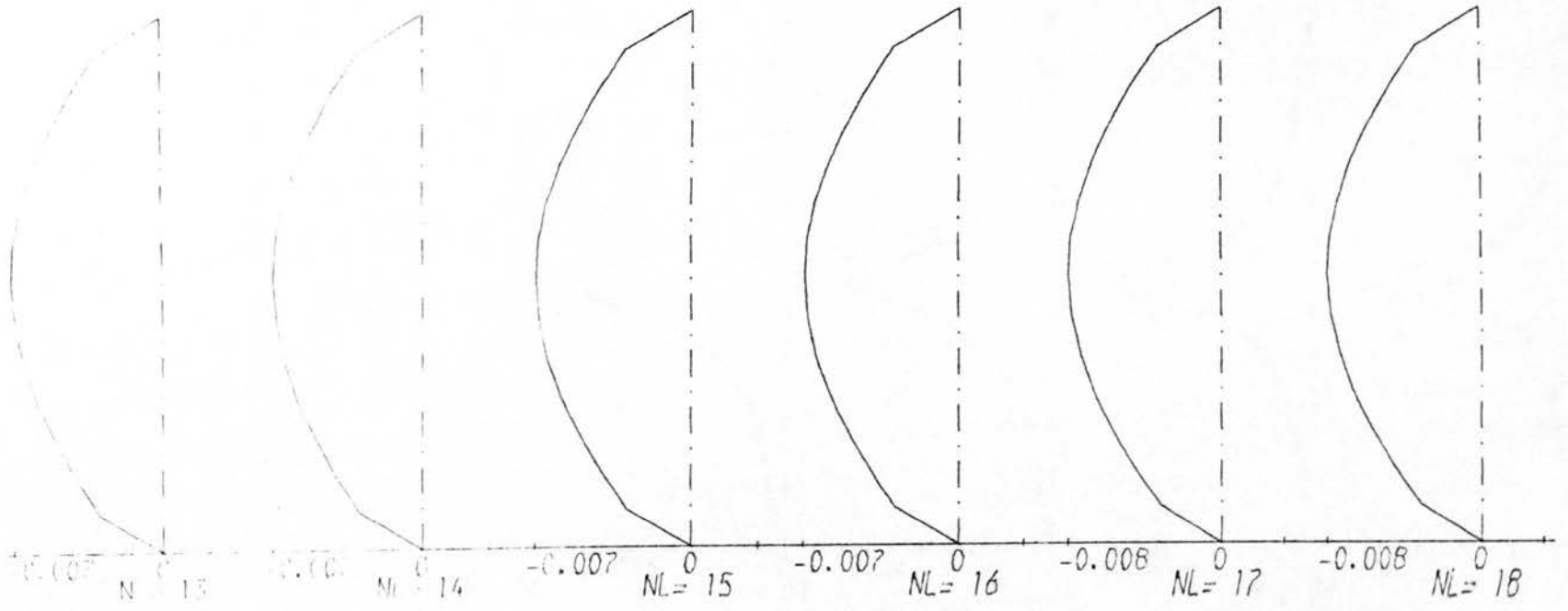
-0.007
0
NL= 15
-0.007
0
NL= 16
-0.008
0
NL= 17
-0.008
0
NL= 18